

N O T I C E

THIS DOCUMENT HAS BEEN REPRODUCED FROM
MICROFICHE. ALTHOUGH IT IS RECOGNIZED THAT
CERTAIN PORTIONS ARE ILLEGIBLE, IT IS BEING RELEASED
IN THE INTEREST OF MAKING AVAILABLE AS MUCH
INFORMATION AS POSSIBLE

11
NASA Contractor Report 165333

(NASA-CR-165333) STAGNATION REGION GAS FILM
COOLING: SPANWISE ANGLED INJECTION FROM
MULTIPLE ROWS OF HOLES Final Report (Purdue
Univ.) 81 p HC A05/MF A01 CSCI 20D

N81-25333

Unclas

G3/34 26546

STAGNATION REGION GAS FILM COOLING - SPANWISE
ANGLED INJECTION FROM MULTIPLE ROWS OF HOLES

D. W. Luckey and M. R. L'Ecuyer

Purdue University
Thermal Sciences and Propulsion Center
West Lafayette, Indiana

April 1981



Prepared for
Office of Naval Research
Under Contract N00014-75-C-0873

and

NATIONAL AERONAUTICS AND SPACE ADMINISTRATION
Lewis Research Center
Under Grant NSG-3071

FOREWARD

The study reported herein was conducted under the sponsorship of the Office of Naval Research, Power Program, Contract No. N00014-75-C-0873. The experimental apparatus used was fabricated with partial support from the NASA Lewis Research Center under Grant No. NSG 3071. The subject study was performed under the technical cognizance of Mr. James R. Patton, Jr., Office of Naval Research.

A follow-on study (to be reported in 1981) was conducted under the sponsorship of the National Aeronautics and Space Administration, Grant No. NSG 3071, with technical cognizance of Mr. F.S. Stepka, NASA Lewis Research Center, Turbine Cooling Branch.

The authors express their appreciation for the support provided by the aforementioned agencies. The authors also wish to acknowledge the assistance of: Dr. B.A. Reese, Chief Scientist, AEDC(AFSC), formerly Professor and Head, School of Aeronautics and Astronautics, Purdue University; Mr. C.E. Brockley, Thermogage, Inc.; Mr. G. Tekulve, J.C. Wilson Engineering Corp.; Mr. F.G. Risser, Electronics Shop, School of Mechanical Engineering, Purdue University. The manuscript was prepared with the assistance of Ms. L.K. Vadyak and Ms. S.L. Nejfelt, Thermal Sciences and Propulsion Center, Purdue University.

TABLE OF CONTENTS

	Page
NOMENCLATURE	vi
I. INTRODUCTION	1
I.A. General Discussion	1
I.B. Introduction to Film Cooling Parameters	4
I.C. Review of the Literature	9
I.C.1. Film Cooling Performance Parameters	9
I.C.2. Film Cooling Geometry	15
I.C.3. Mass Flux Ratio and Angle of Injection	20
I.C.4. Freestream Conditions	25
I.D. Scope of the Investigation	28
II. EXPERIMENTAL INVESTIGATION	31
II.A. Modeling of Gas Turbine Environment	31
II.B. General Description of Experimental Apparatus	32
II.B.1. Flow System	32
II.B.2. Test Cylinder	39
II.B.3. Instrumentation and Measurements	48
II.C. Description of Experiment	55
II.D. Data Reduction	61
III. FREESTREAM CONDITIONS AND HEAT TRANSFER WITHOUT FILM COOLING	64
III.A. Freestream Conditions	64
III.B. Cylinder Temperature Distribution	71
III.C. Cylinder Pressure Distribution	72
III.D. Cylinder Heat Flux Distribution	79
IV. SINGLE ROW COOLANT INJECTION	91
IV.A. Introduction	91

	Page
IV.B. Presentation of Single Row Data	93
IV.B.1. Spanwise Injection at $\theta_1 = 5^\circ$	93
IV.B.2. Spanwise Injection at $\theta_1 = 22.9^\circ$	100
IV.B.3. Spanwise Injection at $\theta_2 = 40.8^\circ$	105
IV.B.4. Spanwise Injection at $\theta_3 = 58.7^\circ$	117
IV.B.5. Upstream Effects for Single Row Injection	124
IV.C. Discussion of Results	124
IV.C.1. Introduction	124
IV.C.2. Coolant Jet Behavior	127
IV.C.3. Film Cooling Effectiveness	129
IV.C.4. Spanwise Averaged Film Cooling Results	133
IV.D. Summary	137
V. MULTIPLE ROW INJECTION WITH A UNIFORM BLOWING DISTRIBUTION	139
V.A. Introduction	139
V.B. Presentation of the Data	139
V.B.1. Five Row Configuration with First Row at $\theta_1 = 5^\circ$, $S/d = P/d = 5$	140
V.B.2. Three Row Configuration with First Row at $\theta_1 = 5^\circ$, $S/d = P/d = 10$	150
V.B.3. Two Row Configuration with First Row at $\theta_2 = 22.9^\circ$, $S/d_0 = P/d_0 = 10$	152
V.C. Discussion of the Results	160
V.C.1. Introduction	160
V.C.2. Five Row Configuration ($\theta_1 = 5^\circ$, $S/d_0 = P/d = 5$)	162
V.C.3. Three Row Configuration ($\theta_1 = 5^\circ$, $S/d_0 = P/d = 10$)	169
V.C.4. Two Row Configuration ($\theta_2 = 22.9^\circ$, $S/d_0 = P/d = 10$)	173
V.C.5. Spanwise Averaged Results	179
V.C.6. Prediction of the Results for Multiple Row Injection	191
V.D. Summary	194
VI. MULTIPLE ROW INJECTION WITH A BLOWING DISTRIBUTION SIMULATING PLENUM SUPPLY	197
VI.A. Introduction	197
VI.B. Presentation of the Data	198
VI.B.1. Five Row Configuration with First Row at $\theta_1 = 5^\circ$, $S/d = P/d = 5$	198
VI.B.2. Three Row Configuration with First Row at $\theta_1 = 5^\circ$, $S/d = P/d = 10$	210
VI.B.3. Two Row Configuration with First Row at $\theta_2 = 22.9^\circ$, $S/d_0 = P/d_0 = 10$	215

	Page
VI.C. Discussion of the Results	223
VI.C.1 Five Row Configuration ($\theta_1 = 5^\circ$, $S/d_0 =$ P/d = 5)	223
VI.C.2. Three Row Configuration ($\theta_1 = 5^\circ$, $S/d_0 =$ P/d = 10)	228
VI.C.3. Two Row Configuration ($\theta_2 = 22.9^\circ$, $S/d_0 =$ P/d = 10)	230
VI.D. Summary	232
VII. EFFECT OF FREESTREAM TURBULENCE INTENSITY ON FILM COOLING PERFORMANCE	234
VIII. CONCLUSIONS	242
VIII.A. Single Row Injection	243
VIII.B. Multiple Row Injection with Uniform Blowing . . .	244
VIII.C. Multiple Row Injection with a Blowing Distribution Simulating a Plenum Supply	245
VIII.D. The Influence of Freestream Turbulence Intensity on Film Cooling Performance	246
BIBLIOGRAPHY	247
APPENDICES	
I. Blowing Ratio Distribution Simulating a Plenum Supply	251
II. Surface Roughness of the Test Cylinder	259
III. Experimental Data from the Film Cooling Experiments	264

NOMENCLATURE

C_p	pressure coefficient, $(P_w - P_{\infty,0})/(P_{T\infty,0} - P_{\infty,0})$
c_p	specific heat at constant pressure
D	test cylinder diameter
d_o	coolant hole diameter
Ec	Eckert number, $V_{\infty}^2/c_p(T_{\infty} - T_w)$
h	local heat transfer coefficient
h'	local heat transfer coefficient with film cooling, $q_{FC}''/(T_{adw} - T_{w,FC})$
\bar{h}	laterally averaged heat transfer coefficient
I	momentum flux ratio, $\rho_c V_c^2/\rho_{\infty} V_{\infty}^2$
k	thermal conductivity
K	acceleration parameter, $\frac{V_{\infty}}{V_{\infty}^2} \frac{dV_{\infty}}{dx}$
L	length of coolant hole
M	blowing or mass flux ratio, $\rho_c V_c/\rho_{\infty} V_{\infty}$
Ma	Mach number
\dot{m}	mass flow rate
Nu	Nusselt number
P	Row-to-row spacing on the surface
p	pressure
Pr	Prandtl number
q''	local heat flux

NOMENCLATURE (Cont'd)

Re	Reynolds number with density and viscosity evaluated at mean temperature, $T_m = (T_\infty + T_w)/2$
Re*	Reynolds number with freestream density and viscosity evaluated at $T_m = (T_\infty + T_w)/2$
R	gas constant
S	coolant hole centerline-to-centerline spacing along a row
St	Stanton number
s ₀	coolant slot height or width
T, t	temperature
T _u	turbulence intensity ($\sqrt{u'}/\bar{u}$)
u	x-component of velocity
V	velocity
v	y-component of velocity
x	distance in streamwise direction downstream of coolant holes
x/d ₀	dimensionless distance in streamwise direction downstream of coolant holes
y	vertical distance from surface
z	spanwise or lateral distance
z/S, z/d ₀	dimensionless spanwise distance
$1 - \frac{St_{FC}}{St_0}$	film cooling performance parameter, Stanton Number Reduction (SNR)

NOMENCLATURE (Cont'd)

GREEK

α	coolant injection angle measured along the test surface relative to the x-axis
β	coolant injection angle measured vertically from the test surface
δ	boundary layer thickness
δ^*	boundary layer displacement thickness
η	film cooling effectiveness parameter
θ	angular position along a cylinder relative to stagnation
θ_c	dimensionless coolant temperature ratio, $\frac{T_\infty - T_c}{T_\infty - T_w}$
θ_i	angular position of coolant injection along a cylinder relative to stagnation
θ_{mom}	boundary layer momentum thickness
ρ	density
μ	dynamic viscosity
ν	kinematic viscosity

SUBSCRIPTS

ad, adw	adiabatic wall condition
AVG	spanwise averaged condition
c	coolant condition
D	cylinder diameter
FC	film cooling condition
GAS	condition of freestream gases
i	at injection

NOMENCLATURE (Cont'd)

SUBSCRIPTS

m	downstream of multiple rows
max	spanwise maximum Stanton Number Reduction, $[1 - (St_{FC}/St_0)]_{\max}$, at fixed blowing ratio, M, and downstream distance x/d_0
nom	nominal wall temperature, $T_{w,nom}$, computed as an average of the temperature from the 47 wall thermocouples in the film cooled region
NEG	negative value of Stanton Number Reduction found directly behind the coolant hole ($z/S = 0.0$)
o	without film cooling
opt	for the optimum blowing ratio
s	downstream of a single row
T	total or stagnation condition
w	at the wall
∞	local freestream condition around the test cylinder
$\infty,0$	freestream condition upstream of the test cylinder
1,2,3,4,5	designates the following row locations, 1 = 5° , 2 = 22.9° , 3 = 40.8° , 4 = 58.7° , 5 = 76.6°

I. INTRODUCTION

I.A. General Discussion

A thermodynamic analysis of the gas turbine engine cycle shows that the performance of the gas turbine is strongly influenced by the maximum cycle temperature, i.e. the turbine (gas) inlet temperature. While increasing the inlet temperature will improve the power output and efficiency of the engine, it also results in higher operating temperatures for the turbine vanes and blades. Metallurgical technology has developed new alloys to provide increased strength at higher temperatures, but the demand for higher turbine inlet temperatures has resulted in the development of complex turbine cooling methods.

Two different techniques to cool the turbine vanes and blades can be used to maintain acceptable metal temperature levels. The first involves removing the heat from the inside of the vane after it has been transferred from the hot freestream gases through the vane surface. The second technique reduces the amount of heat transferred to the vane by protecting the outer surface of the vane from the hot freestream gases. Convective cooling within turbine vanes and blades has been used to provide the internal heat removal. The use of labyrinth channels, pin fins, and impingement flow has enhanced the effectiveness of the internal cooling techniques, but the demand for higher turbine inlet temperatures has required the development of more advanced cooling methods.

Transpiration and film cooling are two ways of providing additional cooling protection to the vanes and blades. Both processes involve injecting a relatively cool fluid from the vane interior through the wall and onto the external vane surface. This provides cooling in two ways, by forced convection as the coolant passes through the wall and by thermal protection as the coolant forms a blanket over the outer surface. In transpiration, the coolant is injected uniformly through a porous wall.

After passing through many passages in the wall, the coolant emerges at the surface with approximately the same temperature as the external wall. Although transpiration cooling has been found to be an effective method of providing extra thermal protection, the fabrication of a porous turbine vane poses a complex and expensive problem. In addition, the problems of pore obstruction due to oxidation within the porous material have forced the operating material temperature to be lowered, thus hampering the utilization of this scheme in turbine engines.

Film cooling is similar to transpiration in that it protects the surface from the influence of the hot freestream by injecting a coolant through the vane wall onto the surface. However, for film cooling, the coolant passes through discrete slots or holes machined in the vane. This technique makes the fabrication procedure easier and less costly. The coolant acts like a heat sink, providing a protective layer (blanket) of cool fluid along the surface. However, as the film flows downstream from the point of injection, it deteriorates as it mixes with the freestream. Therefore, an efficient application of film cooling on a turbine vane surface requires a thorough understanding of the film coolant behavior after injection. A poorly designed injection configuration could result in increased heat transfer to the surface.

A variety of ways can be used to film cool a surface. A cool, secondary fluid may be injected onto a surface through slots, interrupted slots, or holes as illustrated in Figure 1. Numerous studies have shown that a continuous slot provides better protection than a row of holes because of the increased mixing that occurs between the freestream and the coolant for hole injection. However, from a practical point of view, while slots and interrupted slots may be excellent for use in large components such as combustor liners, they are more difficult to use in smaller components like turbine vanes. High thermal stresses in the vane can cause structural problems that make the use of slots impractical, except perhaps in the trailing edge region. Therefore, most applications of film cooling on a turbine vane are accomplished using rows of holes in spite of the complex three-dimensional nature of the flow field and the large number of parameters that must be considered in an optimal design.

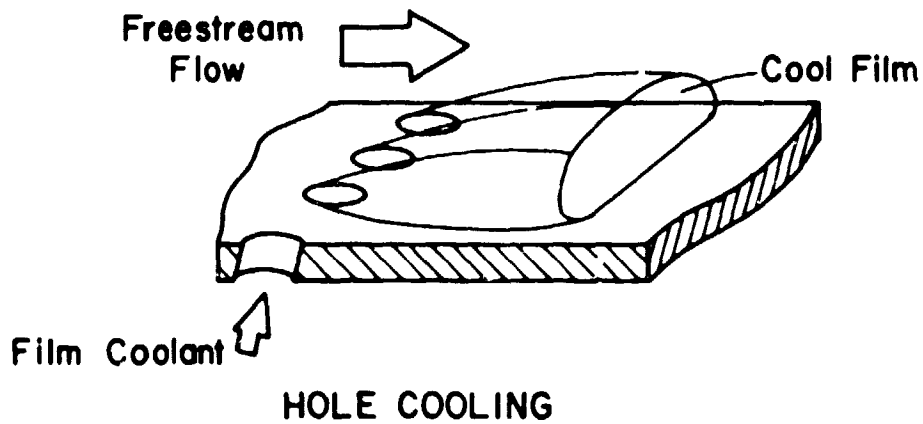
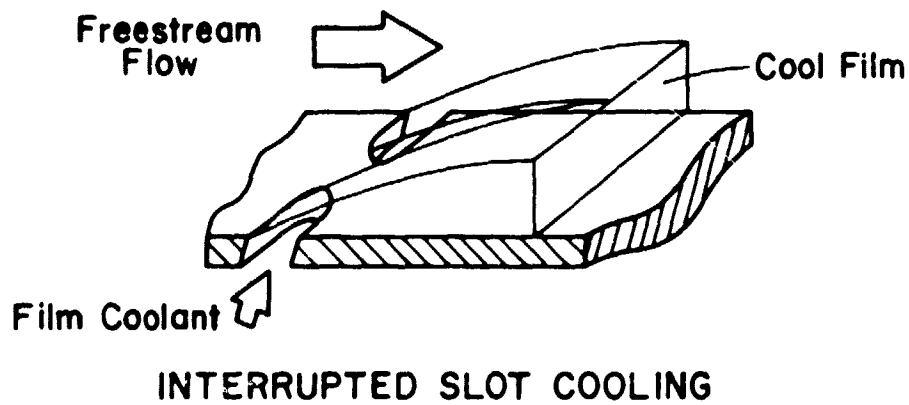
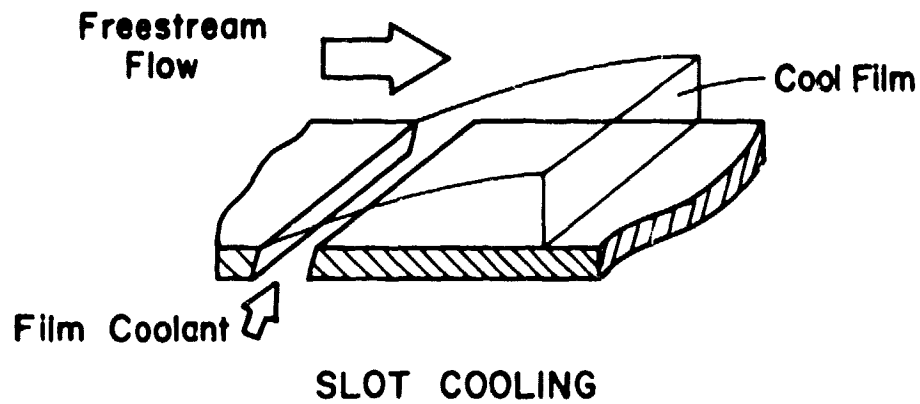


Figure 1. Film Cooling Configurations

Numerous investigations of discrete hole film cooling can be found in the literature describing the effect of coolant blowing, hole geometry, and freestream flow (pressure gradient, turbulence intensity, ...) on the film cooling performance. A large majority of these studies have been conducted on flat surfaces and the results have been used with success on the pressure and suction surfaces of the turbine vane. However, the stagnation or leading edge region of the vane, particularly on the first stage vane, is where the heat flux reaches its highest level and cooling protection is most crucial. A review of the literature reveals that minimal attention has been given to film cooling measurements in the leading edge region.

This study was devoted to providing film cooling data for the stagnation or leading edge region. The objective of this study was to investigate multiple row coolant injection (commonly referred to as full coverage film cooling) in the leading edge region. Using a circular cylinder to model the leading edge, extensive measurements were made downstream and between the injection holes to determine the ability of the film coolant to reduce the surface heat flux. The gas turbine environment was modeled by simulating the Reynolds number and the freestream-to-wall temperature ratio. The investigation encompassed a study of the influence of coolant blowing distribution, coolant hole-to-hole spacing, and freestream turbulence intensity on the film cooling performance in the leading edge region.

I.B. Introduction to Film Cooling Parameters

This section provides a general overview of the film cooling process and introduces a number of film cooling parameters. Film cooling involves the injection of a cool fluid onto a surface to protect it from the hot external freestream. The geometric parameters involved in establishing a coolant film over the surface are illustrated in Figure 2. After injection onto the surface, the coolant jets are turned downstream in the freestream (x) direction while at the same time spreading laterally across the surface in the z direction. If the coolant jets succeed in coalescing, they tend to reinforce each other, thus improving the

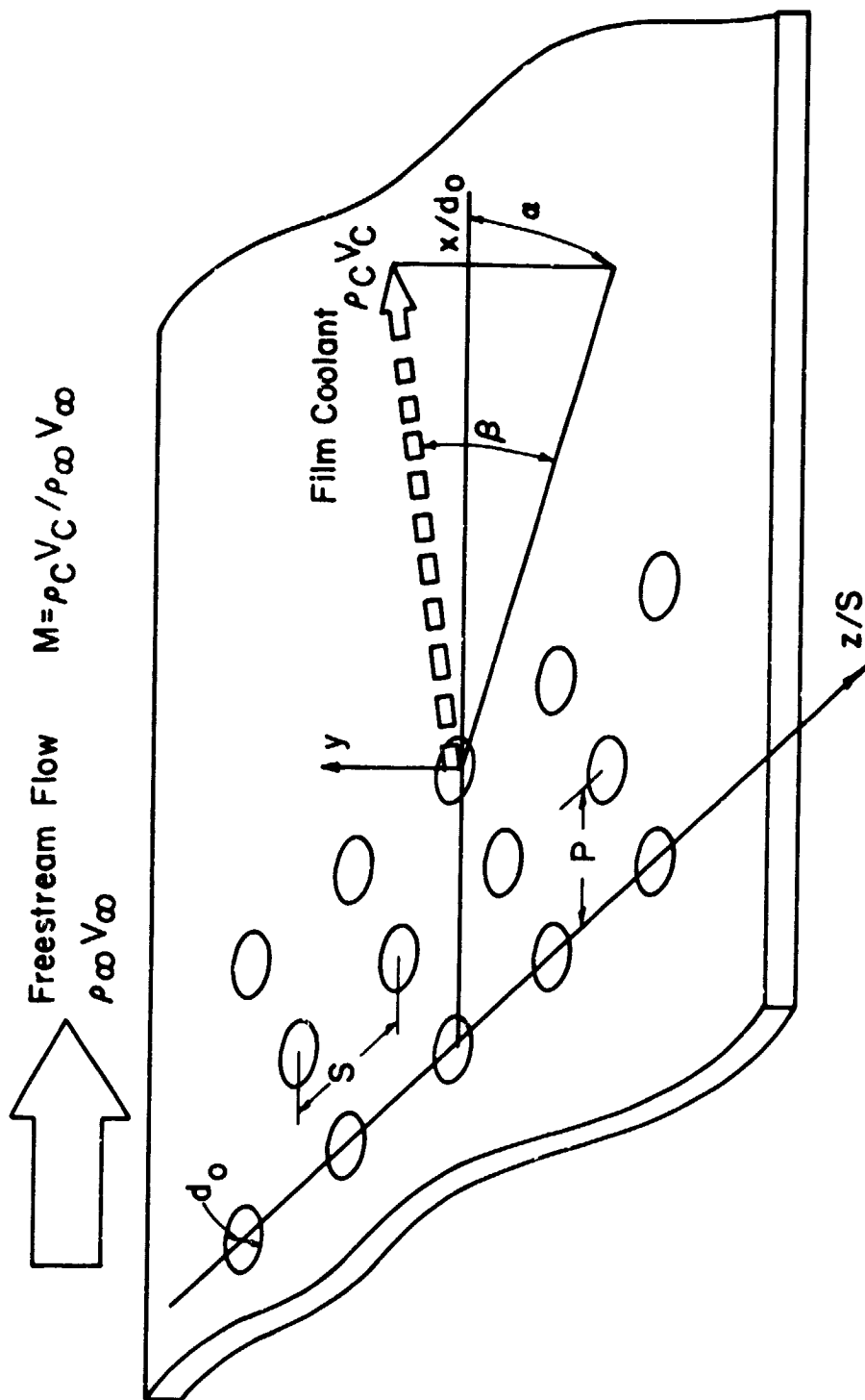


Figure 2. Geometric Parameters along a Film Cooled Surface

uniformity of the protective layer across the surface. The origin of the coordinate system is located at the center of the hole of interest (see Figure 2) and frequently the hole diameter, d_0 , or the center-to-center hole spacing, S , are used to non-dimensionalize the x and z coordinates. With multiple row injection, the row-to-row spacing, P , and the staggering of the holes from row to row can improve the effectiveness of the coolant film as it flows downstream. Additional rows of holes allow consecutive downstream rows to carry on when coolant injected upstream has lost its cooling capacity. By staggering the holes of one row with respect to its adjacent upstream row, the gap in the coolant film created by the hole spacing is filled in by the coolant from the next downstream row. Consequently, multiple rows that are properly staggered can minimize the lateral variation in cooling performance.

With the film coolant acting as a heat sink, the magnitude of the reduction of the surface heat flux depends strongly on the mass of coolant injected (i.e., the coolant thermal capacity). The blowing ratio, a dimensionless mass flux ratio defined as

$$M = \frac{\rho_c V_c}{\rho_\infty V_\infty} \quad (1)$$

is commonly used as a measure of the thermal capacity of the film coolant. As the cool fluid is blown onto the surface, the hot free-stream begins to mix with the emerging coolant jets. This results in a deterioration of the coolant film with the extent of this interaction being strongly influenced by the penetration of the coolant jets away from the surface into the freestream. Two parameters frequently used to characterize the jet penetration and trajectory are the velocity ratio, V_c/V_∞ , and the momentum flux ratio,

$$I = \frac{\rho_c V_c^2}{\rho_\infty V_\infty^2} \quad (2)$$

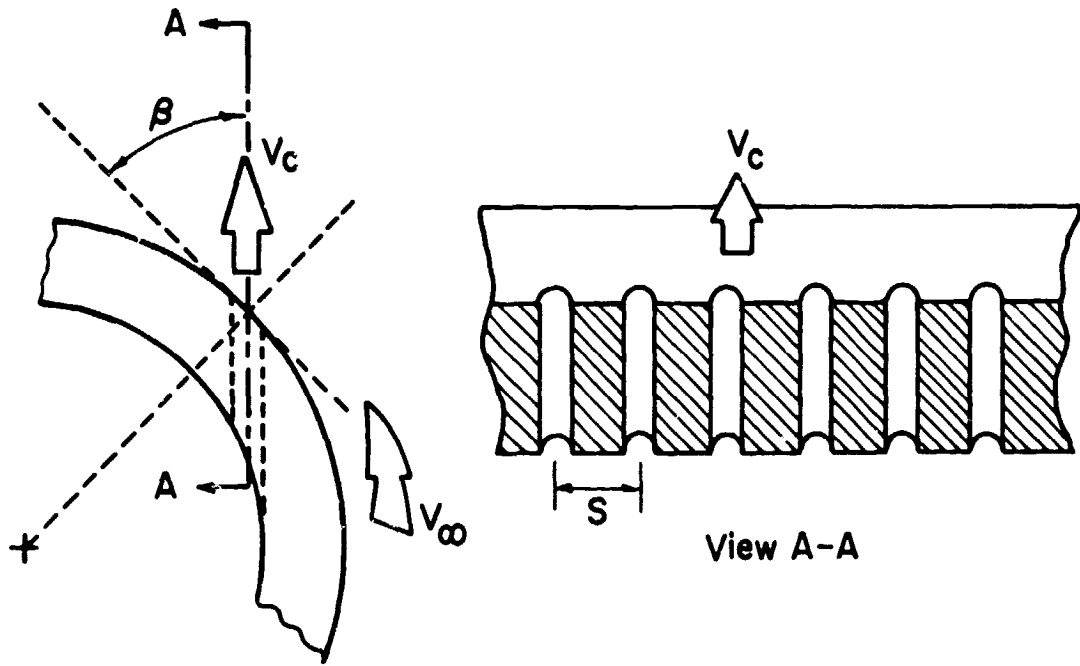
All three of the aforementioned hydrodynamic parameters are interdependent. Therefore, while more blowing will increase the thermal capacity of the coolant, excessive blowing can result in significant

coolant jet penetration away from the surface. This penetration will enhance the mixing process to such an extent that the net effect is a rapid deterioration of the coolant's ability to protect the surface.

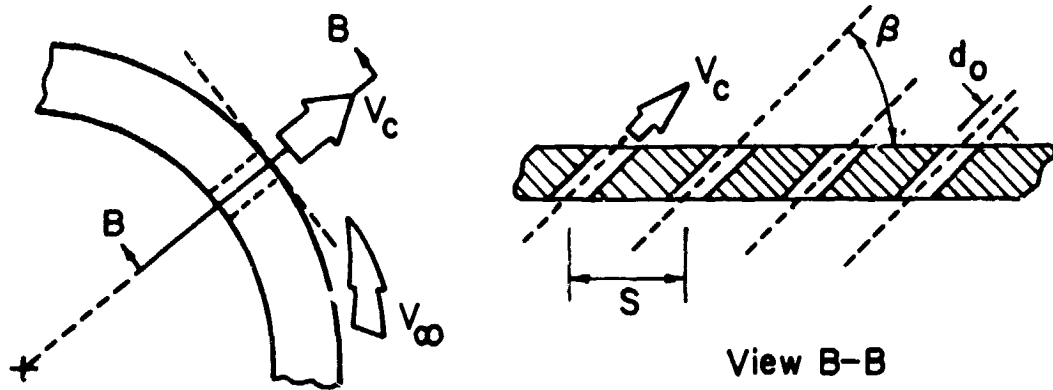
The penetration of the coolant jet into the freestream is also strongly influenced by the injection hole angle as defined in Figure 2. The angle made with respect to the surface is represented by β while the angular position relative the x-axis is represented by α . Therefore, a hole angled at 35° in the streamwise direction would be represented by $\alpha = 0^\circ$, $\beta = 35^\circ$, and a similar hole angled in the spanwise direction would be represented by $\alpha = 90^\circ$, $\beta = 35^\circ$. In order to minimize the penetration of the coolant jet into the freestream and the subsequent mixing that occurs, it is desirable to maintain as shallow an angle, β , as possible. An additional benefit of using shallow injection angles is an increase in the length-to-diameter ratio, L/d_0 , of the coolant hole. Larger L/d_0 values improve the convective heat transfer from the turbine vane wall to the cool fluid passing through it.

Conventionally, film coolant holes on turbine vane surfaces are angled in the freestream direction. However, in the leading edge region, the surface curvature complicates the problem of maintaining a shallow injection angle, β . As Figure 3 demonstrates, the minimum injection angle for streamwise angled holes ($\alpha = 0^\circ$) is limited by the vane wall thickness. To resolve this limitation, and to increase the L/d_0 ratio, coolant holes angled in the spanwise direction ($\alpha = 90^\circ$) are frequently employed for the leading edge region.

The nature of the freestream flow can have a significant effect on the coolant jet penetration and the coolant-freestream mixing process. A thin freestream boundary layer, with high velocity flow close to the surface, improves the film cooling performance because of its ability to more readily deflect the coolant back along the surface. The boundary layer displacement thickness-to-hole diameter ratio, δ^*/d_0 , is frequently used to characterize the boundary layer at the injection point. The coolant-freestream mixing process is also influenced by freestream acceleration and freestream turbulence. The parameter K is used to identify the freestream acceleration where



Streamwise Injection ($\alpha = 0^\circ$)



Spanwise Injection ($\alpha = 90^\circ$)

Figure 3. Leading Edge Cooling Configurations on a Turbine Vane

$$K = \frac{\nu_{\infty}}{V_{\infty}^2} \frac{dV_{\infty}}{dx} \quad (3)$$

where ν_{∞} = kinematic viscosity
 V_{∞} = local velocity
 x = coordinate along the surface

The turbulence intensity and the turbulence scale are both used to characterize the freestream turbulence. The acceleration and turbulence parameters have significant values along the leading edge of the turbine vane and their influence on the film cooling performance can not be overlooked.

This brief discussion was provided to give an introduction to the film cooling process and the parameters that are prevalent throughout the film cooling literature.

I.C. Review of the Literature

A comprehensive review of the film cooling literature has been prepared by Goldstein [1]. Updates of this review can be found in both Hanus and L'Ecuyer [2] and Luckey and L'Ecuyer [3]. Consequently, this literature summary will deal with the areas of specific interest to the application of multiple row film cooling on the leading edge of a turbine vane.

I.C.1 Film Cooling Performance Parameters

As with all convective heat transfer analysis, film cooling requires a knowledge of the heat transfer rate along the surface. A review of the literature reveals that two different methods have been developed for the correlation of film cooling data. The adiabatic effectiveness method is based on the analogy between film heating and film cooling and often a "heated" coolant jet was used in a cold free-stream to model the film cooling process. An examination of the governing equations shows that for small temperature differences (constant

properties) the analogy is valid [1]. Therefore it was postulated that the heat flux to a film cooled surface could be expressed by

$$q''_{w,FC} = h'(T_{adw,FC} - T_{w,FC}) \quad (4)$$

where $T_{adw,FC}$ - adiabatic wall temperature with film cooling
 $T_{w,FC}$ - wall temperature with film cooling
 $q''_{w,FC}$ - heat flux at the wall with film cooling
 h' - heat transfer coefficient with film cooling as defined by Eqn. (4)

The adiabatic wall temperature reflects the extent that the free-stream gas temperature near the wall has been changed by the addition of a cool (or hot) fluid. Film cooling studies are conducted over an adiabatic surface for selected values of the freestream (T_∞) and coolant (T_c) temperatures. The wall temperature distributions that are measured are commonly presented in terms of the dimensionless film cooling effectiveness.

$$\eta_{adw} = \frac{T_\infty - T_{adw,FC}}{T_\infty - T_c} \quad (5)$$

Results of η_{adw} are given as functions of the coolant blowing ratio (M), the injection angle (α, β), the location from injection ($x/d_o, z/s$), the hole geometry ($S/d_o, P/d_o$), and the nature of the local freestream boundary layer.

With a knowledge of the adiabatic effectiveness, the wall heat flux for a non-adiabatic surface can be determined from Eqn. (4) if the heat transfer coefficient (h') can be estimated. As a first approximation, it is frequently assumed that h' is approximately equal to h_o , the heat transfer coefficient without film coolant flow.

To experimentally determine h' , the flow conditions used to find η_{adw} must be applied to a non-adiabatic surface. By measuring the surface heat flux with unheated coolant injection ($T_c = T_\infty = T_{adw}$) and prescribed T_w , Eqn. (4) can be used to compute h' . The use of a heat

transfer coefficient ratio, h'/h_0 , provides a direct indication of the influence of coolant mass addition on the hydrodynamic boundary layer. Investigations of the heat transfer coefficient, h' , have shown that h'/h_0 approaches 1.0 far downstream of the point of injection. However, closer to the coolant hole, studies by Hartnett, Birkebak and Eckert [4], Metzger and Fletcher [5], and Eriksen and Goldstein [6] have all shown a significant influence of coolant blowing on h'/h_0 . To model the film cooling conditions representative of turbine blade applications, Launder, Fish and Suo [7] conducted an experiment using film cooling injection from two staggered rows of holes on a turbine vane. Their results, shown in Figure 4, demonstrate the influence of coolant blowing on the heat transfer coefficient, h' , for distances of 20 or more slot widths downstream. All of these studies demonstrate that the use of the adiabatic effectiveness method to determine the surface heat flux near injection requires experiments to determine both $T_{adw,FC}$ and h' .

Frequently in the literature, η_{adw} and h' data are presented in the spanwise averaged form, $\overline{\eta_{adw}}$ and $\overline{h'}$. To determine the spanwise averaged heat flux, $\overline{q''}$, the term $(\overline{\eta_{adw} h'})$ must be computed and sometimes the approximation

$$\overline{h'} \times \overline{\eta_{adw}} \approx \overline{h' \eta_{adw}} \quad (6)$$

is made. However, this approximation is subject to question and further work needs to be done in this area before this question is resolved.

Although a majority of the film cooling studies found in the literature are based on the adiabatic effectiveness method, an alternate method for correlating film cooling performance was initiated by Metzger [8]. It involves the direct measurement of surface heat transfer with film cooling on an isothermal surface. A heat transfer coefficient is computed by the following equation.

$$q''_{w,FC} = h_{FC}(T_{\infty} - T_{w,FC}) \quad (7)$$

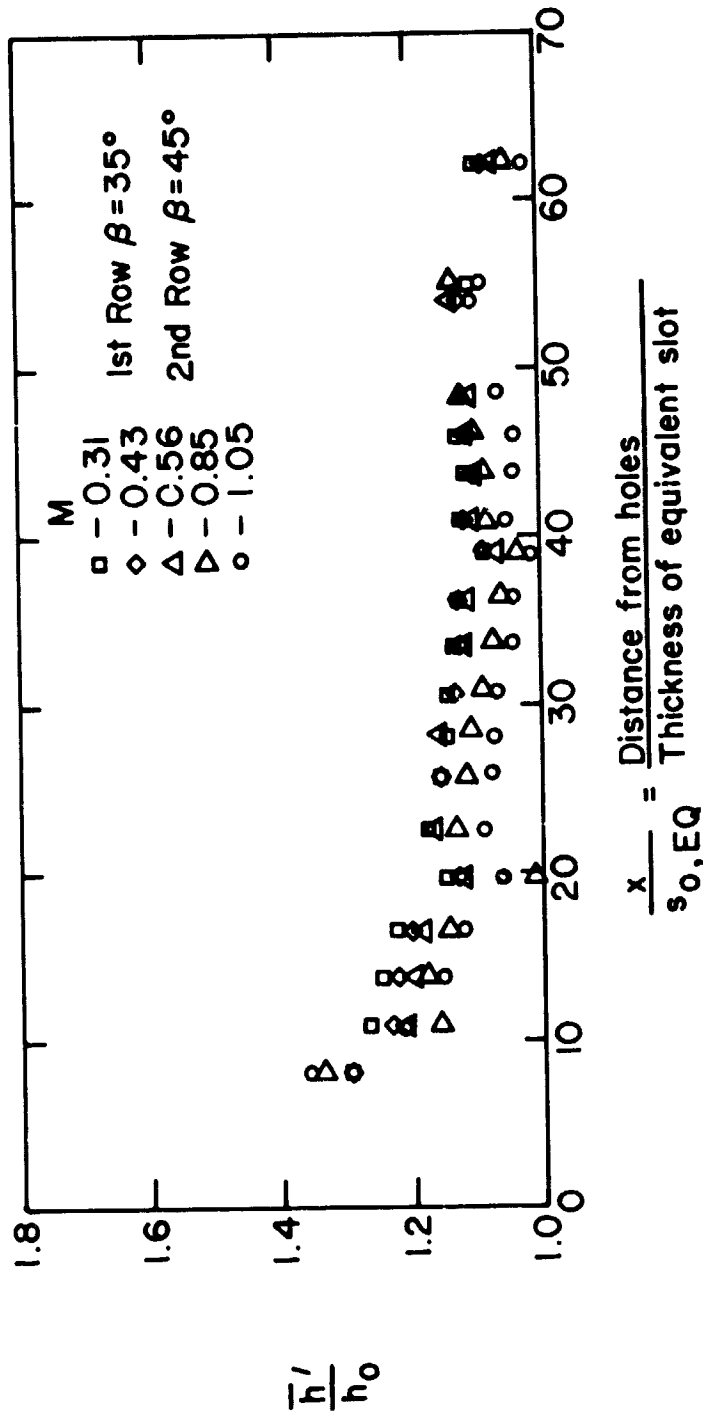


Figure 4. Heat Transfer Coefficient Downstream of Hole Injection on a Film Cooled Turbine Vane Surface (Lander, Fish and Suo [7])

The film cooling performance is then defined in terms of the ratio of the heat transfer coefficients, with and without blowing, h_{FC}/h_o , or the Stanton Numbers, with and without blowing, St_{FC}/St_o . An alternate form of presenting the film cooling data is in terms of the Stanton Number Reduction,

$$SNR = 1 - \frac{St_{FC}}{St_o} \quad (8)$$

For isothermal conditions ($T_{w,FC} \approx T_{w,o}$), Eqn. (8) becomes equivalent to

$$1 - \frac{q''_{FC}}{q''_o} \quad (9)$$

which is commonly referred to as the isothermal film cooling effectiveness, η_{iso} .

These two methods for measuring film cooling performance have been shown by Choe, Kays and Moffat [9] to be directly related. By examining the energy boundary layer equation for constant fluid properties, the heat transfer coefficient with film cooling can be shown to be a linear function of a dimensionless coolant temperature ratio,

$$\theta_c = \frac{T_\infty - T_c}{T_\infty - T_w} \quad (10)$$

The linear dependence of the heat transfer coefficient allows the following relationships to be derived.

$$h(\theta_c) = h(\theta_c = 0) - \theta_c [h(\theta_c = 0) - h(\theta_c = 1)] \quad (11)$$

and

$$\eta_{adw} = \frac{1}{\theta_{c,adw}} = \frac{T_c - T_\infty}{T_{adw,FC} - T_\infty} = \frac{h(\theta_c = 0) - h(\theta_c = 1)}{h(\theta_c = 0)} \quad (12)$$

Therefore starting with Eqn. (7)

$$q_w'' = h(\theta_c)(T_\infty - T_w) \quad (7)$$

and substituting Eqn. (11) into it, produces

$$q_w'' = h(\theta_c = 0)(1 - \theta_c \times \eta_{adw})(T_\infty - T_{w,FC}) \quad (13)$$

Then substitution of the definitions of θ_c and η_{adw} into Eqn. (13) gives

$$q_w'' = h(\theta_c = 0)(T_{adw,FC} - T_{w,FC}) \quad (14)$$

Eqn. (14) has the same driving potential as that used in Eqn. (4) and a comparison of these equations reveals that the heat transfer coefficient with film cooling for $\theta_c = 0$ (i.e. $T_c = T_\infty$) corresponds to h' . Using the relationships developed, the two film cooling performance parameters can be shown to be related in the following manner.

$$\frac{St_{FC}}{St_0} = \frac{h'}{h_0} (1 - \theta_c \eta_{adw}) \quad (15)$$

Because of the linear variation of h_{FC} with θ_c , the measurement of the heat flux at two different coolant temperatures establishes a straight line that can be extrapolated to determine η_{adw} and $h(\theta_c = 0)$, or h at any desired θ_c value. Choe, et al. [9] did conclude their discussion with one caution about comparing the values for η_{adw} found by extrapolating the $h(\theta_c) - \theta_c$ curve with those values obtained by measuring $T_{adw,FC}$ on an adiabatic surface. The linearity of the $h(\theta_c) - \theta_c$ curve was based on a constant wall temperature boundary condition, $T_{w,FC}$. However, for experiments to determine η_{adw} along an adiabatic surface, the wall temperature ($T_{adw,FC}$) is allowed to vary. The derivative of the enthalpy thickness will not be the same in both cases so values of η_{adw} found from the $h(\theta_c) - \theta_c$ plots should not be expected to compare directly with the results from an adiabatic wall approach.

I.C.2. Film Cooling Geometry

To eliminate the development of "hot spots" on the vane, it is desirable to achieve a uniform film cooling coverage across the entire surface. Multiple row film cooling helps to build this uniform coverage in two ways. The use of staggered rows allows the gap in the coolant film, created by the hole spacing in an upstream row, to be filled in by the next downstream row. In addition, the use of multiple rows of holes allows consecutive downstream rows to carry on when upstream coolant injection has lost its cooling capacity.

The earlier phase of this investigation [3] represents a large portion of the limited results that have been reported in the literature for film cooling measurements applicable to the leading edge region. This study involved heat flux measurements made in the stagnation region of a circular cylinder with coolant injection from a single row of spanwise angled holes ($S/d_o = 3.3$). Figure 5 [3] shows a plot of the Stanton Number Reduction versus spanwise location (hole-to-hole) for two separate blowing ratios, and demonstrates the non-uniformity of the film cooling performance for a single row of holes. In view of this lateral variation, data in this study were presented in terms of a spanwise maximum Stanton Number Reduction and a spanwise averaged Stanton Number Reduction (see Figure 5).

Russell [10] conducted flow visualization studies for coolant injection from a single row of spanwise angled holes (2 holes) in the stagnation region of a circular cylinder. For a blowing ratio above 0.4, photographs revealed no spreading of the injected coolant from the injection point (for injection at 15° , 30° , 45°) to a distance of about 80° from the stagnation line. With a M less than 0.4, the injected coolant even "necked down" slightly. In addition, the flow was turned quickly from the spanwise to the freestream direction. Even for M values above 1.0, the angle the coolant made with the freestream one diameter downstream from injection was only 10° . Consequently, the staggering of the rows of holes can be very important in achieving a uniform film across the surface.

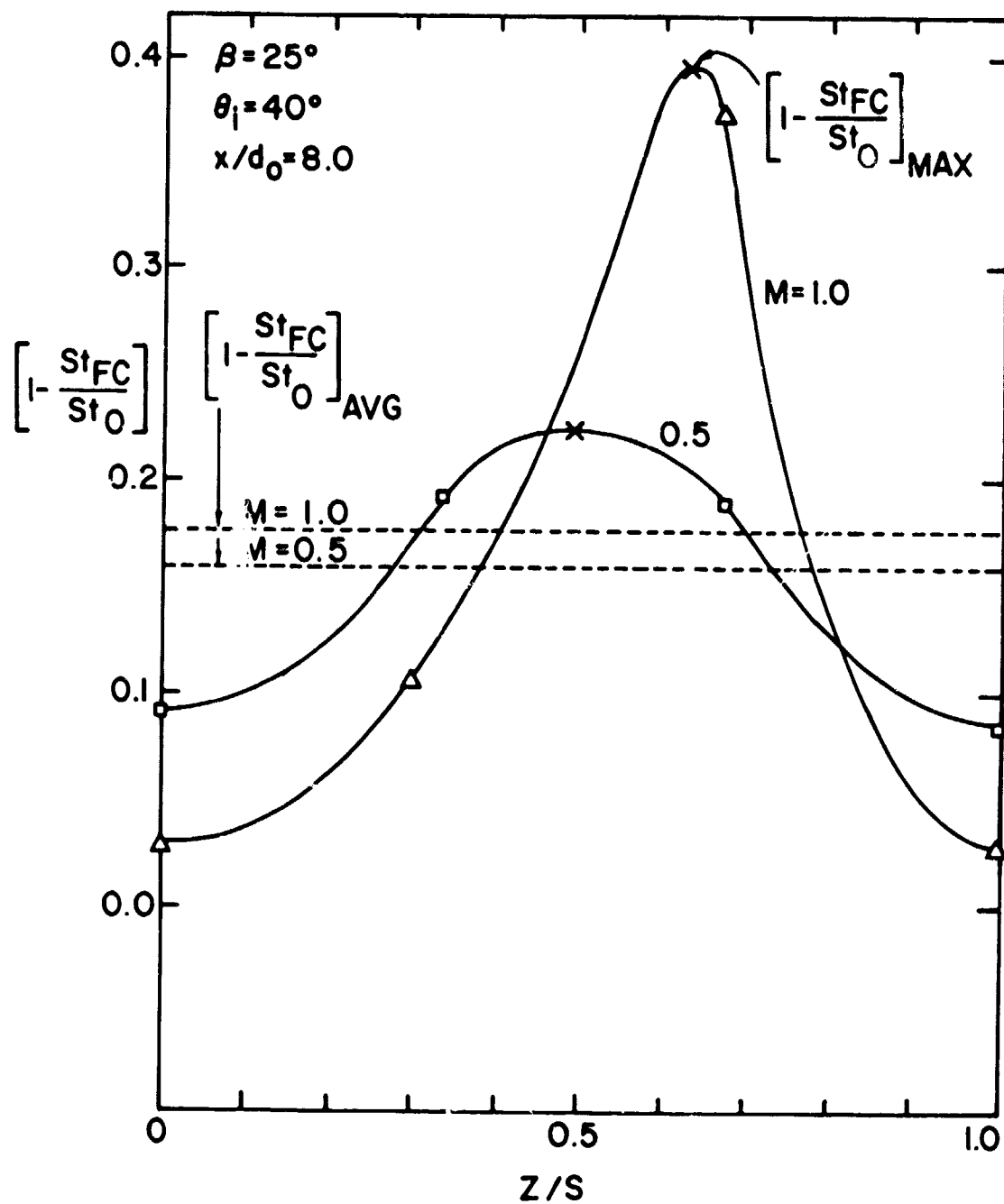


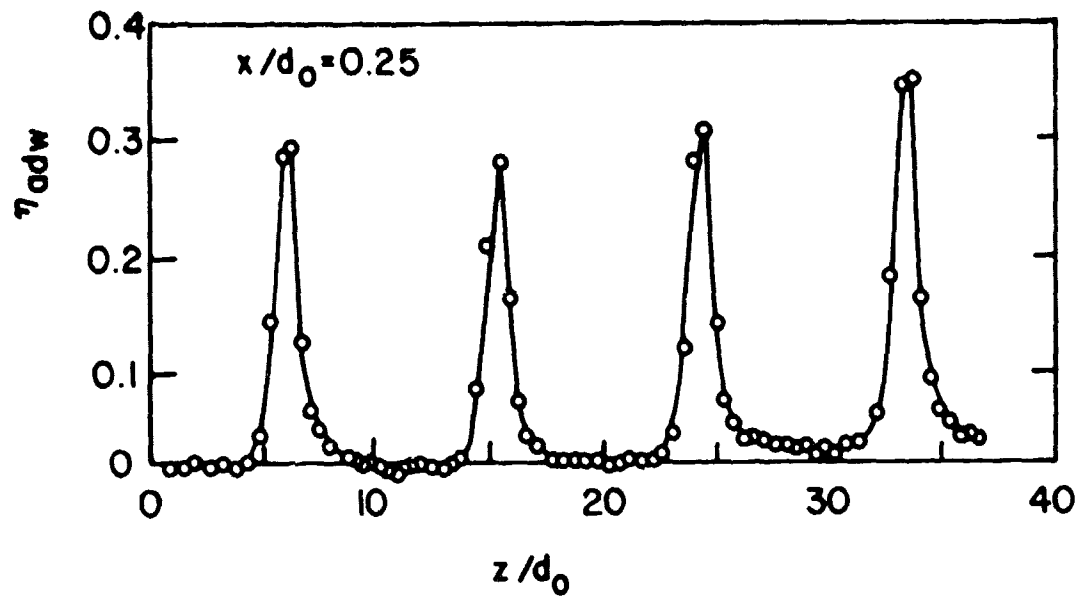
Figure 5. Spanwise Variation of the Stanton Number Reduction Downstream of a Single Row of Film Coolant Holes [3]

Metzger, Takeuchi, and Kuenstler [11] investigated multiple row arrangements, using 10 equally spaced rows of holes ($\beta = 90^\circ$) with a pitch-to-diameter ratio of 4.8 and both staggered and in-line arrangements of the holes. The in-line arrangement proved to be inferior to the staggered array, because the cooling effect from an upstream hole was found to be negated after flowing over two holes in-line downstream. The staggered arrangement used the coolant from an upstream row to fill in the gaps between the holes of the downstream row thus allowing the coolant to pass four rows downstream before its cooling influence became negligible.

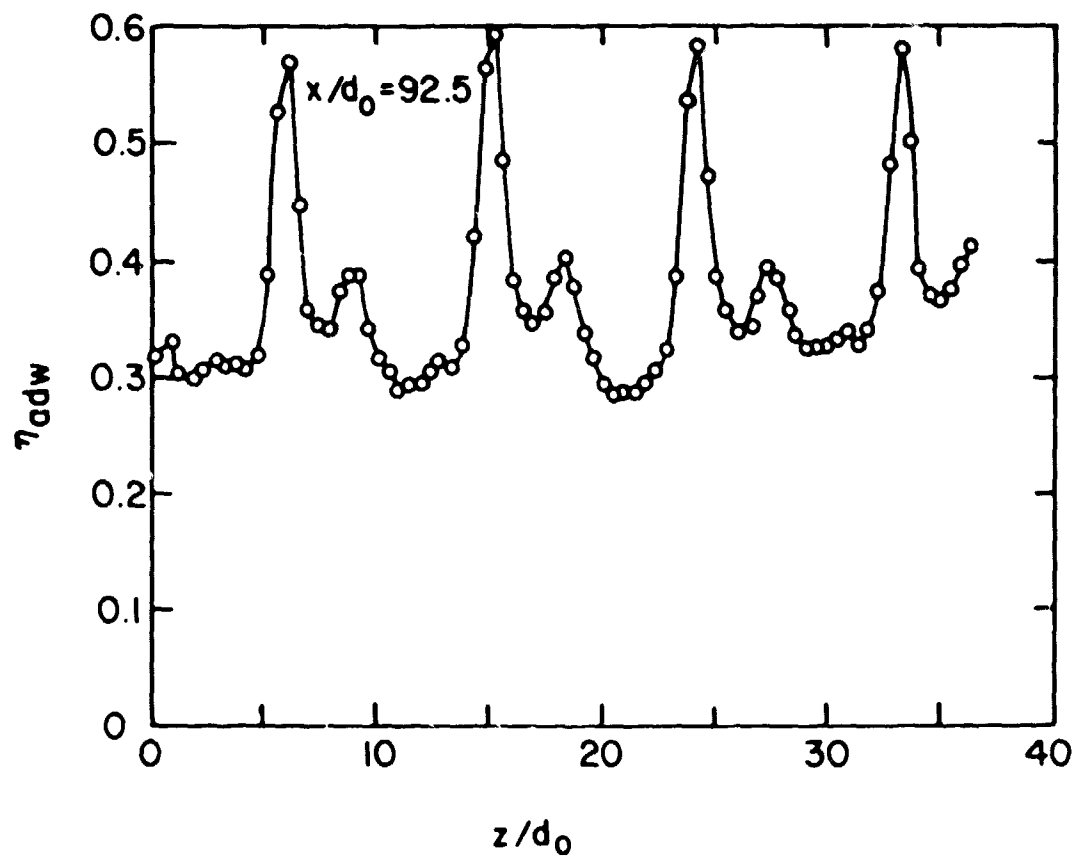
Spanwise measurements within a multiple row configuration were made by Mayle and Camarata [12]. They investigated film coolant injection through a staggered array of streamwise ($\beta = 0^\circ$) angled holes on a flat plate with $S/d_o = 8.7$ and $P/d_o = 10.0$. As Figure 6 demonstrates, the spanwise variation of the adiabatic effectiveness behind the first row was highly non-uniform. Even behind the tenth row where the minimum level of η_{adw} was 0.3, the spanwise non-uniformity was still present.

LeBrocq, Launder, and Pridden [13] also conducted multiple row film cooling studies on a flat plate. Using a hole and row spacing of 8.0, they found lateral variations similar to those observed by Mayle and Camarata [12]. From their results, LeBrocq, Launder, and Pridden [13] recommended a hole spacing (S/d_o) of 5 to eliminate the spanwise non-uniformity. Unfortunately, spanwise variations for small hole spacings (3 to 5) have not been reported in the literature. Therefore, staggering the rows in a multiple row configuration should help to eliminate the gaps created by upstream rows, but for hole spacings of $10 d_o$ or greater, a spanwise non-uniformity in the film cooling performance will probably still be present.

The ability to maintain a high level of film cooling performance over the entire length of the surface has also led to the use of multiple row configurations. Figure 7 shows the results of Mayle and Camarata [12] with the spanwise averaged adiabatic effectiveness $\bar{\eta}_{adw}$ plotted against the downstream distance, x/d_o . The performance of the film coolant is seen to continually increase in the region of the hole



a) Behind first row



b) Behind tenth row

Figure 6. Spanwise Variation of the Adiabatic Effectiveness (Mayle and Camarata [12])

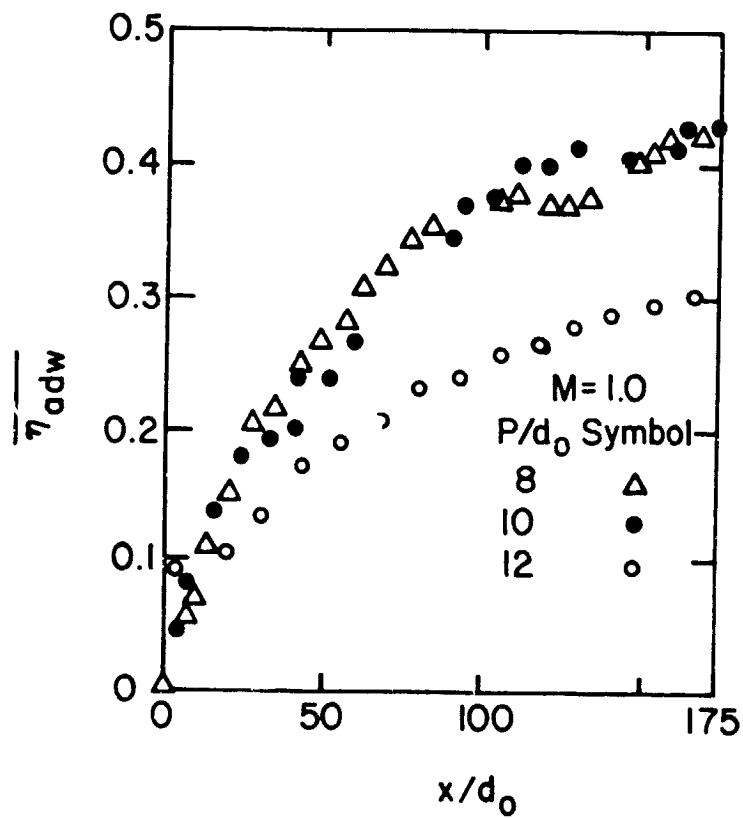
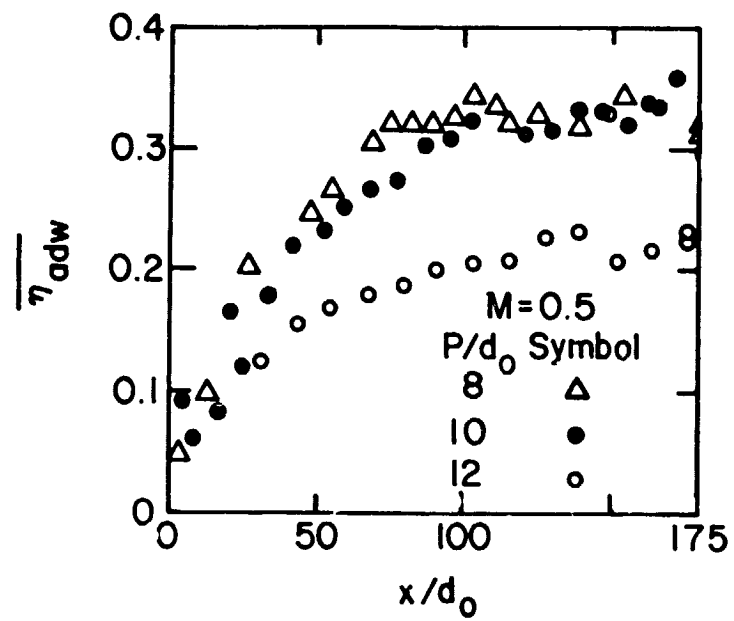


Figure 7. Streamwise Variation of the Adiabatic Effectiveness (Mayle and Camarata [12])

ORIGINAL PAGE IS
OF POOR QUALITY

ORIGINAL PAGE IS
OF POOR QUALITY

pattern. A similar trend was reported by Crawford, Kays, and Moffat [14]. They studied film coolant injection through a staggered array of holes on a flat plate with hole and row spacings of 5 and 10 diameters. Thus, the multiple row configuration was found to be quite successful in maintaining a high level of film cooling performance in the region of the injection holes.

Both of the studies, Mayle and Camarata [12] and Crawford, Kays, and Moffat [14], investigated the influence of different hole and row spacings. Figures 7 and 8, showing the results of Mayle and Camarata [12], demonstrate the improvement in film cooling effectiveness when the row spacing ($S = 0.87 P$) is decreased from $14 d_o$ to $10 d_o$. However, a negligible effect is seen when the spacing is decreased further to $8 d_o$. Crawford, et al. [14] found that the Stanton Number Ratio, St_{FC}/St_o , is significantly decreased (for the same blowing ratio, M) as the hole and row spacing ($S = P$) is decreased from $10 d_o$ to $5 d_o$.

In summary, the multiple row staggered configurations have been shown to be effective in providing a protective film across a flat plate surface. However, studies to determine the effectiveness of applying a multiple row configuration to the leading edge region of a turbine vane have not been presented in the literature.

I.C.3. Mass Flux Ratio and Angle of Injection

The direction and quantity of film coolant being injected onto the surface can be expected to have a strong effect on the film cooling performance. As discussed previously, it is desirable to inject a large amount of coolant onto the surface to increase the thermal capacity of the film. However, it is necessary to keep the coolant jets close to the surface in order to minimize the mixing that occurs between the freestream and the coolant.

The earlier phase of this investigation [3], using a single row of spanwise angled holes, studied the influence of the blowing ratio, M , and the injection angle. Figure 9 shows that for all three angles studied, the Stanton Number Reduction increased with blowing ratio until a maximum level was reached at the optimum blowing ratio, M_{opt} . Increasing the blowing ratio past M_{opt} resulted in a sharp decrease

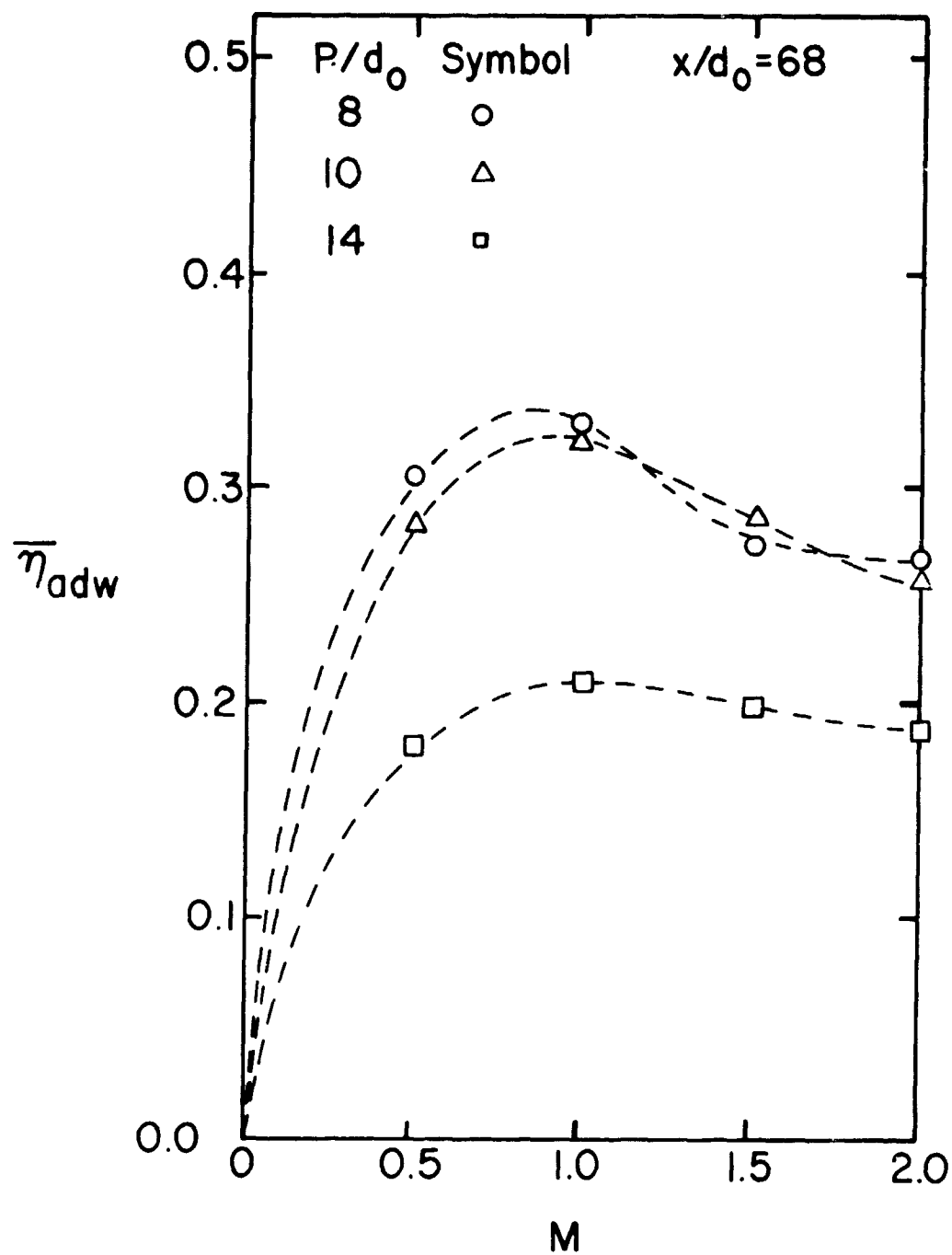


Figure 8. Effect of Row and Hole Spacing on the Adiabatic Effectiveness (Mayle and Camarata [12])

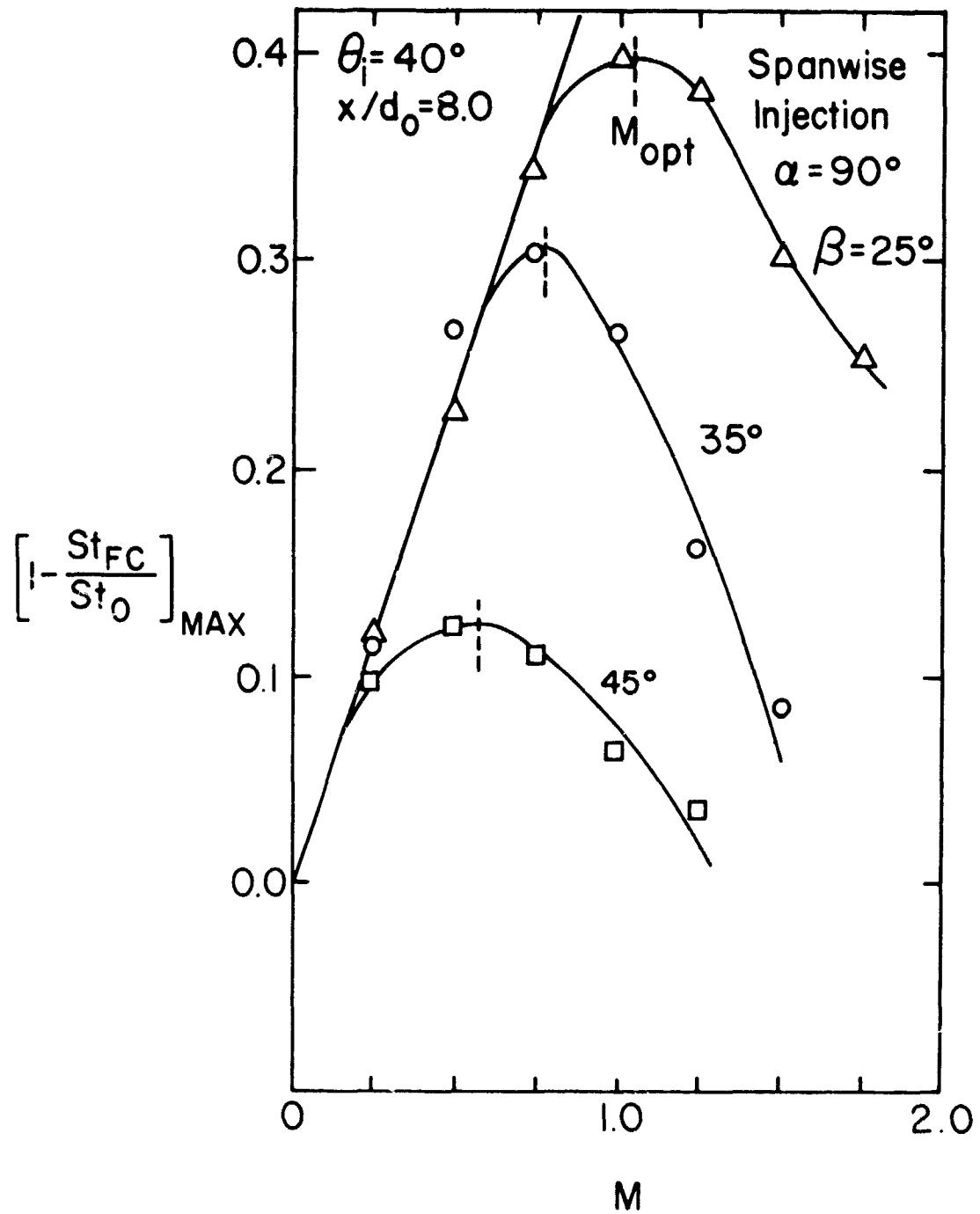


Figure 9. Effect of Coolant Blowing Ratio and Injection Angle on the Spanwise Maximum Stanton Number Reduction (Luckey and L'Ecuyer [3])

in the film cooling performance, which was attributed to coolant jet detachment from the surface and penetration into the freestream. Freestream-coolant mixing increases with penetration and any benefits from additional thermal capacity were overwhelmed by the mixing process. Excessive blowing can augment the mixing to such an extent that the heat flux rises above the level obtained without film cooling.

Pedersen [15] conducted an investigation involving a single row of holes at a fixed angle to study the influence of coolant-to-freestream density ratio ($1.0 \rightarrow 4.0$). He found that the maximum film cooling performance was independent of the density ratio, dependent only on the velocity ratio, V_c/V_∞ . These results were confirmed by LeBrocq, Launder, and Pridden [13] and Launder and York [16] for a multiple row configuration conducted on the same experimental apparatus with streamwise injection ($\alpha = 0^\circ$) along a flat plate. Three different density ratios (1, 1.6, 4) were investigated and the blowing ratio for maximum film cooling performance was found to be independent of the density ratio.

Multiple row studies [12], [16] have shown a similar trend with blowing ratio for the first row, but farther downstream Launder and York [16] and Mayle and Camarata [12] both have found a different trend. After the sixth row, Launder and York [16] discovered that the film cooling effectiveness decreased only slightly and then leveled off to a constant value as the blowing ratio was increased past M_{opt} . As shown in Figure 8, Mayle and Camarata [12] found the same trend when they made measurements of adiabatic effectiveness downstream of the seventh row.

Sasaki, Takahara, Sakata, and Kumagai [17] investigated film cooling in the stagnation region of a circular cylinder with two rows of spanwise angled holes, one row located at 15° from stagnation and the other located at 45° . Near the second row, the adiabatic effectiveness increased until blowing reached an M_{opt} value of 0.5 to 0.6. As the blowing ratio was increased past M_{opt} , the film cooling effectiveness continually decreased. An unfortunate feature of their results is that very few of their measurements were made in the stagnation region of the cylinder.

Except for the two row study of Sasaki, Takahara, Sakata, and Kumagai [17], all other multiple row studies have been confined to a uniform blowing distribution along the surface. However, the leading edge of a turbine vane experiences a large variation in the blowing ratio along the surface when a common plenum is used to feed all of the coolant rows. The influence of a non-uniform blowing distribution on the film cooling performance has yet to be discussed in the literature.

The ability of the coolant jets to remain close to the surface depends greatly on the injection angle. The effect of both the α and β angles on film cooling performance has been reported. Figure 9 from the earlier phase of this investigation [3] demonstrates that increasing the injection angle, β , causes the coolant jet to detach at a lower blowing ratio and results in lower levels of film cooling performance. Similar trends were discovered by Sasaki, Takahara, Sakata, and Kamagai [17] for their two row study of spanwise injection in the stagnation region. By decreasing the β angle from 90° to 30° , both the value of M_{opt} and the level of the film cooling effectiveness were found to increase.

The α angle has also been identified as a significant parameter in determining the optimum blowing ratio. Film cooling flow visualization studies have been conducted at the NASA Lewis Research Center for a variety of injection configurations [10], [18], and [19]. The initial investigation by Colladay and Russell [18] was conducted on a flat plate using a three row staggered array with a $5 d_o$ spacing. For a streamwise angled hole ($\alpha = 0^\circ$) with $\beta = 30^\circ$, the coolant was observed to detach from the surface at an M of 0.5. However, when a compound angle ($\alpha = 45^\circ$, $\beta = 30^\circ$) was employed, the jet remained attached to the surface until the blowing ratio, M , reached 0.9. Photographs showed a single, strong vortex filament downstream of each hole. It was this strong vortex motion that kept the jets attached to the surface at higher blowing rates than those observed for streamwise injection.

Russell [19] continued this work by investigating the difference between spanwise and compound angle injection. While the compound

angle injection was found to produce a relatively tight and smooth vortex, the spanwise injection created a loosely wound and erratic vortex that visibly had more turbulent motion in it. Spanwise injection was observed to have more voids between the jets as they passed downstream than that seen with compound injection. However, both compound and spanwise injection kept the coolant jets close to the surface up to the blowing ratio of 0.9, which is superior to the streamwise injection case where the jets separated at a M of 0.5.

Russell's [10] next investigation consisted of a single row of spanwise angled holes (2 holes) on a circular cylinder. While the film was found to penetrate farther from the surface as the injection angle β was increased from 30° to 45° , photographs also revealed that jet detachment from the surface is influenced by the location of injection from stagnation, θ_i . Russell observed that detachment occurred at $M = 1.13$ for $\theta_i = 30^\circ$, but decreased to 0.86 for $\theta_i = 45^\circ$, and to 0.70 for $\theta_i = 60^\circ$. Consequently, the optimum blowing condition for film cooling in the stagnation region of a turbine vane has been found to be a function of both injection angles, α and β , and the location of injection from stagnation, θ_i , but not the density ratio, ρ_c/ρ_∞ .

I.C.4. Freestream Conditions

Film cooling in the stagnation region is exposed to a large free-stream pressure gradient that varies significantly around the leading edge of a turbine vane. Film cooling studies have investigated the influence of a pressure gradient imposed on a flat plate surface, with the pressure gradient being characterized by an acceleration parameter, $K = (v_\infty/V_\infty^2)(dV_\infty/dx)$. Liess [20], studying injection through a single row of streamwise angled holes ($\beta = 35^\circ$, $S/d_o = 3.0$) found that a favorable pressure gradient (up to $K = 1 \times 10^{-6}$) resulted in a small decrease of the film cooling effectiveness. Similar trends were discovered by earlier slot film cooling studies [21], [22], and by Jabbari [23] who used two staggered rows of streamwise angled holes.

Investigating a single row of streamwise ($\alpha = 0^\circ$) angled holes, Kadotani [24] found that the lateral spreading of the coolant jets decreased as the acceleration parameter, K , was increased. This resulted in highly non-uniform spanwise profiles of the film cooling adiabatic effectiveness. He concluded that as acceleration increased, a decrease in the turbulent mixing within the boundary layer reduced the lateral spreading.

Using a multiple row, streamwise angled coolant configuration, Launder and York [16] applied a constant acceleration of $K = 2 \times 10^{-6}$ over their entire flat plate surface. Like Kadotani, they also observed a decrease in the lateral spreading of the coolant. However, directly behind the holes an increase in the adiabatic effectiveness was discovered. Because the coolant jets were laminar just before they emerged from the injection holes, Launder and York concluded that the streamwise acceleration delayed the transition of the jet from laminar to turbulent. This delay resulted in higher levels of adiabatic effectiveness behind the holes until the coolant jets turned turbulent.

While studies have been conducted to investigate the influence of constant acceleration on film cooling performance, the distribution of the acceleration parameter, K , around a vane leading edge will not be uniform, and the values of K in the front stagnation region (0° to 30°) will be an order of magnitude greater than those studied by Launder and York [16]. Presently, the literature is void of any results pertaining to the influence of non-uniform acceleration across a multiple row film cooling configuration.

The freestream turbulence intensity of the hot gases at the combustor exit/turbine entry could be expected to have an effect on the film cooling performance. Two-dimensional slot studies by Marek and Tacina [25] have shown a decrease in film cooling adiabatic effectiveness by as much as 50% when the freestream turbulence intensity was increased from 7 to 35%. While the majority of multiple row studies have been conducted in a low turbulence level wind tunnel, Launder and York [16] conducted a study on their multiple row flat plate configuration with a turbulence intensity of 6%. They concluded that the main influence of freestream turbulence was on the transition of the coolant

jets from laminar to turbulent flow. Consequently, when the jet emerged from the hole as turbulent flow, the freestream turbulence had little effect on the film cooling effectiveness directly downstream of the hole. They did observe a decrease of the lateral spreading in the flow with higher turbulence intensity (6%). They reasoned that the turbulent mixing at the outer edge of the boundary layer increases the transport of coolant away from the wall, providing less coolant to be spread laterally.

Extensive studies concerning the influence of freestream turbulence on film cooling have been conducted by Kadotani [24] in an effort to isolate the influence of turbulence intensity and of turbulence scale. His investigations were run with a single row of streamwise angled holes ($\alpha = 30^\circ$) on a flat plate. At low blowing ratios when the coolant jets remain attached to the surface, the film cooling performance was found to be sensitive to the turbulence intensity, which governs the mixing process between the secondary flow and the free-stream. For every scale size investigated, Kadotani found the adiabatic effectiveness to continually decrease as the turbulence intensity was increased. However, when the blowing ratio became large enough for the coolant jets to detach from the surface, the jet penetration into the freestream generated enough turbulence by itself that the freestream turbulence intensity did not have much effect on the adiabatic effectiveness.

The effect of scale was established from the adiabatic effectiveness contours measured by Kadotani. When the scale was small, the values of η_{adw} were high close to the injection hole and the contours stretched in the downstream direction. As the scale was increased, the contours did not stretch as far downstream, but spread more laterally. While the turbulence intensity was found to have little effect on the lateral distribution of the adiabatic effectiveness, the turbulence scale clearly did. As the scale was increased, the spanwise non-uniformity of η_{adw} became smaller and smaller. Therefore, while large scale turbulence will promote turbulent mixing between the coolant and mainstream, it will also promote rapid lateral spreading.

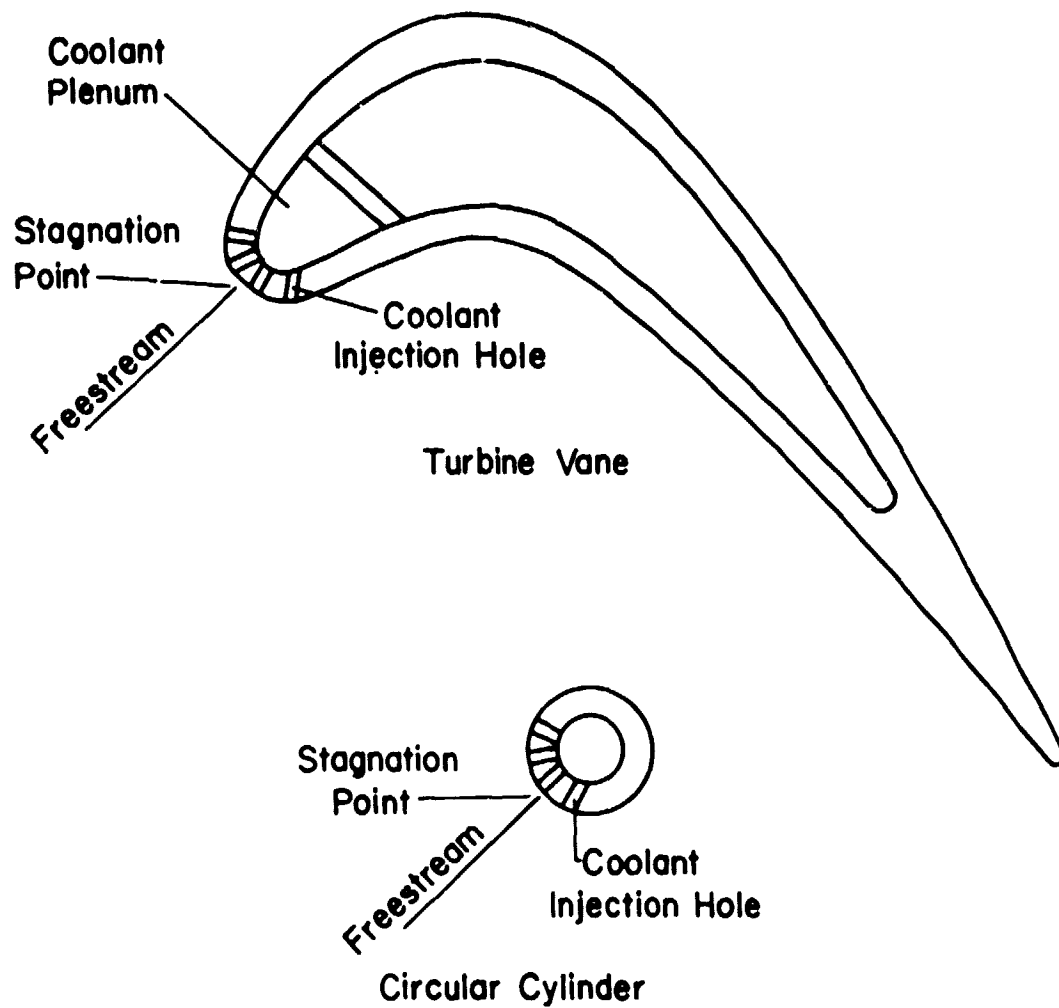
Although the leading edge of a turbine vane will experience high levels of freestream turbulence, the effect of the turbulence on the film cooling process is uncertain. With multiple row film cooling, the turbulence generated by the injection process may be large enough that the freestream turbulence will not have any influence on the film cooling process.

In summary, a review of the film cooling literature reveals that most previous multi-row studies have been confined to flat plate configurations and a majority of these have used negligible freestream-to-coolant temperature ratios. The only reported work conducted in the stagnation region of a circular cylinder or turbine vane has been the flow visualization work of Russell [10], the work of Sasaki, Takahara, Sakata, and Kamagai [17] for two rows of coolant holes, and the results for a single row from the earlier phase of this investigation [3]. The leading edge of the turbine vane experiences some unusual freestream and coolant flow conditions that have yet to be investigated. These include non-uniform blowing distributions around the surface, high levels of non-uniform freestream acceleration around the surface, and the combination of high freestream acceleration and turbulence intensity levels. As will be discussed in the next section, the objective of the present investigation was to study the influence of these leading edge conditions on the film cooling performance.

I.D. Scope of Investigation

While almost all of the multi-row film cooling studies in the literature have been confined to flat plate configurations, some of the most severe heat loads are experienced by the leading edge of the turbine vane. The purpose of this investigation was to obtain film cooling data applicable to the stagnation region of a turbine vane using the stagnation region of a circular cylinder, as shown in Figure 10, to model the leading edge.

The primary purpose of the present investigation was to investigate multiple row cooling configurations that are typical of present and future turbine vane leading edge designs, and to simulate the flow conditions typical of the turbine vane environment (e.g. Reynolds



ORIGINAL PAGE IS
OF PAPER 61-1117

Figure 10. Modeling the Stagnation Region of a Turbine Vane with a Circular Cylinder

number, Re_D , freestream-to-wall temperature ratio, T_∞/T_w , blowing level and distribution, turbulence intensity). Hot combustion gases flowing over the cylindrical, film cooled test surface were employed to simulate a Reynolds number (9×10^4) representative of high temperature, high pressure turbine designs. Internal cooling of the test cylinder maintained the wall temperature near room temperature ($\sim 294K$), allowing the use of a moderate gas temperature (500K) to simulate a freestream-to-wall temperature ratio of 1.7.

The film cooling experiments were conducted using either one, three, or five rows of spanwise angled holes ($\beta = 25^\circ$, $\alpha = 90^\circ$). The single row experiments were conducted to help provide an understanding of the multiple row injection process. Hole-to-hole and row-to-row spacings of $5 d_o$ and $10 d_o$ were used for the injection of room temperature air ($T_c \approx T_w$) as film coolant. Miniature heat flux sensors measured the local heat flux both with and without film coolant injection. The film cooling performance was determined in terms of the Stanton Number Reduction, $1 - St_{FC}/St_o$.

The objectives of the present investigation were

- 1) to measure the spanwise (z/S) and streamwise (x/d_o) variation of the Stanton Number Reduction behind the row or rows of holes during coolant injection
- 2) to study the influence of row-to-row (P/d_o) and hole-to-hole (S/d_o) spacing on the Stanton Number Reduction
- 3) to study the influence of uniform blowing (from $M = 0.25$ to 2.0) and non-uniform blowing on the Stanton Number Reduction when multiple rows are used
- 4) to study the influence of the freestream turbulence intensity on the Stanton Number Reduction

II. EXPERIMENTAL INVESTIGATION

II.A. Modeling of Gas Turbine Environment

The objective of this research program was to investigate multiple row film cooling under conditions characteristic of the leading edge of a turbine vane. To model the leading edge region, geometric similarity was obtained using the front stagnation region of a circular cylinder in crossflow. Effective modeling of the convective heat transfer environment on a turbine vane requires the simulation of important dimensionless parameters that govern the flow and heat transfer phenomena.

A dimensional analysis of the continuity, momentum, and energy equations [3] shows that the Nusselt number depends upon the following parameters¹.

$$Nu = f(x, y, z, Re_D, Pr, Ec, c, T_\infty/T_w) \quad (16)$$

where

$$Nu = \frac{hD}{k}$$

$$Re_D = \frac{\rho V D}{\mu}$$

$$Pr = \frac{c_p \mu}{k}$$

$$Ec = \frac{V_\infty^2}{c_p (T_\infty - T_w)}$$

D = cylinder diameter

¹ Due to the large temperature differences characteristic of the turbine environment, viscosity and conductivity were represented as exponentially dependent on temperature (T^E).

Therefore, under conditions where the Prandtl number and the exponent n do not vary significantly, and the freestream kinetic energy available for dissipation is small compared to the thermal energy ($Ec \ll 1.0$), the heat transfer environment at elevated temperatures and pressures can be simulated by reduced flow conditions if the Reynolds number, Re_D , and freestream-to-wall temperature ratio, T_∞/T_w , are maintained the same.

Dimensional analysis has also been conducted for film cooling along a surface [26] [27] and the Nusselt or Stanton number has been shown to be a function of additional parameters when film cooling is employed. Thus,

$$St = f(M, \theta_c, \rho_c/\rho_\infty, \delta^*/d_o, \text{coolant hole geometry}) \quad (17)$$

where

$$\theta_c = \frac{T_\infty - T_c}{T_\infty - T_w}, \quad M = \frac{\rho_c V_c}{\rho_\infty V_\infty}$$

Therefore, to model the influence of film cooling on the heat transfer, the parameters listed in Eqn. (17) must also be duplicated to simulate the stagnation region of a film cooled turbine vane.

II.B. General Description of Experimental Apparatus

The investigation of multiple row film cooling typical of a turbine vane leading edge was conducted using a cylindrical test surface exposed to a crossflow of heated air from a gas turbine combustor. A description of the experimental apparatus is presented in the following sections.

II.B.1. Flow System

Figure 11 is a simplified schematic of the overall flow system used in conducting this investigation. A photograph of the test cell is presented in Figure 12. A blow-down facility provides an air flow rate of ~ 1.4 kg/sec with the air storage facility permitting a typical run time of approximately 60 minutes. The air enters a gas turbine

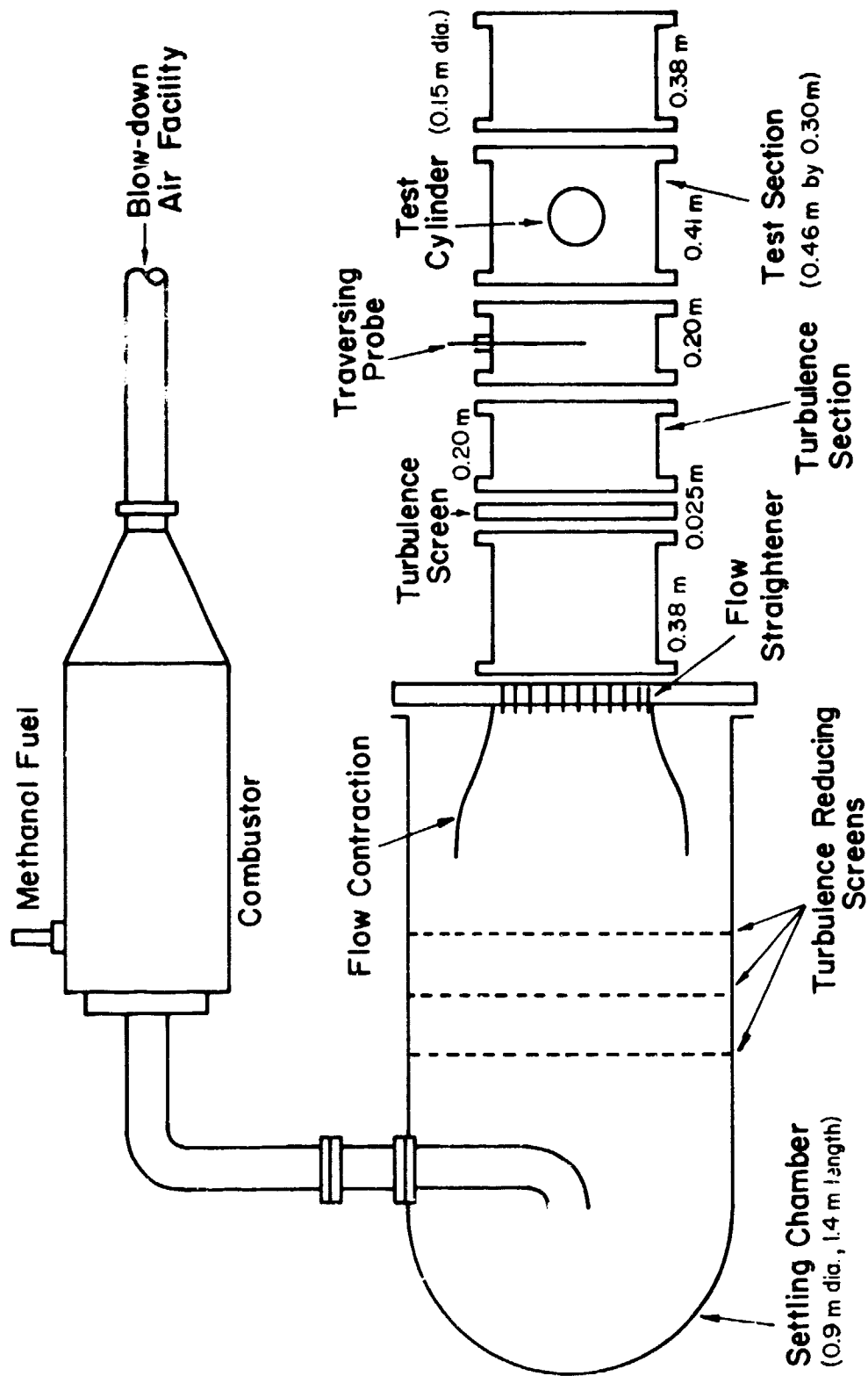


Figure 11. Schematic of the Flow System

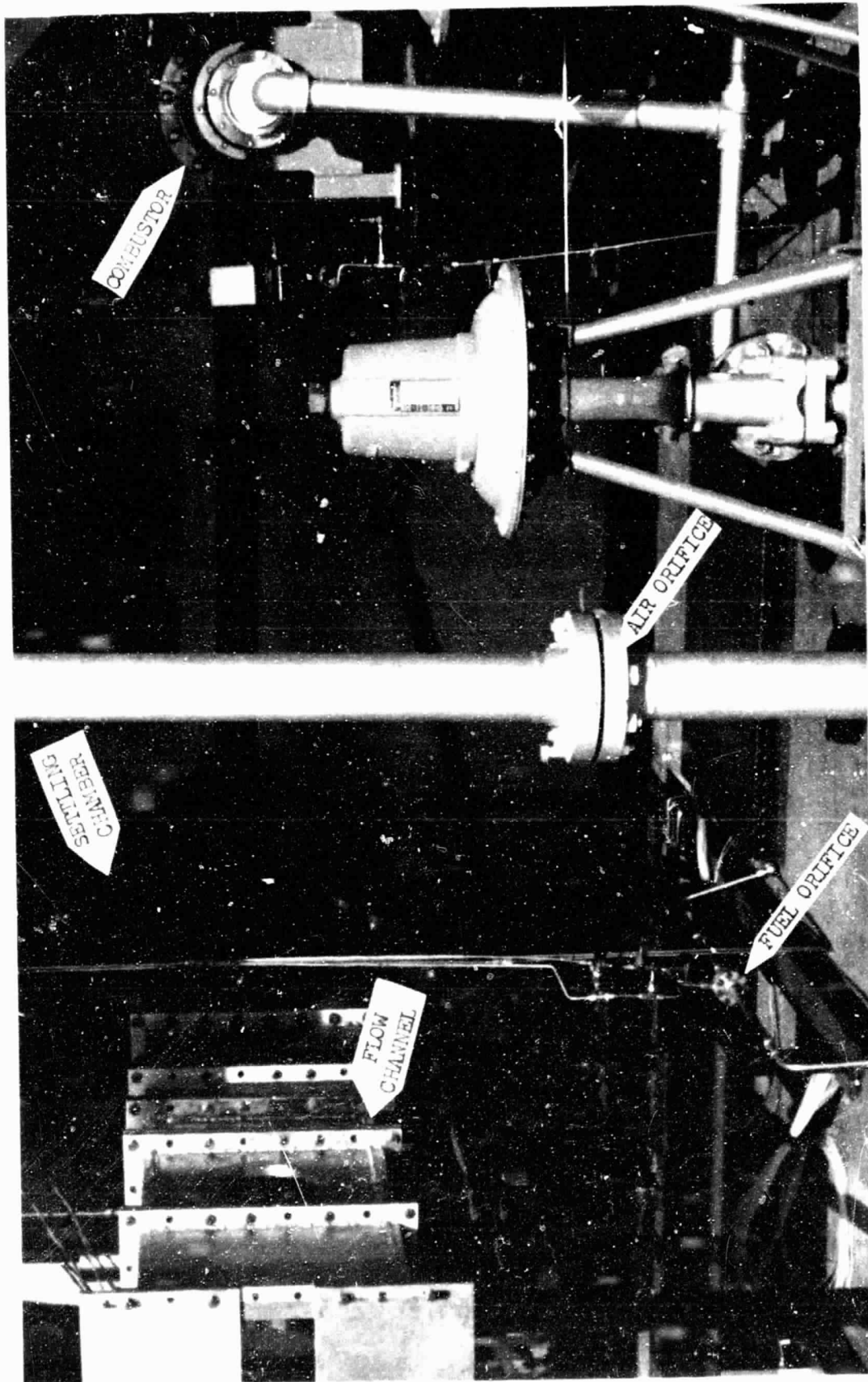


Figure 12. Photograph of the Flow System

combustor, where methyl alcohol is burned to provide the nominal free-stream condition of $T_{\infty} \sim 500$ K.

Downstream of the combustor the flow is dumped into a large settling chamber (0.9 m in diameter and 1.4 m long) which was installed to provide some control of the turbulence intensity passing through the test flow channel. The hot flow from the combustor is directed against the dome end of the chamber and then passes through three stainless steel fine mesh screens (0.43 mm diameter woven wire, 14 x 14 mesh, spaced 0.18 m apart). The flow is accelerated through a 2:1 area contraction (designed following the recommendations of Morel [28]) to the chamber exit.

At the entrance to the flow channel, a stainless steel honeycomb flow straightener (0.06 m long, 6.4 mm hexagonal cells, from 0.10 mm thick stock) is maintained in position by a fine screen (20 x 20 mesh, 0.41 mm wire diameter). The flow channel sections, shown in Figure 11, have an open area of 0.46 m by 0.30 m. The turbulence screen, see Figure 13, can be inserted between any two flow channel sections. Two interchangeable screens were available for use in this investigation: (1) fine screen, 1.60 mm diameter wires and a 4 x 4 mesh, (2) coarse screen, 3.05 mm diameter wires and 4 x 4 mesh. By using the different size screens and by placing the screens at different distances in front of the test cylinder, different levels of turbulence intensity were generated. Using the theory for decay of isotropic turbulence downstream from screens [29] [30], the turbulence intensity approaching the test cylinder was estimated to be as high as 11%.

Upstream of the test section holding the cylinder, a special flow channel section was positioned to allow the insertion of probes into the flow stream. A traversing mechanism attached to the outside of the flow section (see Figure 14) allowed a probe to be traversed across the entire depth or width of the flow field. The schematic drawing in Figure 15 illustrates the port locations where a probe was inserted into the flow. Following the recommendations of Kestin and Wood [31], the traversing ports were located 1 1/2 cylinder diameters (or 0.23 m) upstream of the leading edge of the test cylinder to eliminate any influence of the test cylinder on the flow field.

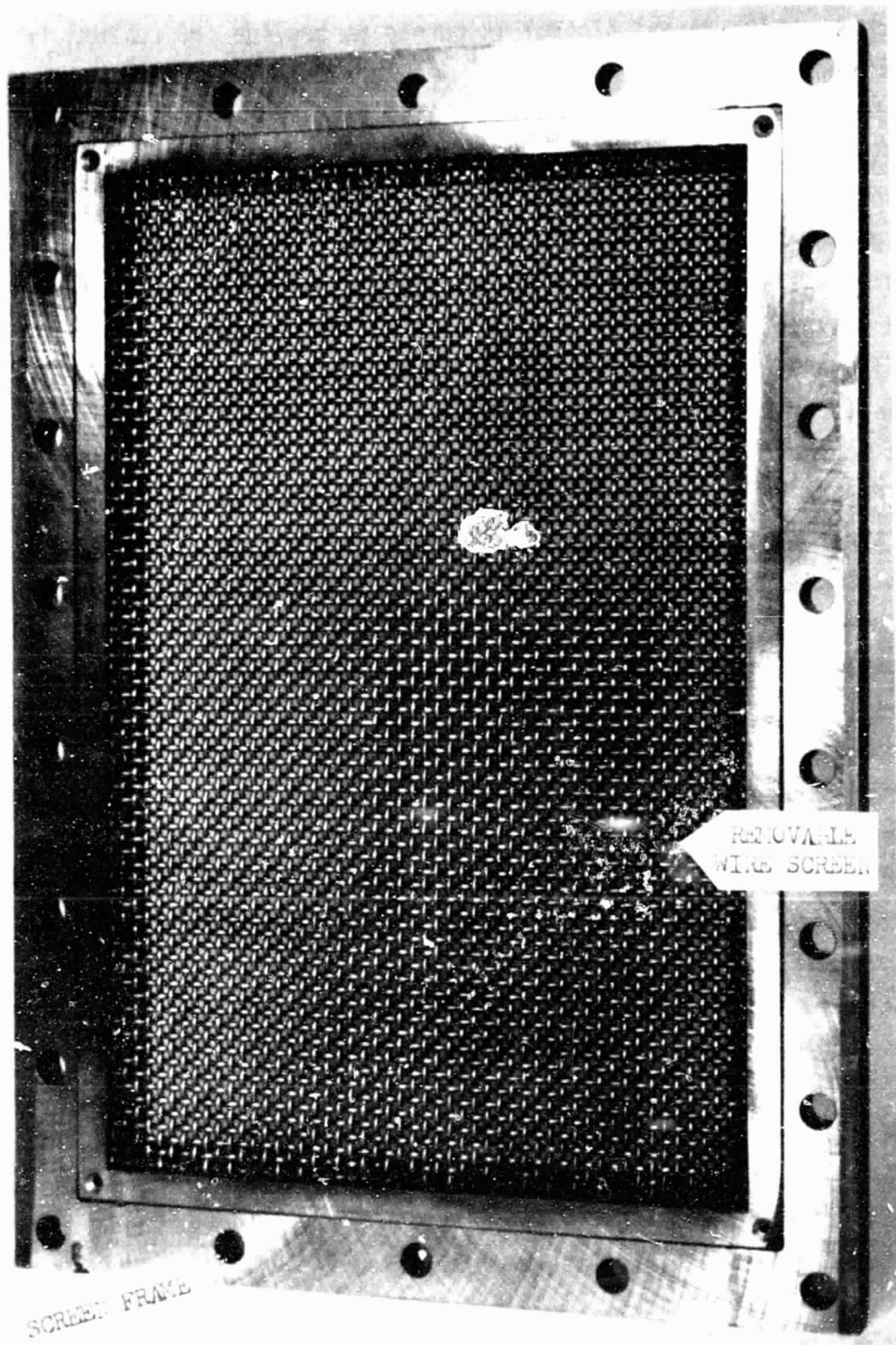


Figure 13. Photograph of the Turbulence Screen

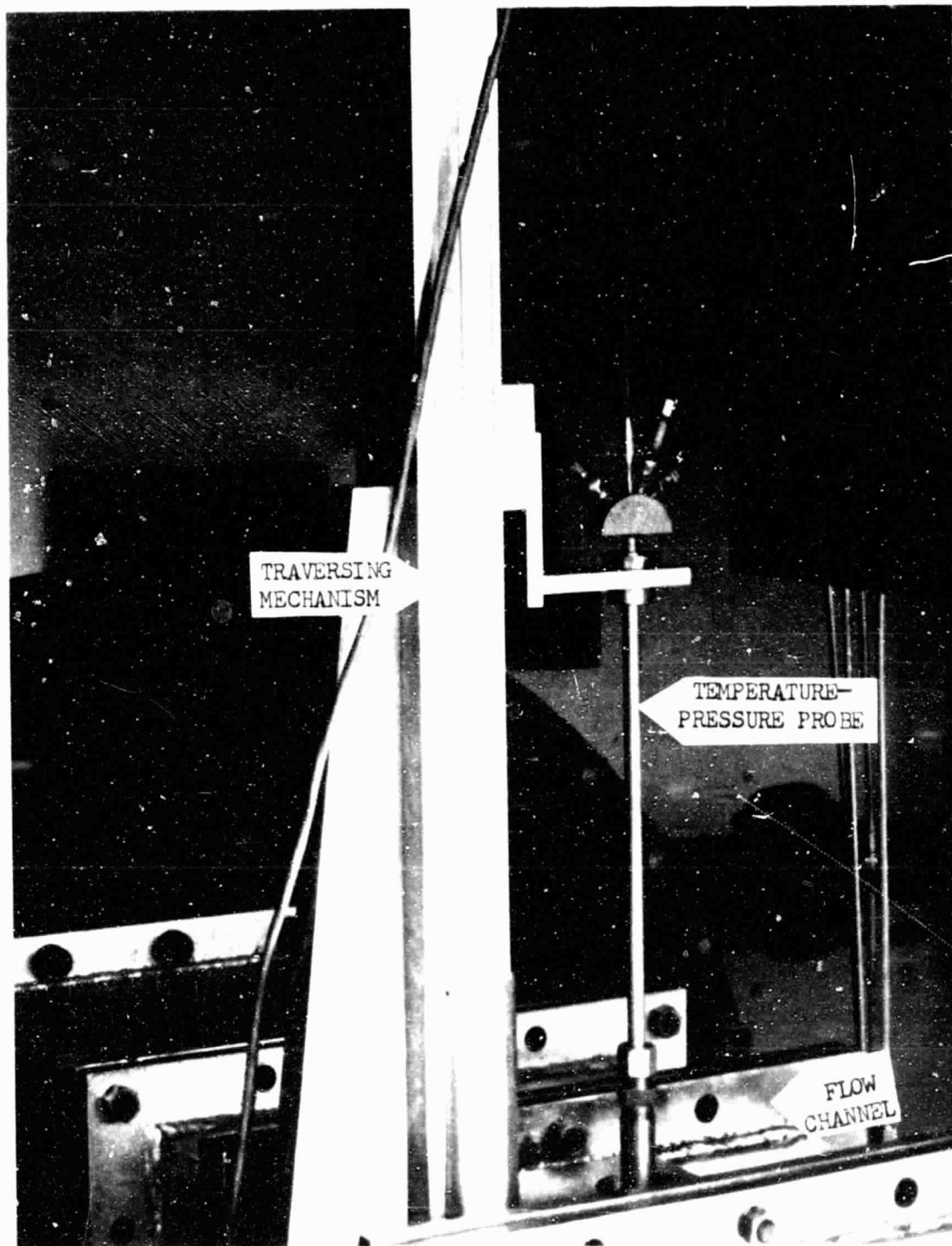


Figure 14. Photograph of the Traversing Mechanism

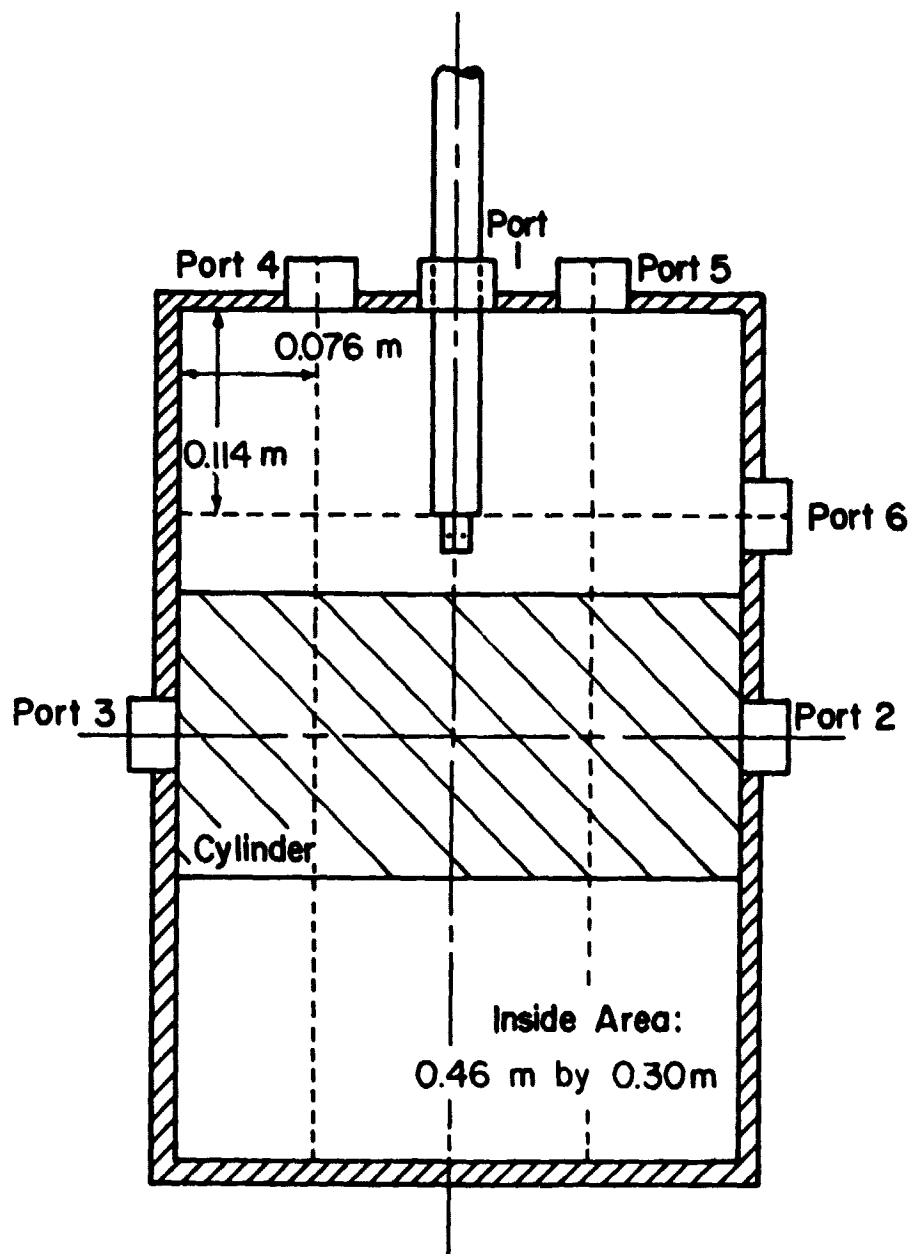


Figure 15. Schematic of the Probe Ports

ORIGINAL PAGE IS
OF POOR QUALITY

Downstream of the traversing probe, the test cylinder was held in the flow channel with circular flanges. Each flange consisted of two separate pieces which were held together by machine screws. As the machine screws were tightened, o'rings between the two flange pieces provided a pressure seal around the cylinder. By loosening the machine screws holding the flange together, it was possible to rotate the cylinder with respect to the flow channel.

The hot freestream flow passed over the test cylinder and was exhausted to the atmosphere.

II.B.2. Test Cylinder

A schematic drawing of the test cylinder is shown in Figure 16. The 0.15 m diameter cylinder, also shown in the photograph in Figure 17, is a scaled up model of the leading edge of a turbine vane. The large increase in size enabled the use of film coolant holes that were large relative to the instrumentation that measured the surface heat flux and temperature.

Three concentric cylinders were used to fabricate the 0.41 m long test cylinder. The inner stainless steel cylinder with a 12.7 mm wall is shown in Figures 18 and 19 at the beginning stages of fabrication. As Figure 18 reveals, 14 channels were milled (6.3 mm deep) along the outside to form coolant channels for internal cooling of the test cylinder. Figure 18 shows 6 channels where the flow area was contracted for a short length. The region where these contracted channels were located corresponds to the film cooled part of the cylinder and the contractions were necessary to provide space for the installation of instrumentation. The holes shown in the photograph in Figure 19 were drilled into each end of the cylinder to provide inlet and exit ports for each coolant channel. The stainless steel tubes emerging from the holes were connected at both ends of the test cylinder to cylindrical liquid coolant manifolds. A centrifugal pump provided 605 liter/min of water to the coolant channels. This maintained the cylinder at room temperature when exposed to the hot (500 K) freestream flow.

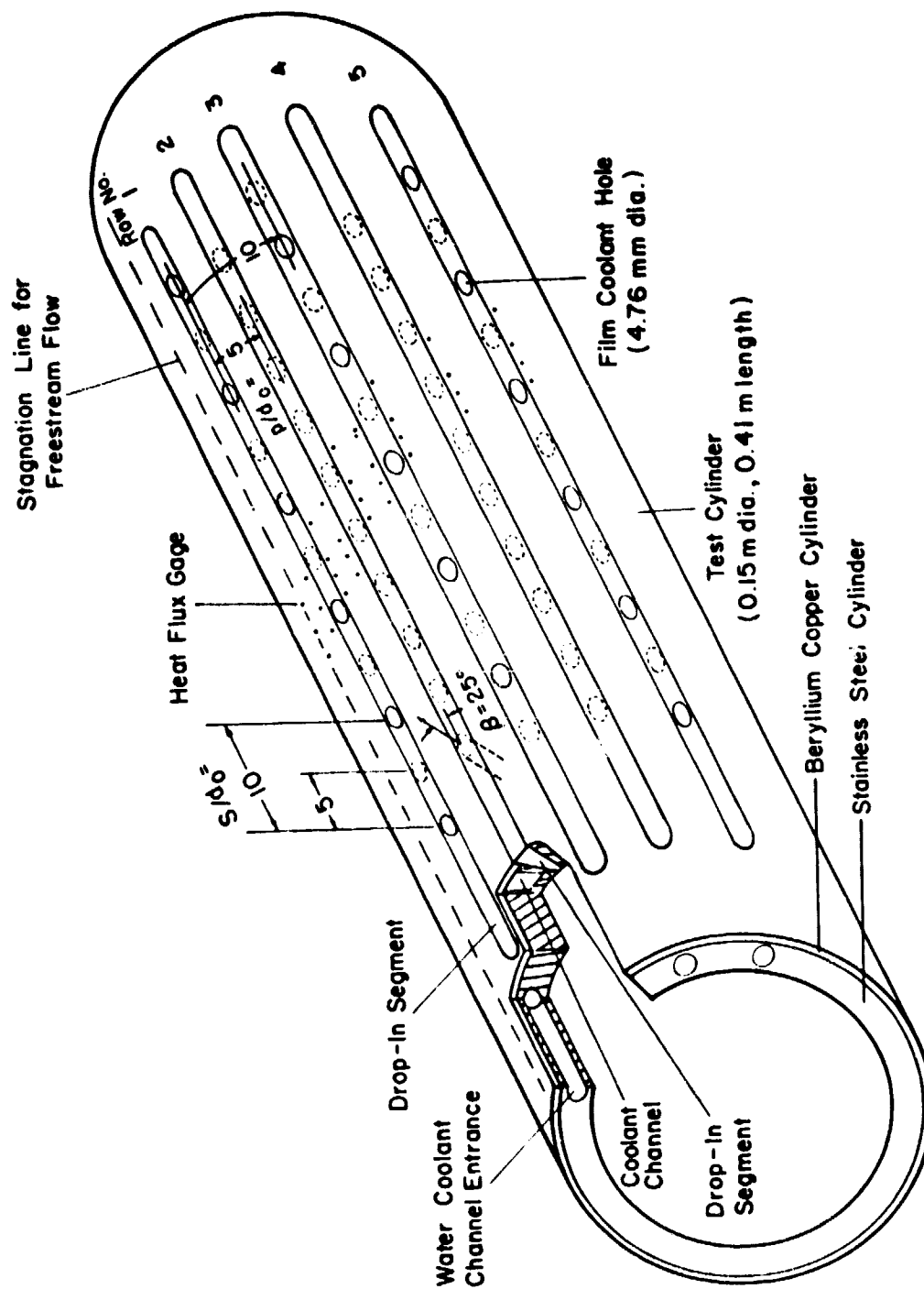


Figure 16. Schematic of the Test Cylinder

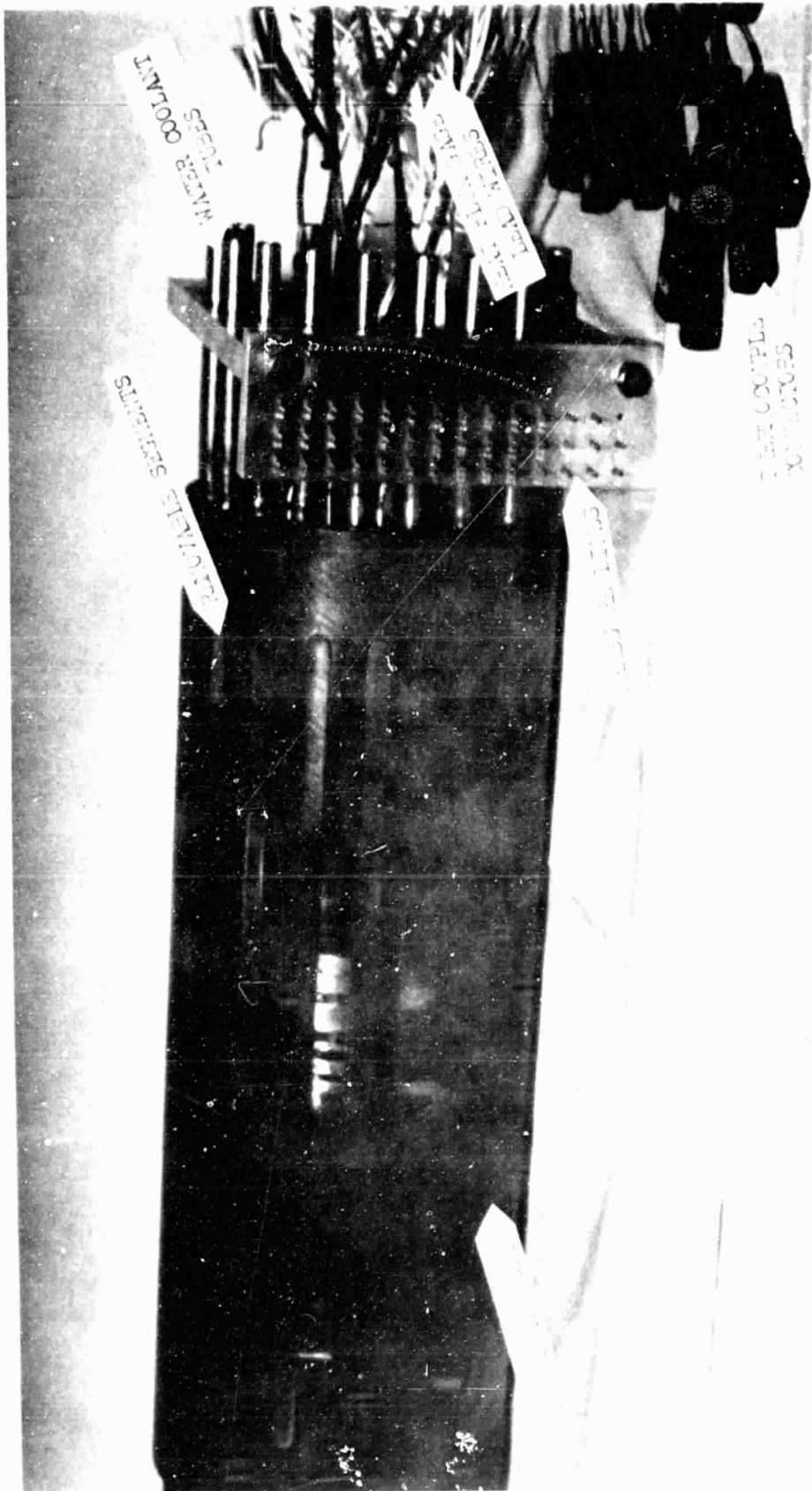


Figure 17. Photograph of the Test Cylinder

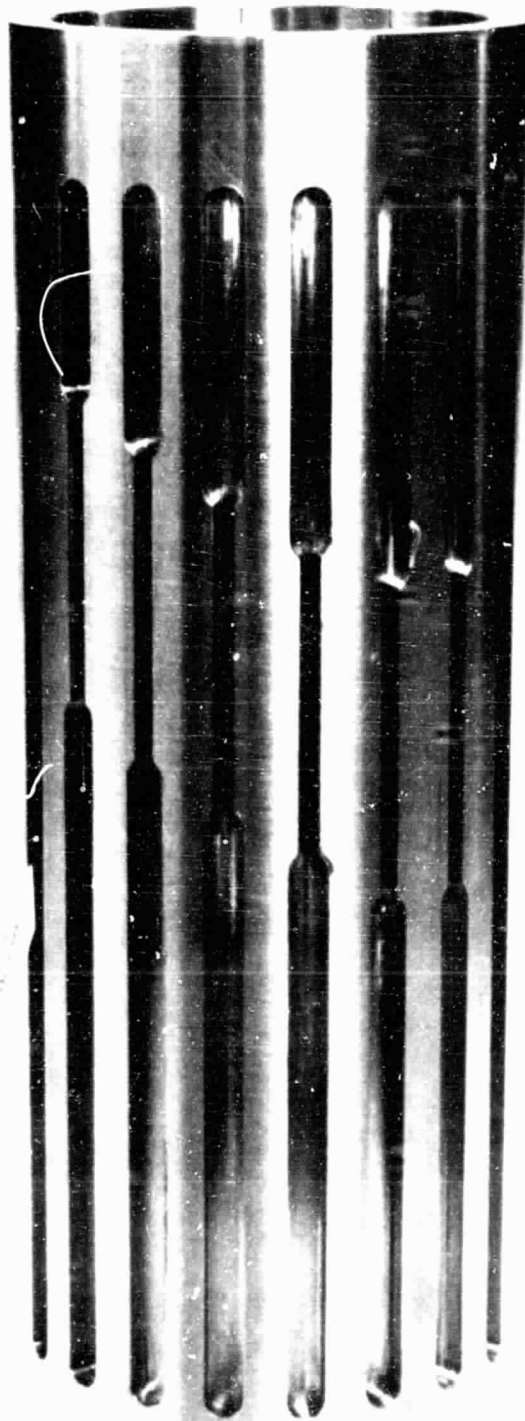


Figure 18. Photograph of the Stainless Steel Inner Cylinder

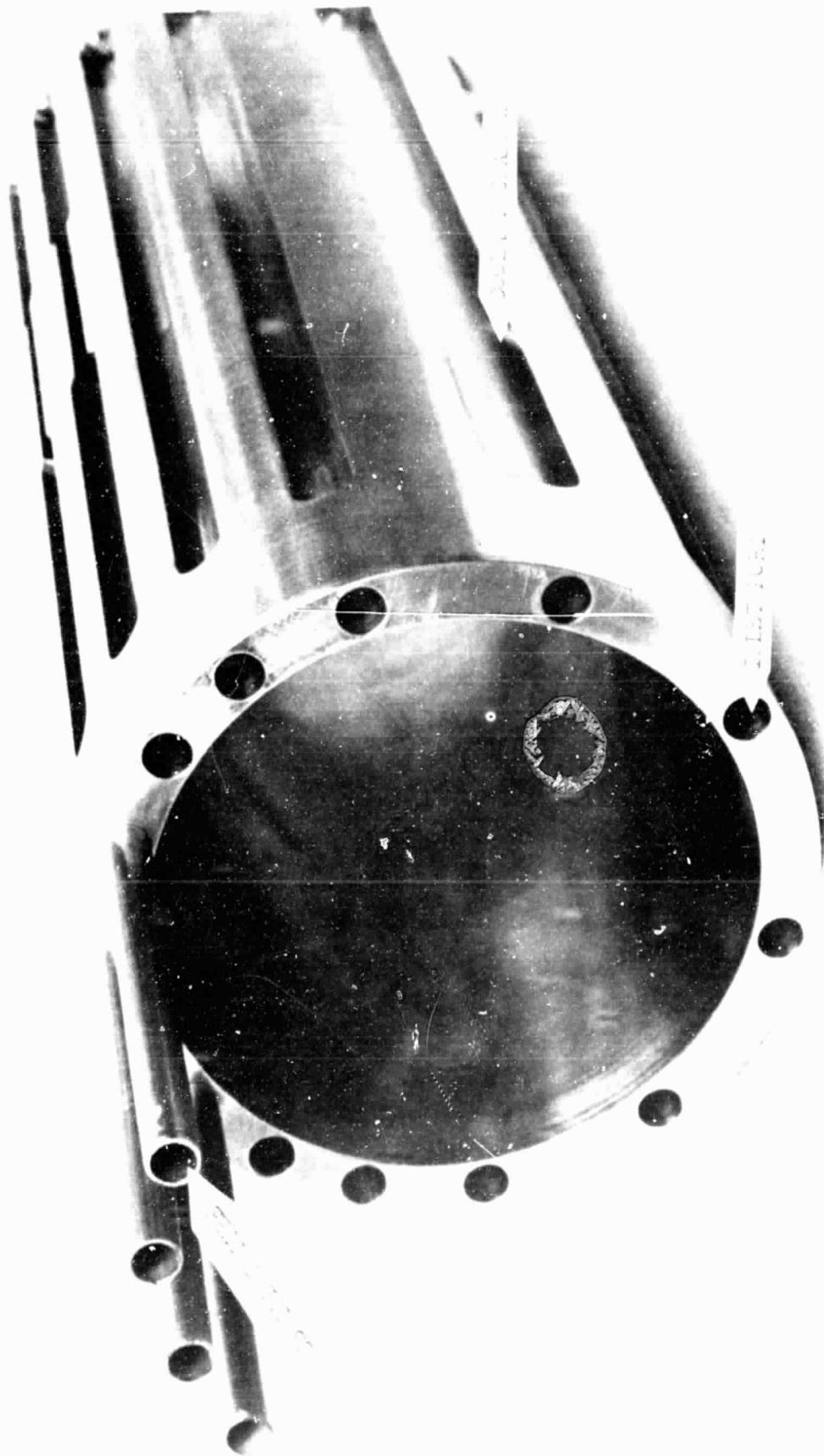


Figure 19. Photograph of the Water Coolant Channels in the Cylinder

A second stainless steel cylinder, 1.59 mm thick, was slipped over the inner cylinder. Electron beam welds were run along the outlines of the coolant channels to seal each coolant channel. The third cylinder, made of beryllium copper, was slipped over the stainless steel inner cylindrical assembly. A copper skin was chosen to help maintain a uniform test surface temperature. The copper and stainless steel cylinders were over brazed together and then electron beam welded along the coolant channel outlines. To obtain the 0.15 m diameter test cylinder, the outer copper skin was turned down to a nominal thickness of 1.59 mm.

Film coolant holes were located in removable drop-in segments that fit into five slots that were milled into the test cylinder (see Figure 16). The cylinder with the segments removed is shown in Figure 20. As will be discussed in the next section, the holes in the surface (seen in Figure 20) were for the installation of instrumentation. An earlier photograph (Figure 17) showed the cylinder with solid segments in place, resulting in a smooth cylindrical test surface. Figure 21 shows the top and bottom view of the three types of segments used in this investigation: (1) the smooth, solid segment, (2) segment with coolant holes at $10 d_o$ spacing, and (3) segment with coolant holes at $5 d_o$ spacing. The segments, made of beryllium copper, have 4.76 mm diameter coolant holes drilled through at an angle of 25° from the surface. The photograph in Figure 22 illustrates the test cylinder with the $10 d_o$ segments installed. This configuration with three rows of holes represents a $10 d_o$ hole-to-hole and row-to-row spacing.

From the back side of the segments, the coolant holes were counterbored to a diameter of 6.3 mm and a short length of copper tubing (6.3 mm OD x 4.76 mm ID x 33.1 mm long) was inserted into each hole. Air film coolant was supplied through plastic tubing connected to the 6.3 mm tubes. The plastic tubing for each row of coolant holes was run through the hollow interior of the test cylinder and was connected to an individual plenum. The air flow to each of five coolant plenums was individually filtered, regulated and measured. This separate control allowed the coolant flowrate from each row of holes to be varied independently. The plastic tubing

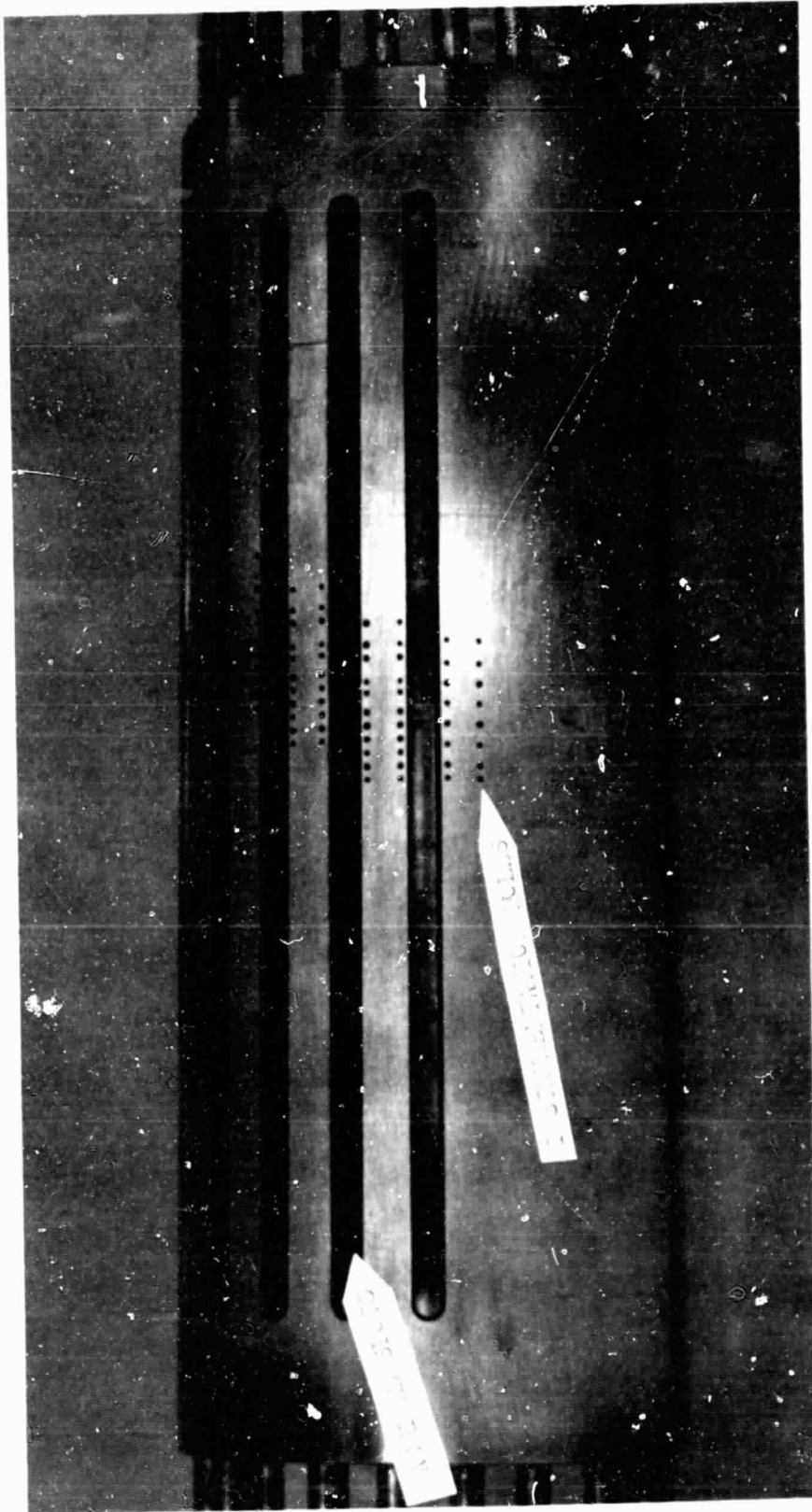


Figure 20. Photograph of the Cylinder with the Segments Removed

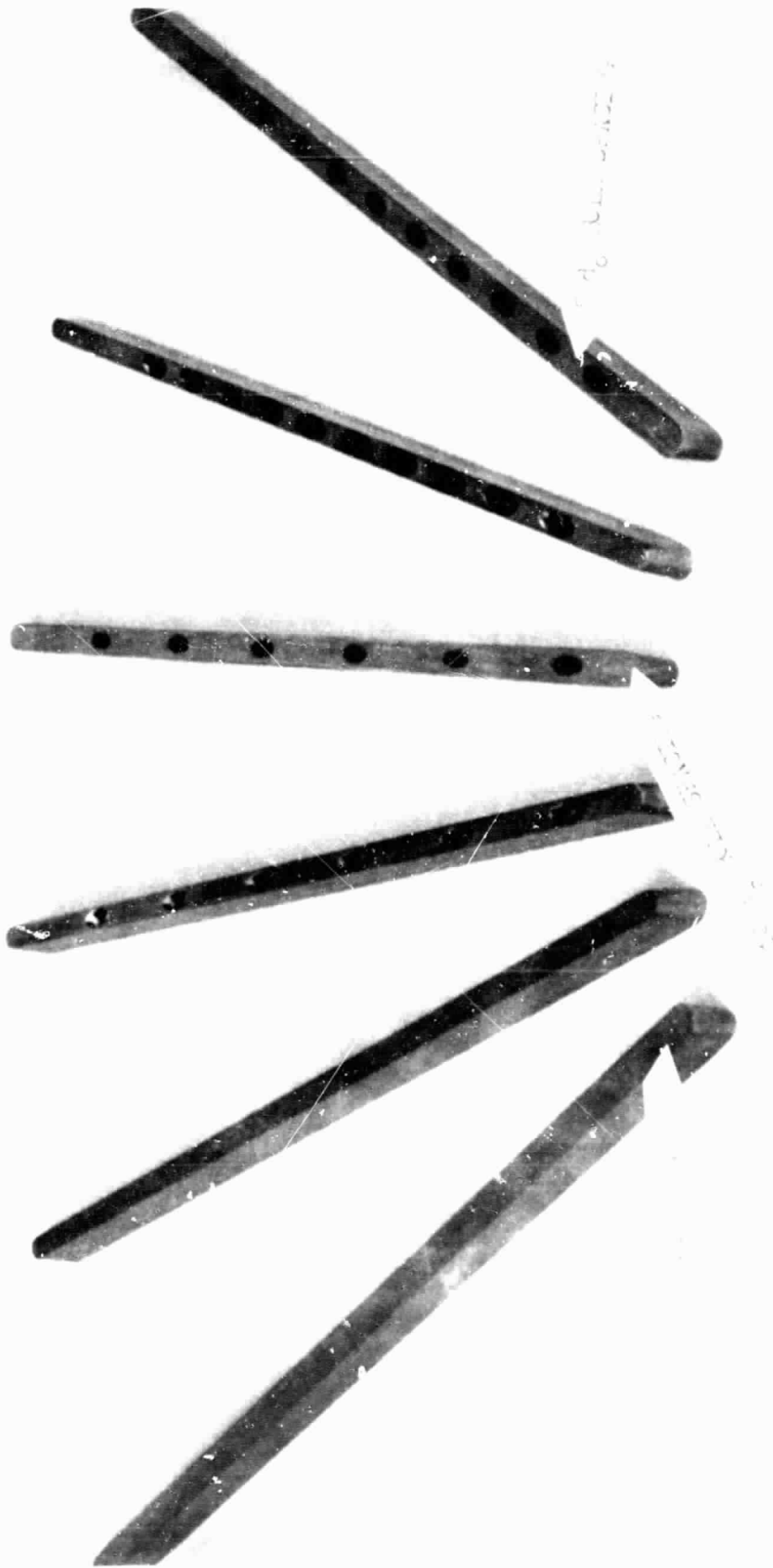


Figure 21. Photograph of the Removable Drop-In Segments

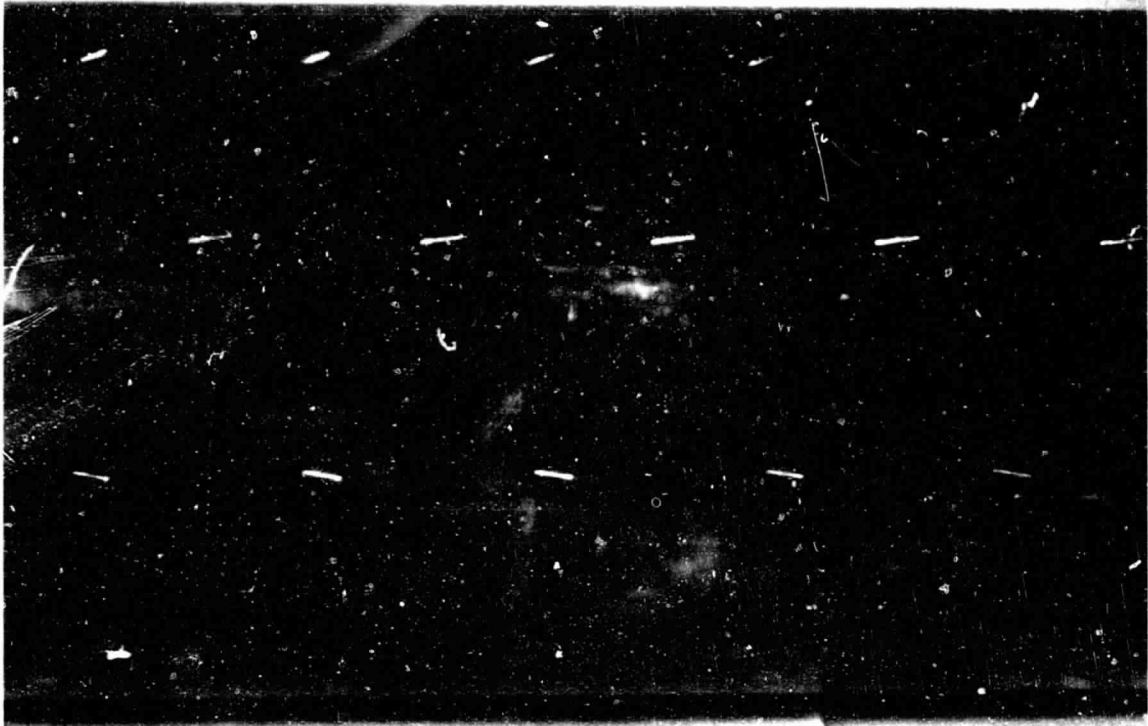


Figure 22. Photograph of the Test Cylinder with a
10 d_o Hole-to-Hole and Row-to-Row Spacing

ORIGINAL PAGE IS
OF POOR QUALITY

supplying each hole in a given row was made identical to ensure equal coolant flow through each hole in a given row.

II.B.3. Instrumentation and Measurements

The mass flow rates of the combustion air and fuel were measured using flat-plate orifices (see Figure 12). Validyne DP15 pressure transducers were used to measure the differential and total pressures. The freestream flow conditions (T_T, P_T, P) were measured in a plane perpendicular to the flow and 0.23 m upstream of the leading edge of the test cylinder. Vertical and horizontal traverses to map the velocity and temperature fields in that plane were made with a wedge-shaped, pitot-static and total temperature probe (United Sensor, 0.61 m long, 4.75 mm dia. head, and 4.53 mm dia. reinforcement tubing). A Meriam inclined manometer was used to measure the pitot-static pressure differential.

A DISA 55A75 hot wire probe was used to conduct turbulence intensity measurements in the freestream. The hot wire signal was processed through a DISA anemometer (55M10) and linearized (55D10) and monitored on a RMS voltmeter. The 0.61 m long hot wire probe had a 4.0 mm head with 9.8 mm diameter reinforcement tubing. The sensor consisted of a 2.21 mm long 10 μ m diameter platinum-rhodium wire.

The photograph in Figure 20 shows the holes drilled in the test cylinder surface for the installation of instrumentation. A view of the instrumentation installed in the film cooled region is shown in the photograph in Figure 23.

A schematic diagram showing the location of the coolant holes and cylinder instrumentation is presented in Figure 24. The coolant holes shown by solid lines represent the hole-to-hole and row-to-row spacing of $S/d_0 = P/d_0 = 10$. The additional holes shown by dashed lines represent $S/d_0 = P/d_0 = 5.0$. The location of the rows of coolant holes relative to stagnation is specified by θ_i where subscript $i = 1, 2, 3, 4, 5$ designates the rows one through five. The location of each row of instrumentation is shown in degrees from stagnation and in terms of the nondimensional coordinate, $(x/d_0)_i$, $i = 1, 2, 3, 4, 5$, downstream

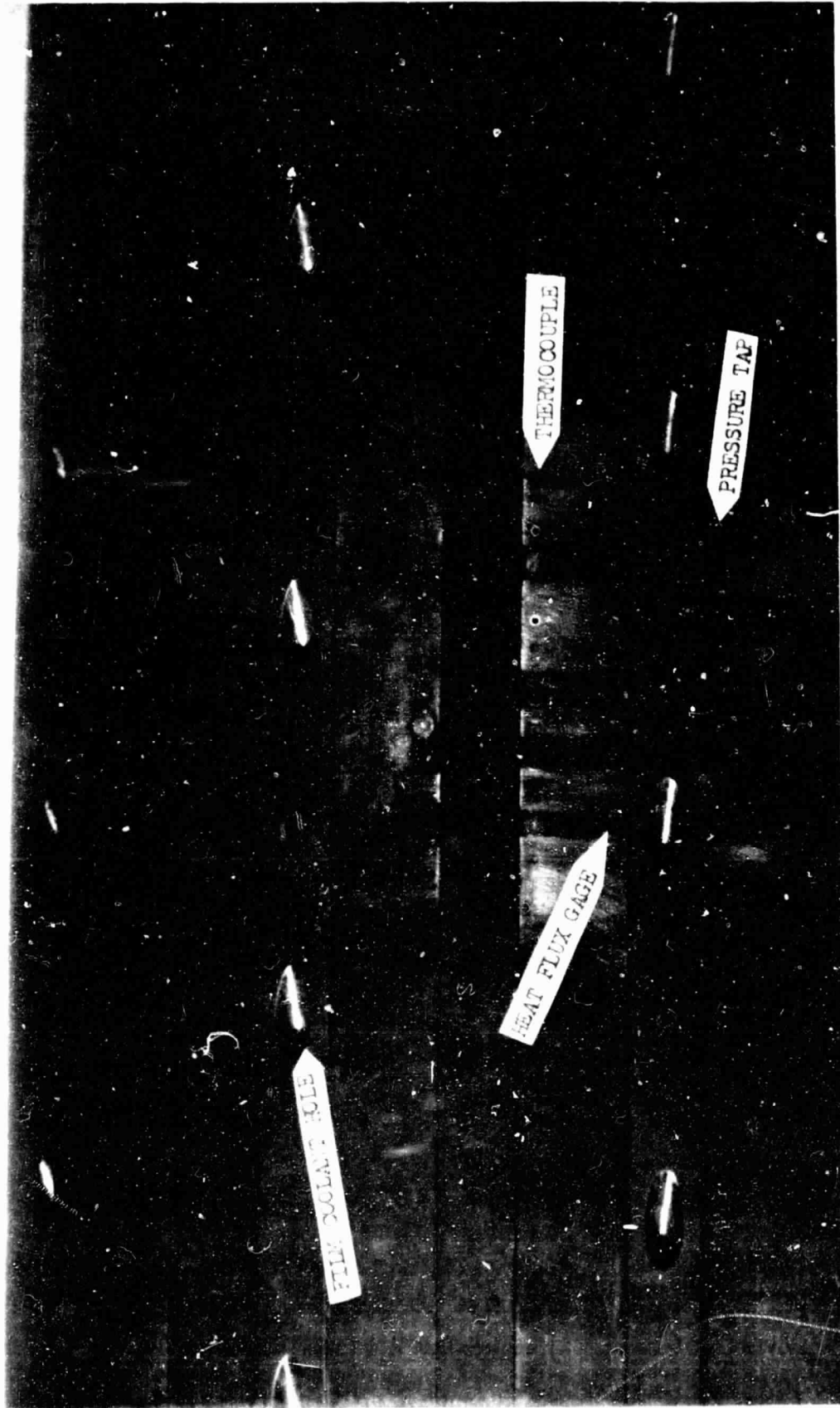


Figure 23. Photograph of the Instrumentation along the Cylinder Surface

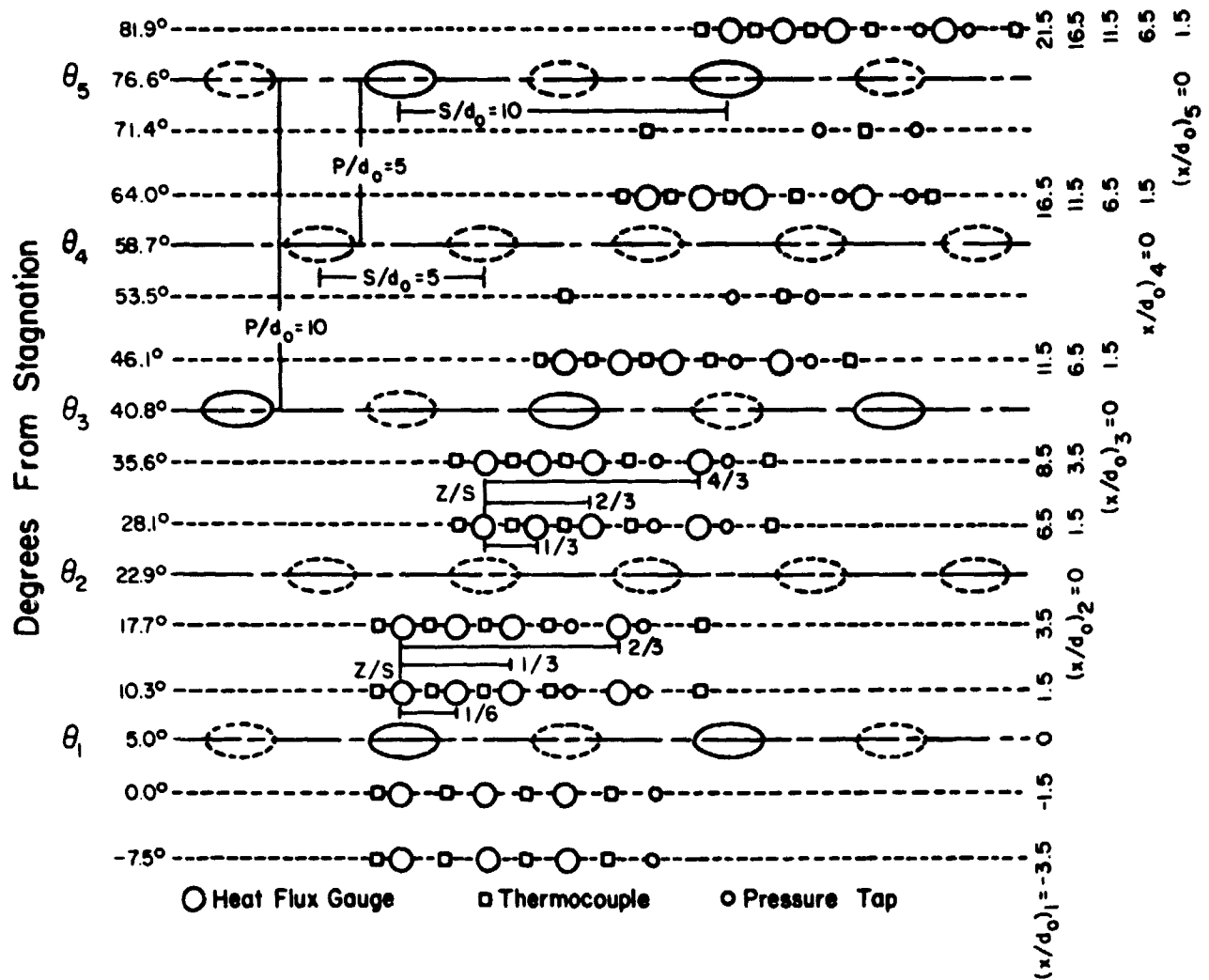


Figure 24. Schematic of the Instrumentation in the Film Cooling Region

(or upstream) from row 1. The spanwise location of the instrumentation relative to the nearest upstream coolant hole is given in terms of the nondimensional coordinate z/S . As Figure 24 demonstrates, the spanwise location of the heat flux gages were chosen so the heat flux would be measured at values of z/S of 0.00, 0.33, and 0.67 for both of the hole-to-hole spacings studied ($S/d = 5$ and 10). The location of all instrumentation in the test cylinder surface is summarized in Table 1.

In designing the test cylinder, the contraction of the water coolant channels was dictated by the closeness of the coolant channels to the slots for the drop-in segments and the need for enough land to drill the instrumentation holes. These contractions, previously shown in Figure 18, fixed the locations, $(x/d_o)_i$, possible for the installation of the heat flux gages. As Figures 23 and 24 revealed, instrumentation holes were drilled so that each heat flux gage would be bordered on either side by a thermocouple

Wall temperature measurements were made using copper-constantan thermocouples mounted flush with the cylinder surface. Four copper-constantan thermocouples were also mounted in each drop-in segment. Holes drilled from the bottom side of each segment allowed the thermocouples to be placed 3.18 mm beneath the surface. The 63 thermocouples along the cylinder surface and the 20 thermocouples in the drop-in segments were monitored by an Esterline Angus (PD2064) data acquisition system. The multi-channel data logger permitted a printed record of the large number of temperature readings to be obtained quickly.

Surface static pressure measurements were made with hyperdermic stainless steel tubing (1.37 mm OD, 0.81 mm ID) inserted flush with the cylindrical surface. Surface pressure measurements were made in a differential form relative to the freestream static pressure upstream of the cylinder. Meriam inclined manometers were used to measure the differential pressure. While a majority of the thermocouples and pressure taps were located in the film cooled region, a limited number were positioned around the entire cylinder surface.

Direct measurements of the surface heat flux were made using miniature, Gardon type, thin foil heat flux gages (Model No. 2000, Thermogage, Inc.). Figure 25 illustrates the operation of the heat

Table 1. Heat Flux, Pressure and Temperature Measurement Locations for $S/d_o=5$

a) Heat Flux Gages			b) Pressure Taps			c) Thermocouples		
	$(x/d_o)_1$	z/s		$(x/d_o)_1$	z/s		$(x/d_o)_1$	z/s
1	-3.5	.00	1	-3.5	.54	1	-3.5	.84
2	-3.5	.50	2	-1.5	.54	2	-3.5	.26
3	-3.5	.00	3	1.5	.04	3	-3.5	.76
4	-1.5	.00	4	1.5	.50	4	-3.5	.26
5	-1.5	.50	5	3.5	.04	5	-1.5	.84
6	-1.5	.00	6	3.5	.50	6	-1.5	.26
7	1.5	.00				7	-1.5	.76
8	1.5	.33		$(x/d_o)_2$	z/s	8	-1.5	.26
9	1.5	.67	7	1.5	.04	9	1.5	.84
10	1.5	.33	8	1.5	.50	10	1.5	.16
11	3.5	.00	9	3.5	.04	11	1.5	.50
12	3.5	.33	10	3.5	.50	12	1.5	.90
13	3.5	.67				13	1.5	.76
14	3.5	.33		$(x/d_o)_3$	z/s	14	1.5	.84
			11	1.5	.04	15	3.5	.16
	$(x/d_o)_2$	z/s	12	1.5	.50	16	3.5	.50
15	1.5	.00	13	3.5	.04	17	3.5	.90
16	1.5	.33	14	3.5	.50	18	3.5	.76
17	1.5	.67						
18	1.5	.33		$(x/d_o)_4$	z/s	19	1.5	.84
19	3.5	.00	15	1.5	.18	20	1.5	.16
20	3.5	.33	16	1.5	.64	21	1.5	.50
21	3.5	.67	17	3.5	.04	22	1.5	.90
22	3.5	.33	18	3.5	.64	23	1.5	.76
						24	3.5	.84
	$(x/d_o)_3$	z/s		$(x/d_o)_5$	z/s	25	3.5	.16
23	1.5	.00	19	1.5	.18	26	3.5	.50
24	1.5	.33	20	1.5	.50 ⁺	27	3.5	.90
25	1.5	.67	21	5.1	C	28	3.5	.76
26	1.5	.33	22	10.1	C			
			23	16.3	C		$(x/d_o)_3$	z/s
	$(x/d_o)_4$	z/s	24	29.4	C	29	1.5	.84
27	1.5	.00	25	42.4	C	30	1.5	.16
28	1.5	.33	26	50.5	C	31	1.5	.50
29	1.5	.67	27	54.0	L	32	1.5	.90
30	1.5	.33	28	54.0	C	33	1.5	.76
			29	54.0	R	34	3.5	.00
	$(x/d_o)_5$	z/s	30	60.7	L	35	3.5	.33
31	1.5	.00	31	60.7	C			
32	1.5	.33	32	60.7	R		$(x/d_o)_4$	z/s
33	1.5	.67	33	64.2	C	36	1.5	.84
34	1.5	.33	34	70.6	L	37	1.5	.16
			35	70.6	C	38	1.5	.50
			36	70.6	R	39	1.5	.90
						40	1.5	.76
						41	3.5	.00
						42	3.5	.33
							$(x/d_o)_5$	z/s
						43	1.5	.84
						44	1.5	.16
						45	1.5	.50
						46	1.5	.90
						47	1.5	.76
						48	5.1	C ⁺
						49	10.0	C
						50	16.3	C
						51	29.4	C
						52	42.4	C
						53	50.5	C
						54	54.0	L
						55	54.0	C
						56	54.0	R
						57	60.7	L
						58	60.7	C
						59	60.7	R
						60	64.2	C
						61	70.6	L
						62	70.6	C
						63	70.6	R

⁺ Outside of the film cooled region, the spanwise location (z/s) of the pressure taps and thermocouples relative to the coolant holes is no longer relevant. Therefore, the C, L, and R designations indicate whether the instrumentation is near the centerline of the cylinder or the left or right end of the cylinder.

ORIGINAL PAGE IS
OF POOR QUALITY

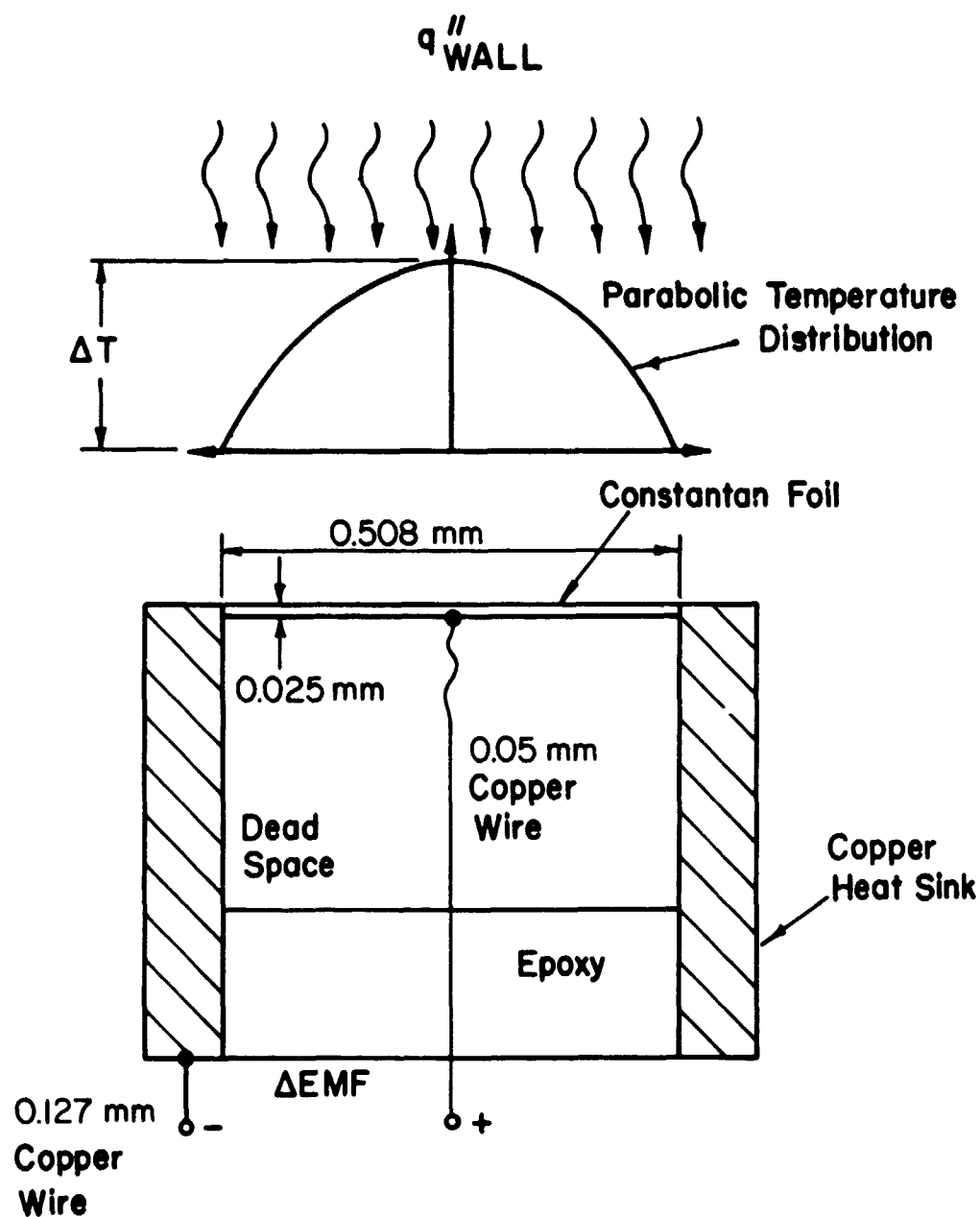


Figure 25. Schematic of the Operation of a Heat Flux Gage

flux gage. The operation of the gage is based on the incident heat flux on the thin constantan foil flowing radially to the cylindrical copper body (heat sink), establishing a parabolic temperature profile over the foil. The Thermogage heat flux gage consisted of a constantan foil (0.025 mm thick, 0.508 mm dia.) silver soldered to the end of a cylindrical, copper tube. The sensor was then press fitted into a 2.54 mm diameter copper plug. The temperature difference that is created between the center and the edge of the foil is dependent on the magnitude of the incident heat flux. A fine copper wire is fused to the center of the coil on its underneath side, while another copper wire is fused to the copper body and the emf from these two thermocouple junctions is dependent on the temperature differences across the foil (i.e. the incident heat flux). Coincidentally, the variation of the thermal conductivity of constantan with temperature and the thermoelectric power of the copper-constantan thermocouple are such that a linear relation between the heat flux and the emf from the copper-constantan gage is produced (assuming the gage temperature remains in the 283 K - 505 K range).

Due to the small size of the gages used, a microvolt signal is produced. Therefore, the sensor must be matched with an operational amplifier (gain ~ 1000) to provide a millivolt level signal. Since 34 gages were installed on the test cylinder, two gages were matched to one amplifier through a switch to reduce the number of amplifiers required. Therefore, seventeen gages were read simultaneously with the output from the amplifiers fed to a multichannel oscillograph and the Esterline Angus data logger. The oscillograph allowed a continuous record of the heat flux to be recorded while a digital printout was obtained from the data logger.

The film coolant air flow rate for each row of holes was measured with a hot wire mass flow meter (Thermo Systems, Inc. Model 1352). A total of five hot wire flow meters allowed the flow through each row to be measured separately. As mentioned in the previous section, copper tubing (6.3 mm OD) was inserted into the counter bore of the coolant holes in the back of each segment. A copper-constantan thermocouple was mounted in the center of the central tube in each

segment to measure the temperature of the coolant as it emerged from the segment.

II.C. Description of Experiment

This experimental program was conducted to investigate the reduction in the local heat flux due to film cooling from multiple row injection on the leading edge of a cylindrical test surface with flow conditions chosen to simulate the film cooling typical of the leading edge of a turbine vane. To ensure that the experiment modeled representative leading edge conditions, a survey of the engine companies was made to determine flow conditions and hole geometry typical of current and future leading edge designs. Table 2 shows the range of parameters important in film cooling the leading edge of turbine vanes and the specific values of each parameter being matched in this investigation.

Although the 0.15m cylinder was scaled up in size, a Reynolds number of 9×10^4 based on the leading edge diameter closely matches typical engine conditions. In the present study, a moderate free-stream gas temperature (~ 500 K) and water cooling of the test cylinder to maintain the surface near room temperature (~ 294 K), provided a freestream-to-wall temperature ratio of 1.7. The use of a copper skin helped maintain an approximately isothermal wall condition. As the discussion in Section II.A revealed, the Reynolds number and free-stream-to-wall temperature ratio are important parameters in modeling the convective heat transfer environment.

The turbulence intensity approaching the leading edge of the cylinder was varied by the use of screens. The screens were sized to increase the clear wind tunnel turbulence intensity of 4% up to as high as 11%.

The freestream Mach number was the one parameter not simulated in the present investigation due to the low flow velocity through the wind tunnel (~ 14.3 m/sec). However, studies by Liess [20] and Papell and Trout [32] have shown that the effect of Mach number (particularly at low subsonic values) has no influence on the film cooling performance.

The film cooling geometry investigated was selected to fall within the range for engine conditions listed in Table 2. A spanwise angle of 25° was chosen, although the versatility of the test cylinder allows new drop-in segments to be made with a different injection angle. Two different hole and row spacings were studied. The first, $S/d_o = P/d_o = 5 d_o$, was selected to closely match engine conditions. The second spacing, $S/d_o = P/d_o = 10 d_o$, was chosen because of the trend in future engine designs toward larger hole spacings. The two spacings, $5 d_o$ and $10 d_o$, also correspond to the spacings used in the numerous investigations conducted at Stanford [14] [26] [33] for multiple row film cooling on a flat plate.

The selection of a hole and row spacing of $5 d_o$ permitted the use of five rows of holes. The angular location of these rows with respect to stagnation (see Figure 24) were: $\theta_1 = 5^\circ$, $\theta_2 = 22.9^\circ$, $\theta_3 = 40.8^\circ$, $\theta_4 = 58.7^\circ$, $\theta_5 = 76.6^\circ$. The first row was positioned slightly away from the stagnation line to avoid the problem of defining the blowing ratio at the stagnation line.

The investigation of a hole and row spacing of $10 d_o$ resulted in 3 rows of holes to cover the same area. The two intermediate slots were filled with smooth, solid segments as illustrated in Figure 22. The angular location of the three row configuration (see Figure 24) were: $\theta_1 = 5^\circ$, $\theta_3 = 40.8^\circ$, $\theta_5 = 76.6^\circ$. Additional experiments with the $10 d_o$ spacing were conducted with two rows of holes by positioning the cylinder with the first row at $\theta_2 = 22.9^\circ$ and the second row at $\theta_4 = 58.7^\circ$. The third row located at 94.5° was not employed.

The acceleration of the freestream in the stagnation region of the test cylinder is characterized by the acceleration parameter, K . For each of the five injection locations, the K values[†] were:

Injection location	5°	22.9°	40.8°	58.7°	76.6°
Acceleration parameter, $K \times 10^5 = 200$	9.4	2.7	1.1	0.37	

[†] The values of K were calculated from incompressible potential flow for a cylinder in cross flow with a correction for blockage.

Table 2. Turbine Gas Stream and Film Cooling Heat Transfer Parameters

<u>Typical Leading Edge Conditions</u> ¹		<u>Purdue Investigation</u>
<u>Freestream Conditions</u>		
Reynolds Number	$4 \times 10^4 - 1 \times 10^5$	9×10^4
T/T_w	1.4 - 1.9	1.7
Turbulence Intensity	7 - 20%	4% (4 - 11%) ²
Mach number	0.1 - 0.2	0.03
<u>Coolant Hole Geometry</u>		
Spanwise Angle	15° - 45°	25°
S/d_o	4 - 10	5, 10
P/d_o	2 - 4	5, 10
<u>Coolant Flow Conditions</u>		
$M(\rho_C V_C / \rho_\infty V_\infty)$	0.5 - 2.0	0 - 2.0
$\theta_C(T_\infty - T_C / T_\infty - T_w)$	1.4 - 2.0	1.0

¹ Information collected from a survey of engine companies to determine conditions typical of current and future leading edge designs.

² A clear wind tunnel turbulence intensity of 4% was increased up to 11% with the insertion of screens in the wind tunnel.

The coolant hole diameter was selected so the local boundary layer displacement thickness-to-coolant hole diameter ratio (δ^*/d_o) would approach the values found on actual leading edge designs. However, the need for internal cooling of the test cylinder and the space required for the installation of instrumentation, the width of the drop-in segment, and subsequently the coolant hole diameter, was restricted. The largest possible coolant hole, 4.76 mm diameter, was used. This resulted in a ratio δ^*/d_o of 0.032^{††} for the test cylinder, while the values of δ^*/d_o on current engines range from 0.01 to 0.025. Although the δ^*/d_o value on the test cylinder was somewhat larger, Liess [20] found in his investigation of single row film cooling that for values of δ^*/d_o less than 0.1, the film cooling performance was unaffected.

One of the most crucial parameters influencing the film cooling performance is the blowing ratio, M . Table 2 shows the M values typically found along a vane leading edge. All multiple row studies conducted on a flat plate have established a uniform M distribution along the rows of holes with M defined as the mass flux of the coolant over the local mass flux of the freestream. The leading edge of a vane presents a very different situation. The multiple rows in the stagnation region are generally fed by a common plenum and the pressure distribution around the vane surface results in a different coolant mass flux at different row locations. In addition, the local velocity of the freestream around the vane varies. Variations in the coolant and local freestream mass velocity result in a non-uniform distribution of M for multiple rows in the stagnation region. The blowing ratio for rows fed from a common plenum was modeled as shown in Appendix 1, and the blowing distribution was shown to be a function of two parameters, the freestream total pressure-to-plenum coolant pressure ratio (P_{T_c}/P_{T_∞}) and the freestream approach Mach number, $Ma_{\infty,0}$. Selecting values for P_{T_c}/P_{T_∞} and $Ma_{\infty,0}$ typical of actual leading edge designs, the non-uniform blowing distributions computed in Appendix 1 are presented in Table 3.

†† The value of δ^*/d_o was calculated for a cylinder in crossflow using the integral momentum boundary layer equation [35].

Table 3. Blowing Ratio, M , for Multiple Rows with Common Plenum
$$M_{\infty,0} = 0.1 \quad S/d_0 = 10 \quad \theta_1 = 5^\circ$$

P_{T_c}/P_{T_∞}	Row 1 $\theta_1 = 5^\circ$	Row 2 $\theta_3 = 40.8^\circ$	Row 3 $\theta_5 = 76.6^\circ$
1.010	5.73	1.17	1.01
1.020	8.16	1.40	1.16
1.030	10.05	1.61	1.27

$$M_{\infty,0} = 0.2$$

P_{T_c}/P_{T_∞}	Row 1 $\theta_1 = 5^\circ$	Row 2 $\theta_3 = 40.8^\circ$	Row 3 $\theta_5 = 76.6^\circ$
1.010	2.96	0.95	0.92
1.020	4.15	1.04	0.96
1.030	5.08	1.14	1.01

$$M_{\infty,0} = 0.1 \quad S/d_0 = 10 \quad \theta_2 = 22.9^\circ$$

P_{T_c}/P_{T_∞}	Row 1 $\theta_2 = 22.9^\circ$	Row 2 $\theta_4 = 58.7^\circ$
1.010	1.54	1.05
1.020	2.02	1.24
1.030	2.41	1.36

$$M_{\infty,0} = 0.2$$

P_{T_c}/P_{T_∞}	Row 1 $\theta_2 = 22.9^\circ$	Row 2 $\theta_4 = 58.7^\circ$
1.010	1.08	0.92
1.020	1.28	0.98
1.030	1.44	1.04

$$M_{\infty,0} = 0.1 \quad S/d_0 = 5 \quad \theta_1 = 5^\circ$$

P_{T_c}/P_{T_∞}	Row 1 $\theta_1 = 5^\circ$	Row 2 $\theta_2 = 22.9^\circ$	Row 3 $\theta_3 = 40.8^\circ$	Row 4 $\theta_4 = 58.7^\circ$	Row 5 $\theta_5 = 76.6^\circ$
1.010	5.73	1.54	1.17	1.05	1.01
1.020	8.16	2.02	1.40	1.24	1.16
1.030	10.05	2.42	1.61	1.36	1.27

$$M_{\infty,0} = 0.2$$

P_{T_c}/P_{T_∞}	Row 1 $\theta_1 = 5^\circ$	Row 2 $\theta_2 = 22.9^\circ$	Row 3 $\theta_3 = 40.8^\circ$	Row 4 $\theta_4 = 58.7^\circ$	Row 5 $\theta_5 = 76.6^\circ$
1.010	2.96	1.08	0.95	0.92	0.92
1.020	4.15	1.27	1.04	0.98	0.96
1.030	5.08	1.44	1.14	1.04	1.01

ORIGINAL PAGE IS
OF POOR QUALITY

The investigation of the influence of coolant blowing ratio was divided into three parts. The first part involved blowing from a single row only. Experiments were conducted using the multiple row configurations to obtain data when each row was blowing along. The results for single row blowing were used to help isolate the row-to-row interactions within the multiple row configurations. The second part used a uniform (i.e. constant M) blowing distribution for the multiple rows of holes with M being varied from 0 to 2.0. The third part of the study investigated non-uniform blowing distributions representative of a common plenum supply.

The dimensionless coolant temperature, θ_c , listed in Table 2 varies from 1.4 to 2.0 in actual leading edge designs. The present investigation employed reduced temperature conditions with the cylinder surface maintained at approximately room temperature ($\sim 70^\circ\text{F}$). To obtain a value of θ_c of 1.5 would have required a coolant temperature of 191 K. The present phase of the investigation was conducted with $\theta_c = 1.0$ ($T_c = T_w$) to avoid the difficulty in obtaining such low coolant exit temperatures. This value of θ_c corresponds to the transpiration case and Colladay [34] has shown that when considering a combination of internal convection cooling and external film cooling, optimum cooling of the vane is achieved when $\theta_c = 1.0$. However, to apply the results from the present investigation to actual design conditions where $\theta_c \neq 1.0$, one would have to use the linear theory developed by Choe, Kays, and Moffat [9] to determine the Stanton number ratio for the pertinent value of θ_c . Using the data for h'/h_0 which has been published in the literature and extrapolating a line through the present results at $\theta_c = 1.0$, it would be possible to estimate the film cooling performance at higher values of θ_c . A follow-on phase of the study of stagnation region film cooling currently in progress is conducting experiments to obtain data for $\theta_c > 1.0$.

II.D. Data Reduction

During each experimental run, the following measurements were recorded: a) the freestream total temperature, the freestream total pressure, and the freestream total-to-static pressure difference, upstream of the cylinder, b) the cylinder wall temperature and wall heat flux distributions, c) the coolant mass flow rate and the coolant exit temperature for each row. These values were then used to compute the parameters needed to evaluate the film cooling performance. To ensure that no changes occurred in the freestream or surface conditions during a run, the dry wall heat flux was measured both before and after the film cooling experiments as well as several times during the experiments (between the heat flux measurements for two different blowing conditions). This provided a check on both the heat transfer environment and the performance of the heat flux gages.

The freestream total temperature and total-to-static pressure ratio were used to determine the freestream Mach number, $Ma_{\infty,0}$, velocity, $V_{\infty,0}$, and static temperature. The Reynolds number was calculated using the cylinder diameter. Following convention in the gas turbine industry, a mean film temperature, $T_m = (T_{\infty} + T_w)/2$, was used to determine the density and viscosity in the Reynolds number. The perfect gas law was used to compute the density and other physical properties of the freestream (μ , k , γ , Mol. Wt.) were determined from Ref. 36.

The local freestream velocity around the cylinder, V_{∞} , was computed from incompressible potential flow theory. The expression for a cylinder in an infinite freestream was corrected to account for tunnel blockage effects yielding

$$V_{\infty} = C \sqrt{2} V_{\infty,0} \sin \theta$$

The tunnel blockage correction, C , was calculated by determining the potential flow over a large number of cylinders (of same diameter) above and below the test cylinder of interest. The spacing between the cylinder axes was chosen to locate the mid-streamline (symmetry line), between the test cylinder and the cylinder above, to coincide with the upper tunnel wall. The correction for the freestream

velocity at the location of the coolant holes was

Degrees from Stagnation $\theta_1=5^\circ$ $\theta_2=22.9^\circ$ $\theta_3=40.8^\circ$ $\theta_4=58.7^\circ$ $\theta_5=76.6^\circ$
 Correction Factor, C = 1.089 1.091 1.093 1.097 1.099

For the experiments without film cooling, the surface heat flux and the freestream-to-wall temperature difference were used to compute the local convective heat transfer coefficient.

$$h_o = \frac{q_{w,o}''}{T_\infty - T_{w,o}} \quad (18)$$

The subscript o designation indicates no film coolant flow (i.e. dry wall). The thermocouples on either side of each heat flux gage were averaged to determine the wall temperature at the gage. Therefore, the dry wall heat transfer coefficient, h_o , was computed directly from the recorded values of heat flux, wall temperature, and freestream temperature. Using a value of thermal conductivity evaluated at the mean film temperature, T_m , the Nusselt number, based on the cylinder diameter, was calculated from h_o .

For the experiments with film coolant flow, the heat flux and the freestream-to-wall temperature difference were used to compute a local convective heat transfer coefficient with film cooling.

$$h_{FC} = \frac{q_{w,FC}''}{T_\infty - T_{w,FC}} \quad (19)$$

The subscript FC designation indicates with film cooling.

The influence of film cooling was determined by the ratio of the heat transfer coefficients, h_{FC}/h_o . Since the freestream parameters do not change with film cooling (i.e. $\rho_\infty, V_\infty, c_p$ remain constant with or without coolant injection), the heat transfer coefficient ratio is equivalent to the Stanton number ratio.

$$\frac{h_{FC}}{h_o} = \frac{St_{FC}}{St_o} \quad (20)$$

where

$$St = \frac{h}{\rho_{\infty} V_{\infty} c_{p_{\infty}}}$$

and

V_{∞} = local freestream velocity along the cylinder

The film cooling results in this investigation are given as a percentage reduction in the Stanton number due to film cooling which is defined as

$$1 - \frac{St_{FC}}{St_0} = \text{the Stanton Number Reduction} \quad (21)$$

Computation of the film cooling blowing parameters, $M, V_c/V_{\infty}$ and I , was based on the assumption of equal flow through all of the coolant holes in a particular row. The mass flux of the coolant ($\rho_c V_c$) was determined from the measured coolant flow rate and the number and diameter of the coolant holes. The local freestream mass flux, $\rho_{\infty} V_{\infty}$, was determined from the local freestream velocity, V_{∞} , at the location of the row of coolant holes and the freestream density, $\rho_{\infty,0}$, assuming incompressible flow. The local injection blowing ratio was calculated as $M = (\rho_c V_c)/(\rho_{\infty} V_{\infty})$. The freestream-to-coolant density ratio was determined by using the perfect gas law and assuming the pressure of the coolant emerging from the hole (P_c) equals the local static pressure (P_{∞}). Having determined the values of M and ρ_c/ρ_{∞} , the coolant-to-freestream velocity ratio (V_c/V_{∞}) and the momentum flux ratio ($\rho_c V_c/\rho_{\infty} V_{\infty}$) were computed.

Each experimental test was limited to a steady state run time of approximately 1 hour due to the capacity of the air supply facility. The data collected from each test was inserted into a data reduction computer program to perform all of the calculations described in this section.

A detailed discussion of the results from the experimental investigation is given in the next four sections.

III. Freestream Conditions and Heat Transfer without Film Cooling

The present investigation was denoted to matching important parameters typical of the turbine vane environment such as the Reynolds number, Re_D , and the freestream-to-wall temperature ratio, T_∞/T_w . For all experimental runs, the following nominal test conditions were maintained: (a) Reynolds number (based on leading edge diameter) of 9×10^4 ($\pm 2.5\%$), and (b) freestream-to-wall temperature ratio of 1.7 ($\pm 1.5\%$) using a freestream gas temperature of 500 K (± 3 K) and a nearly uniform wall temperature of 294 K (± 3 K). A preliminary investigation was conducted to survey the freestream flow conditions and the cylinder wall temperature distribution, and to determine the cylinder pressure and heat flux distributions (without film cooling) characteristic of the experimental apparatus. The results of the preliminary investigation are presented in this section.

III.A. Freestream Conditions

All experiments were conducted with the wind tunnel exhausting directly to the atmosphere. All freestream profile data were measured 1 1/2 cylinder diameters (0.23 m) upstream of the leading edge of the cylinder following the recommendations of Kestin and Wood [31]. The port locations where each traverse was obtained are shown in Figure 15.

The freestream vertical and horizontal velocity profiles are shown in nondimensional form in Figures 26 and 27, respectively. The velocity profiles in Figure 26 are presented as a function of the wind tunnel height. The profile at Port 1, traversing along the centerline of the tunnel, shows a variation of less than 3% across the entire tunnel. Within the cross-sectional region covered by the frontal area of the cylinder (the shaded region in Figure 26), the variation was less than 1%. The profile at Port 5, located halfway between Port 1 and the tunnel side wall, shows a slightly larger variation across

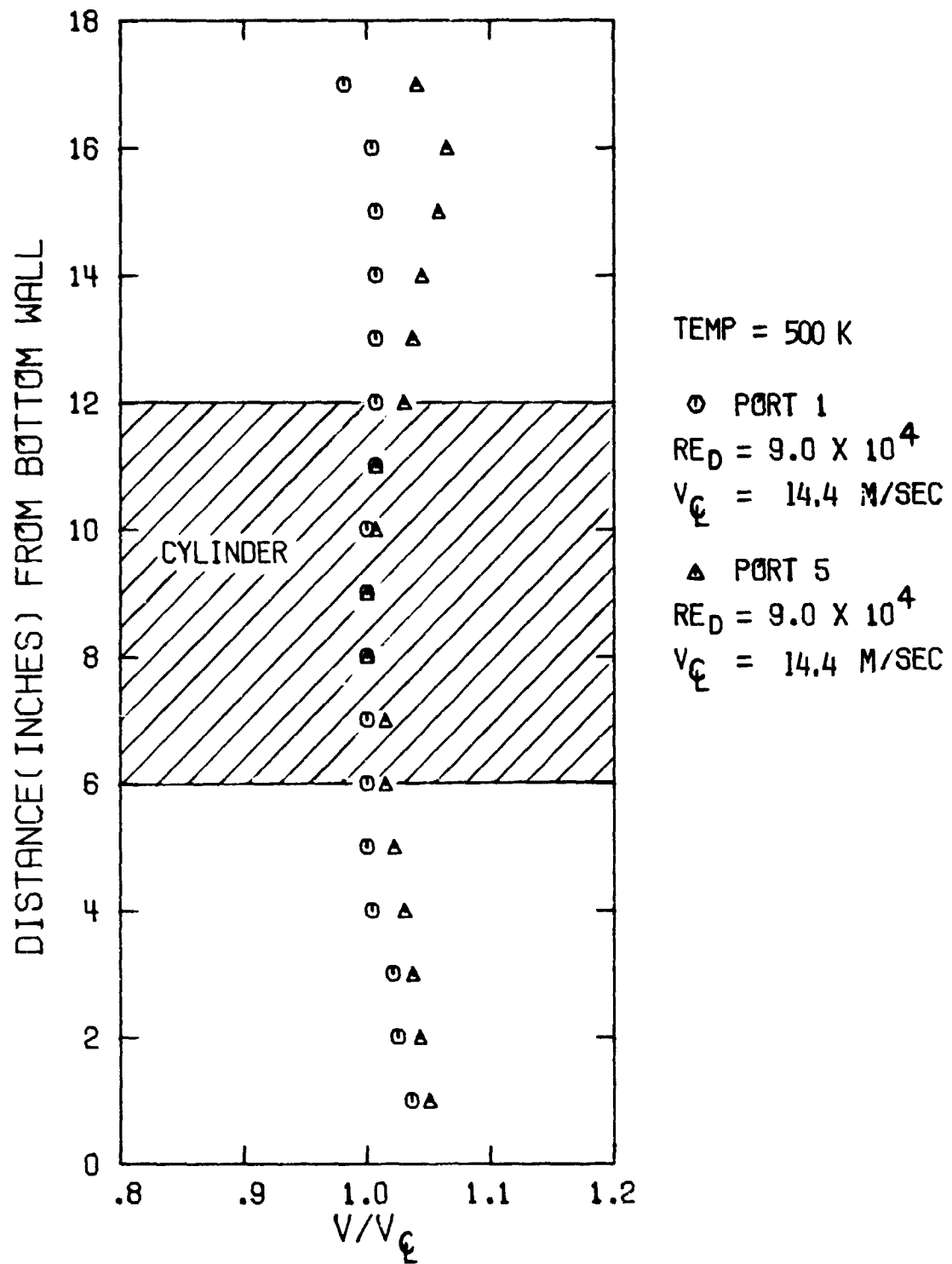


Figure 26. Vertical Freestream Velocity Profiles

ORIGINAL PAGE IS
 OF POOR QUALITY

TEMP = 500 K

○ PORT 2
 $RE_D = 9.0 \times 10^4$
 $V_{\infty} = 14.4 \text{ M/SEC}$

△ PORT 6
 $RE_D = 8.9 \times 10^4$
 $V_{\infty} = 14.2 \text{ M/SEC}$

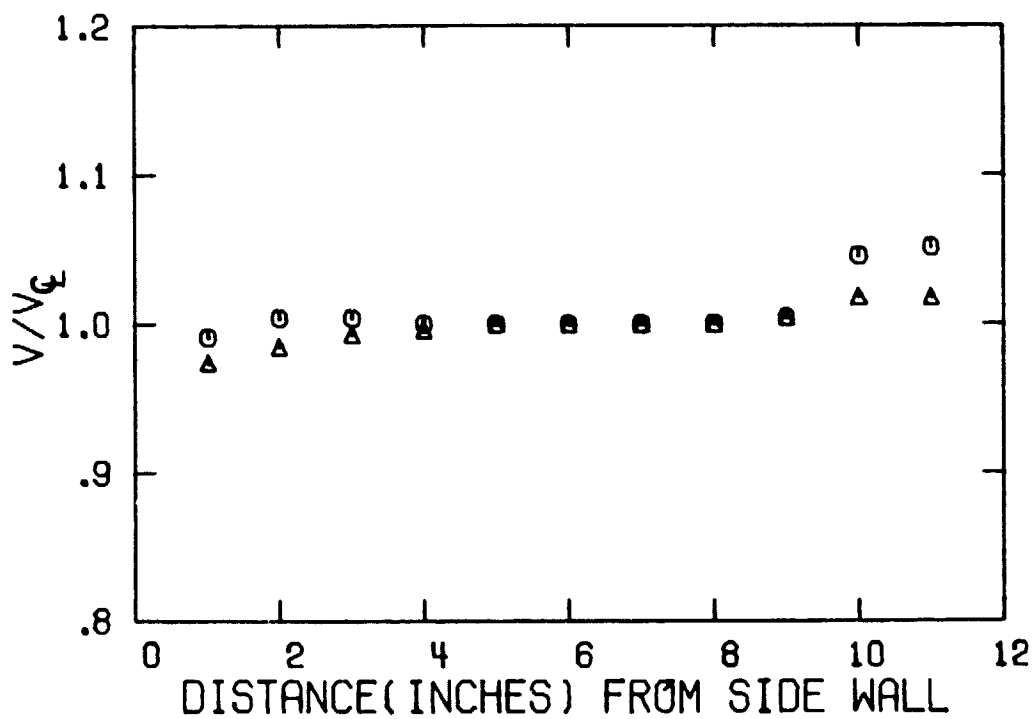


Figure 27. Horizontal Freestream Velocity Profiles

the tunnel, but never exceeded 6%. Within the cylinder frontal region, the variation was less than 3%. Therefore, the vertical velocity profile, particularly the region covered by the cylinder frontal area, was very uniform.

The horizontal velocity profiles in Figure 27 are presented as a function of the wind tunnel width. Referring back to Figure 15, Port 2 enabled a traverse along the centerline of the tunnel, while Port 6 is located halfway between Port 2 and the top of the wind tunnel. The profile at Port 2 was very flat in the center of the tunnel, and only as it approached the walls (within 2 in.) did any variation occur. However, this variation did not exceed 5%. Similar results were obtained for the horizontal profile from Port 6. A flat profile was measured in the center of the tunnel, with the variation not exceeding 2% as the side walls were approached. Figures 26 and 27 confirm that a uniform freestream velocity approached the test cylinder.

Figures 28 and 29, showing the vertical and horizontal non-dimensional freestream total temperature profiles are presented in the same format as the velocity profiles. The profiles from Ports 1 and 5, Figure 28, are in close agreement. Across the entire tunnel, the variation of temperature never exceeded 2%. Within the region covered by the frontal area of the cylinder, the variation was less than 1%. The data for horizontal traverses in Figure 29 also shows the profiles from Ports 2 and 6 in close agreement. Again, the variation of temperature across the entire tunnel never exceeded 2%. Figures 28 and 29 confirm that a uniform freestream total temperature approached the test cylinder.

To complete the documentation of the freestream flow conditions, the turbulence intensity, $T_u(\sqrt{u'}/\bar{u})$, was measured under cold flow conditions in the vertical plane (Port 1) with different types of screens inserted into the tunnel. Figure 30 presents profiles of turbulence intensity as a function of tunnel height with the frontal area of the cylinder represented by the shaded region. A wind tunnel Reynolds number per length, defined as $(\rho V/\mu)_{\infty,0}$ with properties evaluated at $T_{\infty,0}$, identical to the wind tunnel Reynolds number used in all of the experiments, was maintained at 1.2×10^5 per ft. for all

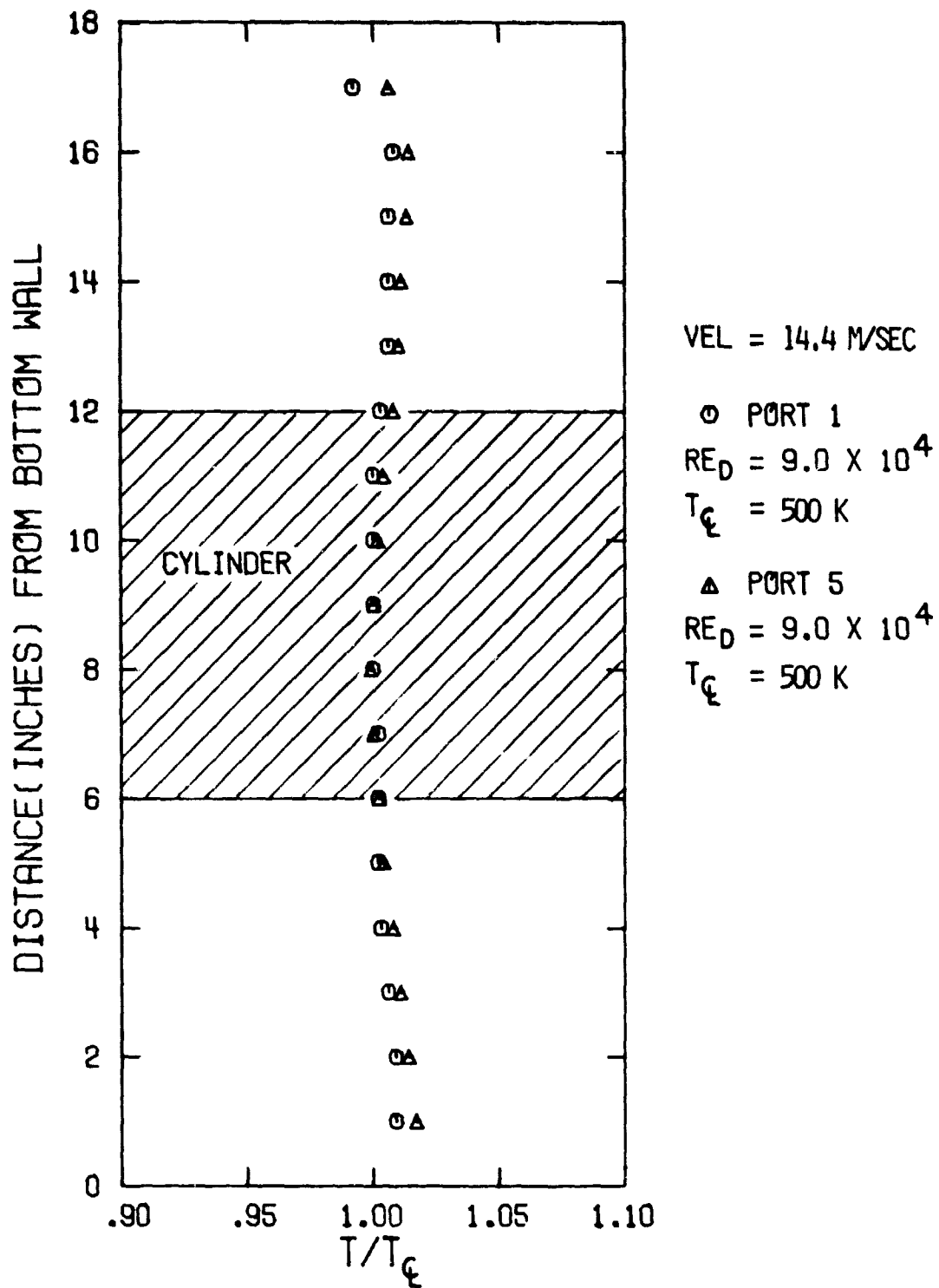


Figure 28. Vertical Freestream Temperature Profiles

VEL = 14.3 M/SEC

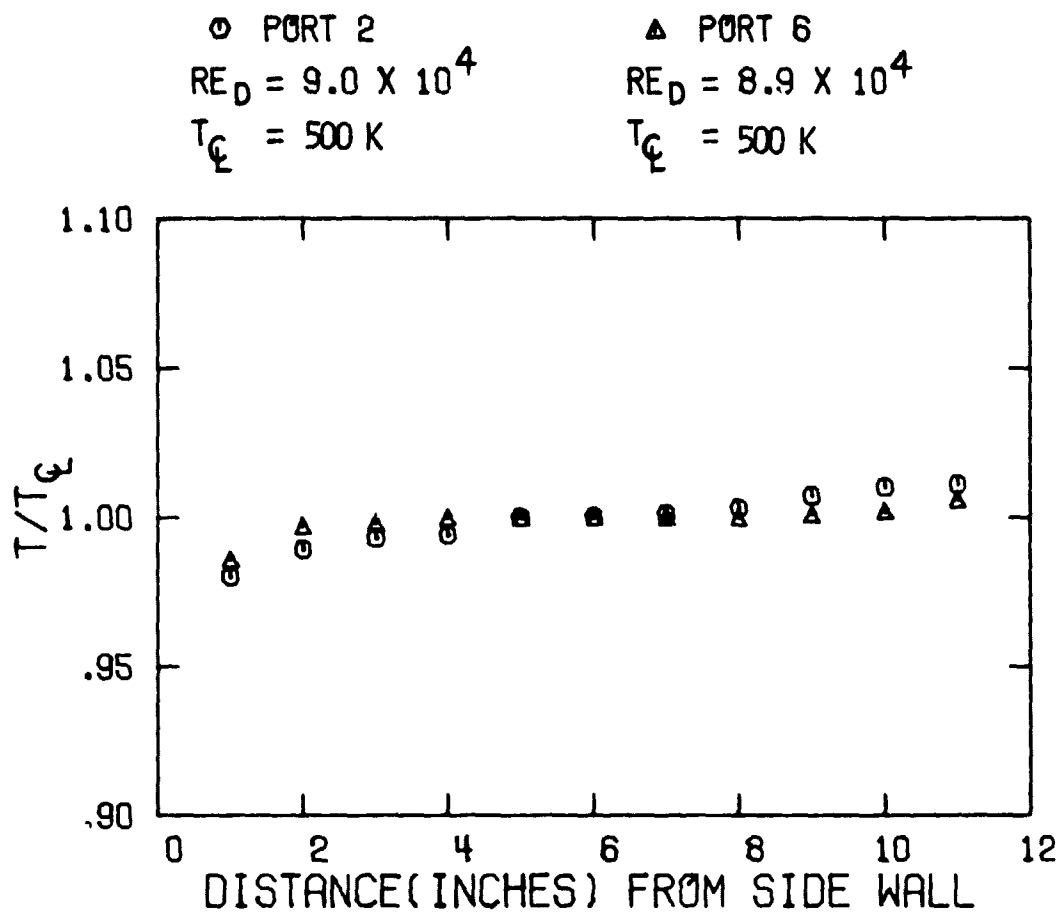


Figure 29. Horizontal Freestream Temperature Profiles

ORIGINAL PAGE IS
OF POOR QUALITY

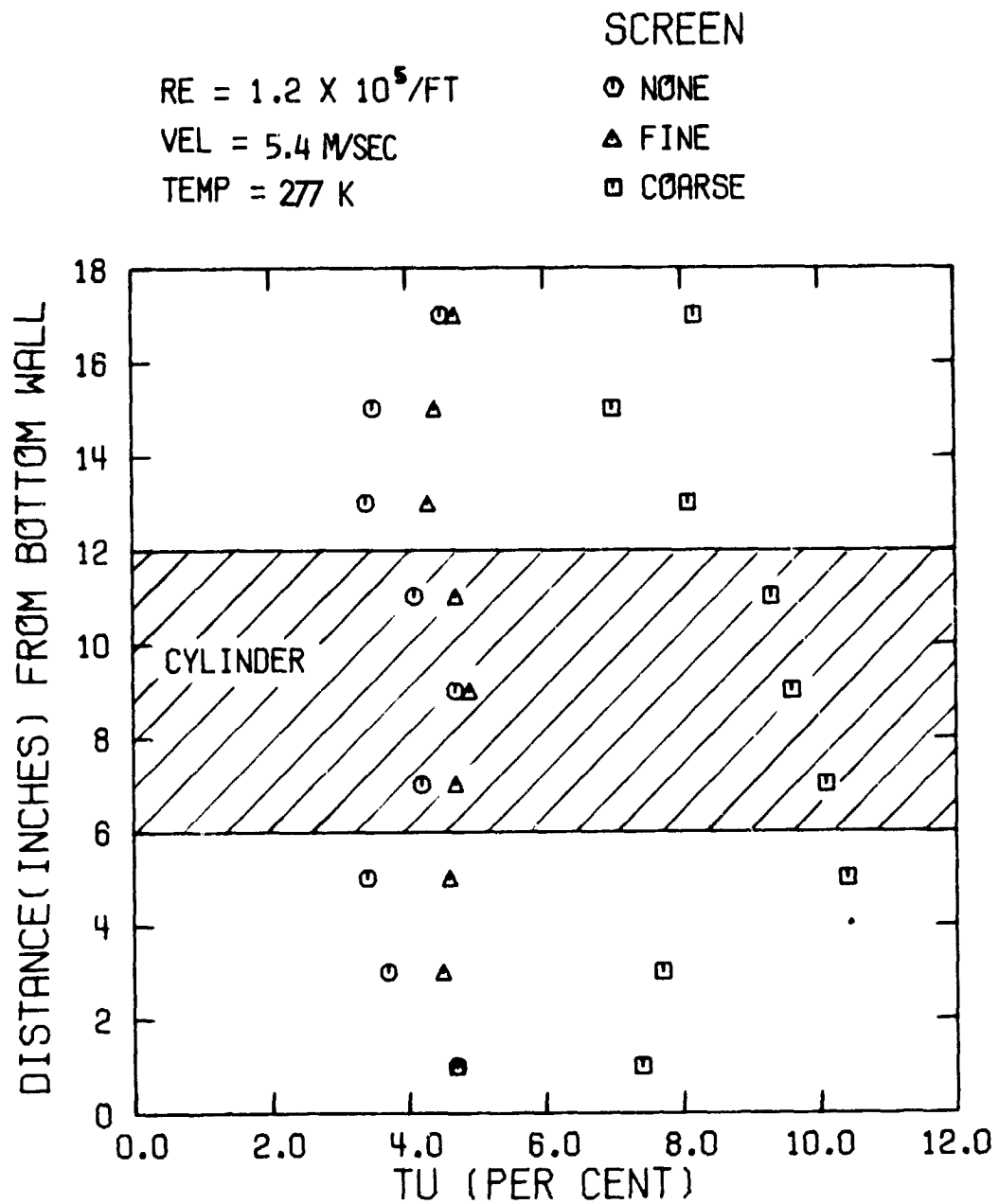


Figure 30. Vertical Turbulence Intensity Profiles

three profiles. With the open wind tunnel (no screen inserted), the hot wire measurements show a turbulence intensity of $4.4\% \pm 0.3\%$ within the region approaching the cylinder. Outside of this region, the intensity dropped to between 3.5 to 3.7%, but increased to $\sim 4.5\%$ as the top and bottom walls were approached.

Insertion of the screens into the tunnel was made 0.11 m upstream of the traversing hot wire. The fine screen, consisting of 1.60 mm diameter wire with a 4 x 4 mesh, was predicted to generate a turbulence intensity of 5.5%. The hot wire measurements within the region approaching the cylinder showed a turbulence intensity of $4.8\% \pm 0.1\%$. Outside of this region, the turbulence intensity decreased slightly (minimum value of 4.3%). Therefore, while the fine screen provided a slightly higher level of turbulence intensity compared to the open wind tunnel, the fine screen did generate a more uniform profile.

The coarse screen, consisting of 3.05 mm diameter wire with a 4 x 4 mesh, was predicted to generate a turbulence intensity of 11%. To produce this high level of turbulence, a coarse screen with a high area blockage ratio was used. While the profile for the coarse screen was more non-uniform, in the region covered by the frontal area of the cylinder the turbulence intensity was fairly uniform at $9.7\% \pm 0.4\%$. Although this value is slightly less than the predicted value of 11%, it still represents a substantial increase in the turbulence intensity over that measured with the open tunnel or with the fine screen inserted.

III.B. Cylinder Temperature Distribution

The fourteen internal coolant channels distributed around the cylinder surface and the use of a copper skin and copper segments resulted in a cylinder surface temperature that was approximately isothermal. Thermocouples, distributed along the cylinder surface, were used to measure the wall temperature around the circumference of the cylinder. Figure 24 shows the location (θ) of the wall thermocouples arranged in rows at selected angular positions relative to stagnation. In addition, four thermocouples were located in each drop-in segment to measure the segment wall temperature in the film cooled region.

For each experimental test, a nominal wall temperature, $T_{w,nom}$, was computed as the average of the temperature from the 47 wall thermocouples shown in Figure 24. For each row of thermocouples at a particular θ , the temperatures were averaged to obtain a local T_{avg} . Figure 31 shows the average wall temperature distribution, $(T_{avg} - T_{w,nom})/T_{w,nom}$, along the film cooled region of the cylinder for one representative experimental test. For this case, the variation of $T_{w,avg}$ from $T_{w,nom}$ did not exceed 1.9% (i.e. $10^\circ R$). For all experimental tests, the variation of $T_{w,avg}$ from $T_{w,nom}$ did not exceed 2.3% (i.e. $12^\circ R$). For the thermocouples in a row at a particular θ , the maximum-to-minimum variation in local temperature was typically 2 to 3 K and was never greater than 7 K. The four thermocouples in each segment were averaged to compute a segment temperature. As demonstrated in Figure 31, the segment temperatures were typically 6 - 7 K less than the $T_{w,nom}$ value. For all experimental tests, this difference was never greater than 9 K.

III.C Cylinder Pressure Distribution

The nature of the boundary layer development on the film cooled region of the cylinder was investigated by measurements of the pressure distribution around the cylinder using the solid segments (i.e. no film cooling holes). Before discussing the data from the present study, a short review of some previous cylinder drag and pressure distribution measurements is presented to help in understanding the relationship to the boundary layer development.

Numerous studies concerning the drag on a cylinder (which are summarized in Schlichting [35]) have shown that the drag coefficient, C_D , remains constant between a Reynolds number of 1×10^4 and 2×10^5 . However, between the Reynolds numbers of 2×10^5 and 5×10^5 , C_D drops rapidly, and the Re_D range where this rapid drop occurs is referred to as the critical range. Flow with Reynolds numbers less than the minimum value of the critical range are called subcritical, while flow with Re_D values in excess of the maximum value of the critical range are called supercritical.

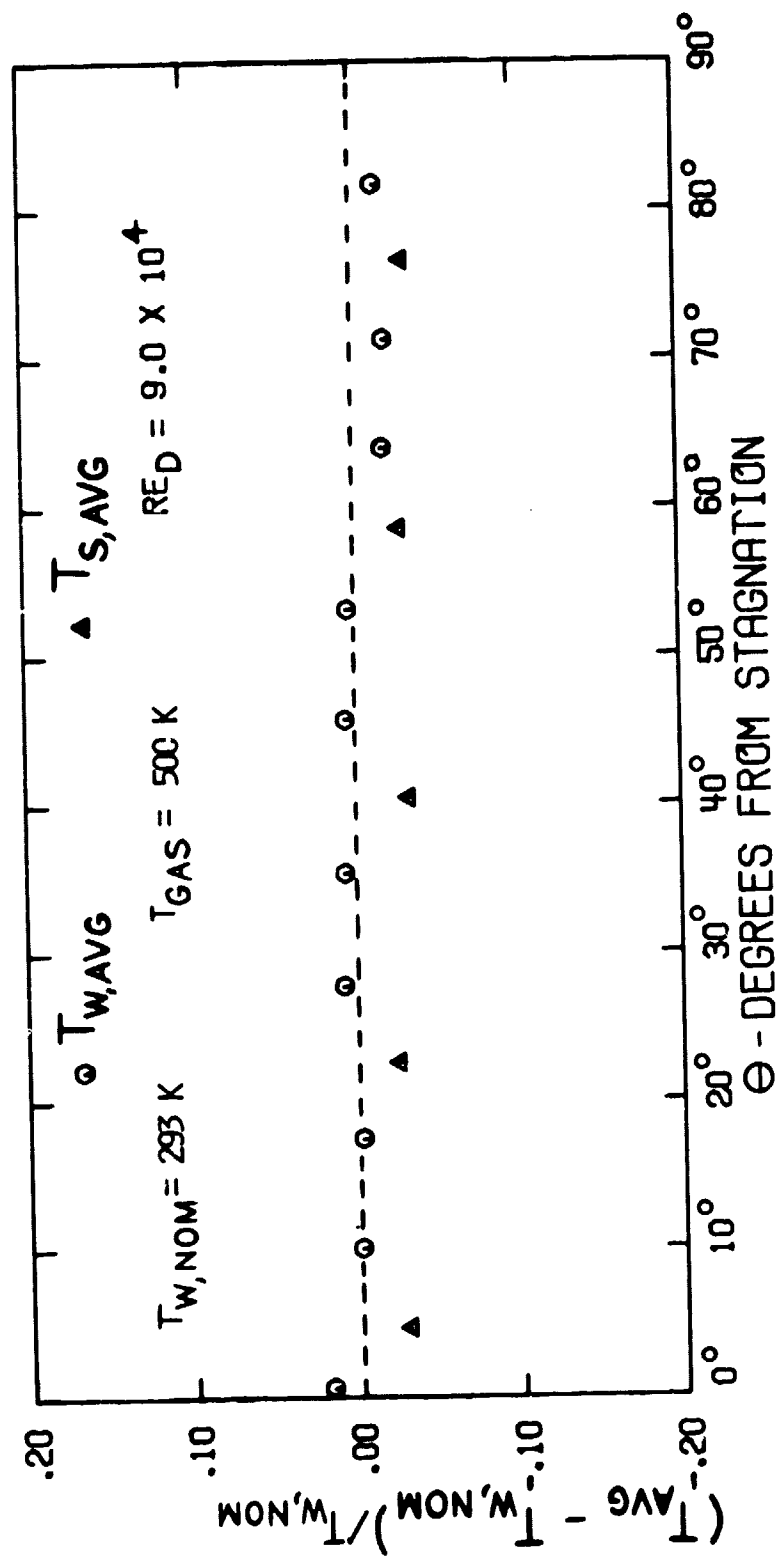


Figure 31. Cylinder Average Wall Temperature Distribution

This sharp decrease in drag is related to the boundary layer development on the cylinder. The favorable pressure gradient on the front portion of the cylinder aids in maintaining an attached boundary layer while the adverse pressure gradient characteristic of the rear portion promotes boundary layer separation. As with all blunt bodies, a laminar boundary layer develops from the front stagnation line on the cylinder.

For a subcritical Re_D , the laminar boundary layer develops until the adverse pressure gradient on the rear portion of the cylinder causes the boundary layer to separate about 80° from stagnation. This leaves the rear portion of the cylinder in a low pressure wake, causing a high form drag. When the Reynolds number is in the supercritical range, the developing laminar boundary layer transitions to a turbulent one before experiencing the influence of the adverse pressure gradient. The turbulent boundary layer subsequently remains attached further along the surface, and the point of separation moves downstream on the cylinder surface (beyond the 90° point) reducing the low pressure wake and resulting in a lower drag force. Consequently, it is the transition of the boundary layer from laminar to turbulent that results in the sharp decrease in drag when Re_D is in the critical range.

The critical Reynolds number range listed above (2×10^5 to 5×10^5) corresponds to a smooth cylinder in a wind tunnel with a low level of turbulence intensity ($\sim 0.5\%$). Both surface roughness and freestream turbulence will influence the critical Reynolds number range where the laminar to turbulent transition occurs. An increase in either the roughness or the turbulence will reduce the Reynolds number defining the critical range.

The cylinder pressure distribution from this investigation is presented in Figure 32, $C_p = (P_w - P_{\infty,0}) / (P_{T_\infty} - P_{\infty})_0$, along with the data of Achenbach [37]. Achenbach's data were obtained in a wind tunnel with a turbulence intensity of 0.7% and cylinder blockage-to-tunnel area ratio of 1:6. The pressure data for the present investigation were obtained in a wind tunnel with a turbulence intensity of $\sim 4.4\%$ and a cylinder blockage-to-tunnel area ratio of 1:3.

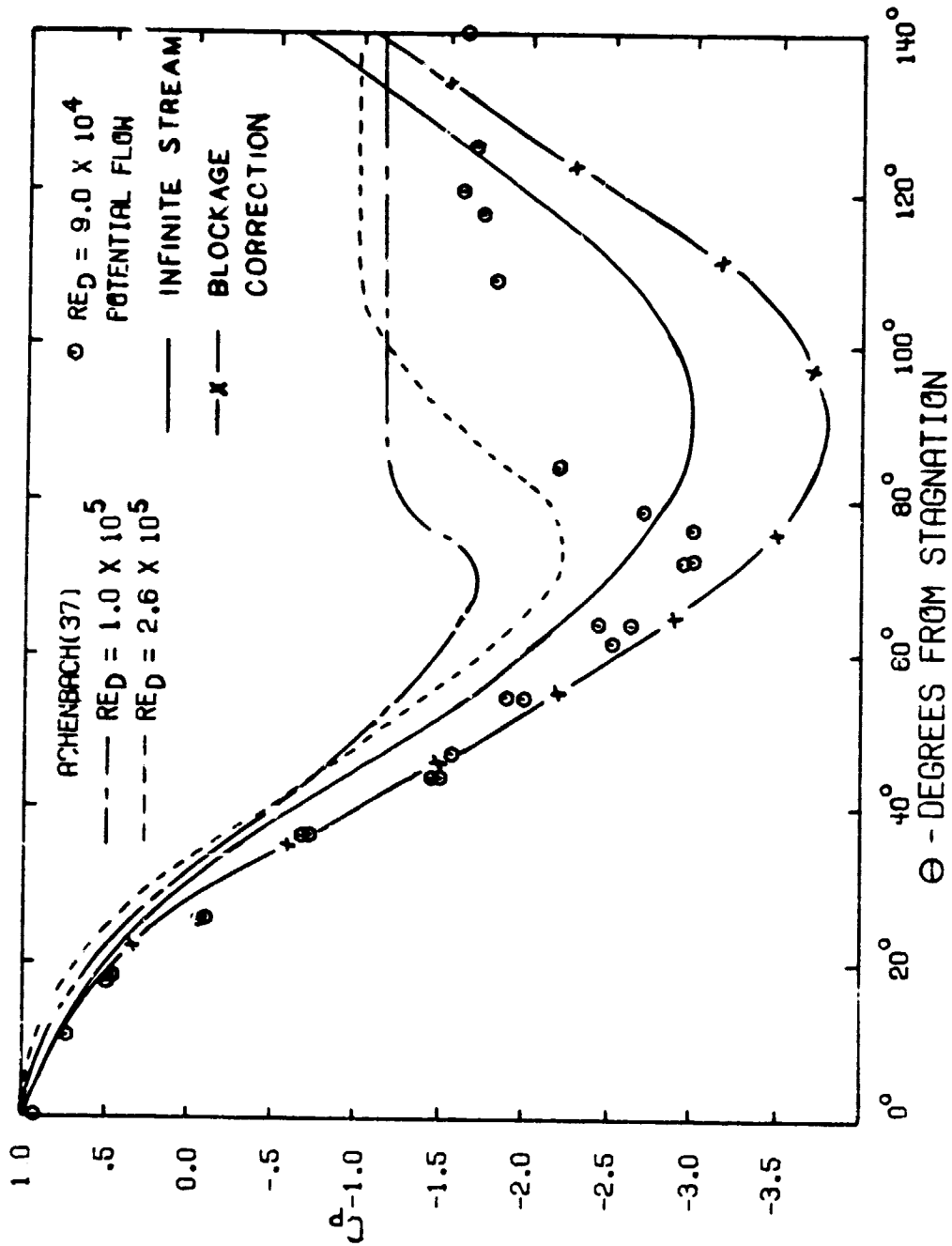


Figure 32. Cylinder Surface Pressure Distributions

The potential flow pressure distribution computed for incompressible flow over a cylinder is presented in Figure 32 for both an infinite freestream and a freestream within a wind tunnel. The potential flow solution for the infinite freestream was corrected to account for the cylinder-to-tunnel blockage ratio, 1:3, used in the present study. The results of Achenbach [37] are represented by the two dashed lines. The Achenbach data for $Re_D = 1.0 \times 10^5$ corresponds to subcritical flow. The C_p distribution is seen to decrease continually as θ increases from the stagnation line until a minimum C_p of -1.75 is reached at $\theta \approx 70^\circ$. With the laminar boundary layer separating at $\theta \approx 80^\circ$, the wake region behind the cylinder obtains a C_p value of -1.15. The Achenbach data for $Re_D = 2.6 \times 10^5$, represented by the dashed line, corresponds to flow approaching the critical range. The C_p distribution follows the trend established by the subcritical flow for the first 50° from stagnation. However, beyond $\theta = 50^\circ$, the C_p for $Re_D = 2.6 \times 10^5$ continues to decrease reaching a minimum ($C_{p,min} = -2.25$) at $\theta \approx 75^\circ$ with separation effects evident in the range of $\theta \approx 100^\circ$.

The Achenbach data for subcritical flow, $Re_D = 1.0 \times 10^5$, were chosen for comparison with the data from the present study obtained at $Re_D = 9 \times 10^4$. However, the data from the present study, shown in Figure 32, follow the trends established by the Achenbach data for $Re_D = 2.6 \times 10^5$. A minimum point ($C_p = -3.00$) was reached at $\theta \approx 75^\circ$ and the pressure rise to the constant value in the wake occurred in the range of $\theta \approx 100^\circ$. Although the trends are similar, the experimental data do not fall along the Achenbach curve for $Re_D = 2.6 \times 10^5$. The magnitude of the C_p minimum and the C_p value in the wake region are larger than those measured by Achenbach. This difference can be attributed to the larger cylinder blockage-to-tunnel area ratio used in this study, 1:3, as compared with the 1:6 ratio for the Achenbach study. As Figure 32 demonstrates, the experimental data for the first 60° from stagnation closely

follow the potential flow curve when it has been corrected for the cylinder-tunnel blockage effect. While the magnitudes of the C_p values may differ, the patterns established by the experimental data from this investigation and the Achenbach curve for $Re_D = 2.6 \times 10^5$ are the same (location of C_p minimum, location of boundary layer separation, etc.). Therefore, it was concluded that the boundary layer development on the test cylinder in the present investigation was typical of that observed for flow approaching the critical range. This flow behavior at $Re_D = 9 \times 10^4$ is attributed to the higher freestream turbulence intensity and the larger cylinder-to-tunnel blockage in the present study. The data for cylinder surface pressure distribution confirm the existence of an attached boundary layer on the front portion of the test cylinder covering the entire film cooled region.

Some wall pressure data also were obtained with the turbulence screens inserted in the wind tunnel. During these experiments, the solid segments in the cylinder were replaced by segments with film cooling holes with a spacing of $S/d_o = 5$. Figure 33 shows the data for the fine and coarse screens in addition to the open wind tunnel results previously shown in Figure 32. The data with the turbulence screens follows the trend previously established by the open tunnel data.

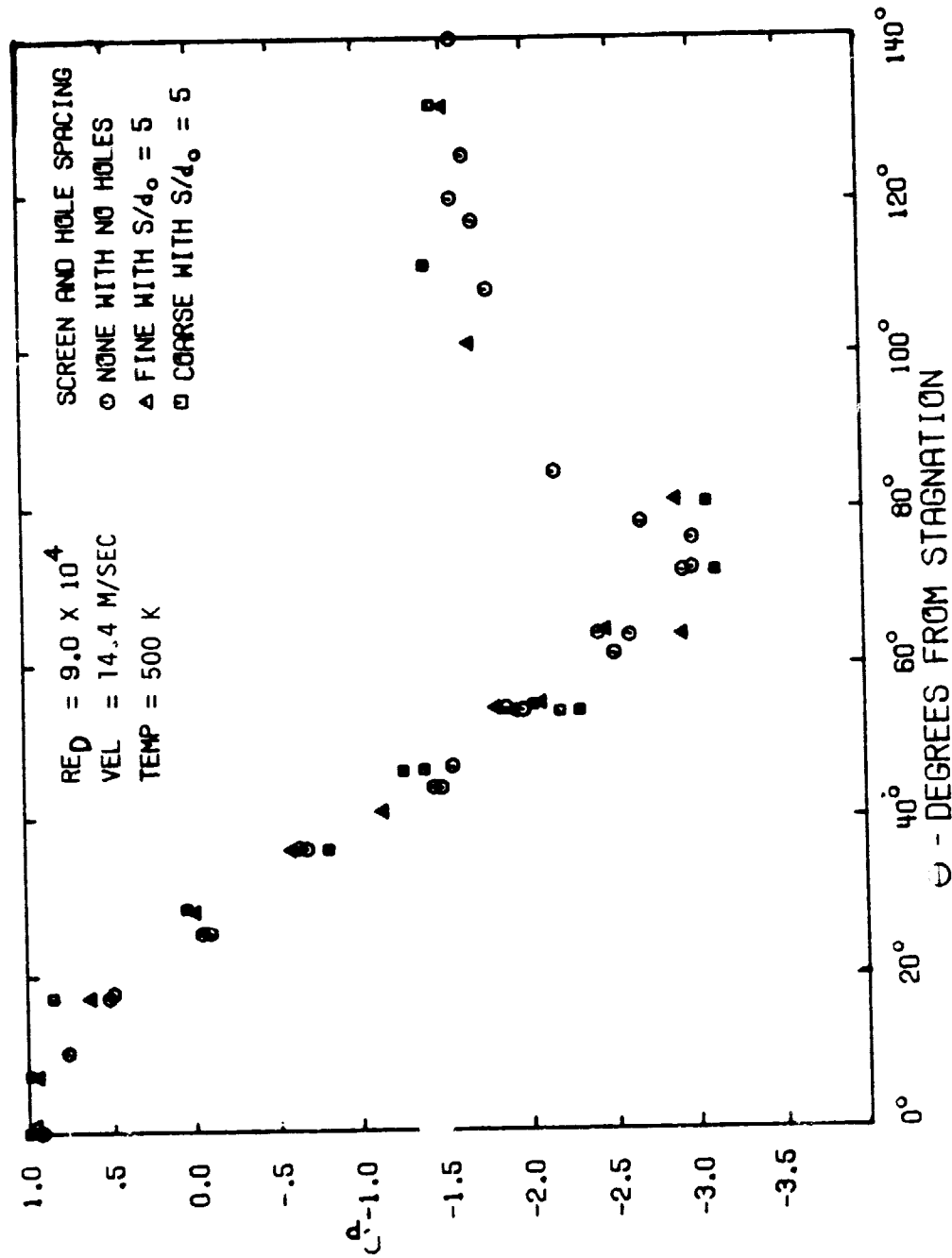


Figure 33. Cylinder Pressure Distribution for Different Freestream and Surface Conditions

III.D. Cylinder Heat Flux Distribution

The next phase of the preliminary investigation was a study of the heat transfer to the cylindrical test surface without film cooling; hereafter referred to as dry wall heat transfer. By changing the orientation of the cylinder, it was possible to position the heat flux gages at different locations relative to stagnation and thereby determine the dry wall heat transfer as a function of position relative to stagnation, θ . The objectives of this phase of the study were:

- 1) to establish a standard calibration curve for the heat flux gages to detect any deterioration in gage performance during the course of the investigation
- 2) to compare the data from this study with previous investigations of cylinder heat transfer
- 3) to determine the influence of freestream turbulence intensity on the dry wall transfer
- 4) to determine the influence of surface roughness on the heat transfer due to the fit of the drop-in segments in the cylinder and the film coolant holes drilled in the segments.

In general, the heat transfer distribution around a cylinder is correlated with the Nusselt and Reynolds numbers, and the results are commonly presented in the form of $Nu_D/\sqrt{Re_D}$ as a function of the angular position on the cylinder, θ . The Reynolds number defined earlier in this study, which is commonly used in the gas turbine industry, was based on the density and viscosity being evaluated at a mean temperature, $T_m = (T_\infty + T_w)/2$. However, past investigators of dry wall heat transfer around a cylinder have correlated their results using a Reynolds number based on the freestream density with the viscosity in the Reynolds number and the conductivity in the Nusselt number evaluated at the mean temperature. In the discussion of the dry wall heat transfer results from this investigation, a Reynolds number based on the freestream density, Re_D^* , is employed. For the present investigation, with $Re_D = 9 \times 10^4$, the Reynolds number used to present the dry wall results is $Re_D^* = 7.1 \times 10^4$. The use of this alternate definition of Reynolds number, Re_D^* , is limited to the discussion of the dry wall heat transfer.

Previous investigations have measured the local heat transfer on cylindrical test surfaces. Figure 34 presents the results from five different studies at Reynolds numbers close to the value $Re_D^* = 7.1 \times 10^4$ characterizing the present investigation. The heat transfer data of Seban [38], Giedt [39], and Zapp [40] were all obtained in wind tunnels with a freestream turbulence intensity of approximately 1%. The study by Achenbach [41] had a freestream turbulence intensity of 0.45% and the mass transfer study by Kestin and Wood [42] had a freestream turbulence intensity of 0.2%. The mass transfer results of Kestin and Wood [42] were converted using the heat-mass transfer analogy where

$$\frac{Nu_D}{\sqrt{Re_D^*}} = \frac{Sh}{\sqrt{Re_D^*}} \left(\frac{Pr}{Sc} \right)^{1/3} \quad (22)$$

$$Sh = \frac{bD}{D}, \text{ Sherwood number}$$

$$Sc = \frac{\nu}{D}, \text{ Schmidt number}$$

b = mass transfer coefficient

D = coefficient of binary diffusion

The results from all five investigations are in good agreement at the stagnation line on the cylinder where the $Nu_D/\sqrt{Re_D^*}$ ratio is approximately 1.0. The data of Seban are somewhat higher for $\theta \geq 50^\circ$. The results represent the trend of $Nu_D/\sqrt{Re_D^*}$ versus θ characteristic of the development of a laminar boundary layer along the front portion of the cylinder.

The heat flux levels on the test cylinder of the present investigation were measured with heat flux gages (see Section II.B.3) permitting local heat transfer measurements on the cylindrical surface. Experiments were conducted to verify the manufacturer's gage calibration as follows. The cylinder was tested in the wind tunnel with a nominal Reynolds number (Re_D^*) of 7.1×10^4 , a nominal freestream gas temperature of $900^\circ R$ and a nominal wall temperature of $530^\circ R$, to

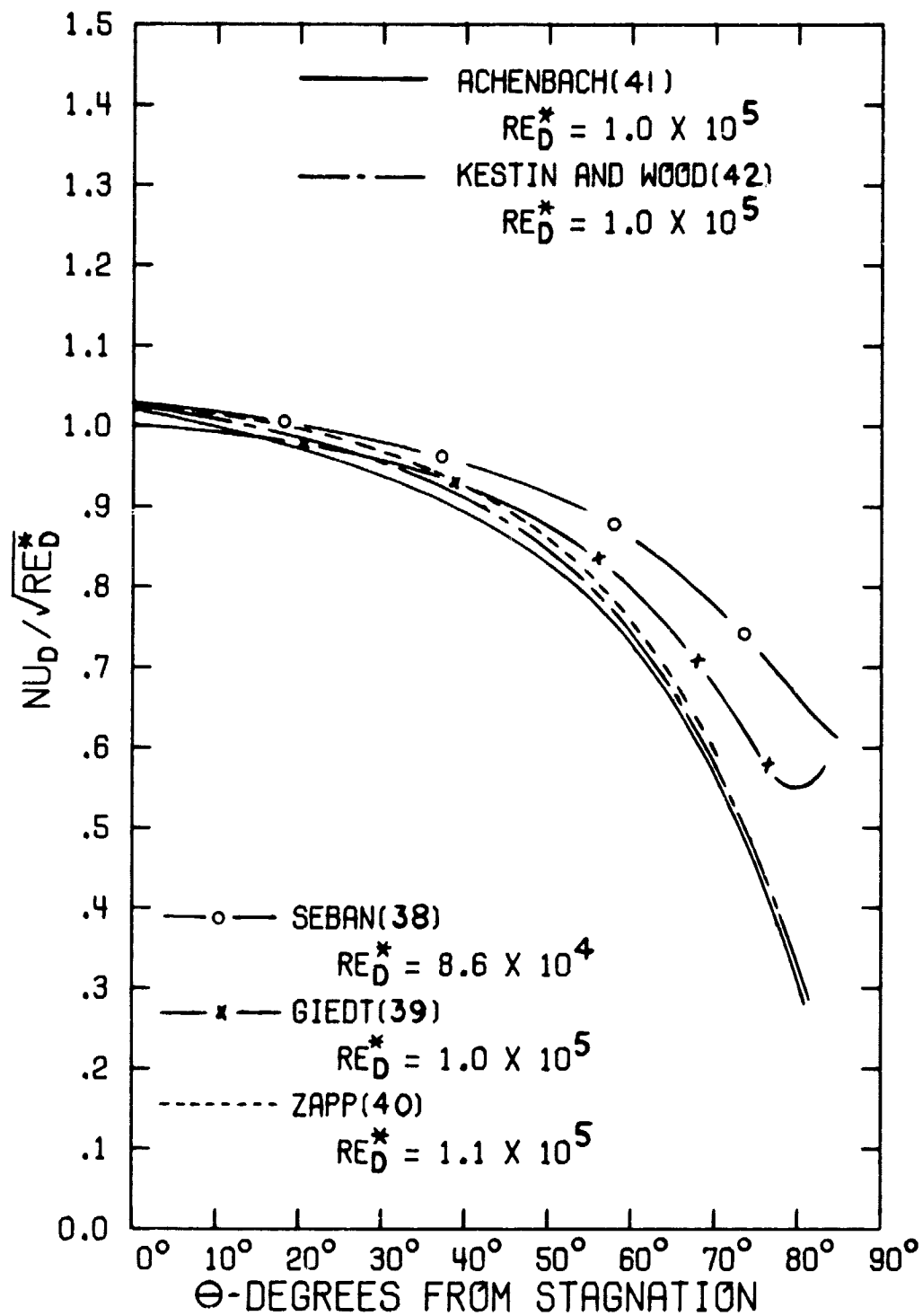


Figure 34. Heat Flux Distribution Around a Circular Cylinder

measure the heat transfer rate indicated by each gage when it was positioned at the stagnation line. The gages were installed in the test cylinder with three or four gages located in a row (spanwise direction) with a total of nine rows of gages covering the film cooled region of the cylinder. A series of experiments were conducted with each row positioned at the stagnation line, and Figure 35 shows the results obtained. The position of the gage in a row is indicated by the different data symbols. (Refer back to Section II.B.3. for a more detailed description of the heat flux gage locations on the cylinder surface.)

Figure 35 shows that the results for row nine have a calibration error and, therefore, those results were deleted from the following discussion of gage calibration standardization. The results for the gages in rows 1 through 8 show that 80% of them yield data in a bandwidth of $\pm 12.5\%$ around the value $Nu_D/\sqrt{Re_D^*} = 1.2$. The cause of this data scatter is attributed to several sources. First, while the Reynolds number (Re_D^*), freestream gas temperature, and wall temperature were maintained constant for each experimental run, the reproducibility of the results for a particular gage was determined to be $\pm 6\%$. Second, possible errors in the manufacturer's calibration for some of the gages could have contributed to increased data scatter. Finally, the heat flux gages made local measurements of the heat flux to the surface. Although all the gages in a row were at the stagnation line simultaneously, any local variations in the external flow or the cylinder surface conditions in the spanwise direction would lead to different heat flux levels along the row of gages. It is expected that a combination of these three factors contributed to the data scatter seen in Figure 35.

A least squares fit of the data in Figure 35 (excluding row nine) was conducted first of the data inside the $\pm 12.5\%$ data band and second of all the data points. The least squares value for both cases gave a stagnation line value of $Nu_D/\sqrt{Re_D^*} = 1.25$. To standardize the output for all heat flux gages, the calibration factor for each gage was adjusted so that each gage indicated a stagnation line value of

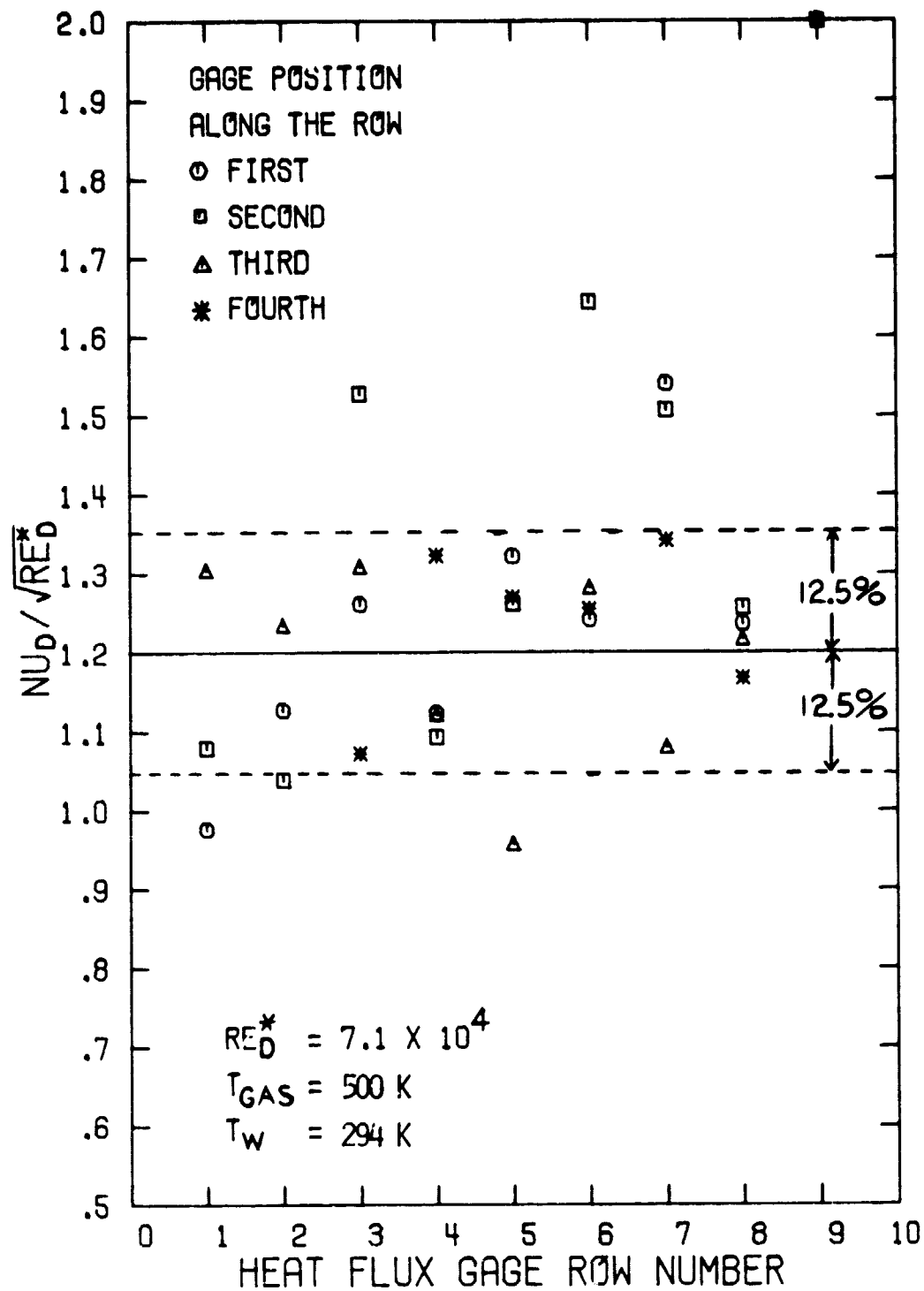


Figure 35. Dry Wall Stagnation Line Heat Flux Calibration

ORIGINAL PAGE IS
OF POOR QUALITY

$Nu_D/\sqrt{Re_D^*} = 1.25$. The adjusted heat flux gage calibration was used in all subsequent results in the present investigation.

Repositioning the cylinder on subsequent experiments allowed each row of gages to be placed on the stagnation line. While one row of gages was at stagnation, the other eight rows were at various θ locations around the cylinder. This provided data for $Nu_D/\sqrt{Re_D^*}$ as a function of angular distance from stagnation, θ , as shown in Figure 36. A least squares fit of the data yielded

$$\frac{Nu_D}{\sqrt{Re_D^*}} = 1.22 - (3.26 \times 10^{-3})\theta + (8.48 \times 10^{-5})\theta^2 - (1.54 \times 10^{-6})\theta^3 \quad (23)$$

with data bandwidth of $\pm 7\%$ of the stagnation value. The heat flux distribution shown in Figure 36 provided a standard against which the indication from each heat flux gage was checked to monitor any deterioration in the performance of the gages.

Figure 37 shows the least squares fit of the dry wall heat transfer from the present study compared to the results from previous investigations. The freestream turbulence intensity in the present study was $4.4\% \pm 0.3\%$. This is considerably above the levels ($Tu \leq 1\%$) used in the previous investigations for the data shown in Figure 34. The Reynolds number values for the previous investigations were selected to match as closely as possible the value (7.1×10^4) of the present investigation. Consequently the results shown in Figure 37 from previous investigations are those corresponding to elevated levels of turbulence intensity as shown on the figure¹. The results from the present investigation are in reasonable agreement with similar data obtained by previous investigations.

The stagnation values for $Nu_D/\sqrt{Re_D^*}$ in Figure 37, 1.22 to 1.32, are considerably larger than the value of 1.0 observed in Figure 34.

¹ The freestream turbulence intensity for Seban [38] was estimated from the screen grid size reported.

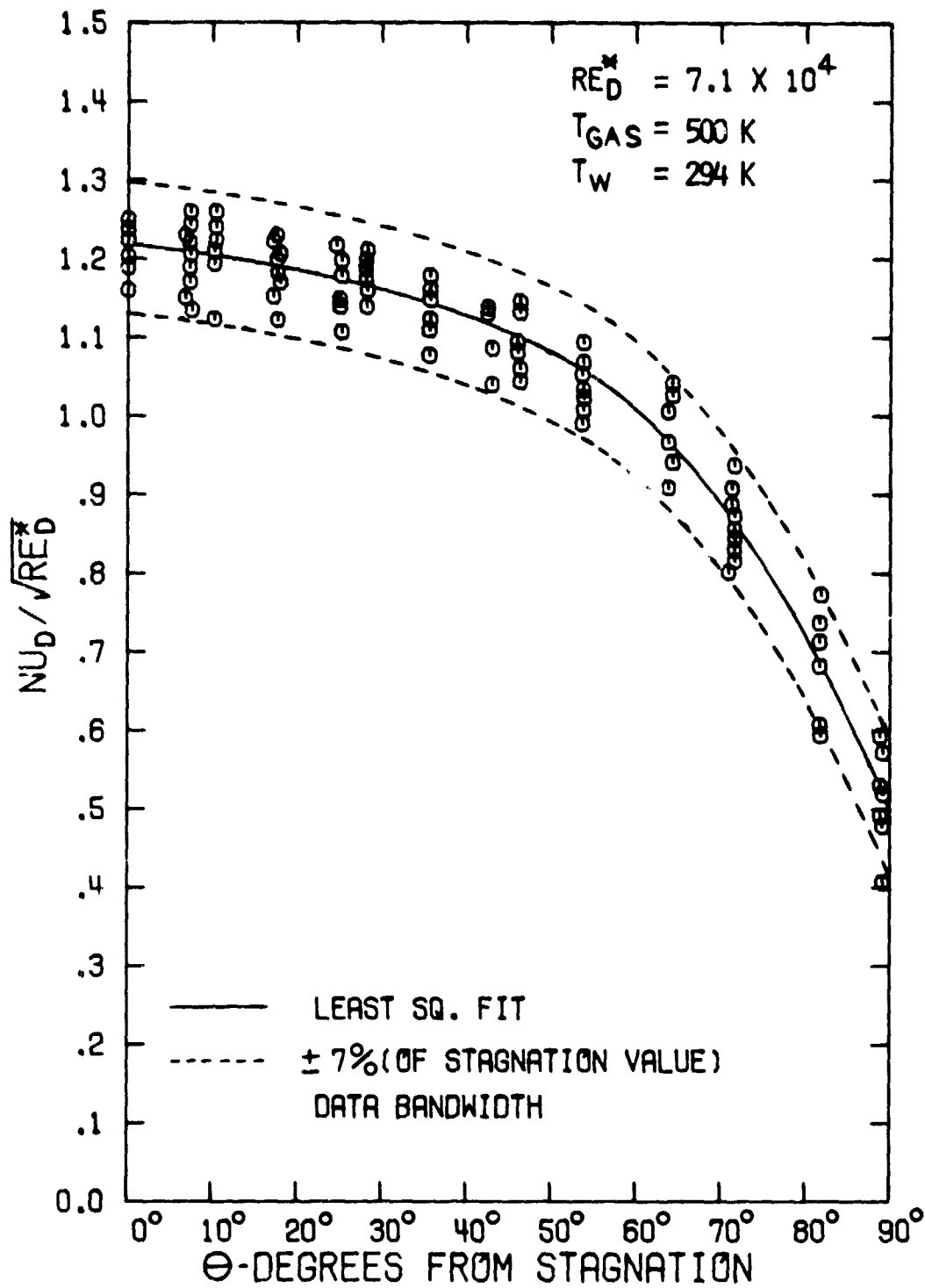


Figure 36. Heat Flux Distribution Around the Test Cylinder

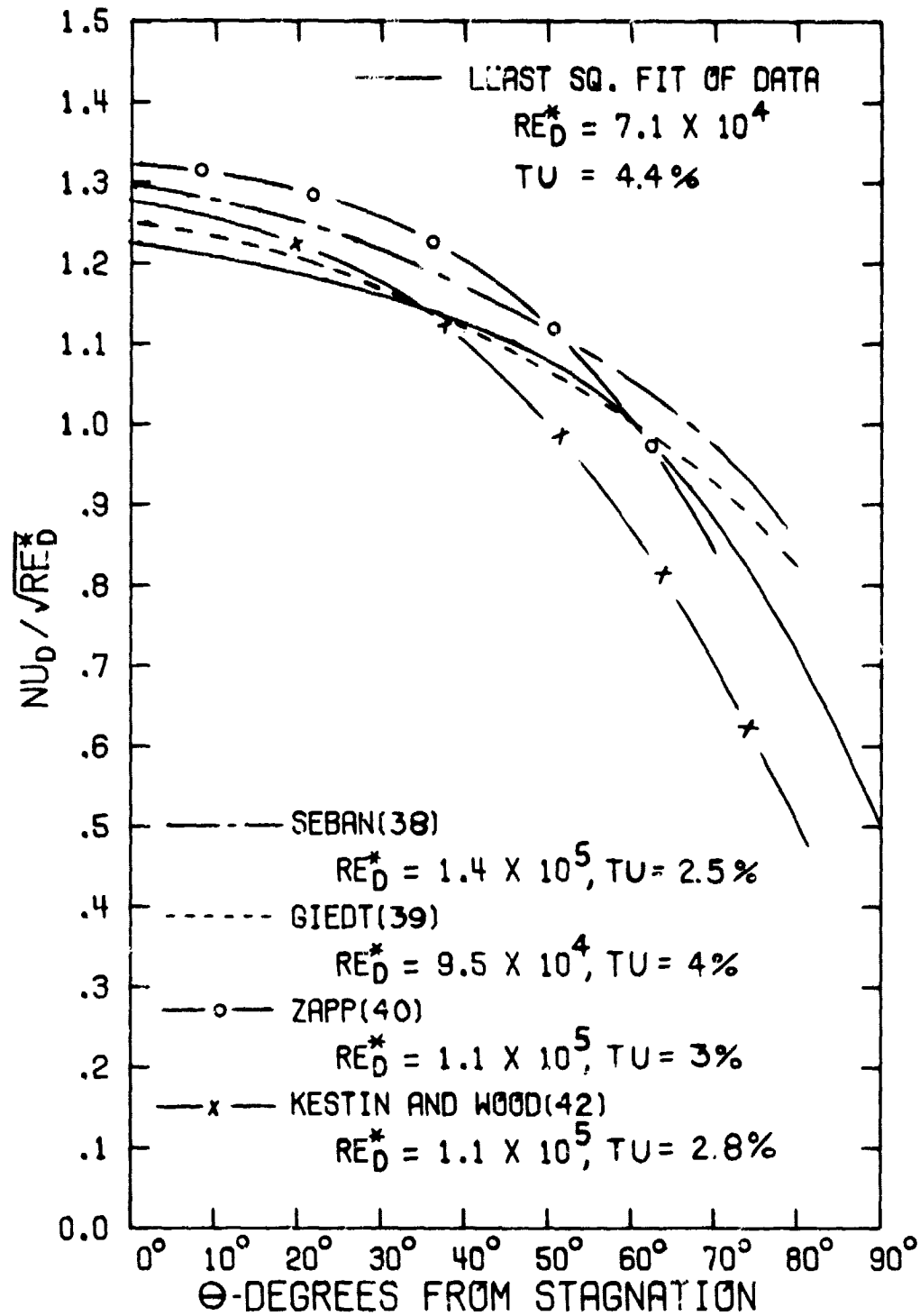


Figure 37. Test Cylinder Heat Flux Distribution Compared with Other Cylinder Studies

Obviously, the freestream turbulence intensity has an effect on the dry wall heat transfer. In the present investigation, turbulence screen was inserted into the wind tunnel to study the influence of freestream turbulence intensity on the film cooling performance. This also allowed the dry wall heat transfer rates to be measured at higher levels of freestream turbulence intensity. The freestream turbulence intensity for the fine screen was found to be $4.8\% \pm 0.1\%$, while the coarse screen gas an intensity of $9.7\% \pm 0.4$ (Section III.A.) The dry wall heat transfer results with and without the turbulence screens are shown in Figure 38. The solid line represents the least squares fit (equation 23) for the data with no screen. The results clearly show an increase in the heat transfer as the freestream turbulence intensity increased. For the first 40° from stagnation, the fine screen produced a 5 to 7% increase in the heat transfer rate, while the coarse screen produced a 15 to 18% increase in the heat transfer rate. Beyond 40° , the increase in heat transfer was smaller.

Another consideration governing the boundary layer development along the front portion of the cylinder is the surface roughness. The test cylinder was designed to use drop-in segments (for coolant holes) and this created a surface roughness when the segments were not flush with the cylinder surface. To determine the size of the roughness produced by the use of the drop-in segments, a dial indicator was passed over the cylinder surface each time a new set of segments was installed in the cylinder. Appendix II gives a description of the procedure used to determine the roughness height, K , and figures showing all the measurements made. With the solid segments installed (no coolant holes), the largest roughness anywhere along the cylinder was, $K/D = 5.0 \times 10^{-4}$, where D is the cylinder diameter. When the segments with a hole spacing of $10 d_o$ were installed, the largest roughness, $K/D = 11.7 \times 10^{-4}$, was located near the end of the cylinder (within 25.4mm of the tunnel wall). Excluding this location within 25.4mm from either side wall, the largest roughness in the central region instrumented for heat flux measurements was $K/D = 6.7 \times 10^{-4}$. Finally, when the segments with a hole spacing of $5 d_o$ were installed into the cylinder, the largest roughness of $K/D = 13.3 \times 10^{-4}$ was

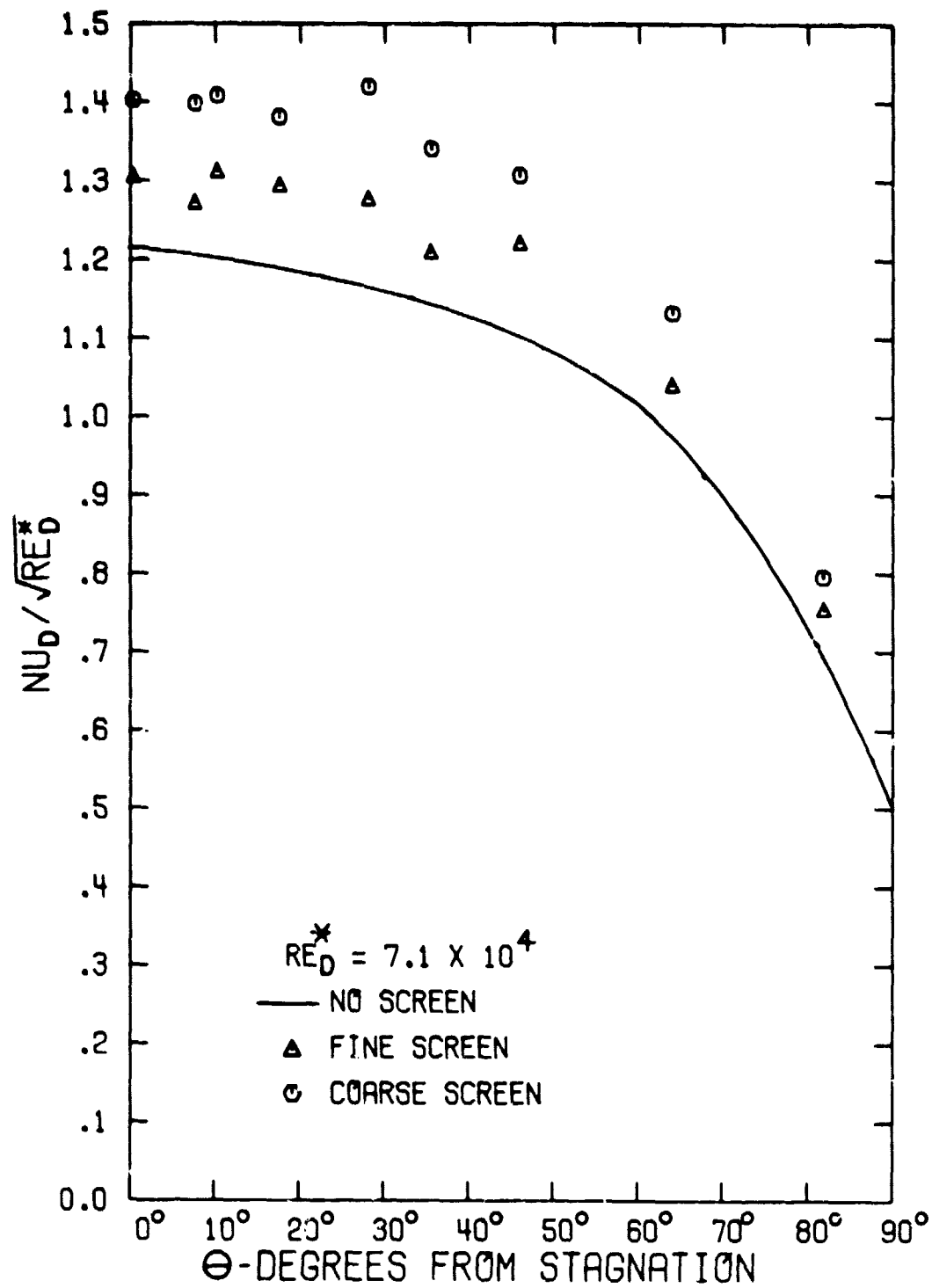


Figure 38. The Influence of Freestream Turbulence Intensity on the Dry Wall Heat Transfer

again located within 1 in. of the tunnel side wall. Excluding this location within 1 in. from either side wall, the largest roughness was $K/D = 8.3 \times 10^{-4}$. Therefore, in the central portion of the cylinder instrumented for the heat flux measurements, the maximum surface roughness due to the drop-in segments varied from 5.0 to 8.3×10^{-4} for the three segment configurations used.

Achenbach [43] has conducted extensive studies on the influence of surface roughness on heat transfer around a cylinder. The cylinders investigated by Achenbach had emery paper attached so that the roughness elements covered the entire cylinder surface. Pressure and heat flux measurements, taken with a Reynolds number, Re_D^* , of 8.3×10^4 and a sand grain roughness of $K_s/D = 7.5 \times 10^{-4}$, showed subcritical flow and no influence of the roughness elements on the flow around the cylinder. Even for a sand grain roughness of 30×10^{-4} , the pressure and heat flux measurements for $Re_D^* = 6.3 \times 10^{-4}$ showed similar results. Consequently the roughness of 5 to 8.3×10^{-4} found on the cylinder for the present investigation was not expected to influence the cylinder heat transfer. Indeed, the dry wall heat transfer results shown in Figure 36 revealed no discontinuities indicative of the influence of local surface roughness on the heat transfer.

An additional surface roughness effect is introduced by the presence of film coolant holes drilled in the segments. To determine the influence of the coolant holes, a comparison was made of the heat transfer measurements with solid segments (i.e. no film coolant holes) and those with segments containing drilled film coolant holes. The comparison revealed no effect of the holes on the surface heat transfer with the exception of gages located directly behind the hole. The heat flux gage located directly behind a coolant hole ($x/d_o = 1.5$ only) registered approximately a 5% increase in the heat transfer rate. Further downstream of the holes or anywhere between the holes, the effect of the drilled coolant holes was negligible.

As a result of the preliminary experiments reported in this section, it was concluded that the surface pressure and dry wall heat flux measurements established the development of an attached boundary layer over the front portion of the test cylinder, i.e. the film cooled

C-2

region. The dry wall heat transfer was found to increase as the free-stream turbulence intensity increased, particularly in the region close to the stagnation line. The influence of drop-in segments or coolant hole roughness was found to be negligible. The next chapter presents a discussion of the results for film cooling with injection from a single row of holes.

IV. SINGLE ROW COOLANT INJECTION

IV.A Introduction

The film cooling experiments were divided into three phases: (a) single row injection, (b) multiple row injection with a uniform blowing distribution, and (c) multiple row injection with a blowing distribution simulating a plenum supply. While the primary purpose of this investigation was to study multiple row film cooling typical of the leading edge of a turbine vane, it was concluded that an investigation of the film cooling performance with injection from a single row would be helpful in understanding the performance for multiple row injection. Experiments were conducted with blowing from a single row of holes with the row located at each of the positions (θ_i) occupied by the film coolant rows in the multiple row configurations. This procedure allowed the film cooling performance in the region of one particular row of a multiple row configuration to be compared with the results for single row injection to determine the effect of row-to-row interaction between the film coolant jets. Also, the investigation of single row injection permitted a study of the influence of injection location on film cooling performance without the additional effects of film cooling from other rows of holes. This chapter presents the results from the study of single row injection, while the results from multiple row injection with a uniform blowing distribution and with a blowing distribution simulating a plenum supply are presented in the following chapters. The experiments for injection from a single row of holes were conducted with the row positioned at the following four locations from stagnation: 5° , 22.9° , 40.8° and 58.7° (see Figure 24). These locations correspond to the angular positions of the first four rows of coolant holes in the multiple row studies. No data were obtained for single row injection from a row located at 76.6° .

The experiments for single row injection were conducted with blowing from the first row of holes in the test cylinder. By changing the angular orientation of the cylinder, the first row of holes was positioned at 5°, 22.9°, 40.8°, and 58.7°. This technique was employed to obtain the maximum amount of heat flux instrumentation downstream of the blowing row. For the injection locations of 22.9°, 40.8°, and 58.7°, the cylinder surface upstream from the blowing row was smooth (i.e. without rows of holes) contrary to the multiple row configurations. The absence of upstream, non-blowing rows of holes had no effect on the results for single row injection. The results for dry-wall heat transfer discussed in Chapter III showed that the influence of a non-blowing hole was negligible beyond $1.5 d_o$ downstream from the hole.

Reference to Figure 24 shows the use of a subscript i to identify: (a) the row location, θ_i , $i = 1, 2, 3, 4, 5$, (b) the distance downstream from a specific row, $(x/d_o)_i$, $i = 1, 2, 3, 4, 5$, and (c) the local blowing ratio, M_i , $i = 1, 2, 3, 4$, for a specific row. At each row location, θ_i , the blowing ratio, M_i , was varied over the same range as that encountered in the multiple row configurations. Two different hole-to-hole spacing ratios, $S/d_o = 5$ and 10, were investigated for the single row of spanwise angled holes, $\beta = 25^\circ$.

The film cooling results are presented in terms of the Stanton Number Reduction defined as

$$\text{Stanton Number Reduction (SNR)} \equiv 1 - \frac{St_{FC}}{St_o} \quad (24)$$

The Stanton number ratio (St_{FC}/St_o) is equal to the heat transfer coefficient ratio (h_{FC}/h_o), as was discussed previously in Section II.B. The SNR value represents the percentage reduction in the Stanton number or heat transfer coefficient due to film cooling.

A complete listing of all SNR data for injection from a single row of holes is presented in tabular and graphical form in Appendix III for all of the parameters studied. A limited sample of the film cooling results are presented and discussed in this chapter to illustrate the important trends observed and the conclusions drawn.

IV.B. Presentation of Single Row Data

The data to be presented are divided into four sections, one section for each of the four row locations, θ_1 , studied. Within each section, the influence of hole spacing, S/d_0 , blowing ratio, M_1 , streamwise location $(x/d_0)_1$ and spanwise location (z/S) is examined.

IV.B.1. Spanwise Injection at $\theta_1 = 5^\circ$

Figures 39 and 40 present the film cooling performance for single row injection at $\theta_1 = 5^\circ$ showing the values of SNR at $(x/d_0)_1 = 1.5$ downstream from row 1. The results in Figures 39 and 40 are plotted with the Stanton Number Reduction (SNR) as a function of spanwise location, z/S , for hole-to-hole spacing ratios, $S/d_0 = 5$ and 10, respectively.¹ The legend in each figure shows the data symbols used to represent each blowing ratio.

One of the most significant features of the performance is the highly localized affect of the film coolant on the surface. The influence of the coolant was restricted to a narrow region, leaving a significant portion between the coolant holes unaffected, particularly for the larger hole spacing of $S/d_0 = 10$. At low values of the blowing ratio ($M_1 \leq 1.0$), the coolant injected in the spanwise direction was turned quickly by the freestream to the streamwise direction, and the maximum cooling effect was observed directly behind the hole. Comparing the results for the two hole spacings, the SNR magnitude behind the hole is found to be considerably larger for the $S/d_0 = 10$ spacing.

As the blowing ratio was increased, the location of the point with maximum SNR shifted in the spanwise direction (direction of coolant injection) for both hole spacings. With this trajectory of the coolant jet, negative values of SNR were observed directly behind the hole for $M_1 > 2.0$. Continued increase in the blowing ratio resulted in higher negative values of SNR behind the hole. At the same

¹ Due to periodicity, the value of SNR at $z/S = 1.0$ was assumed equal to the value at $z/S = 0$.

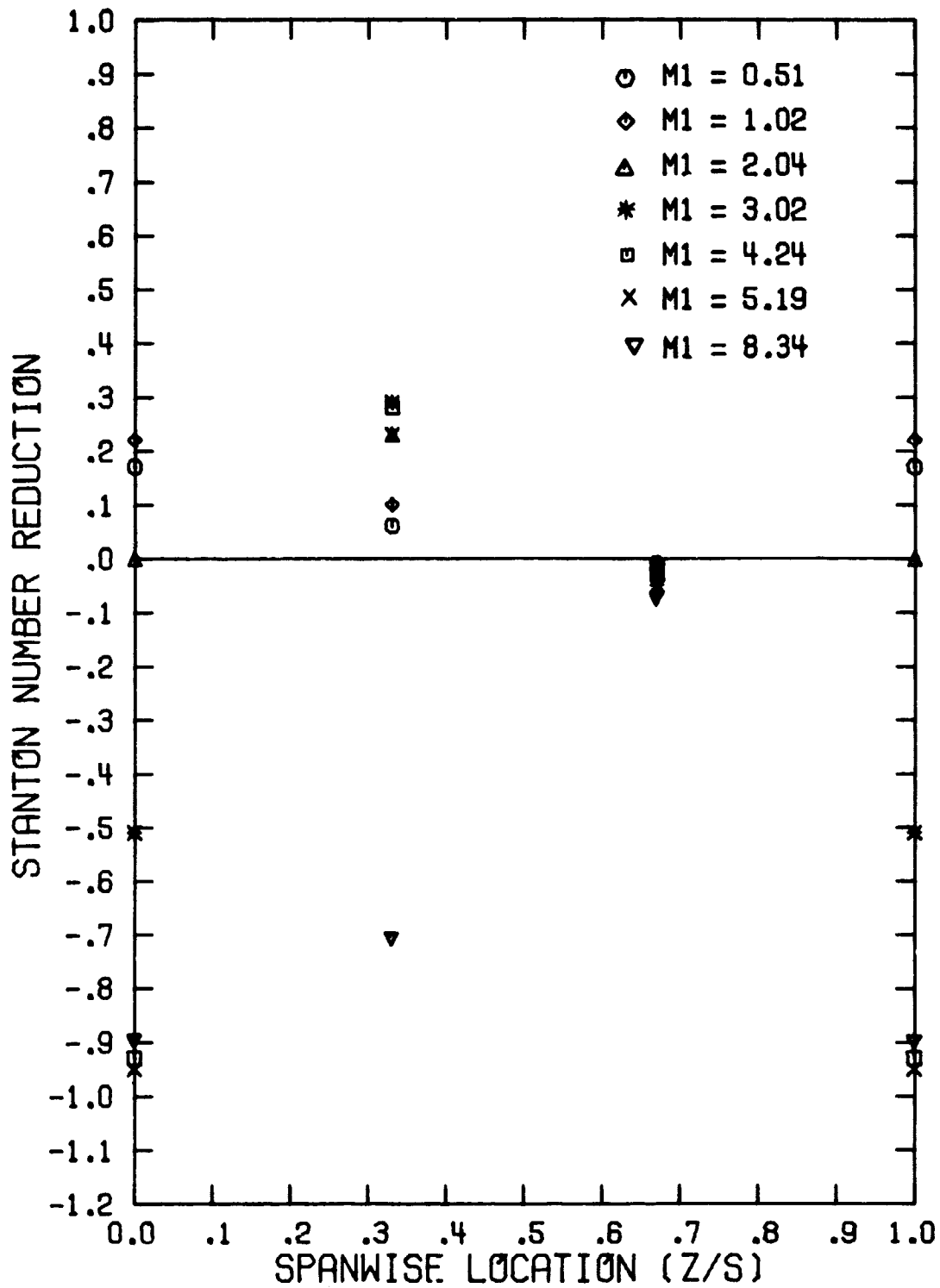


Figure 39. Spanwise Variation of the Stanton Number Reduction with Single Row Injection ($\theta_1 = 5^\circ$, $(x/d_0)_1 = 1.5$, $S/d_0 = 5$)

ORIGINAL PAGE IS
OF POOR QUALITY

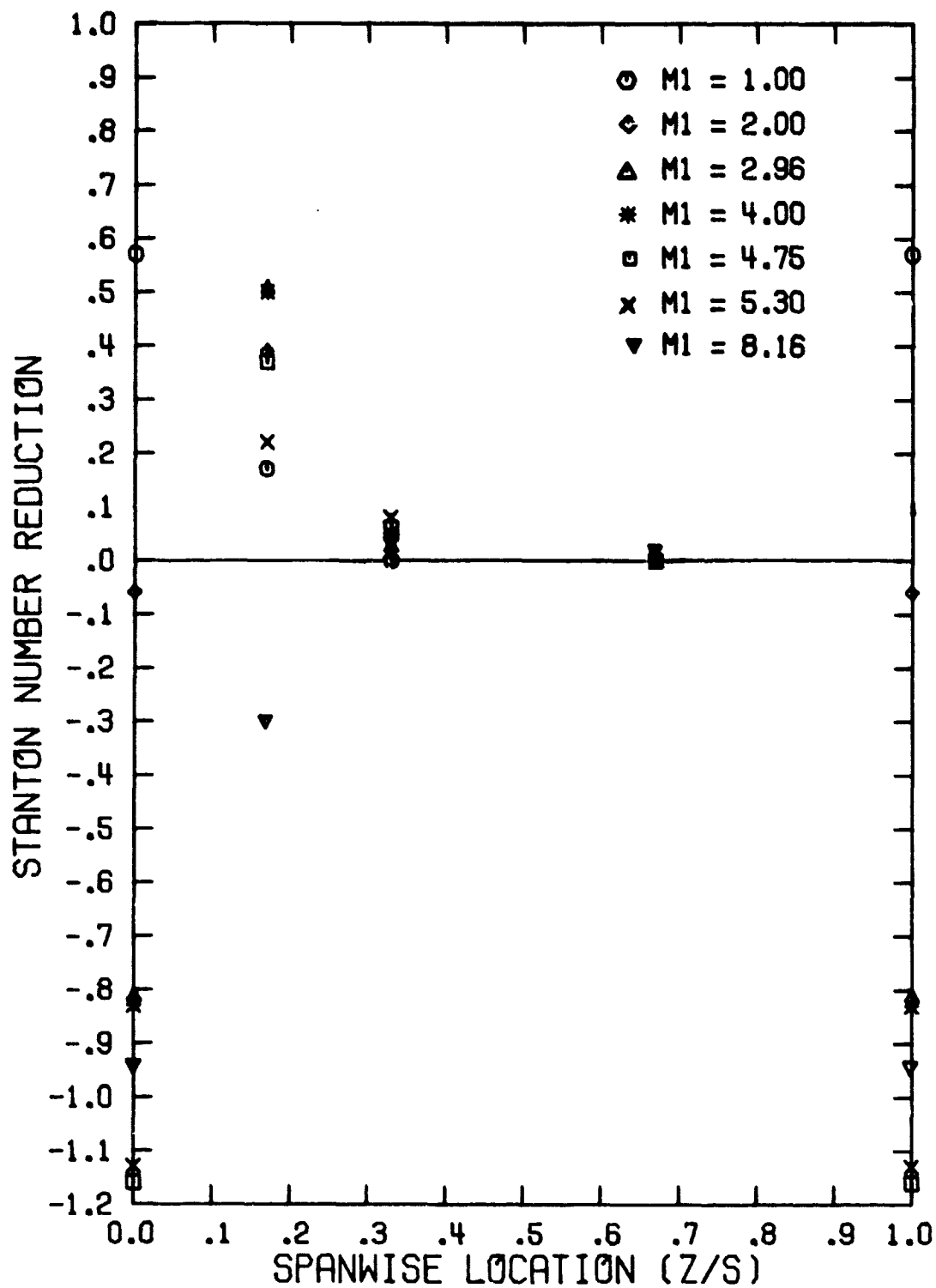


Figure 40. Spanwise Variation of the Stanton Number Reduction with Single Row Injection ($\theta_1 = 5^\circ$, $(x/d_0)_1 = 1.5$, $S/d_0 = 10$)

time, an increase in the blowing ratio up to a certain level also resulted in higher positive values of SNR in the region covered by the coolant. An increase in M_1 above a certain level (e.g. $M_1 > 4.0$ in Figure 40) resulted in a decrease in the positive value of SNR as well.

To simplify the data interpretation process, the following definitions are introduced:

- (a) the negative value of SNR located directly behind the coolant hole is designated as SNR_{neg} ,
- (b) the spanwise maximum value of SNR from the measured data only is designated as SNR_{max} ,
- (c) the blowing ratio that produces the largest value of SNR_{max} is referred to as the optimum blowing ratio, M_{opt} ,
- (d) an approximate location of the trajectory of the coolant jet was identified as the value of z/S where SNR_{max} was observed.

For both values of hole spacing, the optimum blowing ratio was observed in the range, $3 < M_1 < 4$, for $(x/d_o)_1 = 1.5$. Increasing the blowing ratio beyond 4 resulted in a continual decline in the value of SNR_{max} for both hole spacings. The values of SNR for $S/d_o = 10$ were considerably larger than those for $S/d_o = 5$ for a given value of M_1 . For $M_1 \approx 8.2$, the value of SNR_{neg} was approximately -0.9 and $SNR \leq 0$ all along the spanwise direction at $(x/d_o)_1 = 1.5$.¹

Farther downstream from row 1, Figures 41 and 42 present the results for SNR at $(x/d_o)_1 = 3.5$ for the hole spacing $(S/d_o) = 5$ and 10, respectively. The trends observed at $(x/d_o)_1 = 1.5$ were repeated at this downstream location. The influence of the coolant is still very localized, with no noticeable spreading in the spanwise direction. The positive values of SNR diminished with an increase in downstream distance. However, at the same time, the large values of SNR_{neg} behind the hole also decreased in absolute magnitude. The location of the coolant along the surface moved somewhat in the spanwise direction,

¹ Large values of M_1 were investigated for injection at θ_1 since the value of $(\rho_\infty V_\infty)_1$ is so low.

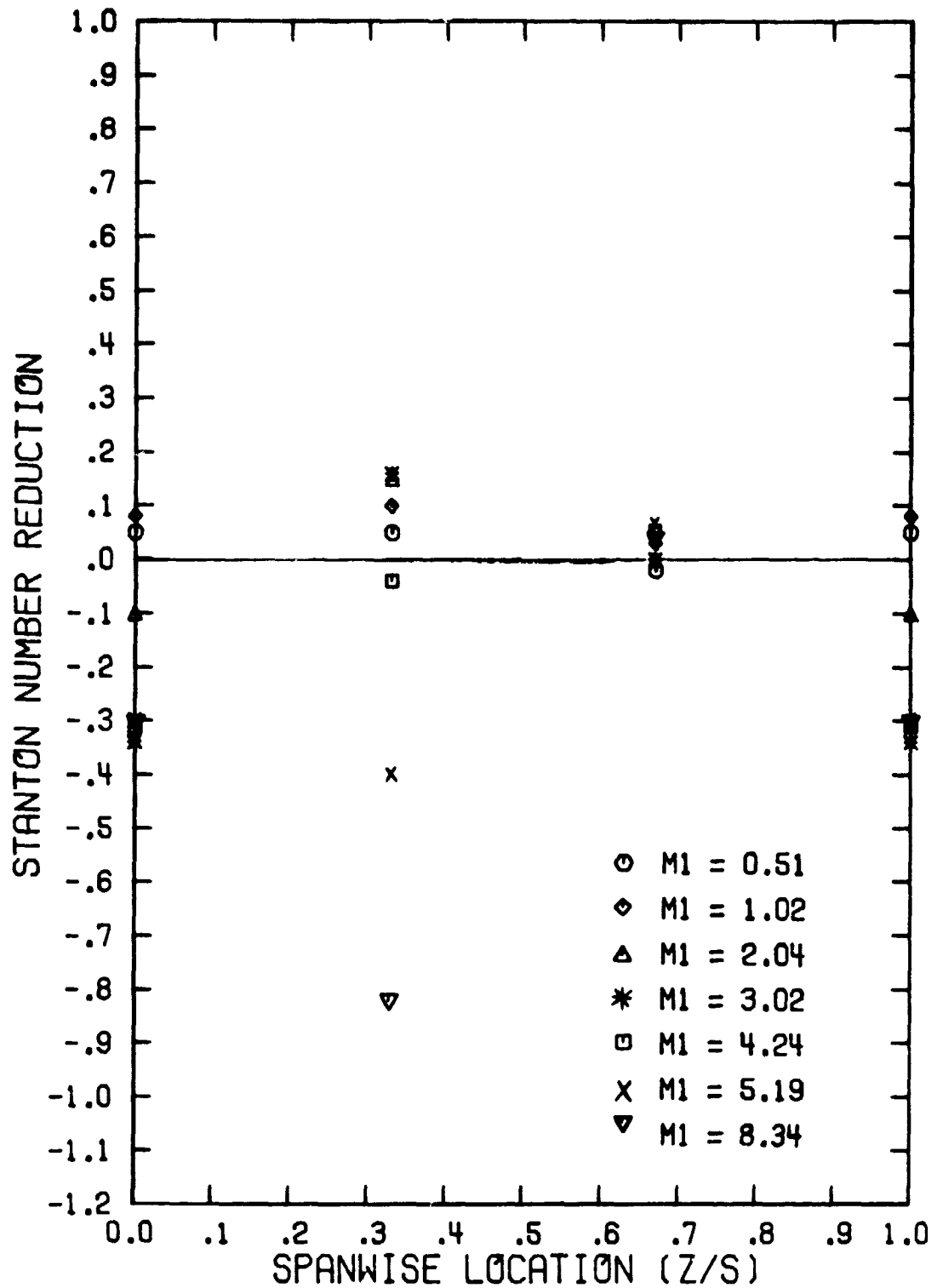


Figure 41. Spanwise Variation of the Stanton Number Reduction with Single Row Injection ($\theta_1 = 5^\circ$, $(x/d_0)_1 = 3.5$, $s/d_0 = 5$)

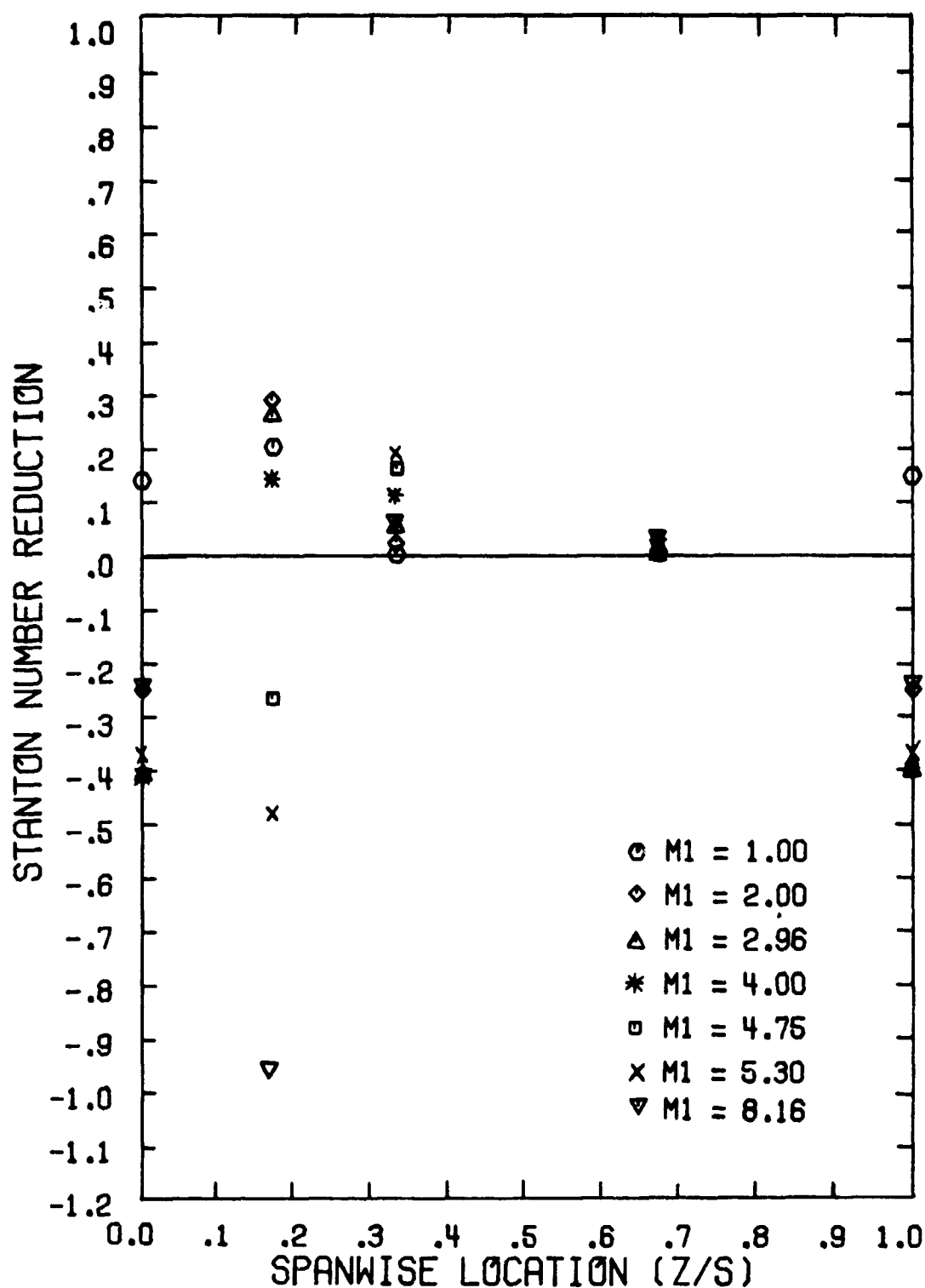


Figure 42. Spanwise Variation of the Stanton Number Reduction with Single Row Injection ($\theta_1 = 5^\circ$, $(x/d_0)_1 = 3.5$, $S/d_0 = 10$)

particularly at the higher values of M_1 , compared with the data for the upstream location of $(x/d_o)_1 = 1.5$. An examination of the additional data for $\theta_1 = 5^\circ$ in Appendix III, Figures A7, A8, etc., shows that farther downstream, $(x/d_o)_1 \geq 6.5$ the coolant was completely turned to the streamwise direction and the spanwise location of the coolant trajectory remained fixed as the coolant continued to flow downstream. As the value of $(x/d_o)_1$ increased, the positive values of SNR continued to diminish and the magnitude of SNR_{neg} behind the hole decreased as well. At large values of the blowing ratio, negative values of SNR were observed at all spanwise locations.

In the application of film cooling data to turbine vane cooling designs, it is convenient to have film cooling performance averaged in the spanwise direction (i.e. average hole-to-hole). Consequently the results from this investigation (Appendix III) were used to determine the spanwise averaged Stanton Number Reduction, SNR_{avg} . The value of SNR_{avg} for a particular $(x/d_o)_1$ location was computed as follows:

- (a) a series of straight line segments were fit through the data points of SNR vs z/S for the range $0 \leq z/S \leq 1$,
- (b) the value for SNR at $z/S = 0$ (when a heat flux gage was not located at that point) was obtained by linear interpolation of the data,
- (c) the value for SNR at $z/S = 1$ was assumed equal to the value for $z/S = 0$, and
- (d) the value of SNR_{avg} was obtained by integration under the straight line segment curve.

$$SNR_{avg} = \int_0^1 SNR d(z/S)$$

A complete tabulation of the computed values of SNR_{avg} is given in Appendix III.

The user of spanwise averaged data should note that averaging tends to smear out localized effects. A low value of SNR_{avg} could result from a large value of SNR_{neg} , a large value of SNR_{max} and a significant portion of the span with $SNR = 0$. Or the value of SNR

could be more uniform across the span with SNR_{avg} a good representation.

Figures 43 and 44 present the values for SNR_{avg} plotted as a function of downstream distance, $(x/d_0)_1$, for the hole spacing of $S/d_0 = 5$ and 10, respectively. The legend in each figure defines the blowing ratio. For both values of hole spacing, the maximum values of SNR_{avg} are reached at $M_1 \approx 1.0$, but the magnitude of SNR_{avg} is ≤ 0.10 except at $(x/d_0)_1 = 1.5$. For $(x/d_0)_1 > 1.5$, the values of SNR_{avg} for both hole spacings are in close agreement. As the blowing ratio exceeds 2.0, the value of SNR_{avg} at all $(x/d_0)_1$ become negative for both values of S/d_0 . This corresponds to the development of large values of SNR_{NEG} behind the hole. The data for $M_1 = 8.2$ reveals larger negative values of SNR_{AVG} for the hole spacing of $S/d_0 = 5$ than for $S/d_0 = 10$.

IV.B.2. Spanwise Injection at $\theta_2 = 22.9^\circ$

The Stanton Number Reduction for injection at $\theta_2 = 22.9^\circ$ is presented in Figures 45 and 46 for $(x/d_0)_2 = 1.5$ and $S/d_0 = 5$ and 10, respectively. As was observed at $\theta_1 = 5^\circ$, with low blowing rates the coolant was turned quickly by the freestream and passed directly behind the hole. As expected, high values of SNR were found behind the hole, with the magnitude being approximately the same for both values of hole spacing. Even though the values of SNR reached 70% behind the hole, the effect of the coolant jets on the entire surface was still very localized.

When the blowing ratio was increased, the coolant trajectory shifted in the spanwise direction. For $S/d_0 = 5$, negative values of SNR occurred directly behind the hole ($(x/d_0)_2 = 1.5$) for $M_2 \geq 1.1$ with value of SNR_{NEG} increasing as M_2 increased. However, for $S/d_0 = 10$, the negative values were not observed until $M_2 > 2.0$. The data farther downstream $(x/d_0)_2 = 3.5$, Figure 48, reveal that for $S/d_0 = 10$, negative values of SNR were observed directly behind the hole for $M_2 = 1.1$. This peculiarity is discussed in greater detail later.

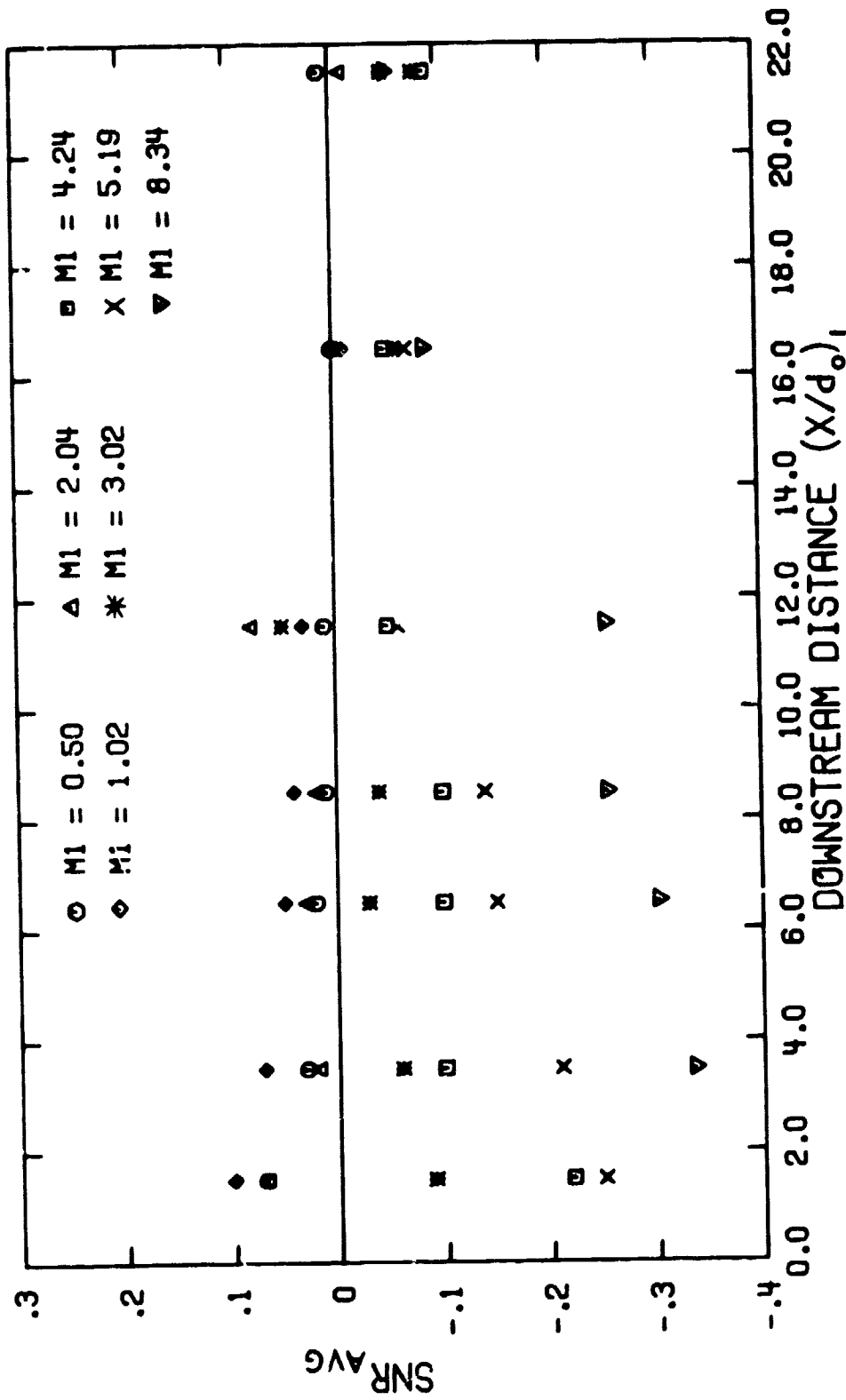


Figure 43. Variation of the Spanwise Averaged Stanton Number Reduction with Downstream Distance for Single Row Injection ($\theta_i = 5^\circ$, $S/d_o = 5$)

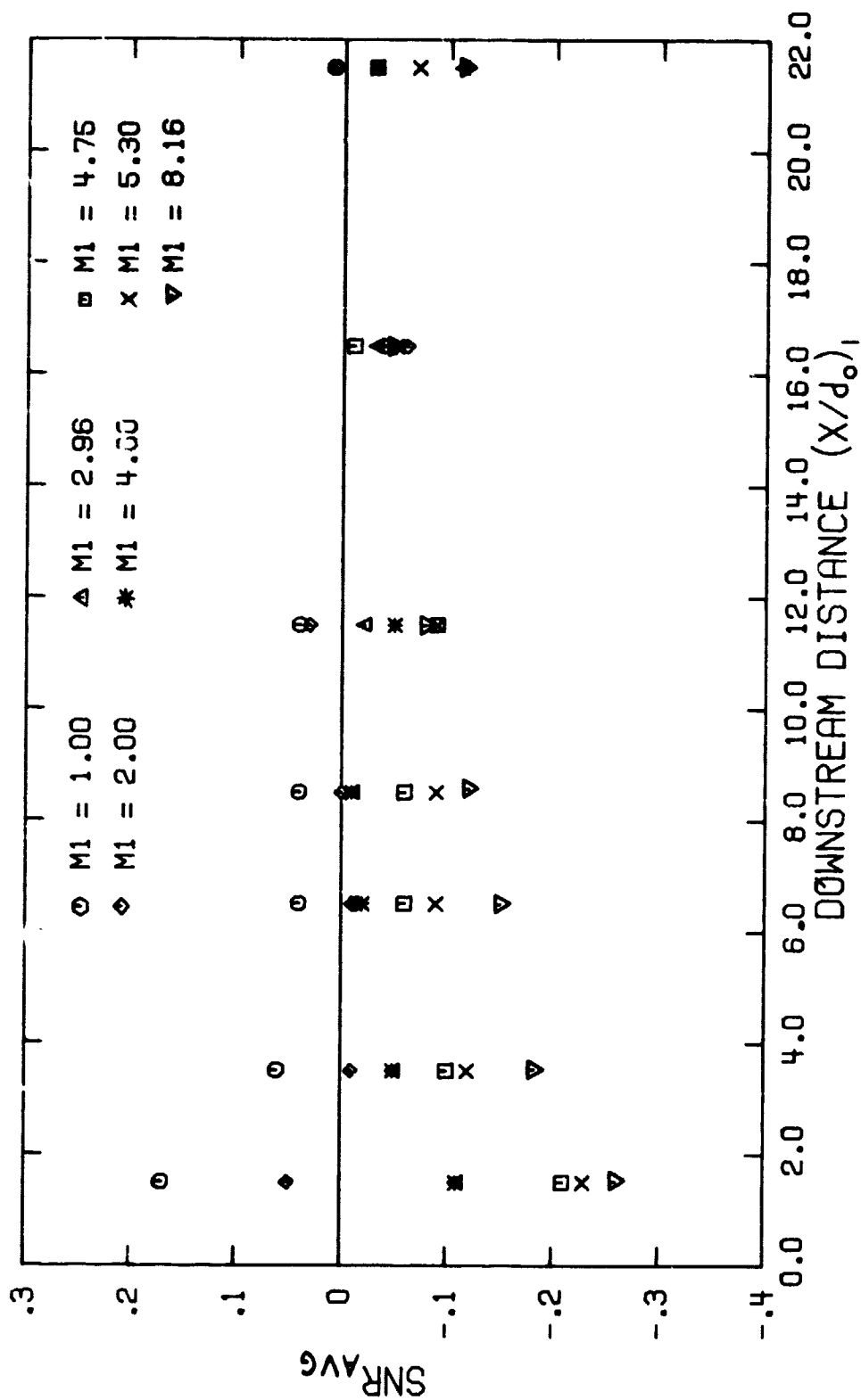


Figure 44. Variation of the Spanwise Averaged Stanton Number Reduction with Downstream Distance for Single Row Injection ($\theta_1 = 5^\circ$, $S/d_o = 10$)

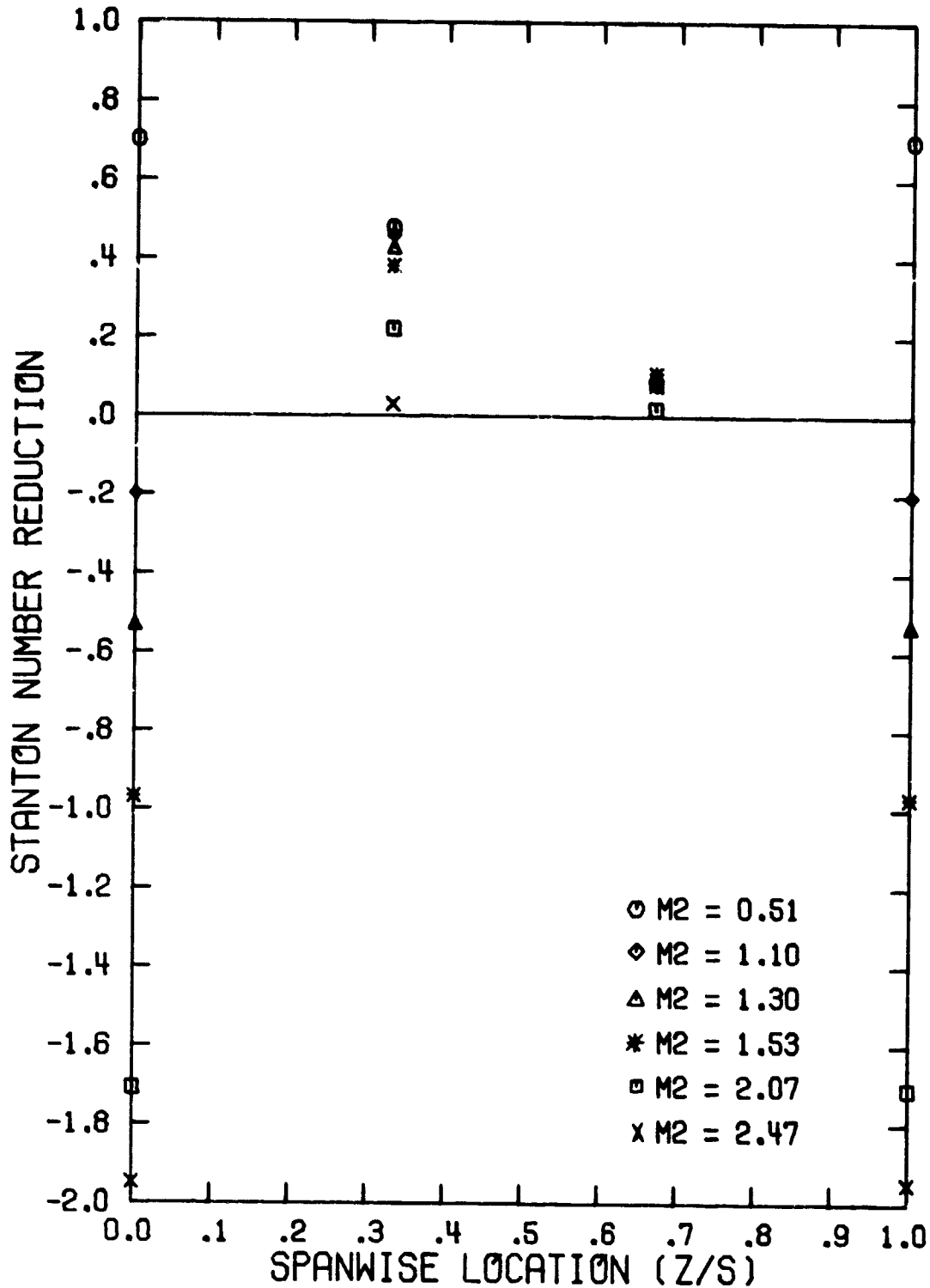


Figure 45. Spanwise Variation of the Stanton Number Reduction with Single Row Injection ($\theta_2 = 22.9^\circ$, $(x/d_0)_2 = 1.5$, $s/d_0 = 5$)

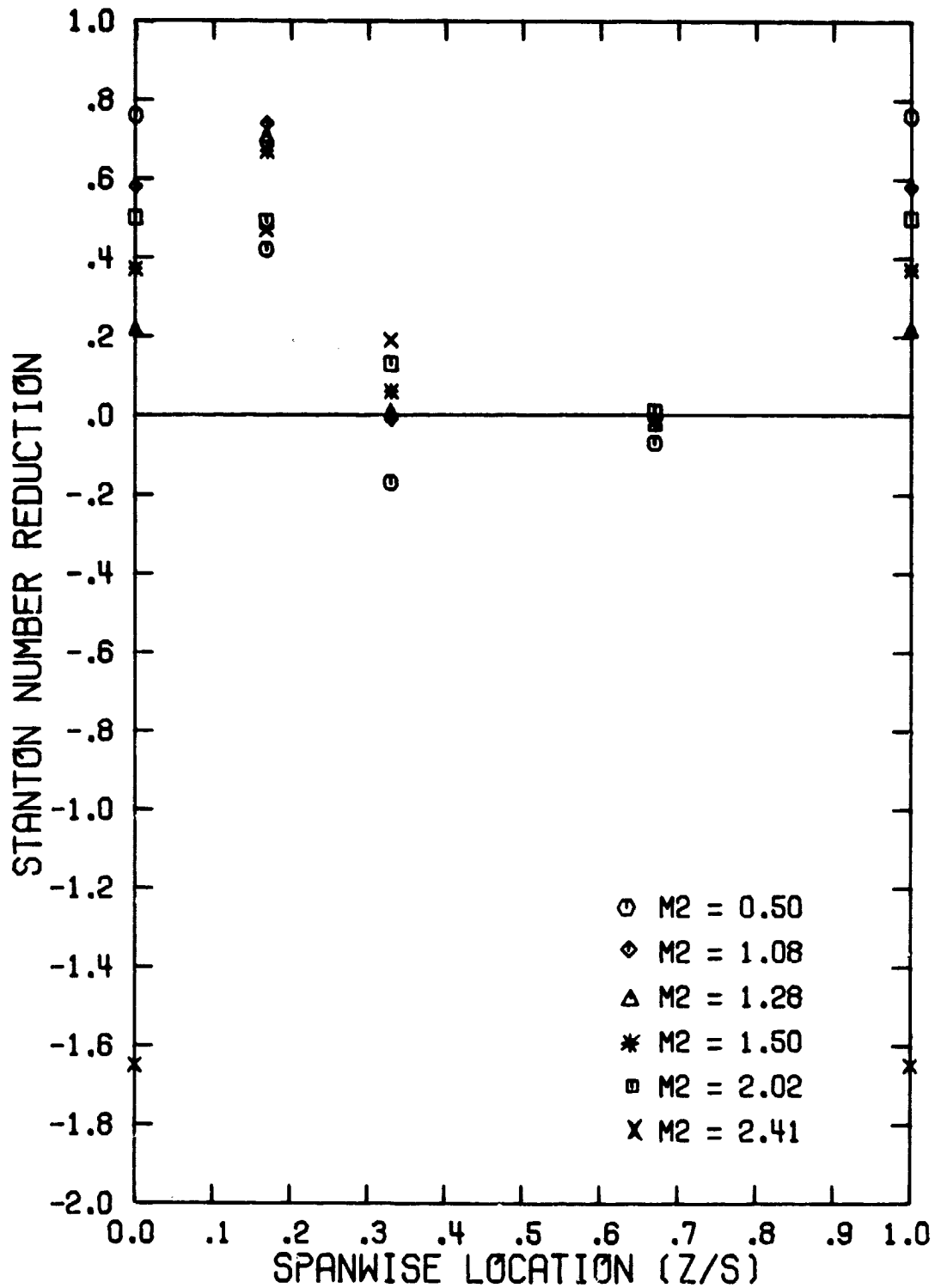


Figure 46. Spanwise Variation of the Stanton Number Reduction with Single Row Injection ($\theta_2 = 22.9^\circ$, $(x/d_0)_2 = 1.5$, $S/d_0 = 10$)

An optimum blowing ratio yielding the highest SNR_{MAX} was $M_2 \approx 0.75$ for both hole spacings. However, for a value of the blowing ratio greater than 1.0, the coolant with a hole spacing of $10d_0$ was able to maintain higher values of SNR than those achieved for the smaller hole spacing of $5d_0$.

Downstream at $(x/d_0)_2 = 3.5$, the results for SNR for the hole spacing of 5 and 10 are presented in Figures 47 and 48, respectively. Following the trend established at $\theta_1 = 5^\circ$, the values of SNR decreased from the upstream levels. The large negative values behind the hole were observed for both hole spacings for $(x/d_0)_2 = 3.5$.

The spanwise averaged results for $\theta_2 = 22.9^\circ$ are shown in Figures 49 and 50 for S/d_0 of 5 and 10, respectively. The data for both spacing ratios exhibit the same trend, with the maximum value of SNR_{AVG} located near the hole and a continual decrease of SNR_{AVG} in the downstream direction. As M_2 was increased, the best film cooling performance was observed at $M_2 \approx 0.50$ for both hole spacings. However, the magnitude of SNR_{AVG} for $S/d_0 = 5$ exceeded that for $S/d_0 = 10$ at the optimum blowing condition.

With the blowing ratio, $M_2 > 1.3$, generally negative values of SNR_{AVG} were found for $S/d_0 = 5$. A similar trend occurred for $S/d_0 = 10$, except at $(x/d_0)_2 = 1.5$ where SNR_{NEG} was not observed until $M_2 > 2.0$. As was discovered previously for $\theta_1 = 5^\circ$, the negative values of SNR_{AVG} for $S/d_0 = 5$ were larger than those for $S/d_0 = 10$. Using the spanwise averaged results for comparison, the film cooling performance for $\theta_2 = 22.9^\circ$ shows a somewhat higher level of SNR_{AVG} at the optimum blowing condition, $M_2 \approx 0.50$, than for $M_1 = 1.00$ at $\theta_1 = 5^\circ$.

IV.B.3. Spanwise Injection at $\theta_3 = 40.8^\circ$

The trends established for the injection locations of 5° and 22.9° continued for injection at $\theta_3 = 40.8^\circ$. Figures 51 and 52 present the data for SNR at $(x/d_0)_3 = 1.5$ for $S/d_0 = 5$ and 10, respectively. Again, for low values of M_3 , the coolant was turned quickly behind the hole

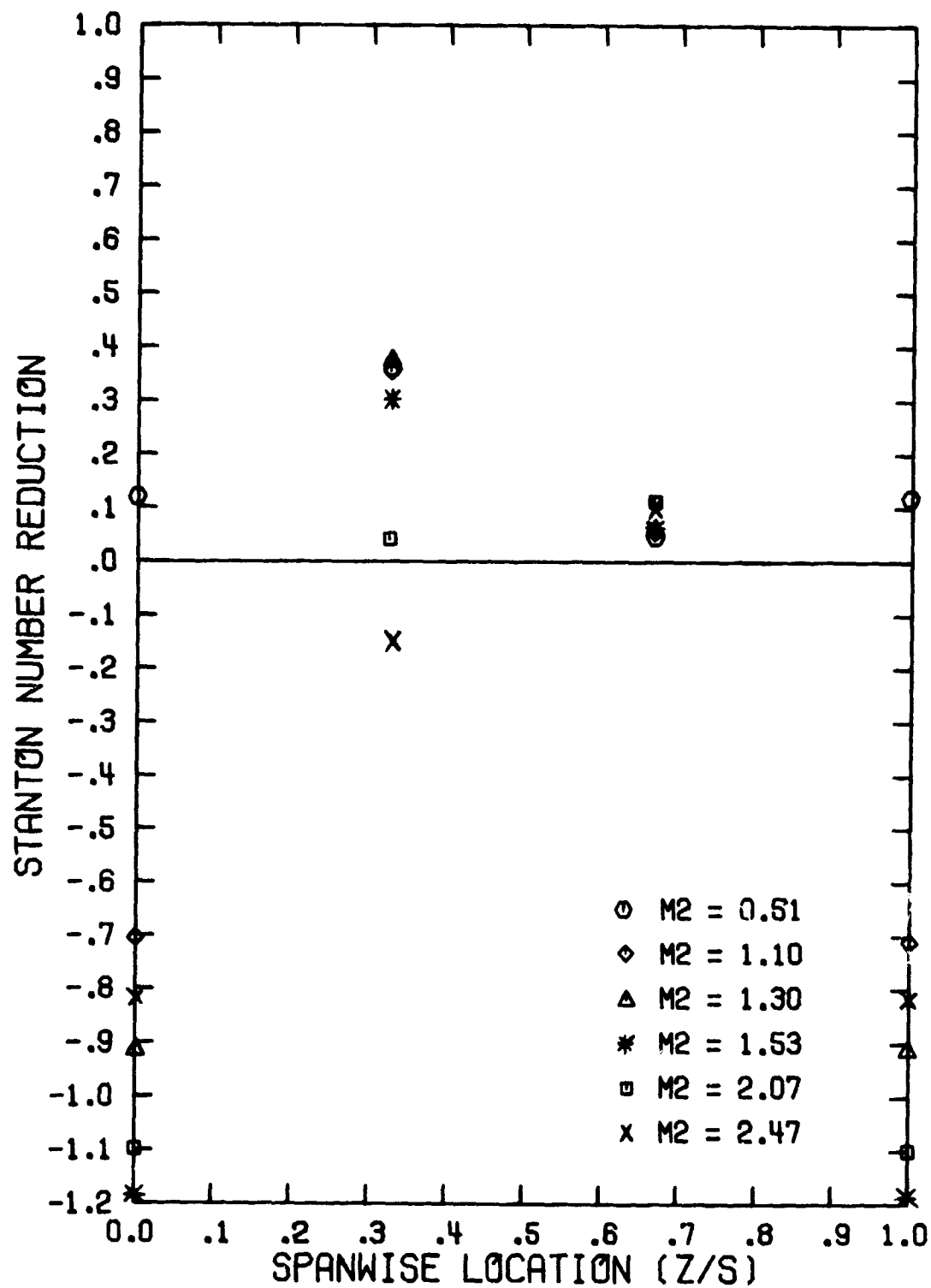


Figure 47. Spanwise Variation of the Stanton Number Reduction with Single Row Injection ($\theta_2 = 22.9^\circ$, $(x/d_0)_2 = 3.5$, $S/d_0 = 5$)

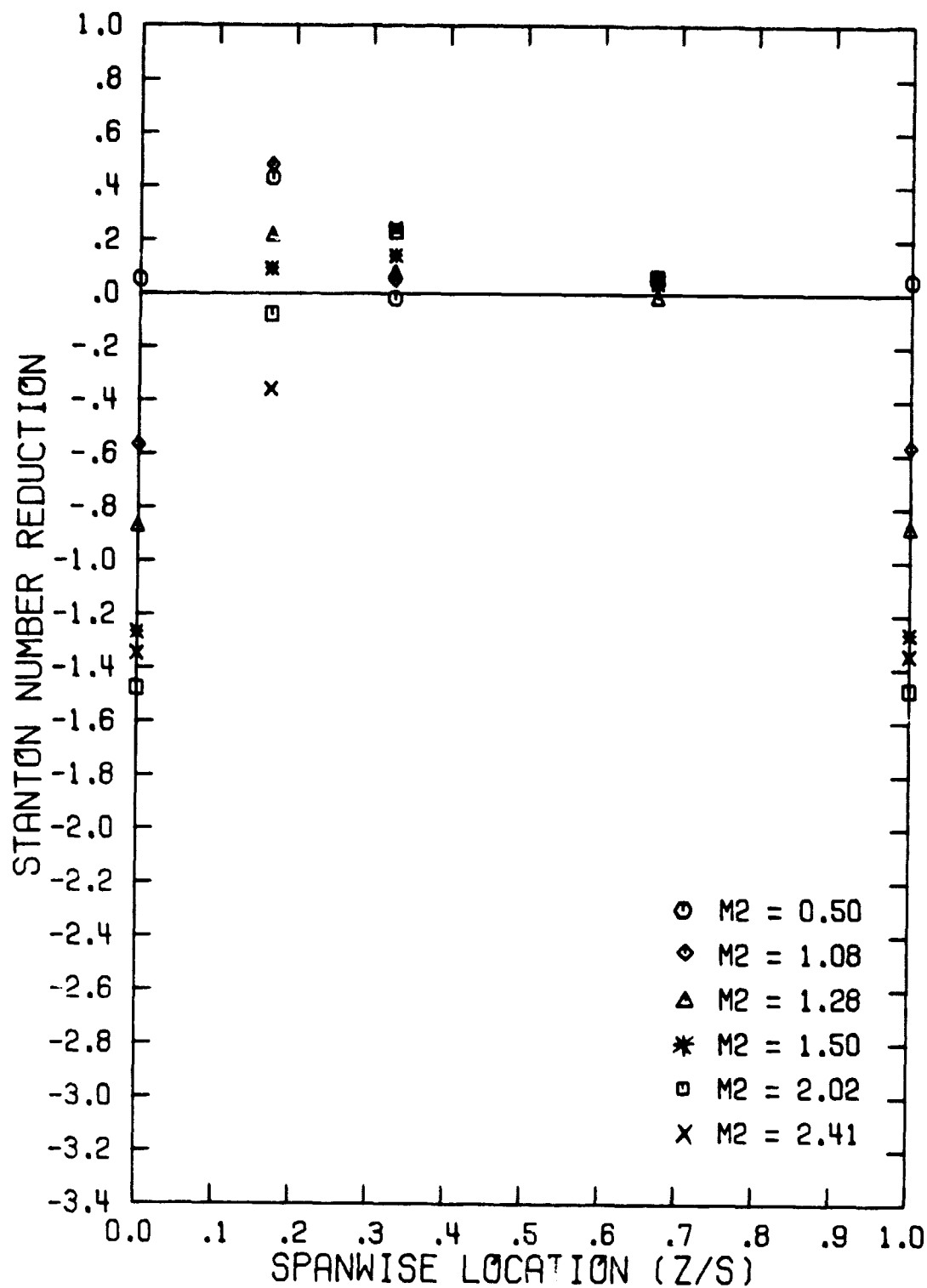


Figure 43. Spanwise Variation of the Stanton Number Reduction with Single Row Injection ($\theta_1 = 22.9^\circ$, $x/d_0)_2 = 3.5$, $S/d_0 = 10$)

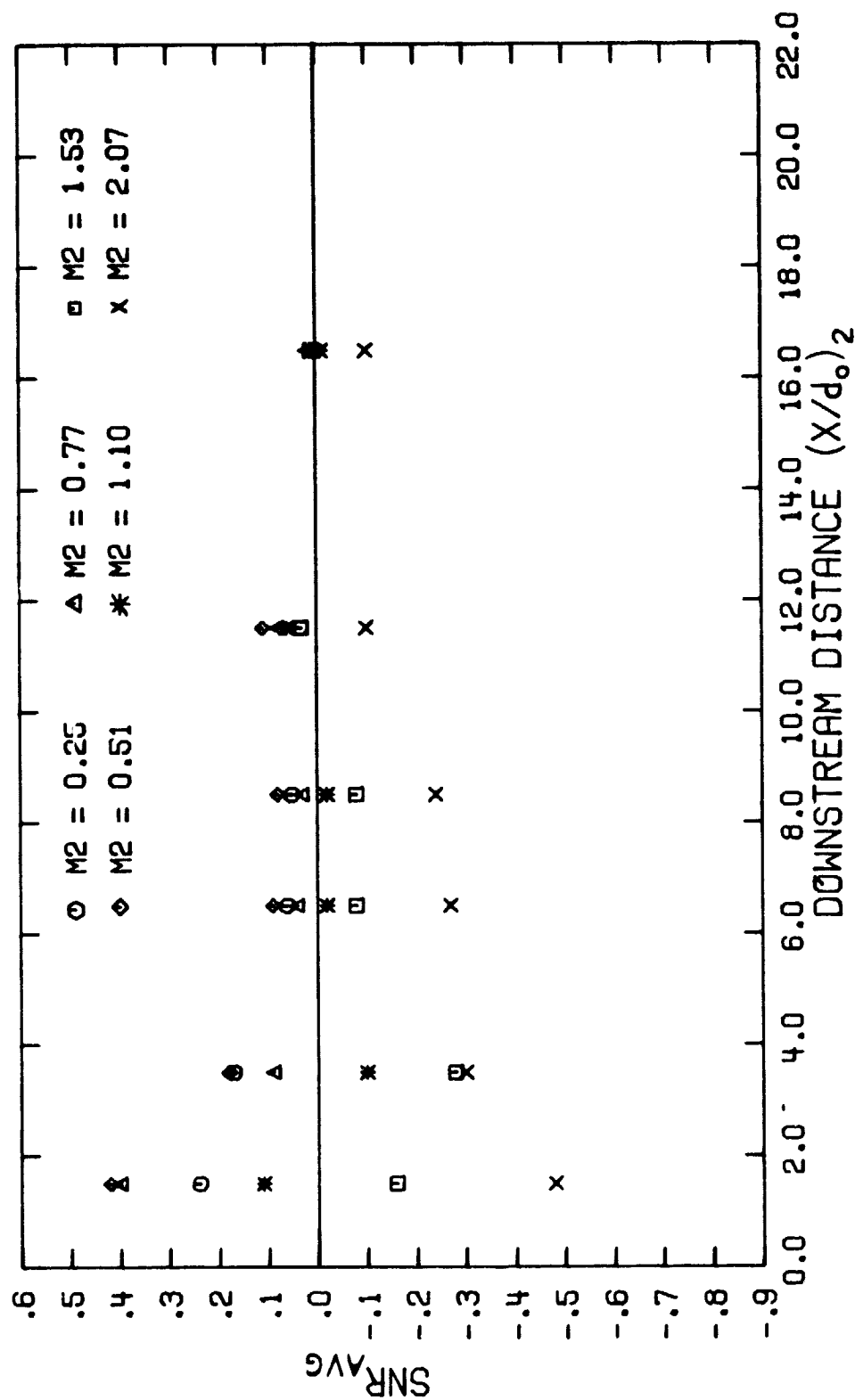


Figure 49. Variation of the Spanwise Averaged Stanton Number Reduction with Downstream Distance for Single Row Injection ($\theta_2 = 22.9^\circ$, $S/d_o = 5$)

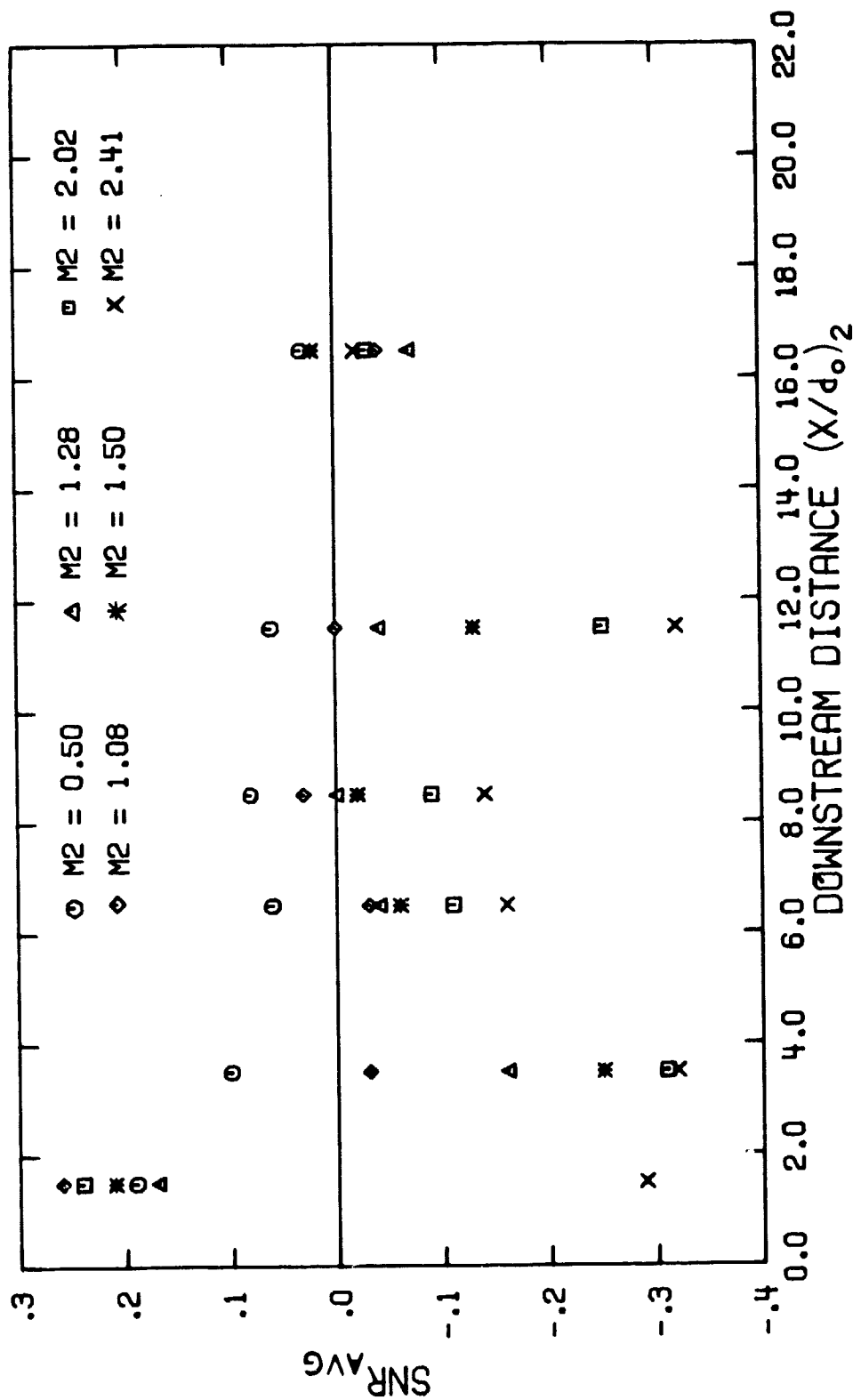


Figure 50. Variation of the Spanwise Averaged Stanton Number Reduction with Downstream Distance for Single Row Injection ($\theta_2=22.9^\circ$, $S/d_o=10$)

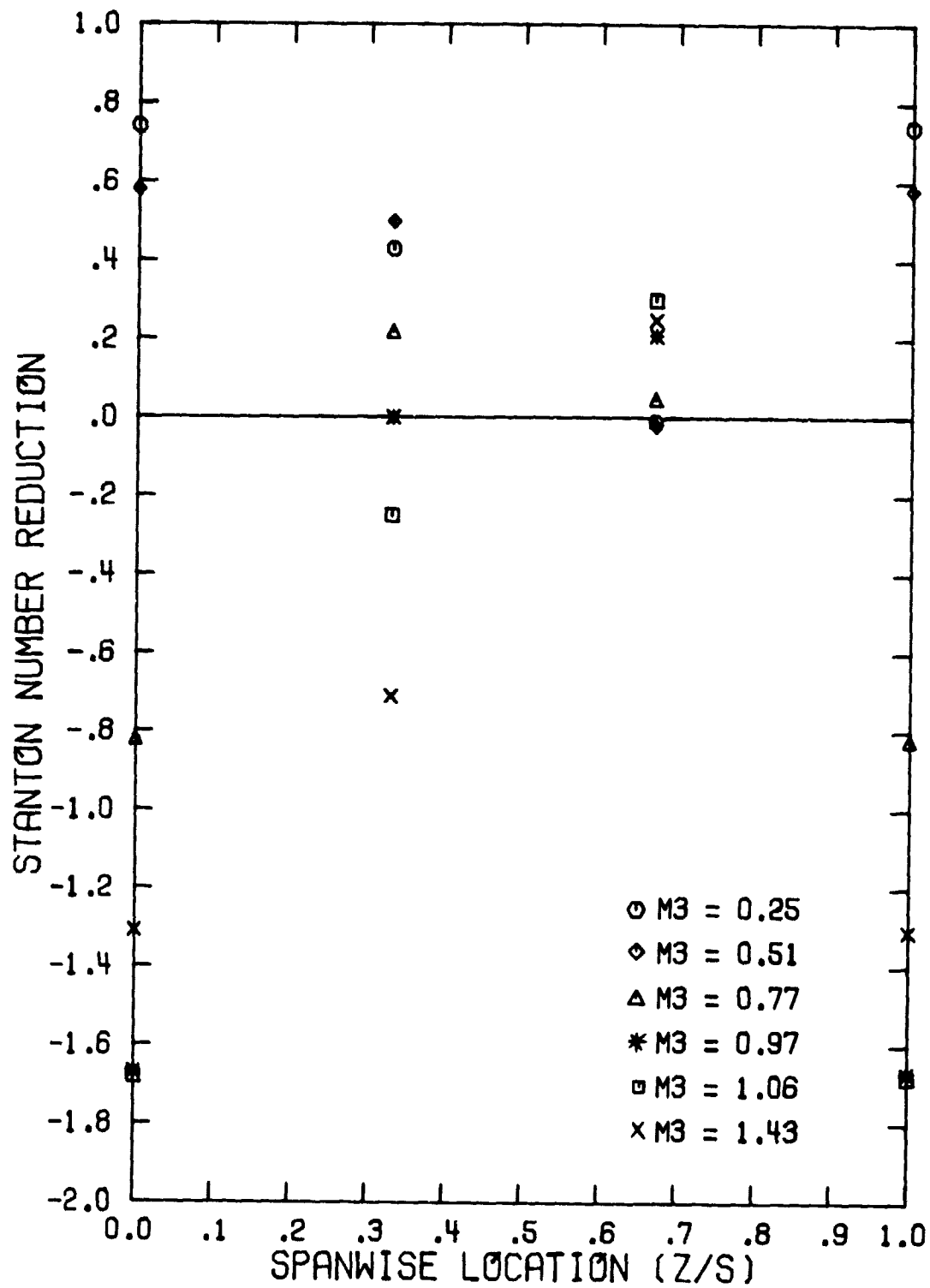


Figure 51. Spanwise Variation of the Stanton Number Reduction with Single Row Injection ($\theta_3 = 40.8^\circ$, $(x/d_0)_3 = 1.5$, $S/d_0 = 5$)

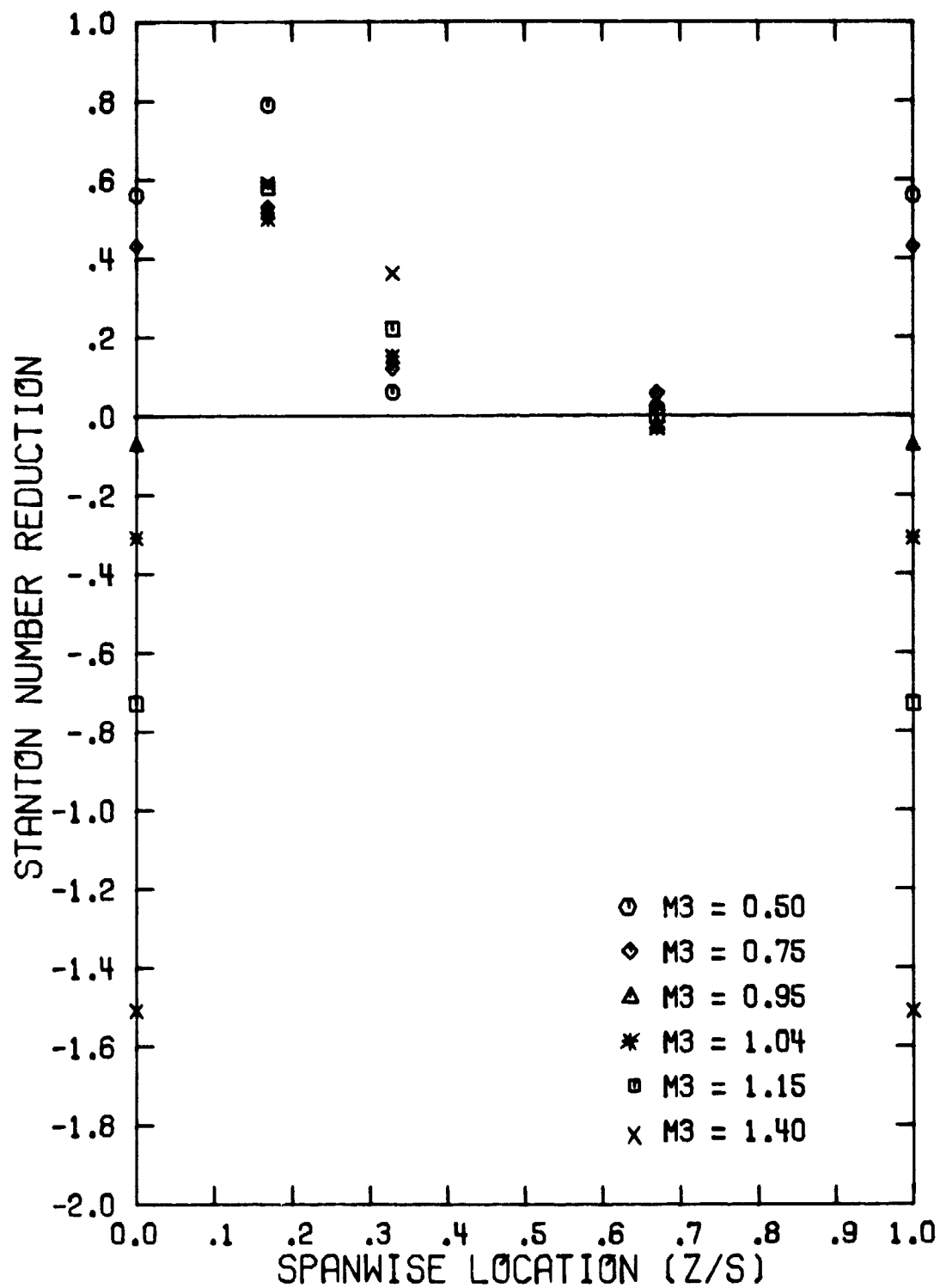


Figure 52. Spanwise Variation of the Stanton Number Reduction with Single Row Injection ($\theta_3=40.9^\circ$, $(x/d_0)_3=1.5$, $s/d_0=10$)

giving the highly localized cooling effect found throughout this study. The magnitude of SNR was approximately the same for both values of hole spacing, with the optimum SNR_{MAX} occurring at $M_3 \approx 0.50$.

As the blowing ratio was increased, negative values of SNR were observed behind the hole for $M \geq 0.75$ for $S/d_0 = 5$. With the larger hole spacing, the development of SNR_{NEG} values was not observed until $M_3 \approx 1.0$. When $M_3 > 1.0$ the coolant from the larger hole spacing maintained higher values of SNR than that for $S/d_0 = 5$ similar to the pattern developed at $\theta_2 = 22.9^\circ$ for high blowing ratios.

The results downstream are shown in Figure 53 for $(x/d_0)_3 = 3.5$, $S/d_0 = 5$ and in Figure 54 for $(x/d_0)_3 = 6.5$, $S/d_0 = 10$. To expedite the experiment, the data for $S/d_0 = 10$ were obtained with the test cylinder in a fixed orientation. Blowing occurred from a single row at $\theta_3 = 40.8^\circ$. For this orientation, there was a row of non-blowing holes at $\theta_1 = 5^\circ$. The influence of upstream non-blowing holes was found to be negligible (see Section III.D). This orientation resulted in heat flux data at $(x/d_0)_3 = 1.5, 6.5$, and 11.5 only for $S/d_0 = 10$ (see Figure 24).

The data for both values of S/d_0 show SNR diminishing with increasing $(x/d_0)_3$ and SNR_{NEG} values that generally decrease in magnitude. The location of the coolant trajectory moved in the spanwise direction from the position established at $(x/d_0)_3 = 1.5$, but the location remained constant for $(x/d_0)_3 \geq 6.5$. Figure 53 shows that for $M_3 \geq 1.2$, the values of SNR were negative all along the surface for $S/d_0 = 5$. However, for $S/d_0 = 10$, some positive values of SNR were observed even at the highest blowing ratio investigated, $M_3 = 1.75$.

Figures 55 and 56 show the spanwise averaged results for the hole spacing of 5 and 10, respectively. The heat flux data extend only to $(x/d_0)_3 = 11.5$ at this injection site because measurements beyond 90° from the stagnation line were not considered. The optimum film cooling performance for $S/d_0 = 5$ occurred when $M_3 = 0.25$, while for $S/d_0 = 10$, the optimum was reached at $M_3 = 0.50$ (no measurements were made at $S/d_0 = 10$ for the blowing ratio of 0.25). When $M_3 = 0.50$, the value of SNR_{AVG} was approximately the same for both values of S/d_0 . Increasing

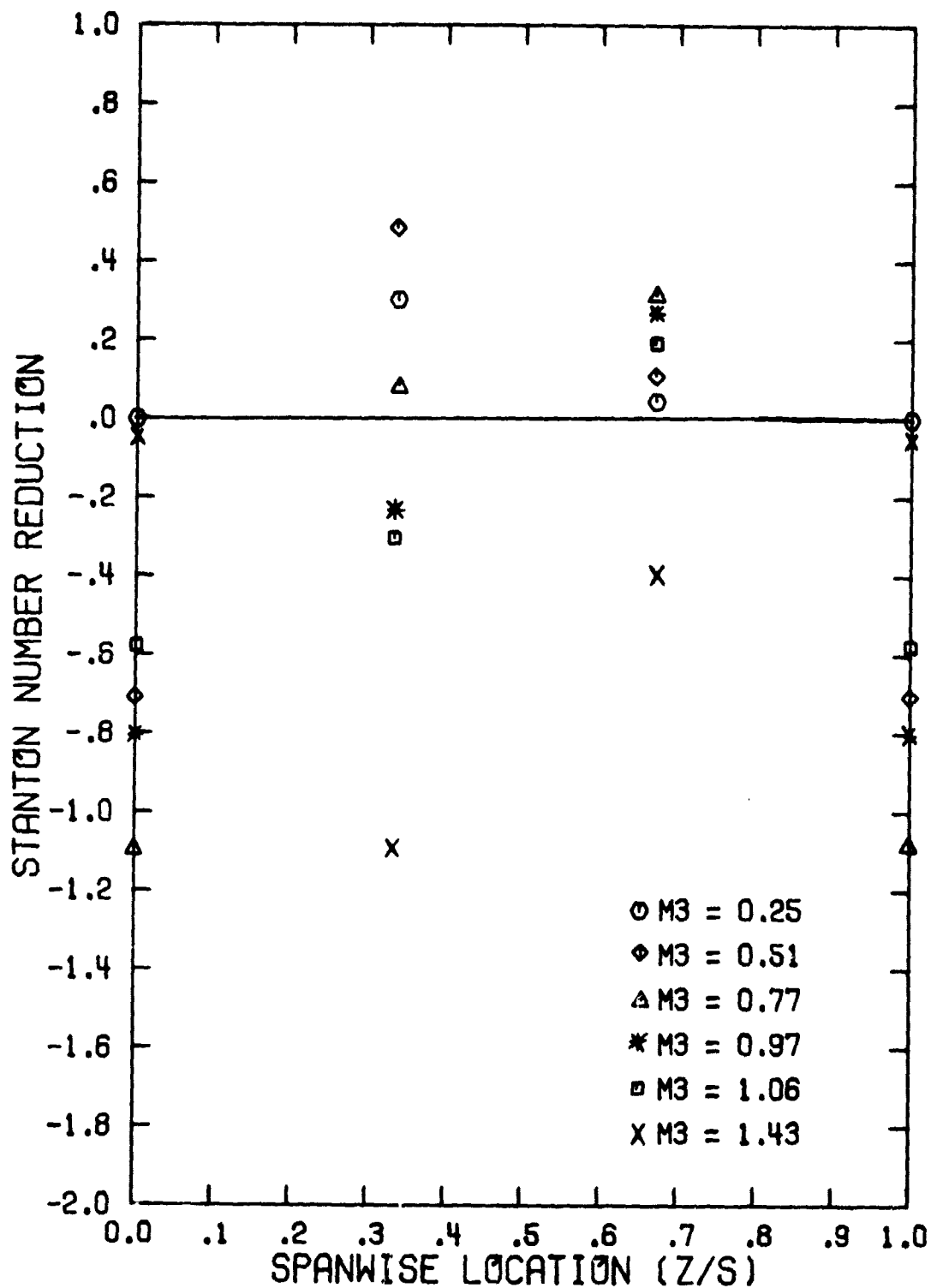


Figure 53. Spanwise Variation of the Stanton Number Reduction with Single Row Injection ($\theta_3 = 40.8^\circ$, $(x/d_0)_3 = 3.5$, $S/d_0 = 5$)

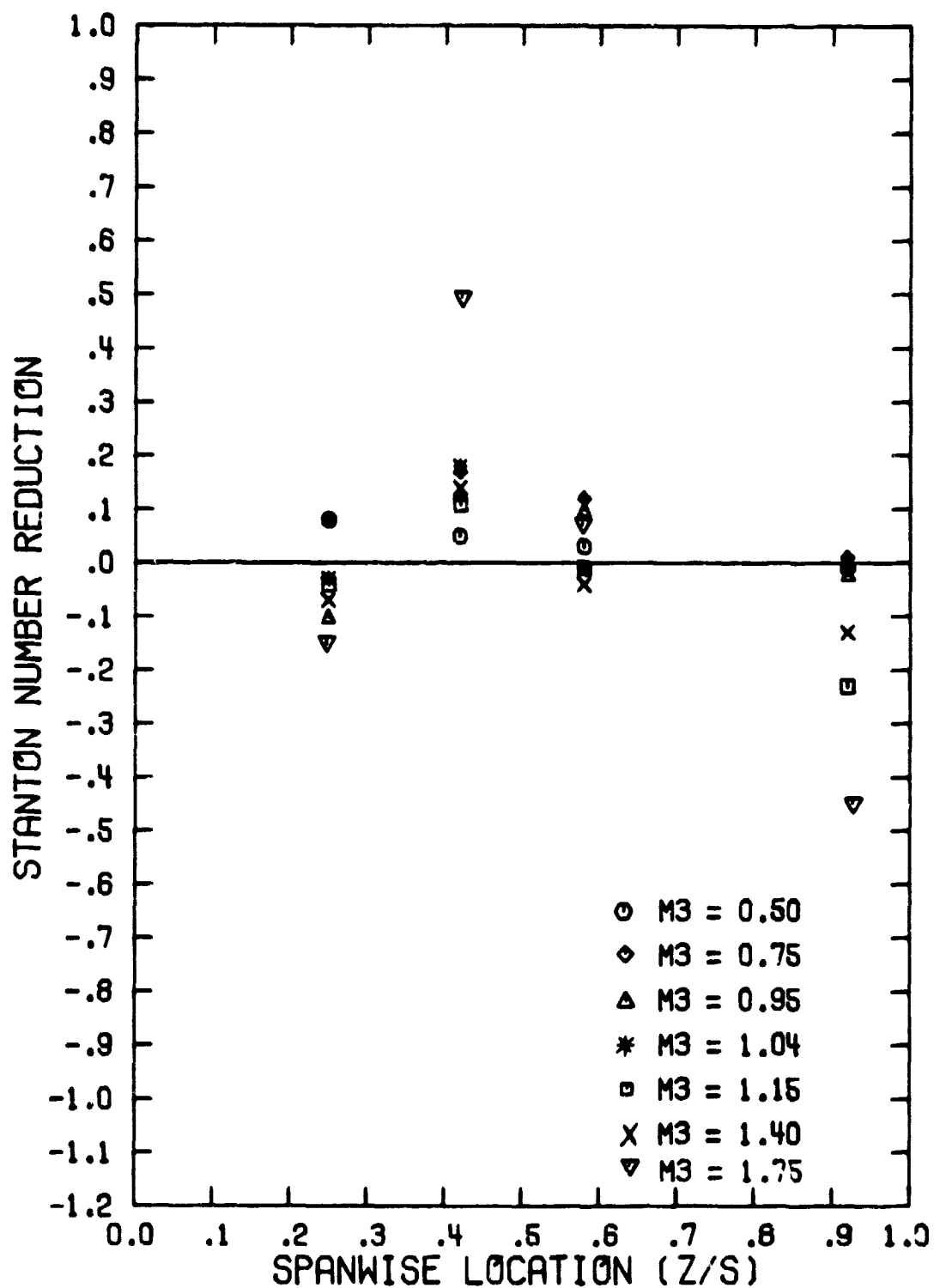


Figure 54. Spanwise Variation of the Stanton Number Reduction with Single Row Injection ($\theta_3 = 40.8^\circ$, $(x/d_0)_3 = 6.5$, $S/d_0 = 10$)

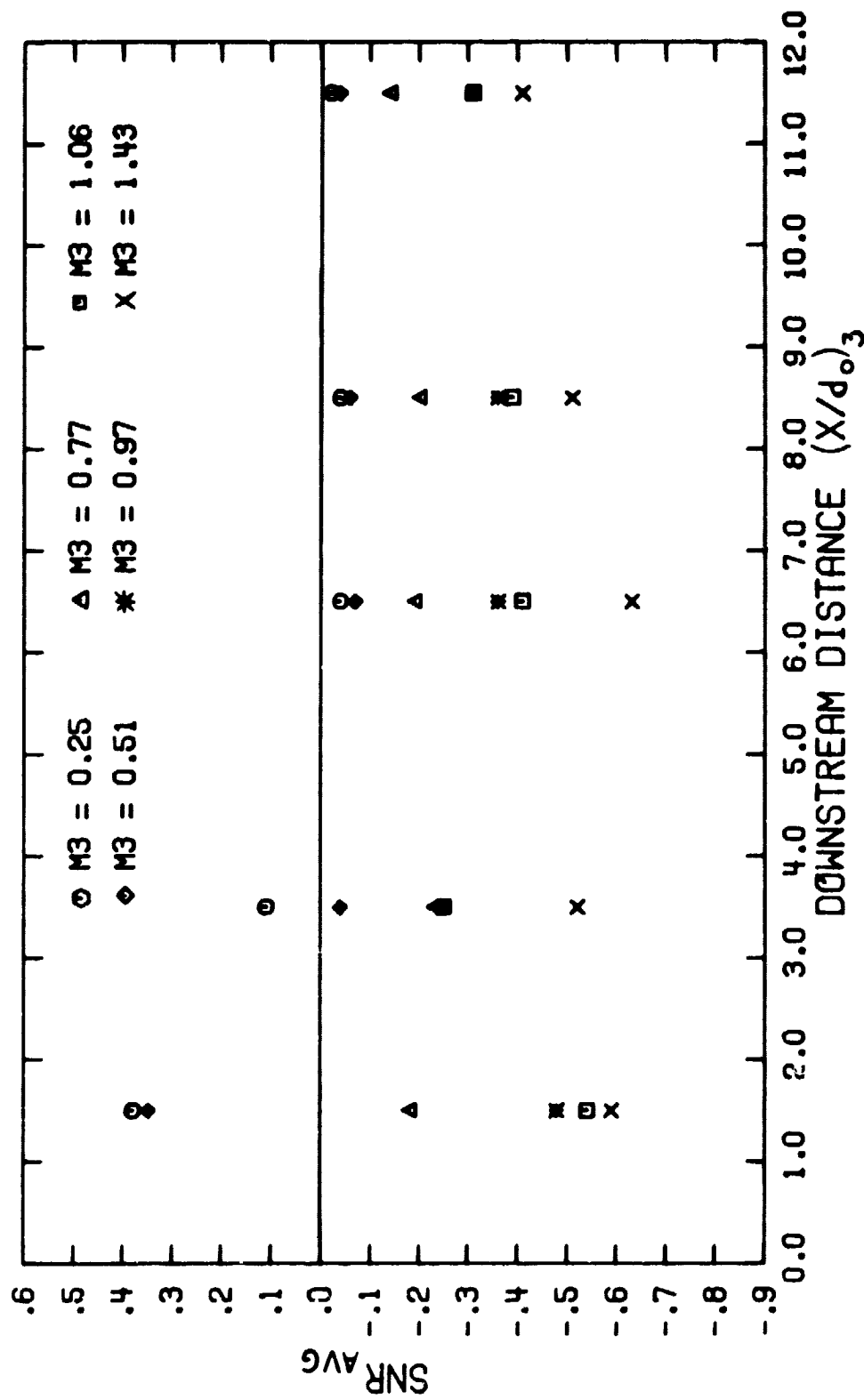


Figure 55. Variation of the Spanwise Averaged Stanton Number Reduction with Downstream Distance for Single Row Injection ($\theta_3 = 40.8^\circ$, $S/d_o = 5$)

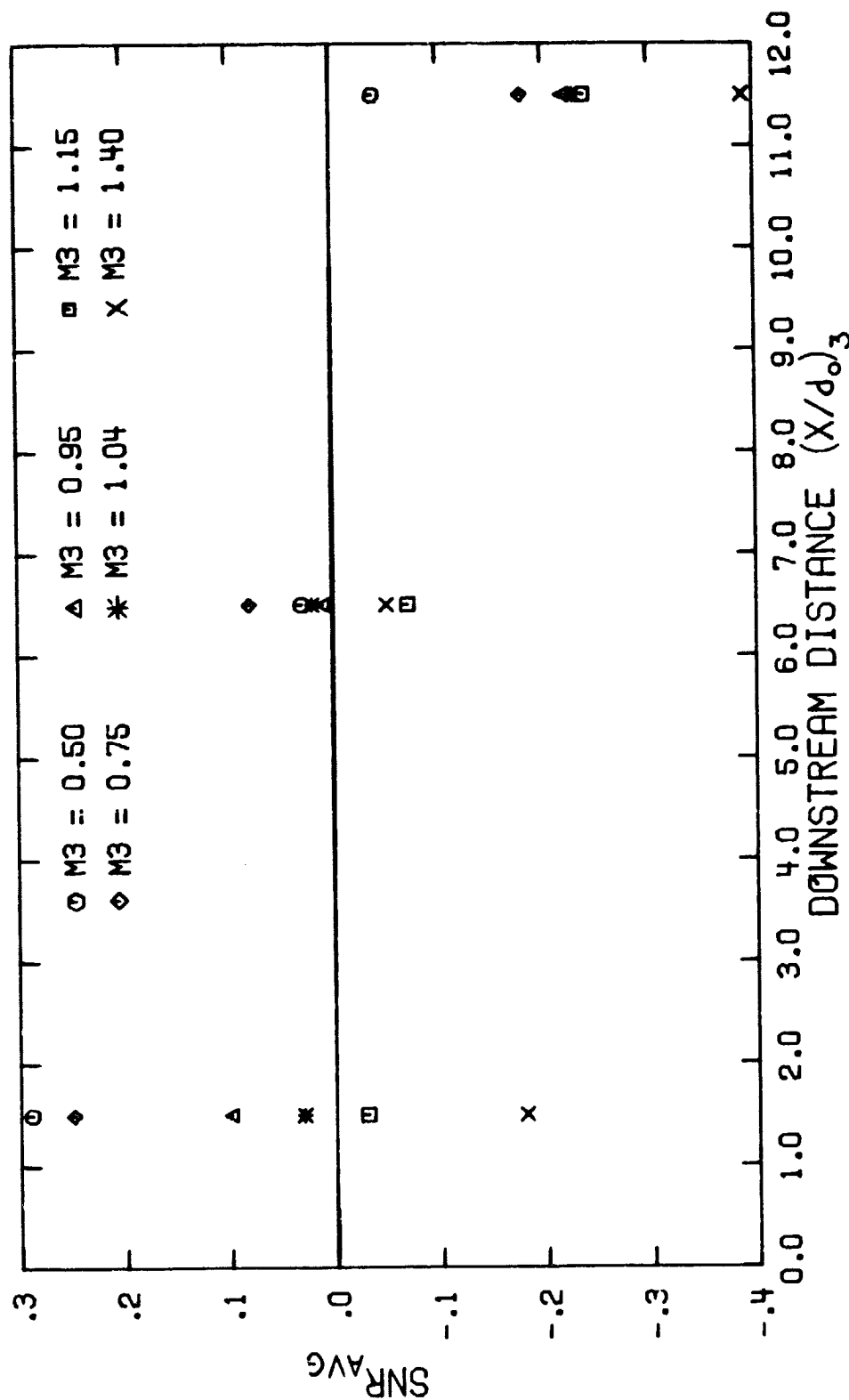


Figure 56. Variation of the Spanwise Averaged Stanton Number Reduction with Downstream Distance for Single Row Injection ($\theta_3 = 40.8^\circ$, $S/d_o = 10$)

the blowing ratio to $M_3 \geq 0.75$ resulted in negative values of SNR_{AVG} along the entire surface for $S/d_0 = 5$. The same pattern was observed for $S/d_0 = 10$ when $M_3 \geq 1.15$. As has been established at the upstream injection locations of 5° and 22.9° , for high blowing ratio ($M_3 \geq 1.4$), the smaller hole spacing ($S/d_0 = 5$) had larger negative values of SNR_{AVG} than for $S/d_0 = 10$.

IV.B.4. Spanwise Injection at $\theta_4 = 58.7^\circ$

The results for the single row injection at $\theta_4 = 58.7^\circ$ are illustrated in Figures 57 and 58 for $(x/d_0)_4 = 1.5$ and the hole spacings of 5 and 10, respectively. At low values of the blowing ratio, the trends established by the previous injection locations were repeated. The coolant was quickly turned in the freestream direction with the coolant passing directly behind the hole producing a very localized cooling effect. For $S/d_0 = 5$, the highest value of SNR_{MAX} was observed for $M_4 \approx 0.50$, while for $S/d_0 = 10$ the optimum blowing condition occurred with $M_4 \approx 0.75$. For $M_4 \geq 1.0$, negative values of SNR were found behind the coolant hole for both hole spacings. Contrary to the pattern established for injection at 22.9° and 40.8° , the smaller hole spacing ($S/d_0 = 5$) maintained a higher SNR value than for $S/d_0 = 10$ when higher blowing ratios were used.

The results downstream are presented in Figure 59 for $(x/d_0)_4 = 3.5$, $S/d_0 = 5$ and in Figure 60 for $(x/d_0)_4 = 6.5$, $S/d_0 = 10$. To expedite the experiment, the data for $S/d_0 = 10$ were obtained with blowing from a single row at $\theta_4 = 58.7^\circ$ with a row of non-blowing holes located at $\theta_2 = 22.9^\circ$. The influence of upstream non-blowing holes was found to be negligible (see Section III.D). This cylinder configuration resulted in heat flux data at $(x/d_0)_4 = 1.5$ and 6.5 only for $S/d_0 = 10$ (see Figure 24). The data for $S/d_0 = 5$ show slightly diminished values of SNR as $(x/d_0)_4$ increased. For $M_4 \geq 1.0$, large values of SNR_{NEG} were observed behind the hole.

Figures 61 and 62 present the spanwise averaged results for $\theta_4 = 58.7^\circ$, for $S/d_0 = 5$ and 10 , respectively. The heat flux data extend only to $(x/d_0)_4 = 8.5$ at this injection site because measurements

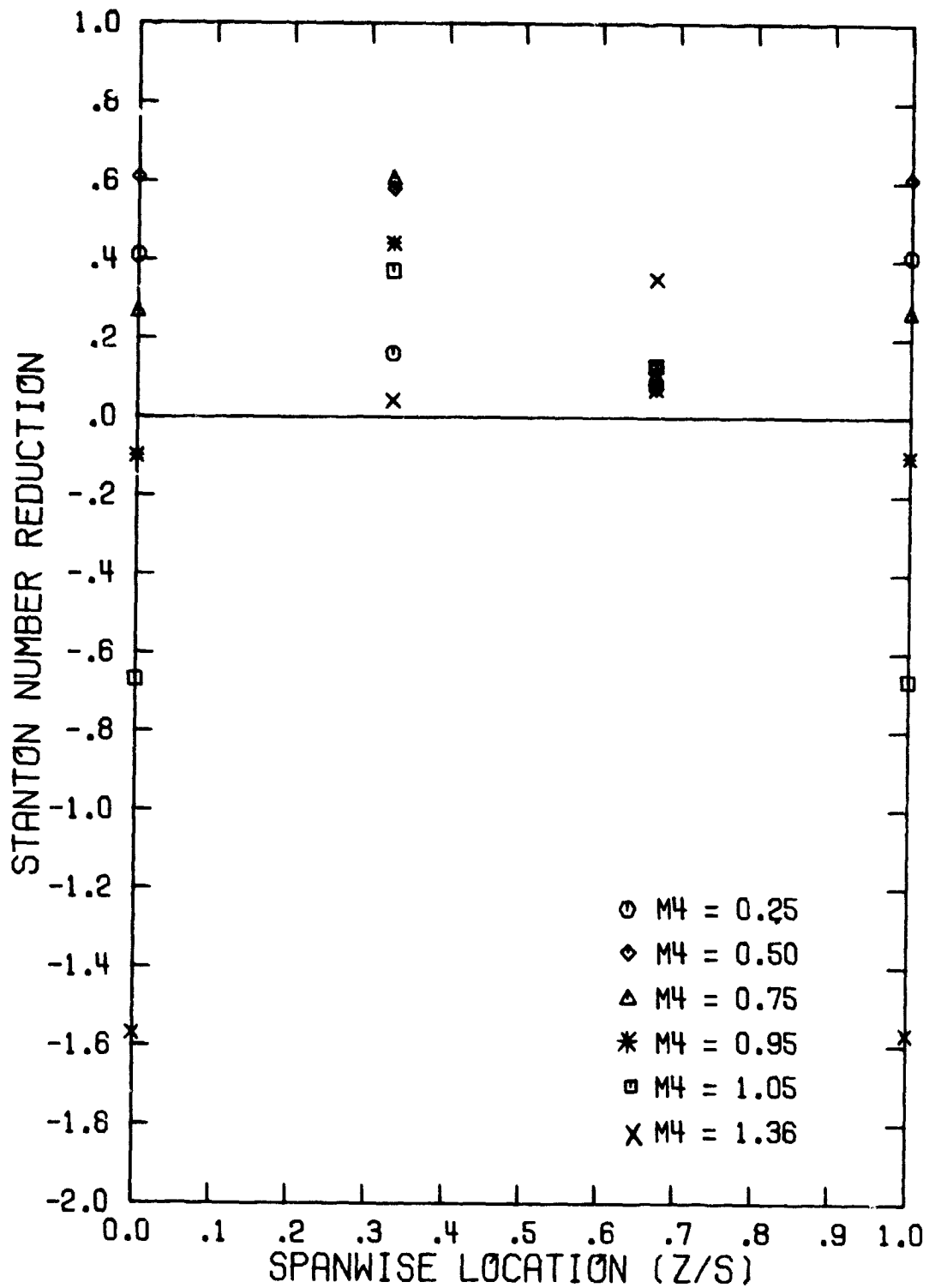


Figure 57. Spanwise Variation of the Stanton Number Reduction with Single Row Injection ($\theta_4 = 58.7^\circ$, $(x/d_0)_4 = 1.5$, $S/d_0 = 5$)

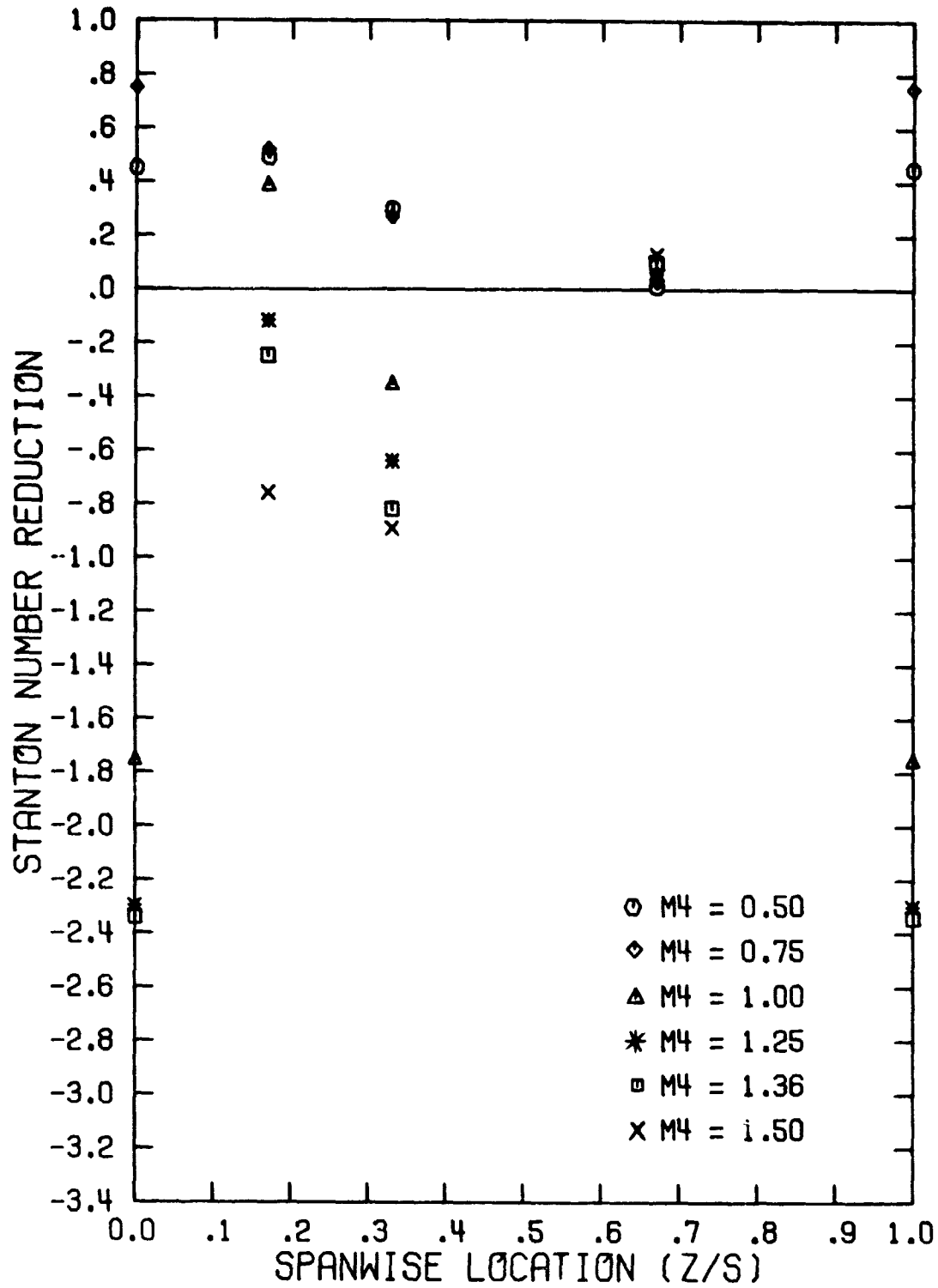


Figure 58. Spanwise Variation of the Stanton Number Reduction with Single Row Injection ($\theta_4 = 58.7^\circ$, $(x/d_0)_4 = 1.5$, $S/d_0 = 10$)

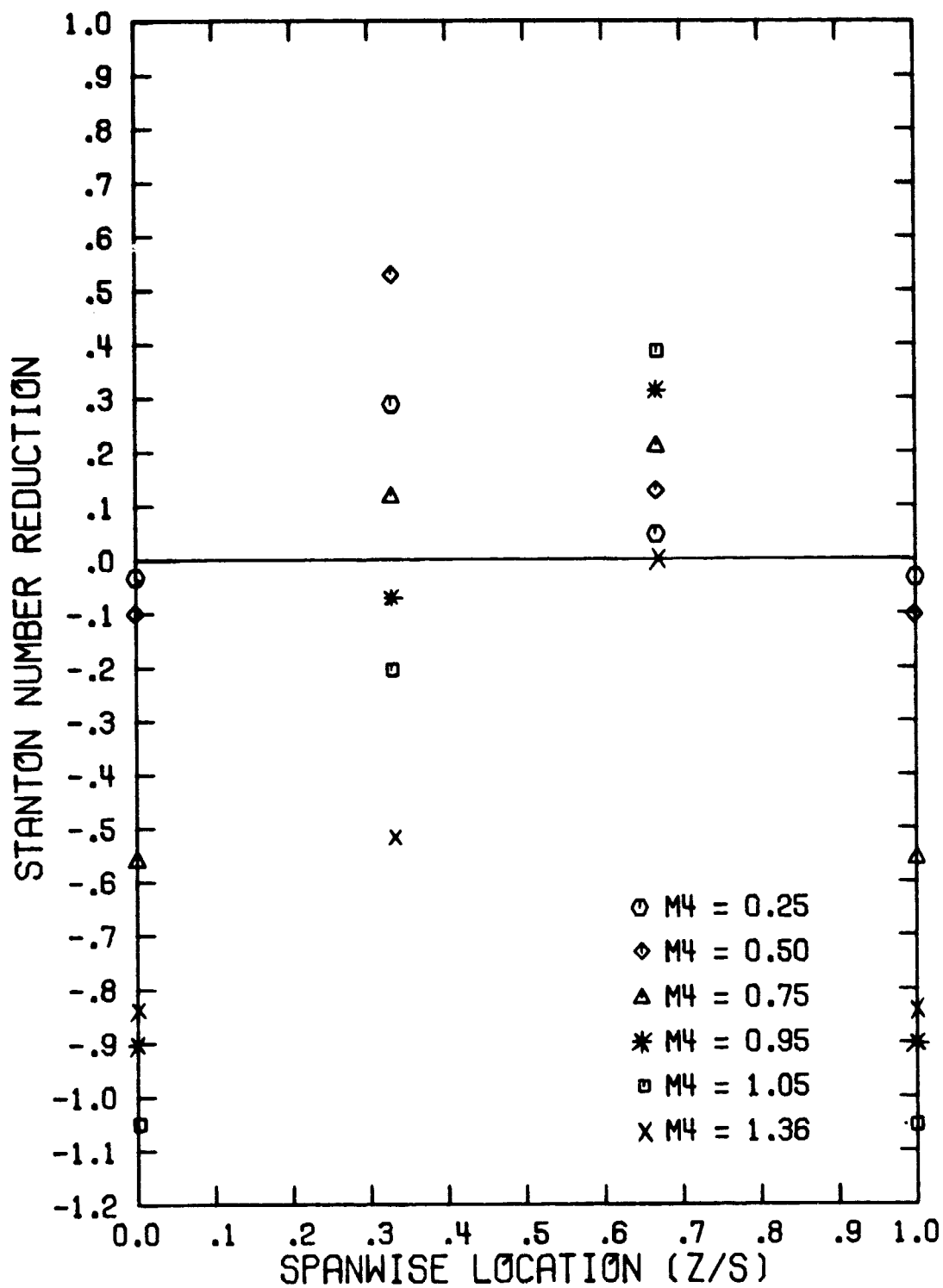


Figure 59. Spanwise Variation of the Stanton Number Reduction with Single Row Injection ($\theta_4 = 58.7^\circ$, $(x/d_0)_4 = 3.5$, $S/d_0 = 5$)

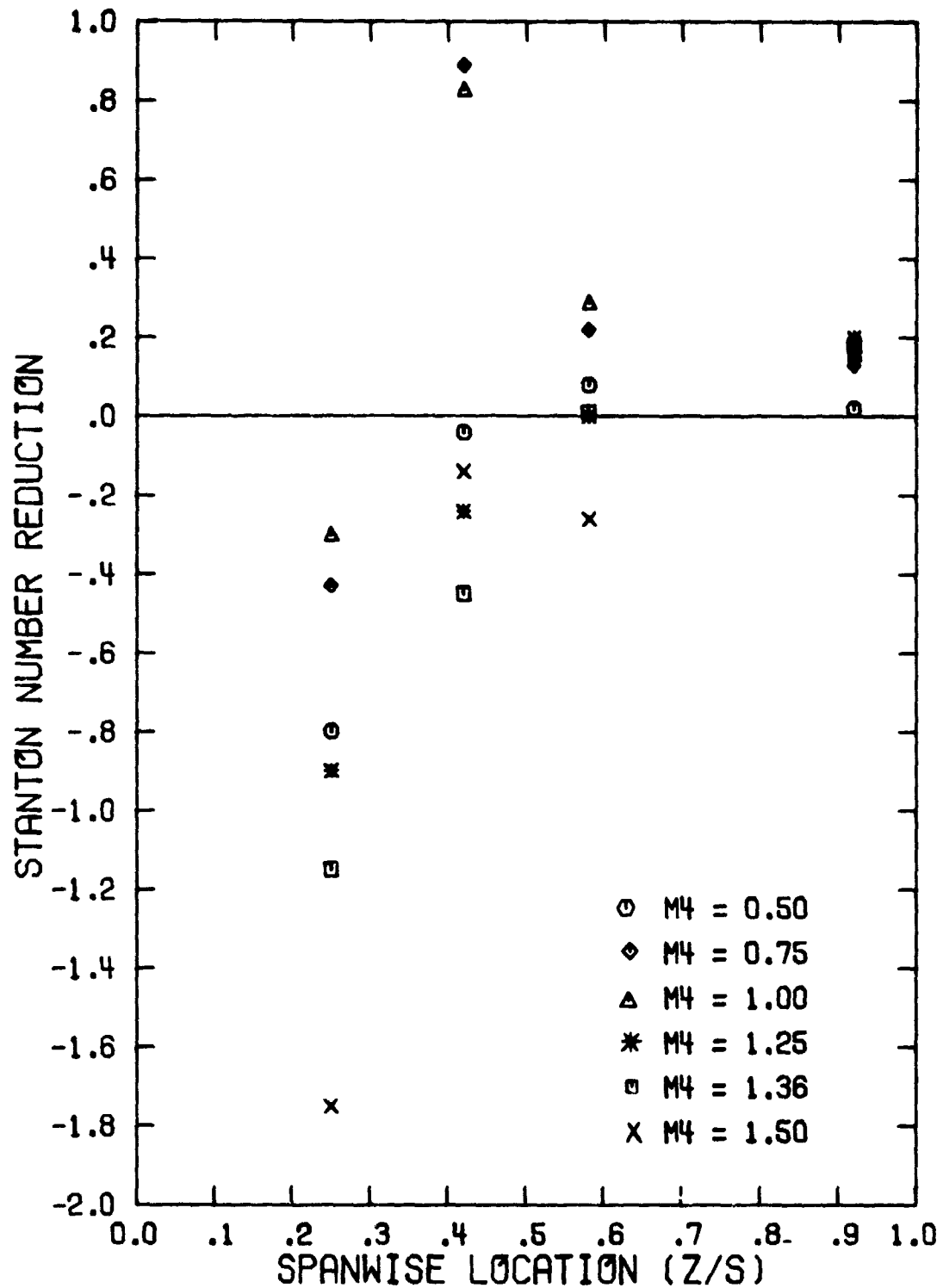


Figure 60. Spanwise Variation of the Stanton Number Reduction with Single Row Injection ($\theta_4 = 58.7^\circ$, $(x/d_0)_4 = 6.5$, $s/d_0 = 10$)

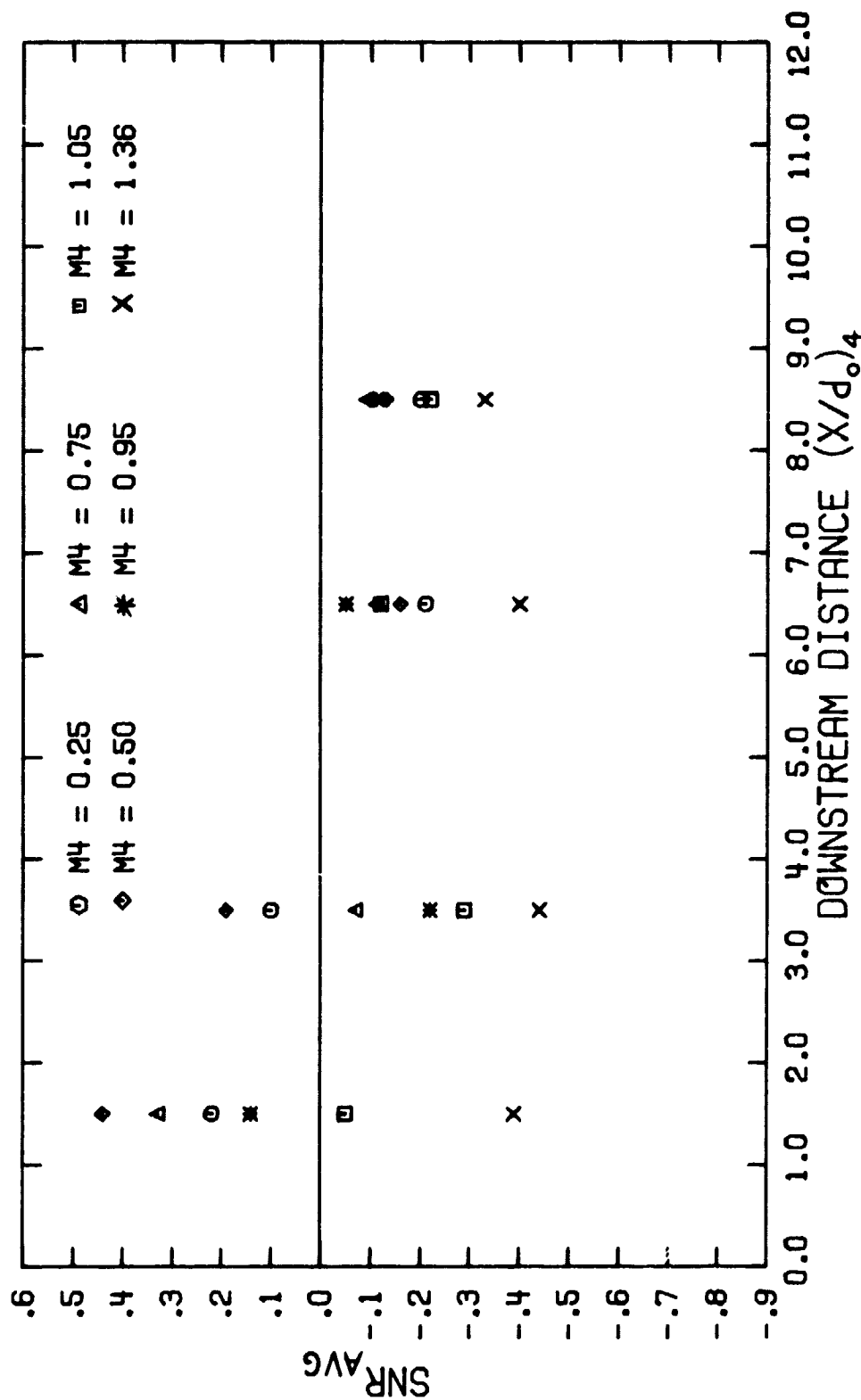


Figure 61. Variation of the Spanwise Averaged Stanton Number Reduction with Downstream Distance for Single Row Injection ($\theta_4 = 58.7^\circ$, $S/d_o = 5$)

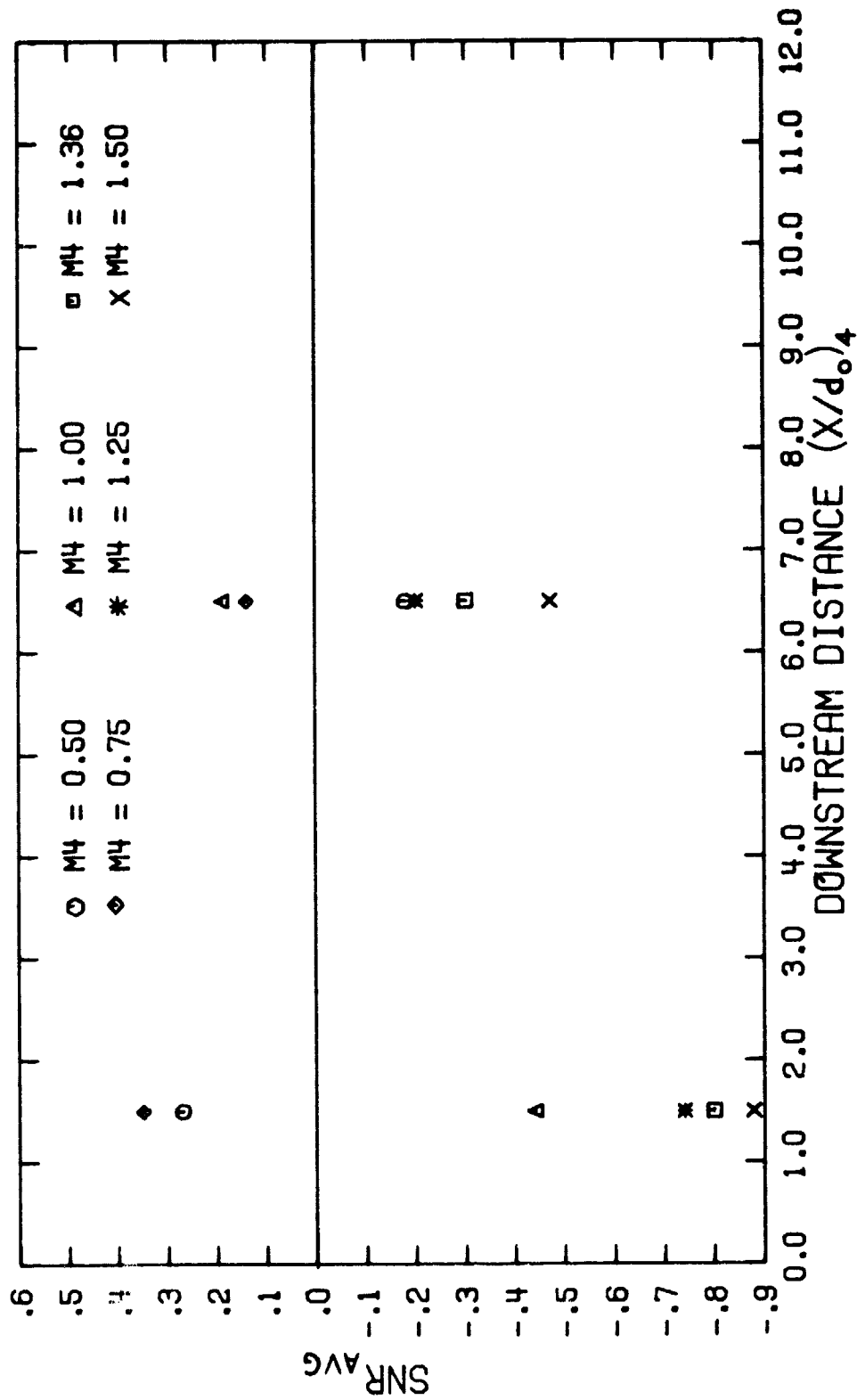


Figure 62. Variation of the Spanwise Averaged Stanton Number Reduction with Downstream Distance for Single Row Injection ($\theta_4 = 58.7^\circ$, $S/d_o = 10$)

beyond 90° from the stagnation line were not considered.

The optimum film cooling performance occurred at $M_4 \approx 0.50$ for $S/d_0 = 5$, and at $M_4 \approx 0.75$ for $S/d_0 = 10$. Increasing the blowing ratio beyond 1.0 resulted in negative values of SNR_{AVG} across the entire surface. With $M_4 > 1.0$ the negative values for SNR_{AVG} for $S/d_0 = 10$ exceed those for $S/d_0 = 5$, contrary to the trend observed at the upstream injection locations of 5° , 22.9° , and 40.8° .

IV.B.5. Upstream Effects for Single Row Injection

One additional observation regarding the influence of single row injection on surface heat flux was the effect of coolant injection on the surface heat flux upstream from the injection site. A review of the data in Appendix III revealed that the heat flux levels directly upstream from a coolant hole, $(x/d_0)_i = -1.5$ (and near the same spanwise location as the coolant hole) are influenced when coolant is blown from the hole. Figure 63 illustrates some typical results upstream from a single row at $\theta_3 = 40.8^\circ$. The results show that the largest upstream effect of injection occurred near the edge of the coolant hole in the same spanwise direction as that of the emerging coolant. The data show SNR values of 0.10 to 0.15 for the higher values of blowing ratio. This effect is restricted to the upstream area close to the coolant holes.

IV.C. Discussion of Results

IV.C.1. Introduction

One of the most important features observed in the data for single row injection was the highly localized influence of the coolant and the very limited spreading of the coolant over the surface. At low values of the blowing ratio, the coolant was turned quickly in the streamwise direction so that the cooling effectiveness was largest directly behind the hole. As the blowing ratio was increased, the coolant moved somewhat in the spanwise direction and large negative values of SNR (i.e. increased heat flux level) were observed directly behind the coolant hole.

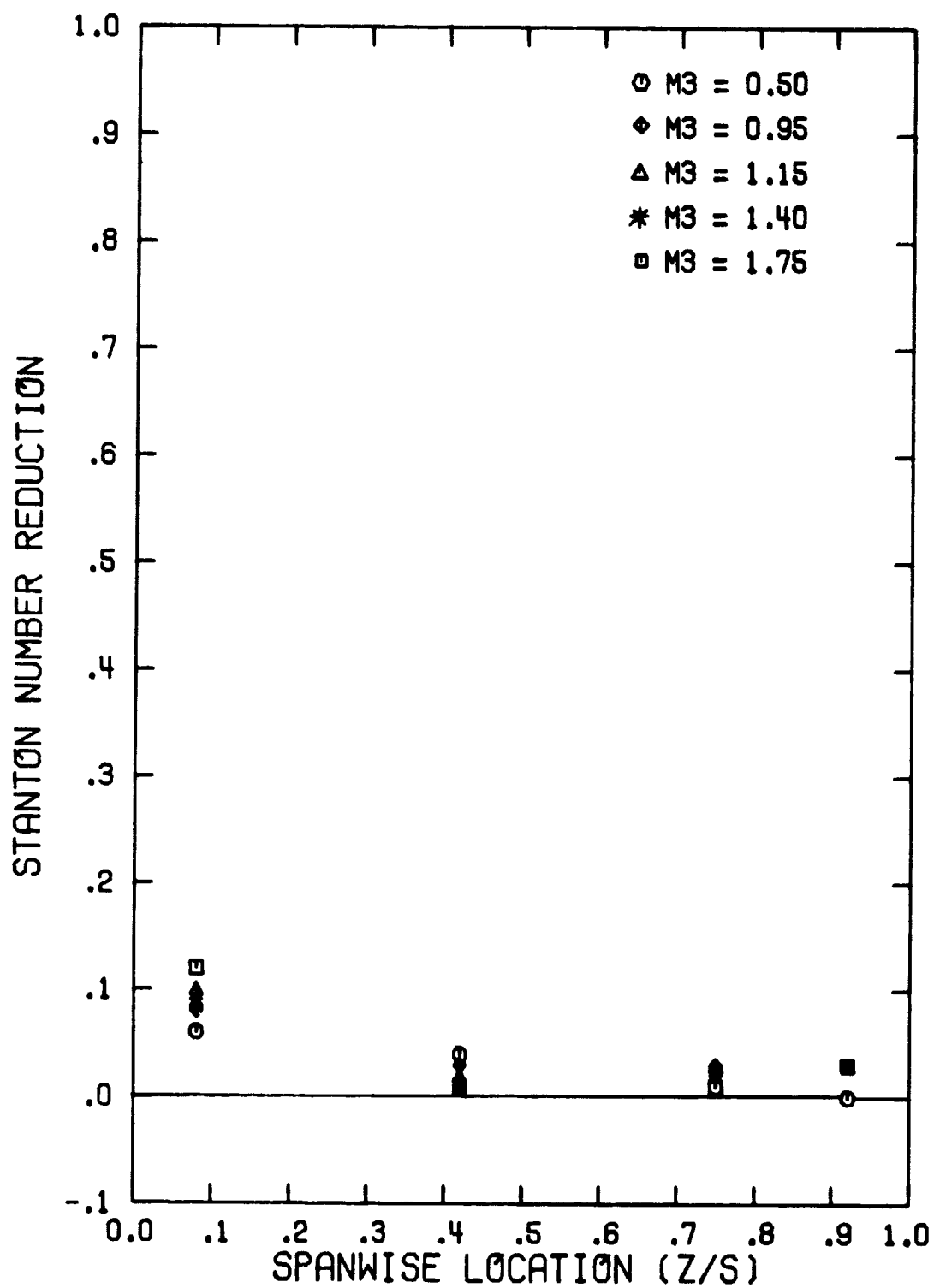


Figure 63. Spanwise Variation of the Stanton Number Reduction with Single Row Injection ($\theta_3 = 40.8^\circ$, $(x/d_0)_3 = -1.5$, $S/d_0 = 10$)

In flow visualization studies of both compound and spanwise injection along a flat plate, Russell [19] observed the development of a vortex downstream of the coolant hole. The compound injection angle produced a smooth, tightly wound vortex, while for spanwise injection the vortex was less smooth, more loosely wound and more erratic. In similar flow visualization experiments for spanwise injection from a single row of holes on a cylinder, Russell [10] found that the injected coolant was turned almost immediately in the streamwise direction with no observable change in the width (i.e. no spreading) of the coolant jet from the injection point to about 80° from stagnation. It can be expected that the development of this complex flow pattern around the coolant jet has an important effect on the effectiveness of the coolant in reducing the heat flux along the surface. The limited amount of coolant spreading and the large heat flux levels observed behind the coolant holes are, no doubt, influenced by this complex flow pattern.

In any discussion of film cooling results, a parameter of particular interest is the local blowing ratio, M , defined as the ratio of the coolant mass flux to the local freestream mass flux. With a flat plate configuration, the freestream velocity remains constant along the surface and the blowing ratio is an indication of the amount of coolant being blown from each row of coolant holes. However, in the subject investigation the local freestream velocity around the test cylinder surface varied with the position from stagnation, θ . An alternate definition of the blowing ratio can be based on the free-stream velocity approaching the test cylinder, thus

$$M_{\infty,0} = \frac{\rho_c V_c}{\rho_{\infty,0} V_{\infty,0}} \quad (25)$$

Then $M_{\infty,0}$ for a given row of holes will vary with the amount of coolant blown from the row. In the following discussion of results, values are quoted for both of these blowing parameters to illustrate their utility in correlating the results.

IV.C.2. Coolant Jet Behavior

An examination of the film cooling data in Appendix III revealed two features that were used to characterize the behavior of the coolant jet. The first was the occurrence of negative values of SNR (i.e. increased heat flux) directly behind the coolant hole when the blowing ratio was increased above a certain level. The second was the identification of the location of the coolant jet trajectory indicating the region downstream between hole centerlines where the film cooling influence was the largest.

For low values of the blowing ratio, the coolant was turned quickly by the freestream and the largest values of SNR were observed directly behind the holes. As the blowing ratio was increased, the coolant jet trajectory shifted somewhat in the spanwise direction eventually resulting in large negative values of SNR behind the holes. Table 4 summarizes the blowing condition when negative values of SNR behind the holes were first observed. Results are included for the four injection locations and the two values of hole spacing studied. With the exception of the data for $\theta_2 = 22.9^\circ$, $S/d_0 = 10$, the results indicate that the value of $M_{\infty,0}$ initiating SNR_{NEG} was independent of S/d_0 and the value of $M_{\infty,0}$ increased as θ_i increased. Moving the injection location farther from stagnation allowed a higher coolant velocity to be used before the SNR_{NEG} values started to occur. Once the blowing ratio was large enough to create the SNR_{NEG} values, any further increase in blowing ratio resulted in excessively large SNR_{NEG} values, with heat flux levels directly behind the coolant holes 100 to 200% greater than they were without film cooling. Moving downstream the large values of SNR_{NEG} diminished rather rapidly with the exception of injection at $\theta_4 = 58.7^\circ$.

The data for $\theta_2 = 22.9^\circ$, $S/d_0 = 10$ exhibited a peculiar trend at $(x/d_0)_2 = 1.5$ with SNR_{NEG} only occurring when $M_2 \approx 2.4$. However, the data for $(x/d_0)_2 = 3.5$ were consistent with the trends shown in Table 4.

The trajectory of the coolant jet plays a significant role in determining the heat flux distribution between the coolant holes. At low values of the blowing ratio when the coolant was turned quickly in

Table 4. Blowing Ratio that Initiated Negative SNR
Behind the Coolant Hole at $(x/d_0)_1=1.5$

M				
	$\theta_1=5^\circ$	$\theta_2=22.9^\circ$	$\theta_3=40.8^\circ$	$\theta_4=58.7^\circ$
$S/d_0=5$	2.0	1.10	0.77	0.95
$S/d_0=10$	2.0	2.41*	0.95	1.00

$M_{\infty,0}$				
	$\theta_1=5^\circ$	$\theta_2=22.9^\circ$	$\theta_3=40.8^\circ$	$\theta_4=58.7^\circ$
$S/d_0=5$.38	.94	1.11	1.78
$S/d_0=10$.38	2.05*	1.36	1.88

*Although the negative values of SNR were delayed at $(x/d_0)_2=1.5$ they occurred at $M=0.77$ and $M_{\infty,0}=0.65$ for $(x/d_0)_2=3.5$.

the streamwise direction, the jet trajectory passed downstream directly behind the coolant hole. As the blowing ratio was increased, the jet trajectory was shifted somewhat in the spanwise direction. The data from this investigation showed that the trajectory reached its maximum spanwise location for $(x/d_o)_i \geq 6.5$. Beyond this downstream distance, the coolant continued downstream at approximately the same spanwise location.

The coolant jet trajectory was determined at $(x/d_o)_i = 6.5$ where the maximum spanwise location was established. The data in Appendix III were examined to determine the z/S location where the measured SNR value was a maximum. If two adjacent measurement points had approximately the same value of SNR, the location midway between them was chosen. The results are presented in Table 5 in terms of $z/d_o = (z/S) \cdot (S/d_o)$, which is a physical distance in the spanwise direction independent of hole spacing. The results in Table 5 indicate a general increase in the trajectory z/d_o as the blowing ratio is increased. Larger values of the blowing ratio provide more spanwise momentum for the coolant jet, and as a result, the jet moves farther in the spanwise direction. The results for $S/d_o = 10$ indicate that the trajectory z/d_o approached the midpoint between the holes for $\theta_i = 5^\circ$, 22.9° , and 40.8° . The results for $S/d_o = 5$ show similar trends for $\theta_i = 5^\circ$ and 22.9° . However, as the distance from stagnation was increased, the trajectory z/d_o approached the next coolant hole.

IV.C.3. Film Cooling Effectiveness

Although the cooling effect for single row injection was very localized, a significant reduction in heat flux was observed on some areas of the surface. Behind the holes large negative values of SNR may have occurred, while at the same time a few diameters outward in the spanwise direction the coolant was providing a 50 to 70% reduction in the heat flux to the surface. Concentrating on the region where the coolant was most effective, the data showed the Stanton Number Reduction increased as the blowing ratio was increased until optimum blowing condition was observed. The blowing ratio where the highest

Table 5. Spanwise Location of the Coolant Jet Trajectory $(x/d_0)_1=6.5$

Value of z/d_0 at $\theta_1=5^\circ$

$M=1.0$ 2.0 4.0 5.85
 $M_{\infty,0}=0.19$ 0.38 0.76 1.11

$S/d_0=10$	2.5	2.5	2.5	4.2
$S/d_0=5$	0.9	1.65	2.5	—*

Value of z/d_0 at $\theta_2=22.9^\circ$

$M=0.5$ 1.0 1.3 2.0
 $M_{\infty,0}=0.43$ 0.86 1.1 1.7

$S/d_0=10$	2.5	2.5	2.5	4.2
$S/d_0=5$	0.9	2.5	2.5	2.5

Value of z/d_0 at $\theta_3=40.8^\circ$

$M=0.5$ 0.75 0.90 1.20
 $M_{\infty,0}=0.72$ 1.08 1.29 1.72

$S/d_0=10$	2.5	4.2	4.2	4.2
$S/d_0=5$	2.5	2.5	4.2	4.2

Value of z/d_0 at $\theta_4=58.7^\circ$

$M=0.5$ 0.75 1.0 1.20
 $M_{\infty,0}=0.94$ 1.41 1.88 2.25

$S/d_0=10$	5.8	4.2	4.2	9.2
$S/d_0=5$	2.5	2.5	4.2	4.2

*There was no positive value for SNR.

level of SNR was found was defined as the optimum blowing condition, M_{opt} . Increasing M past M_{opt} resulted in a decrease in the value of SNR. The results in Appendix III were used to determine M_{opt} for the different injection locations and hole spacings studied. The data for SNR vs z/S at $(x/d_o)_i = 1.5$ were examined to determine the value of SNR_{MAX} for each particular blowing ratio. Recall, the SNR_{MAX} value was obtained from the measured heat flux values only. No attempt was made to curve fit and interpolate between heat flux gages. The values of SNR_{MAX} vs M were examined to determine the optimum blowing condition. If two values of M had similar values of SNR_{MAX} , an examination of the SNR vs z/S distributions at these blowing ratios was made. If one blowing ratio had significantly higher values of SNR, it was chosen as M_{opt} . If there was no clear distinction between the distributions, M_{opt} was taken as the average of the two values of M . As a consequence, the values for M_{opt} were selected only from the experimentally measured values of M in this investigation. No attempt was made to interpolate between the measured values of SNR_{MAX} vs M to determine the exact optimum condition. The results are shown in Table 6 with the optimum blowing condition given in terms of the local M and $M_{\infty,0}$ based on approach velocity.

The data for $\theta_i = 5^\circ, 22.9^\circ$, and 40.8° show a continual decrease in M_{opt} as the injection location was increased with no effect of the hole spacing ratio. Use of the approach velocity to define the blowing ratio shows that $(M_{\infty,0})_{opt}$ was approximately constant for $\theta_i = 5^\circ, 22.9^\circ$, and 40.8° , particularly for $S/d_o = 10$. The data for $\theta_4 = 58.7^\circ$ do not follow the trend observed for the three other injection locations. Instead, a larger value of M_{opt} and $(M_{\infty,0})_{opt}$ was observed. This may be due to the proximity of the injection location to the region where boundary layer separation and/or transition effects become important. Table 6 also contains data from flow visualization studies by Russell [10] showing the relationship between the coolant jet separation phenomena and the injection location. At a particular blowing ratio, the coolant jet was observed to separate from the surface and penetrate into the freestream. The blowing ratio

Table 6. Optimum Coolant Blowing Conditions and Jet Separation

 M_{opt} for SNR_{MAX} at $(x/d_o)_i=1.5$ $\theta_1=5^\circ$ $\theta_2=22.9^\circ$ $\theta_3=40.8^\circ$ $\theta_4=58.7^\circ$

$S/d_o=10$	3.5	0.77	0.50	0.75
$S/d_o=5$	3.5	0.50	0.38	0.50

 $(M_{\infty,o})_{opt}$ for SNR_{MAX} at $(x/d_o)_i=1.5$ $\theta_1=5^\circ$ $\theta_2=22.9^\circ$ $\theta_3=40.8^\circ$ $\theta_4=58.7^\circ$

$S/d_o=10$	0.67	0.66	0.72	1.41
$S/d_o=5$	0.67	0.45	0.54	0.94

Blowing Ratio Initiating Jet Separation, Russell [10]

	$\theta=30^\circ$	$\theta=45^\circ$	$\theta=60^\circ$
M	1.18	.86	.70
$M_{\infty,o}$	1.18	1.22	1.21

for jet separation is given in terms of local M and $M_{\infty,0}$ based on the approach velocity. Russell's data show that the M for separation decreased as the injection location increased, while the $M_{\infty,0}$ for separation was essentially constant. These trends are in good agreement with those observed for the optimum blowing condition in the present investigation.

The data in Appendix III also were examined to determine the magnitude of the Stanton Number Reduction as a function of blowing ratio, injection location, and hole spacing. Table 7 summarizes the results for SNR_{MAX} at $(x/d_0)_i = 1.5$ for the four injection locations and the two different hole spacings studied. The data for $\theta_i = 5^\circ, 22.9^\circ$, and 40.8° show that for $M > M_{opt}$ (see Table 6), the values of SNR_{MAX} for $S/d_0 = 10$ were substantially larger than the values for $S/d_0 = 5$. For $M < M_{opt}$, the values of SNR_{MAX} for $S/d_0 = 10$ and 5 were essentially the same for $\theta_i = 22.9^\circ$ and 40.8° . Closer to stagnation ($\theta_i = 5^\circ$) the value of SNR_{MAX} for $S/d_0 = 10$ was always greater than for $S/d_0 = 5$. The data for $\theta_i = 5^\circ, 22.9^\circ$, and 40.8° also indicate a relatively small decrease in SNR_{MAX} for $S/d_0 = 10$ as M was increased while the value of SNR_{MAX} for $S/d_0 = 5$ showed a significant decrease with increasing M .

The data for $\theta_4 = 58.7^\circ$ show, for $M \leq M_{opt}$, little difference between the values of SNR_{MAX} for $S/d_0 = 10$ and 5. However, for $M > M_{opt}$ there was a difference and, contrary to the trend for the other three injection locations, the $S/d_0 = 5$ yielded significantly larger values of SNR_{MAX} .

IV.C.4. Spanwise Averaged Film Cooling Results

The spanwise averaging of the film cooling performance tends to smear out the local characteristics of the Stanton Number Reduction across the surface. A low value of SNR_{AVG} could be the result of a high negative value of SNR behind the hole and a high positive value of SNR between the holes. At the same time, it could be the result of a fairly uniform, low value of SNR across the surface. Therefore, the detail of the spanwise distribution of SNR is lost with spanwise

Table 7. Values of SNR_{MAX} at $(x/d_0)_i = 1.5$

$$\theta_1 = 5^\circ$$

$$\begin{array}{ccccc} M=1.0 & 2.0 & 3.0 & 4.0 & 5.73 \\ M_{\infty,0}=0.19 & 0.30 & 0.57 & 0.76 & 1.09 \end{array}$$

$S/d_0=10$.57	.39	.51 *	.50	.28
$S/d_0=5$.22	.23	.29 *	.29	.11

$$\theta_2 = 22.9^\circ$$

$$\begin{array}{ccccc} M=0.5 & 1.1 & 1.5 & 2.1 & 2.4 \\ M_{\infty,0}=0.43 & 0.94 & 1.28 & 1.79 & 2.0 \end{array}$$

$S/d_0=10$.76 *	.74	.67	.49	.47
$S/d_0=5$.70 *	.46	.38	.22	.08

$$\theta_3 = 40.8^\circ$$

$$\begin{array}{ccccc} M=0.5 & 0.75 & 1.05 & 1.20 & 1.60 \\ M_{\infty,0}=0.72 & 1.08 & 1.51 & 1.72 & 2.30 \end{array}$$

$S/d_0=10$.79 *	.53	.50	.58	.54
$S/d_0=5$	* .58	.22	.30	.35	.09

$$\theta_4 = 58.7^\circ$$

$$\begin{array}{ccccc} M=0.50 & 0.75 & 1.05 & 1.36 & 1.50 \\ M_{\infty,0}=0.94 & 1.41 & 1.97 & 2.55 & 2.81 \end{array}$$

$S/d_0=10$.49	.75 *	.39	.10	.13
$S/d_0=5$.61 *	.61	.37	.35	.39

The star () indicates the values of M bracketing M_{opt} . See Table 6.

averaging. Nevertheless, spanwise averaged film cooling performance is convenient for the turbine vane designer when computing a mean wall temperature as a function of streamwise distance. The averaged performance is also a convenient method of interpreting the general influence of blowing ratio, hole spacing, and injection location.

An examination of the data in Appendix III shows that for four injection locations, the maximum value of SNR_{AVG} occurred at $(x/d_o)_i = 1.5$. Moving downstream, the value of SNR_{AVG} continually decreased in magnitude. Occasionally, a slight increase in SNR_{AVG} was found at $(x/d_o)_i = 8.5$ or 11.5 which was due to the fact that the value of SNR_{NEG} diminished faster than the values of SNR decayed.

The results for SNR_{AVG} for the hole spacing of $S/d_o = 5$ were equal to or greater than SNR_{AVG} for $S/d_o = 10$ (except for $\theta_i = 5^\circ$ at $(x/d_o)_i = 1.5$). The influence of the coolant jet was found to be very localized, so that some area between the holes is frequently unaffected by the coolant. This dead region with $SNR \approx 0.0$ was larger for $S/d_o = 10$ than for $S/d_o = 5$. When computing SNR_{AVG} , the dead region acted as a weighting factor that reduced the influence of high positive values of SNR and/or large negative values of SNR. Although the values of SNR_{AVG} for $S/d_o = 5$ were somewhat larger than those for $S/d_o = 10$, the smaller hole spacing required that twice as much coolant mass be blown onto the surface.

The data in Appendix III were examined to determine the optimum blowing ratio for the spanwise averaged film cooling performance. The optimum blowing condition, $M_{opt,AVG}$, was determined as the measured value of blowing ratio that yielded the highest value of SNR_{AVG} for all measurement locations downstream from injection. Table 8 shows the conditions in terms of local M and $M_{\infty,o}$ based on approach velocity. The results in Table 8 for $\theta_i = 5^\circ, 22.9^\circ$, and 40.8° show that $M_{opt,AVG}$ was essentially the same for $S/d_o = 10$ and 5 . The value of $M_{opt,AVG}$ decreased as the injection location (θ_i) was moved further from stagnation. Most of the values of $M_{opt,AVG}$ were smaller than the values for M_{opt} shown in Table 6. The value of $(M_{\infty,o})_{opt,AVG}$ was found generally to increase with θ_i indicating that the coolant flow required for maximum SNR_{AVG} increased as the row of holes was moved away from

Table 8. Optimum Cooling Blowing Conditions for Spanwise Averaged Film Cooling Performance

	$M_{opt,AVG}$			
	$\theta_1=5^\circ$	$\theta_2=22.9^\circ$	$\theta_3=40.8^\circ$	$\theta_4=59^\circ$
$S/d_o=10$	1.00	.50	$\leq .50^*$.75
$S/d_o=5$	1.00	.50	.25	.50

	$(M_{\infty,o})_{opt,AVG}$			
	$\theta_1=5^\circ$	$\theta_2=22.9^\circ$	$\theta_3=40.8^\circ$	$\theta_4=59^\circ$
$S/d_o=10$	0.19	0.43	$\leq 0.72^*$	1.41
$S/d_o=5$	0.19	0.43	0.36	0.94

*Data were not obtained for $S/d_o=10$ with $M=0.25$.

stagnation. With injection at $\theta_4 = 58.7^\circ$, the value of $M_{opt,AVG}$ did not follow the trend observed for the other injection locations; the value of $(M_{\infty,0})_{opt,AVG}$ did continue to increase.

At very high values of the blowing ratio, the data for a hole spacing of $S/d_0 = 5$ was found to have consistently larger negative values for SNR_{AVG} than those for $S/d_0 = 10$. This is a result of the averaging process. Even though the two values of hole spacing might have had similar magnitudes of negative SNR values across the surface, the larger area of $SNR \approx 0.0$ for $S/d_0 = 10$ makes that spanwise averaged value less negative than the value for $S/d_0 = 5$.

In conclusion, an important point factor to remember when using spanwise averaged results is that all details of the film cooling performance distribution across the surface are eliminated. The spanwise averaging process does allow a convenient comparison of the film cooling performance as a function of blowing ratio, hole spacing, and injection location. While the smaller hole spacing was found to have higher SNR_{AVG} values, the coolant flow required was twice that for $S/d_0 = 10$.

IV.D. Summary

The study of single row injection was conducted to provide an understanding of the film cooling performance for different injection locations and different hole spacings. One of the most significant features of the study was the highly localized nature of the coolant jet as it passed over the surface. The lack of spreading by the coolant agreed with the flow visualization studies of Russell [10]. Of equal importance in the present study was the measurement of increased heat flux levels behind the coolant hole when the jet began to move outward in the spanwise direction. The blowing ratio (based on upstream freestream velocity) that initiated the negative values of SNR behind the hole was found to increase in magnitude as the injection location was moved away from stagnation. This coolant jet behavior resulted in large negative values of SNR behind the hole with positive values of SNR between the holes.

The optimum coolant blowing condition yielding the largest local SNR was found to be independent of S/d_o and to be correlated in terms of the blowing parameter based on approach velocity, $(M_{\infty,o})_{opt} \approx$ constant. These trends were in agreement with flow visualization data by Russell [10] characterizing the blowing condition for coolant jet separation from the surface.

The magnitude of the maximum local film cooling performance, SNR_{MAX} was found to vary with hole spacing ratio when $M > M_{opt}$, with SNR_{MAX} for $S/d_o = 10$ significantly larger than for $S/d_o = 5$. The spanwise averaged results showed that, for a given M , the smaller hole spacing of $S/d_o = 5$ gave generally higher values of SNR_{AVG} than those for $S/d_o = 10$. However, twice as much coolant was injected for $S/d_o = 5$, while the corresponding SNR_{AVG} values did not approach a 100% increase over the $S/d_o = 10$ results.

V. MULTIPLE ROW INJECTION WITH A UNIFORM BLOWING DISTRIBUTION

V.A. Introduction

The chapter presents the results for coolant injection from multiple rows of holes with a uniform (i.e. constant) blowing ratio, M , for all rows. Three different configurations were studied. The first consisted of 5 rows with $S/d_0 = P/d_0 = 5$ and with the first row placed at $\theta_1 = 5^\circ$. The other two configurations had $S/d_0 = P/d_0 = 10$; one with three rows of holes with the first row at $\theta_1 = 5^\circ$. The second configuration had two rows of holes with the first row at $\theta_2 = 22.9^\circ$. The value of M was varied from 0.25 to 2.00 in intervals of 0.25.

As in the previous chapter, the film cooling results are introduced in the next section and discussed only in a qualitative fashion. A complete discussion of the data is presented in the following section. A complete listing of the data for multiple row coolant injection with uniform blowing is presented in tabular and graphical form in Appendix III.

The purpose of using multiple rows of coolant holes is to improve the uniformity of the film cooling performance across the surface by allowing coolant from downstream holes to fill in the deficient areas left by coolant from upstream rows. The results for multiple row injection are presented and comparisons are made with the data from single row injection (Chapter IV).

V.B. Presentation of the Data

The data presented are split into three sections, one section for each multiple row configuration studied. Within each section, the influence of injection location, θ_i , blowing ratio, M , and streamwise (x/d_0) and spanwise (z/S) location is examined. The film cooling

performance is presented in terms of the Stanton Number Reduction and the spanwise averaged results are computed in a manner identical to that outlined in the previous chapter.

V.B.1. Five Row Configuration with First Row at $\theta_1 = 5^\circ$, $S/d_0 = P/d_0 = 5$

Figure 64 presents the film cooling performance at $(x/d_0)_1 = 1.5$ downstream from the first row of spanwise angled holes, showing SNR vs z/s for selected values of M .

Downstream from the first row in the five row configuration, the highly localized nature of the coolant jet is still evident. At low values of the blowing ratio ($M \leq 1.0$), the coolant was quickly turned in the streamwise direction and positive values of SNR were observed directly behind the coolant hole. As the blowing was increased, the coolant trajectory moved slightly in the spanwise direction. At $M = 1.50$, negative values of SNR (SNR_{NEG}) were initiated.

The maximum local value of SNR, SNR_{MAX} , was small, never exceeding 0.20 for all values of M . A comparison of these results with the data for single row injection at $\theta_1 = 5^\circ$ shows good agreement on the level of SNR and the trends for both cases. The only exception was the blowing ratio that initiated the SNR_{NEG} values. For the multiple row injection, SNR_{NEG} occurred at $M = 1.50$, while for the single row injection, SNR_{NEG} occurred at $M_1 = 2.00$.

From the study of single row injection, the optimum coolant blowing condition for $\theta_1 = 5^\circ$ was observed when $M_1 \approx 3.5$. With the multiple row configuration, there was negligible change in SNR_{MAX} for $M = 1.01, 1.51, 2.01$. The largest value of M investigated for the multiple row configuration was limited to $M \approx 2.0$ since, with all five rows having the same blowing ratio, to exceed this value for the first row would have caused excessive blowing from the other downstream rows.

The results at the downstream location, $(x/d_0)_1 = 3.5$, (see Appendix III) closely match those for single row injection. There was still no noticeable spreading of the coolant across the surface although the values of SNR diminished slightly from the level upstream at $(x/d_0)_1 = 1.5$. A review of the data for SNR in Appendix III, for five row and

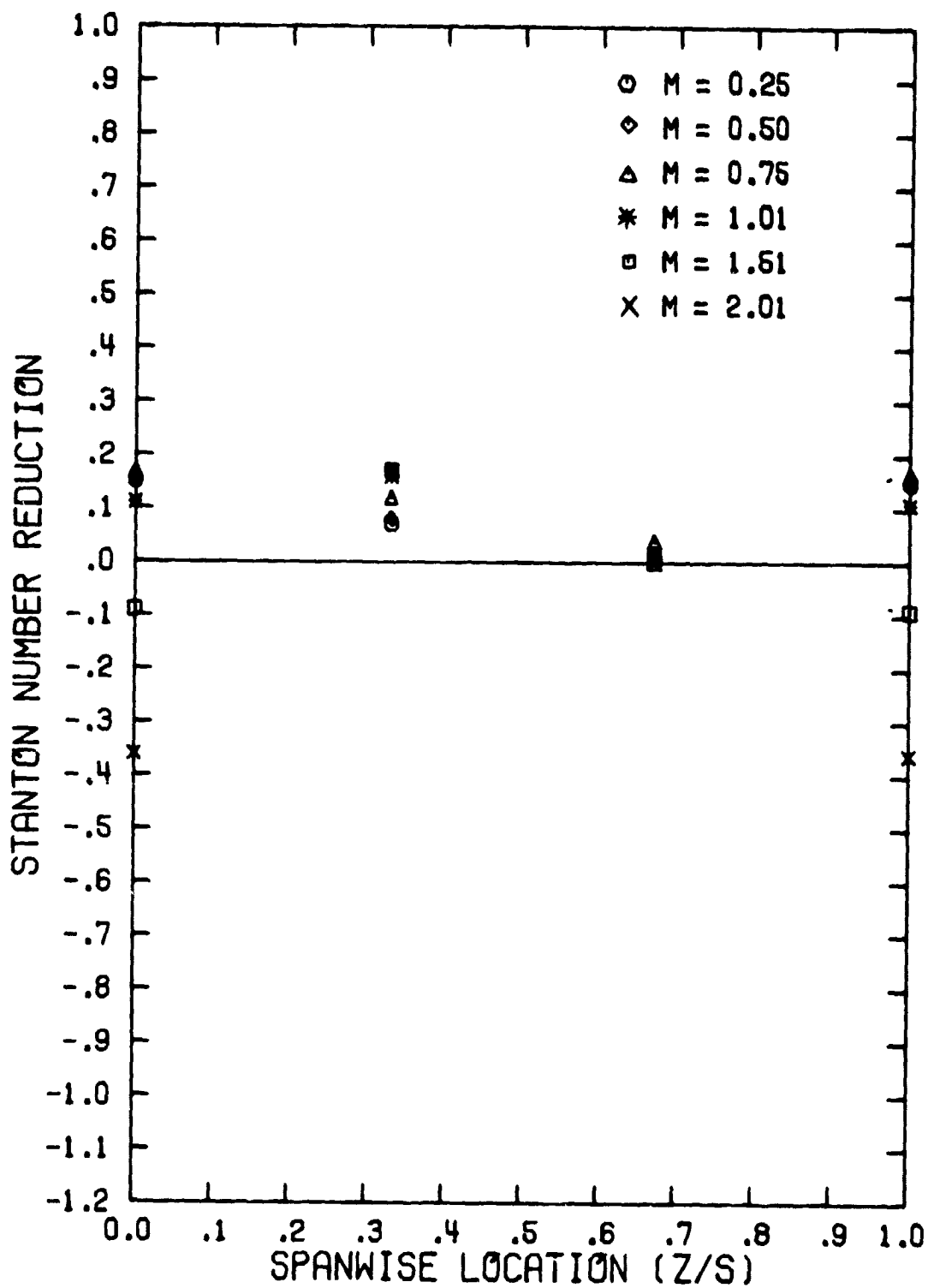


Figure 64. Spanwise Variation of the Stanton Number Reduction for a Five Row Configuration ($\theta_1 = 5^\circ$, $(x/d_0)_1 = 1.5$, $S/d_0 = P/d_0 = 5$)

single row injection, shows that the only difference for the two configurations was measured by the heat flux gage at $(x/d_o)_1 = 3.5$ and $z/S = 0.67$. That gage was positioned upstream of a coolant hole in the second row (see Figure 24). A value of $SNR \approx 0.05$ to 0.10 was observed for the five row configuration while SNR was approximately zero for the single row study. The study of single row injection showed a comparable increase in the heat flux level in the region directly in front of a hole as discussed in Chapter IV.

The spanwise averaged data for the five row configuration (see Appendix III) showed close agreement with the results for the single row at $(x/d_o)_1 = 1.5$, with $M = 1.0$, yielding $SNR_{AVG} \approx 0.10$. When the blowing ratio was increased to $M = 2.0$, the value of SNR_{AVG} for the five row configuration (-0.06) was smaller than that for single row injection (0.07).

Figure 65 presents the film cooling performance at $(x/d_o)_2 = 1.5$, downstream from the second row ($\theta_2 = 22.9^\circ$) in the five row configuration. At low values of the blowing ratio ($M \leq 0.5$), the coolant was quickly turned in the freestream direction resulting in positive values of SNR directly behind the hole. As was discovered with single row injection at θ_2 , very little spreading of the coolant was evident.

The largest value of SNR_{MAX} occurred with $M = 0.50$ compared with the value of $M_{opt} \approx 0.50$ for the single row study. As M increased, the coolant trajectory shifted in the spanwise direction. When the blowing ratio reached $M = 1.25$ (see Appendix III), negative values of SNR appeared behind the coolant hole. This blowing ratio was close to the value $M_2 \approx 1.1$ initiating SNR_{NEG} for the single row study. A comparison of the data at $(x/d_o)_2 = 1.5$ for multiple and single row injection showed the only differences occurring when $M > 1.0$, with the multiple row configuration giving larger values of SNR_{MAX} (~ 0.5) than those found with single row injection (~ 0.3). Also, the magnitude of SNR_{NEG} was smaller when the multiple row configuration was used.

The patterns developed at $(x/d_o)_2 = 1.5$ were repeated downstream at $(x/d_o)_2 = 3.5$. The magnitude of SNR was diminished, but at the same time, the magnitude of SNR_{NEG} also decreased. As was discovered upstream,

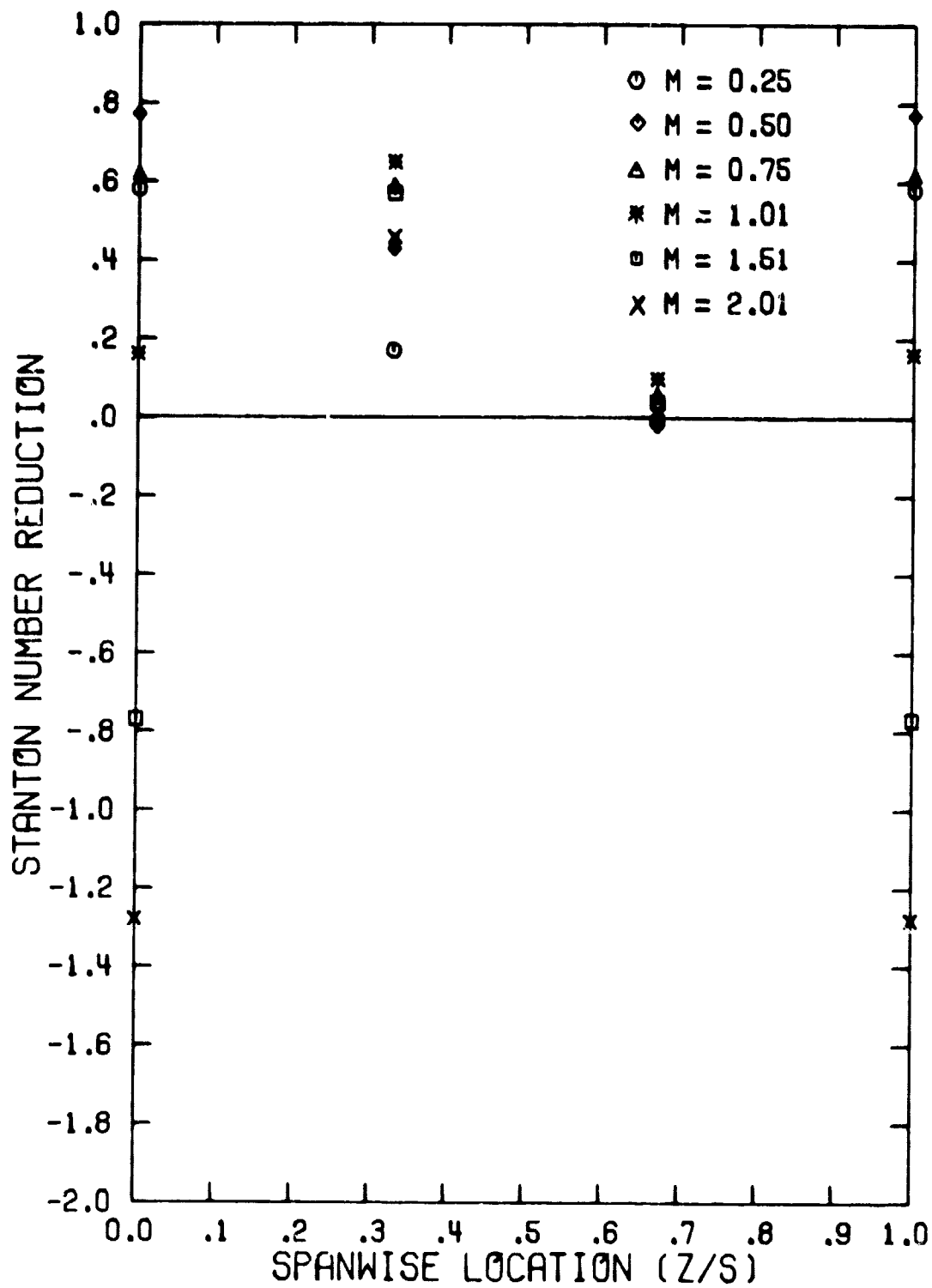


Figure 65. Spanwise Variation of the Stanton Number Reduction for a Five Row Configuration ($\theta_1 = 5^\circ$, $\theta_2 = 22.9^\circ$, $(x/d_0)_2 = 1.5$, $s/d_0 = p/d_0 = 5$)

the results at $(x/d_o)_2 = 3.5$ were in close agreement with the results for single row injection for $M \leq 1.0$. At the higher values of blowing ratio, multiple row injection maintained higher values of SNR and lower values of SNR_{NEG} than single row injection. While the magnitude of SNR for single and multiple row injection differed somewhat, the spanwise patterns established across the surface were essentially the same. One final distinction between the data for the two configurations occurred at the heat flux gage located upstream of a coolant hole in the third row (see Figure 24) yielding a positive value of SNR as a result of blowing from the hole downstream.

Figure 66 presents the data for SNR_{AVG} at $(x/d_o)_2 = 1.5$ as a function of blowing ratio for the multiple and single row configurations. As might be expected, there is close agreement between the two configurations when $M \leq 0.75$. However, when $M \geq 1.0$, multiple row injection yielded larger values than for the single row. Beyond $M = 1.5$, the value of SNR_{AVG} was negative. A similar pattern was repeated at the downstream location of $(x/d_o)_2 = 3.5$.

The film cooling performance downstream from the third row ($\theta_3 = 40.8$) is presented in Figure 67 for $(x/d_o)_3 = 1.5$. At blowing ratio, $M = 0.25$, the coolant was turned quickly by the freestream and the positive value of SNR behind the hole was similar in magnitude to that for single row injection at θ_3 . However, injection from rows θ_1 , θ_2 , and θ_3 provided more uniform film coverage across the surface when $M = 0.25$. A value of SNR of 0.27 was measured behind the third row at $(x/d_o)_3 = 1.5$, $z/S = 0.67$, while the SNR for the single row configuration at θ_3 was found to be approximately zero at $(x/d_o)_3 = 1.5$, $z/S = 0.67$.

Increasing the blowing ratio to 0.50 showed SNR_{NEG} behind the coolant hole. The occurrence of SNR_{NEG} for single row injection at θ_3 was not initiated until $M_3 = 0.75$. A comparison of the data for the five row and single row configurations, $(x/d_o)_3 = 1.5$, in the range $1.0 < M \leq 1.6$, showed the single row data with positive values of SNR on the surface. This was not the case with injection from five rows. For $M \geq 1.0$, only negative values of SNR were found across the surface. For $M \geq 1.25$, the negative values for SNR were evenly distributed across the surface.

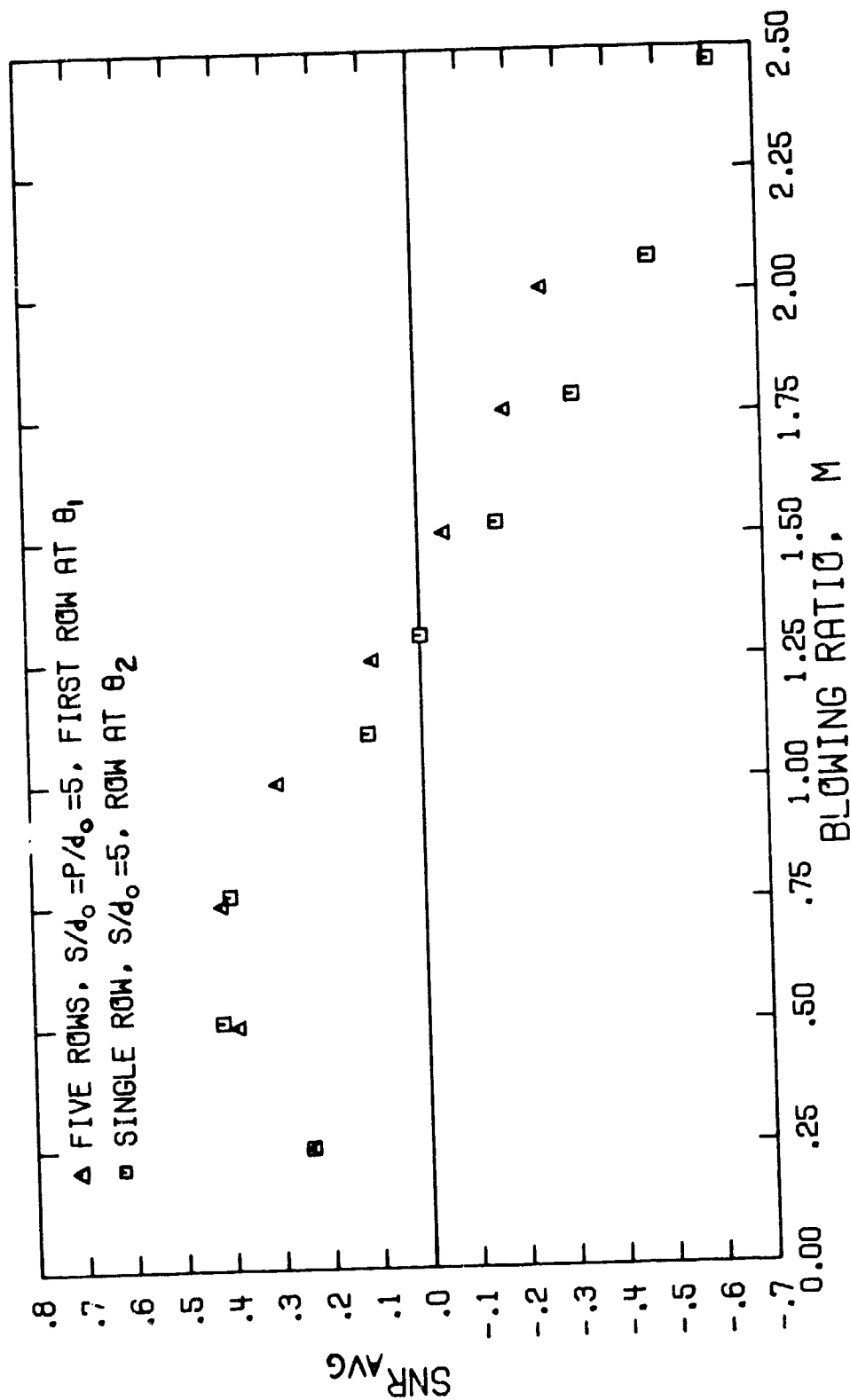


Figure 66. Variation of the Spanwise Averaged Stanton Number Reduction with Blowing Ratio for a Five Row Configuration ($\theta_1 = 5^\circ$, $\theta_2 = 22.9^\circ$, $(x/d_o)_2 = 1.5$, $S/d_o = P/d_o = 5$)

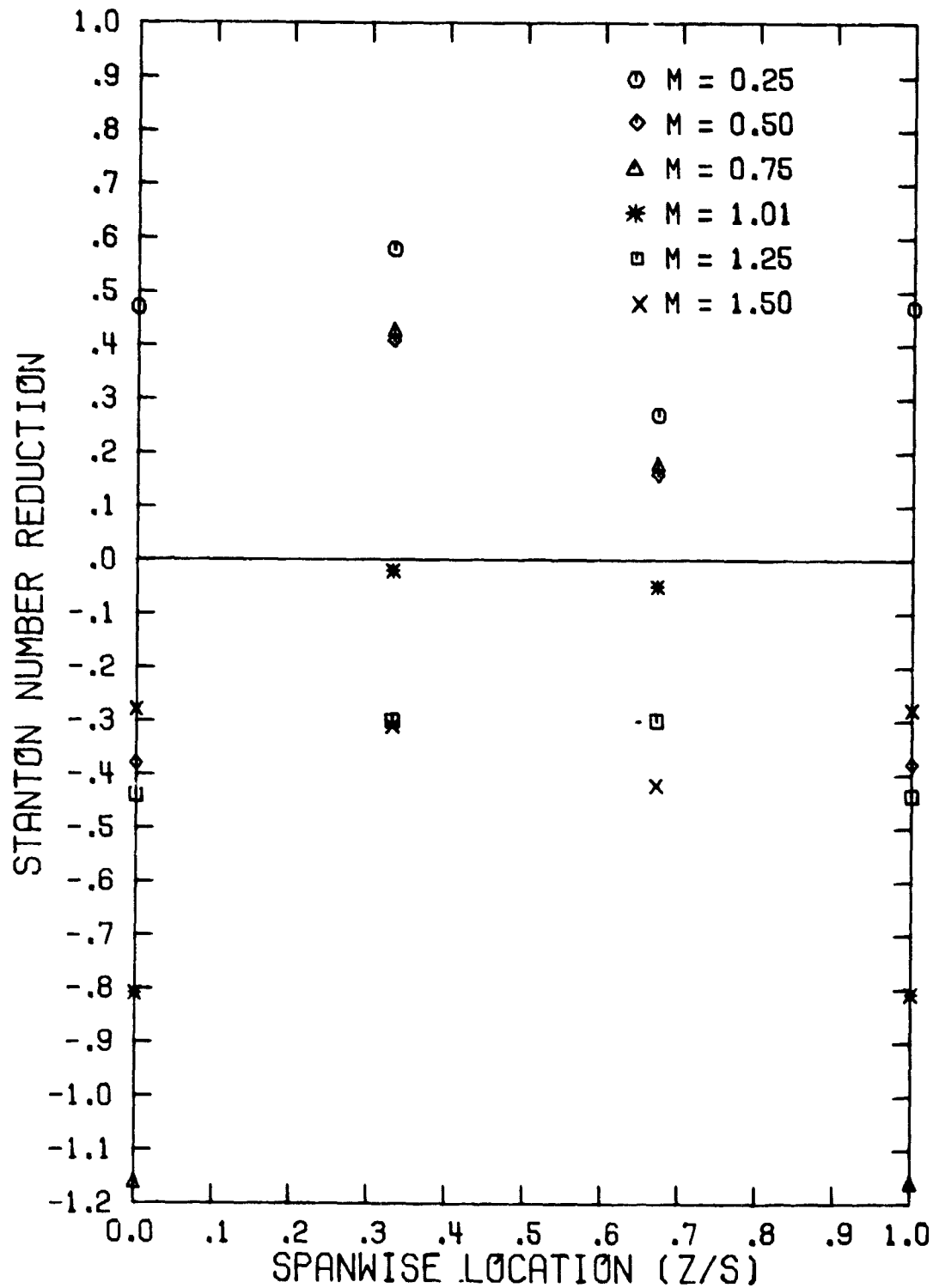


Figure 67. Spanwise Variation of the Stanton Number Reduction for a Five Row Configuration ($\theta_1 = 5^\circ$, $\theta_2 = 22.9^\circ$, $\theta_3 = 40.8^\circ$, $(x/d_0)_3 = 1.5$, $S/d_0 = P/d_0 = 5$)

The data for SNR_{AVG} at $(x/d_o)_3 = 1.5$ are shown in Figure 68 as a function of blowing ratio for the multiple and single row configurations. At the blowing ratio of 0.25, the two configurations achieved a comparable level of film cooling effectiveness, but at $M = 0.50$, data for single row injection was higher. For $M \geq 0.75$, the value for SNR_{AVG} is negative for both configurations but the data for single row injection are substantially lower.

Figure 69 presents the film cooling performance downstream of the fourth row ($\theta_4 = 58.7^\circ$) with $(x/d_o)_4 = 1.5$. For a blowing ratio, $M \leq 0.5$, the coolant was turned quickly in the streamwise direction resulting in positive values of SNR behind the coolant hole with magnitudes similar to the data for single row injection. The optimum coolant blowing condition was between 0.25 and 0.50 compared to a value of $M_{opt} \approx 0.50$ for single row injection at θ_4 .

Injection with the five row configuration previously was shown to provide good spanwise coverage downstream of the third row when $M = 0.25$. However, downstream of the fourth row, at $z/S = 0.67$, the value of SNR was approximately zero for $M = 0.25$. As the blowing ratio increased to 0.75, negative SNR was observed behind the coolant hole, and when $M \geq 1.25$, SNR was negative across the surface. A review of the data for single row injection showed SNR_{NEG} initiated at $M_4 \approx 0.95$.

The spanwise averaged results for $(x/d_o)_4 = 1.5$ showed positive values for SNR_{AVG} ($\sim .35$) occurring when $M \leq 0.50$ and negative SNR_{AVG} for larger M . The data for SNR_{AVG} for the five row configuration was superior to the single row configuration only at $M = 0.25$. For $M \geq 0.50$, the single row configuration consistently had higher SNR_{AVG} values.

The data downstream of the fifth row was limited due to a failure of one heat flux gage ($z/S = 0.67$). The data from the remaining gages (see Appendix III) show positive values of SNR behind the coolant hole for $M \leq 0.50$. As the blowing ratio was increased to $M = 0.75$, SNR_{NEG} was initiated. With $M = 1.25$, only negative values of SNR were observed for the gages that were operational. The data from the five row configuration are discussed in more detail in Section V.C.

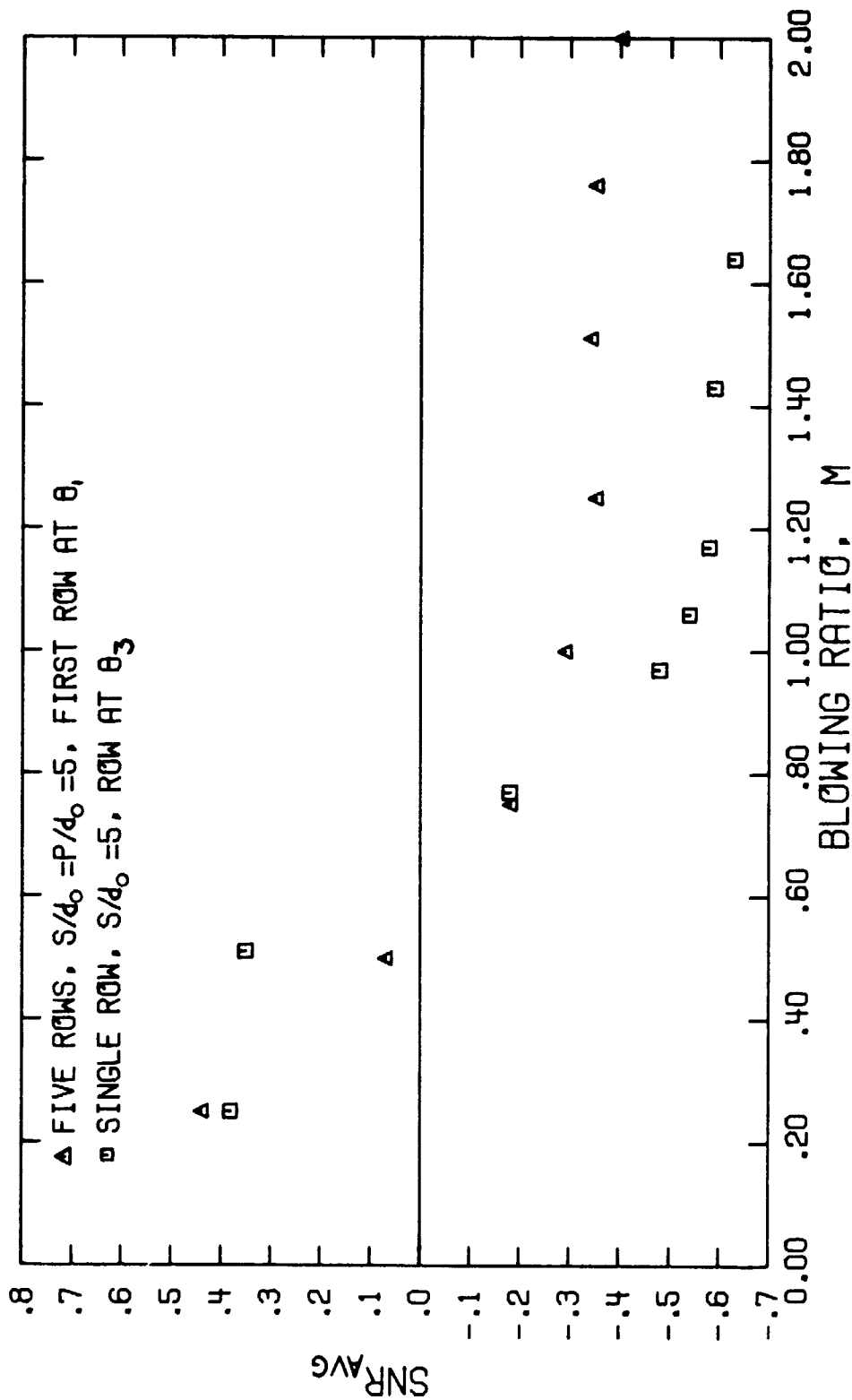


Figure 68. Variation of the Spanwise Averaged Stanton Number Reduction with Blowing Ratio for a Five Row Configuration ($\theta_1 = 5^\circ$, $\theta_2 = 22.9^\circ$, $\theta_3 = 40.8^\circ$, $(x/d_o)_3 = 1.5$, $S/d_o = P/d_o = 5$)

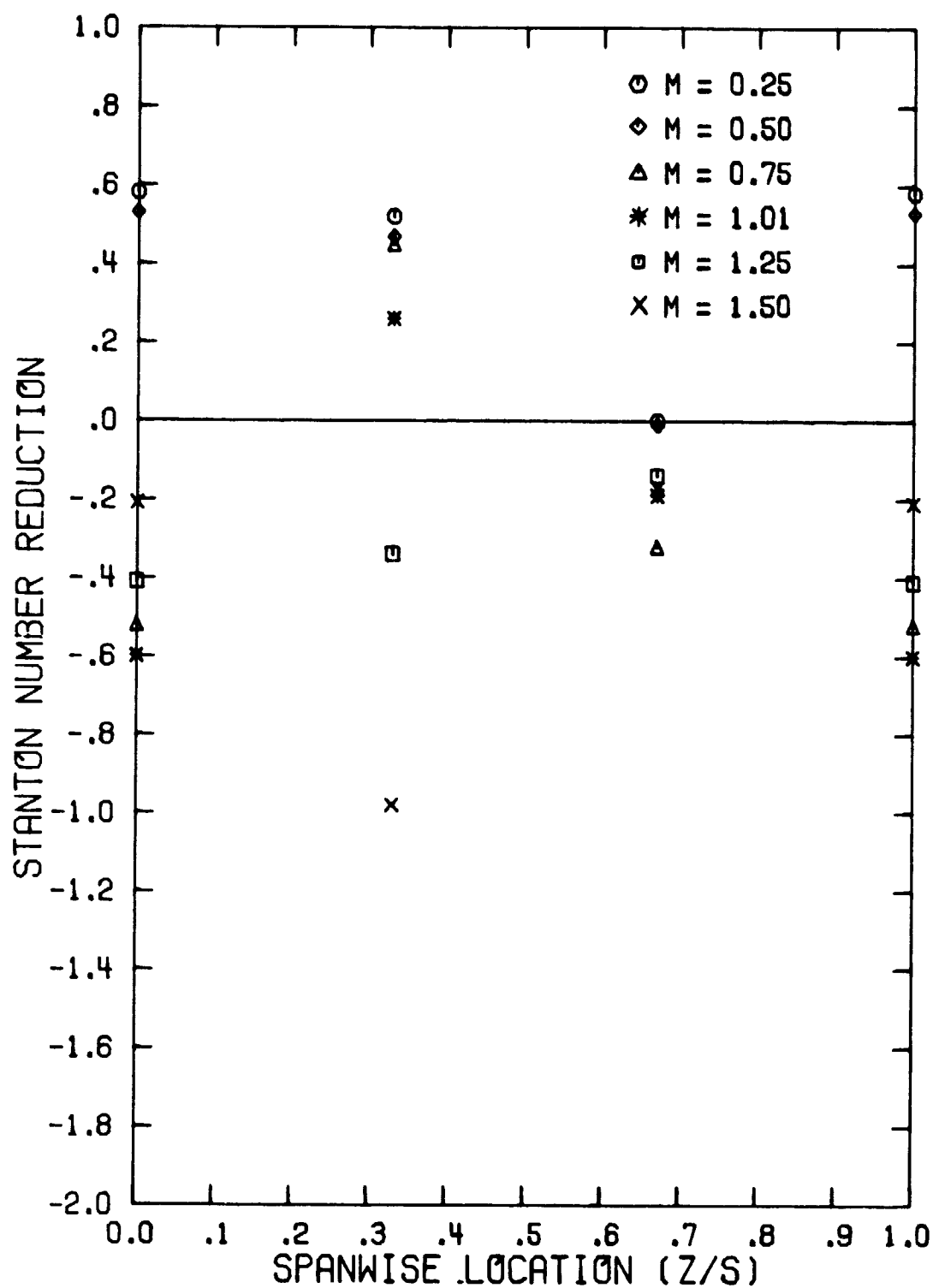


Figure 69. Spanwise Variation of the Stanton Number Reduction for a Five Row Configuration ($\theta_1=5^\circ$, $\theta_2=22.9^\circ$, $\theta_3=40.8^\circ$, $\theta_4=58.7^\circ$, $(x/d_0)_4=1.5$, $S/d_0=P/d_0=5$)

V.B.2. Three Row Configuration with First Row at $\theta_1 = 5^\circ$, $S/d_0 = P/d_0 = 10$

Figure 70 presents the film cooling performance for the three row configuration at $(x/d_0)_1 = 1.5$ downstream of the first row ($\theta_1 = 5^\circ$). For a blowing ratio, $M < 2.0$, the coolant was turned quickly in the streamwise direction resulting in positive values of SNR directly behind the coolant hole. The magnitude of the values of SNR show close agreement with the data for single row injection.

As the blowing ratio increased, the coolant trajectory shifted somewhat in the spanwise direction. The occurrence of SNR_{NEG} was initiated at $M \approx 2.5$ compared with 2.0 observed for single row injection. A comparison of the data at $(x/d_0)_1 = 1.5$ for single and multiple row injection showed the magnitude of the positive values of SNR in good agreement for all values of the blowing ratio.

Downstream from the first row at $(x/d_0)_1 = 3.5$ and 6.5^1 , the value of SNR diminished from the levels at $(x/d_0)_1 = 1.5$, but the patterns developed upstream were repeated. The results at $(x/d_0)_1 = 3.5$ and 6.5 showed good agreement with the data for single row injection. The values for SNR at $(x/d_0)_1 = 8.5$, and $z/S = 0.42$ and 0.58 , show a range from 0.05 to 0.10 for all values of the blowing ratio studied. With single row injection, the SNR values at these two spanwise locations were approximately zero. This difference results from the location of these two gages in front of a coolant hole (see Figure 24). Previous results have shown that the region in front of a coolant hole experiences a reduced heat flux when coolant is emerging from the hole.

The data for SNR_{AVG} (Appendix III) show the film cooling performance at $(x/d_0)_1 = 1.5$ to be $SNR_{AVG} \approx 0.05$ at $M = 0.25$, with SNR_{AVG} continuously increasing with M to a maximum of $SNR_{AVG} \approx 0.18$ at $M = 1.25$. Further increases in the blowing ratio resulted in a steady decrease in SNR_{AVG} to a level of 0.04 at $M = 2.5$. Moving downstream, $(x/d_0)_1 \geq 3.5$, the magnitude of SNR_{AVG} diminished to 0.06 or less for all values of M . A comparison of the values of SNR_{AVG} for the three row and single row configurations showed excellent agreement at $M = 1.0$. However, when $M \geq 2.0$, the value of SNR_{AVG} for the three row configuration (0.08) was larger than that for single row injection (0.04).

¹ See Appendix III.

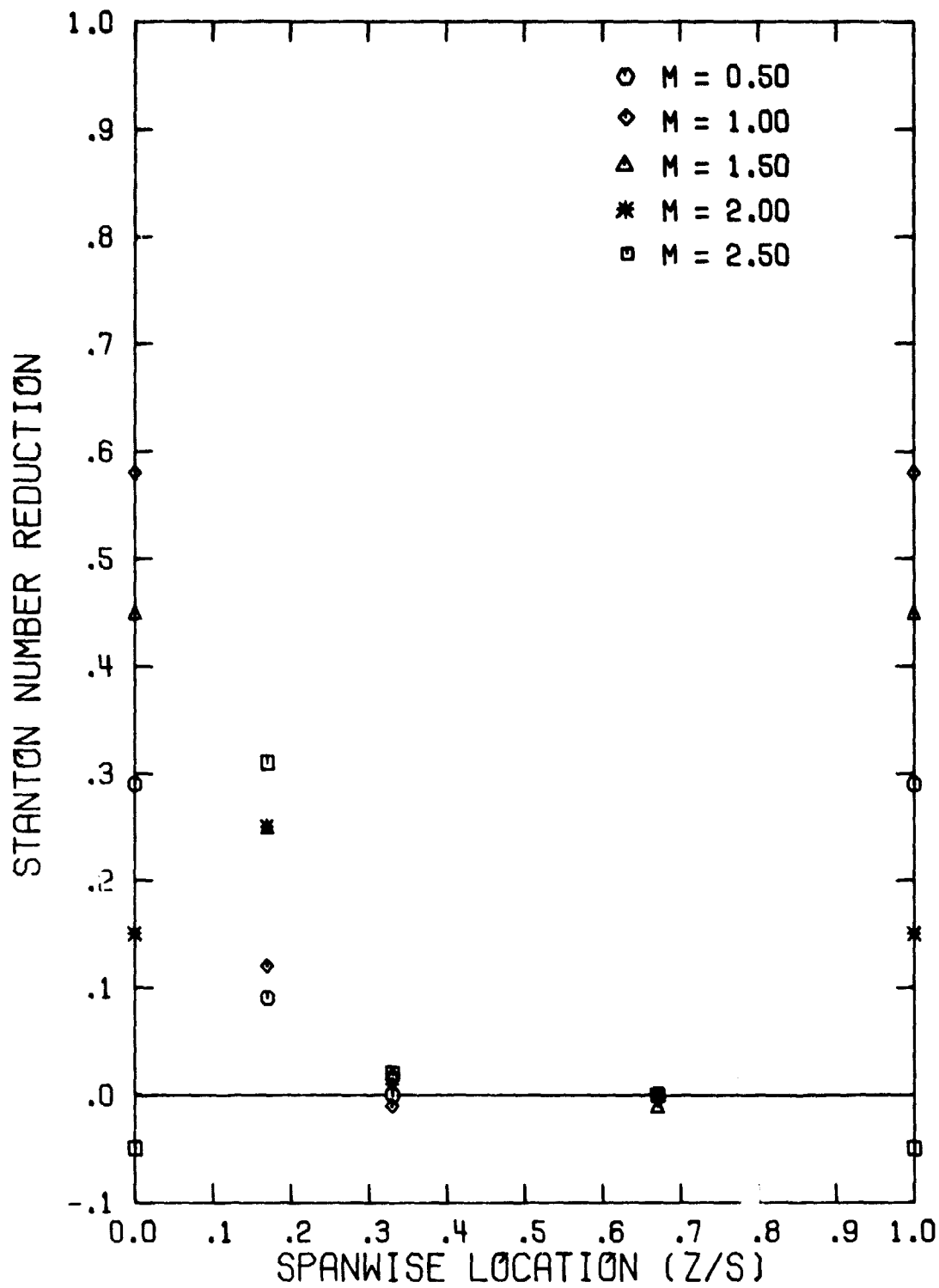


Figure 70. Spanwise Variation of the Stanton Number Reduction for a Three Row Configuration ($\theta_1 = 5^\circ$, $(x/d_0)_1 = 1.5$, $S/d_0 = P/d_0 = 10$)

The film cooling performance at $(x/d_o)_3 = 1.5$ behind the second row ($\theta_3 = 40.8^\circ$) is presented in Figure 71. For values of $M \leq 0.75$, high levels of SNR were observed behind the hole. A comparison of the data for the three row and single row injection shows similar results for $M \leq 0.75$, although the positive values of SNR for the three row configuration are slightly larger. Both configurations indicate a $M_{opt} \approx 0.5$.

As the blowing ratio was increased, the coolant trajectory shifted in the spanwise direction. When M reached a level of 1.0, SNR_{NEG} was initiated, in close agreement with the data for single row injection. A comparison of the data for the three row and single row configurations showed the values of SNR_{NEG} and SNR_{MAX}^1 in good agreement.

Further downstream at $(x/d_o)_3 = 6.5$, the value of SNR diminished although the spanwise trends established upstream were repeated. The values of SNR_{MAX} for the three row configuration ($\sim .65$) are slightly larger than those for single row injection ($\sim .55$).

Figure 72 presents the spanwise averaged results at $(x/d_o)_3 = 1.5$ for both the three row and single row configurations. The data show a maximum SNR_{AVG} of 0.35 at $M \approx 0.50$. Increasing the blowing ratio beyond 0.50 leads to a continual decrease in SNR_{AVG} with negative values for $M \geq 1.25$. Similar trends are shown downstream at $(x/d_o)_3 = 6.5$.

The data downstream from the third row, $\theta_5 = 76.6^\circ$, were limited due to an inoperable heat flux gage at $z/S = 0.67$. The data from the remaining gages at $(x/d_o)_5 = 1.5$ show positive values of SNR ($\sim .70$) directly behind the coolant hole for $M \leq 0.5$. As the blowing ratio was increased, negative values of SNR behind the hole were observed, with $M \geq 1.0$ yielding negative SNR from all operational gages.

V.B.3. Two Row Configuration with First Row at $\theta_2 = 22.9^\circ$, $S/d_o = P/d_o = 10$

The film cooling performance for the two row configuration, $S/d_o = 10$, at $(x/d_o)_2 = 1.5$ downstream of the first row at ($\theta_2 = 22.9^\circ$) is presented in Figure 73. For values of $M \leq 0.75$, the coolant was turned quickly by the freestream resulting in large positive values of SNR behind the coolant hole. At these values of blowing ratio, lateral spreading of the coolant across the surface was minimal. A comparison of the data

¹ See Appendix III.

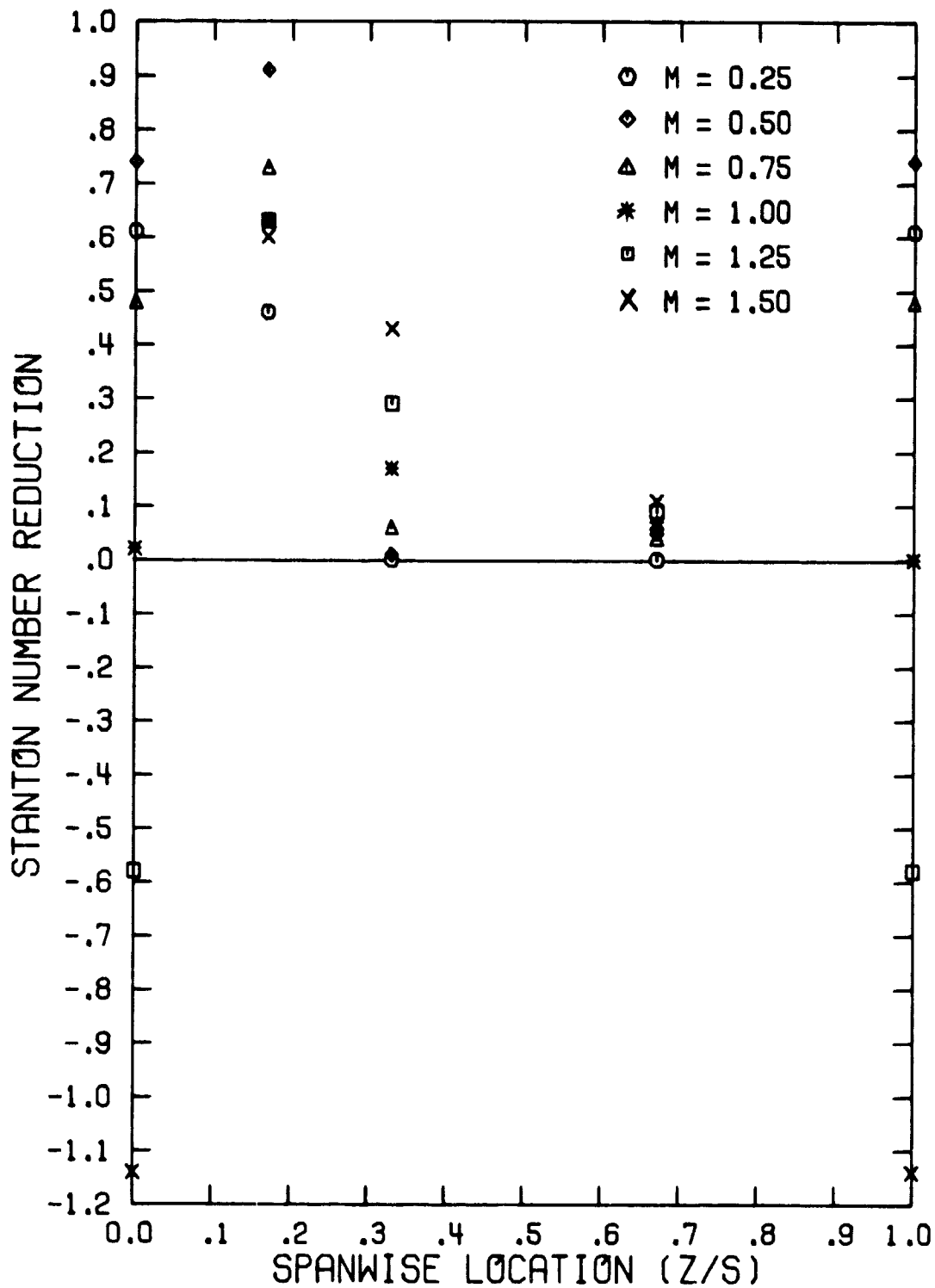


Figure 71. Spanwise Variation of the Stanton Number Reduction for a Three Row Configuration ($\theta_1 = 5^\circ$, $\theta_3 = 40.8^\circ$, $(x/d_0)_3 = 1.5$, $S/d_0 = P/d_0 = 10$)

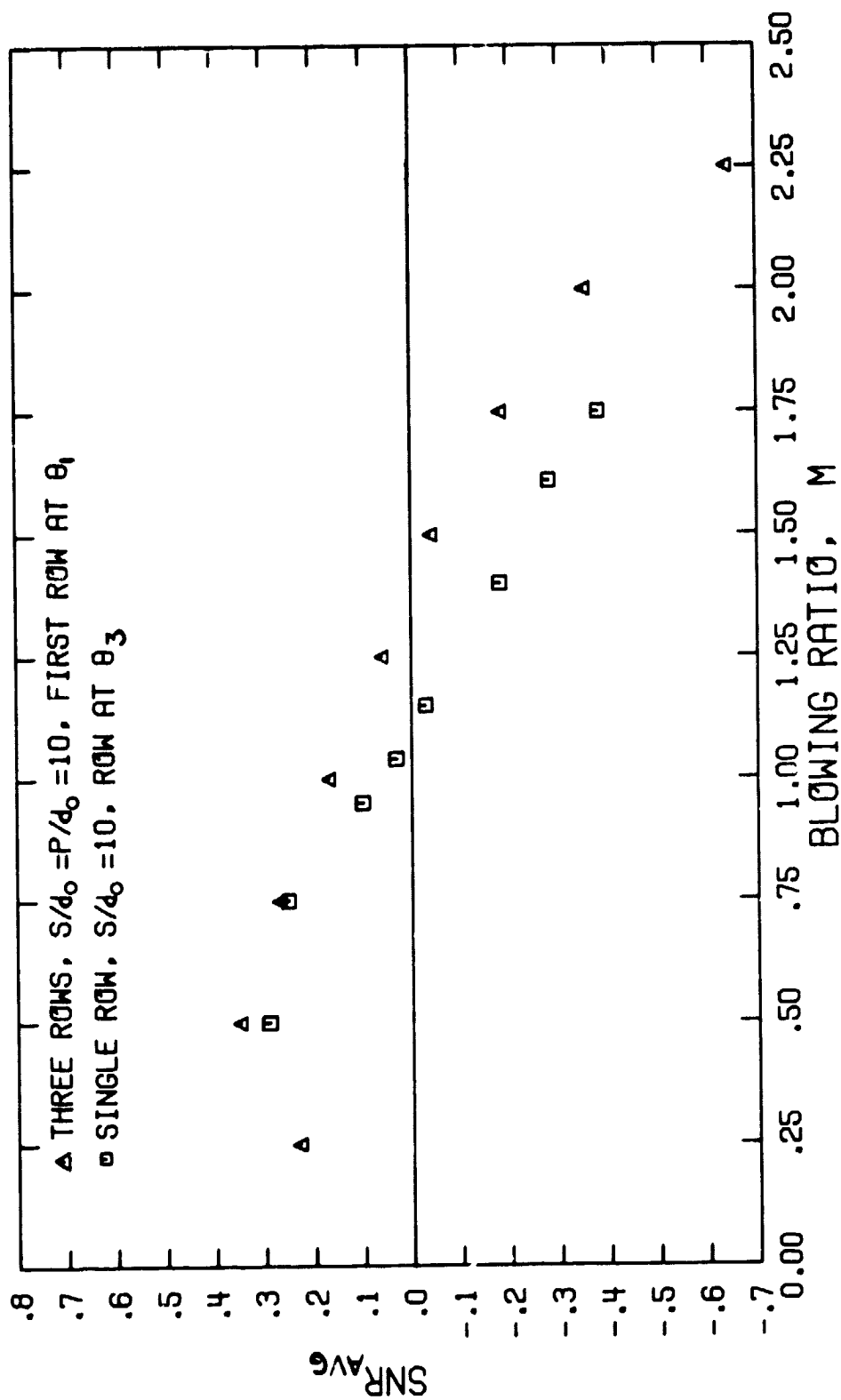


Figure 72. Variation of the Spanwise Averaged Stanton Number Reduction with Blowing Ratio for a Three Row Configuration ($\theta_1 = 5^\circ$, $\theta_3 = 40.8^\circ$, $(x/d_0)_3 = 1.5$, $S/d_0 = P/d_0 = 10$)

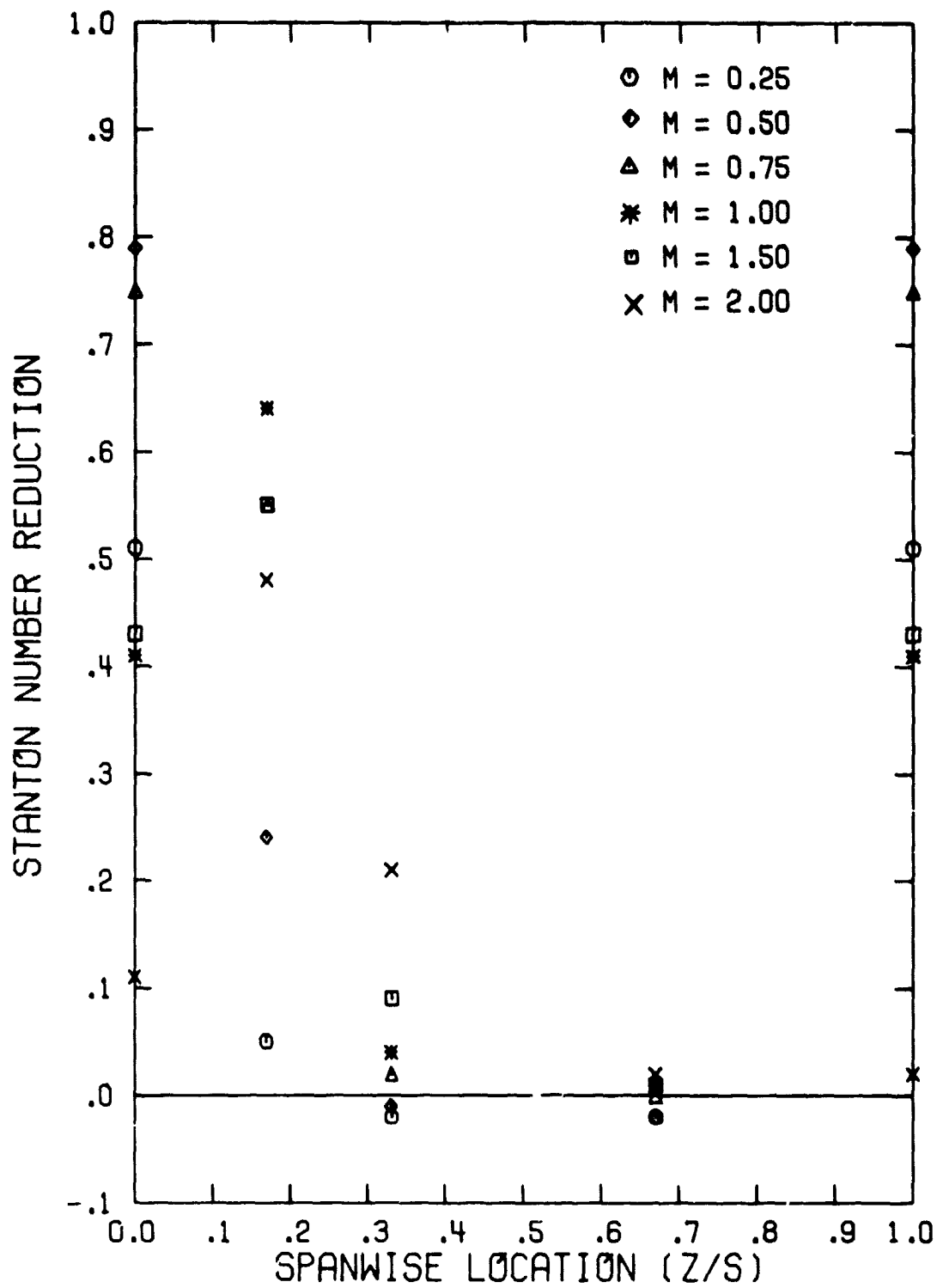


Figure 73. Spanwise Variation of the Stanton Number Reduction for a Two Row Configuration ($\theta_2 = 22.9^\circ$, $(s/d_0)_2 = 1.5$, $S/d_0 = P/d_0 = 10$)

for two row injection and that for single row injection at θ_2 shows good agreement between the values of SNR along the surface. The optimum blowing condition, $M \approx 0.5$ to 0.75 , for the two row configuration agreed well with the value (≈ 0.75) for single row injection.

As the blowing ratio was increased, $M > 0.5$, the coolant trajectory shifted but SNR_{NEG} values did not occur for values of M up to 2.0 . This corresponded exactly to the pattern found with single row injection. An increase in the blowing ratio decreased the value of SNR_{MAX} , but did not result in negative values of SNR behind the coolant hole.

Moving downstream to $(x/d_0)_2 = 3.5^1$, the values of SNR diminished from the upstream levels, although they remained high (0.3 to 0.5) for $M \leq 1.0$. Downstream from the hole, SNR_{NEG} was found at $M \approx 0.75$. Increasing the blowing ratio beyond this point caused the magnitude of SNR_{NEG} to grow. The data for single row injection demonstrated a similar pattern with SNR_{NEG} initiated at $M_2 \approx 1.0$. A comparison of the data for two row and single row injection shows close agreement in the values of SNR_{MAX} and SNR_{NEG} at each blowing ratio greater than 0.75 .

Downstream further at $(x/d_0)_2 = 6.5^1$, the values of SNR decreased slightly from the level at $(x/d_0)_2 = 3.5$. The region covered by the coolant showed $SNR \approx 0.20$ to 0.30 but the coolant effect remained very localized and a large portion of the distance between the holes was unaffected. Again the data for two row and single row injection show good agreement for both the values of SNR_{MAX} and SNR_{NEG} .

The final downstream location, $(x/d_0)_2 = 8.5^1$ before the second row of coolant holes showed a repetition of the patterns established at $(x/d_0)_2 = 3.5$ and 6.5 , with the exception of the data at $z/S = 0.58$. With two row injection, the heat flux gage at $(x/d_0)_2 = 8.5$, $z/S = 0.58$ was positioned in front of a coolant hole in the next row. As previous results have shown, the value of SNR at this location increased when there was blowing from a downstream hole. Comparing the results for two row and single row injection, the heat flux gage in front of the blowing hole showed an increase in SNR of approximately 0.10 .

The spanwise averaged data at $(x/d_0)_2 = 1.5$ is presented in Figure 74 as a function of the blowing ratio for both the multiple and single row configurations. The results for the two row configuration

¹ See Appendix III.

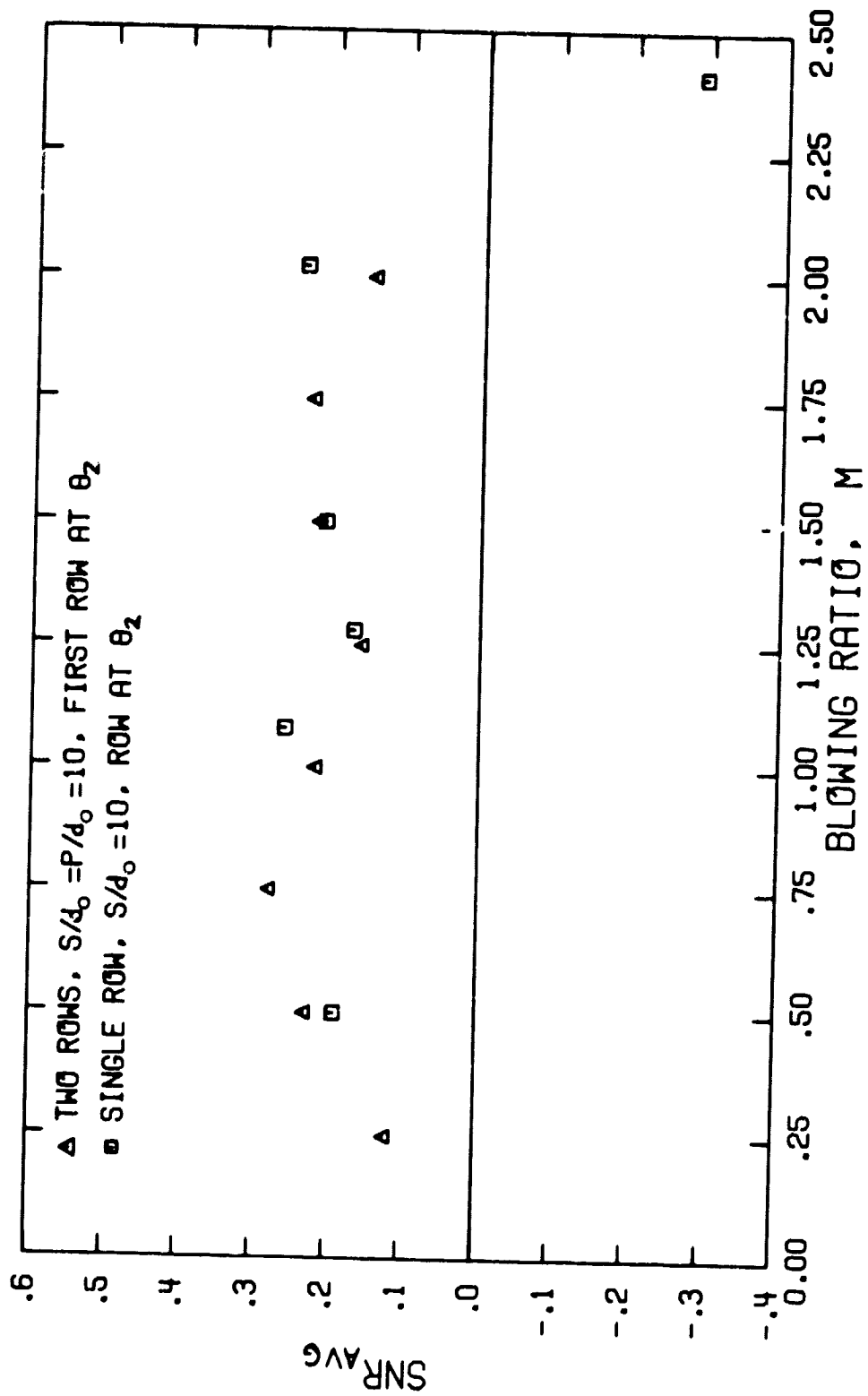


Figure 74. Variation of the Spanwise Averaged Stanton Number Reduction with Blowing Ratio for a Two Row Configuration ($\theta_2 = 22.9^\circ$, $(x/d_0)_2 = 1.5$, $s/d_0 = P/d_0 = 10$)

reveal a steady increase in SNR_{AVG} as the blowing ratio is increased, with maximum value of $SNR_{AVG} = 0.28$ reached at $M = 0.75$. Further increase in the blowing ratio results in a slight decrease in SNR_{AVG} , to a level of approximately 0.2. Excellent agreement is found between the data for SNR_{AVG} from the two row and single row configurations.

Moving downstream to $(x/d_o)_2 = 3.5$ ¹, the data for the two row configuration show the value of SNR_{AVG} reduced sharply in magnitude (i.e. -0.4 at $M = 1.0$ and -0.30 at $M = 2.0$) when compared to the upstream results. This corresponds to the development of SNR_{NEG} values at $(x/d_o)_2 = 3.5$ that were not found at $(x/d_o)_2 = 1.5$. Further downstream at $(x/d_o)_2 = 6.5$ and 8.5, the value of SNR_{AVG} does increase somewhat in magnitude from the levels found at $(x/d_o)_2 = 3.5$. But it does not come close to reaching the levels attained at $(x/d_o)_2 = 1.5$. This downstream trend at $M = 1.0$ shows $SNR_{AVG} = 0.22$ at $(x/d_o)_2 = 1.5$, dropping to -0.04 at $(x/d_o)_2 = 3.5$, and increasing to 0.08 at $(x/d_o)_2 = 8.5$.

The film cooling performance at $(x/d_o)_4 = 1.5$, downstream of the second row at θ_4 is presented in Figure 75. For $M \leq 0.5$, positive values of SNR cover the entire surface with the maximum value around $z/S = 0.17$. The unique feature about the film cooling results in this range of M is the nearly uniform spanwise coverage. This coverage is apparently a result of the upstream injection at θ_2 . The data for single row injection at θ_4 did not show the film coolant covering the region near $z/S = 0.67$.

As the blowing ratio is increased to $M = 0.75$, the occurrence of SNR_{NEG} values behind the second row was observed. When $M = 1.25$, the value of SNR was negative over the entire span. The data for single row injection show that SNR_{NEG} was initiated at $M \approx 1.0$. Both the single row and two row configurations had large values of SNR_{NEG} (-2.0 to -2.5) when $M \geq 1.25$.

Downstream at $(x/d_o)_4 = 6.5$ ¹, the value of SNR was almost negligible for $M = 0.25$. However, at $M = 0.50$ and 0.75, large values of SNR (0.8 - 0.9) were observed at $z/S = 0.42$. Additional increase in the blowing ratio caused the value of SNR to decrease in magnitude (~0.4) with the location shifting spanwise to $z/S = 0.92$. This pattern was also observed with single row injection at θ_4 .

¹ See Appendix III.

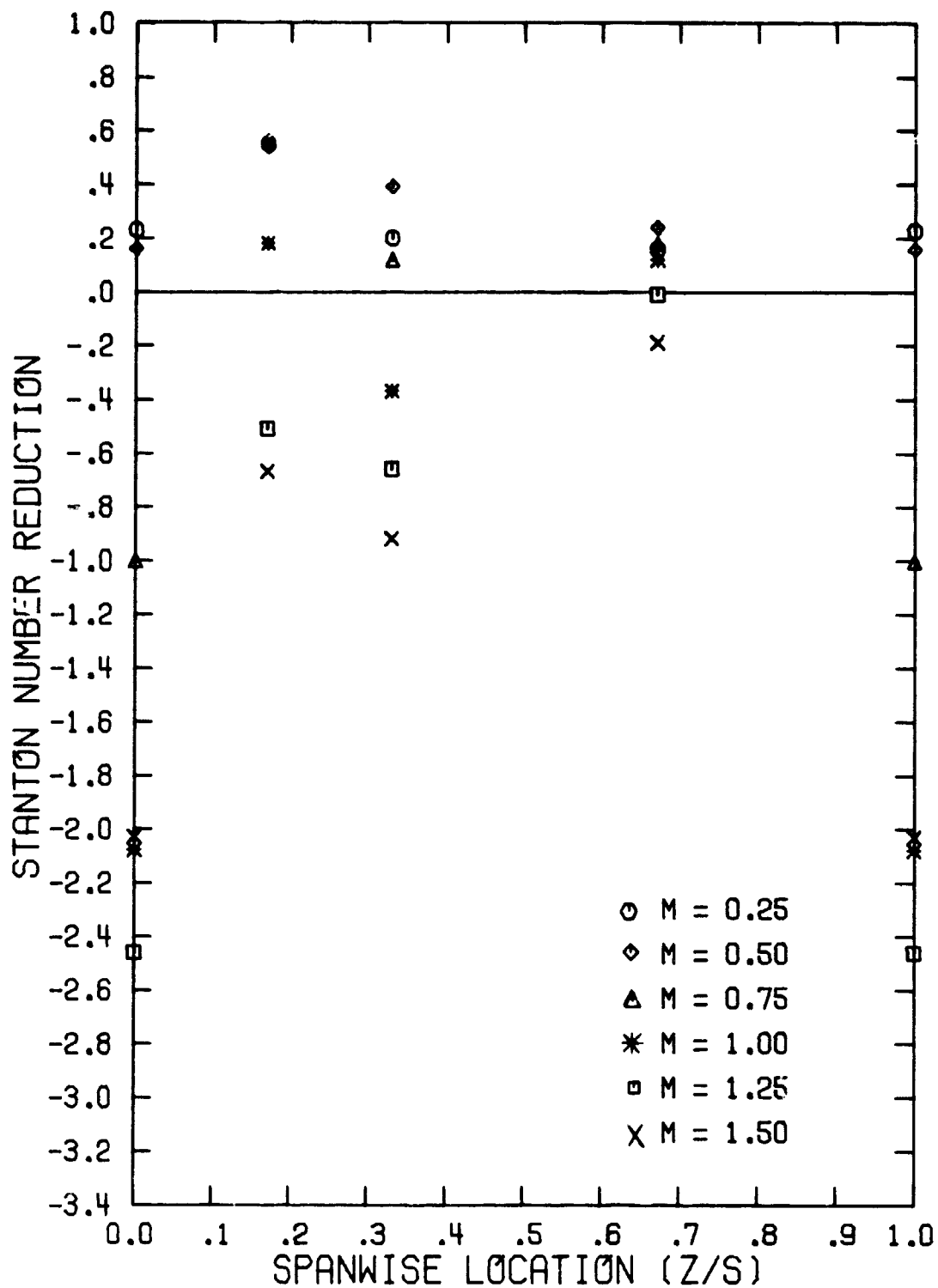


Figure 75. Spanwise Variation of the Stanton Number Reduction for a Two Row Configuration
 $(\theta_2 = 22.9^\circ, \theta_4 = 58.7^\circ, (x/d_0)_4 = 1.5, s/d_0 = P/d_0 = 10)$

The spanwise averaged data at $(x/d_o)_4 = 1.5$ is presented in Figure 76 as a function of blowing ratio for both the multiple and single row configurations. The data for SNR_{AVG} for the two row configurations shows the optimum film cooling performance (0.31) occurring at $M = 0.5$. Negative values of SNR_{AVG} were observed for a blowing ratio, $M = 0.75$. The negative values of SNR_{AVG} become excessive as the blowing is increased, reaching a level of approximately -0.9 for $M \geq 1.25$. A similar pattern was found for single row injection, although one difference between the two configurations is noticeable. The optimum film cooling performance (0.35) for single row injection occurred at $M = 0.75$, and negative values of SNR_{AVG} did not begin until $M = 1.00$.

V.C. Discussion of the Results

V.C.1 Introduction

The study of single row injection demonstrated that there was very little lateral spreading of the coolant jet across the surface. It also showed a rapid decrease in the heat flux reduction (SNR) by the film coolant as it passed downstream. Multiple row film cooling configurations are frequently employed in an attempt to improve the lateral coverage by the coolant. The injection rows are staggered with respect to the upstream row so that the coolant can fill the gap in coverage between the coolant holes. The placement of additional rows downstream from the first row is intended to sustain a level of film cooling performance along the surface in the streamwise direction.

One of the most significant features that evolved from the data for multiple row injection was the continued lack of good film coolant coverage across the surface (i.e. spanwise). Many areas between the holes were still unaffected by the film coolant. Russell's [19] flow visualization studies included an investigation of spanwise injection on a flat plate using a three row array, $S/d_o = P/d_o = 5$. His results also showed voids between the coolant streams, particularly at higher values of the blowing ratio ($M \sim 0.8$). For the hole spacing studied in this investigation, $S/d_o = 5$ and 10, multiple row injection resulted

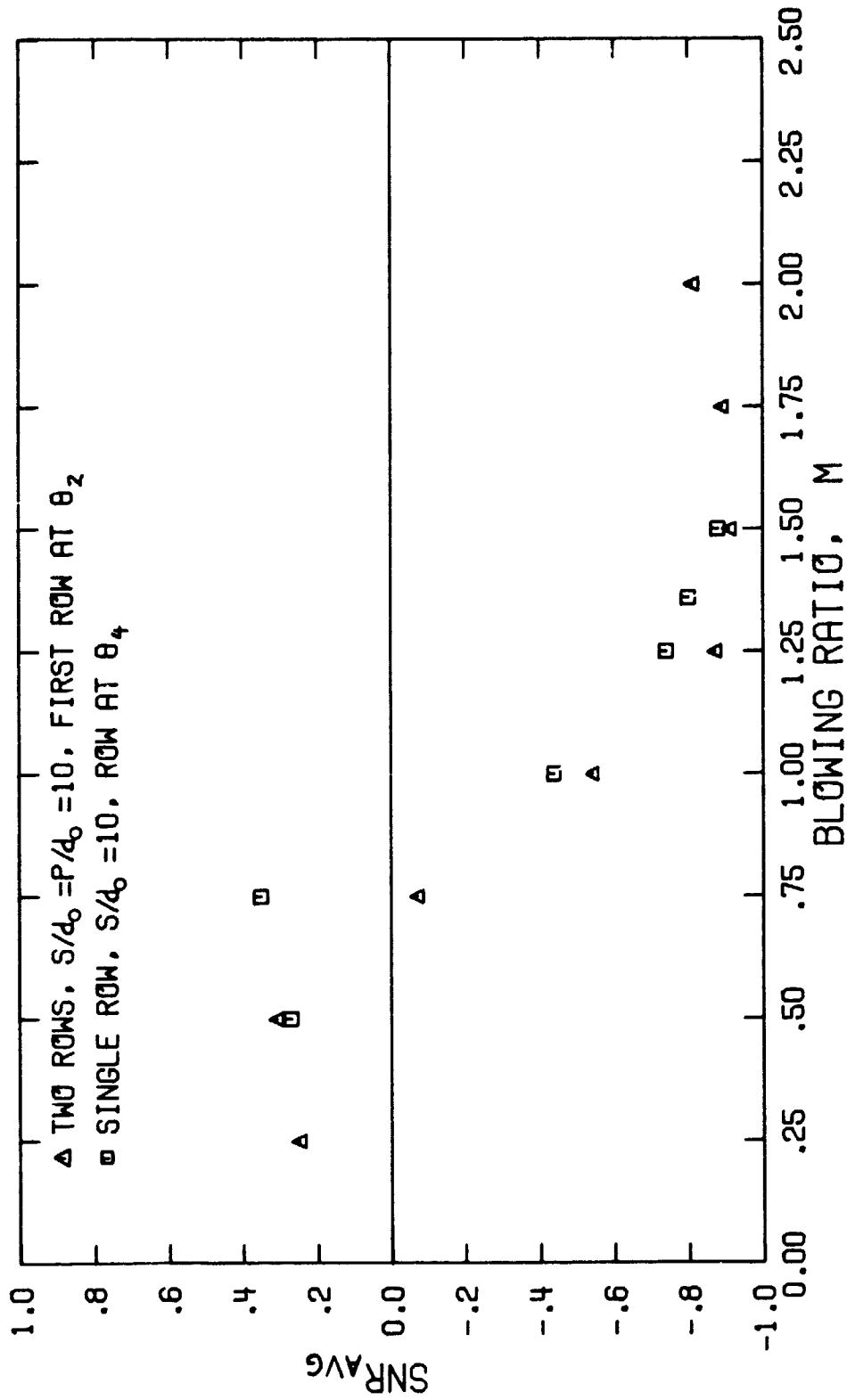


Figure 76. Variation of the Spanwise-Averaged Stanton Number Reduction with Blowing Ratio for a Two Row Configuration
 ($\theta_2 = 22.9^\circ$, $\theta_4 = 58.7^\circ$, $(x/d_o)_4 = 1.5$, $x/d_o = P/d_o = 10$)

in very limited spreading of the coolant across the surface. Another important feature observed from the data was the close agreement found between the data for multiple row and single row injection, particularly when $S/d_0 = 10$. While there was some influence of upstream or downstream rows on the film cooling performance for a particular row, it was not a dominate factor. Both of these features concerning multiple row coolant injection will be discussed in detail in the following sections.

The discussion of the results for multiple row injection is divided into individual sections for each of the three configurations studied. The final two sections in this chapter discuss the spanwise averaged results. The data for SNR_{AVG} allows comparisons to be made between the data for the different multiple row configurations and single row injection.

V.C.2 Five Row Configuration ($\theta_1 = 5^\circ$, $S/d_0 = P/d_0 = 5$)

To aid in the discussion of film cooling with five rows of holes, three tables were compiled to compare the results for single and multiple row injection. Table 9 lists the values of M corresponding to the blowing ratio where SNR_{NEG} behind the coolant hole was first observed. Values of the blowing ratio presented in all three tables are given for both M and $M_{\infty,0}$ corresponding to local and upstream freestream velocities. The values of blowing ratio that produce the optimum film cooling performance; M_{opt} , are presented in Table 10. Finally, the spanwise location of the coolant jet, i.e. where the largest SNR_{MAX} occurred, is presented in Table 11 for selected values of blowing ratio. Behind the first two rows, the data for z/d_0 are presented for $(x/d_0)_i = 3.5$, while behind the last two rows the data are presented for $(x/d_0)_i = 1.5$, the only measurement location downstream of these rows. The downstream position of $(x/d_0)_i = 3.5$ was selected to provide an indication of the coolant jet location as it approached the next downstream row.

The main feature of the results behind the first row of holes (θ_1) is the good agreement found with the data for a single row of holes at θ_1 . The magnitudes of SNR from these two configurations are in good

Table 9. Blowing Ratio that Initiated SNR_{NEG}
 $(x/d_0)_1 = 1.5, S/d_0 = P/d_0 = 5$

M

 $\theta_1 = 5^\circ$ $\theta_2 = 22.9^\circ$ $\theta_3 = 40.8^\circ$ $\theta_4 = 58.7^\circ$

Single Row	2.0	1.10	0.77	0.95
Multiple Row	1.5	1.26	0.50	0.75

 $M_{\infty,0}$

Single Row	.38	.94	1.11	1.78
Multiple Row	.29	1.08	.72	1.41

Table 10. Blowing Ratio for Largest SNR_{MAX}
 $(x/d_0)_i = 1.5, S/d_0 = P/d_0 = 5$

	M_{opt}			
	$\theta_1 = 5^\circ$	$\theta_2 = 22.9^\circ$	$\theta_3 = 40.8^\circ$	$\theta_4 = 58.7^\circ$
Single Row	3.5	0.50	0.38	0.50
Multiple Row	— *	0.50	0.25	0.38

	$M_{\infty, opt}$			
	$\theta_1 = 5^\circ$	$\theta_2 = 22.9^\circ$	$\theta_3 = 40.8^\circ$	$\theta_4 = 58.7^\circ$
Single Row	.67	0.45	0.54	0.94
Multiple Row	— *	0.45	0.36	.57

*Data were not taken beyond $M_1 = 2.0$ for the uniform blowing study.

Table 11. Spanwise Location, z/d_0 , of the Coolant,
 $S/d_0 = P/d_0 = 5$

$\theta_1 = 5^\circ$, $(x/d_0)_1 = 3.5$

	$M=0.50$ $M_{\infty,0}=0.10$	$M=1.00$ $M_{\infty,0}=0.19$	$M=1.50$ $M_{\infty,0}=0.29$	$M=2.00$ $M_{\infty,0}=0.38$
Single Row	0.8	1.7	—*	1.7
Multiple Row	1.7	1.7	1.7	1.7

$\theta_2 = 22.9^\circ$, $(x/d_0)_2 = 3.5$

	$M=0.50$ $M_{\infty,0}=0.43$	$M=0.75$ $M_{\infty,0}=0.64$	$M=1.5$ $M_{\infty,0}=1.29$	$M=2.0$ $M_{\infty,0}=1.71$
Single Row	1.7	1.7	1.7	3.3
Multiple Row	0.8	1.7	1.7	2.5

$\theta_3 = 40.8^\circ$, $(x/d_0)_3 = 1.5$

	$M=0.25$ $M_{\infty,0}=0.36$	$M=0.50$ $M_{\infty,0}=0.72$	$M=0.75$ $M_{\infty,0}=1.08$	$M=1.25$ $M_{\infty,0}=1.80$
Single Row	0.0	0.8	1.7	3.3
Multiple Row	0.8	1.7	1.7	—†

$\theta_4 = 58.7^\circ$, $(x/d_0)_4 = 1.5$

	$M=0.25$ $M_{\infty,0}=0.47$	$M=0.50$ $M_{\infty,0}=0.94$	$M=0.75$ $M_{\infty,0}=1.41$	$M=1.00$ $M_{\infty,0}=1.87$
Single Row	0.0	0.8	1.7	1.7
Multiple Row	0.8	0.8	1.7	1.7

*No single row measurements were taken at this blowing ratio.

†Only negative SNR values covered the surface at this blowing ratio.

agreement. (Appendix III) Table 9 shows approximately the same value of M initiating SNR_{NEG} for both cases. Also, good agreement for the coolant jet position along the surface is shown in Table 11 except for $M = 0.5$.

The first row in the configuration does not appear to be influenced by the blowing from downstream rows. The only discrepancy occurs with the heat flux gage positioned directly in front of the coolant hole in the second row. This increase in SNR has been noted previously to be a direct result of the blowing from a coolant hole in the next downstream row. This represents the only film cooling effect in the multiple row results not seen in the single row study. According to Table 11, the position of the coolant jet as it approaches the second row of holes is approximately $1.7 d_0$ from the hole centerline, while the coolant hole in the second row is located at $2.5 d_0$.

The results behind the second row (θ_2) are also similar to those found with single row injection at θ_2 . A comparison of the multiple and single row data for θ_2 shows the values of M_{opt} in Table 10 to be similar. Good agreement is also shown in Table 9 where the values of M initiating SNR_{NEG} are approximately the same. The coolant locations listed in Table 11 were in reasonable agreement.

Some differences between the data for single and multiple row injection at θ_2 were observed when $M_2 > M_{opt}$. As was mentioned in the data presentation section, the values for SNR_{MAX} for the five row configuration remained high (0.5 to 0.6) for $0.5 \leq M \leq 2.0$, while for the single row SNR_{MAX} decreased steadily to ~ 0.2 at $M_2 = 2.0$. For this same range of blowing ratio, the magnitude of SNR_{NEG} behind the coolant hole was not as large for multiple row injection as that found with single row injection. It was concluded that the results downstream from θ_2 were influenced by upstream blowing when $M_1 \geq 0.75$.

The only other difference between the results for five row and single row injection was the heat flux measured just upstream of a coolant hole in the third row. As has been discussed numerous times herein, blowing from a downstream hole reduced the heat flux in the region immediately in front of the coolant hole.

Downstream from the third row (θ_3) in the five row configuration,

the influence of upstream blowing was more pronounced. Better film coverage across the surface was achieved for $M \leq 0.5$ because of the coolant flow from the upstream rows. For a low blowing ratio, $M = 0.25$, the value of SNR behind the hole was similar to that for single row injection. The major difference between the two configurations was the added film cooling protection at $z/S = 0.67$ provided by the coolant from upstream rows in the five row configuration.

While good film coverage across the surface was achieved for $M = 0.25$, the occurrence of SNR_{NEG} was initiated at $M_3 = 0.50$ for multiple row injection. Table 9 shows the blowing ratio for SNR_{NEG} to be smaller than that observed with single row injection. Table 10 also shows that the value of M_{opt} at θ_3 for multiple row injection decreased from the level found with single row injection. Apparently, the disturbance created by upstream blowing alters the coolant jet-freestream interaction in a manner that is detrimental to film cooling performance. The appearance of SNR_{NEG} values occurs at a lower blowing ratio and M_{opt} is substantially reduced.

The position of the jet along the surface, listed in Table 11, does not differ significantly from the results for single row injection, but increasing M to 1.0 resulted in negative SNR across the surface. The data for single row injection show that the influence of the coolant jet produced local values of $SNR > 0$ up to the highest blowing ratio studied, $M_3 = 1.6$. For multiple row injection, an approximately uniform distribution of negative values of SNR resulted for $M > 1.0$. The magnitude of these negative values of SNR was less than the values found for single row injection. This pattern was previously seen downstream of the second row. At high blowing ratios, the negative SNR values for the five row configuration were smaller in magnitude than those for single row injection.

With only one row of heat flux gages downstream from the third row, the estimate of the coolant jet position approaching the fourth row was at $(x/d_0)_3 = 1.5$. The results in Table 11 indicate that the coolant centers about a spanwise position between 1.7 and 3.3 d_0 for the higher values of M . With the coolant hole in the fourth row positioned at

$2.5 d_0$ with respect to the hole in the third row, the coolant jet is directed toward the coolant hole in the fourth row resulting in poorer film coverage across the surface behind the fourth row.

Downstream of the fourth row (θ_4), the film cooling results do not show many benefits from upstream blowing. For $M \leq 0.50$, the film coverage is still very localized and the values for SNR behind the hole are similar to those found with single row injection. By increasing M to 0.75, the initiation of SNR_{NEG} behind the coolant hole was observed. Table 9 reveals that this blowing ratio for multiple row injection was smaller than that discovered with single row injection. Table 10 also shows a smaller value of M_{opt} than that for the single row configuration. In addition, the values of SNR behind the hole for $M = 0.75$ and 1.0 were approximately 30% lower for the multiple row injection. Apparently, the flow disturbance created by upstream blowing was large enough for $M \geq 1.25$ that the coolant jet separated from the surface resulting in $SNR < 0$ at $(x/d_0)_4 = 1.5$. By comparison, the data for single row injection show the influence of the coolant still present along the surface at $(x/d_0)_4 = 1.5$, (i.e. $SNR > 0$), up to the highest blowing ratio studied, $M = 1.5$.

The coolant jet location, Table 11, was relatively unaffected by the change from single row to multiple row injection. Once again the value of z/d_0 in Table 11 was measured at $(x/d_0)_4 = 1.5$, giving an estimate of the coolant location approaching the fifth row.

Results downstream of the fifth row (θ_5) repeat the patterns established at the fourth row. The negative value, SNR_{NEG} , was initiated at $M = 0.75$, and at blowing ratios greater than 1.25, only negative values of SNR were measured along the surface.

The foregoing results for injection with the five row configuration ($S/d_0 = P/d_0 = 5$) have shown that the performance for the first two rows are relatively unaffected by the multiple row arrangement, indicating good agreement with the results for single row injection. The first row is unaffected primarily because no injection occurs upstream of it. With a uniform distribution of M for all rows the second row feels little influence of the first row because of the low coolant flow rate at θ_1 .

Although the performance for the first two rows was unaffected by the multiple row arrangement, the performance for rows 3 and 4 definitely was influenced by the effects of upstream blowing. Downstream of rows 3 and 4, the disturbance created by upstream blowing caused a reduction in the value of M_{opt} and the value of M initiating SNR_{NEG} from the levels observed with single row injection. In effect, upstream blowing decreased the blowing range where negative values of SNR were not present along the surface. At high values of blowing ratio, the flow disturbance from upstream blowing apparently was large enough to result in $SNR < 0$ over the entire surface downstream from rows 3 and 4.

The following two sections in this chapter discuss the data for multiple row injection with a hole spacing, $S/d_0 = P/d_0 = 10$.

V.C.3 Three Row Configuration ($\theta_1 = 5^\circ$, $S/d_0 = P/d_0 = 10$)

To aid in this discussion, tables similar to those presented in the last section, were compiled to provide a comparison between the results for single row injection and those for 3 row injection with $S/d_0 = P/d_0 = 10$. Table 12 lists the values of M initiating SNR_{NEG} while Table 13 presents the values for M_{opt} for the first row at θ_1 and the second row at θ_3 . Data for the third row at θ_5 are not presented. The coolant jet location along the surface, z/d_0 , is presented in Table 14. The data in Table 14 are presented for $(x/d_0)_1 = 8.5$, $(x/d_0)_3 = 6.5$ corresponding to the last row of heat flux gages before the rows at θ_3 and θ_5 , respectively.

The most significant feature of the film cooling performance downstream of the first row at θ_1 is the close agreement found with the results for single row injection. When the three row and single row data are compared, the magnitude of the SNR values and the value of M initiating SNR_{NEG} are approximately equal. As was discovered with the configuration, with $S/d_0 = 5$ the film coolant jet from the first row was unaffected by the downstream blowing at other rows. The only difference observed was for the heat flux gage located directly in front of the coolant hole in the second row at θ_3 , where an increase in the magnitude of SNR was found due to blowing from the downstream hole.

Table 12. Blowing Ratios that Initiated SNR_{NEG}
 $(x/d_0)_i = 1.5$, $S/d_0 = P/d_0 = 10$

M

	$\theta_1 = 5^\circ$	$\theta_3 = 40.8^\circ$
Single Row	2.0	0.95
Multiple Row	2.5	1.25

 $M_{\infty,0}$

	$\theta_1 = 5^\circ$	$\theta_3 = 40.8^\circ$
Single Row	.38	1.36
Multiple Row	.48	1.80

Table 13. Blowing Ratio for Largest SNR_{MAX}
 $(x/d_0)_i=1.5$, $S/d_0=P/d_0=10$

M_{opt}		
	$\theta_1=50^\circ$	$\theta_3=40.8^\circ$
Single Row	3.5	0.50
Multiple Row	—*	0.50

$M_{\infty, opt}$		
	$\theta_1=50^\circ$	$\theta_3=40.8^\circ$
Single Row	.67	0.72
Multiple Row	—*	0.72

*Data not taken beyond $M_1=2.0$ for the uniform blowing study.

Table 14. Spanwise Location, z/d_0 , of the Coolant,
 $S/d_0 = P/d_0 = 10$

$\theta_1 = 5^\circ$, $(x/d_0)_1 = 8.5$

$M = 0.50$ $M = 1.00$ $M = 1.50$ $M = 2.00$
 $M_{\infty,0} = 0.10$ $M_{\infty,0} = 0.19$ $M_{\infty,0} = 0.29$ $M_{\infty,0} = 0.38$

Single Row	— *	2.5	— *	2.5
Multiple Row	2.5	2.5	2.5	2.5

$\theta_3 = 40.8^\circ$, $(x/d_0)_3 = 6.5$

$M = 0.25$ $M = 0.50$ $M = 0.75$ $M = 1.25$
 $M_{\infty,0} = 0.36$ $M_{\infty,0} = 0.72$ $M_{\infty,0} = 1.08$ $M_{\infty,0} = 1.80$

Single Row	— *	2.5	4.2	4.2
Multiple Row	1.7	2.5	4.2	4.2

*No single row measurements were taken at this blowing ratio.

From Table 14, the coolant jet issuing from the row at θ_1 had a location of $2.5 d_0$ just upstream from the second row at θ_3 , placing the coolant midway between the coolant holes at θ_1 and θ_3 .

The results downstream from the second row (θ_3) also demonstrate reasonable agreement with the data from the study of single row injection. The magnitude of SNR and the values of M_{opt} (Table 13) were approximately equal for the two configurations. Table 12 reveals that the value of M initiating SNR_{NEG} for the three row configuration was somewhat larger than that for single row injection. For both configurations, the magnitudes of SNR_{NEG} were approximately the same. For single row injection at θ_3 with $S/d_0 = 10$, SNR at $z/S = 0.67$ was negligible for $(x/d_0)_3 = 1.5$. However, for injection from rows at θ_1 and θ_3 with $M \geq 1.0$, values of SNR in the range of 0.1 and 0.2 were observed at $(x/d_0)_3 = 1.5$, $z/S = 0.67$. Therefore, for $S/d_0 = 10$, although the coolant flow from the first row (θ_1) did not alter the coolant injection process at θ_3 , the coolant from the upstream row did increase the values of SNR downstream of the second row at θ_3 . This situation differs from the study of five row injection ($S/d_0 = 5$). With five rows, the injection process at the third row (θ_3) was altered by upstream blowing from the second row (θ_2).

V.C.4 Two Row Configuration ($\theta_2 = 22.9^\circ$, $S/d_0 = P/d_0 = 10$)

In this section, the results for injection from a two row configuration with the first row at θ_2 are presented. Results for the values of M initiating SNR_{NEG} , M_{opt} , and the coolant jet location are summarized in Tables 15, 16, and 17 respectively. The results for the first two multiple row configurations have shown that the performance for the first row in the injection pattern is relatively unaffected by downstream blowing. This trend also was observed for the two row configuration with the first row at θ_2 . The film cooling performance behind the first row (θ_2) compared with the results for single row injection at θ_2 show that the magnitudes of the value of SNR behind the hole are in good agreement and the values of M_{opt} (Table 16) are approximately equal.

Table 15. Blowing Ratios that Initiated SNR_{NEG} ,
 $(\lambda/d_0)_i=1.5$, $S/d_0 = P/d_0 = 10$

M		
	$\theta_2=22.9^\circ$	$\theta_4=58.7^\circ$
Single Row	2.40	1.00
Multiple Row	>2.0	0.75

$M_{\infty,0}$		
	$\theta_2 = 22.9^\circ$	$\theta_4=58.7^\circ$
Single Row	2.05	1.88
Multiple Row	>1.71	1.41

Table 16. Blowing Ratio for Largest SNR_{MAX} ,
 $(x/d_0)_1=1.5$, $S/d_0=P/d_0=10$

	M_{opt}	
	$\theta_2=22.9^\circ$	$\theta_4=58.7^\circ$
Single Row	0.77	0.75
Multiple Row	0.625	0.38

	$M_{\infty,0 opt}$	
	$\theta_2=22.9^\circ$	$\theta_4=58.7^\circ$
Single Row	0.66	1.41
Multiple Row	0.55	.57

Table 17. Spanwise Location, z/d_0 of the Coolant,
 $S/d_0 = P/d_0 = 10$

$\theta_2 = 22.90^\circ, (x/d_0)_2 = 8.5$

$M = 0.50$ $M = 1.00$ $M = 1.50$ $M = 2.00$
 $M_{\infty,0} = 0.43$ $M_{\infty,0} = 0.86$ $M_{\infty,0} = 1.29$ $M_{\infty,0} = 1.71$

Single Row	2.5	2.5	2.5	4.2
Multiple Row	2.5	2.5	2.5	4.2

$\theta_4 = 58.70^\circ, (x/d_0)_4 = 6.5$

$M = 0.25$ $M = 0.50$ $M = 0.75$ $M = 1.00$
 $M_{\infty,0} = 0.47$ $M_{\infty,0} = 0.94$ $M_{\infty,0} = 1.41$ $M_{\infty,0} = 1.88$

Single Row	*	5.8	4.2	4.2
Multiple Row	5.8	4.2	4.2	9.2

*No single row measurements were taken at this blowing ratio.

At the highest blowing ratio studied, $M = 2.0$, the initiation of SNR_{NEG} behind the coolant hole had not occurred. This agrees with the results for single row injection where SNR_{NEG} was first observed at $M_2 = 2.4$. Both configurations showed negative values of SNR at $M \sim 1.0$ at $(x/d_0)_2 = 3.5$. The magnitude of SNR_{NEG} behind the coolant hole showed good agreement between the two row and single row configurations. While the film cooling performance downstream from the first row (θ_2) is in good agreement with the results for single row injection, the heat flux gage located in front of a coolant hole in the second row (θ_4) showed a positive value of SNR of 0.10 to 0.20.

The location of the coolant jet approaching the second row (Table 17) was found to be $2.5 d_0$ for $M \leq 1.50$, whereas for $M \geq 2.0$, the coolant location was greater than $4 d_0$, which is close to the coolant hole in the second row. Therefore, when $M \leq 1.5$, the film coverage between the coolant holes downstream from the second row (θ_4) should be aided by the blowing from the row at θ_2 .

Behind the second row (θ_4), low values of blowing ratio, $M \leq 0.5$, produced the same level of SNR behind the coolant hole as found with single row injection. However, the two row configuration showed a positive value of SNR at $z/S = 0.67$. As expected, blowing from the upstream row (θ_2) aided the performance between the coolant holes. A comparison with the results for single row injection shows SNR near zero at this spanwise location.

It was found that upstream blowing also can have an adverse effect, especially at the higher values of blowing ratio ($M > 0.50$). Comparing the results for the single and two row configurations downstream from θ_4 , Table 15 shows a smaller value for M initiating SNR_{NEG} and Table 16 a smaller value for M_{opt} for the two row configuration. While upstream blowing can be beneficial at low values of the low blowing ratio, it has a detrimental effect on the film cooling performance behind downstream rows when the blowing ratio is increased.

In conclusion, the foregoing results show that some of the trends established with the five row configuration ($S/d_0 = P/d_0 = 5$) have been observed with the three and two row configurations ($S/d_0 = P/d_0 = 10$).

Blowing from a row at θ_1 was found to have very little effect on the film cooling performance at the next downstream row. This was attributed to the small amount of coolant being blown from the row at θ_1 when a uniform blowing distribution ($M = \text{constant}$) is employed. However, the blowing from a row at θ_2 did influence the performance downstream from downstream rows. For both the five row and two row configurations, with injection at θ_2 , the next row downstream showed lower values for M_{opt} and M initiating SNR_{NEG} than for single row injection at the same downstream location. Furthermore, blowing at θ_2 with high values of M ($M_2 > 1.0$) generally resulted in only negative values of SNR downstream from the following row.

One objective for the use of multiple row injection is to promote more uniform film cooling performance across the surface. However, the results from this study indicate that the disturbance created by upstream blowing can effectively reduce the range of M available to downstream rows before negative values of SNR appear on the surface. If a uniform blowing distribution is held below M initiating SNR_{NEG} , the film cooling performance directly behind the coolant hole shows good agreement with the results for single row injection. Therefore, within this range of M , the data for single row injection can be used to predict values of SNR for the multiple row configurations.

The coolant spanwise location approaching the next downstream row, indicates whether the coolant will flow between the coolant holes or over the top of them. The results in Tables 11, 14 and 17 show very little difference between the value of z/d_0 for single and multiple row injection. Therefore, for a given blowing distribution, the results for single row injection enable an estimate of coolant location relative to holes in downstream rows.

When the blowing ratio is increased, the injection from downstream rows is disturbed by upstream blowing. This disturbance can result in only negative values of SNR across the surface following the downstream rows. Thus, a large blowing ratio at one row not only affects the film cooling performance immediately downstream of that row, but the interference also affects the film cooling performance at other downstream rows. The results indicate that the proper selection of a

blowing distribution is a critical factor in the design of a multiple row injection configuration. Although the film cooling performance remains very localized along the surface with multiple row injection, a carefully chosen blowing distribution and row staggering arrangement could provide high levels of film cooling effectiveness along the surface. At the same time, a poorly conceived blowing distribution can result in heat transfer rates that significantly exceed the values observed when coolant injection is not present.

V.C.5 Spanwise Averaged Results

As described in Chapter IV, the local values of SNR vs. z/S were averaged in the spanwise direction to allow comparisons to be made between the different injection configurations. However, it should be noted that spanwise averaging eliminates the detail of the local heat flux variation. Predictions of wall temperatures based on SNR_{AVG} would not reveal the hot (or cold) spots that are typical of the local heat flux distribution. Figures 77, 78, 79 and 80 present a comparison of the data for SNR_{AVG} for multiple and single row injection. Each figure presents SNR_{AVG} as a function of downstream distance, x/d_0 . The data shown in Figures 77 and 78 represent coolant injection with a hole spacing of $S/d_0 = 5$, showing SNR_{AVG} for the 5 row configuration with the first row at θ_1 . Data for uniform value of $M = 0.25$ were selected because that corresponded to the highest level of SNR_{AVG} for the entire surface. The results for multiple row injection shown in Figure 77 are compared with the values of SNR_{AVG} for single row injection at θ_1 . A blowing ratio of $M_1 = 1.0$ was chosen for the single row because that produced the best film cooling performance

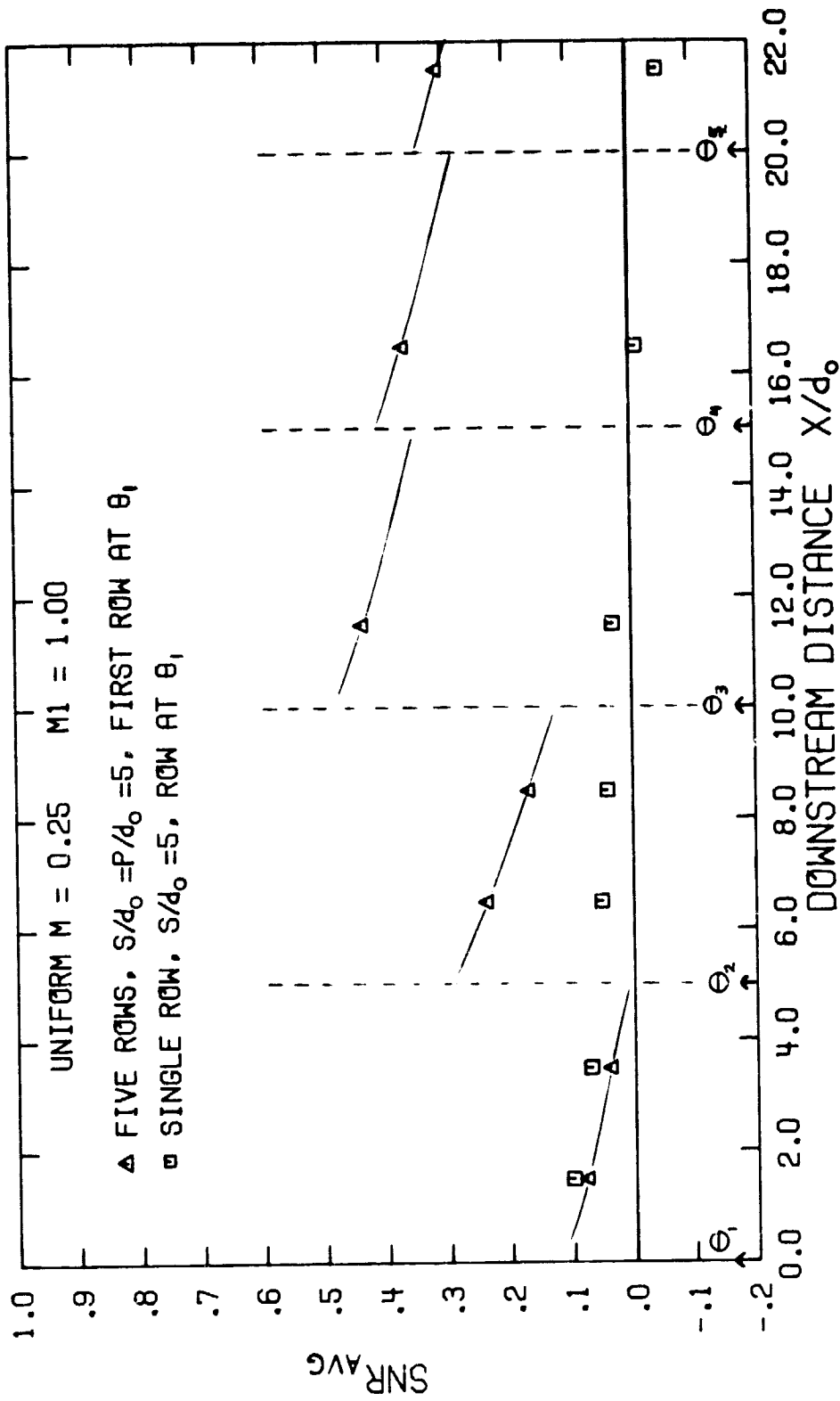


Figure 77. Comparison of the Spanwise Averaged Stanton Number Reduction for the Five Row Configuration and the Single Row Configuration at θ_1 .

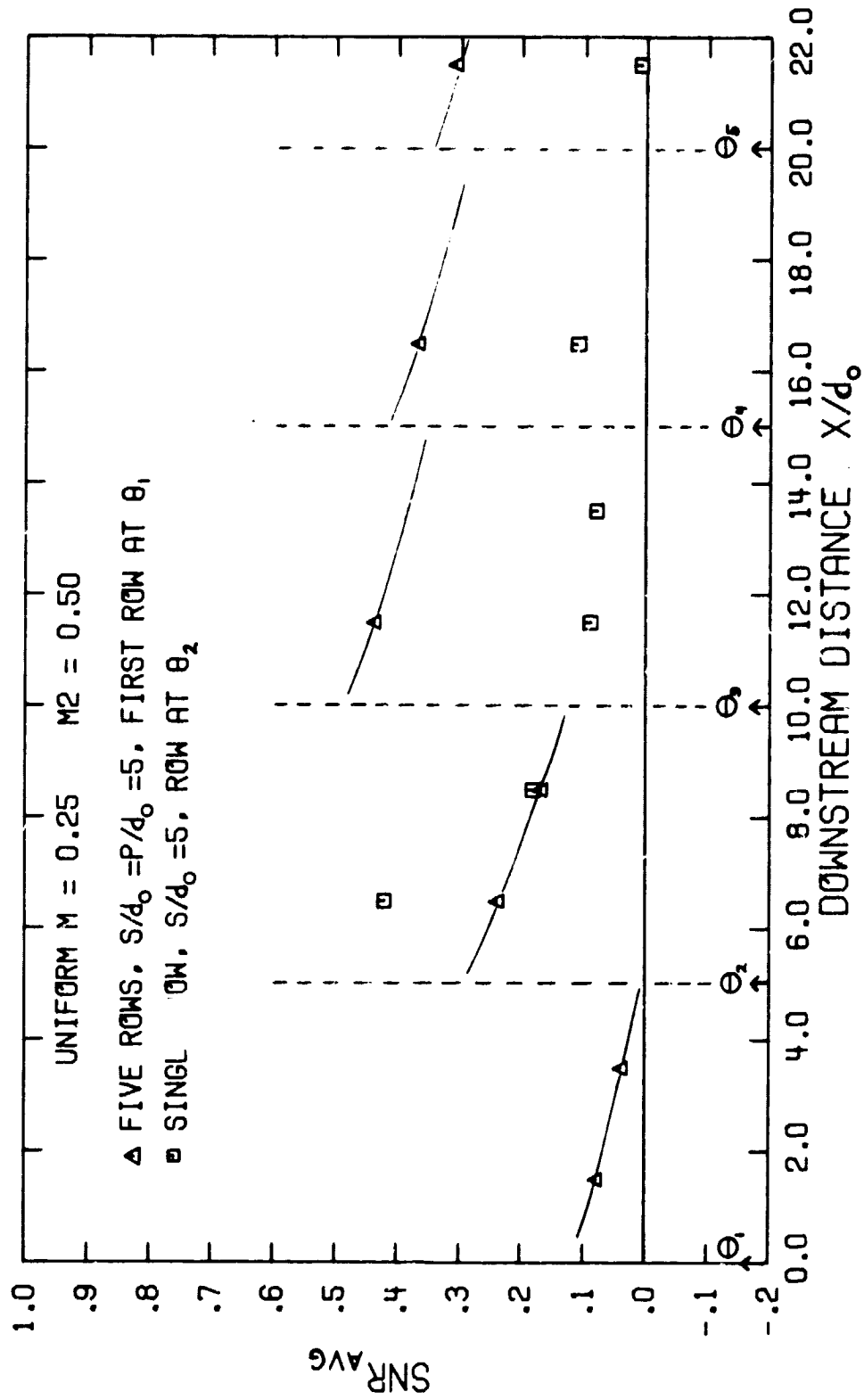


Figure 78. Comparison of the Spanwise Averaged Stanton Number Reduction for the Five Row Configuration and the Single Row Configuration at θ_2 .

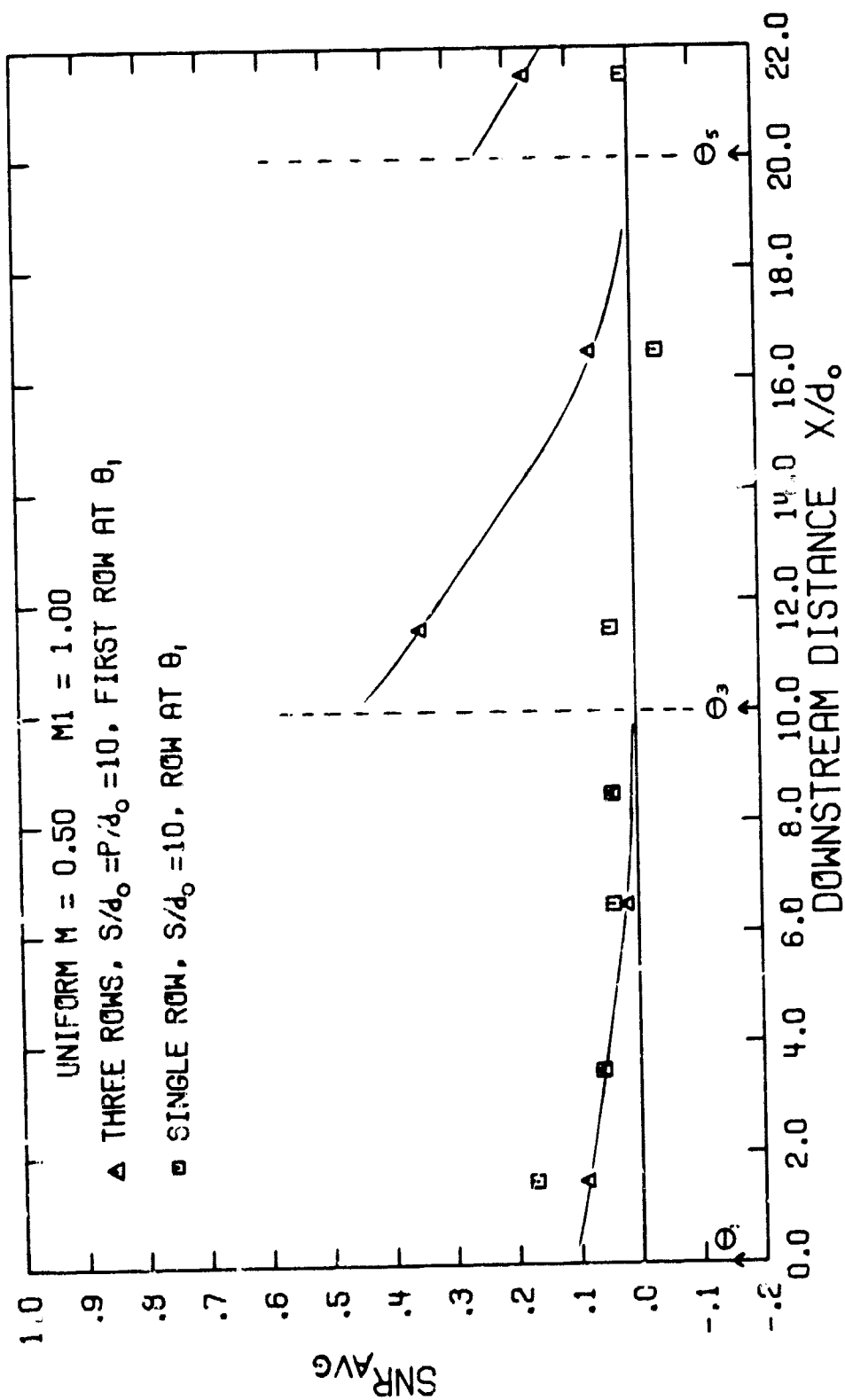


Figure 79. Comparison of the Spanwise Averaged Stanton Number Reduction for the Three Row Configuration and the Single Row Configuration at θ_1 .

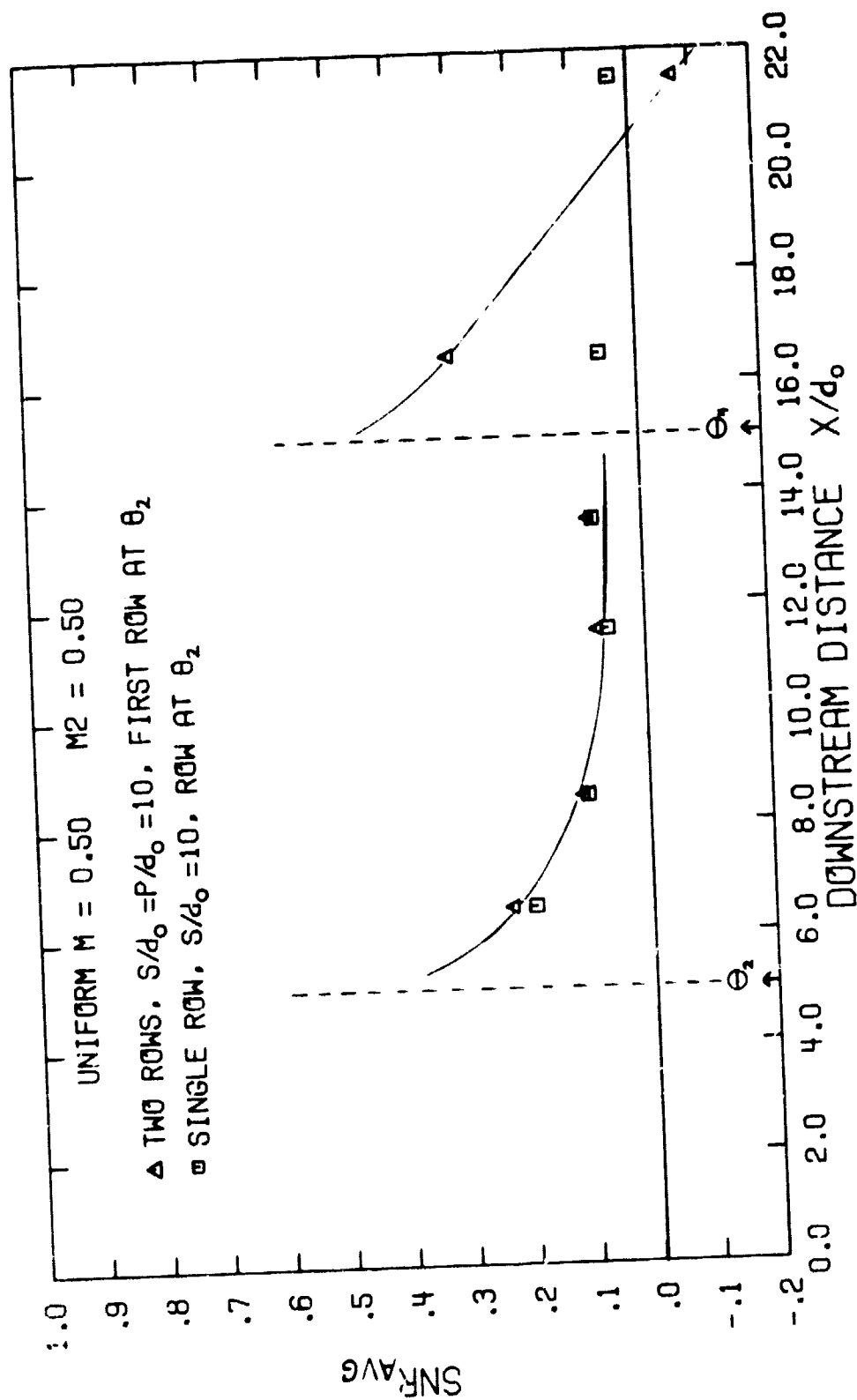


Figure 80. Comparison of the Spanwise Averaged Stanton Number Reduction for the Two Row Configuration and the Single Row Configuration at θ_2 .

from θ_1^1 . The results in Figure 77 demonstrate the superiority of the multiple row configuration, however the total coolant flow rate for the single row is only 0.12 times that for the five row configuration (see footnote). An increase in $M_1 > 1.0$ would not improve SNR_{AVG} for the single row as shown by the data in Table A-17.

The investigation of single row injection for $S/d_0 = 5$ revealed that injection at θ_2 produced much larger values of SNR_{MAX} than for injection at θ_1 . Therefore, Figure 78 compares the data for five row injection with data for single row injection at θ_2 with $M_2 = 0.50$, corresponding to M_{opt} . Note, this combination of M_2 and M corresponds to a coolant flow rate for the single row that is 0.25 times the total coolant flow rate for the five row configuration. Large values of SNR_{AVG} are observed directly behind the single row at θ_2 injection. This is primarily a result of the single row coolant flow rate being twice as large as that from the second row in the five row configuration.

¹ Note, the total coolant flow rate for the single row configuration is significantly less than for the five row configuration. If one considers the variation of the freestream flow as defined in Section II.D ($\rho_\infty V_\infty i = \rho_\infty V_\infty 0.2 C_i \sin \theta_i$), the ratio of single row-to-multiple row total coolant flow rates can be written as

$$\frac{\dot{M}_{Cj}}{\dot{M}_{Ctot}} = \frac{M_j}{M} \left\{ \frac{N_j C_j \sin \theta_j}{\sum_{i=1}^5 N_i C_i \sin \theta_i} \right\}$$

where N = number of coolant holes per row
 M = uniform blowing ratio for five row configuration
 M_j = blowing ratio for single row at θ_j
 \dot{M}_{Cj} = coolant flow rate for single row
 \dot{M}_{Ctot} = total coolant flow rate for all rows

The value of the term $\{ \}$ for single row injection at θ_j is:

θ_j	5°	22.9°	40.8°	58.7°	76.6°
{2 rows}	---	0.3521	---	0.6479	---
{3 rows}	0.0540	---	0.3383	---	0.6077
{5 rows}	0.0305	0.1238	0.2292	0.2734	0.3431

However, downstream from the single row (θ_2), the value of SNR_{AVG} decays rapidly while the multiple row injection maintained SNR_{AVG} at 0.3 to 0.4. Figures 77 and 78 both demonstrate the ability of the multiple row configuration to maintain a level of spanwise averaged film cooling performance across the surface long after the effect of single row injection has decayed to values of SNR_{AVG} near zero.

Figures 79 and 80 compare the data for SNR_{AVG} with coolant injection with a hole spacing $S/d_o = 10$. The data for the three row configuration with the first row at θ_1 is presented in Figure 79 for a uniform value of $M = 0.5$. Also included in this figure are the data for single row injection at θ_1 with $M_1 = 1.0$. Note, this combination of M_1 and M corresponds to a coolant flow rate for the single row that is 0.11 times the total coolant flow rate for the three row configuration (see previous footnote). Figure 80 presents the data for SNR_{AVG} for the two row configuration with the first row at θ_2 . Data for a uniform value of $M = 0.5$ are shown. The data for the single row correspond to injection at θ_2 with $M_2 = 0.5$. This combination of M_1 and M_2 , selected because they produced the optimum film cooling performance for the respective configurations, corresponds to a coolant flow rate for the single row that is 0.35 times the total coolant flow rate for the two row configuration.

Both figures show little difference in the value of SNR_{AVG} downstream of the first row located at θ_1 , or θ_2 . This is to be expected because of the close agreement that was found between the local values of SNR for the multiple and single row configurations. The beneficial effects of multiple row injection are seen downstream of the second row located at θ_3 , or θ_4 . These results indicate the difficulty in maintaining film cooling performance using a multiple row injection pattern with a row spacing, $P/d_o = 10$.

The results presented in Figures 77 through 80 are reproduced in Figures 81 through 84 to provide a direct comparison between the five row, three row and two row configurations. The five row and three row configurations are compared in Figures 81 and 82 for uniform values of $M = 0.25$ and 0.50 , respectively. Figure 81 shows that the five row

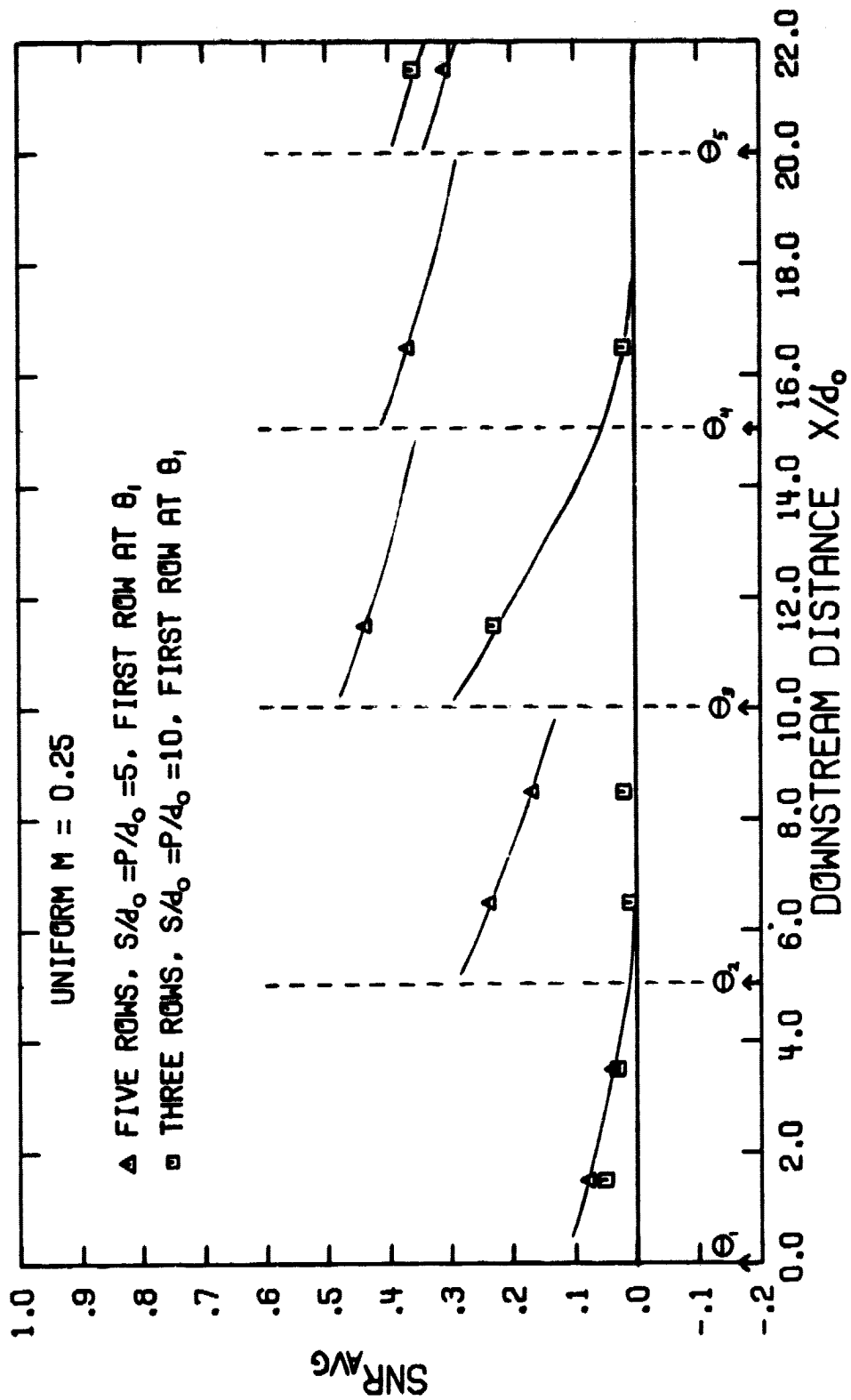


Figure 81. Comparison of the Spanwise Averaged Stanton Number Reduction for the Five Row and Three Row Configurations ($M = 0.25$).

C-3

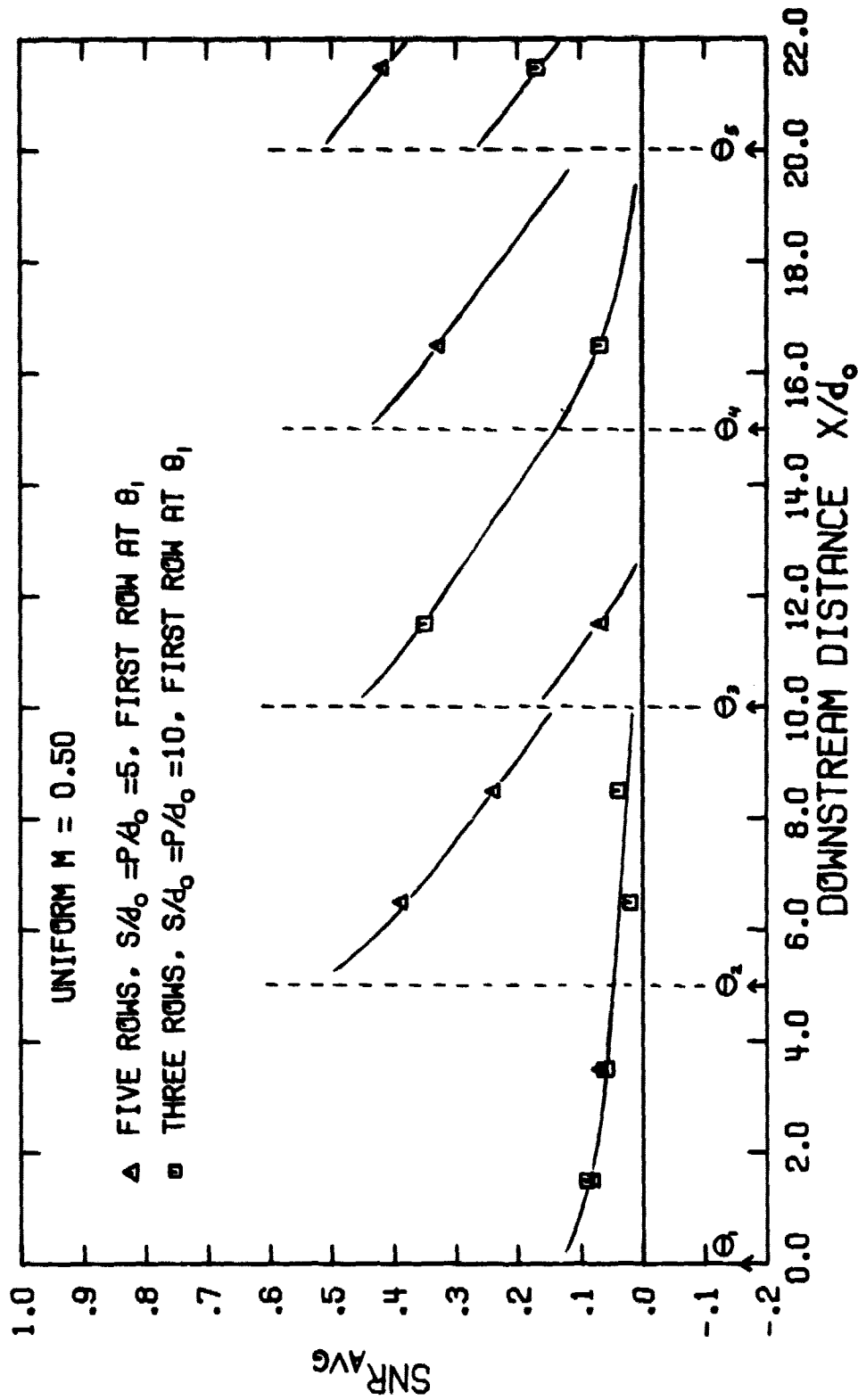


Figure 82. Comparison of the Spanwise Averaged Stanton Number Reduction for the Five Row and Three Row Configurations ($M = 0.50$).

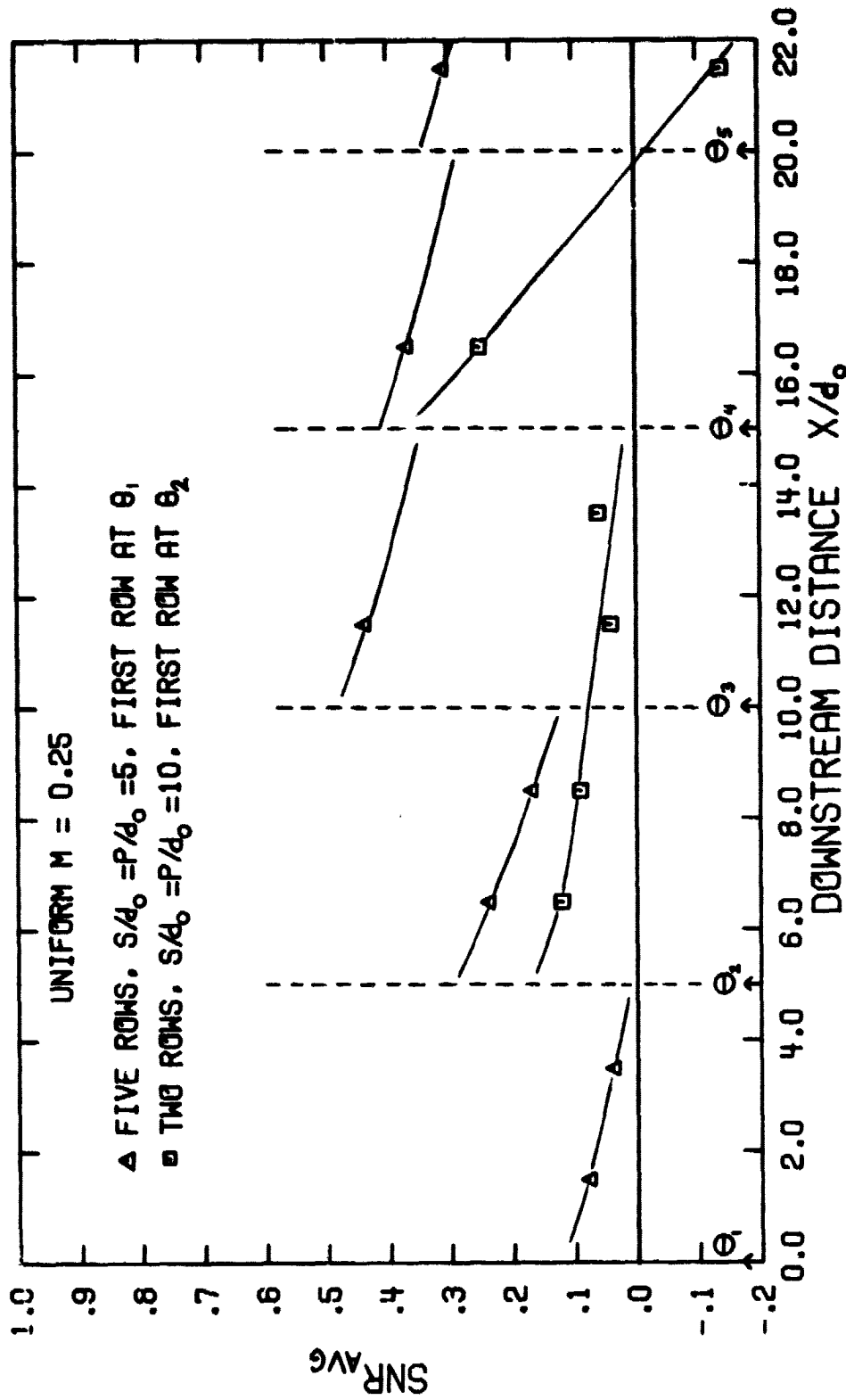


Figure 83. Comparison of the Spanwise Averaged Stanton Number Reduction for the Five Row and Two Row Configurations ($M = 0.25$).

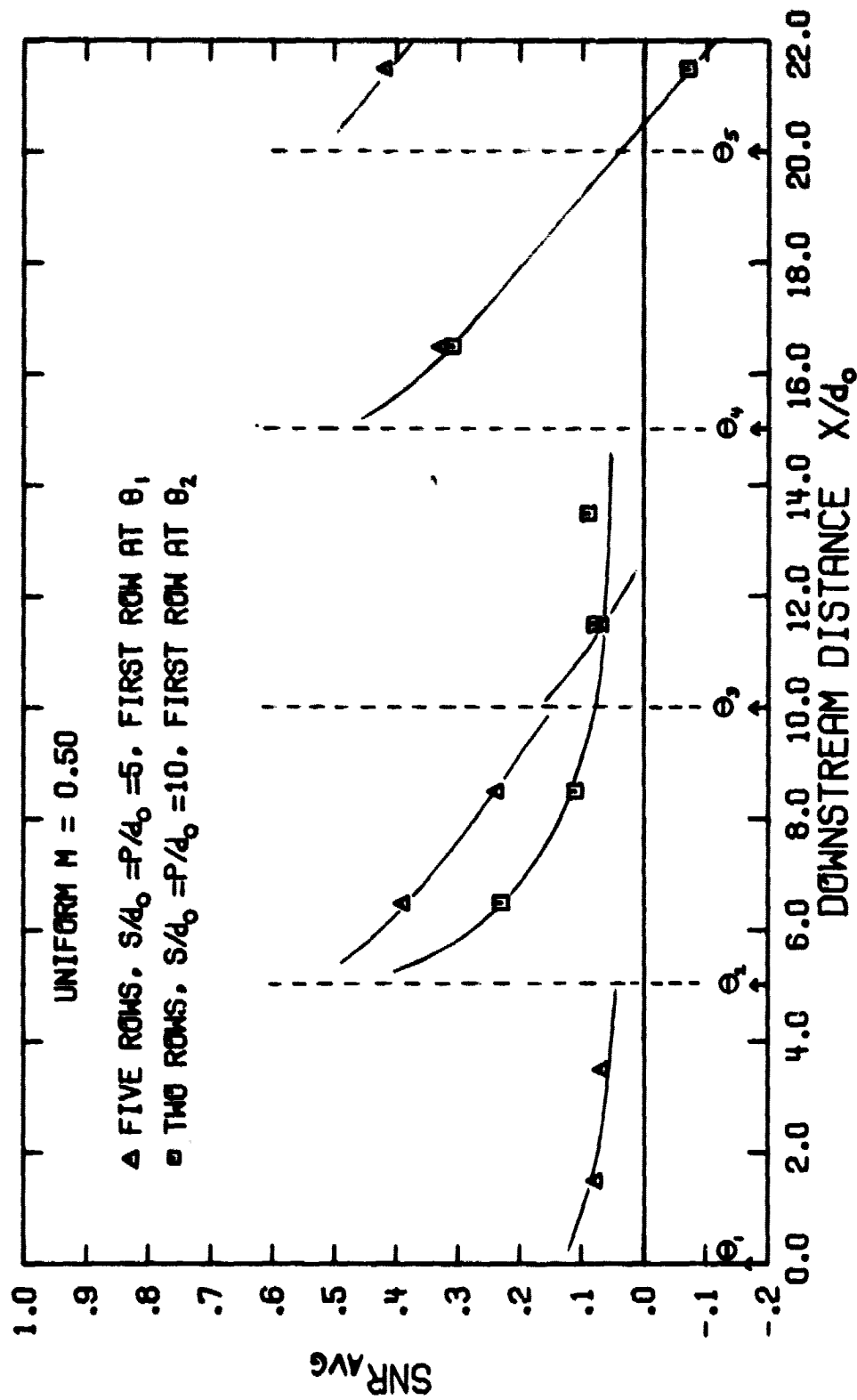


Figure 84. Comparison of the Spanwise Averaged Stanton Number Reduction for the Five Row and Two Row Configurations ($M = 0.50$).

configuration yields significantly better film cooling performance in the region downstream from θ_2 . However, the total coolant flow rate for the five row configuration ($S/d_0 = 5$) is 3.25 times that for the three row configuration ($S/d_0 = 10$) for the same value of M . The results for $M = 0.50$ in Figure 82* still show generally better film cooling performance for the five row configuration. However, the SNR_{AVG} value downstream from the third row at θ_3 is low for the five row configuration as a consequence of negative values of SNR behind the third row beginning at $M = 0.50$. The negative SNR results in a low value for SNR_{AVG} . The three row configuration did not show SNR_{NEG} until $M = 1.25$.

The performance for the five row and two row configurations is compared in Figures 83 and 84 for uniform values of $M = 0.25$ and 0.50 , respectively. For a low value of M , Figure 83, the five row configuration yields superior film cooling performance. However, the total coolant flow rate for the five row arrangement is 4.74 times that for the two row. The performance for higher M , Figure 84, shows the five row configuration somewhat better than the two except for the region downstream from θ_3 as discussed previously.

The basic limitation with the row spacing, $P/d_0 = 10$, is the rapid decay of the film cooling performance after injection. The film cooling performance decreases significantly before additional coolant is added by the next row. However, when the blowing ratio is kept low, the five row configuration with $S/d_0 = P/d_0 = 5$ is capable of maintaining a level of SNR_{AVG} of 0.2 to 0.3 over the major portion of the surface.

* Data for the five row configuration for $M = 0.5$, not shown previously, were obtained from Table A-25.

V.C.6 Prediction of the Results for Multiple Row Injection Using Superposition Theory

At low values of the blowing ratio, the results for multiple row injection were in good agreement with those for single row injection. This suggested that a superposition model might be effective in estimating the multiple row film cooling performance with single row injection data. Sellers [44] developed a superposition model to predict the adiabatic effectiveness, η_{adw} , for a multiple row configuration. Figure 85 presents a schematic representation of the model. The features of the model are outlined for two rows of holes.

It is assumed that adiabatic effectiveness data have been obtained for blowing from row 1 alone and from row 2 alone, with the film effectiveness for each row defined as

$$\eta_{1,s} = \frac{T_{\infty} - T_{ad1,s}}{T_{\infty} - T_{c,1}} \quad (27)$$

$$\eta_{2,s} = \frac{T_{\infty} - T_{ad2,s}}{T_{\infty} - T_{c,2}} \quad (28)$$

where the subscript s designates injection from a single row only and 1 (or 2) identifies the region downstream from row 1 (or row 2). The adiabatic effectiveness for two rows blowing simultaneously is defined as

$$\eta_{2,m} = \frac{T_{\infty 2,m} - T_{ad2,m}}{T_{\infty 2,m} - T_{c,2}} \quad (29)$$

where the subscript m designates multiple row injection. In the superposition model, it is assumed that $T_{ad2,m} = T_{ad2,s}$ and $T_{\infty 2,m} = T_{ad1,s}$. Then equation (28) can be rearranged to give

$$T_{ad2,m} = \eta_{2,s} T_{c,2} + (1 - \eta_{2,s}) T_{ad1,s} \quad (30)$$

Using equations (29) and (30) it can be shown that for two rows blowing

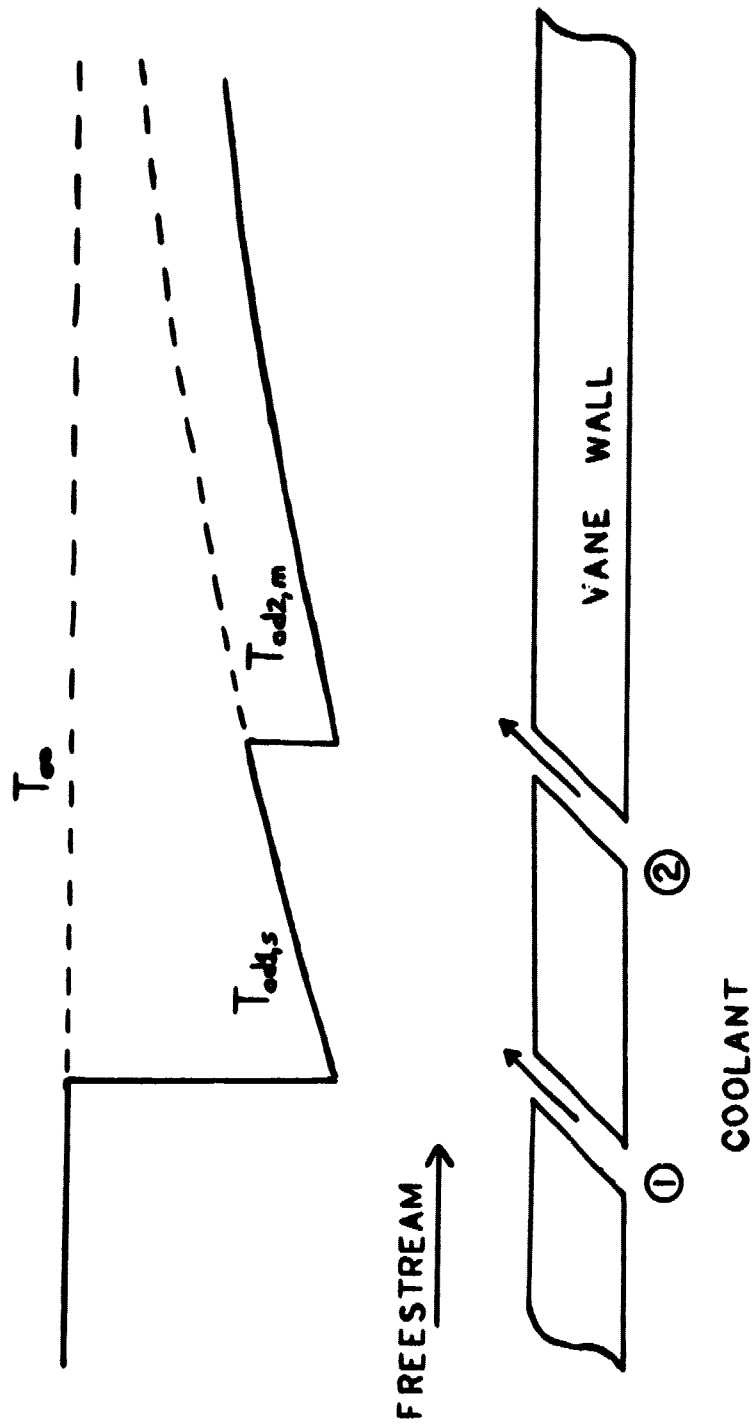


Figure 85. Schematic of the Superposition Model

$$\eta_{2,m} = \eta_{1,s} + \eta_{2,s} (1 - \eta_{1,s}) \quad (31a)$$

The format of equation (31a) can be generalized for the effectiveness downstream from N rows of holes.

$$\eta_{N,m} = \sum_{i=1}^N \eta_{i,s} \prod_{j=0}^{i-1} (1 - \eta_{j,s}) \quad (31b)$$

where $\eta_{0,s} = 0$. This superposition model can also be applied to the Stanton number ratio which is related to the adiabatic effectiveness by the following equation (see Section I.C.1).

$$\frac{St_{FC}}{St_0} = \frac{h'}{h_0} (1 - \theta_c \eta_{adw}) \quad (15)$$

Rearranging equation (15) gives

$$\frac{(1 - \frac{St_{FC}}{St_0}) + (\frac{h'}{h_0} - 1)}{(\frac{h'}{h_0}) \theta_c} = \eta_{adw} \quad (32)$$

Equation (32) can be substituted for $\eta_{i,s}$ and $\eta_{N,m}$ in equation (31b) to predict the Stanton number ratio for multiple rows.

The experiments for this investigation were conducted with $\theta_c = 1.0$. For simplicity, and due to a lack of data for h'/h_0 in the stagnation region, it was further assumed that $h'/h_0 \approx 1.0$, and then equation (32) reduces to

$$(1 - \frac{St_{FC}}{St_0})_{i,s} = (SNR)_{i,s} = \eta_{i,s} \quad (33)$$

The results for SNR_{AVG} for single row injection were used in conjunction with equations (33) and (31b) to predict SNR_{AVG} for multiple row injection. The application of the superposition theory was limited to values of M where $(SNR_{AVG})_{i,s} > 0$ due to the necessity of information

on h'/h_0 to handle negative values of SNR.

Table 18 shows the experimental results from the investigation of injection from five rows of holes compared with the predictions made with the superposition model. For $M = 0.25$, the predictions from the model compare well with the experimental data except downstream from the fourth row where the model underpredicts the value of SNR_{AVG} . The predictions for $M = 0.50$ show reasonable agreement downstream from the first two rows. The large discrepancy downstream from the row at $\theta_3 = 40.8^\circ$ is due to large negative values (SNR_{AVG}) downstream from the third row when $M = 0.50$ for the five row configuration. With injection from a single row, negative values of $(SNR_{AVG})_{3,s}$ did not occur until $M_3 = 0.75$. Therefore, the superposition model appears useful to estimate multiple row performance when the blowing ratio is low enough that negative values of SNR do not appear on the surface. Additional information on realistic values of h'/h_0 would be required to extend the use of the superposition model.

V.D. Summary

The foregoing discussions show that coolant injection from multiple rows can result in attractive levels of film cooling performance in the stagnation region when the blowing ratio is relatively low. With a uniform distribution of M , values of $M < 0.5$ are needed to avoid negative values of SNR behind the coolant holes. For low values of M , the best film cooling performance was obtained with the five row configuration ($S/d_0 = P/d_0 = 10$). Although the three row and two row configurations ($S/d_0 = P/d_0 = 10$) represent an improvement over injection from a single row, the rows are spaced too far apart. The lack of spreading by the coolant across the surface and the rapid decay in performance downstream would suggest a closer row spacing.

For higher values of blowing ratio ($M > 1.0$), large negative values, SNR_{NEG} , begin to dominate the film cooling performance. Heat flux levels exceed those without film coolant flow as SNR approaches -1.0 to -2.0 in some locations. For moderate values of the blowing ratio, $M \approx 0.75 - 1.0$, multiple row injection creates a disturbance

Table 18. Prediction of SNR_{AVG} from Superposition Model
Five Row Configuration ($S/d_0 = P/d_0 = 5$)

$M = 0.25$

	$\theta_1 = 5^\circ^*$		$\theta_2 = 22.9$		$\theta_3 = 40.8$	$\theta_4 = 58.7$
x/d_0	1.5	3.5	1.5	3.5	1.5	1.5
SNR_{AVG} Experiment	.08	.04	.24	.17	.44	.37
SNR_{AVG} Predicted	.07	.03	.26	.18	.42	.25

$M = 0.50$

	$\theta_1 = 5^\circ$		$\theta_2 = 22.9$		$\theta_3 = 40.8$	$\theta_4 = 58.7$
x/d_0	1.5	3.5	1.5	3.5	1.5	1.5
SNR_{AVG} Experiment	.08	.07	.39	.24	.07	.33
SNR_{AVG} Predicted	.07	.03	.43	.19	.41	.47

* Values for $(SNR_{AVG})_{1.5}$ at $M = 0.5$ were used for the prediction since that was the lowest value of M investigated at $\theta_1 = 5^\circ$.

such that the film cooling performance at downstream rows is adversely affected. While injection at $\theta_1 = 5^\circ$ was found to have little effect on the performance downstream from the row at $\theta_2 = 22.9^\circ$, injection at θ_2 had noticeable effects on the performance downstream from the row at $\theta_3 = 40.8^\circ$. When blowing was applied at θ_2 in the multiple row configurations, the development of SNR_{NEG} downstream from θ_3 occurred at lower values of M than with single row injection at θ_3 .

Multiple row injection continued to exhibit the highly localized cooling effect found previously with single row injection. However, by using multiple rows and by staggering them, it was possible to achieve a more uniform coverage and an improved SNR_{AVG} than with single row injection. But this improvement was always contingent upon maintaining a low blowing ratio.

VI. MULTIPLE ROW INJECTION WITH A BLOWING DISTRIBUTION SIMULATING PLENUM SUPPLY

VI.A. Introduction

This chapter presents the results for multiple row coolant injection with a blowing distribution typical of that resulting when all rows are supplied from a common plenum. The three different hole and row spacing configurations studied were (same as in Chapter V) (a) five row configuration ($S/d_0 = P/d_0 = 5$) with the first row at $\theta_1 = 5^\circ$, (b) three row configuration ($S/d_0 = P/d_0 = 10$) with the first row at $\theta_1 = 5^\circ$, and (c) two row configuration ($S/d_0 = P/d_0 = 10$) with the first row at $\theta_2 = 22.9^\circ$.

Typical cooling configurations for the leading edge of a turbine vane, with multiple rows of holes fed from a common plenum, result in a nonuniform blowing distribution since the coolant flow rate per row is governed by the plenum-to-external surface pressure difference. In addition to the variation of the coolant flow rate row to row, the local blowing ratio is influenced by the variation of the freestream mass velocity ($\rho_\infty V_\infty$) along the surface.

A model was developed to predict the blowing ratio as a function of the row location (θ_1) for coolant holes fed by a common plenum (see Appendix I). The blowing distribution, predicted for specified row locations, was found to depend on two parameters, the approach Mach number, $Ma_{\infty,0}$ and the plenum total pressure-to-freestream total pressure ratio, $P_{Tc}/P_{T\infty}$. Calculation of the blowing distribution representative of engine design conditions were performed for $Ma_{\infty,0} = 0.1$ and 0.2 , and $P_{Tc}/P_{T\infty} = 1.010$, 1.020 , and 1.030 . The six blowing distributions that resulted from these combinations are listed in Section II.C., Table 3, for each of the three hole spacing configurations studied.

A complete listing of the experimental values of SNR for multiple row coolant injection with the blowing distribution simulating a plenum supply is presented in tabular and graphical form in Appendix III. The results are discussed qualitatively in Section VI.B. and the analysis

of the data is presented in section VI.C.

Frequent reference is made to the data from Chapters IV and V to illustrate the influence of the nonuniform blowing distribution.

VI.B. Presentation of the Data

The presentation of the data is divided into three sections, one for each multiple row configuration studied. The data are examined to illustrate the influence of the film cooling parameters: injection location, θ_1 , blowing ratio, M , and streamwise (x/d_0) and spanwise location (z/S). Comparisons with the results for single row injection and multiple row injection with uniform M are presented to determine the influence of blowing from upstream and downstream rows on the film cooling performance at a particular location.

VI.B.1. Five Row Configuration with First Row at $\theta_1 = 5^\circ$, $S/d_0 = P/d_0 = 5$

Figure 86 presents the film cooling performance at $(x/d_0)_1 = 1.5$ downstream from the first row of coolant holes showing the Stanton Number Reduction (SNR) as a function of spanwise location, z/S . The legend in the figure defines the blowing distribution for the six combinations of $Ma_{\infty,0}$, $P_{TC}/P_{T\infty}$ studied (see Table 3, Section II.C). The blowing distribution yields the lowest values of M with $P_{TC}/P_{T\infty} = 1.010$ and $Ma_{\infty,0} = 0.2$. The blowing ratio then increases in magnitude as $P_{TC}/P_{T\infty}$ is increased to 1.030 (with $Ma_{\infty,0} = 0.2$). By changing the Mach number to 0.1, the blowing distribution for $P_{TC}/P_{T\infty} = 1.010$ exceeds the largest blowing distribution for $Ma_{\infty,0} = 0.2$. The blowing ratio for $Ma_{\infty,0} = 0.1$ also increases as $P_{TC}/P_{T\infty}$ is increased to 1.030.

Reference to Figure 86 shows, as might be expected, the highly localized influence of the coolant behind the first row of the five row configuration. Even at the lowest blowing ratio studied, $M_1 \approx 3.0$, large negative values of SNR were observed. As the blowing ratio was increased, the magnitude of the negative SNR remained fairly constant. However, the value of SNR at $(x/d_0)_1 = 1.5$ was about one-half that found with single row injection at $\theta_1 = 5^\circ$. The positive value of SNR never exceeded 0.21. The previous data for single row injection at $\theta_1 = 5^\circ$

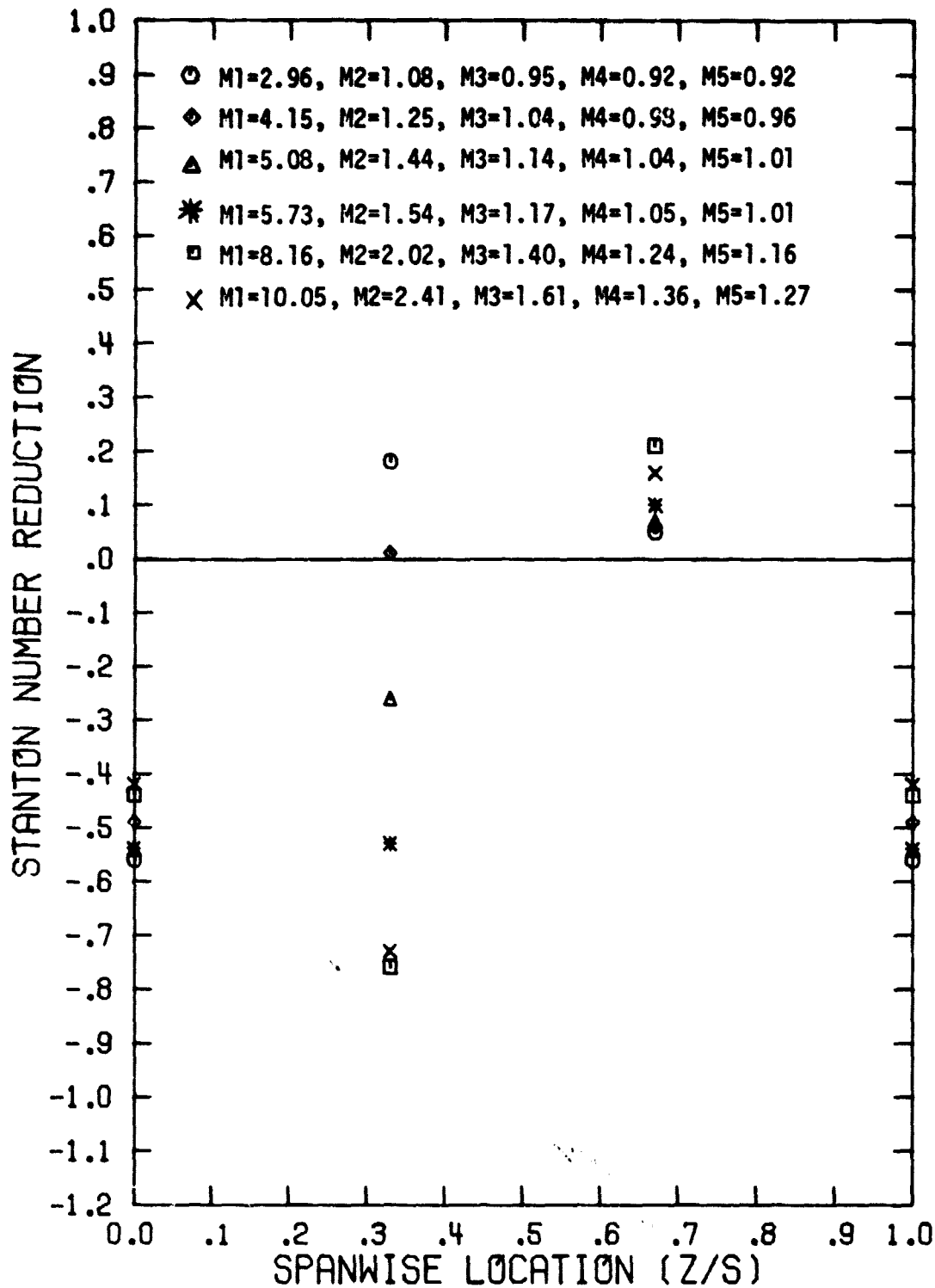


Figure 86. Spanwise Variation of the Stanton Number Reduction for a Five Row Configuration with Blowing Distribution Simulating Plenum Supply ($\theta_1=5^\circ$, $(x/d_0)_1=1.5$, $S/d_0=P/d_0=5$)

showed comparable levels for SNR for high values of M_1 .

Downstream at $(x/d_0)_1 = 3.5$, the negative values of SNR behind the coolant hole diminished somewhat and the positive values of SNR tended to increase slightly from the values at $(x/d_0)_1 = 1.5$. Lateral spreading of the coolant did not materialize and the trends and patterns established by the data for single row injection were repeated behind the first row of the five row configuration with the variable blowing distribution. The main difference between the two configurations was the smaller negative value of SNR that occurred with the five row configuration at the higher values of blowing ratio.

Figure 87 presents the data for SNR_{AVG} as a function of the blowing ratio for the downstream locations of $(x/d_0)_1 = 1.5$ and 3.5. The data for $(x/d_0)_1 = 1.5$ show $SNR_{AVG} < 0$ for every blowing ratio investigated with values in close agreement with the data for single row injection for $M_1 < 5.7$. However, for $M_1 = 8.2$ and 10.1, the negative values for SNR_{AVG} for single row injection were substantially larger than those for the five row configuration. Downstream at $(x/d_0)_1 = 3.5$, Figure 87 shows values of SNR_{AVG} that are also negative at all values of the blowing ratio. Compared with the data for single row injection at $(x/d_0)_1 = 3.5$, the values of SNR_{AVG} for multiple row injection are less negative, and the difference is most noticeable at $M = 8.2$ and 10.1.

Figure 88 presents the film cooling performance at $(x/d_0)_2 = 1.5$ downstream from the second row of holes. For the lowest value of blowing ratio used at the second row ($M_2 = 1.08$) negative values of SNR were observed behind the coolant hole. The negative value of SNR increased in magnitude as the blowing ratio was increased for $1.08 \leq M_2 \leq 1.54$ and then decreased for $M_2 > 1.5$. Although the film cooling effect was highly localized, values of SNR_{MAX} of 0.7 to 0.5 were observed for up to $M_2 = 2.02$. A review of the data for single row injection shows that SNR_{NEG} was initiated at $M_2 = 1.1$ and increased in magnitude up to $M_2 = 2.47$. The magnitude of the SNR_{MAX} for single row injection were approximately one-half that shown in Figure 88.

Downstream of the second row for the plenum blowing simulation,

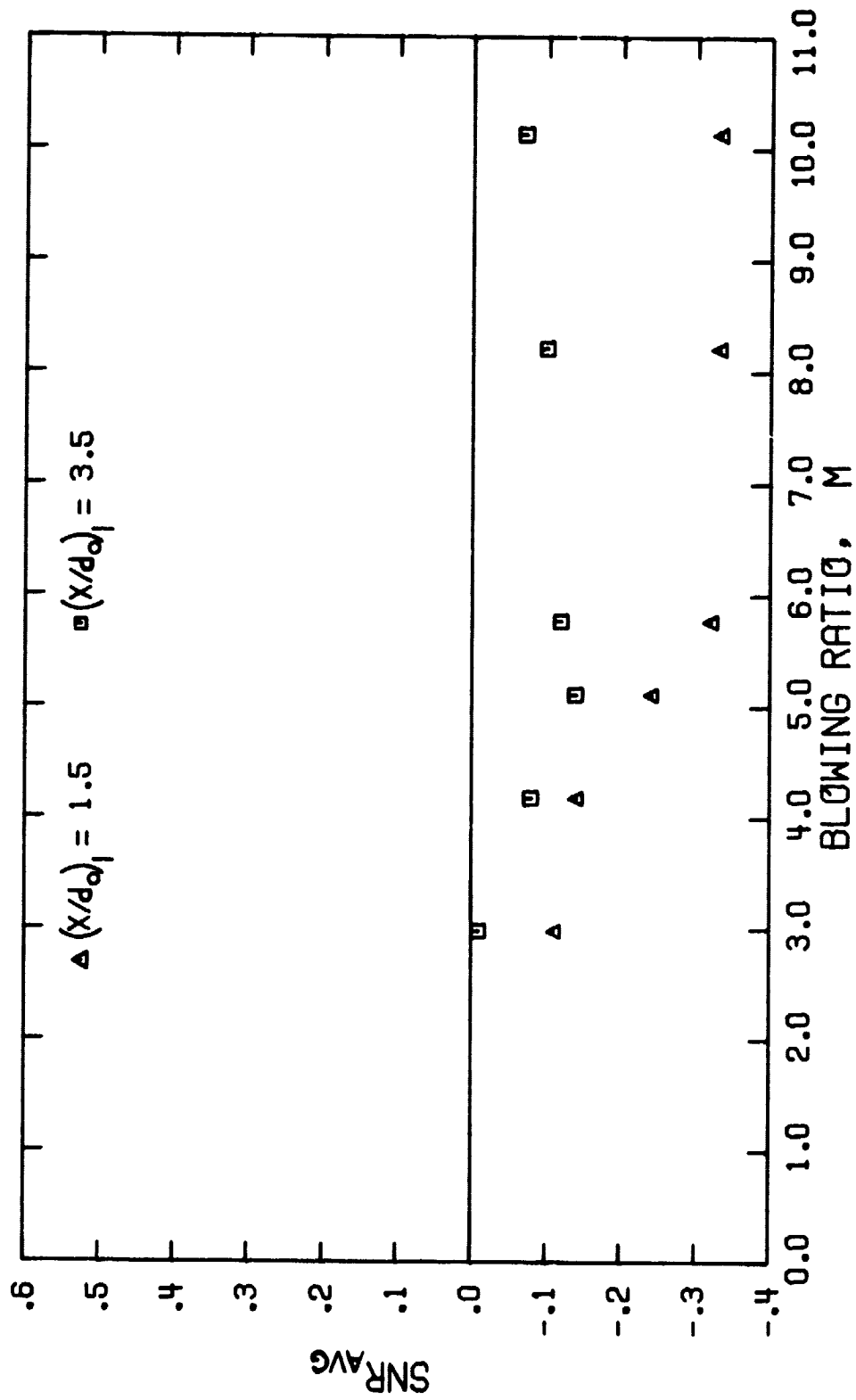


Figure 87. Variation of the Spanwise Averaged Stanton Number Reduction for a Five Row Configuration with Blowing Distribution Simulating Plenum Supply ($\theta_1 = 5^\circ$, $S/d_0 = P/d_0 = 5$)

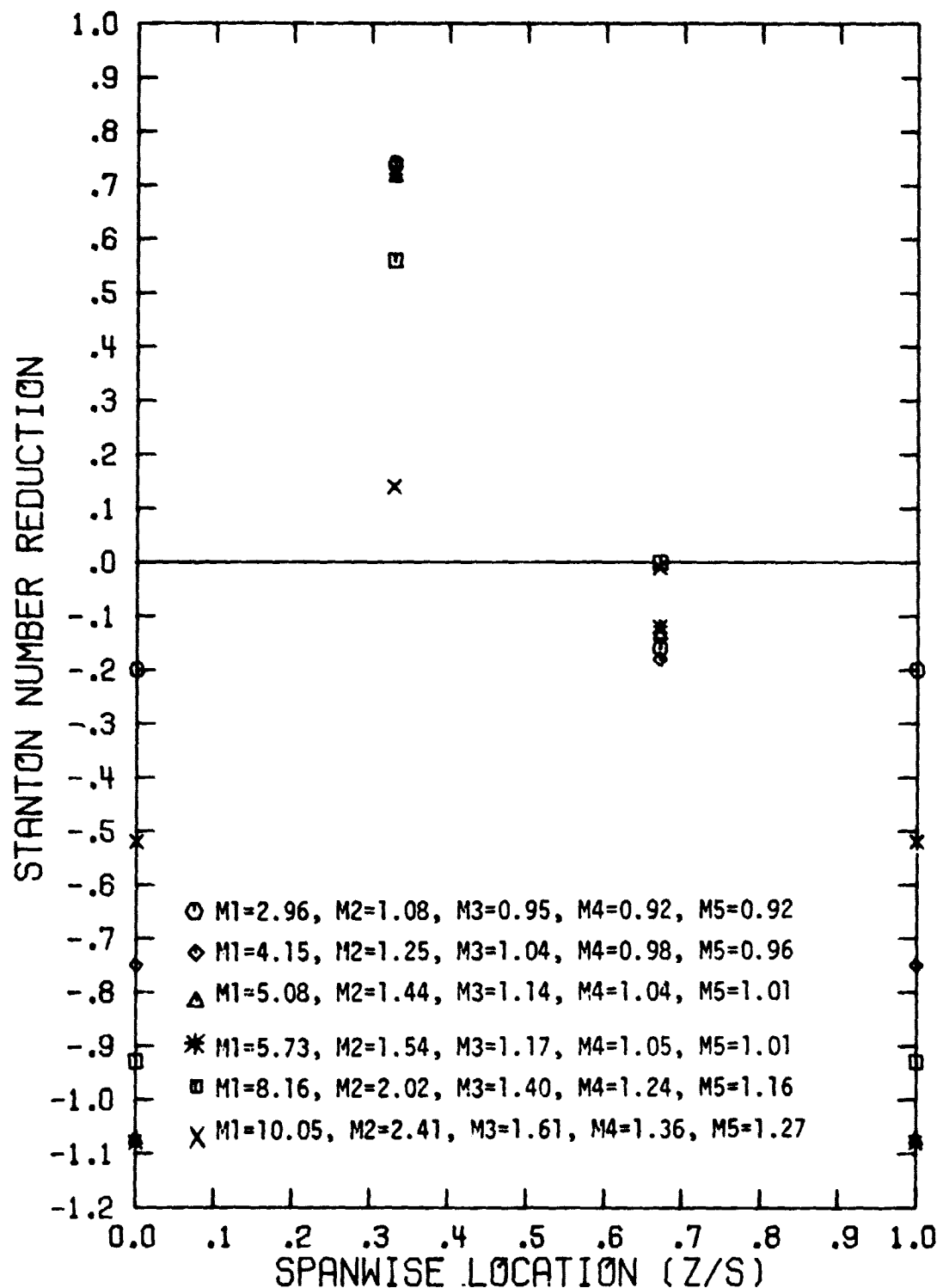


Figure 88. Spanwise Variation of the Stanton Number Reduction for a Five Row Configuration with Blowing Distribution Simulating Plenum Supply ($\theta_2=22.9^\circ$, $(x/d_0)_2=1.5$, $S/d_0=P/d_0=5$)

negative values of SNR were observed at $z/S = 0.67$ for $M_2 = 1.08$, persisting until $M_2 = 1.54$. The data for single row injection and multiple row injection with uniform blowing show $SNR \sim 0$ at this spanwise location for the same range of blowing ratio. The levels of SNR_{MAX} for the plenum blowing simulation were somewhat larger than that for single row injection and multiple row injection with uniform blowing. Downstream at $(x/d_0)_2 = 3.5$, the positive values of SNR decreased and were located at $z/S = 0.67$ near the hole in the next row downstream.

Figure 89 presents the data for SNR_{AVG} as a function of the blowing ratio for the downstream locations of $(x/d_0)_2 = 1.5$ and 3.5 . The spanwise averaged data at $(x/d_0)_2 = 1.5$ show $SNR_{AVG} > 0$ for $M_2 \leq 1.08$ with negative values of SNR_{AVG} for higher blowing ratio. The data for single row injection at $(x/d_0)_2 = 1.5$ are in good agreement with the results for the plenum blowing simulation for $M_2 \leq 1.54$. Downstream at $(x/d_0)_2 = 3.5$, SNR_{AVG} is near zero for all values of the blowing ratio shown. With single row injection, SNR_{AVG} was significantly less than zero, -0.10 to -0.34 for all values of blowing ratio studied.

The film cooling performance downstream from the third row (θ_3) is presented in Figure 90 for $(x/d_0)_3 = 1.5$. At this location, the study of single row injection at θ_3 indicated that $SNR < 0$ for $M_3 \geq 0.75$ and the study with multirow injection with a uniform blowing distribution showed that $SNR < 0$ for $M_3 \geq 1.0$. These trends are repeated by the results for the plenum blowing simulation in Figure 90. The lowest value of blowing ratio for the third row was $M_3 = 0.95$ and, as can be seen, SNR was negative over most of the span. The value of SNR_{MAX} was 0.08 and increasing the blowing ratio to $M_3 = 1.04$ resulted in negative values of SNR over the entire span.

The magnitude of SNR_{NEG} (behind the hole) was approximately constant up to $M_3 = 1.17$. Increasing the blowing ratio beyond this point actually caused SNR_{NEG} to be less negative although a large negative value of SNR was observed at the spanwise location, $z/S = 0.33$.

Figure 91 presents the data for SNR_{AVG} at $(x/d_0)_3 = 1.5$ as a function of the blowing ratio for both the multiple row configuration with the plenum blowing simulation and the single row configuration.

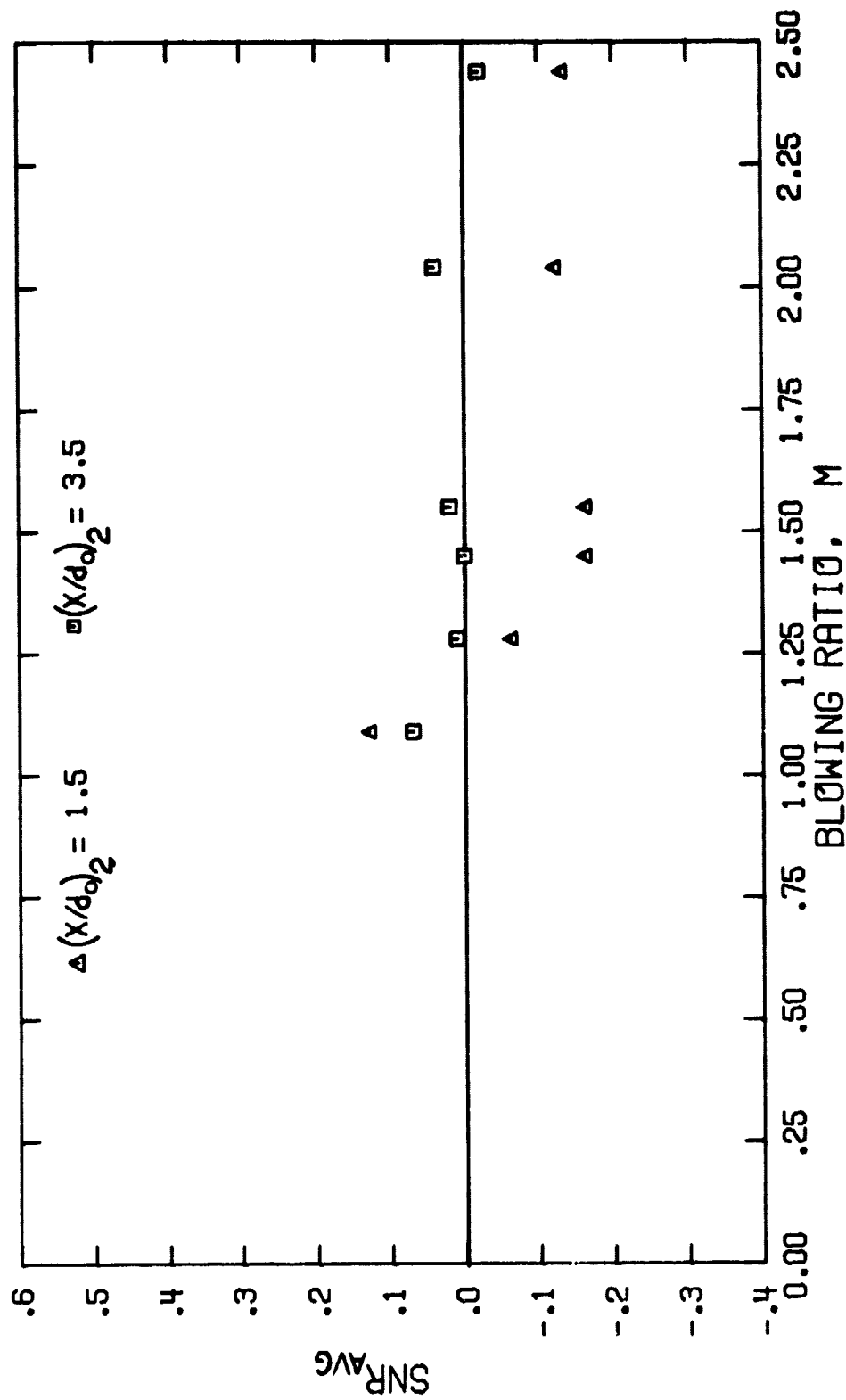


Figure 89. Variation of the Spanwise Averaged Stanton Number Reduction for a Five Row Configuration with Blowing Distribution Simulating Plenum Supply ($\theta_2 = 22.9^\circ$, $S/d_o = P/d_o = 5$)

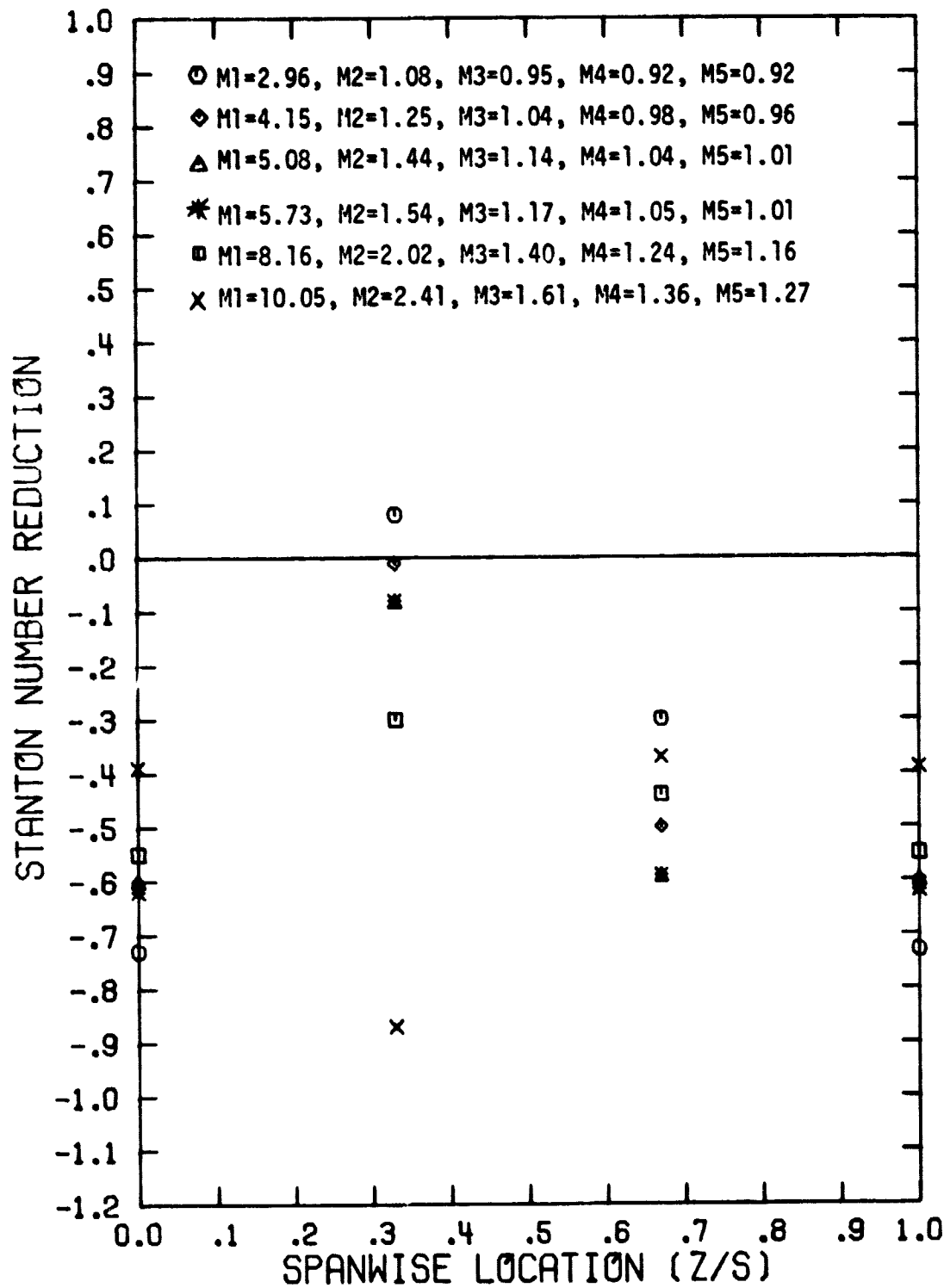


Figure 90. Spanwise Variation of the Stanton Number Reduction for a Five Row Configuration with Blowing Distribution Simulating Plenum Supply ($\theta_3 = 40.8^\circ$, $(x/d_0)_3 = 1.5$, $S/d_0 = P/d_0 = 5$)

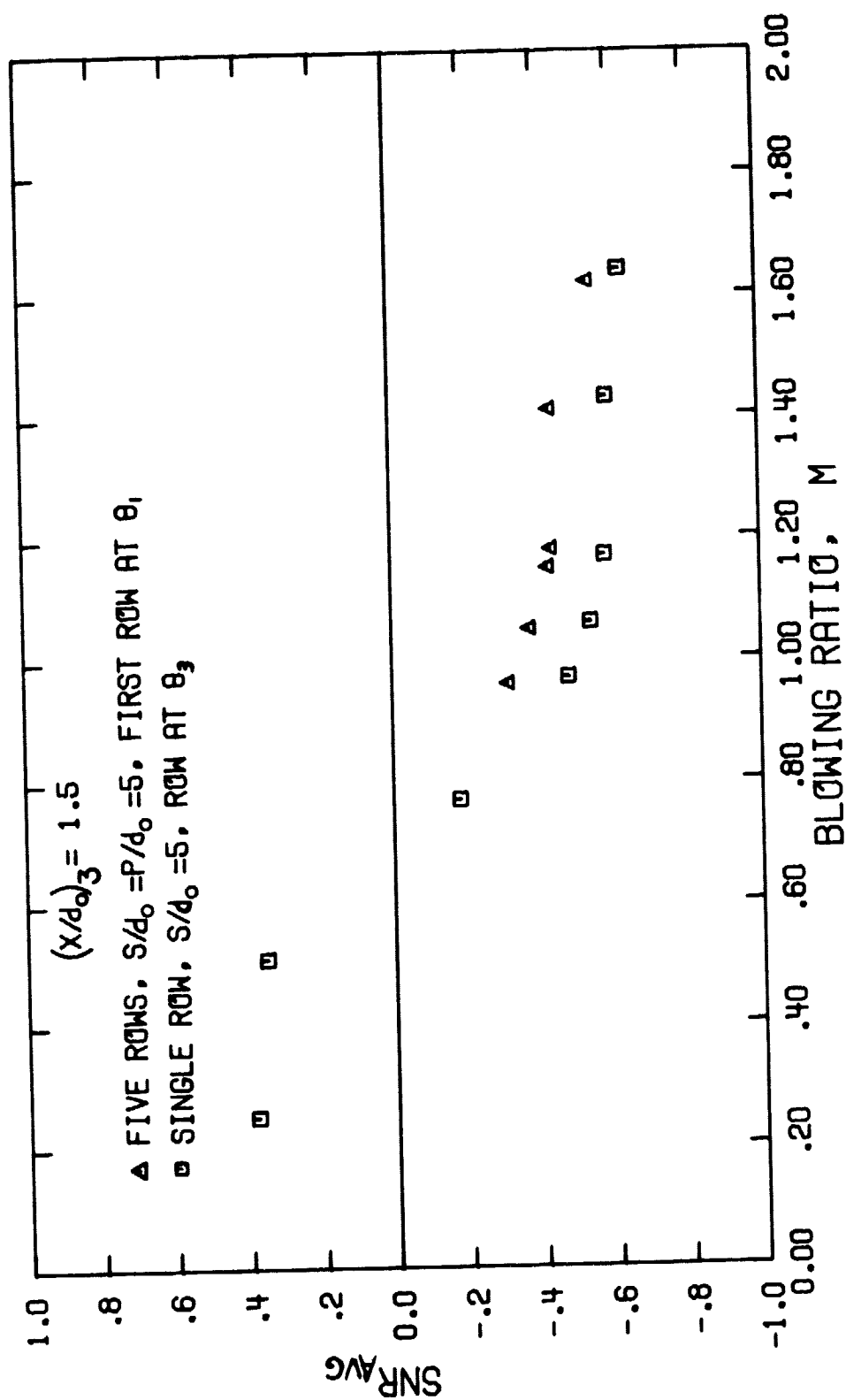


Figure 91. Comparison of the Spanwise Averaged Stanton Number Reduction for the Five Row Configuration and the Single Row Configuration at θ_3 ($S/d_0 = 5$, $(x/d_0)_3 = 1.5$)

The spanwise averaged results for the plenum blowing simulation reflect the influence of generally negative values of SNR for $M_3 > 0.95$, with SNR_{AVG} varying from -0.31 for $M_3 = 0.95$ to -0.54 at $M_3 = 1.61$. However, for $M_3 \leq 0.70$ the data trends suggest that $SNR_{AVG} > 0$ at this location. It is noted that negative values of SNR_{AVG} for the plenum blowing simulation are not as severe as for single row injection, apparently due to upstream injection in the former case.

The film cooling performance downstream from the fourth row (θ_4) is presented in Figure 92 for $(x/d_o)_4 = 1.5$. It is noted that for the value of M_4 (and M_5) did not vary significantly as the values of $P_{TC}/P_{T\infty}$ and $Ma_{\infty,0}$ were changed. Therefore, a narrow range of blowing ratio was examined for rows four and five, $0.92 \leq M \leq 1.36$.

The data for single row injection at θ_4 showed SNR_{NEG} ($SNR < 0$ behind the hole) for $M_4 = 0.95$. The data for multiple row injection with uniform blowing showed SNR_{NEG} for $M_4 = 0.75$. Since the lowest value of blowing ratio studied for the plenum blowing simulation was $M_4 = 0.93$, negative values of SNR behind the coolant hole, as shown in Figure 92, were expected. The localized coolant effect shows $SNR_{MAX} \approx 0.3$ for $M_4 \leq 1.05$. The trends shown in Figure 92 repeat the pattern found previously behind the second and third rows of coolant holes. With the blowing ratio $M_4 = 0.98$, the spanwise distribution of SNR for the plenum blowing simulation is in excellent agreement with the results for uniform blowing for $M = 1.0$. However, a review of the data for single row injection at θ_4 shows some differences from the multiple row data, with values of SNR_{NEG} that are less negative and values of SNR_{MAX} that are somewhat larger (~ 0.4).

For $M_4 \geq 1.24$, the data for the plenum blowing simulation show that SNR is generally negative across the span, although the value of SNR_{NEG} (behind the coolant hole) was less severe for $M_4 = 1.36$.

Figure 93 presents the data for SNR_{AVG} at $(x/d_o)_4 = 1.5$ as a function of the blowing ratio for both the multiple row configuration with the plenum blowing simulation and the single row configuration. The values of SNR_{AVG} were negative for all values of blowing ratio, varying from -0.17 at $M_4 = 0.92$ to -0.28 at $M_4 = 1.24$. The data in Figure 93 illustrate different trends for

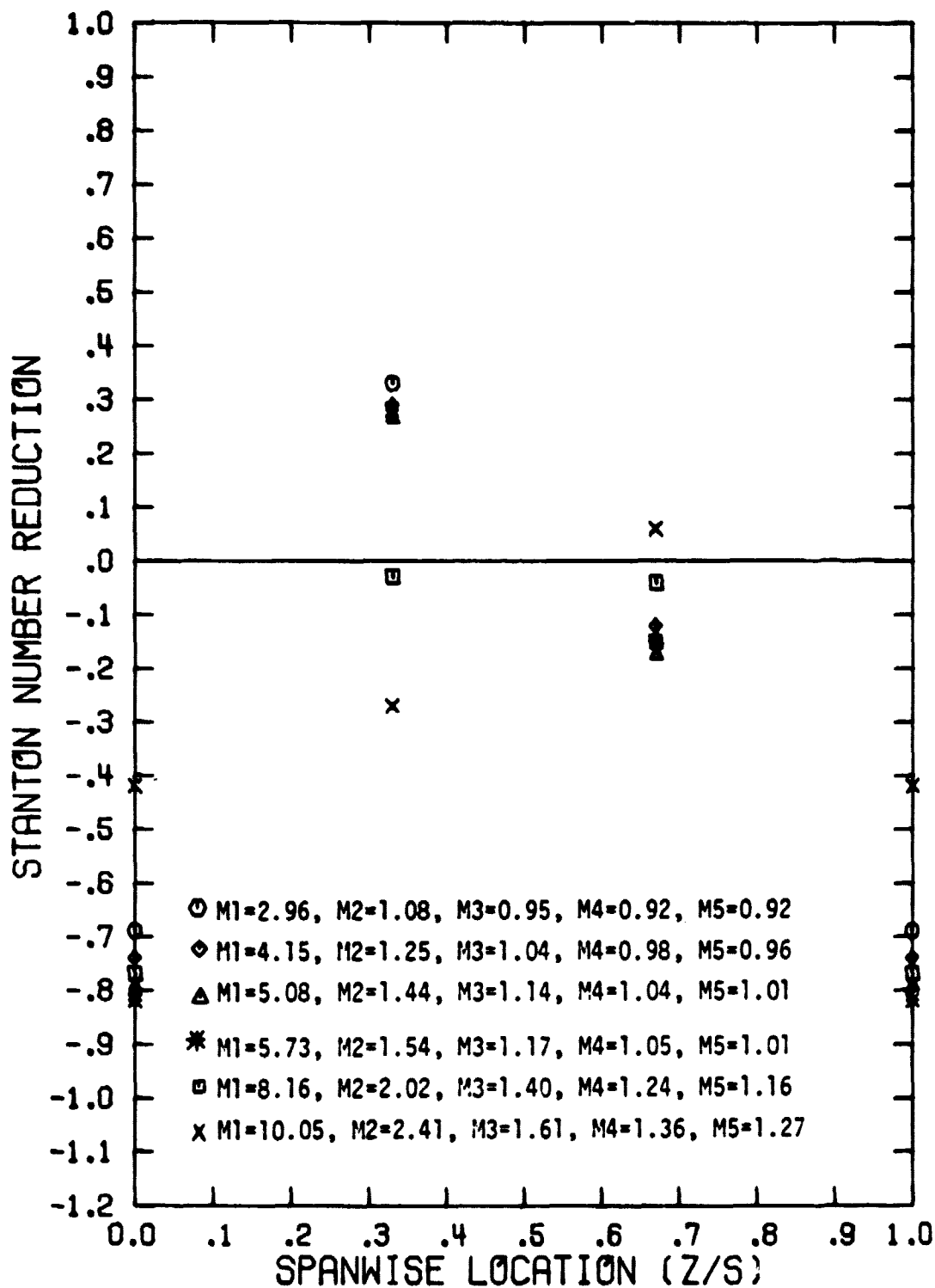


Figure 92. Spanwise Variation of the Stanton Number Reduction for a Five Row Configuration with Blowing Distribution Simulating Plenum Supply ($\theta_4=58.7^\circ, (x/d_0)_4=1.5, S/d_0=P/d_0=5$)

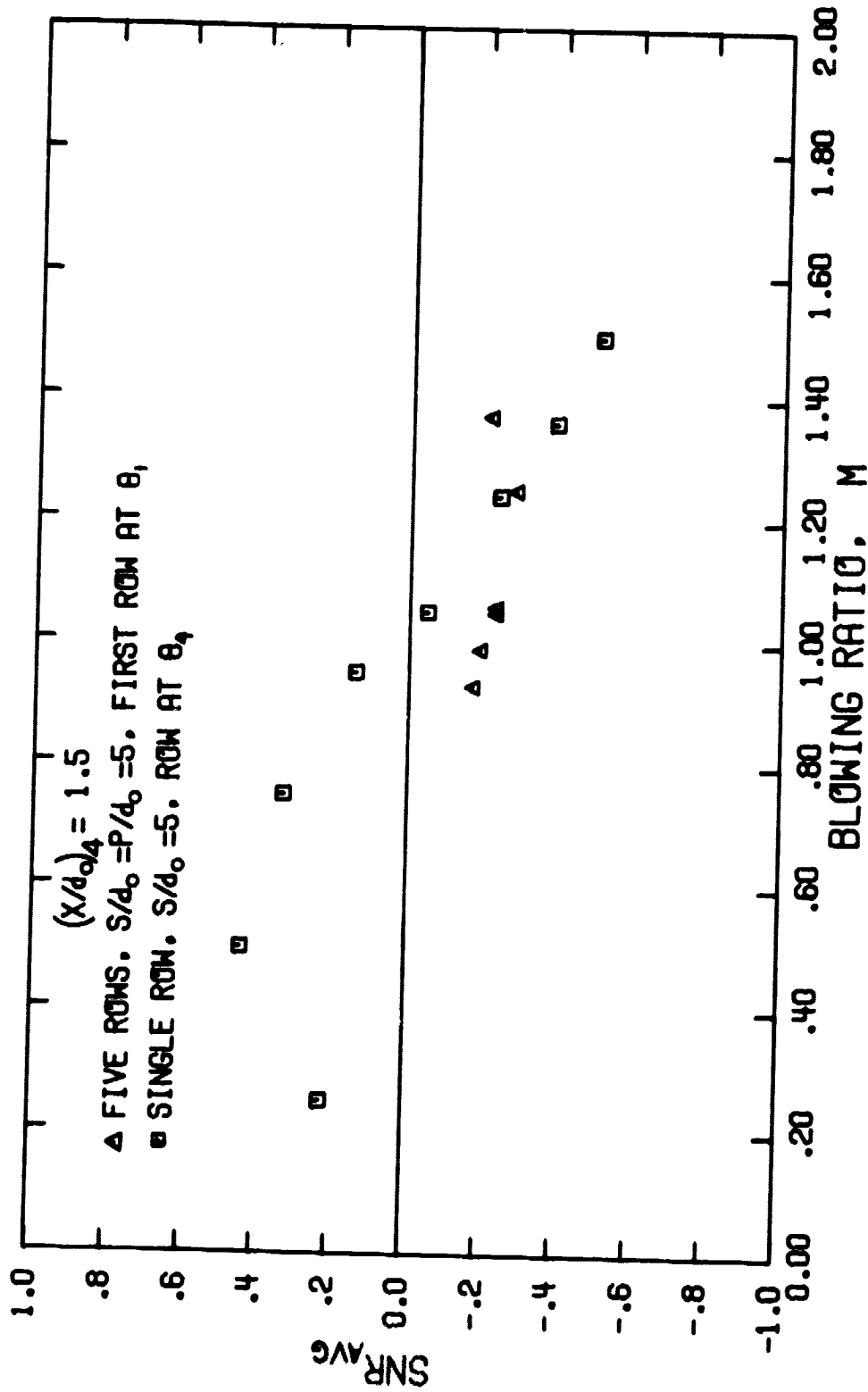


Figure 93. Comparison of the Spanwise Averaged Stanton Number Reduction for the Five Row Configuration and the Single Row Configuration at θ_4 ($S/d_0 = 5$, $(x/d_0)_4 = 1.5$)

the two configurations. The results for the plenum blowing simulation did not change significantly as the blowing ratio was increased, but the data for single row injection show a decreasing trend from $SNR_{AVG} = 0.44$ at $M_4 = 0.50$ to $SNR_{AVG} = -0.51$ at $M_4 = 1.50$. The data for film cooling performance behind the fifth row of coolant holes are limited because of the failure of one of the heat flux gages. The data show trends similar to those established behind the fourth row of holes. The values of SNR_{MAX} are approximately the same as those behind the fourth row. The value of SNR_{NEG} behind the fifth row was not as severe. Negative values of SNR across the span were observed for $M_5 = 1.16$.

VI.B.2. Three Row Configuration with First Row at $\theta_1 = 5^\circ$, $S/d_0 = P/d_0 = 10$

Figure 94 presents the film cooling performance at $(x/d_0)_1 = 1.5$ for the plenum blowing simulation for the three row configuration. The data show that for the lowest blowing ratio studied, $M_1 = 2.96$, negative values (SNR_{NEG}) were observed behind the coolant hole. Initially, the blowing ratio was increased ($2.96 \leq M_1 \leq 5.08$) the value of SNR_{NEG} increased in magnitude; for $M_1 \geq 5.08$, SNR_{NEG} remained relatively constant. The value of SNR_{MAX} approached 0.50 for the low values of M_1 ratios, far exceeding the values for SNR found with the five row configuration ($S/d_0 = P/d_0 = 5$). As the blowing ratio was increased beyond $M_1 = 4.15$, the value of SNR_{MAX} decreased. The values for SNR_{MAX} and SNR_{NEG} , and all of the values for SNR across the span at all values of the blowing ratio show remarkably close agreement with the results for single row injection.

Downstream at $(x/d_0)_1 = 3.5$, the values of SNR_{NEG} behind the hole diminished and the values of SNR_{MAX} decreased. Very little lateral spreading of the coolant across the surface was observed. A comparison with the results for single row injection ($S/d_0 = 10$) once again shows excellent agreement at all spanwise locations and for all values of blowing ratio. Further downstream at $(x/d_0)_1 = 6.5$, the trends established upstream are repeated, and excellent agreement with the results for single row injection was observed.

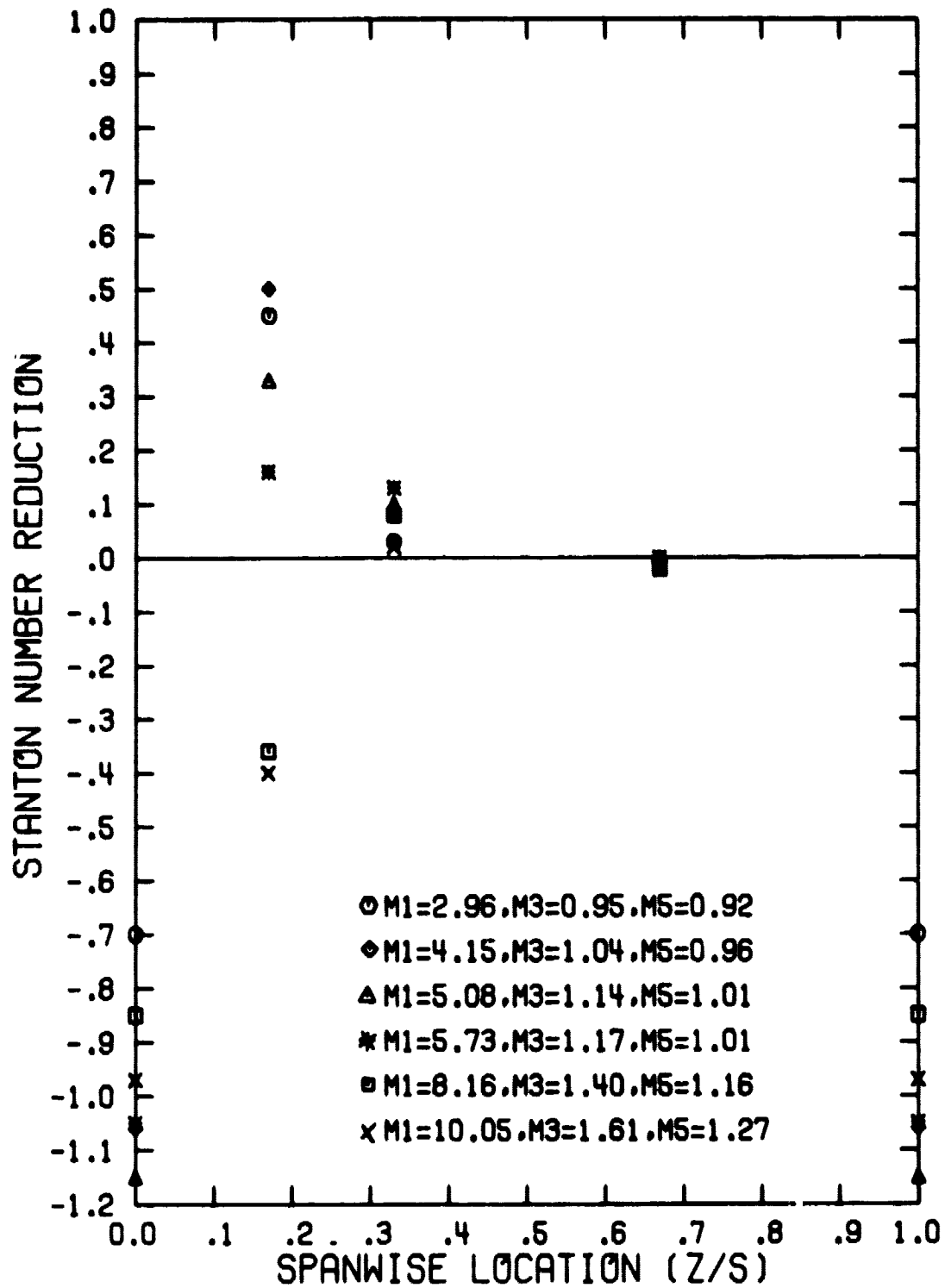


Figure 94. Spanwise Variation of the Stanton Number Reduction for a Three Row Configuration with Blowing Distribution Simulating Plenum Supply ($\theta_1=5^\circ$, $(x/d_0)_1=1.5$, $S/d_0=P/d_0=10$)

At the final downstream location before the next row of coolant holes (at θ_3) $(x/d_0)_1 = 8.5$, the values of SNR (positive and negative) were approximately the same magnitude as at $(x/d_0)_1 = 6.5$. The values of SNR across the span showed good agreement with the data for single row injection with one difference, at $z/S = 0.58$, where the heat flux gage was located in front of a coolant hole in the next row. Blowing from that hole caused the heat flux gage to read higher values of SNR than those for single row injection.

The data for SNR_{AVG} are presented in Figure 95 as a function of the blowing ratio for the downstream locations of $(x/d_0)_1 = 1.5, 3.5, 6.5$ and 8.5 . The results show generally negative values of SNR_{AVG} with SNR_{AVG} decreasing as M_1 increases. The largest negative value for SNR_{AVG} was observed immediately downstream from the injection location at $(x/d_0)_1 = 1.5$. The value of SNR_{AVG} increased (became less negative) continually as $(x/d_0)_1$ increased for any M_1 . As might be expected, the spanwise averaged data show very close agreement with the results for single row injection. Figure 96 presents the results downstream from the second row of holes (θ_3). For low values of blowing ratio ($M_3 \leq 1.04$), positive values of SNR were observed behind the coolant hole. The occurrence of negative values (SNR_{NEG}) behind the coolant hole was observed at $M_3 = 1.14$. This value of blowing ratio is larger than that observed for single row injection ($M = 0.95$) but close to the value found with the uniform blowing distribution ($M = 1.25$). The value of SNR behind the hole decreased continually as the blowing ratio was increased. However, the negative values (SNR_{NEG}) were not as severe as that observed for single row injection. The values of SNR_{MAX} (at $z/S = 0.17$) were constant over the range of M_3 studied while SNR at $z/S = .33$ increased continuously as the blowing ratio was increased, indicating local values as high as 0.4 to 0.6. This pattern was observed previously with single row injection and multiple row with uniform blowing.

Downstream at $(x/d_0)_3 = 6.5$, the values of SNR_{MAX} decreased from the upstream level accompanied by a small decrease in the magnitude of the negative values of SNR. The values of SNR_{MAX} and negative SNR

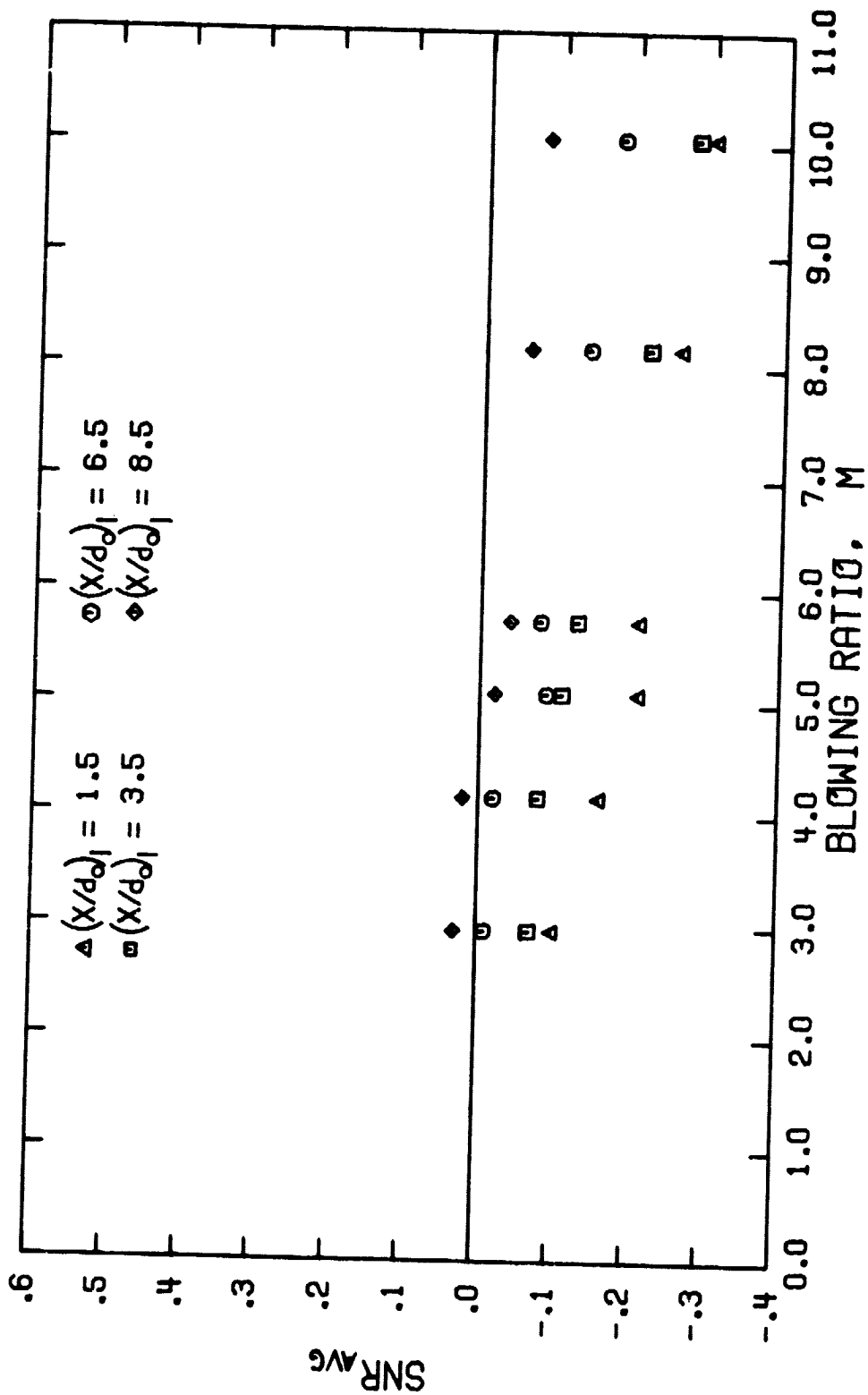


Figure 95. Variation of the Spanwise Averaged Stanton Number Reduction for a Three Row Configuration with Blowing Distribution Simulating Plenum Supply ($\phi_1 = 5^\circ$, $S/d_0 = P/d_0 = 10$)

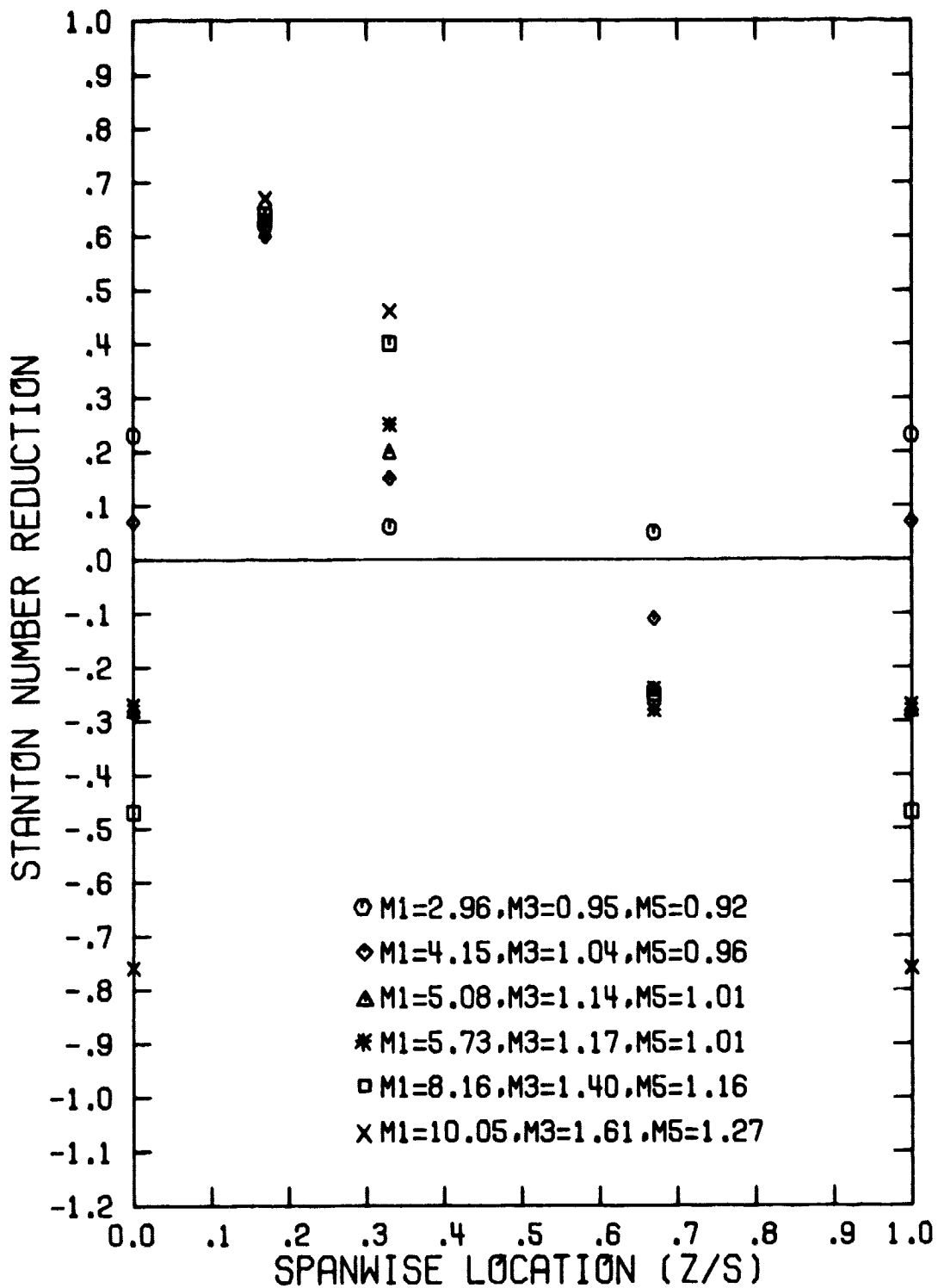


Figure 96. Spanwise Variation of the Stanton Number Reduction for a Three Row Configuration with Blowing Distribution Simulating Plenum Supply ($\theta_3=40.8^\circ$, $(x/d_0)_3=1.5$, $S/d_0=P/d_0=10$)

across the span were approximately the same as those found with single row injection and multiple row injection with the uniform blowing distribution.

Figure 97 presents the data for SNR_{AVG} as a function of the blowing ratio at $(x/d_0)_3 = 1.5$ for the three row configuration with the plenum blowing simulation and the single row configuration. The spanwise averaged data show SNR_{AVG} decreasing as M_3 was increased, with a level of 0.19 at $M_3 = 0.95$ and $SNR_{AVG} \leq 0$ for $M_3 \geq 1.14$. The data for single row injection show similar trends. However, for $M_1 \geq 1.15$, SNR_{AVG} for the plenum blowing simulation is substantially higher apparently due to upstream blowing effects.

Further downstream at $(x/d_0)_3 = 6.5$, the values of SNR_{AVG} were small in magnitude, with neither positive nor negative values exceeding 0.05, which is in good agreement with the results for single row injection.

Because of the limited number of heat flux gages behind the fifth row of holes (at θ_5), a complete spanwise distribution of the film cooling performance was not to be measured. The data obtained show only large negative values of SNR across the span at all values of the blowing ratio studied.

VI.B.3. Two Row Configuration with First Row at $\theta_2 = 22.9^\circ$, $S/d_0 = P/d_0 = 10$

The results for the two row plenum blowing simulation are presented in Figure 98 for $(x/d_0)_2 = 1.5$ downstream from the first row of coolant holes (at θ_2). At the lowest blowing ratio studied, $M_2 = 1.08$, SNR_{MAX} is located directly behind the coolant hole with a level of $SNR \sim 0.60$ in the region $0 < z/S < 0.2$ and the remainder of the span with SNR near zero. As the blowing was increased, the coolant jet shifted outward from the hole, with SNR_{MAX} located near $z/S = 0.17$. With a blowing ratio $M_2 \geq 1.44$, negative values of SNR were observed behind the coolant hole increasing in severity as the blowing ratio was increased. The values of SNR_{MAX} remained relatively constant, decreasing when $M_2 > 2.0$. The spanwise distribution of the data shows good agreement with the results for single row injection and multiple row with the uniform blowing distribution. The only difference was found behind

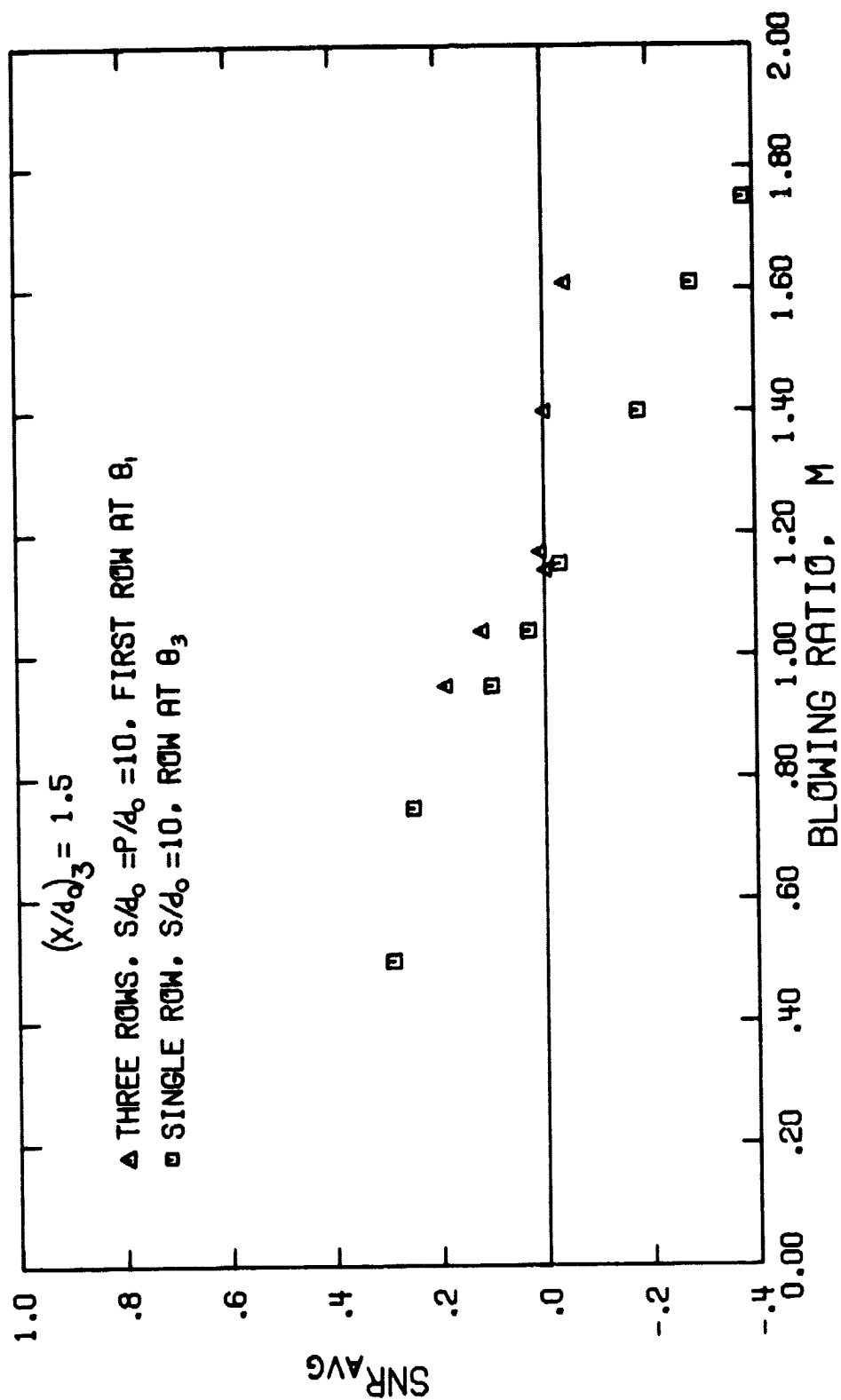


Figure 97. Comparison of the Spanwise Averaged Stanton Number Reduction for the Three Row Configuration and the Single Row Configuration at θ_3 ($S/d_0 = 10$, $(x/d_0)_3 = 1.5$)

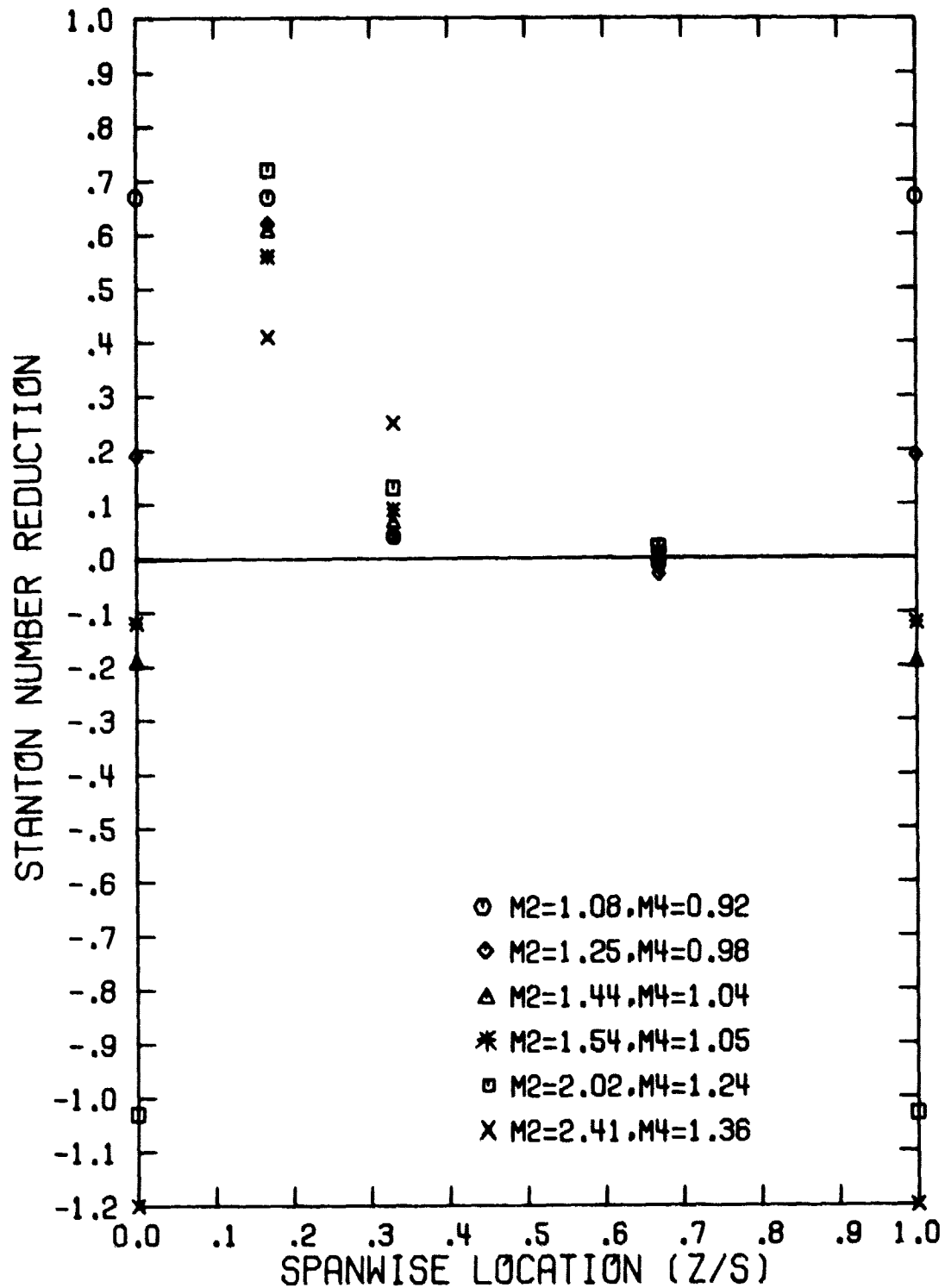


Figure 98. Spanwise Variation of the Stanton Number Reduction for a Two Row Configuration with Blowing Distribution Simulating Plenum Supply ($\theta_2=22.9^\circ$, $(x/d_0)_2=1.5$, $S/d_0=P/d_0=10$)

the coolant hole, where for the plenum blowing simulation, SNR_{NEG} was initiated when $M_2 = 1.44$. This did not occur until $M_2 > 2.0$ for single row injection or multiple row injection with a uniform blowing distribution.

Downstream at $(x/d_0)_2 = 3.5$, SNR_{NEG} was observed behind the coolant hole for $M_2 = 1.08$. This trend of SNR_{NEG} at $(x/d_0)_2 = 3.5$ occurring at a lower value of M_2 than SNR_{NEG} at $(x/d_0)_2 = 1.5$ was also observed for the single row injection and multiple row with uniform blowing configurations. With the plenum blowing simulation, the magnitude of SNR_{NEG} becomes more negative as the blowing ratio was increased. The negative values of SNR were as large or larger as the negative values of SNR located just upstream at $(x/d_0)_2 = 1.5$. The values for SNR_{MAX} decreased from the upstream levels, remaining approximately constant for $M_2 < 2.0$. Very little lateral spreading of the coolant was indicated.

Further downstream at $(x/d_0)_2 = 6.5$, the values of SNR_{MAX} remained at approximately the same level as observed upstream at $(x/d_0)_2 = 3.5$, but the value of SNR_{NEG} diminished. There was no evidence of lateral spreading of the coolant. The values of SNR at each blowing ratio showed good agreement with the data for single row injection.

At the final downstream location before the second row of holes, $(x/d_0)_2 = 8.5$, upstream trends were repeated. The value of SNR_{MAX} decreased to ~ 0.3 while the negative value of SNR continued to diminish. The values of SNR across the span showed good agreement with the results for single row injection with the exception of data at $z/S = 0.58$, corresponding to the heat flux gage directly in front of a coolant hole in the second row.

The data for SNR_{AVG} are presented in Figure 99 as a function of blowing ratio for the downstream locations of $(x/d_0)_2 = 1.5, 3.5, 6.5$ and 8.5 . The data illustrates SNR_{AVG} decreasing with increasing M_2 for any given $(x/d_0)_2$. For $M_2 \leq 1.54$, SNR_{AVG} is positive near the hole, $(x/d_0) = 1.5$, and further downstream $6.5 \leq (x/d_0)_2 \leq 8.5$. Negative values of SNR_{AVG} were obtained at $(x/d_0) = 3.5$ for all M_2 . A comparison with the data for SNR_{AVG} for single row injection shows good agreement

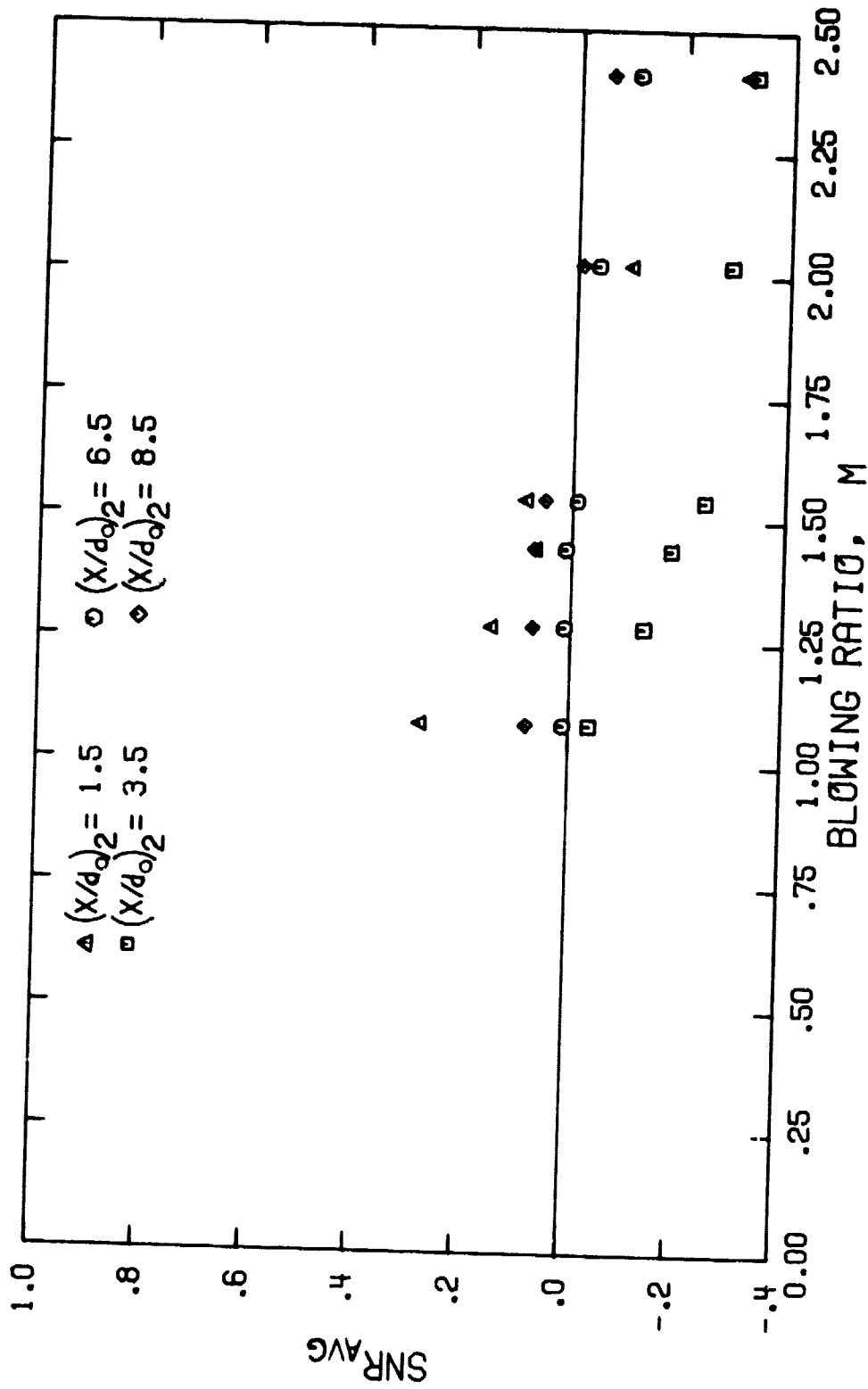


Figure 99. Variation of the Spanwise Averaged Stanton Number Reduction for a Two Row Configuration with Blowing Distribution Simulating Plenum Supply ($\theta_2 = 22.9^\circ$, $S/d_o = P/d_o = 10$)

for $M_2 \leq 1.28$. The only differences are downstream at $(x/d_0)_2 = 6.5$ and 8.5 where the plenum blowing simulation yielded somewhat larger values for SNR_{AVG} . For $1.28 \leq M_2 \leq 2.0$, the data for single row injection did not show SNR_{NEG} behind the hole at $(x/d_0)_2 = 1.5$. Consequently, the data for the single row shows SNR_{AVG} substantially larger (~ 0.2) than that for the plenum blowing simulation (~ 0.1) at the same downstream location. When $M_2 = 2.4$, both single row blowing and the plenum blowing simulation result in $SNR < 0$ behind the coolant hole and then the data for SNR_{AVG} for both blowing studies are again in reasonable agreement.

The film cooling performance downstream from the second row of holes at θ_4 is presented in Figure 100 for $(x/d_0)_4 = 1.5$. For the lowest blowing ratio studied, $M_4 = 0.92$, large negative values (SNR_{AVG}) were observed behind the coolant hole. The results for both single row blowing and multiple row with uniform blowing showed SNR_{NEG} initiated for $M_4 \sim 1.0$. The value at SNR_{NEG} with the plenum blowing simulation remained fairly constant as M was increased, which agrees well with the results for both single row blowing and multiple row with uniform blowing.

While a value of SNR_{MAX} was observed for $M_4 = 0.92$, SNR decreased as the blowing ratio was increased such that near zero or negative values of SNR existed for $M_4 \geq 1.05$. These trends and levels are in good agreement with the data for single row injection and multiple row injection with uniform blowing.

Further downstream, $(x/d_0)_4 = 6.5$, values of SNR_{MAX} near 0.7 were found ($z/S = 0.25$) for $M_4 \leq 0.98$ which is greater than SNR_{MAX} at $(x/d_0)_4 = 1.5$.

Figure 101 presents the data for SNR_{AVG} as a function of the blowing ratio at $(x/d_0)_4 = 1.5$ for the two row configuration with the plenum blowing simulation and the single row configuration. The data for the two configurations are in reasonable agreement showing SNR_{AVG} decreasing as M_4 was increased with $SNR_{AVG} < 0$ for $M_4 \geq 0.95$. Additional data downstream, $(x/d_0)_4 = 6.5$, indicate $SNR_{AVG} \sim 0.23$ for $M_4 \sim 0.95$ with $SNR_{AVG} < 0$ for $M_4 \geq 1.04$.

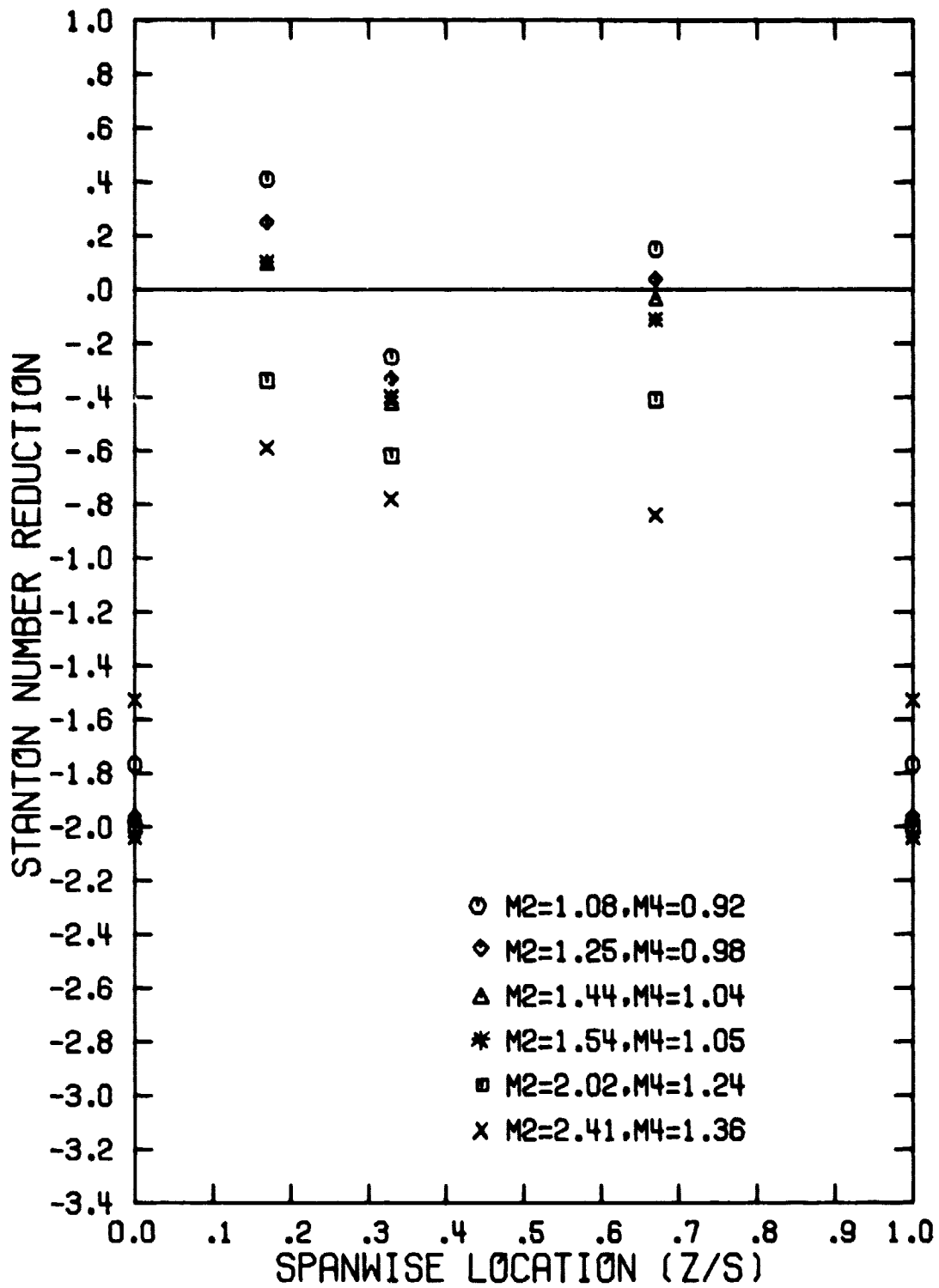


Figure 100. Spanwise Variation of the Stanton Number Reduction for a Two Row Configuration with Blowing Distribution Simulating Plenum Supply ($\theta_4=58.7^\circ$, $(x/d_0)_4=1.5$, $S/d_0=P/d_0=10$)

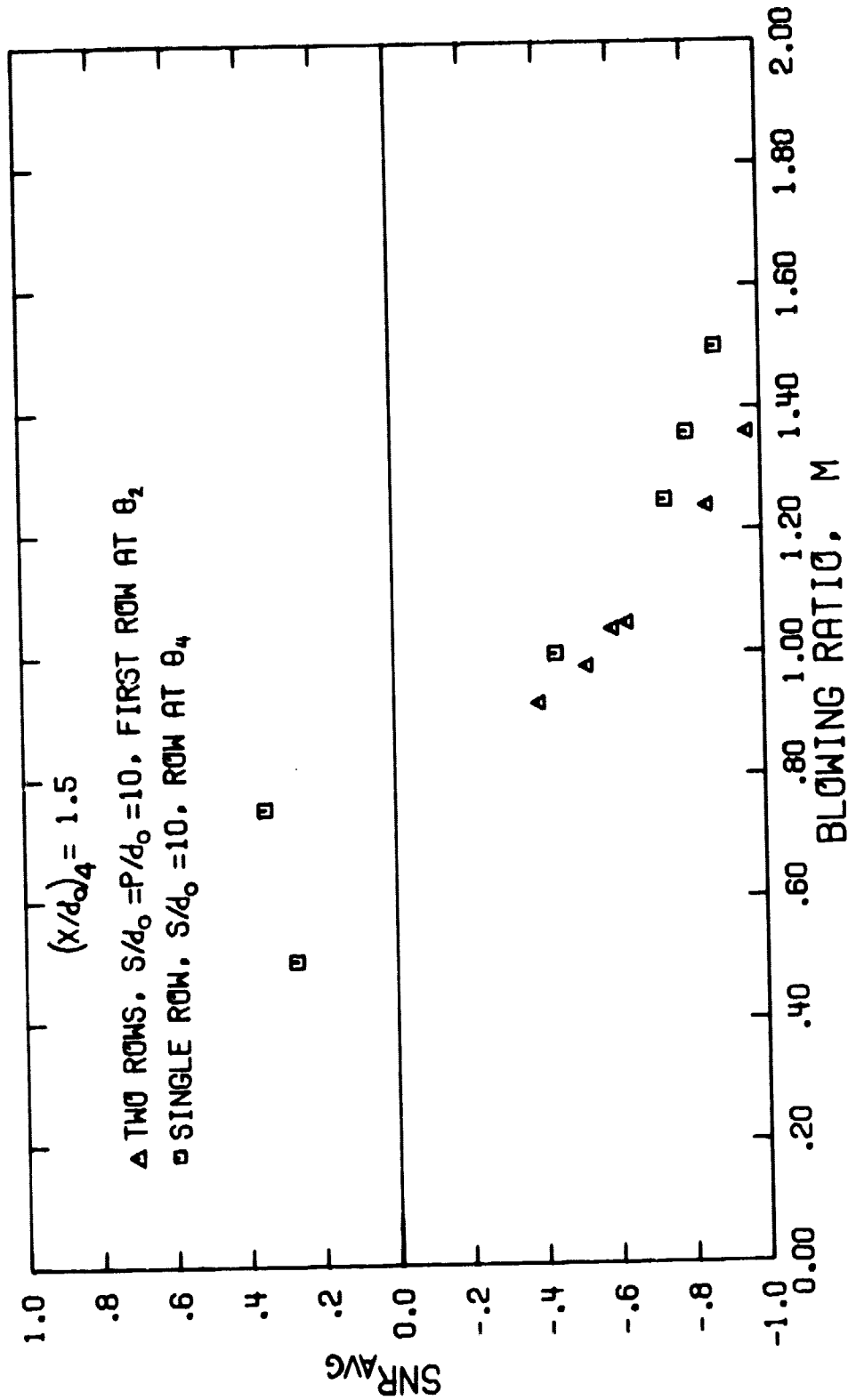


Figure 101. Comparison of the Spanwise Averaged Stanton Number Reduction for the Two Row Configuration and the Single Row Configuration at θ_2 ($S/d_0 = 10$, $(x/d_0)_4 = 1.5$)

VI.C. Discussion of the Results

Experiments were conducted with three different multiple row injection configurations to simulate the coolant blowing distribution for rows of holes supplied by a common plenum. A model for the plenum blowing simulation (see Appendix I) shows that the distribution of the blowing ratio depends on the location of the rows of holes, the approach Mach number, $Ma_{\infty,0}$, and the total pressure ratio, $P_{TC}/P_{T\infty}$. Three values of $P_{TC}/P_{T\infty}$ and two values of $Ma_{\infty,0}$, typical of engine design conditions, were selected to predict six different blowing ratio distributions to be investigated. The film cooling results for the six blowing distributions and three multiple row configurations are discussed in this section.

The most significant feature revealed in the presentation of the data was the large negative values of SNR resulting from the large level of the blowing ratio typical of design conditions. Even for the distribution with the lowest levels of blowing ratio, the values of M were large enough to produce SNR_{NEG} behind the coolant holes. Since the effect of the coolant was very localized, the negative values of SNR tended to dominate the spanwise averaged data such that SNR_{AVG} was generally negative.

Following the format used in Chapter V, the discussion of the results is split into sections for each multiple row configuration. The discussion includes comparisons with the results for single row injection where upstream blowing was not present and multiple row injection with the uniform blowing where upstream blowing was a factor.

VI.C.1. Five Row Configuration ($\theta_1 = 5^\circ$, $S/d_0 = P/d_0 = 5$)

A major feature of the film cooling performance downstream from the first row of holes at θ_1 is the large negative values of SNR that result from the excessive values of blowing ratio when holes are located so close to the stagnation point. The previous experiments with single row injection and multiple row injection with uniform blowing showed that SNR_{NEG} was initiated at $M_1 = 2.0$ and 1.5, respectively.

Therefore, the plenum blowing simulation with $P_T/P_{T_\infty} = 1.010$ and $Ma_{\infty,0} = 0.2$, yielding $M_1 = 2.96$, was well beyond the blowing condition required to initiate SNR_{NEG} behind the coolant holes. Although local positive values of SNR were observed, the magnitude of SNR_{NEG} dominated the spanwise distribution resulting in generally negative values for SNR_{AVG} . The data downstream from the first row (θ_1) for the plenum blowing simulation were in close agreement with the data for single row injection at θ_1 and the data for multiple row injection with uniform blowing. There were two minor areas of difference between the data for the plenum blowing simulation and single row injection. First, the values for SNR_{NEG} for plenum blowing were not as large as those for single row injection at the higher values of blowing ratio, $M_1 > 5$. Second, the value of SNR at $(x/d_0)_1 = 3.5$ in front of the downstream coolant hole was larger for plenum blowing than for single row injection as noted previously.

The spanwise location of the coolant jet (z/d_0) approaching the second row of holes was determined as described in Chapter IV and is listed in Table 19 compared with the values for single row injection. Downstream from the first row, the coolant location was at $z/d_0 \sim 3.3$, in close agreement with the data for single row injection except for the lowest value of M_1 . Since the coolant hole in the second row is located at $z/d_0 = 2.5$ with respect to the first row, the coolant jet flowing downstream from the first row is directed in close proximity to the coolant jet emerging from the second row.

The results downstream from the second row of holes also reveal values of SNR_{NEG} behind the coolant hole even for the minimum value of blowing ratio ($M_2 = 1.08$) studied. This was not surprising since the data for single row injection and multiple row injection with uniform blowing showed SNR_{NEG} for $M_2 = 1.1$ and 1.25 , respectively. The influence of the coolant jet was still very localized behind the second row which is consistent with the location of the coolant jet from the first row in close proximity with the coolant jet from the second row. The upstream injection of coolant does result in large values of SNR_{MAX} (~ 0.70) at $(x/d_0)_2 = 1.5$ that remain fairly constant up to $M_2 = 1.61$.

Table 19. Spanwise Location, z/d_0 , of the Coolant,
 $S/d_0 = P/d_0 = 5$

$\theta_1 = 5^\circ$, $(x/d_0)_1 = 3.5$

$M=2.96$ $M=4.15$ $M=5.73$ $M=8.16$
 $M_{\infty,0}=0.57$ $M_{\infty,0}=0.78$ $M_{\infty,0}=1.08$ $M_{\infty,0}=1.56$

Single Row	1.7	3.3	3.3	—*
Plenum Blowing Simulation	3.3	3.3	3.3	—*

$\theta_2 = 22.9^\circ$, $(x/d_0)_2 = 3.5$

$M=1.08$ $M=1.54$ $M=2.02$ $M=2.41$
 $M_{\infty,0}=0.92$ $M_{\infty,0}=1.28$ $M_{\infty,0}=1.71$ $M_{\infty,0}=2.05$

Single Row	1.7	1.7	3.3	3.3
Plenum Blowing Simulation	1.7	1.7	3.3	3.3

$\theta_3 = 40.8^\circ$, $(x/d_0)_3 = 1.5$

$M=0.95$ $M=1.14$ $M=1.40$ $M=1.61$
 $M_{\infty,0}=1.37$ $M_{\infty,0}=1.66$ $M_{\infty,0}=2.02$ $M_{\infty,0}=2.30$

Single Row	3.3	3.3	3.3	3.3
Plenum Blowing Simulation	1.7	—*	—*	—*

$\theta_4 = 58.7^\circ$, $(x/d_0)_4 = 1.5$

$M=0.98$ $M=1.05$ $M=1.24$ $M=1.36$
 $M_{\infty,0}=1.84$ $M_{\infty,0}=1.97$ $M_{\infty,0}=2.32$ $M_{\infty,0}=2.55$

Single Row	1.7	1.7	3.3	3.3
Plenum Blowing Simulation	1.7	1.7	—*	—*

* Only negative SNR values covered the surface at this blowing ratio.

In contrast, the data for single row injection showed SNR_{MAX} decreasing with M_2 for $M_2 > 0.75$. With multiple row injection, the upstream jet reinforces the coolant jet from the second row resulting in large values of SNR_{MAX} at high values of blowing ratio. This pattern also was observed for multiple row injection with uniform blowing although the magnitudes of SNR_{MAX} (~ 0.6) were less than those for the plenum blowing simulation (~ 0.75). This difference is attributed to the higher coolant flow rate emerging from the first row for the plenum blowing simulation.

The large value of SNR_{MAX} for the lowest blowing ratio, $M_2 = 1.08$ resulted in $SNR_{AVG} > 0$ at $(x/d_0)_2 = 1.5$. However, for larger M_2 , the level of SNR_{MAX} remained relatively constant, but SNR_{NEG} increased in magnitude resulting in negative values for SNR_{AVG} .

A comparison of the results for the two multiple row blowing distributions (plenum simulation vs. uniform) revealed a difference at the spanwise location $z/S = 0.67$ for the second row. The plenum blowing simulation resulted in negative values of SNR at $z/s = 0.67$, a pattern not seen in the study of multiple row injection with uniform blowing. The negative values of SNR are attributed to the large SNR_{NEG} generated behind the hole in the first row (at $z/S = 0.5$ relative to holes in the second row). This flow disturbance propagates downstream deteriorating the film cooling performance ($SNR < 0$) at $z/S = 0.67$, $(x/d_0)_2 = 1.5$ downstream from the second row. Farther downstream at $(x/d_0)_2 = 3.5$, positive values of SNR at $z/S = 0.67$ are attributed to the heat flux gage being located in front of a coolant hole in the third row of holes. Blowing from a downstream hole has been shown previously

to increase the value of SNR in the region in front of the coolant hole.

The location of the coolant jet from the second row of holes (z/d_0) as it approaches the third row is listed in Table 19. A comparison of the data for z/d_0 for multiple and single row injection show excellent agreement. The coolant jet, located at $z/d_0 \sim 1.7$ to 3.3, once again is in close proximity to the coolant hole in the third row which is located at $z/d_0 = 2.5$ with respect to the second row.

The plenum blowing simulation with the lowest values of blowing ratio resulted in $M_3 = 0.95$, yielding near zero or large negative values of SNR across the span downstream from row three. For $M_3 = 1.04$, only negative values of SNR were observed. This is in contrast with the data for single row injection where $SNR > 0$ was observed over a portion of the span for the same level of blowing from row three. Apparently, upstream blowing creates enough of a disturbance that only negative values of SNR are observed. However, it is noted that the value of SNR_{NEG} behind the hole for the plenum blowing simulation was not as large as for single row injection, especially at higher values of the blowing ratio.

Downstream from the third row, large negative values of SNR were observed at $z/S = 0.67$ as a consequence of the large values of SNR_{NEG} generated behind the coolant hole in the second row propagating downstream. The generally negative values of SNR result in spanwise averaged data that vary from $SNR_{AVG} = -0.31$ at $M_3 = 0.95$ to -0.54 at $M_3 = 1.61$. However, the negative level of SNR_{AVG} for the plenum blowing simulation was not as severe as for single row injection at θ_3 for a given value of M_3 .

Table 19 indicates that the coolant jet location downstream from the third row is in close proximity to the holes in the fourth row as observed for upstream rows. Values for z/d_0 are only shown for $M_3 = 0.95$ since $SNR < 0$ across the span for higher values of M_3 .

Following the pattern established by upstream rows, large values of SNR_{NEG} behind the coolant hole in the fourth row were observed at the lowest blowing ratio studied, $M_4 = 0.92$. Only negative values of

SNR across the span were found for $M_4 = 1.24$. Negative values of SNR were again observed at $z/S = 0.67$ downstream from the fourth row as a result of the propagation of the large value of SNR_{NEG} generated behind the hole in the third row. Although the generally negative values of SNR lead to $SNR_{AVG} < 0$ downstream of the fourth row, the level of SNR_{AVG} was not as severe as found for single row injection at θ_4 .

VI.C.2. Three Row Configuration ($\theta_1 = 5^\circ$, $S/d_0 = P/d_0 = 10$)

The location of the coolant jet (z/d_0) downstream from a row of holes is shown in Table 20 for rows at θ_1 and θ_3 for the three row configuration with $S/d_0 = P/d_0 = 10$. A comparison with the data for single row injection shows good agreement. The coolant jet from the first row was located at $z/d_0 = 3.3$ to 5.8 , in close proximity to the hole in the second row which is located at $z/d_0 = 0.5$ relative to the first row.

The lowest value of blowing ratio studied, $M_1 = 2.96$, was large enough to produce negative values of SNR behind the coolant hole. The values of SNR_{NEG} and SNR_{MAX} downstream from the first row, show close agreement with the data for single row injection. A review of the data for the plenum blowing simulation for the two different hole spacings shows that SNR_{MAX} for $S/d_0 = 10$ was significantly larger than for $S/d_0 = 5$. This pattern was observed earlier with single row injection at θ_1 .

The film cooling performance downstream from the second row (θ_3) again shows good agreement with the results for single row injection. The value of SNR behind the coolant hole was positive at the lowest blowing ratio studied, $M_3 = 0.95$. When M_3 was increased to 1.14 , SNR_{NEG} behind the coolant hole was observed. This agrees well with the results for multiple row injection with uniform blowing for $S/d_0 = P/d_0 = 10$. Recall that the data for the five row injection

Table 20. Spanwise Location, z/d_0 , of the Coolant,
 $S/d_0 = P/d_0 = 10$

$$\theta_1 = 5^\circ, (x/d_0)_1 = 1.5$$

$$\begin{array}{cccc} M=2.96 & M=4.15 & M=5.73 & M=8.16 \\ M_{\infty,0}=0.57 & M_{\infty,0}=0.78 & M_{\infty,0}=1.08 & M_{\infty,0}=1.56 \end{array}$$

Single Row	2.5	2.5	4.2	5.8
Plenum Blowing Simulation	3.3	4.2	4.2	5.8

$$\theta_3 = 40.8^\circ, (x/d_0)_3 = 6.5$$

$$\begin{array}{cccc} M=0.95 & M=1.14 & M=1.40 & M=1.61 \\ M_{\infty,0}=1.37 & M_{\infty,0}=1.66 & M_{\infty,0}=2.02 & M_{\infty,0}=2.30 \end{array}$$

Single Row	4.2	4.2	4.2	4.2
Plenum Blowing Simulation	4.2	4.2	4.2	4.2

configuration ($S/d_0 = P/d_0 = 5$) with the plenum blowing simulation showed SNR_{NEG} at $M_3 = 0.95$. Thus, as was observed previously for uniform blowing, injection at θ_1 had little influence on the film cooling injection process downstream, whether the second row was at θ_2 or θ_3 . However, coolant injection at θ_2 apparently created a flow disturbance such that SNR_{NEG} downstream from the next row occurred at a lower value of M_3 than with no blowing at θ_2 . Downstream from the second row (θ_2), negative values of SNR were observed at $(x/d_0)_3 = 1.5$, $z/s = 0.67$, corresponding to the propagation of SNR_{NEG} initiated behind the hole in the first row (θ_1). Similarly, positive values of SNR were observed at $(x/d_0)_3 = 6.5$, $z/s = 0.92$ (when $2.96 \leq M_1 \leq 5.7$) corresponding approximately to the trajectory of the coolant from the first row.

VI.C.3. Two Row Configuration ($\theta_2=22.9^\circ$, $S/d_0=P/d_0=10$)

The location of the coolant jet (z/d_0) downstream from the holes at θ_2 and θ_4 , presented in Table 21, shows good agreement with the data for single row injection. The coolant jet from the first row was located at $z/d_0 = 2.5$ to 4.2 , corresponding to $z/S = 0.75$ to 0.92 relative to the second row of holes (θ_4). The values of SNR downstream from the first row (θ_2) showed good agreement with the results for single row injection at θ_2 except that negative values (SNR_{NEG}) were observed behind the hole at a considerably lower blowing ratio ($M_2 = 1.44$) for the plenum blowing simulation.

Downstream from the second row (θ_4), large negative values of SNR were observed for the lowest value of blowing ratio studied, $M_4 = 0.98$. Only negative values of SNR across the span were found with $M_4 = 1.24$. When $M_4 < 1.24$, the values of SNR_{NEG} and SNR_{MAX} show generally good agreement with the data for single row injection. In the region $(x/d_0)_4 = 6.5$, the observed values for SNR were very sensitive to changes in the blowing ratio (M_4) apparently due to the proximity of the boundary layer separation region.

Table 21. Spanwise Location, z/d_o , of the Coolant,
 $S/d_o = P/d_o = 10$

$$\theta_2 = 22.9^\circ, (x/d_o)_2 = 8.5$$

$$\begin{array}{cccc} M=1.08 & M=1.54 & M=2.02 & M=2.41 \\ M_{\infty,o}=0.92 & M_{\infty,o}=1.28 & M_{\infty,o}=1.71 & M_{\infty,o}=2.05 \end{array}$$

Single Row	2.5	2.5	4.2	4.2
Plenum Blowing Simulation	2.5	2.5	4.2	4.2

$$\theta_4 = 58.7^\circ, (x/d_o)_4 = 6.5$$

$$\begin{array}{cccc} M=0.98 & M=1.05 & M=1.24 & M=1.36 \\ M_{\infty,o}=1.84 & M_{\infty,o}=1.97 & M_{\infty,o}=2.32 & M_{\infty,o}=2.55 \end{array}$$

Single Row	4.2	—*	9.2	9.2
Plenum Blowing Simulation	2.5	9.2	9.2	9.2

* No measurements for single row injection were taken at this blowing ratio.

VI.D. Summary

The dominate feature throughout all of the results for the plenum blowing simulation was the large negative level of SNR due to the large values of blowing ratio for typical design values of plenum-to-freestream total pressure ratio (P_{T_C}/P_{T_∞}) and approach Mach number ($Ma_{\infty,0}$). The patterns and trends established by the results for the plenum blowing simulation show generally good agreement with the data for single row injection. However, with the spanwise injection angle, the coolant from upstream row passed in close proximity to the coolant hole in the next row downstream resulting in very localized cooling performance. Generally, the large values of SNR_{NEG} observed behind the upstream coolant hole propagated downstream resulting in negative values of SNR downstream from the next row. For injection with $S/d_0 = P/d_0 = 5$ and, or injection at θ_2 , blowing apparently created a flow disturbance that reduced the value of M initiating SNR_{NEG} at downstream rows.

Figure 102 presents the spanwise averaged data, SNR_{AVG} , for the three multiple row configurations studied in the plenum blowing simulation, with $P_{T_C}/P_{T_\infty} = 1.010$ and $Ma_{\infty,0} = 0.2$ yielding the smallest values of blowing ratio. The results for the five row configuration ($S/d_0 = P/d_0 = 5$) show $SNR_{AVG} \leq 0.13$ behind the second row and, generally, SNR_{AVG} less than zero, for most of the surface. The trends for the three row configuration ($S/d_0 = P/d_0 = 10$) were similar with improved performance downstream from θ_3 . The two row configuration was comparable. The very localized film cooling performance and the large negative values of SNR tended to dominate the value of SNR_{AVG} . Increasing the value of P_{T_C}/P_{T_∞} and/or decreasing $Ma_{\infty,0}$ resulted in higher values of blowing ratio, larger negative values of SNR and, therefore, lower values (i.e. negative) of SNR_{AVG} .

The results from the plenum blowing simulation illustrate the poor film cooling performance resulting from the high levels of blowing ratio typical of leading edge designs. A reduction in the level of blowing ratio (i.e. reduced P_{T_C}/P_{T_∞}) would provide more effective film cooling over the surface with less coolant consumption.

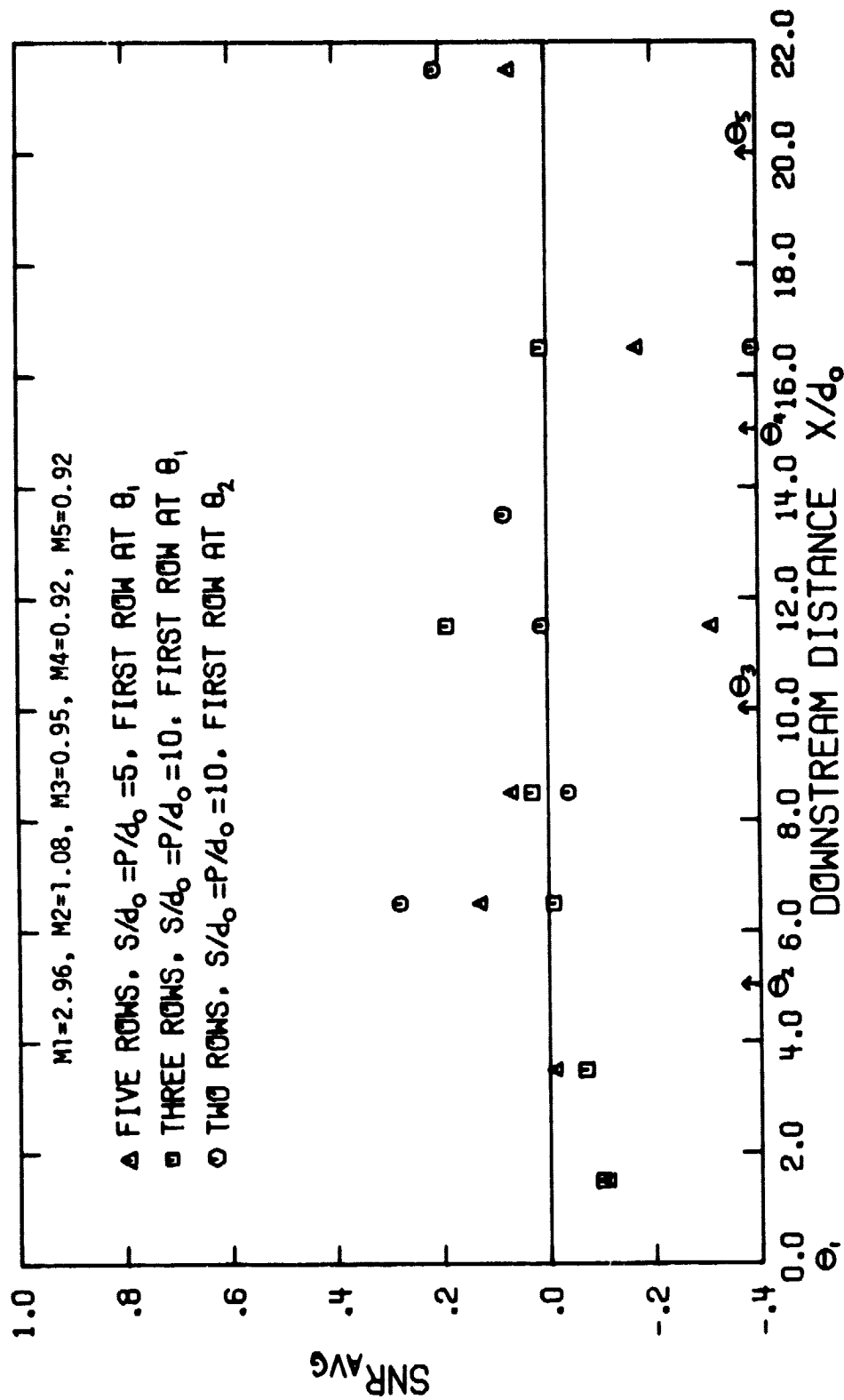


Figure 102. Comparison of the Spanwise Averaged Stanton Number Reduction Data for the Multiple Row Configurations with Plenum Blowing

VII. EFFECT OF FREESTREAM TURBULENCE INTENSITY ON FILM COOLING PERFORMANCE

The influence of changes in freestream turbulence intensity on the heat transfer without film cooling (dry wall) was discussed in Chapter III. An additional study was conducted to determine the influence of freestream turbulence intensity on the film cooling performance. Since previous experiments [18][19] have shown that injection of the coolant through discrete holes can generate a high level of turbulence, it was of interest to examine the importance of changes in the freestream intensity.

Experiments were conducted with the five row configuration ($S/d_0 = P/d_0 = 5$) using different levels of freestream turbulence intensity with (a) a blowing distribution simulating a plenum supply, and (b) a uniform blowing distribution. The turbulence intensity was changed by inserting a screen with a different mesh size and/or a different wire diameter in the wind tunnel. The two different screens employed yielded turbulence intensities of $4.8\% \pm 0.1\%$ for the fine screen and $9.7\% \pm 0.4\%$ for the coarse screen (see Section III.A.). The clear tunnel intensity was measured as $4.4\% \pm 0.3\%$. The film cooling performance was measured for the three levels of freestream turbulence intensity for the plenum blowing simulation with $P_{T_C}/P_{T_\infty} = 1.010$ and $Ma_{\infty,0} = 0.2$ and for the uniform blowing distribution with $M = 0.75$. These levels of blowing ratio were selected so that both positive and negative values of SNR across the span were present.

The results for the plenum blowing simulation show good agreement of the data for SNR for all three intensities investigated. Figures 103, 104 and 105 present the film cooling performance at $(x/d_0)_1 = 1.5$ downstream from the rows at θ_1 , θ_3 and θ_4 , respectively. The data presented are representative of all of the results obtained for the plenum blowing simulation (see Appendix I). Values of SNR as a function of spanwise location, z/S , are presented for each screen configuration.

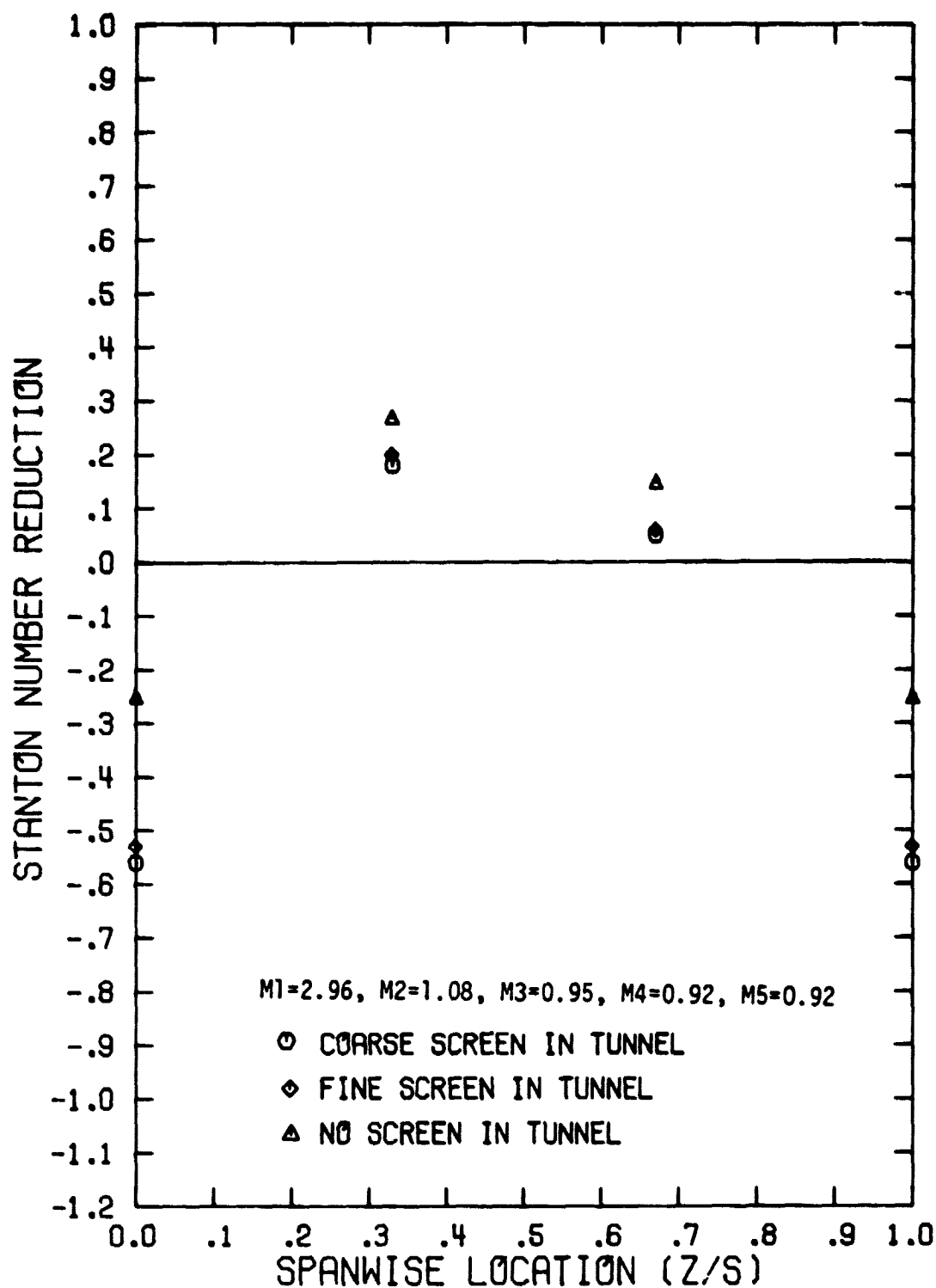


Figure 103. The Influence of Freestream Turbulence on the Film Cooling Performance with a Blowing Distribution Simulating Plenum Supply ($\theta_1=5^\circ$, $(x/d_0)_1=1.5$, $S/d_0=P/d_0=5$)

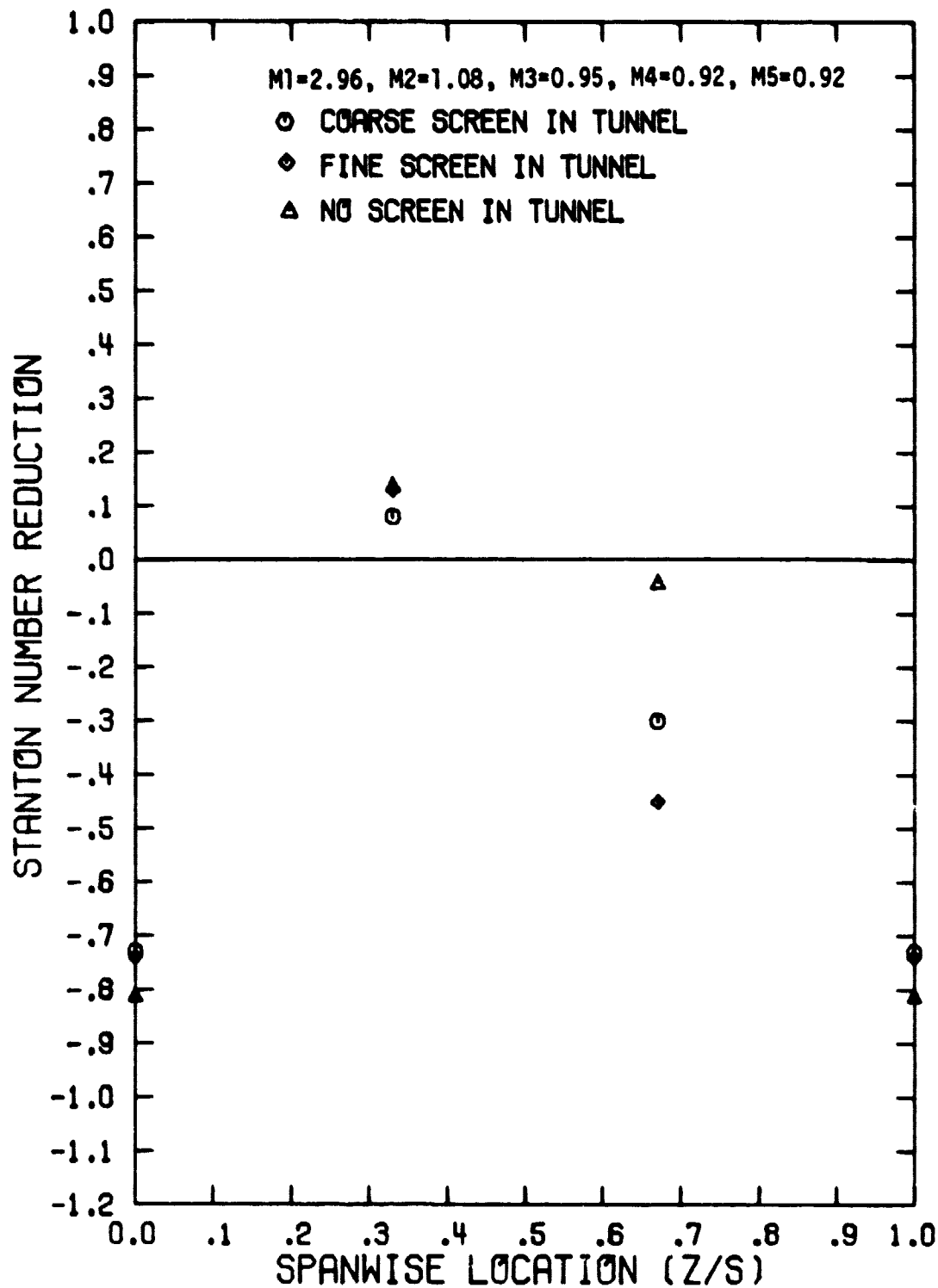


Figure 104. The Influence of Freestream Turbulence on the Film Cooling Performance with Blowing Distribution Simulating Plenum Supply ($\theta_3=40.8^\circ$, $(x/d_0)_3=1.5$, $S/d_0=P/d_0=5$)

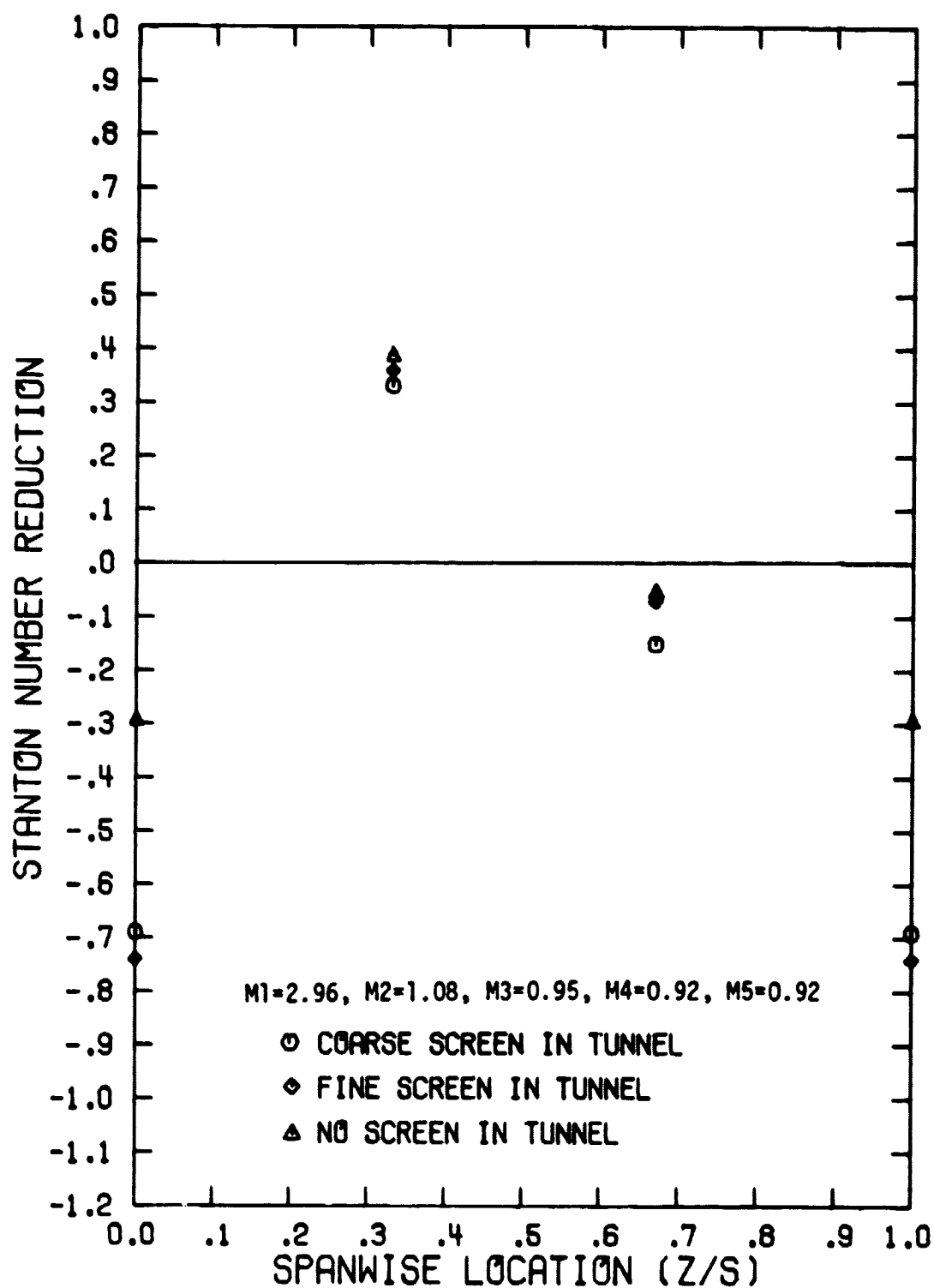


Figure 105. The Influence of Freestream Turbulence on the Film Cooling Performance with a Blowing Distribution Simulating Plenum Supply ($\theta_4=58.7^\circ$, $(x/d_0)_4=1.5$, $S/d_0=P/d_0=5$)

The experiments for No Screen and the Fine Screen had turbulence intensities that were practically the same, and the film cooling data for these two cases show good agreement. The data for the coarse screen shows generally good agreement with the other two screen configurations except for the value of SNR behind the coolant hole at θ_1 and θ_3 . The magnitude of SNR_{NEG} was not as large for the higher level of turbulence intensity (see Figures 103, 105). In Figure 104, the film cooling data downstream from the third row (θ_3) show good agreement for the three screen configurations with the exception of the data at $z/S = 0.67$. A review of all the data for the plenum blowing simulation indicates little influence of freestream turbulence level for the range investigated.

Figures 106, 107 and 108 present the film cooling performance at $(x/d_o)_i = 1.5$ downstream from the rows at θ_1 , θ_2 , and θ_4 , respectively for the uniform blowing distribution. The data show good agreement for all three screen configurations indicating little influence of freestream turbulence intensity for the range investigated.

In general, the results for the three different turbulence screen configurations show no significant influence of the freestream turbulence intensity on the film cooling performance for both the plenum blowing simulation and the uniform blowing distribution. This finding was not surprising since previous experiments with flow visualization [19] have shown a highly turbulent flow resulting from the vortex pattern generated by the coolant jet - freestream interaction. Thus, changes in the freestream turbulence level were of little consequence at least for the range investigated.

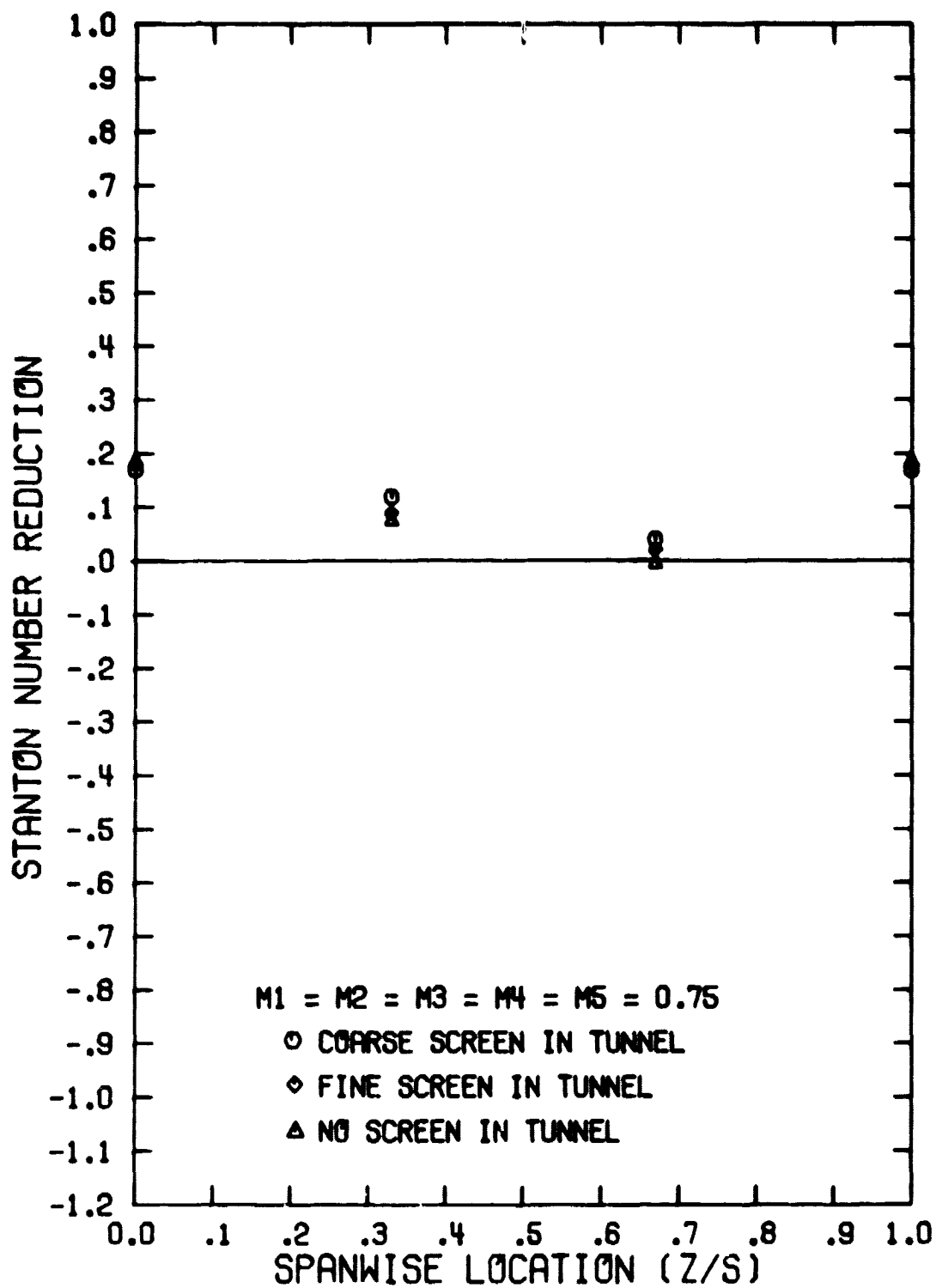


Figure 106. The Influence of Freestream Turbulence on the Film Cooling Performance with Uniform Blowing ($\theta_1 = 5^\circ$, $(x/d_0)_1 = 1.5$, $S/d_0 = P/d_0 = 5$)

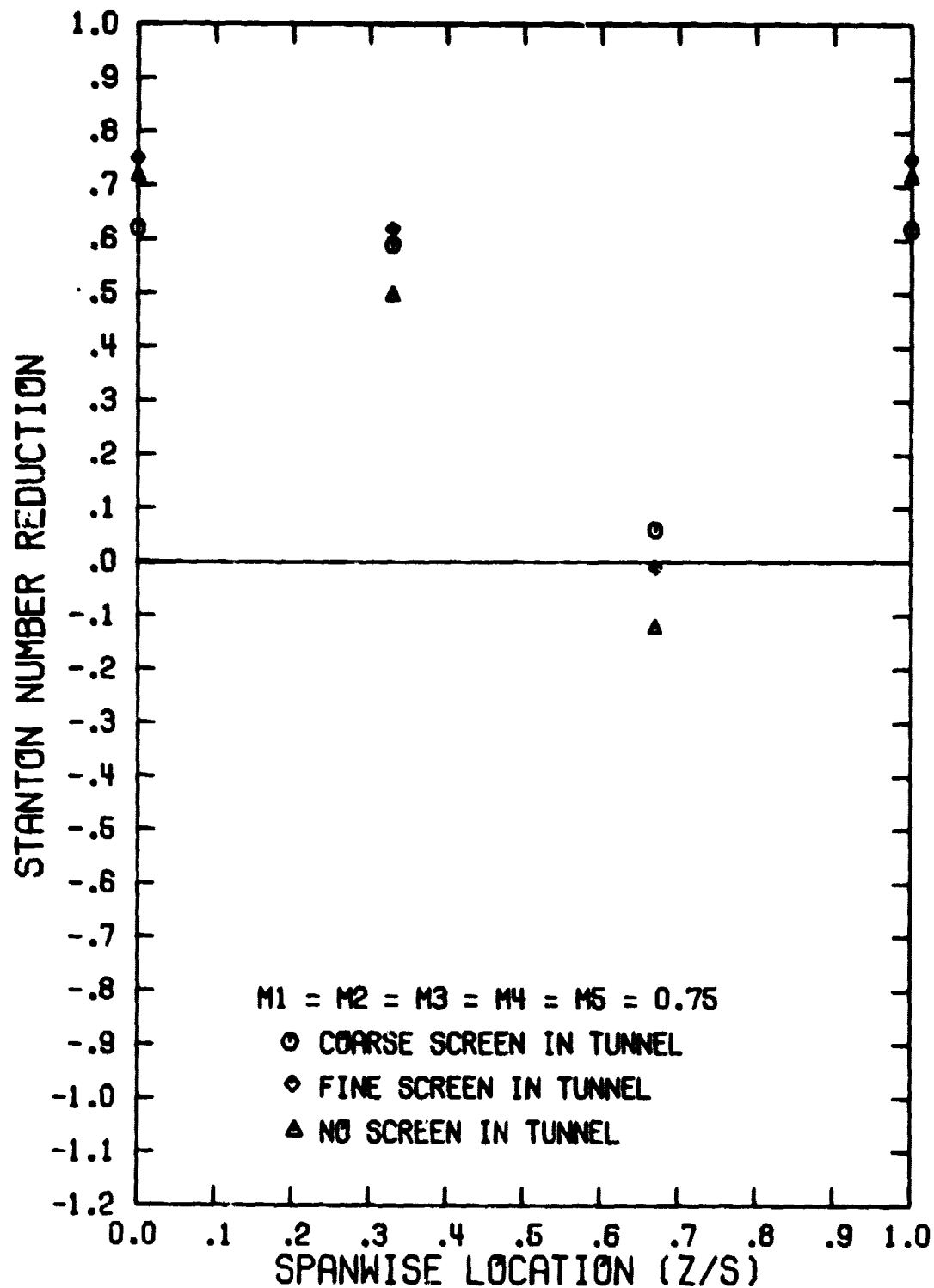


Figure 107. The Influence of Freestream Turbulence on the Film Cooling Performance with Uniform Blowing ($\theta_2 = 22.9^\circ$, $(x/d_0)_2 = 1.5$, $S/d_0 = P/d_0 = 5$)

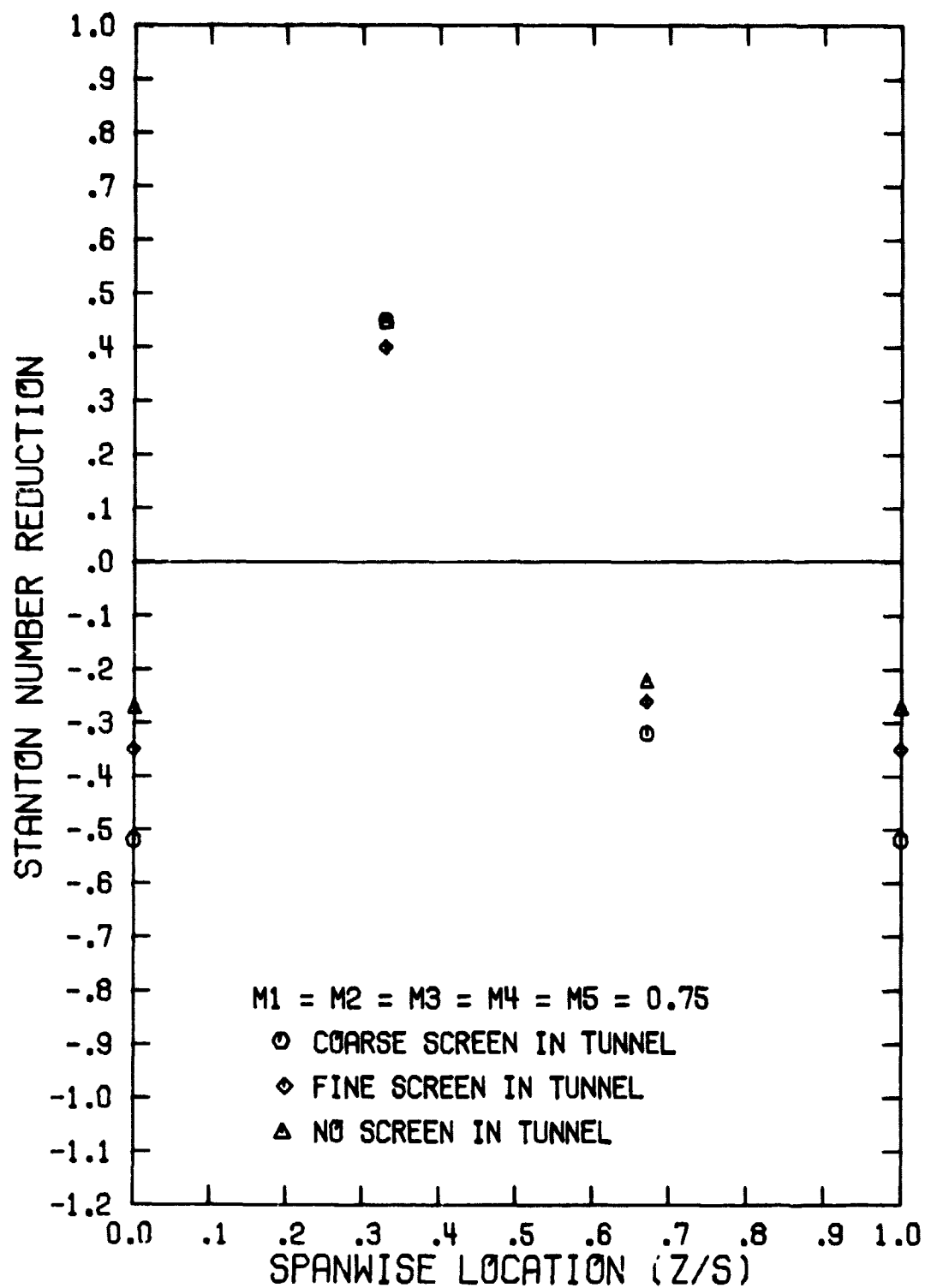


Figure 108. The Influence of Freestream Turbulence on the Film Cooling Performance with Uniform Blowing ($\Theta_4 = 58.7^\circ$, $(x/d_0)_4 = 1.5$, $S/d_0 = P/d_0 = 5$)

VIII. CONCLUSIONS

This investigation was conducted using the stagnation region of a cylinder in cross-flow to investigate the film cooling performance typical of a turbine vane leading edge. Experiments were conducted with film coolant injection from a single row and from multiple rows of coolant holes angled in the spanwise direction with $\beta = 25^\circ$. A freestream-to-wall temperature ratio of $T_\infty/T_w = 1.7$ and a Reynolds number of $Re_D = 9 \times 10^4$ were maintained throughout the investigation to simulate the gas turbine environment.

The test cylinder was instrumented with miniature heat flux gages and thermocouples to determine the local Stanton number, St , the Stanton number ratio with film cooling, St/St_0 , and the Stanton number reduction with film cooling, $SNR = 1 - (St/St_0)$. The data are presented in terms of SNR as a function of the distance x downstream from injection (x/d_0) and the location between adjacent coolant holes (z/S). The local values of SNR were integrated to determine the spanwise averaged Stanton number reduction, SNR_{AVG} as well.

The primary objectives of this investigation were to study the influence of: the coolant blowing ratio, M , the injection location relative to stagnation, θ_i , hole-to-hole (S/d_0) and row-to-row (P/d_0) spacing, and the effect of multiple rows of coolant holes. Data for single row injection were measured at the first four row locations, $\theta_i = 5^\circ, 22.9^\circ, 40.8^\circ, 58.7^\circ$ relative to stagnation, using a hole spacing of $S/d_0 = 5$ and 10.

Data were obtained for three multiple row configurations (a) a five row configuration with $S/d_0 = P/d_0 = 5$ and the first row at $\theta_1 = 5^\circ$, (b) a three row configuration with $S/d_0 = P/d_0 = 10$ and the first row at $\theta_1 = 5^\circ$, and (c) a two row configuration with $S/d_0 = P/d_0 = 10$ and the first row at $\theta_2 = 22.9^\circ$. Experiments were conducted with the multiple row configurations using a uniform blowing distribution and a blowing distribution simulating a plenum supply. Experiments also were conducted to determine the influence of freestream turbulence intensity on the film cooling performance.

From the analysis of the data, the following observations and conclusions were drawn concerning the effects of film cooling in the stagnation region. This summary is divided into four sections corresponding to the following topics: single row injection, multiple row injection with uniform blowing, multiple row injection with a plenum blowing simulation, and multiple row injection with increased freestream turbulence intensity.

VIII.A. Single Row Injection

- 1) The data revealed a very localized influence of the film coolant on the surface heat transfer. Lateral spreading of the coolant as it flowed downstream was minimal and a large portion of the region between the coolant holes remained unaffected.
- 2) The spanwise averaged data (SNR_{AVG}) demonstrated a rapid deterioration in the film cooling performance with downstream distance, x/d_0 .
- 3) The region that was covered by the coolant experiences high levels of film cooling performance ($SNR \approx 0.5$ to 0.7). At low values of blowing ratio, M , the coolant was turned quickly in the freestream direction and the area directly behind the coolant hole experienced large values of SNR . However, as M was increased, the coolant location shifted in the spanwise direction resulting in large negative values of SNR (i.e. increased heat flux) behind the coolant hole. The blowing ratio that produced the negative values of SNR behind the hole increased in magnitude as the injection location was moved away from stagnation.
- 4) In the region covered by the coolant, the blowing ratio that produced the largest value of SNR_{MAX} was referred to as the optimum blowing condition, M_{opt} . The value of SNR_{MAX} decreased as the blowing ratio was increased beyond M_{opt} . A blowing ratio defined with the upstream approach velocity, $M_{\infty,0}$, was found to provide the best correlation of the optimum blowing condition.
- 5) The effect of hole spacing on the local film cooling

performance was small for $M < M_{opt}$, except for injection at $\theta_1 = 5^\circ$ with $S/d_0 = 5$. The data for $S/d_0 = 5$ at θ_1 exhibited very low values of SNR when compared with the data for $S/d_0 = 10$. For $M > M_{opt}$, injection at θ_1 , θ_2 and θ_3 , produced larger values of SNR for $S/d_0 = 10$ than for $S/d_0 = 5$. However, for injection at $\theta_4 = 58.7^\circ$, the trend with respect to hole spacing was reversed.

6) The spanwise averaged film cooling performance (SNR_{AVG}) for $S/d_0 = 5$ was usually larger than for $S/d_0 = 10$. However, the improvement obtained by doubling the total coolant flow rate was typically less than 30 percent.

VIII.B. Multiple Row Injection with Uniform Blowing

1) Multiple row injection resulted in a high level of spanwise averaged film cooling performance when the blowing ratio was maintained at an appropriate level. With a uniform blowing distribution, a value of $M < 0.5$ was necessary, for all multiple row configurations, to avoid negative values of SNR behind the coolant hole.

2) The five row configuration with $S/d_0 = P/d_0 = 5$ exhibited the best film cooling performance. The three and two row configurations with $S/d_0 = P/d_0 = 10$ represented some improvement over single row injection, but the lack of spreading by the coolant across the surface and the rapid decay of the film cooling performance downstream indicated a closer hole and row spacing is necessary to maintain film cooling performance in the range of $SNR_{AVG} \approx 0.3 \rightarrow 0.4$.

3) The film cooling performance downstream from the first row of all multiple row configurations showed good agreement with the results for single row injection at the same injection location. Although the results for the downstream rows showed reasonable agreement with the single row data, some effects of upstream blowing were found. Blowing from upstream rows created a flow disturbance that reduced the optimum blowing condition and the blowing condition that produced negative SNR behind the hole for downstream rows. At

high values of blowing ratio, $M > 1.0$, the flow disturbance became large enough such that SNR was negative across the span. This was not observed with single row injection.

4) The staggering of holes from row-to-row used in this investigation did not yield the spanwise uniformity in film cooling performance expected downstream from the second and subsequent downstream rows. The trajectory of the coolant from the first row (inferred from the data) passed in close proximity to the hole in the second row, and so on. The trajectory of the coolant was found to be essentially the same for single row and multiple row injection.

5) A superposition method using data for SNR_{AVG} for single row injection was used to predict results for multiple row injection showing good agreement with measured data as long as M was restricted such that SNR was positive across the span. The accuracy of the prediction was poor for values of M that resulted in negative SNR behind the hole.

VIII.C. Multiple Row Injection with a Blowing Distribution Simulating a Plenum Supply

1) A model to predict the nonuniform blowing distribution for multiple rows of holes supplied by a common plenum showed the blowing distribution was primarily dependent on the plenum coolant-to-freestream total pressure ratio, $P_{TC}/P_{T\infty}$, and the approach Mach number, $Ma_{\infty,0}$. The blowing distributions, calculated for values of $P_{TC}/P_{T\infty}$ and $Ma_{\infty,0}$ typical of engine conditions, resulted in very large values of M for the first two or three rows of coolant holes. This resulted in large negative values of SNR behind the coolant holes with moderate positive values of SNR between the hole centerlines.

2) Even for the lowest values of blowing ratio ($P_{T,C}/P_{T,\infty} = 1.010$, $Ma_{\infty,0} = 0.2$), the large negative values of SNR tended to dominate the value of SNR_{AVG} . The results for the five row configuration ($S/d_0 = P/d_0 = 5$) show $SNR_{AVG} \leq 0.13$ behind the second row and, generally, SNR_{AVG} was less than zero for most of the surface. The trends for the three row configuration ($S/d_0 = P/d_0 = 10$) were similar with improved performance downstream at θ_3 . The two row configuration was comparable. Increasing the value of $P_{T,C}/P_{T,\infty}$ and/or decreasing $Ma_{\infty,0}$ resulted in higher values of blowing ratio, larger negative values of SNR and, therefore, lower values (i.e. more negative) of SNR_{AVG} .

VIII.D. The Influence of Freestream Turbulence Intensity on Film Cooling Performance

1) The five row configuration ($S/d_0 = P/d_0 = 5$) was used to investigate the influence of freestream turbulence intensity on the film cooling performance. An increase in the turbulence intensity from 4.4% to 9.5% was found to have little influence on the film cooling performance for either the plenum blowing simulation ($P_{T,C}/P_{T,\infty} = 1.010$, $Ma_{\infty,0} = 0.2$) or the uniform blowing distribution ($M = 0.75$).

BIBLIOGRAPHY

1. Goldstein, R.J., *Film Cooling, Advances in Heat Transfer*, New York, Academic Press, 1971, Vol. 7, pp. 321-379.
2. Hanus, G.J., and L'Ecuyer, M.R., *Turbine Vane Gas Film Cooling with Injection in the Leading Edge Region from a Single Row of Spanwise Angled Holes*, Thermal Sciences & Propulsion Center, Purdue University Technical Report No. TSPC-TR-76-1, May, 1976.
3. Luckey, D.W., and L'Ecuyer, M.R., *Stagnation Region Gas Film Cooling - Spanwise Angled Coolant Injection*, Thermal Sciences & Propulsion Center, Purdue University, Technical Report No. TSPC-TR-76-2, December, 1976.
4. Hartnett, J.P., Birkebak, R.C., and Eckert, E.R.G., *Velocity Distributions, Effectiveness, and Heat Transfer in Film Cooling of a Surface with a Pressure Gradient*, Proceedings of 1961 International Heat Transfer Conference, Part IV, Section A, Paper No. 81, 1961.
5. Metzger, D.E., and Fletcher, D.D., *Surface Heat Transfer with Film Cooling Near Non-Tangential Injection Slots*, AIAA Paper No. 69-523, 1969.
6. Eriksen, V.L., and Goldstein, R.J., *Heat Transfer and Film Cooling Following Injection Through Inclined Circular Tubes*, ASME Paper No. 74-HT-V, July, 1973.
7. Lander, R.D., Fish, R.W., and Suo, M., *The External Heat Transfer Distribution on a Film Cooled Turbine Vane*, AIAA 10th Aerospace Sciences Meeting, AIAA Paper No. 72-9, 1972.
8. Metzger, D.E., *A Summary and Design Recommendations - Film Cooling*, Airesearch Report No. TR-5025, Airesearch Manufacturing Company of Arizona, May, 1968.
9. Choe, H., Kays, W.M., and Moffat, R.J., *The Superposition Approach to the Film Cooling of a Uniform Temperature Wall*, ASME Paper No. 74-WA/HT-27, November, 1974.
10. Russell, Louis M., *Flow Visualization of Discrete-Hole Film Cooling With Spanwise Injection Over a Cylinder*, NASA Technical Paper 1491, Lewis Research Center, Cleveland, Ohio, July, 1979.

11. Metzger, D.E., Takeuchi, D.I., and Kuenstler, P.A., *Effectiveness and Heat Transfer with Full Coverage Film Cooling*, Journal of Engineering for Power, July, 1973, pp. 180-184.
12. Mayle, R.E., and Camarata, F.J., *Multihole Cooling Film Effectiveness and Heat Transfer*, ASME Paper No. 74-HT-9, July, 1974.
13. LeBrocq, P.V., Launder, B.E., and Priddin, C.H., *Discrete Hole Injection As A Means of Transpiration Cooling - An Experimental Study*, Proceedings of the Institute of Mechanical Engineers, Thermodynamics and Fluid Mechanics Group, Vol. 187-17/73, 1973, pp. 149-157.
14. Crawford, M.E., Kays, W.M., and Moffat, R.J., *Heat Transfer to a Full-Coverage Film-Cooled Surface with 30° Slant-Hole Injection*, NASA CR-2786, December, 1976.
15. Pedersen, D.R., Eckert, E.R.G., and Goldstein, R.J., *Film Cooling With Large Density Differences Between the Mainstream and the Secondary Fluid Measured by the Heat-Mass Transfer Analogy*, ASME Journal of Heat Transfer, Vol. 99, November, 1977, pp. 620-627.
16. Launder, B.E., and York, J., *Discrete Hole Cooling in the Presence of Freestream Turbulence and Strong Favorable Pressure Gradient*, International Journal of Heat and Mass Transfer, Vol. 17, 1974, pp. 1403-1409.
17. Sasaki, M., Takahara, K., Sakata, K., and Kumagai, T., *Study on Film Cooling of Turbine Blades*, Bulletin of the JSME, Vol. 19, No. 137, November, 1976, pp. 1344-1352.
18. Colladay, R.S., and Russell, L.M., *Flow Visualization of Discrete Hole Film Cooling for Gas Turbine Applications*, NASA Technical Memorandum X-71766, Lewis Research Center, Cleveland, Ohio, 1975.
19. Russell, L.M., *Flow Visualization of Film Cooling with Spanwise Injection From a Small Array of Holes and Compound-Angle Injection From a Large Array*, NASA Technical Paper 1195, Lewis Research Center, Cleveland, Ohio, 1978.
20. Liess, C., *Experimental Investigation of Film Cooling With Ejection from a Row of Holes for the Application to Gas Turbine Blades*, ASME Paper No. 74-GT-5, April, 1974.
21. Seban, R.W., and Back, L.H., *Effectiveness and Heat Transfer for a Turbulent Boundary Layer with Tangential Injection and Variable Freestream Velocity*, ASME Journal of Heat Transfer, Vol. 84, No. 3, August, 1962, pp. 235-242.

22. Pai, B.R., and Whitelaw, J.H., *The Influence of Strong Pressure Gradients on Film Cooling Effectiveness*, Heat Transfer, Vol. 2, FC 1.11, 1970, pp. 1-10.
23. Jabbari, M.Y., *Film Cooling and Heat Transfer with Air Injection Through a Staggered Row of Holes into an Accelerating Flow*, Ph.D. Thesis, University of Minnesota, 1973.
24. Kadotani, K., *Effect of Main Stream Variables on Heated and Unheated Jets Issuing from a Row of Inclined Round Holes*, Ph.D. Thesis, University of Minnesota, 1975.
25. Marek, C.J., and Tacina, R.R., *Effect of Freestream Turbulence on Film Cooling*, NASA TN D-7958, 1975.
26. Crawford, M.E., Choe, H., Kays, W.M., and Moffat, R.J., *Full-Coverage Film Cooling Heat Transfer Study - Summary of Data for Normal-Hole Injection and 30° Slant-Hole Injection*, NASA CR-2648, March, 1976.
27. Ito, S., *Film Cooling and Aerodynamic Loss in a Gas Turbine Cascade*, Ph.D. Thesis, University of Minnesota, 1976.
28. Morel, T., *Comprehensive Design of Axisymmetric Wind Tunnel Contractions*, Journal of Fluids Engineering, June, 1975, pp. 225-233.
29. Hinze, J.O., *Turbulence*, McGraw-Hill, New York, 1959, pp. 204-219.
30. Batchelor, G.K., and Townsend, A.A., *Decay of Isotropic Turbulence in the Initial Period*, *Proceedings of Royal Society, London*, Vol. 193A, 1948, p. 539.
31. Kestin, J., and Wood, R. T., *The Influence of Turbulence on Mass Transfer From Cylinders*, *ASME Journal of Heat Transfer*, November, 1971, pp. 321-327.
32. Papell, S.S., and Trout, A.M., *Experimental Investigation of Air Film Cooling Applied to a Adiabatic Wall by Means of an Axially Discharging Slot*, NASA TN D-9, 1959.
33. Choe, H., Kays, W.M., and Moffat, R.J., *Turbulent Boundary Layer on a Full-Coverage Film-Cooled Surface - An Experimental Heat Transfer Study with Normal Injection*, NASA CR-2642, January, 1976.
34. Colladay, R.S., *The Importance of Combining Convection with Film Cooling*, AIAA Paper No. 72-8, January, 1972.
35. Schlichting, H., *Boundary Layer Theory*, 6th Edition, New York, McGraw-Hill Book Company, 1968, pp. 202.

36. Poferl, D., Suehla, R., and Lewandowski, K., Thermodynamic and Transport Properties of Air and the Combustion Products of Natural Gas and of ASTM-A-1 Fuel with Air, NASA TN D-5452, Lewis Research Center, Cleveland, Ohio, October, 1969.
37. Achenbach, E., Distribution of Local Pressure and Skin Friction Around a Circular Cylinder in Cross-Flow up to $Re = 5 \times 10^6$, Journal of Fluid Mechanics, 1968, Vol. 34, pp. 625-639.
38. Seban, R.A., The Influence of Freestream Turbulence on the Local Heat Transfer from Cylinders, Journal of Heat Transfer, ASME Transactions, Vol. 82, No. 4, November, 1960, pp. 305-312.
39. Giedt, W.H., The Effect of Turbulence Level in Incident Air Stream on Local Heat Transfer and Skin Friction on a Cylinder, Journal of Aeronautical Sciences, November, 1951, pp. 725-730.
40. Zapp, G.M., The Effect of Turbulence on Local Heat Transfer Coefficients Around a Cylinder Normal to an Air Stream, M.S. Thesis, Oregon State College (1950).
41. Achenbach, Elmar, Total and Local Heat Transfer From a Smooth Circular Cylinder in Cross-Flow at High Reynolds Number, International Journal of Heat and Mass Transfer, Vol. 18, 1975, pp. 1387-1396.
42. Kestin, J., and Wood, R.T., The Influence of Turbulence on Mass Transfer from Cylinders, ASME Journal of Heat Transfer, November, 1971, pp. 321-327.
43. Achenbach, Elmar, The Effect of Surface Roughness on the Heat Transfer from a Circular Cylinder to the Cross Flow of Air, International Journal of Heat and Mass Transfer, Vol. 20, 1977, pp. 359-369.
44. Sellers, J.P., Gaseous Film Cooling with Multiple Injection Stations, AIAA Journal, Vol. 1, No. 9, December 1963, pp. 2154-2156.

Appendix I Blowing Ratio Distribution Simulating a Plenum Supply

Most of the multiple row film cooling studies published to date have investigated flat test surfaces with a uniform distribution of the blowing ratio row-to-row. With a flat surface, the constant freestream mass velocity ($\rho_\infty V_\infty$) and uniform blowing distribution corresponds to equal coolant flow rates for each row of holes. For turbine blade cooling applications, it is common to feed different rows of holes from a common plenum. This results in a nonuniform blowing distribution due to (a) the variation of ($\rho_\infty V_\infty$) along the surface and (b) the variation of plenum-to-freestream pressure difference governing the flow through each hole.

Figure A-1 illustrates a diagram representing multiple rows of holes fed from a common plenum typical of turbine vane leading edge designs and the test cylinder used in the present study. The mass flow rate from each hole is governed by the ratio of the plenum coolant total pressure, $P_{T,C}$, to the coolant hole exit static pressure (assumed equal to the local freestream static pressure, P_∞). In the leading edge region, the freestream static pressure and velocity vary as the flow accelerates away from the stagnation point. Therefore, each row of holes will have a unique pressure ratio, $(P_{T,C}/P_\infty)_i$, and mass flow rate depending on its location (θ_i). With both the coolant mass flow rate and the local freestream mass velocity, $(\rho_\infty V_\infty)_i$, dependent on θ_i , the blowing ratio distribution in the leading edge region will be non-uniform row-to-row. This appendix describes the model developed to predict the blowing ratio distribution for multiple rows fed from a common plenum.

The mass flux from a coolant hole can be expressed by the continuity equation as

$$(\dot{m}V)_C = \frac{P_C}{R_C T_C} M_C a_C C_D \quad (A-1)$$

where P_c = coolant static pressure
 T_c = coolant static temperature
 M_c = coolant Mach number
 a_c = coolant speed of sound
 C_D = discharge coefficient
 R_c = coolant gas constant

By replacing static properties in terms of stagnation properties and Mach number, equation (A-1) can be written as

$$(\rho V)_c = C_D P_{T_c} \sqrt{\frac{\gamma_c}{R_c T_c}} \left(\frac{M_c}{[1 + (\gamma_c - 1)/2 M_c^2]^{(\gamma_c + 1)/2(\gamma_c - 1)}} \right) \quad (A-2)$$

where γ_c = specific heat ratio for coolant

The coolant Mach number can be expressed in terms of pressure ratio as

$$M_c = \sqrt{\left\{ \frac{2}{(\gamma_c - 1)} \right\} \left\{ (P_{T_c}/P_c)^{(\gamma_c - 1)/\gamma_c} - 1 \right\}} \quad (A-3)$$

Substituting Equation (A-3) into Equation (A-2) gives

$$(\rho V)_c = C_D P_{T_c} \sqrt{\frac{\gamma_c}{R_c T_c}} \frac{\sqrt{\left\{ \frac{2}{(\gamma_c - 1)} \right\} \left\{ (P_{T_c}/P_c)^{(\gamma_c - 1)/\gamma_c} - 1 \right\}}}{(P_{T_c}/P_c)^{(\gamma_c + 1)/2\gamma_c}} \quad (A-4)$$

The static pressure of the coolant emerging from the hole (P_c) is assumed equal to the local freestream static pressure (P_∞). Then Equation (A-4) can be written as

$$(\rho V)_c = C_D F P_{T_\infty} \sqrt{\frac{\gamma_c}{R_c T_c}} \frac{\sqrt{\left\{ \frac{2}{\gamma_c - 1} \right\} \left\{ (F)^{\frac{\gamma_c - 1}{\gamma_c}} (P_{T_\infty}/P_\infty)^{\frac{\gamma_c - 1}{\gamma_c}} - 1 \right\}}}{(F)^{(\gamma_c + 1)/2\gamma_c} (P_{T_\infty}/P_\infty)^{(\gamma_c + 1)/2\gamma_c}} \quad (A-5)$$

where F = coolant plenum total-to-freestream total pressure ratio, P_{T_c}/P_{T_∞} .

Therefore, the mass flux of the coolant was determined for specified values of the coolant total temperature ($T_{T,c}$), freestream total pressure ($P_{T,\infty}$), freestream total-to-static pressure ratio, C_D , and F .

The freestream total-to-static pressure ratio was determined from the local Mach number distribution.

$$\frac{P_{T,\infty}}{P_\infty} = \left[1 + \frac{\gamma_H - 1}{2} M_\infty^2 \right]^{\gamma_H / (\gamma_H - 1)} \quad (A-6)$$

where γ_H = freestream gas constant
 M_∞ = local Mach number

The local freestream velocity (V_∞) was determined from potential flow accounting for tunnel blockage due to the test cylinder as described in Section II.D. Therefore, assuming incompressible flow for $Ma_{\infty,0} \leq 0.2$ the local freestream velocity around the test cylinder was given as

$$V_\infty = 2V_{\infty,0} C_i \sin \theta_i \quad (A-7)$$

where C_i = correction for tunnel blockage

The local surface Mach number for a given coolant hole location (θ_i) was determined from

$$M_\infty = 2 M_{\infty,0} \sqrt{\frac{1 + \frac{\gamma-1}{2} M_\infty^2}{1 + \frac{\gamma-1}{2} M_{\infty,0}^2}} C_i \sin \theta_i \quad (A-8)$$

The discharge coefficient, C_D , with blowing through holes near the leading edge of a turbine vane was approximated by the results of Sasaki, Takahara, Sakata and Kamagai [17], reporting on an experimental study of the blowing characteristics from a single hole on a circular in a freestream. The discharge coefficient without freestream flow was correlated with the coolant Reynolds number based on hole diameter, $(\frac{\rho_c V_{c,d_0}}{\mu_c})$. A least squares fit of the data gave

$$C'_D = 0.526 + 0.0685 (\log_{10} Re_{d_0}) \quad (A-9)$$

where C'_D = discharge coefficient without freestream flow
 With freestream flow over the cylinder surface, the discharge coefficient was affected by the coolant-freestream interaction.
 Sasaki et al defined a loss coefficient for flow through a hole as

$$\zeta = \frac{1}{(C'_D)^2} - 1 \quad (A-10)$$

The additive loss created when the freestream flow was applied was defined as

$$\begin{aligned} \zeta^* &= \zeta - \zeta_0 \\ \text{where } \zeta_0 &= \frac{1}{(C'_D)^2} - 1 \end{aligned} \quad (A-11)$$

Rearranging these equations gives

$$C_D = \left[\frac{(C'_D)^2}{\zeta^* (C'_D)^2 + 1} \right]^{\frac{1}{2}} \quad (A-12)$$

Sasaki et al found that the loss coefficient, ζ^* , was a function of the local coolant-to-freestream momentum flux ratio, I_∞ . Their data are presented in the following functional form.

For $\log_{10} I_\infty < 0.080$

$$\begin{aligned} \zeta^* &= 0.0006 - 0.6414 (\log_{10} I_\infty) \\ &\quad + 0.1739 (\log_{10} I_\infty)^2 - 0.5562 (\log_{10} I_\infty)^3 \\ &\quad + 0.2853 (\log_{10} I_\infty)^4 \end{aligned} \quad (A-13)$$

For $\log_{10} I_\infty \geq 0.080$

$$\zeta^* = 0.0 \quad (A-14)$$

The coolant mass flux was computed by iteration by initially setting $C_D = 1$, and using Equation (A-5) to estimate $(\rho V)_c$. The coolant Reynolds number, Re_{d_0} , and the local momentum flux ratio, I_∞ , were approximated and Equations (A-9), (A-13) and (A-14) were used to calculate C'_D and ζ^* . The values for C'_D and ζ^* were used in Equation

(A-12) to revise the value of C_D . With a value for C_D less than 1, a revised coolant mass flux was computed from Equation (A-5) and the procedure was repeated until the change in $(\rho V)_C$ was $\leq 0.5\%$.

The foregoing procedure shows that the blowing ratio for a particular row location (θ_i) on the test cylinder is a function of $Ma_{\infty,0}$, F , and $T_{T,\infty}/T_{T,C}$. The values of $T_{T,\infty}$ and $T_{T,C}$ influence the specific heat ratio (γ_H , γ_C), and the values of $P_{T,\infty}$ and $T_{T,C}$ affect Re_{d_0} and C_D , but these effects are of secondary importance. In the present study, the ratio, $T_{T,\infty}/T_{T,C}$ was held constant so that values of $F = P_{T,C}/P_{T,\infty}$ and $Ma_{\infty,0}$ governed the blowing ratio for a particular row location (θ_i).

The blowing ratio for each of the five coolant hole locations ($\theta_1, \dots, \theta_5$) was computed for three values of $P_{T,C}/P_{T,\infty}$ (1.01, 1.02 and 1.03) and two values of $Ma_{\infty,0}$ (0.1 and 0.2) representative of values typically found in leading edge designs. The blowing ratio distributions were calculated for: (a) the experimental conditions in this study,

$$P_{T,\infty} = 101 \text{ kPa}, \quad T_{T,\infty} = 500 \text{ K}, \quad T_{T,\infty}/T_{T,C} = 1.7, \quad d_0 = 4.76 \text{ mm}$$

and (b) typical engine conditions,

$$P_{T,\infty} = 862 \text{ kPa}, \quad T_{T,\infty} = 1610 \text{ K}, \quad T_{T,\infty}/T_{T,C} = 1.7, \quad d_0 = 0.51 \text{ mm}$$

A comparison between the blowing ratio distributions for both cases showed the largest margin of difference to be 4%. The blowing ratio distributions computed for the typical engine conditions were chosen for use in this investigation.

The computed values of blowing ratio, M_i , (typical engine conditions) were compared with the blowing ratio distributions for selected leading edge turbine vane designs for the same $P_{T,C}/P_{T,\infty}$ and $Ma_{\infty,0}$. The values for M_i computed for the present study were approximately 15% higher than the design comparisons, possibly due to a difference in the value of C_D when going from a single hole configuration to a multiple row configuration. Consequently, the values of M_i calculated using data from Sasaki, Takahara, Sakata, and Kamagai [17] data for C_D were reduced by 15% to arrive at the

blowing ratio distribution used in the present study. Table A-1 summarizes the values of the blowing ratio for each multiple row configuration and for each combination of $P_{T,c}/P_{T,\infty}$ and $Ma_{\infty,0}$ used in the study of film cooling with a blowing distribution simulating a plenum supply (see Chapter VI).

Table A-1. Blowing Ratio, M , for Multiple Rows with Common Plenum
$$M_{\infty,0} = 0.1 \quad S/d_0 = 10 \quad \theta_1 = 5^\circ$$

P_{T_c}/P_{T_∞}	Row 1 $\theta_1 = 5^\circ$	Row 2 $\theta_3 = 40.8^\circ$	Row 3 $\theta_5 = 76.6^\circ$
1.010	5.73	1.17	1.01
1.020	8.16	1.40	1.16
1.030	10.05	1.61	1.27

$$M_{\infty,0} = 0.2$$

P_{T_c}/P_{T_∞}	Row 1 $\theta_1 = 5^\circ$	Row 2 $\theta_3 = 40.8^\circ$	Row 3 $\theta_5 = 76.6^\circ$
1.010	2.96	0.95	0.92
1.020	4.15	1.04	0.96
1.030	5.08	1.14	1.01

$$M_{\infty,0} = 0.1 \quad S/d_0 = 10 \quad \theta_2 = 22.9^\circ$$

P_{T_c}/P_{T_∞}	Row 1 $\theta_2 = 22.9^\circ$	Row 2 $\theta_4 = 58.7^\circ$
1.010	1.54	1.05
1.020	2.02	1.24
1.030	2.41	1.36

$$M_{\infty,0} = 0.2$$

P_{T_c}/P_{T_∞}	Row 1 $\theta_2 = 22.9^\circ$	Row 2 $\theta_4 = 58.7^\circ$
1.010	1.08	0.92
1.020	1.28	0.98
1.030	1.44	1.04

$$M_{\infty,0} = 0.1 \quad S/d_0 = 5 \quad \theta_1 = 5^\circ$$

P_{T_c}/P_{T_∞}	Row 1 $\theta_1 = 5^\circ$	Row 2 $\theta_2 = 22.9^\circ$	Row 3 $\theta_3 = 40.8^\circ$	Row 4 $\theta_4 = 58.7^\circ$	Row 5 $\theta_5 = 76.6^\circ$
1.010	5.73	1.54	1.17	1.05	1.01
1.020	8.16	2.02	1.40	1.24	1.16
1.030	10.05	2.42	1.61	1.36	1.27

$$M_{\infty,0} = 0.2$$

P_{T_c}/P_{T_∞}	Row 1 $\theta_1 = 5^\circ$	Row 2 $\theta_2 = 22.9^\circ$	Row 3 $\theta_3 = 40.8^\circ$	Row 4 $\theta_4 = 58.7^\circ$	Row 5 $\theta_5 = 76.6^\circ$
1.010	2.96	1.08	0.95	0.92	0.92
1.020	4.15	1.27	1.04	0.98	0.96
1.030	5.08	1.44	1.14	1.04	1.01

ORIGINAL PAGE IS
OF POOR QUALITY

Appendix II Surface Roughness of the Test Cylinder

The test cylinder was machined with five slots to allow for the placement of removable drop-in segments. The segments were incorporated to permit a variation of the coolant hole spacing (S/d_0) and row-to-row spacing (P/d_0) while still using the same instrumented cylinder. Since surface roughness affects the boundary layer development on the test cylinder, precautions were taken to measure and control the surface roughness due to the misalignment of the drop-in segments and the cylindrical test surface.

The surface roughness produced by the drop-in segments was measured each time a new set of segments were installed in the cylinder. A dial indicator (0.0127 mm divisions) was used to measure the roughness of each segment at selected locations along the span. Figures A-2, A-3, and A-4 show the roughness measurements, K (in millimeters) when the cylinder was equipped with solid segments (i.e., no holes), with segments having a hole spacing of $S/d_0 = P/d_0 = 10$, and with segments having a hole spacing of $S/d_0 = P/d_0 = 5$, respectively. Each figure indicates the location of the heat flux gages along the surface.

The data in Figure A-2 shows, when the solid segments were installed, the largest roughness on the test surface was $K = -0.076$ mm corresponding to a dimensionless roughness height of $K/D = 5.0 \times 10^{-4}$, where D is the cylinder diameter. It is noted that the largest roughness occurs approximately 50.8 mm from the wind tunnel wall. In the central region near the heat flux instrumentation, $K \leq 0.0635$ mm, $K/D \leq 4.1 \times 10^{-4}$.

When the film cooling experiments were initiated, the solid segments S_1 , S_3 , S_5 were replaced with segments having coolant holes drilled at a spacing of $S/d_0 = 10$. The surface roughness measurements shown in Figure A-3 indicate the largest roughness, $K = -0.178$ mm, $K/D = 11.7 \times 10^{-4}$, located 25.4 mm from the wind tunnel wall and $K \leq +0.101$ mm, $K/D \leq 6.7 \times 10^{-4}$, in the central region.

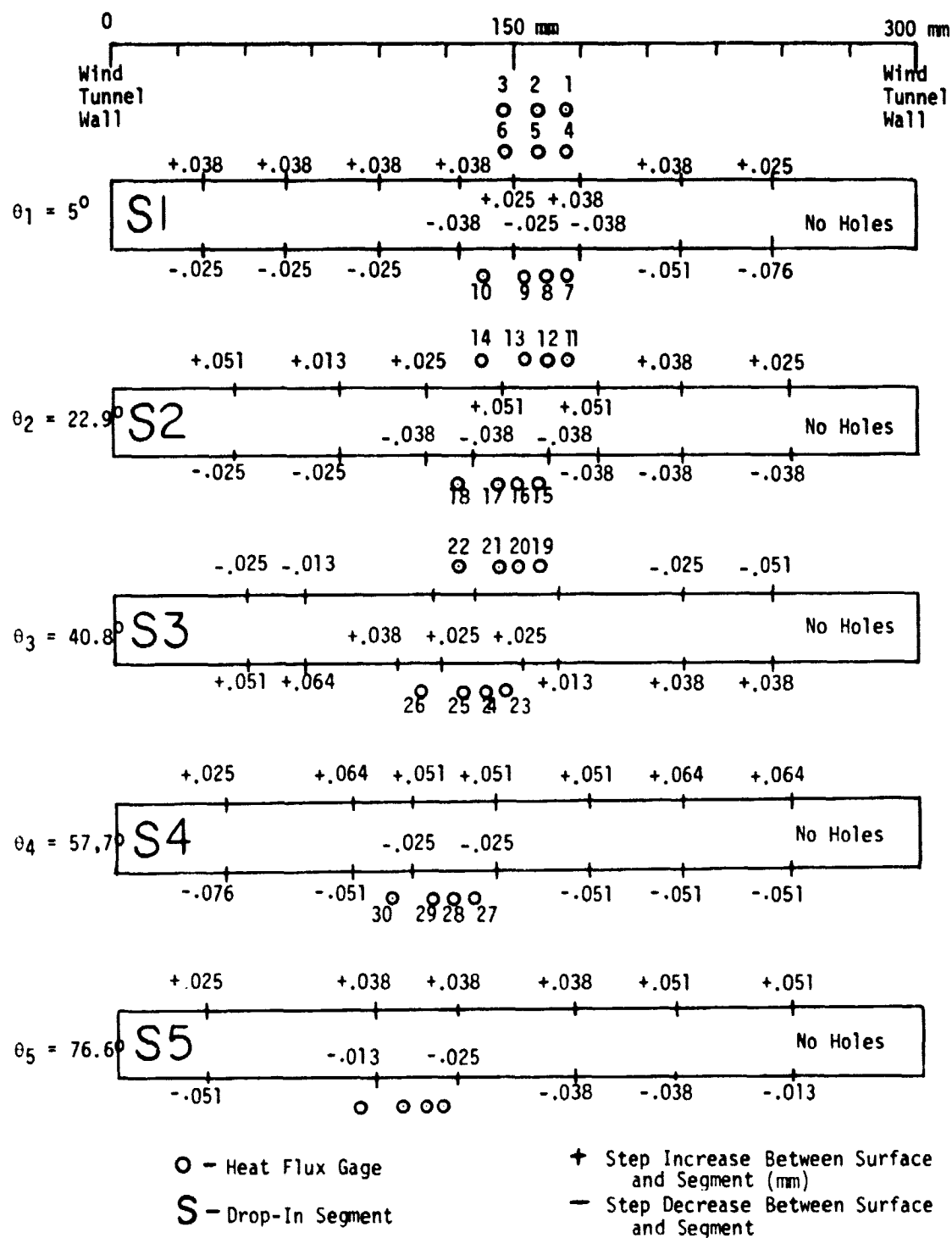


Figure A-2. Surface Roughness of Test Cylinder with Solid Segments Installed

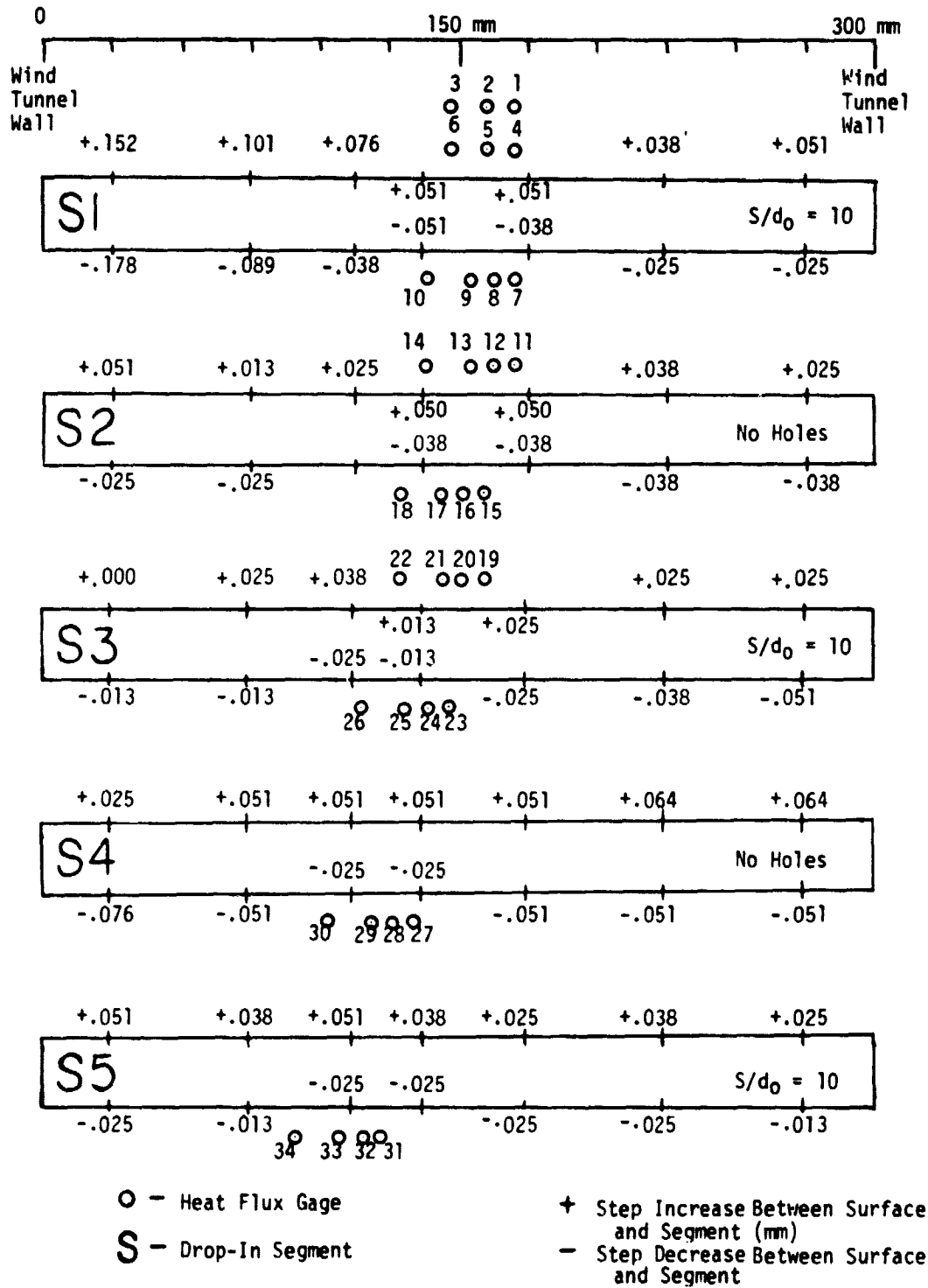
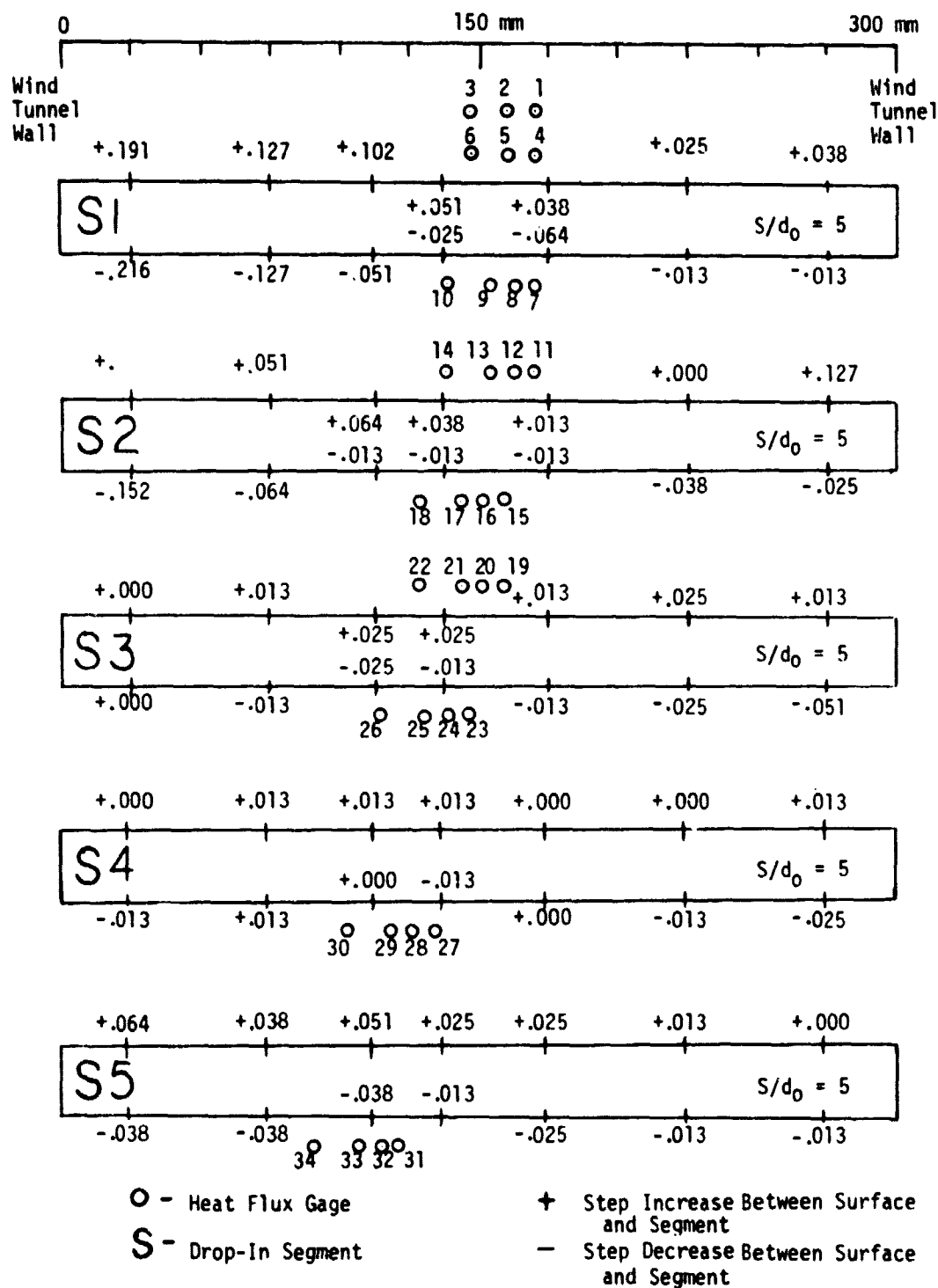


Figure A-3. Surface Roughness of Test Cylinder with Drilled Segments ($S/d_0 = P/d_0 = 10$)



The test configuration with $S/d_0 = P/d_0 = 5$ required a row of coolant holes at all five segment locations. The drilled segments at $\theta_1, \theta_3, \theta_5$ ($S/d_0 = 10$) were removed and drilled for a hole spacing of $S/d_0 = 5$. The solid segments at θ_2, θ_4 were replaced with segments drilled for $S/d_0 = 5$. The surface roughness measurements shown in Figure A-4, indicate the largest surface roughness, $K = 0.216$ mm, $K/D = 13.3 \times 10^{-4}$, near the tunnel wall, and $K \leq 0.127$ mm, $K/D \leq 8.3 \times 10^{-4}$ in the central region.

The foregoing measurements show that for all the experiments, the surface roughness was $K/D \leq 5.0 \times 10^{-4}$ to 8.3×10^{-4} in the central region of the test cylinder where the heat flux measurements were made. The influence of roughness size on heat transfer was investigated by Achenbach [34] using a cylindrical test surface with emery paper to create a selected sand grain roughness. Heat flux measurements made at a Reynolds number, $Re_D^* = 8.3 \times 10^4$ and a sand grain roughness of $K_s/D = 7.5 \times 10^{-4}$ showed no influence of the roughness on the heat transfer when compared with the results for a smooth cylinder. Experiments at $Re_D^* = 6.3 \times 10^4$ with $K_s/D = 30 \times 10^{-4}$ also showed no influence of the roughness on the heat transfer. Therefore, for the present investigation conducted at $Re_D^* = 7.1 \times 10^4$, it was concluded that the surface roughness, $K/D \leq 5.0 \times 10^{-4}$ to 8.3×10^{-4} , had no influence on the measured heat transfer in the central region of the test cylinder. Further evidence in support of this conclusion is indicated by the dry wall heat transfer data presented in Figure 36 where $N_{uD}/\sqrt{Re_D^*}$ decreases monotonically with θ in good agreement with published data for smooth cylinders [38] [39][40].

Appendix III. Experimental Data from the Film Cooling Experiments

The purpose of this appendix is to document the values of Stanton Number Reduction, SNR, measured during the present investigation. A complete listing of the values of SNR is presented in a tabular and graphical form for each heat flux gage location (z/s , x/d_0), for all parameters investigated (S/d_0 , P/d_0 , M_1 , θ_1). The spanwise averaged Stanton Number Reduction, SNR_{AVG} , calculated as described in Chapter also is presented.

An index of the tables and figures follows.

Single Row Injection

<u>Table or Figure</u>	<u>Condition</u>
Figures A-5 → A-11 Table A-2, Table A-17 (SNR_{AVG})	Single Row Injection ($\theta_1 = 5^\circ$, $S/d_0 = 5$)
Figures A-12 → A-18 Table A-3, Table A-18 (SNR_{AVG})	Single Row Injection ($\theta_1 = 5^\circ$, $S/d_0 = 10$)
Figures A-19 → A-24 Table A-4, Table A-19 (SNR_{AVG})	Single Row Injection ($\theta_2 = 22.9^\circ$, $S/d_0 = 5$)
Figures A-25 → A-30 Table A-5, Table A-20 (SNR_{AVG})	Single Row Injection ($\theta_2 = 22.9^\circ$, $S/d_0 = 10$)
Figures A-31 → A-35 Table A-6, Table A-21 (SNR_{AVG})	Single Row Injection ($\theta_3 = 40.8^\circ$, $S/d_0 = 5$)
Figures A-36 → A-39 Table A-7, Table A-22 (SNR_{AVG})	Single Row Injection ($\theta_3 = 40.8^\circ$, $S/d_0 = 10$)
Figures A-40 → A-43 Table A-8, Table A-23 (SNR_{AVG})	Single Row Injection ($\theta_4 = 58.7^\circ$, $S/d_0 = 10$)

<u>Table or Figure</u>	<u>Condition</u>
Figures A-44, A-45 Table A-9, Table A-24 (SNR_{AVG})	Single Row Injection ($\theta_4 = 58.7^\circ$, $S/d_0 = 10$)

Multiple Row Injection with Uniform Blowing

<u>Table or Figure</u>	<u>Condition</u>
Figures A-46 → A-52 Table A-10 Table A-25 (SNR_{AVG})	Five Row Injection with Uniform Blowing ($\theta_1 = 5^\circ$, $S/d_0 = P/d_0 = 5$)
Figures A-53 → A-59 Table A-11 Table A-26 (SNR_{AVG})	Three Row Injection with Uniform Blowing ($\theta_1 = 5^\circ$, $S/d_0 = P/d_0 = 10$)
Figures A-60 → A-65 Table A-12 Table A-27 (SNR_{AVG})	Two Row Injection with Uniform Blowing ($\theta_2 = 22.9^\circ$, $S/d_0 = P/d_0 = 10$)

Multiple Row Injection with Blowing Distribution
Simulating Plenum Supply

<u>Table or Figure</u>	<u>Condition</u>
Figures A-66 → A-72 Table A-13 Table A-28 (SNR_{AVG})	Five Row Injection with Plenum Blowing Simulation ($\theta_1 = 5^\circ$, $S/d_0 = P/d_0 = 5$)
Figures A-73 → A-79 Table A-14 Table A-29 (SNR_{AVG})	Three Row Injection with Plenum Blowing Simulation ($\theta_1 = 5^\circ$, $S/d_0 = P/d_0 = 10$)

<u>Table or Figure</u>	<u>Condition</u>
Figures A-80 → A-85 Table A-15 Table A-30 (SNR_{AVG})	Two Row Injection with Plenum Blowing Simulation ($\theta_2 = 22.9^\circ$, $S/d_0 = P/d_0 = 10$)

Influence of Turbulence Intensity

<u>Table or Figure</u>	<u>Condition</u>
Figures A-86 → A-92 Table A-16 Table A-31 (SNR_{AVG})	Influence of Turbulence Intensity on SNR with Plenum Blowing Simulation (Five Rows, $\theta_1 = 5^\circ$, $S/d_0 = P/d_0 = 5$)
Figures A-93 → A-99 Table A-16 Table A-31 (SNR_{AVG})	Influence of Turbulence Intensity on SNR with Uniform Blowing (Five Rows, $\theta_1 = 5^\circ$, $S/d_0 = P/d_0 = 5$)

Table A-2. Stanton Number Reduction for Single Row Injection,
 $\theta_1 = 50^\circ$, $S/d_0 = 5$

$M_1 =$		0.51	1.02	2.04	3.02	4.24	5.19	5.85	8.34	10.28
$(x/d_0)_1$	z/s									
1.5	.00	.17	.22	.00	-.51	-.93	-.95	-.88	-.89	-1.00
1.5	.33	.06	.10	.23	.29	.28	.23	.11	-.70	-1.21
1.5	.67	-.01	-.01	-.02	-.05	-.03	-.03	-.04	-.06	.09
1.5	1.33	.05	.07	.23	.28	.28	.26	.10	-.72	-1.28
3.5	.00	.05	.08	-.10	-.34	-.32	-.30	-.25	-.29	-.10
3.5	.33	.05	.10	.15	.16	-.04	-.40	-.58	-.82	-.77
3.5	.67	-.02	.03	.00	.00	.05	.07	.11	.05	-.28
3.5	1.33	.05	.12	.16	.17	-.07	-.38	-.59	-.85	-.83
6.5	.50	.00	.03	.04	.06	.06	-.05	-.15	-.50	-.46
6.5	.83	.01	.01	-.02	-.05	-.05	.00	.00	-.10	-.40
6.5	1.17	.06	.13	.08	-.08	-.32	-.42	-.40	-.32	-.15
6.5	1.83	.03	.00	-.03	-.05	-.08	-.02	-.03	-.11	-.38
8.5	.50	-.01	.02	.03	.01	-.04	-.16	-.26	-.47	-.36
8.5	.83	.00	.03	-.03	-.05	-.02	.00	-.01	-.08	-.32
8.5	1.17	.03	.07	.04	-.08	-.23	-.29	-.27	-.17	-.01
8.5	1.83	.01	.02	-.02	-.06	-.04	-.02	-.02	-.06	-.30
11.5	.00	.03	.01	.03	.00	-.09	-.04	-.04	-.21	-.23
11.5	.33	.00	.02	.17	.15	-.10	-.14	-.13	-.26	-.04
11.5	.67	.01	.06	.05	.01	.03	.00	-.01	-.27	-.33
11.5	1.33	.00	.04	.16	.12	-.13	-.16	-.16	-.28	-.07
16.5	.50	.02	.06	.08	.01	.00	-.02	-.06	-.18	-.08
16.5	.83	-.04	-.07	-.06	-.10	-.05	-.07	-.08	-.05	-.11
16.5	1.17	.01	-.02	-.02	-.10	-.10	-.11	-.07	-.05	.02
16.5	1.83	-.04	-.04	-.03	-.09	-.05	-.09	-.04	-.04	-.11
21.5	.00	.00	-.15	-.13	-.25	-.11	-.02	-.02	-.01	-.02
21.5	.33	.02	.04	.10	.08	-.07	-.09	.00	-.12	-.11
21.5	1.33	-.04	.04	.12	.09	-.11	-.07	-.04	-.10	-.14

Table A-3. Stanton Number Reduction for Single Row Injection,
 $\theta_1 = 50^\circ$, $S/d_0 = 10$

$M_1 =$		1.00	2.00	2.50	2.96	4.00	4.75	5.30	5.73	7.50	8.16	9.40	10.05
$(x/d_0)_1$	z/s												
1.5	.00	.57	-.06	-.51	-.81	-.83	-1.16	-1.13	-1.12	-.90	-.94	-.96	-.80
1.5	.17	.17	.39	.43	.51	.50	.37	.22	.28	-.14	-.30	-.48	-.80
1.5	.33	.00	.00	.01	.03	.05	.06	.08	.12	.05	.04	.02	.03
1.5	.67	.00	.00	-.01	.00	.00	.00	.00	.02	.02	.02	.00	.01
3.5	.00	.14	-.25	-.37	-.41	-.41	-.41	-.37	-.28	-.26	-.24	-.27	-.19
3.5	.17	.20	.29	.23	.26	.14	-.27	-.48	-.59	-.93	-.95	-1.01	-.91
3.5	.33	.00	.02	.02	.05	.11	.16	.19	.19	.10	.04	-.09	-.29
3.5	.67	-.01	.00	-.01	-.01	.02	.02	.01	.05	.04	.04	-.01	-.06
6.5	.25	.10	.10	.10	.14	.12	.00	-.14	-.25	-.55	-.71	-.71	-.68
6.5	.42	.00	-.01	.01	.05	.04	.10	.10	.17	.12	.07	.01	-.19
6.5	.58	.00	-.01	.00	.02	.01	.01	.01	.02	.06	.05	.04	.04
6.5	.92	.02	-.10	-.12	-.09	-.07	-.07	-.06	-.04	-.04	-.03	-.07	-.04
8.5	.25	.08	.09	.06	.09	.10	-.03	-.17	-.23	-.46	-.52	-.47	-.46
8.5	.42	.02	.01	.01	.05	.03	.08	.10	.14	.07	-.02	-.12	-.30
8.5	.58	.03	-.01	.00	.02	.02	.01	-.04	.06	.10	.12	.10	.17
8.5	.92	.00	-.06	-.09	-.06	-.04	-.04	-.04	-.01	-.03	-.01	-.05	-.02
11.5	.50	.05	.08	.07	.03	-.02	.01	.02	.04	-.02	.00	-.13	-.22
11.5	.67	.01	.01	-.02	.02	-.02	.01	-.01	.00	.07	.08	.03	.12
11.5	.83	.02	-.02	-.01	.00	.02	.01	.02	.01	.00	.00	-.04	.01
11.5	1.17	.08	.07	.03	.03	-.05	-.29	-.30	-.34	-.29	-.31	-.31	-.22
16.5	.75	-.16	-.16	-.33	-.22	.00	-.03	-.03	-.09	-.09	-.09	-.07	-.09
16.5	.92	.00	-.01	-.02	-.10	-.21	-.04	-.07	-.09	-.05	-.04	-.06	-.03
16.5	1.08	.00	.02	-.05	.06	-.07	-.09	-.21	-.02	-.06	-.02	-.06	-.02
16.5	1.42	.01	-.06	.00	.07	.01	.08	.05	.07	-.04	-.06	-.20	-.23
21.5	.00	-.02	.01	.00	-.14	-.01	-.02	-.04	-.05	-.04	-.08	-.02	-.09
21.5	.17	.00	-.02	.04	.05	-.03	-.08	-.17	-.25	-.01	-.17	-.18	-.19
21.5	.67	.04	.03	.01	-.21	-.04	.01	.00	-.05	-.02	-.07	-.05	-.03

Table A-4. Stanton Number Reduction for Single Row Injection,
 $\theta_2 = 22.9^\circ$, $S/d_0 = 5$

$M_2 =$		0.25	0.51	0.77	1.10	1.30	1.53	1.79	2.07	2.47
(x/r)	z/s									
1.5	.00	.49	.70	.56	-.20	-.53	-.97	-1.40	-1.71	-1.95
1.5	.33	.23	.48	.57	.46	.43	.38	.30	.22	.03
1.5	.67	-.01	.09	.07	.08	.09	.11	.11	.02	.08
1.5	1.33	.27	.51	.59	.44	.49	.38	.28	.19	.06
3.5	.00	.18	.12	-.14	-.71	-.93	-1.19	-1.25	-1.08	-.83
3.5	.33	.26	.36	.37	.37	.36	.27	.17	.03	.15
3.5	.67	.06	.05	.04	.04	.06	.07	.06	.13	.14
3.5	1.33	.25	.35	.36	.37	.35	.30	.19	.03	-.15
6.5	.50	.02	.05	.14	.20	.24	.24	.21	.08	-.24
6.5	.83	.01	.02	-.05	-.11	-.08	-.08	-.07	-.07	-.01
6.5	1.17	.16	.20	.10	-.02	-.05	-.28	-.58	-.85	-.99
6.5	1.83	.02	.04	-.05	-.12	-.09	-.08	-.08	-.10	-.02
8.5	.50	.06	.06	.11	.17	.23	.22	.19	.01	-.30
8.5	.83	.01	-.01	-.07	-.12	-.10	-.10	-.08	-.05	.00
8.5	1.17	.11	.18	.06	-.08	-.14	-.36	-.57	-.80	-.81
8.5	1.83	.00	-.02	-.06	-.11	-.13	-.10	-.07	-.03	-.02
11.5	.00	-.01	.10	.00	-.03	-.01	.00	-.01	-.02	-.01
11.5	.33	.10	.23	.19	.16	.10	-.04	-.20	-.45	-.71
11.5	.67	-.01	.01	.04	.06	.11	.14	.20	.17	.13
11.5	1.33	.08	.21	.20	.16	.11	-.04	-.24	-.46	-.68
16.5	.50	-.01	.01	.00	.11	.19	.11	.03	-.08	-.39
16.5	.83	-.03	.03	.02	-.07	-.01	.04	.03	.04	.03
16.5	1.17	.03	-.01	.03	-.07	-.05	-.11	-.19	-.25	-.32
16.5	1.83	-.01	.03	-.01	-.03	.01	.05	.03	.05	.02

Table A-5. Stanton Number Reduction for Single Row Injection,
 $\theta_2 = 22.9^\circ$, $S/d_0 = 10$

$M_2 =$		0.50	1.08	1.28	1.50	2.02	2.41
$(x/d_0)_2$	z/s						
1.5	.00	.76	.58	.22	.37	.50	-1.65
1.5	.17	.42	.74	.71	.67	.49	.47
1.5	.33	-.17	-.01	.01	.06	.13	.19
1.5	.67	-.07	-.01	-.02	-.01	.01	-.01
3.5	.00	.05	-.57	-.87	-1.27	-1.48	-1.35
3.5	.17	.43	.48	.22	.09	-.08	-.36
3.5	.33	-.02	.05	.08	.14	.23	.24
3.5	.67	.05	.06	-.01	.04	.06	.06
6.5	.25	.19	.24	.26	.28	.09	-.16
6.5	.42	.04	.09	.15	.17	.21	.23
6.5	.58	-.07	-.06	-.04	-.01	.02	.08
6.5	.92	-.02	-.24	-.23	-.23	-.18	-.17
8.5	.25	.12	.30	.31	.30	.09	-.20
8.5	.42	.06	.07	.08	.12	.18	.23
8.5	.58	.06	.06	.06	.07	.08	.11
8.5	.92	.01	-.15	-.17	-.17	-.15	-.12
11.5	.50	-.03	-.01	.01	-.06	-.05	-.06
11.5	.67	.02	-.02	.01	-.13	-.10	-.09
11.5	.83	.01	-.02	-.05	-.10	-.08	-.17
11.5	1.17	.24	.10	.07	-.11	-.51	-.76
16.5	.75	.01	.01	-.04	.01	-.01	.03
16.5	.92	-.03	-.05	.00	-.03	.00	-.02
16.5	1.08	.17	-.09	-.23	-.15	-.36	-.36
16.5	1.42	-.04	-.04	-.01	.18	.18	.20

Tabl. A-6. Stanton Number Reduction for Single Row Injection
 $\theta_3 = 40.8^\circ$, $S/d_0 = 5$

$M_3 =$		0.25	0.50	0.77	0.97	1.06	1.17	1.43	1.64
$(x/d_0)_3$	z/s								
1.5	.00	.74	.58	-.82	-1.67	-1.68	-1.70	-1.31	-1.18
1.5	.33	.43	.50	.22	.00	-.25	-.41	-.71	-.80
1.5	.67	-.01	-.02	.05	.21	.30	.35	.25	.09
1.5	1.33	.41	.49	.21	-.01	-.30	-.46	-.73	-.86
3.5	.00	.00	-.69	-1.08	-.80	-.58	-.40	-.05	-.01
3.5	.33	.31	.48	.05	-.23	-.33	-.56	-1.10	-1.43
3.5	.67	.03	.08	.33	.26	.15	-.04	-.39	-.54
3.5	1.33	.30	.47	.06	-.21	-.34	-.54	-1.10	-1.45
6.5	.50	.17	.32	.10	-.20	-.36	-.54	-.90	-1.07
6.5	.83	-.24	-.35	.01	.22	.21	.05	-.42	-.66
6.5	1.17	-.13	-.15	-.67	-1.21	-1.23	-1.20	-.89	-.84
6.5	1.83	-.26	-.38	.03	.21	.18	.01	-.42	-.64
8.5	.50	.13	.27	.02	-.23	-.43	-.60	-.83	-.88
8.5	.83	-.20	-.20	.07	.09	.08	-.03	-.37	-.44
8.5	1.17	-.15	-.26	-.83	-1.09	-.94	-.85	-.53	-.49
8.5	1.83	-.24	-.16	.05	.11	.11	.00	-.35	-.48
11.5	.00	.01	-.15	-.13	-.11	-.04	-.03	-.08	-.14
11.5	.33	-.10	-.18	-.00	-1.06	-1.09	-1.12	-1.08	-1.08
11.5	.67	.04	.20	.32	.23	.19	.11	-.08	-.17
11.5	1.33	-.10	-.18	-.56	-1.05	-1.08	-1.15	-1.11	-1.11

Table A-7. Stanton Number Reduction for Single Row Injection,
 $\theta_3 = 40.8^\circ$, $S/d_0 = 10$

$M_3 =$		0.50	0.75	0.95	1.04
$(x/d_0)_2$	z/s				
1.5	.00	.56	.43	-.07	-.31
1.5	.17	.79	.53	.52	.50
1.5	.33	.06	.12	.15	.15
1.5	.67	.02	.06	-.02	-.03
6.5	.25	.08	.08	-.10	-.03
6.5	.42	.05	.17	.13	.18
6.5	.58	.03	.12	.10	-.01
6.5	.92	-.01	.01	-.02	.00
11.5	.50	-.16	.01	.09	.06
11.5	.67	.06	.01	-.04	-.09
11.5	1.17	-.06	-.45	-.55	-.52
M_3		1.15	1.40	1.61	1.75
$(x/d_0)_3$	z/s				
1.5	.00	-.73	-1.51	-1.95	-2.50
1.5	.17	.58	.59	.54	.55
1.5	.33	.22	.36	.45	.53
1.5	.67	.00	.04	.03	.06
6.5	.25	-.04	-.07	-.10	-.15
6.5	.42	.11	.14	.25	.49
6.5	.58	-.01	-.04	-.01	.08
6.5	.92	-.23	-.13	-.10	-.44
11.5	.50	.08	.07	.07	.14
11.5	.67	-.02	-.03	.01	.09
11.5	1.17	-.01	-.95	-1.07	-1.18

Table A-8. Stanton Number Reduction for Single Row Injection,
 $\theta_4 = 58.7^\circ$, $S/d_0 = 5$

$M_4 =$		0.25	0.50	0.75	0.95	1.05	1.24	1.36	1.50
$(x/d_0)_4$	z/s								
1.5	.00	.41	.61	.27	-.10	-.67	-1.17	-1.57	-1.83
1.5	.33	.16	.58	.61	.44	.37	.17	.04	-.12
1.5	.67	.08	.13	.11	.07	.13	.27	.35	.39
1.5	1.33	.16	.56	.62	.47	.37	.18	.07	-.08
3.5	.00	-.03	-.10	-.55	-.90	-1.05	-.95	-.83	-.58
3.5	.33	.29	.53	.12	-.07	-.21	-.37	-.51	-.61
3.5	.67	.05	.13	.21	.31	.38	.18	.00	-.31
3.5	1.33	.31	.49	.11	-.05	-.16	-.36	-.45	-.58
6.5	.50	.29	.19	.14	.17	.03	-.12	-.25	-.42
6.5	.83	-.49	-.25	-.10	.09	.21	.28	.13	-.10
6.5	1.17	-.41	-.40	-.37	-.40	-.61	-.89	-1.07	-1.05
6.5	1.83	-.47	-.25	-.11	.09	.23	.30	.11	-.12
8.5	.50	.23	.23	.19	.20	-.02	-.05	-.11	-.28
8.5	.83	-.32	-.11	.06	.16	.22	.20	.08	-.06
8.5	1.17	-.49	-.51	-.52	-.70	-.87	-.98	-.97	-.91
8.5	1.83	-.33	-.10	.07	.17	.25	.21	.12	-.02

Table A-9. Stanton Number Reduction for Single Row
Injection , $\theta_4 = 58.7^\circ$, $S/d_0 = 10$

$M_4 =$		0.50	0.75	1.00	1.25	1.36	1.50
$(x/d_0)_4$	z/s						
1.5	.00	.45	.75	-1.75	-2.30	-2.34	-2.30
1.5	.17	.49	.52	.39	-.12	-.25	-.76
1.5	.33	.30	.27	-.35	-.64	-.82	-.89
1.5	.67	.01	.03	.06	.04	.10	.13
6.5	.25	-.80	-.43	-.30	-.90	-1.15	-1.75
6.5	.42	-.04	.89	.83	-.24	-.45	-.14
6.5	.58	.08	.22	.29	.00	.01	-.26
6.5	.92	.02	.13	.16	.20	.18	.17

Table A-10. Stanton Number Reduction for Multiple Row
Injection with Uniform Blowing,
Five Rows , $\theta_1 = 5^\circ$, $S/d_0 = P/d_0 = 5$

$M_{1+5} =$		0.25	0.50	0.75	1.01	1.26	1.51	1.76	2.01
$(x/d_0)_1$	z/s								
1.5	.00	.15	.15	.17	.11	.03	-.09	-.21	-.36
1.5	.33	.07	.08	.12	.16	.15	.17	.16	.17
1.5	.67	.01	.01	.04	.01	.00	.00	-.02	.00
1.5	1.33	.06	.08	.13	.13	.14	.15	.16	.15
3.5	.00	.05	.05	.07	.05	.02	-.05	-.10	-.12
3.5	.33	.07	.10	.14	.14	.11	.17	.18	.17
3.5	.67	.01	.05	.07	.09	.06	.06	.09	.07
3.5	1.33	.07	.07	.12	.14	.10	.15	.22	.18
$(x/d_0)_2$	z/s								
1.5	.00	.58	.77	.62	.16	-.37	-.77	-1.11	-1.28
1.5	.33	.17	.43	.59	.65	.61	.57	.51	.46
1.5	.67	-.01	-.02	.06	.10	.05	.04	.04	.02
1.5	1.33	.17	.44	.59	.65	.57	.53	.50	.42
3.5	.00	.32	.30	.12	-.17	-.45	-.61	-.67	-.64
3.5	.33	.17	.34	.47	.46	.42	.37	.30	.23
3.5	.67	.03	.08	.14	.16	.20	.21	.26	.26
3.5	1.33	.20	.35	.45	.43	.38	.33	.28	.20
$(x/d_0)_3$	z/s								
1.5	.00	.47	-.38	-1.16	-.81	-.44	-.28	-.38	-.51
1.5	.33	.58	.41	.43	-.02	-.30	-.31	-.30	-.31
1.5	.67	.27	.16	.18	-.05	-.30	-.42	-.38	-.38
1.5	1.33	.60	.40	.39	-.01	-.31	-.36	-.34	-.36
$(x/d_0)_4$	z/s								
1.5	.00	.58	.53	-.52	-.60	-.41	-.21	-.17	-.19
1.5	.33	.52	.47	.45	.26	-.34	-.98	-1.57	-1.72
1.5	.67	.00	-.01	-.32	-.19	-.14	-.17	-.27	-.43
1.5	1.33	.51	.47	.48	.28	-.32	-1.01	-1.61	-1.74
$(x/d_0)_5$	z/s								
1.5	.00	.36	.40	-.07	-.26	-.11	-.13	-.22	-.28
1.5	.33	.27	.44	.39	.14	-.44	-1.11	-1.78	-2.15
1.5	1.33	.24	.46	.40	.12	-.44	-1.20	-1.74	-1.99

Table A-11. Stanton Number Reduction for Multiple Row Injection with Uniform Blowing,
Three Rows , $\theta_1 = 50^\circ$, $S/d_0 = P/d_0 = 10$

$M_{1,3,5}$		0.25	0.50	0.75	1.00	1.25	1.50	1.75	2.00	2.25	2.50
$(x/d_0)_1$	z/s										
1.5	.00	.17	.29	.43	.58	.57	.45	.36	.15	.06	-.05
1.5	.17	.06	.09	.14	.12	.20	.25	.23	.25	.30	.31
1.5	.33	.00	.00	.00	-.01	.00	.02	.02	.01	.01	.02
1.5	.67	.00	.00	-.02	.00	.01	-.01	.00	.00	.02	.00
3.5	.00	.07	.11	.16	.13	.07	.05	-.05	-.03	-.17	-.21
3.5	.17	.06	.08	.12	.14	.22	.24	.19	.20	.26	.24
3.5	.33	.02	.03	.01	-.03	-.02	.02	.03	-.01	-.01	.02
3.5	.67	.00	.03	-.02	.00	.03	-.02	.00	-.02	.03	.01
6.5	.25	.05	.05	.11	.09	.09	.10	.10	.10	.13	.09
6.5	.42	.00	.01	.01	.02	.04	.00	.01	.02	.03	.00
6.5	.58	.01	-.02	-.03	.00	.00	.03	.03	.01	.02	.01
6.5	.92	.00	.00	.01	-.02	-.01	-.07	-.12	-.08	-.10	-.13
8.5	.25	.05	.05	.06	.06	.06	.10	.09	.05	.07	.05
8.5	.42	.02	.04	.03	.05	.06	.05	.12	.09	.08	.05
8.5	.58	.02	.03	.05	.06	.08	.08	.11	.09	.08	.08
8.5	.92	.03	.03	.01	.01	.00	-.04	-.06	-.03	-.02	-.04
$(x/d_0)_3$	z/s										
1.5	.00	.61	.74	.48	.02	-.58	-1.14	-1.86	-2.37	-2.90	-3.04
1.5	.17	.46	.91	.73	.63	.63	.60	.56	.41	.00	-.28
1.5	.33	.00	.01	.06	.17	.29	.43	.57	.43	.14	-.07
1.5	.67	.00	.05	.04	.07	.09	.11	.16	.20	.15	.12
6.5	.25	-.01	.14	.11	-.05	-.06	-.06	-.02	-.29	-.45	-.63
6.5	.42	.02	.02	.27	.24	.23	.25	.33	.31	.03	-.30
6.5	.58	.02	.08	.09	.09	.12	.13	.20	.17	.18	.20
6.5	.92	.04	.02	-.13	-.07	-.09	-.05	-.11	-.10	-.10	-.13
$(x/d_0)_5$	z/s										
1.5	.00	.74	.72	.39	-2.12	-1.53	-.89	-.52	-.58	-.68	-.60
1.5	.17	.75	.24	-.21	-1.01	-1.69	-1.92	-1.98	-2.02	-1.47	-1.85
1.5	.67	.07	-.21	-.31	-.56	-.72	-1.14	-.79	-.53	-.68	-.65

ORIGINAL PAGE IS
OF POOR QUALITY

Table A-12. Stanton Number Reduction for Multiple Row Injection with Uniform Blowing,
Two Rows, $\theta_2 = 22.90^\circ$, $S/d_0 = P/d_0 = 10$

$M_{2,4} =$		0.25	0.50	0.75	1.00	1.25	1.50	1.75	2.00
$(x/d_0)_2$	z/s								
1.5	.00	.51	.79	.75	.41	.18	.43	.48	.11
1.5	.17	.05	.24	.55	.64	.62	.55	.46	.48
1.5	.33	-.02	-.01	.02	.04	.05	.09	.13	.21
1.5	.67	-.02	-.02	.00	.01	.00	.01	.01	.02
3.5	.00	.27	.15	-.16	-.51	-.89	-1.24	-1.37	-1.39
3.5	.17	.09	.36	.55	.49	.33	.10	.01	-.06
3.5	.33	.01	-.03	.01	.04	.02	.06	.11	.23
3.5	.67	.03	.07	.01	.00	-.01	.02	.01	.01
6.5	.25	-.04	.14	.32	.33	.27	.20	.08	.16
6.5	.42	-.14	-.03	.02	.00	.02	.05	-.02	-.02
6.5	.58	.01	.07	.02	.00	.03	-.05	.05	.06
6.5	.92	.11	.01	-.18	-.20	-.20	-.21	-.21	-.18
8.5	.25	.01	.12	.24	.29	.27	.23	.11	.02
8.5	.42	.01	.06	.06	.06	.09	.12	.09	.06
8.5	.58	.07	.12	.17	.19	.20	.19	.19	.26
8.5	.92	.02	.00	-.06	-.09	-.09	-.08	-.07	-.03
$(x/d_0)_4$	z/s								
1.5	.00	.23	.16	-1.00	-2.08	-2.46	-2.03	-1.38	-.89
1.5	.17	.55	.54	.56	.18	-.51	-.67	-.80	-.90
1.5	.33	.20	.39	.12	-.37	-.66	-.92	-1.08	-1.08
1.5	.67	.16	.24	.18	.12	-.01	-.19	-.44	-.49
6.5	.25	-.89	-.91	.88	-.31	-.90	-2.42	-2.40	-2.33
6.5	.42	-.12	.93	.87	-.66	-.99	-1.15	-1.04	-.63
6.5	.58	.10	.02	.11	.19	-.02	-.45	-.67	-.73
6.5	.92	-.33	-.07	.22	.30	.43	.48	.38	.26

Table A-13. Stanton Number Reduction for Multiple Row Injection with
Blowing Distribution Simulating Plenum Supply,
Five Rows, $\theta_1 = 5^\circ$, $S/d_0 = P/d_0 = 5$

$Ma_{\infty}/(P_{T,c}/P_{T,w})$		0.2/1.010	0.2/1.020	0.2/1.030	0.1/1.010	0.1/1.020	0.1/1.030
	$M_1 = 2.96$		4.15	5.08	5.73	8.16	10.05
	$M_2 = 1.08$		1.27	1.44	1.54	2.02	2.42
	$M_3 = 0.95$		1.04	1.14	1.17	1.40	1.61
	$M_4 = 0.92$		0.98	1.04	1.05	1.24	1.36
	$M_5 = 0.92$		0.96	1.01	1.01	1.16	1.27
$(x/d_0)_1$	z/s						
1.5	.00	-.56	-.49	-.54	-.54	-.44	-.42
1.5	.33	.18	.01	-.26	-.53	-.76	-.73
1.5	.67	.05	.06	.07	.10	.21	.16
1.5	1.33	.16	.01	-.29	-.58	-.79	-.71
3.5	.00	-.12	-.10	-.37	-.65	-.92	-.91
3.5	.33	-.06	-.30	-.47	-.46	-.21	-.10
3.5	.67	.15	.15	.13	.14	-.11	-.13
3.5	1.33	-.02	-.26	-.42	-.45	-.22	-.10
$(x/d_0)_2$	z/s						
1.5	.00	-.20	-.75	-1.07	-1.08	-.93	-.52
1.5	.33	.74	.74	.72	.72	.56	.14
1.5	.67	-.16	-.10	-.13	-.12	.00	-.01
1.5	1.33	.71	.71	.68	.69	.56	.15
3.5	.00	-.34	-.53	-.60	-.55	-.27	-.07
3.5	.33	.49	.48	.42	.39	.02	-.29
3.5	.67	.05	.06	.17	.21	.36	.30
3.5	1.33	.50	.50	.40	.39	.02	-.30
$(x/d_0)_3$	z/s						
1.5	.00	-.73	-.60	-.60	-.62	-.55	-.29
1.5	.33	.08	-.01	-.08	-.08	-.30	-.67
1.5	.67	-.30	-.50	-.59	-.59	-.44	-.37
1.5	1.33	.03	.01	-.37	-.08	-.30	-.84
$(x/d_0)_4$	z/s						
1.5	.00	.69	-.74	-.79	-.82	-.77	-.52
1.5	.33	.29	.29	.27	.29	-.03	-.27
1.5	.67	-.15	-.12	-.17	-.15	-.04	.06
1.5	1.33	.33	.29	.23	.27	-.01	-.27
$(x/d_0)_5$	z/s						
1.5	.00	-.24	-.23	-.22	-.25	-.23	-.16
1.5	.33	.37	.29	.19	.18	-.06	-.45
1.5	1.33	.35	.30	.17	.19	-.05	-.48

ORIGINAL PAGE IS
OF POOR QUALITY

Table A-14. Stanton Number Reduction for Multiple Row Injection with
Blowing Distribution Simulating Plenum Supply,
Three Rows, $\theta_1 = 5^\circ$, $S/d_0 = P/d_0 = 10$

$Ma_{\infty,0}/(P_{T,0}/P_{T,\infty})$		0.2/1.010	0.2/1.020	0.2/1.030	0.1/1.010	0.1/1.020	0.1/1.030
		$M_1 = 2.96$	4.15	5.08	5.73	8.16	10.05
		$M_2 = 0.95$	1.04	1.14	1.17	1.40	1.61
$(x/d_0)_1$	z/s	$M_3 = 0.92$	0.96	1.01	1.01	1.16	1.27
1.5	.00	-.70	-1.06	-1.15	-1.05	-.85	-.97
1.5	.17	.45	.50	.33	.16	-.36	-.40
1.5	.33	.33	.08	.10	.13	-.08	-.02
1.5	.67	-.01	.00	-.01	-.02	-.02	.00
3.5	.00	-.39	-.41	-.36	-.34	-.25	-.32
3.5	.17	.18	-.09	-.47	-.67	-.99	-1.09
3.5	.33	.05	.13	.22	.24	.01	-.06
3.5	.67	-.03	.02	.02	.02	.02	-.02
6.5	.25	.09	.03	-.23	-.27	-.66	-.78
6.5	.42	.02	.09	.12	.15	.05	.07
6.5	.58	.03	.04	.01	.03	.08	.05
6.5	.92	-.10	-.07	-.06	-.04	-.03	-.04
8.5	.25	.08	.01	-.14	-.27	-.53	-.61
8.5	.42	.07	.11	.14	.17	.03	.01
8.5	.58	.10	.14	.13	.14	.22	.22
8.5	.92	-.04	-.03	-.02	.00	-.01	.00
$(x/d_0)_2$	z/s						
1.5	.00	.23	.07	-.28	-.27	-.47	-.76
1.5	.17	.62	.60	.63	.63	.64	.67
1.5	.33	.06	.15	.20	.25	.40	.46
1.5	.67	.05	-.11	-.24	-.28	-.25	-.24
6.5	.25	-.10	-.11	-.13	-.06	-.08	-.14
6.5	.42	.12	.16	.27	.23	.22	.27
6.5	.58	.07	-.01	-.31	-.06	.05	-.02
6.5	.92	.00	.08	.11	.07	-.25	-.17
$(x/d_0)_3$	z/s						
1.5	.00	-1.54	-1.47	-1.36	-1.48	-.98	-.84
1.5	.17	-.52	-.34	-1.05	-.36	-1.50	-1.77
1.5	.67	-.67	-.73	-.86	-.99	-.77	-.96

Table A-15. Stanton Number Reduction for Multiple Row Injection with
Blowing Distribution Simulating Plenum Supply,
Two Rows, $\theta = 22.9^\circ$, $S/d_o = P/d_o = 10$

$Ma_{\infty}/(P_{T,C}/P_{T,\infty})$		0.2/1.010	0.2/1.020	0.2/1.030	0.1/1.010	0.1/1.020	0.1/1.030
$(x/d_o)_2$	z/s	$M_2 = 1.08$	1.27	1.44	1.54	2.02	2.42
	z/s	$M_2 = 0.92$	0.98	1.04	1.05	1.24	1.36
1.5	.00	.67	.19	-.19	-.12	-1.03	-1.78
1.5	.17	.67	.62	.61	.56	.72	.41
1.5	.33	.04	.04	.07	.09	.13	.25
1.5	.67	-.01	-.03	.00	.01	.02	.01
3.5	.00	-.49	-.84	-1.04	-1.15	-1.36	-1.24
3.5	.17	.40	.33	.19	.15	-.07	-.40
3.5	.33	.05	.09	.10	.13	.20	.25
3.5	.67	.02	-.01	.03	-.05	.03	-.04
6.5	.25	.32	.35	.41	.36	.20	-.10
6.5	.42	.04	.08	.10	.10	.13	.14
6.5	.58	-.01	.02	.02	.03	.06	.15
6.5	.92	-.18	-.17	-.17	-.16	-.14	-.18
8.5	.25	.29	.32	.32	.30	.06	-.26
8.5	.42	.08	.09	.13	.12	.15	.21
8.5	.58	.16	.18	.18	.19	.20	.27
8.5	.92	-.10	-.11	-.09	-.09	-.08	-.07
$(x/d_o)_4$							
1.5	.00	-1.77	-1.96	-1.57	-2.04	-2.00	-1.53
1.5	.17	.41	.25	.10	.10	.34	-.59
1.5	.33	-.25	-.33	-.42	-.40	-.62	-.78
1.5	.67	.15	.04	-.03	-.11	-.41	-.84
6.5	.25	.63	.78	-1.21	-1.25	-1.31	-2.21
6.5	.42	-.52	-.69	-.74	-.78	-.31	-.31
6.5	.58	.12	.10	-.01	.03	-.09	-.26
6.5	.92	.32	.42	.41	.47	.43	.34

Table A-16. Influence of Turbulence Intensity on Stanton Number Reduction

SCREEN	None	Fine	Coarse	None	Fine	Coarse
$S/d_0 = P/d_0 = 5$ 5 Rows with the First Row at z_1	Plenum Blowing $Ma_{\infty,0}/(P_{T,c}/P_{T,\infty})$	Plenum Blowing	Plenum Blowing	Uniform Blowing $M_{1,2,3,4,5}$	Uniform Blowing	Uniform Blowing
$(x/d_0)_1$ z/s	$= 0.2/1.010$			$= 0.75$		
1.5 .00	-.56	-.53	-.25	.17	.18	.19
1.5 .33	.18	.20	.27	.12	.09	.08
1.5 .67	.05	.06	.15	.04	.02	.00
1.5 1.33	.16	.24	.29	.11	.11	.05
3.5 .00	-.12	-.14	-.13	.07	.10	.10
3.5 .33	-.06	-.11	-.08	.14	.11	.09
3.5 .67	.15	.17	.19	.07	.07	.08
3.5 1.33	-.02	-.09	-.07	.12	.13	.09
$(x/d_0)_2$ z/s						
1.5 .00	-.20	-.27	-.17	.62	.75	.72
1.5 .33	.74	.69	.65	.59	.62	.50
1.5 .67	-.16	-.19	-.09	.06	-.01	-.12
1.5 1.33	.71	.66	.66	.57	.60	.52
3.5 .00	-.34	-.32	-.24	.12	.19	.16
3.5 .33	.49	.52	.48	.47	.43	.32
3.5 .67	.05	.07	.08	.14	.16	-.01
3.5 1.33	.50	.48	.49	.45	.38	.31
$(x/d_0)_3$ z/s						
1.5 .00	-.73	-.74	-.81	-1.16	-1.16	-1.38
1.5 .33	.08	.13	.14	.43	.44	.46
1.5 .67	-.30	-.45	-.04	.18	.19	.21
1.5 1.33	.08	.11	.15	.39	.40	.42
$(x/d_0)_4$ z/s						
1.5 .00	-.69	-.74	-.29	-.52	-.35	-.27
1.5 .33	.33	.36	.39	.45	.40	.45
1.5 .67	-.15	-.07	-.05	-.32	-.26	-.22
1.5 1.33	.33	.39	.42	.48	.47	.40
$(x/d_0)_5$ z/s						
1.5 .00	-.24	-.28	-.05	-.07	.01	.07
1.5 .33	.37	.45	.46	.39	.43	.39
1.5 1.33	.36	.43	.43	.40	.38	.37

Table A-17. Spanwise Averaged Stantri. Number Reduction,
Single Row Injection, $\sigma_1 = 50$, $S/d_0 = 5$

$M_1 =$	0.51	1.02	2.04	3.02	4.24	5.19	5.85	8.34	10.28
	(x/d_0)								
$(x/d_0)_1$	1.5	.07	.10	.07	-.09	-.22	-.25	-.27	-.71
	3.5	.03	.07	.02	-.06	-.10	-.21	-.24	-.38
	6.5	.02	.05	.03	-.03	-.10	-.15	-.17	-.32
	8.5	.01	.04	.02	-.04	-.10	-.14	-.17	-.23
	11.5	.01	.03	.08	.05	-.05	-.06	-.25	-.20
	16.5	.00	-.01	.00	-.06	-.05	-.07	-.09	-.06
	21.5	.01	-.05	-.01	-.08	-.09	-.05	-.06	-.06

Table A-18. Spanwise Averaged Stanton Number Reduction,
Single Row Injection, $\theta_1 = 50^\circ$, $S/d_0 = 10$

$M_1 =$		1.00	2.00	2.50	2.96	4.00	4.75	5.30	5.73	7.50	8.16	9.40	10.05
(x/d_o)													
$(x/d_o)_1$.17	.05	-.06	-.11	-.11	-.21	-.23	-.20	-.23	-.27	-.31	-.32
3.5		.06	-.01	-.05	-.05	-.05	-.10	-.12	-.10	-.18	-.19	-.26	-.29
6.6		.04	-.01	-.02	-.01	-.02	-.06	-.09	-.09	-.14	-.17	-.20	-.21
8.5		.04	.00	-.02	-.01	-.01	-.06	-.09	-.06	-.10	-.12	-.14	-.14
11.5		.04	.03	.01	-.02	-.05	-.09	-.09	-.09	-.08	-.08	-.13	-.10
16.5		-.04	-.06	-.10	-.03	-.05	-.01	-.05	-.02	-.06	-.05	-.11	-.11
21.5		.01	.01	.02	-.11	-.03	-.03	-.07	-.12	-.02	-.11	-.09	-.10

Table A-19. Spanwise Averaged Stanton Number Reduction, Single Row Injection,
 $\theta_2 = 22.9^\circ$, $S/d_0 = 5$

$M_2 =$		0.25	0.51	0.77	1.10	1.30	1.53	1.79	2.07	2.47
(x/d_0)										
$(x/d_0)/2$	1.5	.24	.42	.40	.11	.00	-.16	-.32	-.48	-.61
	3.5	.17	.18	.09	-.10	-.17	-.28	-.34	-.30	-.28
	6.5	.06	.09	.04	-.02	-.02	-.08	-.17	-.27	-.39
	8.5	.05	.08	.03	-.02	-.02	-.08	-.14	-.24	-.33
	11.5	.03	.11	.08	.06	.07	.03	.00	-.10	-.20
	16.5	.00	.01	.02	-.01	.04	.01	-.04	-.10	-.23

Table A-20. Spanwise Averaged Stanton Number Reduction, Single Row Injection,
 $\theta_2 = 22.9^\circ$, $S/d_o = 10$

$M_2 =$		0.50	1.08	1.28	1.50	2.02	2.41
(x/d_o)							
$(x/d_o)^{1/2}$	1.5	.19	.26	.17	.21	.24	-.29
	3.5	.10	-.03	-.16	-.25	-.31	-.32
	6.5	.06	-.03	-.04	-.06	-.11	-.16
	8.5	.08	.03	.00	-.02	-.09	-.14
	11.5	.06	.00	-.04	-.13	-.25	-.32
	16.5	.03	-.04	-.07	.02	-.03	-.02

Table A-21. Spanwise Averaged Stanton Number Reduction, Single Row Injection,
 $\theta_3 = 40.8^\circ$, $S/d_0 = 5$

$M_3 =$		0.25	0.51	0.77	0.97	1.06	1.17	1.43	1.64
(x/d_0)									
$(x/d_0)_3$	1.5	.38	.35	-.18	-.48	-.54	-.58	-.59	-.63
	3.5	.11	-.04	-.23	-.25	-.25	-.33	-.52	-.66
	6.5	-.04	-.07	-.19	-.36	-.41	-.49	-.63	-.74
	8.5	-.04	-.06	-.20	-.36	-.39	-.43	-.51	-.54
	11.5	-.02	-.04	-.14	-.31	-.31	-.35	-.41	-.46

Table A-22. Spanwise Averaged Stanton Number Reduction, Single Row Injection,
 $\theta_3 = 40.8^\circ$, $S/d_0 = 10$

$M_3 =$		0.50	0.75	0.95	1.04	1.15	1.40	1.61	1.75
(x/d_0)									
$(x/d_0)_3$	1.5	.29	.25	.10	.03	-.03	-.18	-.28	-.38
	6.5	.03	.08	.01	.02	-.07	-.05	-.02	-.08
	11.5	-.04	-.18	-.22	-.23	-.24	-.39	-.42	-.42

Table A-23. Spanwise Averaged Stanton Number Reduction, Single Row Injection,
 $\theta_4 = 58.7^\circ$, $S/d_o = 5$

$M_4 =$		0.25	0.50	0.75	0.95	1.05	1.24	1.36	1.50
(x/d_o)									
$(x/d_o)_4$	1.5	.22	.44	.33	.14	-.05	-.24	-.39	-.51
	3.5	.10	.19	-.07	-.22	-.29	-.38	-.44	-.50
	6.5	-.21	-.16	-.11	-.05	-.12	-.24	-.40	-.52
	8.5	-.20	-.13	-.09	-.11	-.22	-.28	-.33	-.42

Table A-24. Spanwise Averaged Stanton Number Reduction Single Row Injection,
 $\theta_4 = 58.7^\circ$, $S/d_0 = 10$

$M_4 =$		0.50	0.75	1.00	1.25	1.36	1.50
(x/d_0)							
$(x/d_0)_4$ ↓	1.5	.27	.35	-.44	-.74	-.80	-.88
	6.5	-.13	.14	.19	-.20	-.30	-.47

Table A-25. Spanwise Averaged Stanton Number Reduction
Multiple Row Injection with Uniform Blowing,
Five Rows, $\theta_1 = 50^\circ$, $S/d_0 = P/d_0 = 5$

$M_{1,2,3,4,5} =$		0.25	0.50	0.75	1.00	1.26	1.51	1.76	2.01
(x/d_0)									
$(x/d_0)_1$ ↓	1.5	.08	.08	.11	.09	.06	.03	-.02	-.06
	3.5	.04	.07	.09	.09	.06	.06	.06	.04
$(x/d_0)_2$ ↓	1.5	.24	.39	.42	.30	.10	-.05	-.18	-.26
	3.5	.17	.24	.24	.15	.06	-.01	-.03	-.05
$(x/d_0)_3$	1.5	.44	.07	-.18	-.29	-.35	-.34	-.35	-.40
	1.5	.37	.33	-.13	-.17	-.30	-.45	-.67	-.78
$(x/d_0)_4$	1.5	.31	.42	.16	-.06	-.27	-.62	-1.00	-1.21
	1.5								

Table A-26. Spanwise Averaged Stanton Number Reduction
Multiple Row Injection with Uniform Blowing,
Three Rows, $\theta_1 = 50^\circ$, $S/d_0 = P/d_0 = 10$

$M_{1,3,5} =$	(x/d_0)	0.25	0.50	0.75	1.00	1.25	1.50	1.75	2.00	2.25	2.50
$(x/d_0)_1$ ↓	1.5	.05	.09	.12	.16	.18	.16	.13	.08	.07	.04
	3.5	.03	.06	.06	.05	.06	.05	.03	.02	.01	.00
	6.5	.01	.02	.03	.03	.04	.03	.01	.02	.01	-.01
	8.5	.02	.04	.04	.05	.05	.05	.05	.05	.05	.03
$(x/d_0)_3$ ↓	1.5	.23	.35	.27	.17	.06	-.04	-.18	-.35	-.64	-.78
	6.5	.02	.07	.05	.03	.02	.04	.07	-.02	-.10	-.20
$(x/d_0)_5$	1.5	.36	.17	-.10	-1.10	-1.25	-1.34	-1.12	-1.04	-.94	-1.04

Table A-27. Spanwise Averaged Stanton Number Reduction
Multiple Row Injection with Uniform Blowing,
Two Rows, $\theta_2 = 22.9^\circ$, $S/d_0 = P/d_0 = 10$

$M_{2,4} =$	(x/d_0)	0.25	0.50	0.75	1.00	1.25	1.50	1.75	2.00
$(x/d_0)_2$ ↓	1.5	.12	.23	.28	.22	.16	.22	.23	.15
	3.5	.09	.11	.06	-.04	-.17	-.27	-.31	-.30
	6.5	.04	.08	.04	.01	-.02	-.08	-.11	-.11
	8.5	.06	.09	.10	.08	.06	.04	.00	.01
$(x/d_0)_4$ ↓	1.5	.25	.31	-.07	-.54	-.87	-.91	-.89	-.81
	6.5	-.14	-.07	.08	-.04	-.25	-.75	-.81	-.78

Table A-28. Spanwise Averaged Stanton Number Reduction Multiple Row Injection with Blowing
 Distribution Simulating Plenum Supply, Five Rows, $\theta_1 = 5^\circ$, $S/d_0 = P/d_0 = 5$

$Ma_{\infty,0}/(P_{T,c}/P_{T,\infty})$	0.2/1.010	0.2/1.020	0.2/1.030	0.1/1.010	0.1/1.020	0.1/1.030
(x/d_0)	$M_1 = 2.96$	4.15	5.08	5.73	8.16	10.05
	$M_2 = 1.08$	1.27	1.44	1.54	2.02	2.42
	$M_3 = 0.95$	1.04	1.14	1.17	1.40	1.61
	$M_4 = 0.92$	0.98	1.04	1.05	1.24	1.36
	$M_5 = 0.92$	0.96	1.01	1.01	1.16	1.27
$(x/d_0)_1$	1.5	-.11	-.14	-.32	-.33	-.33
\downarrow	3.5	-.01	-.08	-.12	-.10	-.07
$(x/d_0)_2$	1.5	.13	-.06	-.16	-.12	-.13
\downarrow	3.5	.07	.01	.02	.04	-.02
$(x/d_0)_3$	1.5	-.31	-.37	-.43	-.43	-.54
$(x/d_0)_4$	1.5	-.17	-.19	-.23	-.28	-.21
$(x/d_0)_5$	1.5	.07	.03	-.03	-.14	-.30

Table A-29. Spanwise Averaged Stanton Number Reduction Multiple Row Injection with Blowing
Distribution Simulating Plenum Supply, Three Rows, $\theta_1 = 50^\circ$, $S/d_0 = P/d_0 = 10$

$Ma_{\infty,0}/(P_{T,c}/P_{T,\infty})$	0.2/1.010	0.2/1.020	0.2/1.030	0.1/1.010	0.1/1.020	0.1/1.030
(x/d_0)	$M_1 = 2.96$	4.15	5.08	5.73	8.16	10.05
	$M_3 = 0.95$	1.04	1.14	1.17	1.40	1.61
	$M_5 = 0.92$	0.96	1.01	1.01	1.16	1.27
$(x/d_0)_1$	1.5	-.10	-.21	-.21	-.26	-.30
$(x/d_0)_2$	3.5	-.07	-.11	-.13	-.22	-.28
$(x/d_0)_3$	6.5	-.01	-.02	-.08	-.14	-.18
$(x/d_0)_4$	8.5	.03	.02	-.04	-.06	-.08
$(x/d_0)_5$	1.5	.19	.12	.01	.00	-.04
$(x/d_0)_6$	6.5	.01	.02	.03	-.05	-.04
$(x/d_0)_7$	1.5	-.84	-.99	-1.10	-1.07	-1.20

Table A-30. Spanwise Averaged Stanton Number Reduction Multiple Row Injection with Blowing
 Distribution Simulating Plenum Supply, Two Rows, $\theta_2 = 22.9^\circ$, $S/d_0 = P/d_0 = 10$

$Ma_{\infty,0}/(P_{T,c}/P_{T,\infty})$	0.2/1.010	0.2/1.020	0.2/1.030	0.1/1.010	0.1/1.020	0.1/1.030
(x/d_0)	$M_2 = 1.08$ $M_4 = 0.92$					
$(x/d_0)/2$						
1.5	.28	.15	.07	.09	-.10	-.31
3.5	-.04	-.14	-.19	-.25	-.29	-.33
6.5	.01	.01	.01	-.01	-.04	-.11
8.5	.08	.07	.07	.05	-.01	-.06
$(x/d_0)/4$						
1.5	-.39	-.52	-.59	-.63	-.85	-.96
6.5	.21	.25	-.29	-.28	-.24	-.55

Table A-31. The Influence of Turbulence Intensity
on Spanwise Averaged Stanton Number Reduction

SCREEN	None	Fine	Coarse	None	Fine	Coarse
5 Rows with the First Row at θ_1	Plenum Blowing	Plenum Blowing	Plenum Blowing	Uniform Blowing	Uniform Blowing	Uniform Blowing
(x/d_o)	$Ma_{\infty,0}/(P_{T,c}/P_{T,\infty})$ $= 0.2/1.010$			$M_1, 2, 3, 4, 5$ $= 0.75$		
$(x/d_o)_1$	- .11	- .09	.06	.11	.10	.09
$(x/d_o)_2$	- .01	- .03	- .01	.09	.09	.09
$(x/d_o)_3$.13	.08	.13	.42	.45	.36
$(x/d_o)_4$.07	.09	.11	.24	.26	.16
$(x/d_o)_5$	- .31	- .35	- .23	- .18	- .17	- .23
$(x/d_o)_6$	- .17	- .15	.02	- .13	- .07	- .01
$(x/d_o)_7$.07	.09	.21	.16	.22	.23

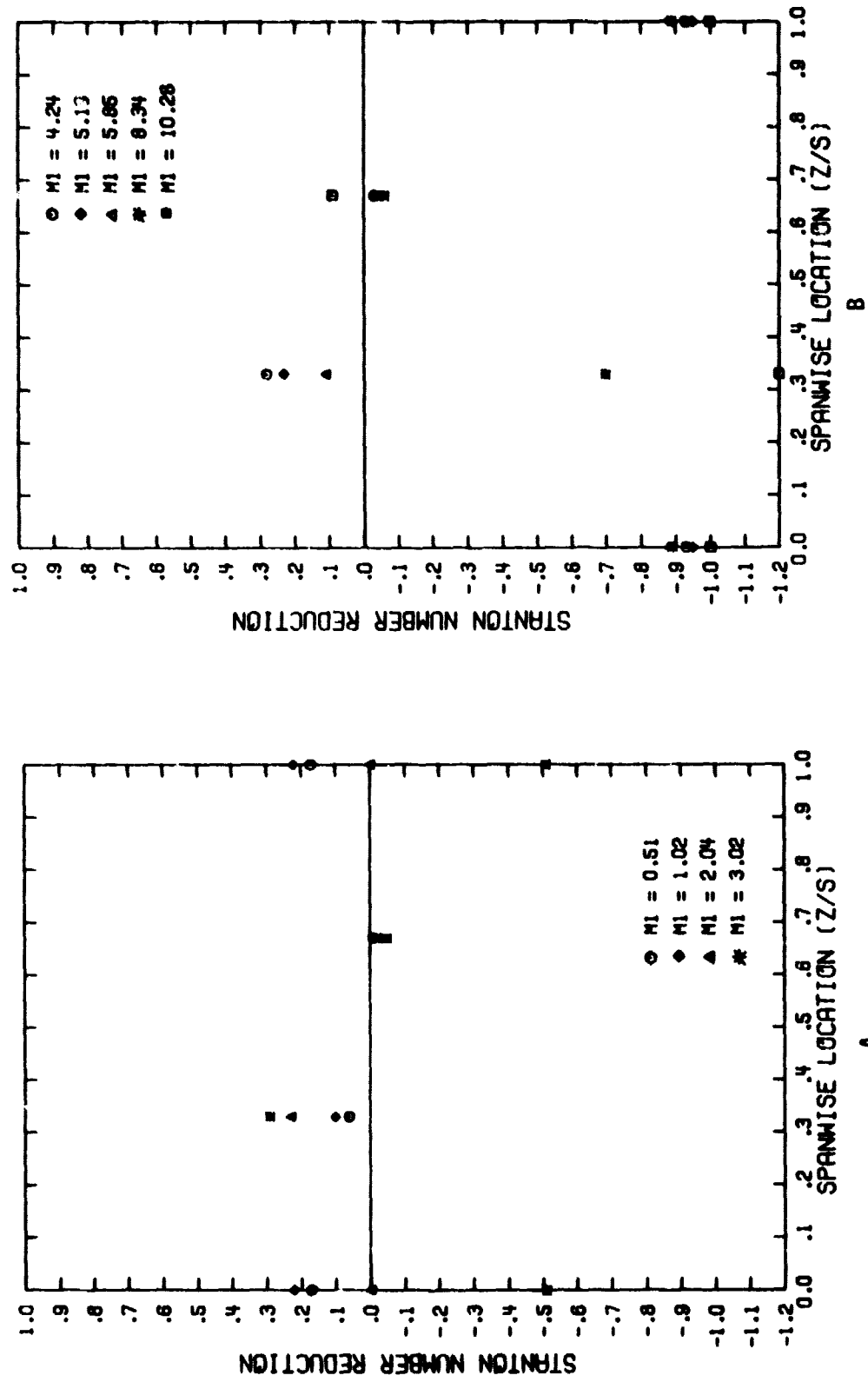


Figure A-5. Spanwise Variation of the Stanton Number Reduction with Single Row Injection
 $(\theta_1 = 5^\circ, s/d_0 = 5, (x/d_0)_1 = 1.5)$

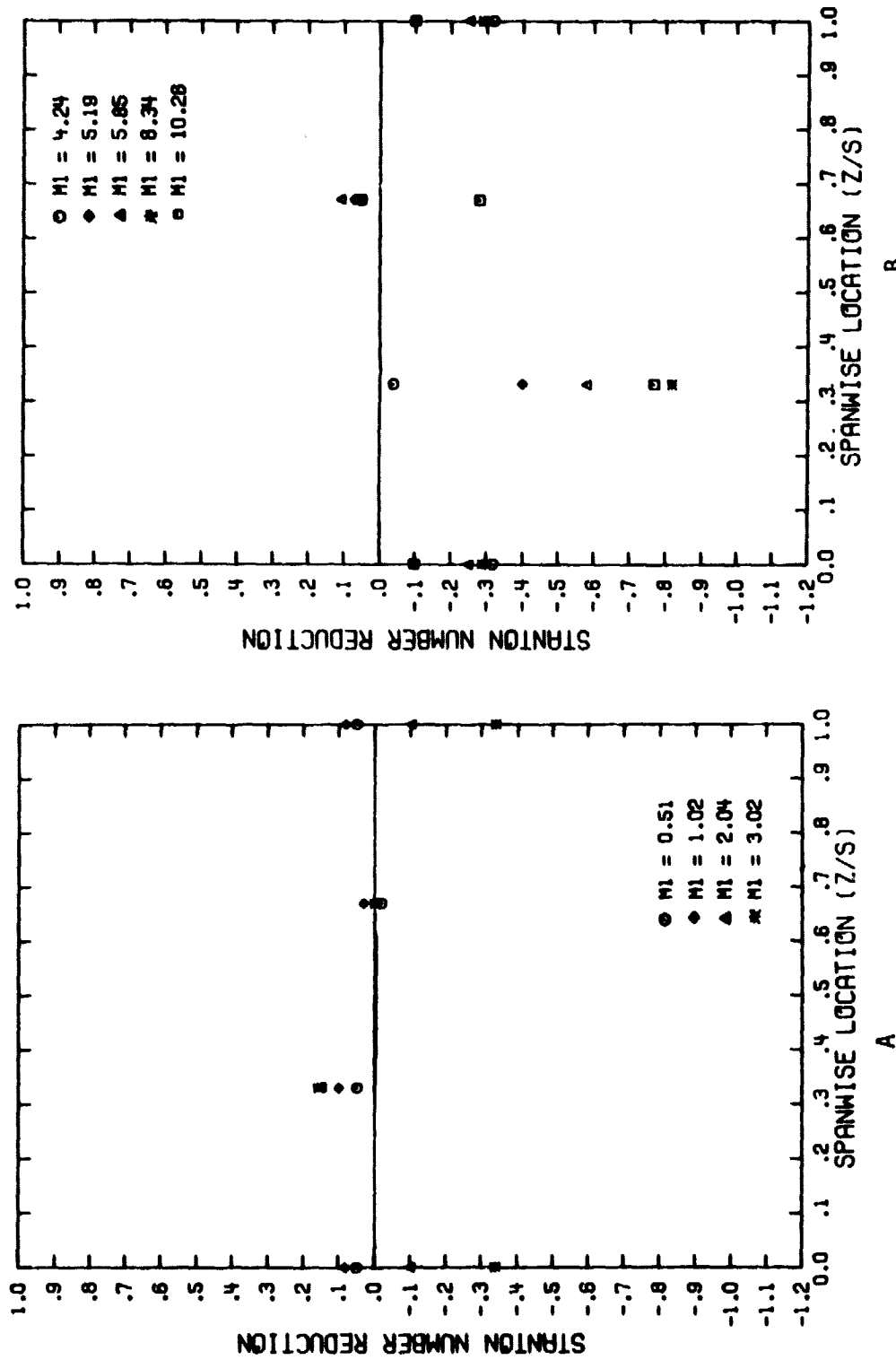


Figure A-6. Spanwise Variation of the Stanton Number Reduction with Single Row Injection
 $(\theta_1=50^\circ, s/d_0=5, (x/d_0)_1=3.5)$

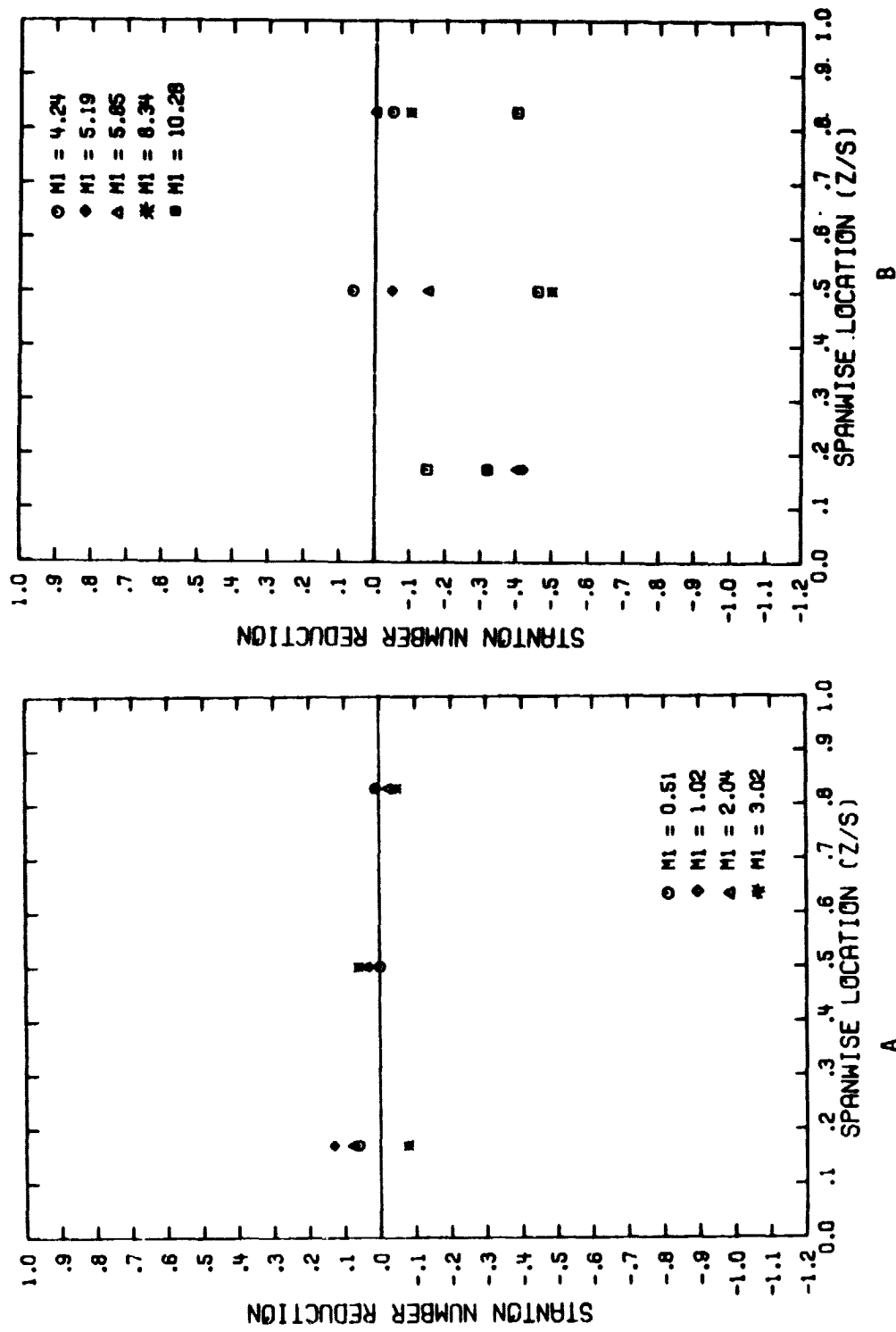


Figure A-7. Spanwise Variation of the Stanton Number Reduction with Single Row Injection
 $(\theta_1 = 50^\circ, s/d_0 = 5, (x/d_0)_1 = 6.5)$

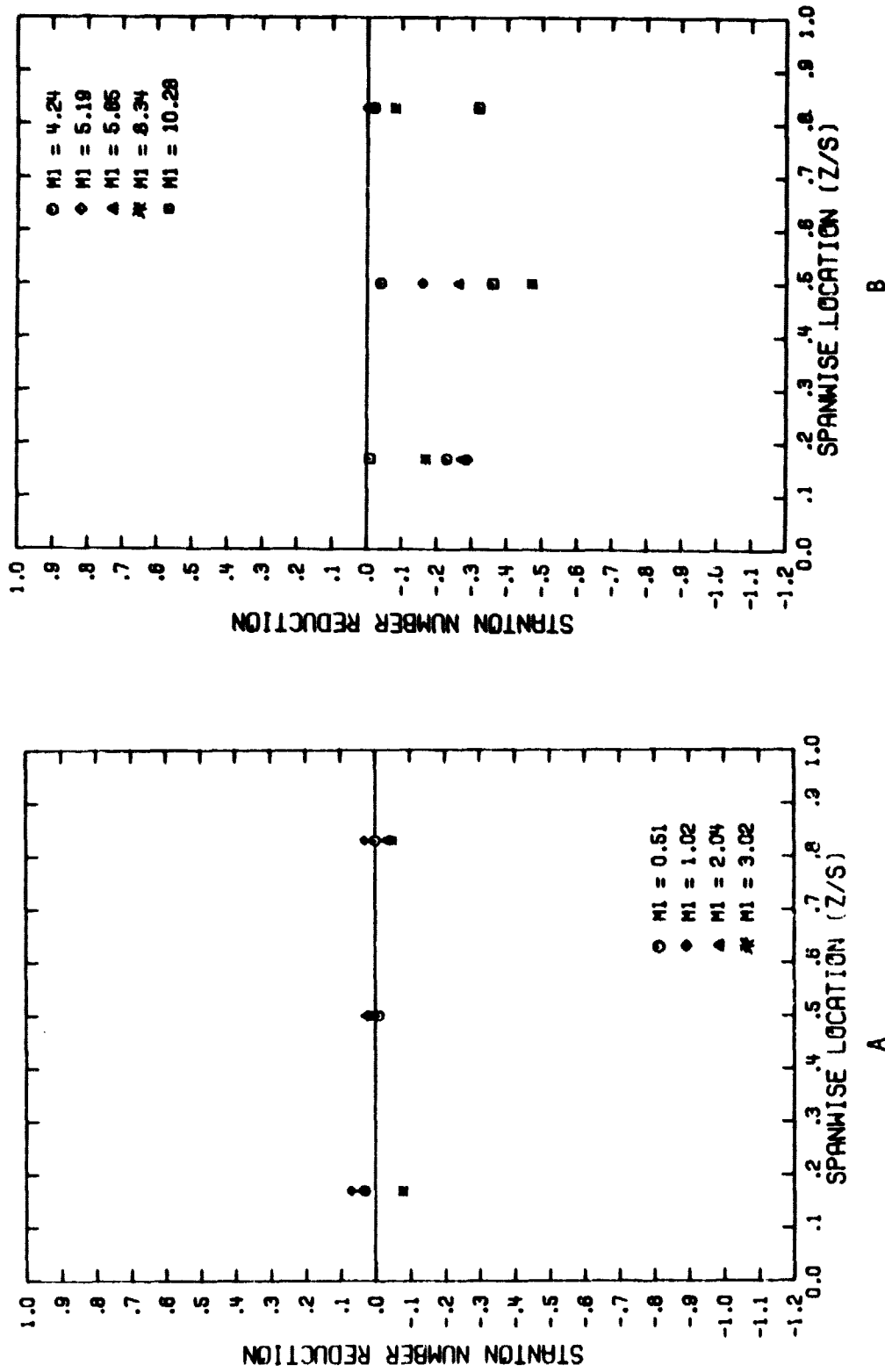


Figure A-8. Spanwise Variation of the Stanton Number Reduction with Single Row Injection
 $(\theta_1 = 50^\circ, s/d_0 = 5, (x/d_0)_1 = 8.5)$

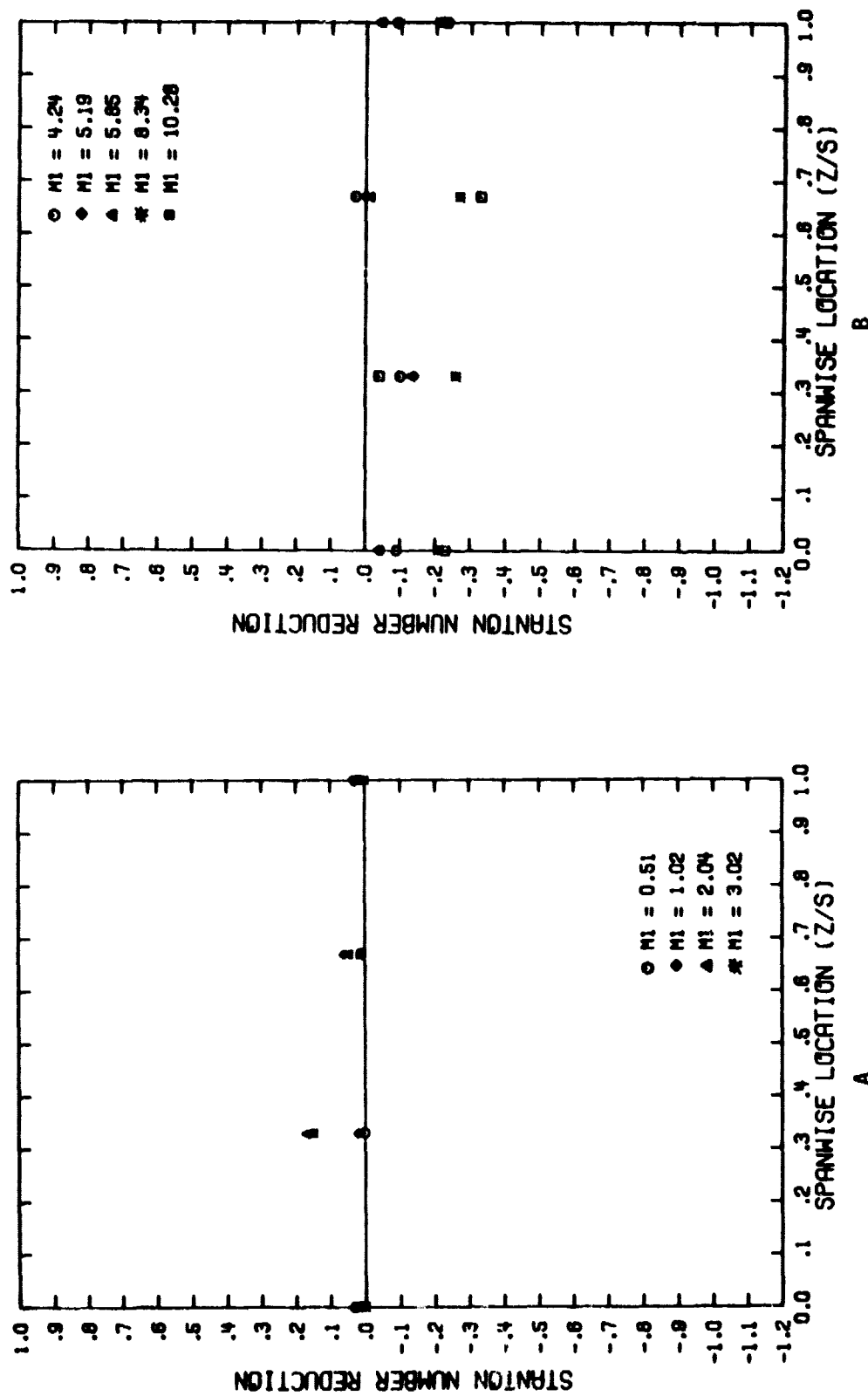


Figure A-9. Spanwise Variation of the Stanton Number Reduction with Single Row Injection
 $(\theta_1=50^\circ, s/d_0=5, (x/d_0)_1=11.5)$

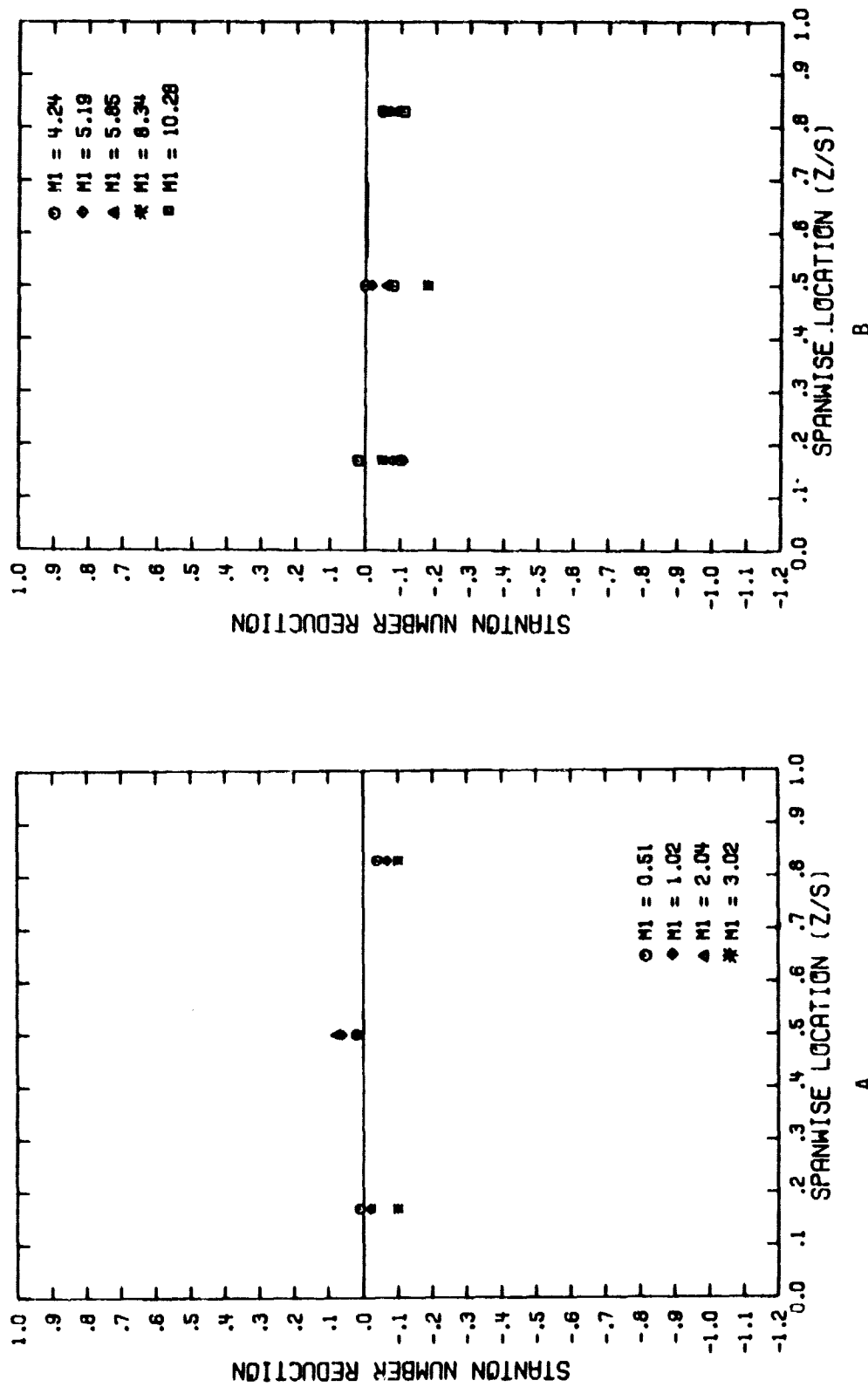


Figure A-10. Spanwise Variation of the Stanton Number Reduction with Single Row Injection
 $(\Theta_1 = 50^\circ, s/d_0 = 5, (x/d_0)_1 = 16.5)$

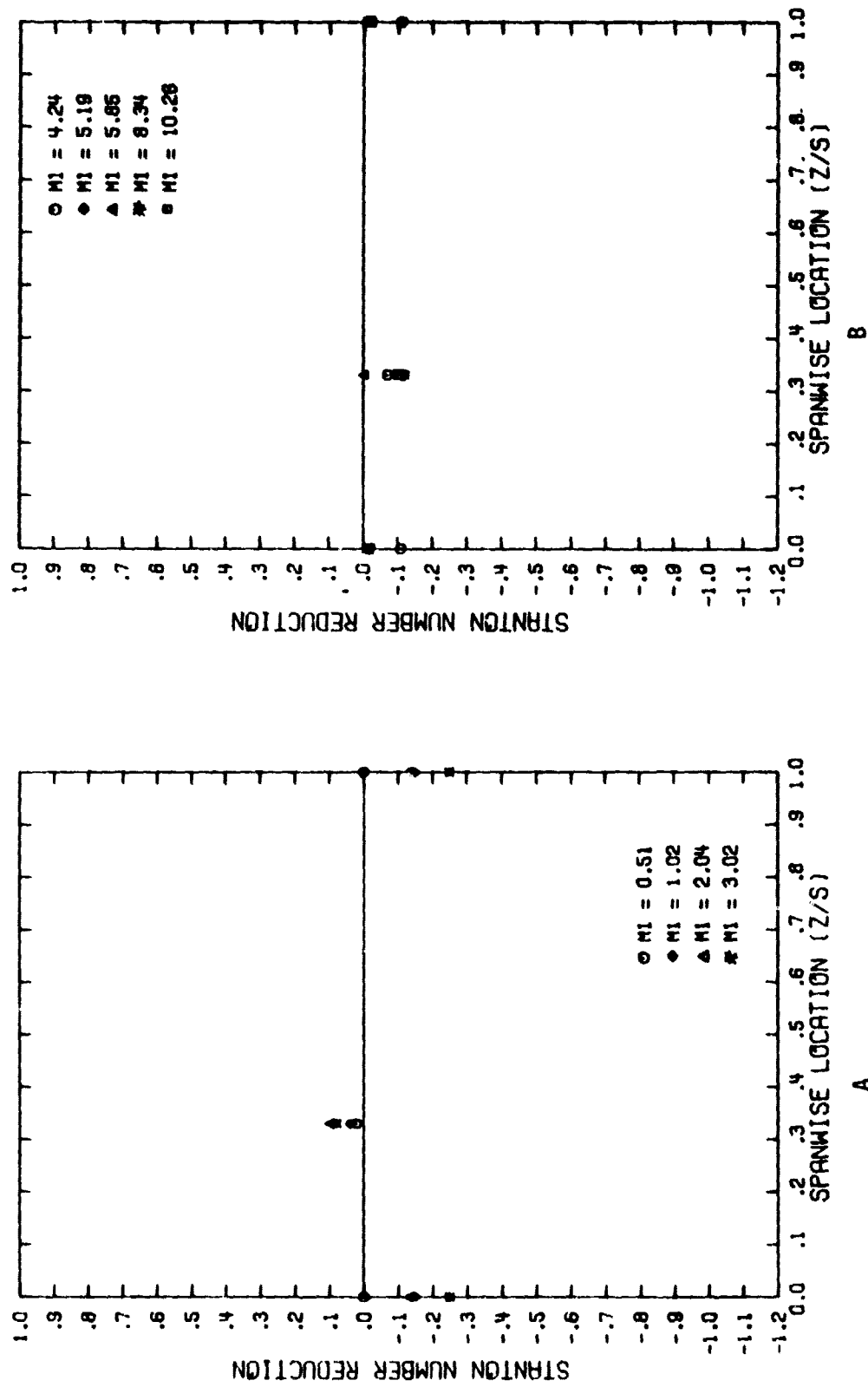


Figure A-11. Spanwise Variation of the Stanton Number Reduction with Single Row Injection
 $(\theta_1 = 5^\circ, s/d_0 = 5, (x/d_0)_1 = 21.5)$

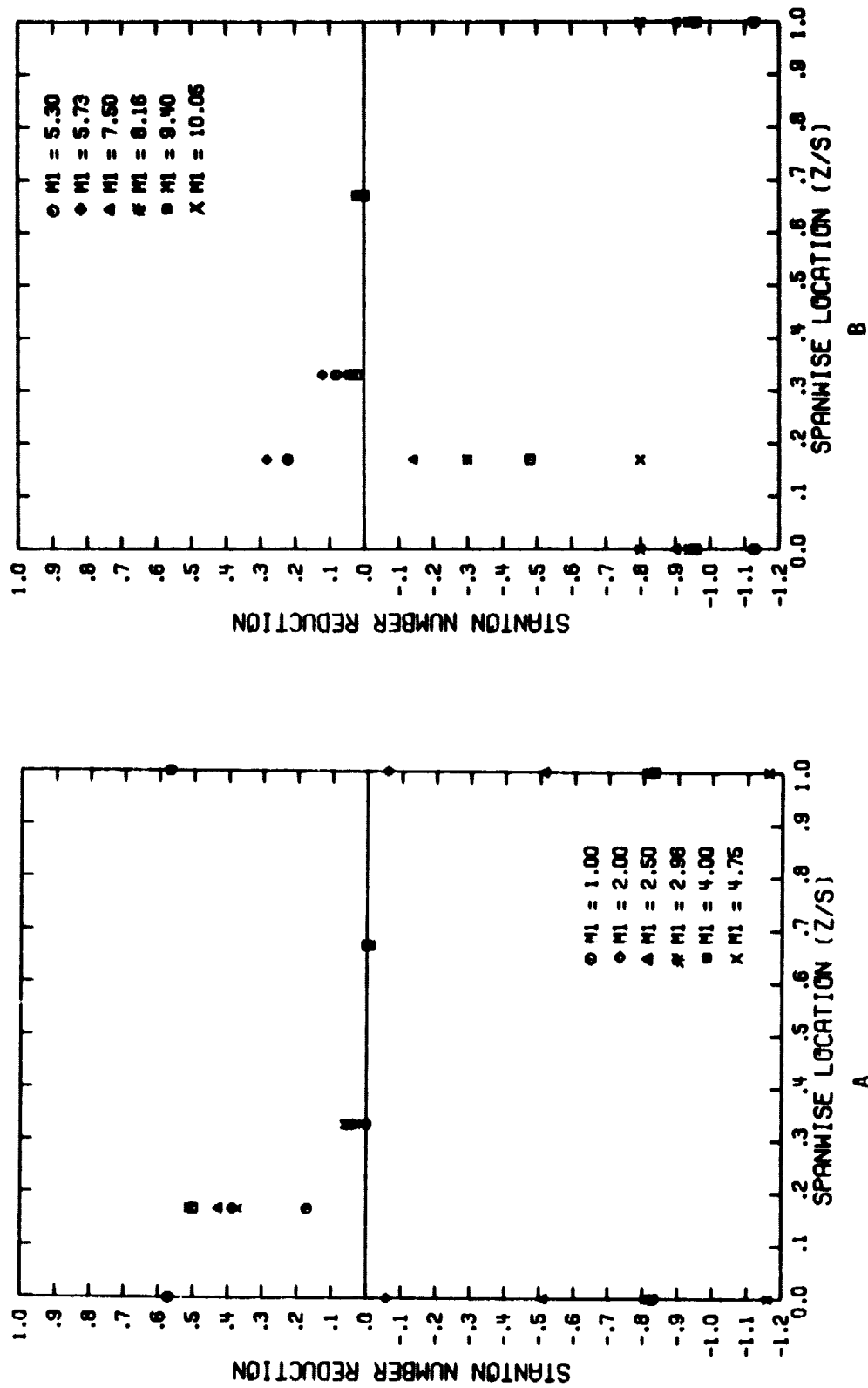


Figure A-12. Spanwise Variation of the Stanton Number Reduction with Single Row Injection
 $(\theta_1 = 50^\circ, s/d_0 = 10, (x/d_0)_1 = 1.5)$

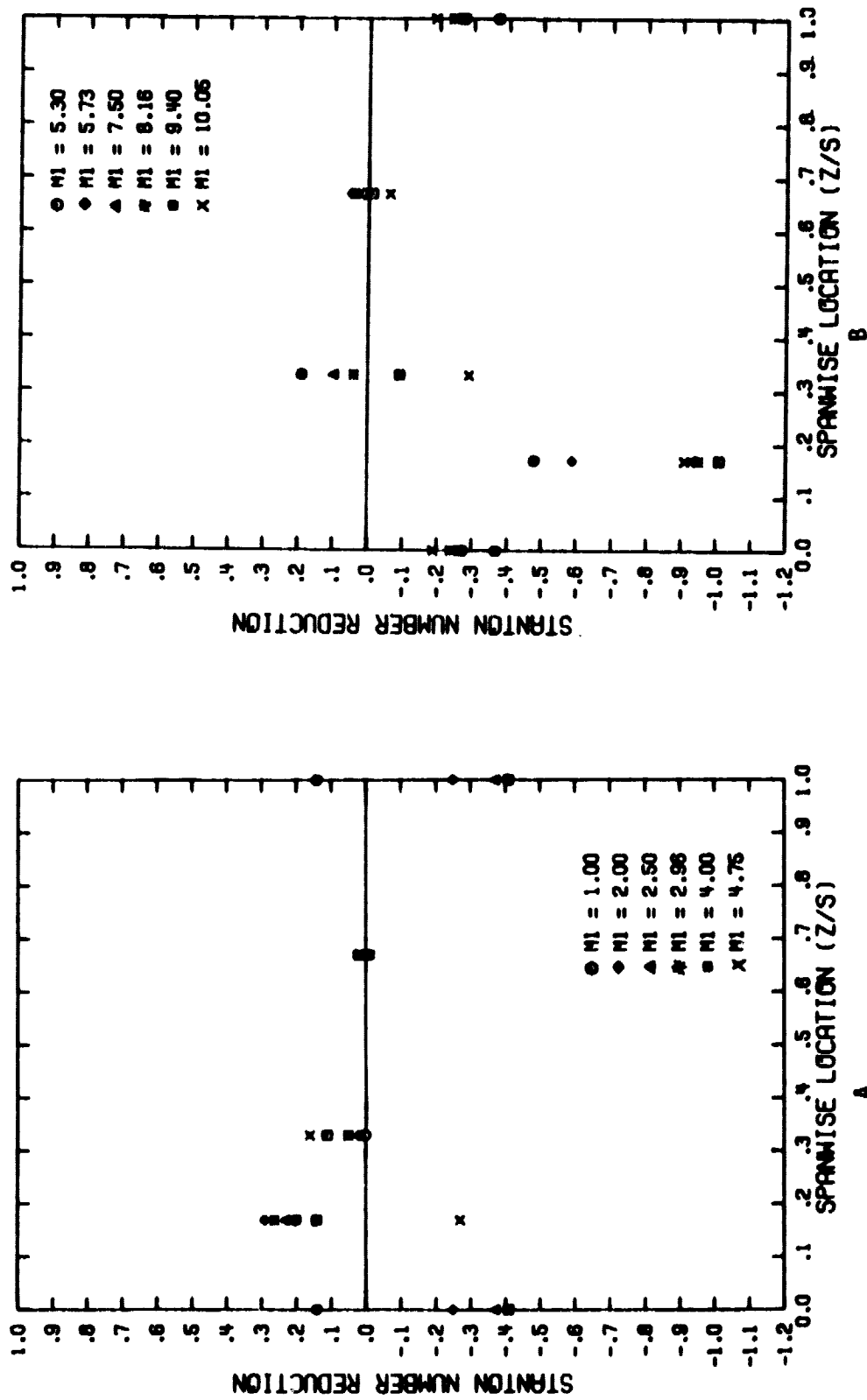


Figure A-13. Spanwise Variation of the Stanton Number Reduction with Single Row Injection
 $(\theta_1 = 50^\circ, s/d_0 = 10, (x/d_0)_1 = 3.5)$

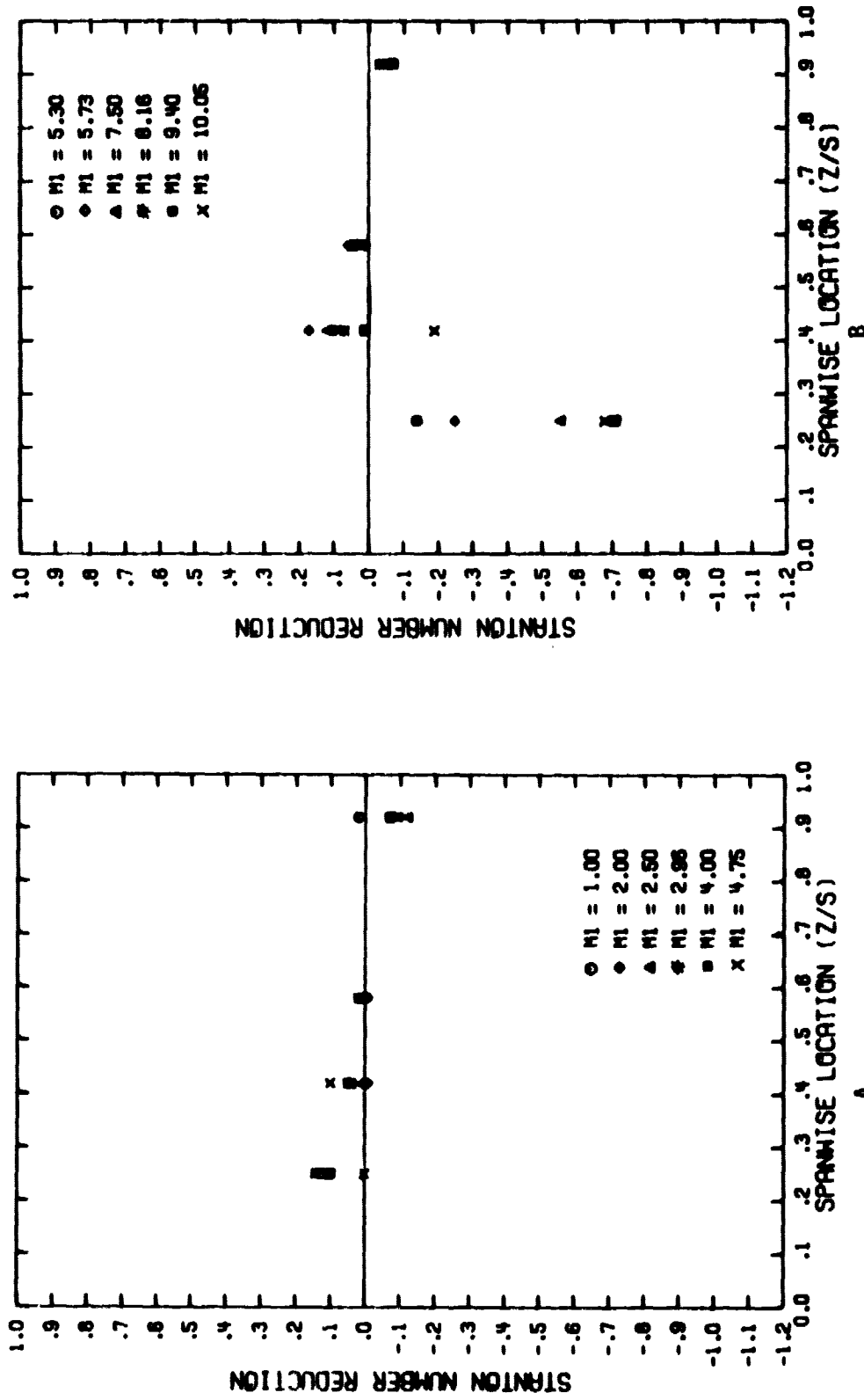


Figure A-14. Spanwise Variation of the Stanton Number Reduction with Single Row Injection
 $(\theta_1=5^\circ, s/d_0=10, (x/d_0)_1=6.5)$

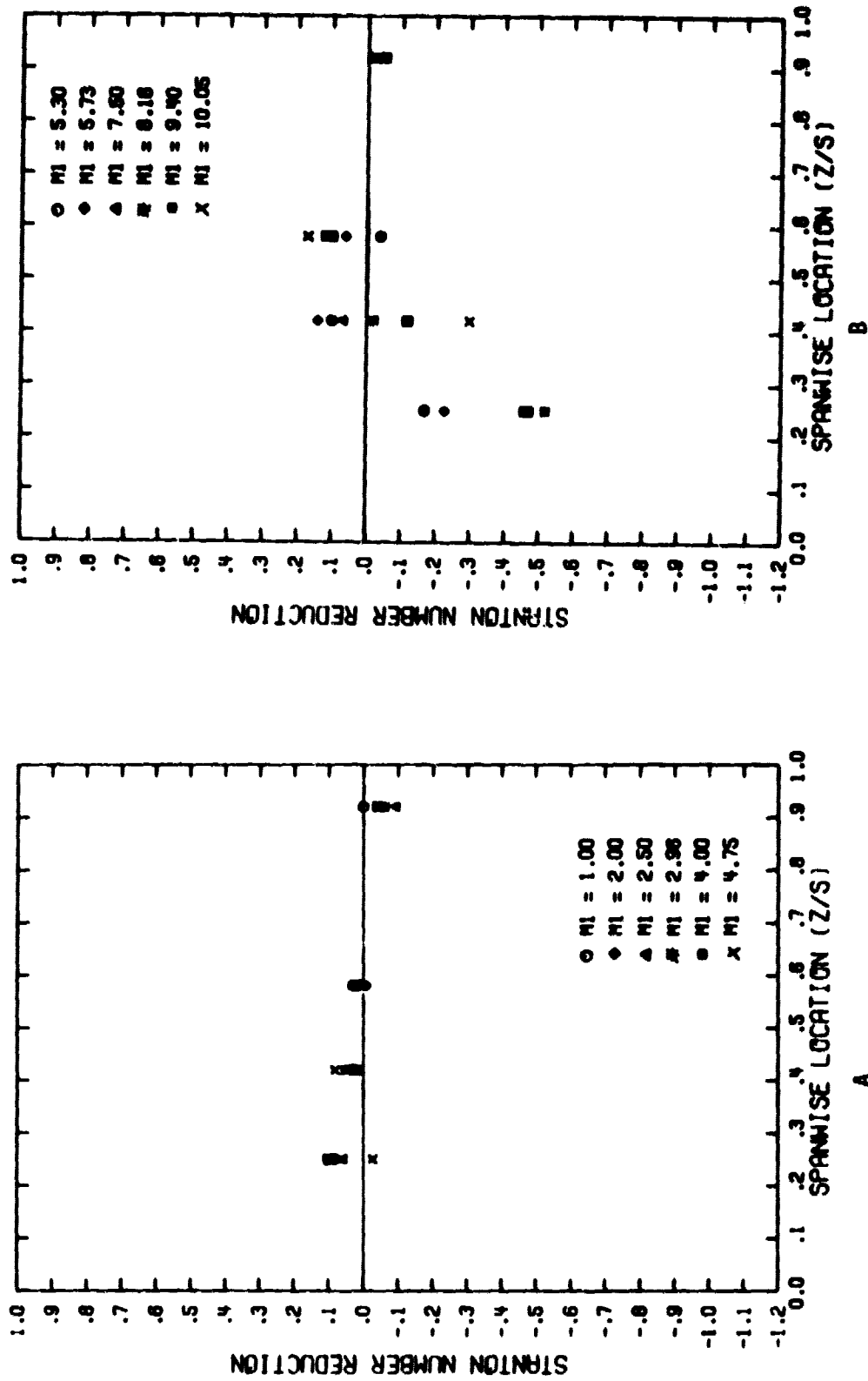


Figure A-15. Spanwise Variation of the Stanton Number Reduction with Single Row Injection
 $(\theta_1=50^\circ, s/d_0=10, (x/d_0)_1=8.5)$

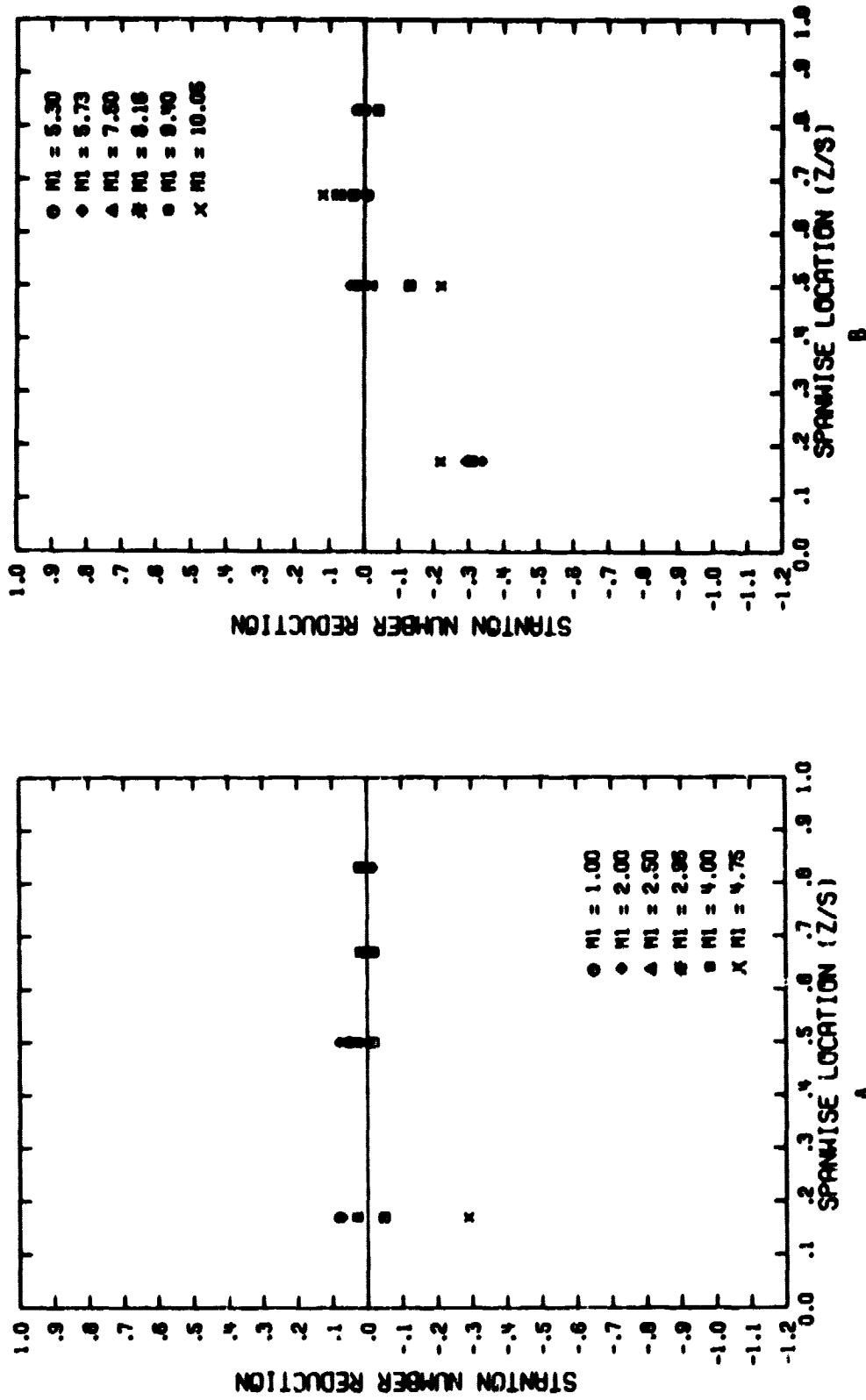


Figure A-16. Spanwise Variation of the Stanton Number Reduction with Single Row Injection
 $(\theta_1 = 5^\circ, s/d_0 = 10, (x/d_0)_1 = 11.5)$

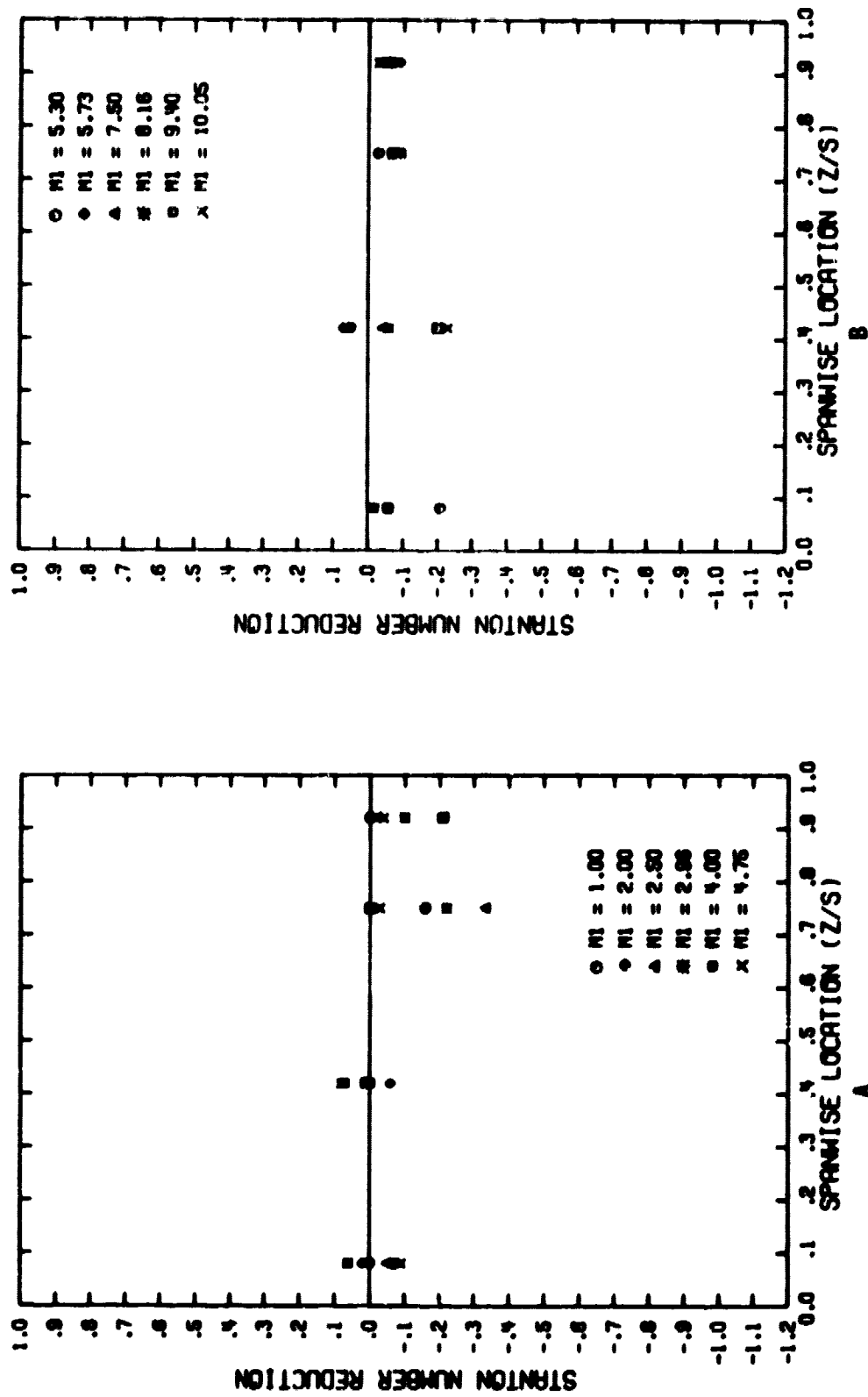


Figure A-17. Spanwise Variation of the Stanton Number Reduction with Single Row Injection
 $(\theta_1 = 50^\circ, s/d_0 = 10, (x/d_0)_1 = 16.5)$

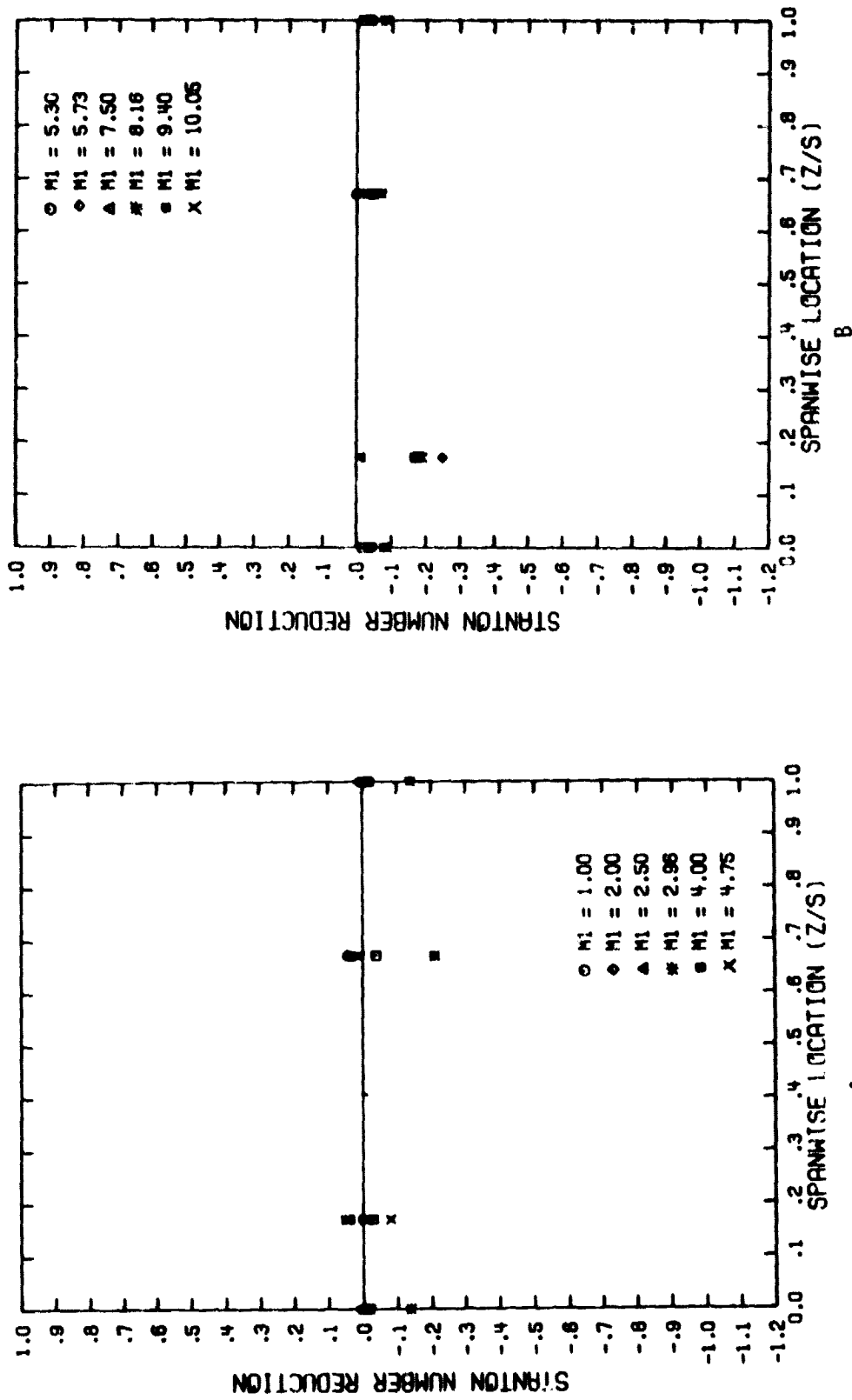


Figure A-18. Spanwise Variation of the Stanton Number Reduction with Single Row Injection
 $(\theta_1 = 50^\circ, s/d_0 = 10, (x/d_0)_1 = 21.5)$

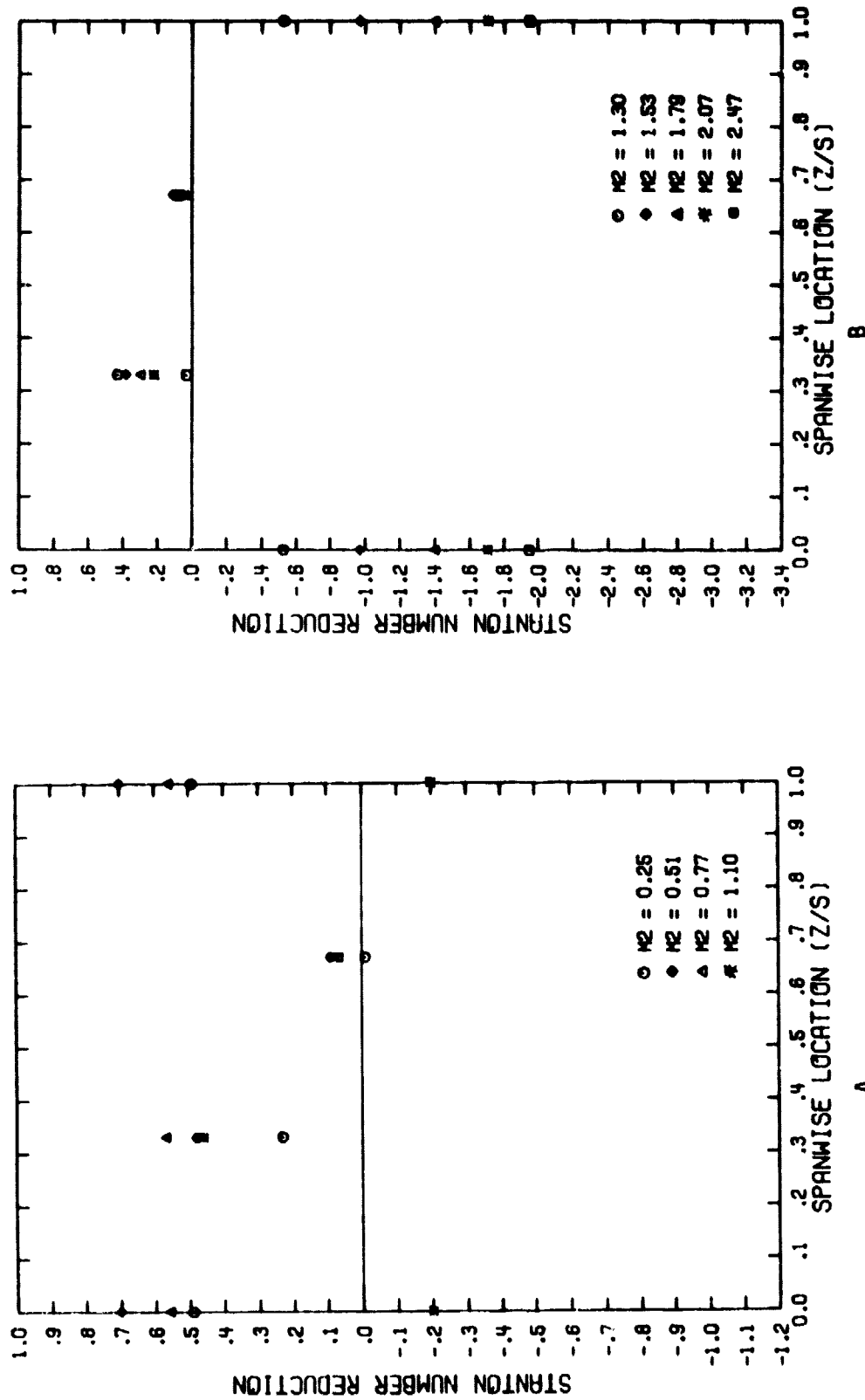


Figure A-19. Spanwise Variation of the Stanton Number Reduction with Single Row Injection
 $(\theta_2=22.9^\circ, s/d_0=5, (x/d_0)_2=1.5)$

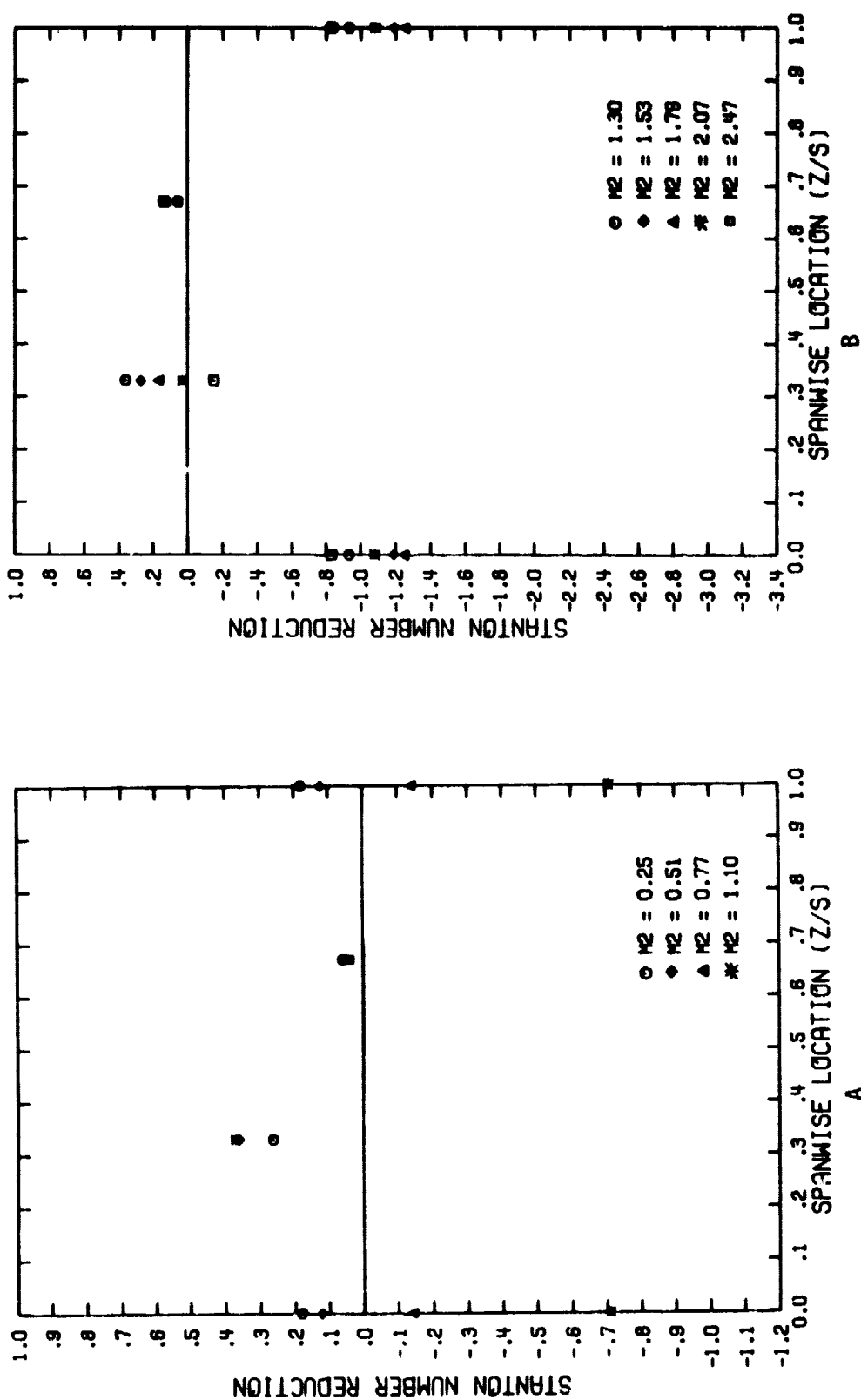


Figure A-20. Spanwise Variation of the Stanton Number Reduction with Single Row Injection
 ($\theta_2 = 22.90^\circ$, $s/d_0 = 5$, $(x/d_0)_2 = 3.5$)

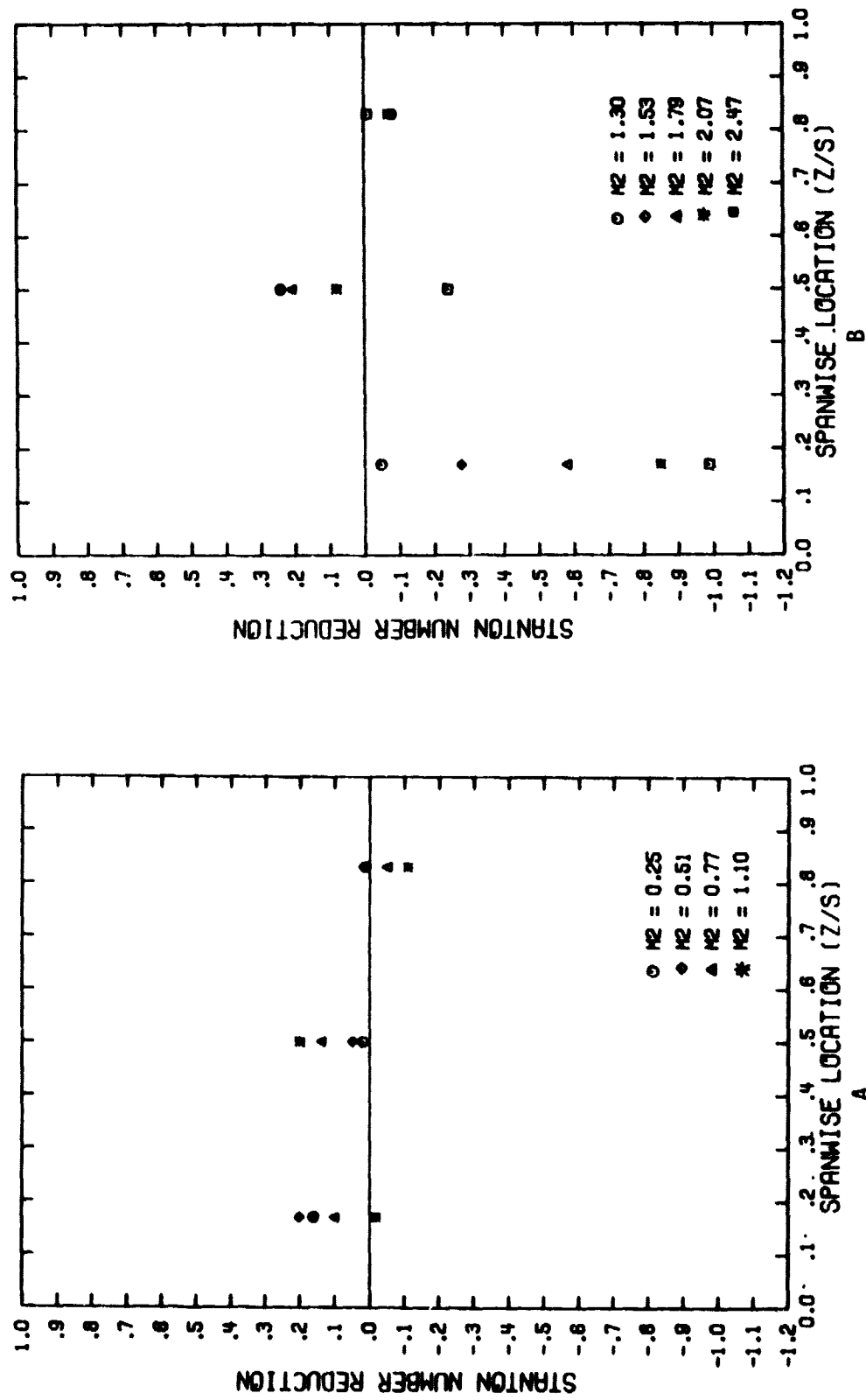


Figure A-21. Spanwise Variation of the Stanton Number Reduction with Single Row Injection
 $(\theta_2=22.9^\circ, s/d_0=5, (x/d_0)_2=6.5)$

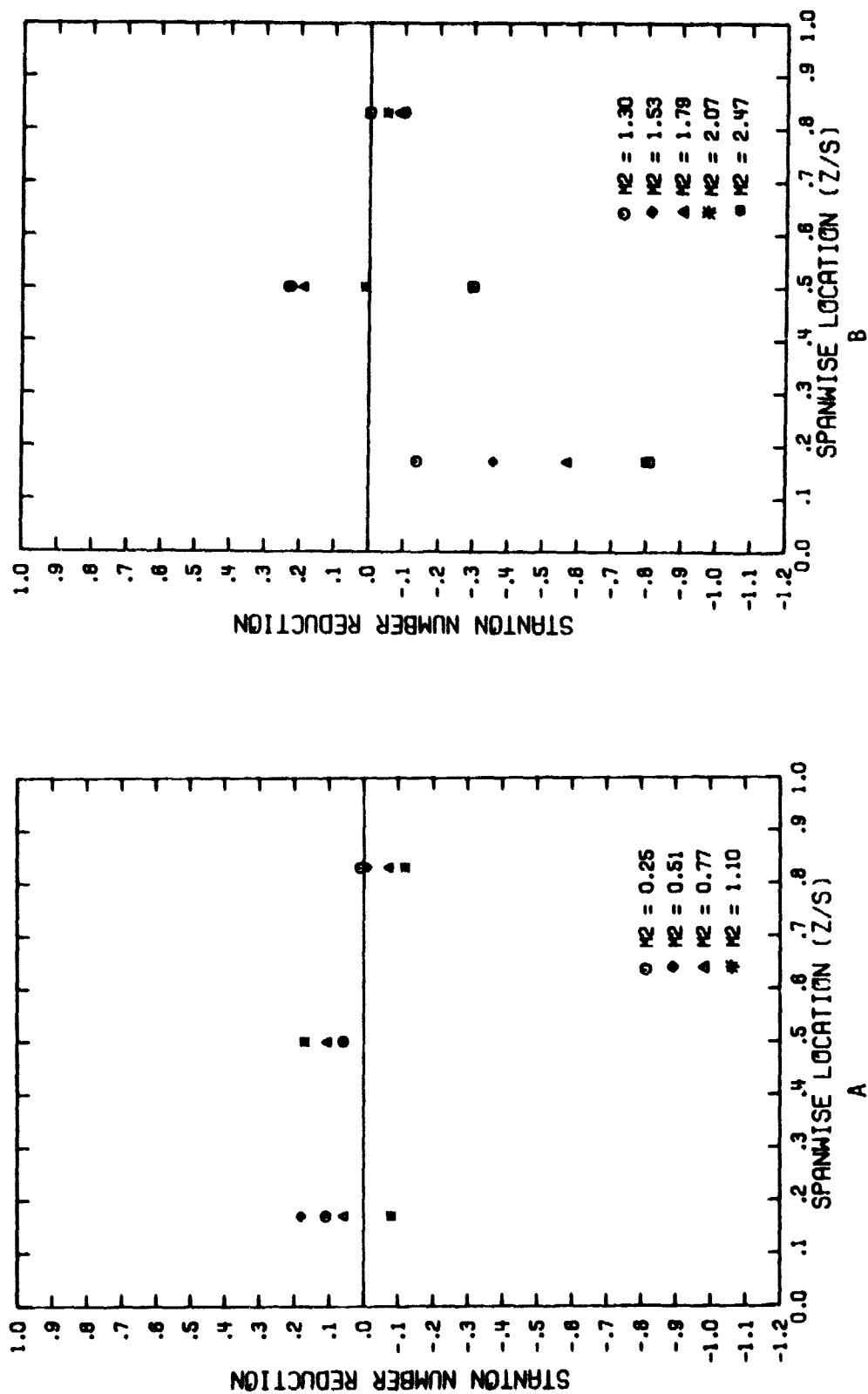


Figure A-22. Spanwise Variation of the Stanton Number Reduction with Single Row Injection
 $(\theta_2 = 22.9^\circ, s/d_0 = 5, (x/d_0)_2 = 8.5)$

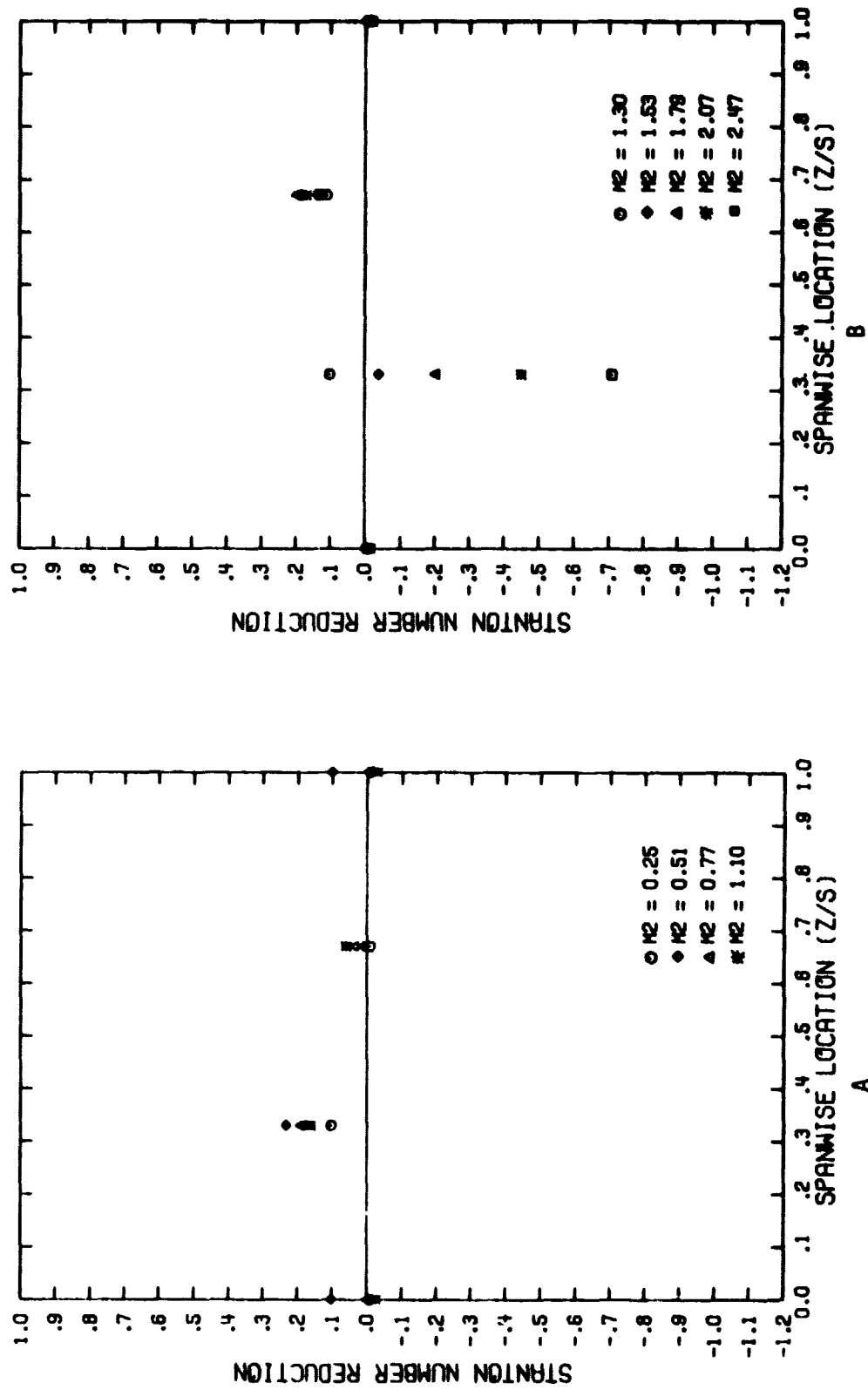


Figure A-23. Spanwise Variation of the Stanton Number Reduction with Single Row Injection
 ($\theta_2 = 22.9^\circ$, $s/d_0 = 5$, $(x/d_0)_2 = 11.5$)

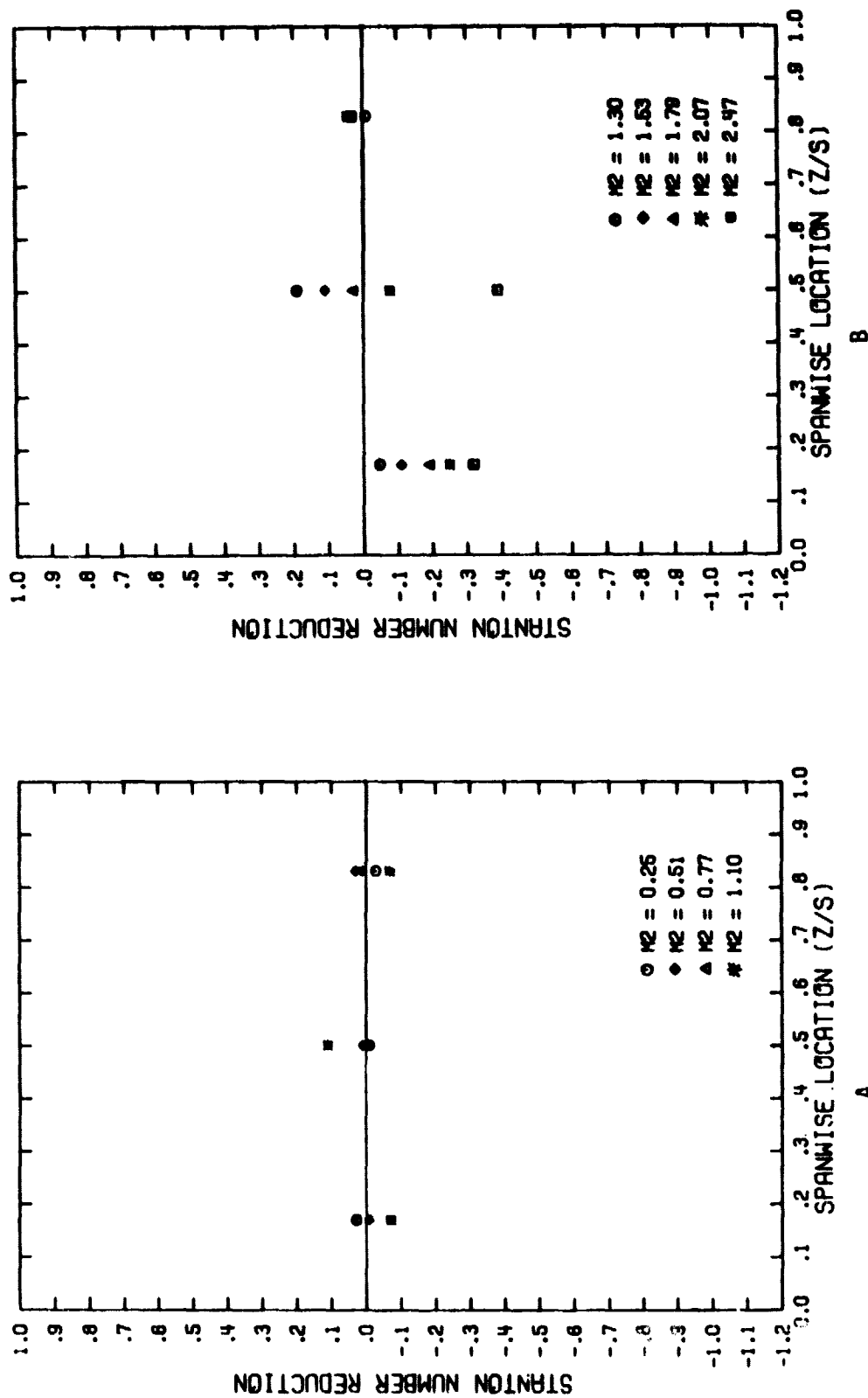


Figure A-24. Spanwise Variation of the Stanton Number Reduction with Single Row Injection
 $(\Theta_2 = 22.9^\circ, s/d_0 = 5, (x/d_0)_2 = 16.5)$

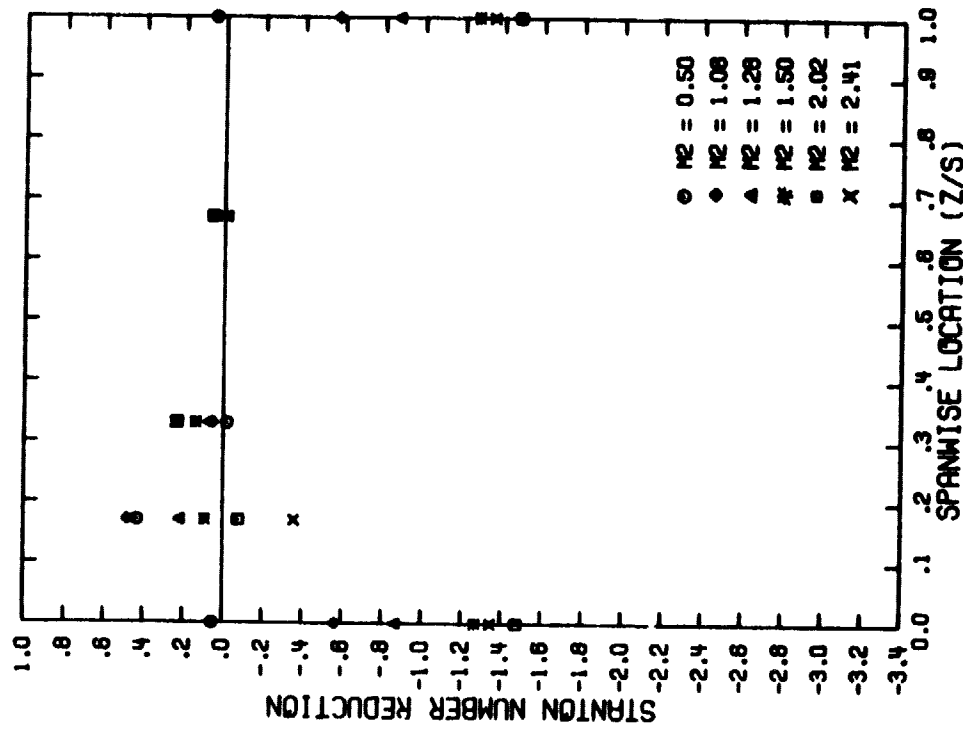


Figure A-25. Spanwise Variation of the Stanton Number Reduction with Single Row Injection ($\theta_2=22.90^\circ$, $s/d_0=10$, $(x/d_0)^2=1.5$)

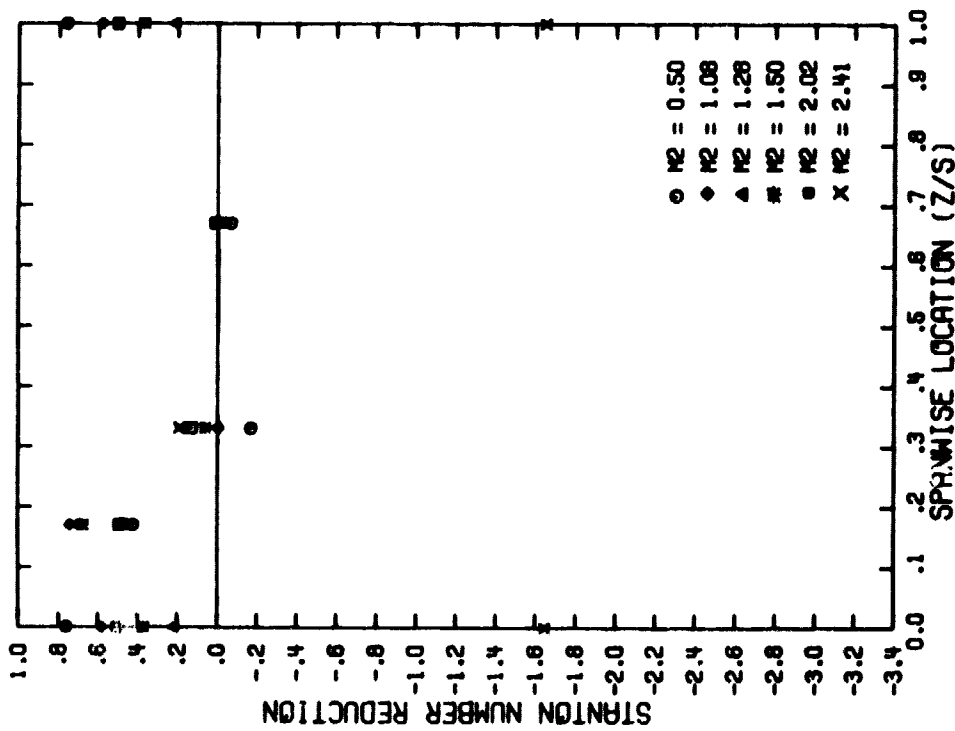


Figure A-26. Spanwise Variation of the Stanton Number Reduction with Single Row Injection ($\theta_2=22.90^\circ$, $s/d_0=10$, $(x/d_0)^2=3.5$)

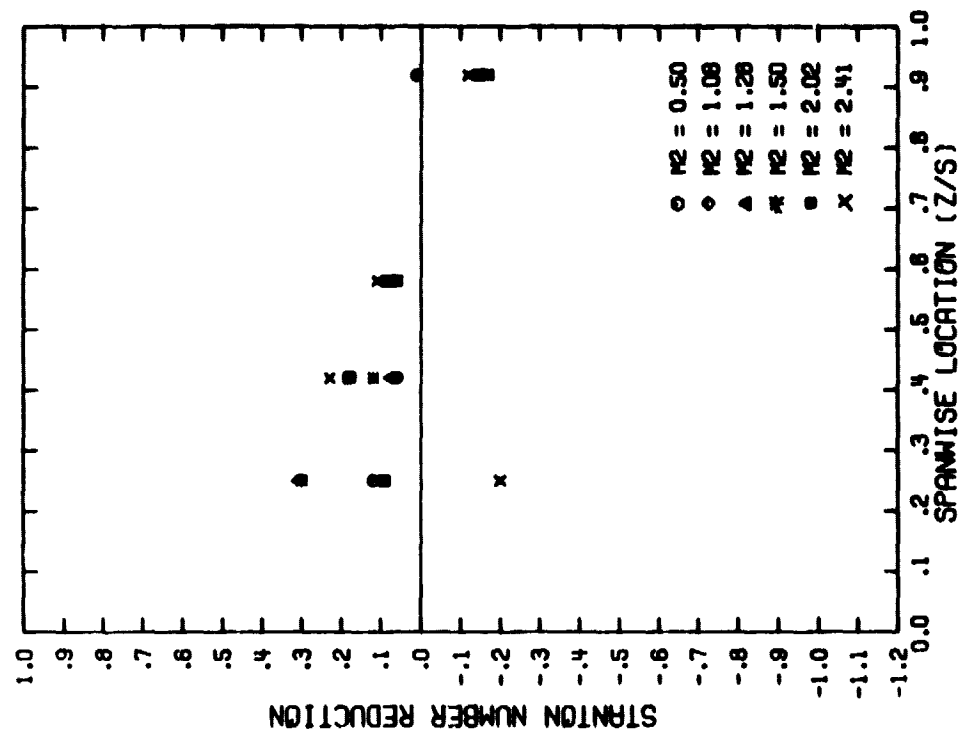


Figure A-27. Spanwise Variation of the Stanton Number Reduction with Single Row Injection ($\theta_2=22.90^\circ$, $s/d_0=10$, $(x/d_0)_2=6.5$)

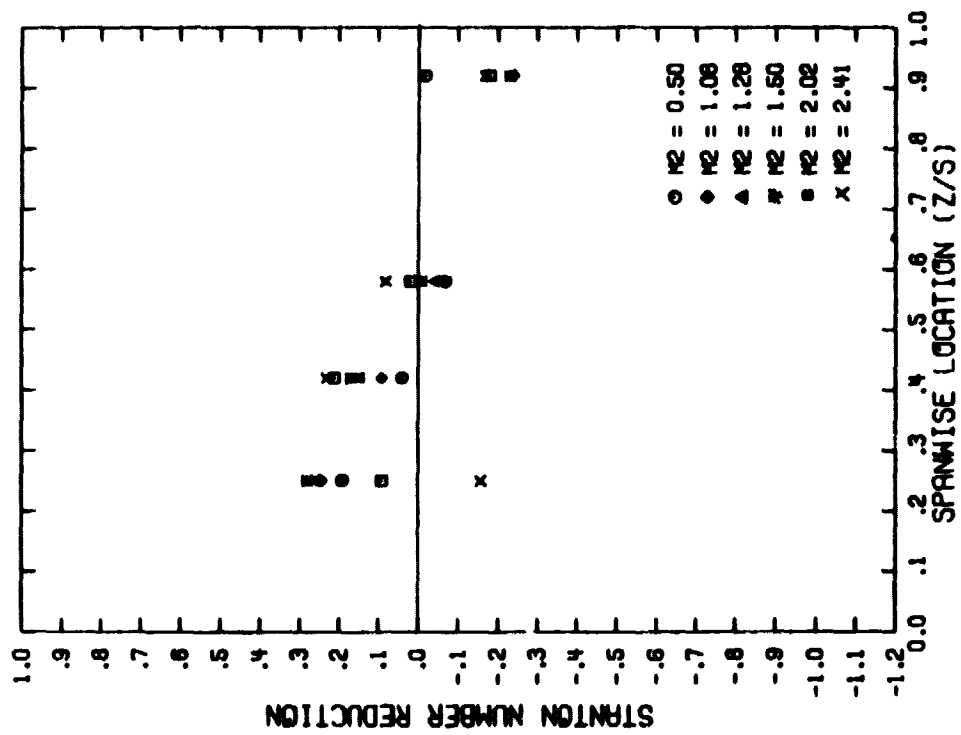


Figure A-28. Spanwise Variation of the Stanton Number Reduction with Single Row Injection ($\theta_2=22.90^\circ$, $s/d_0=10$, $(x/d_0)_2=8.5$)

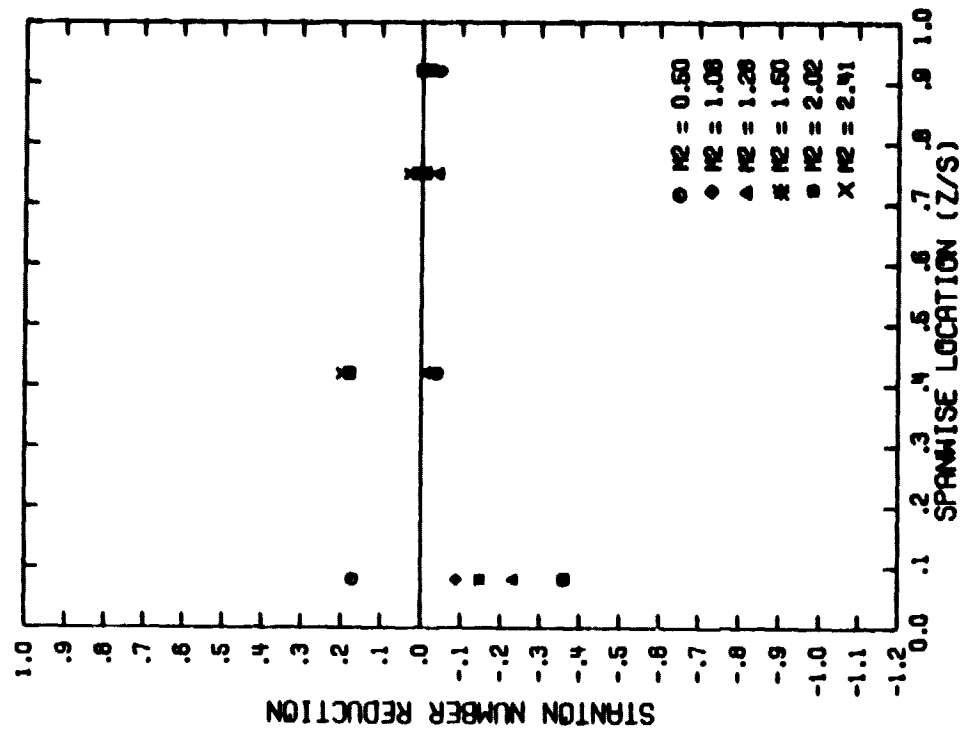


Figure A-29. Spanwise Variation of the Stanton Number Reduction with Single Row Injection ($\theta_2=22.90^\circ$, $s/d_0=10$, $(x/d_0)_2=11.5$)

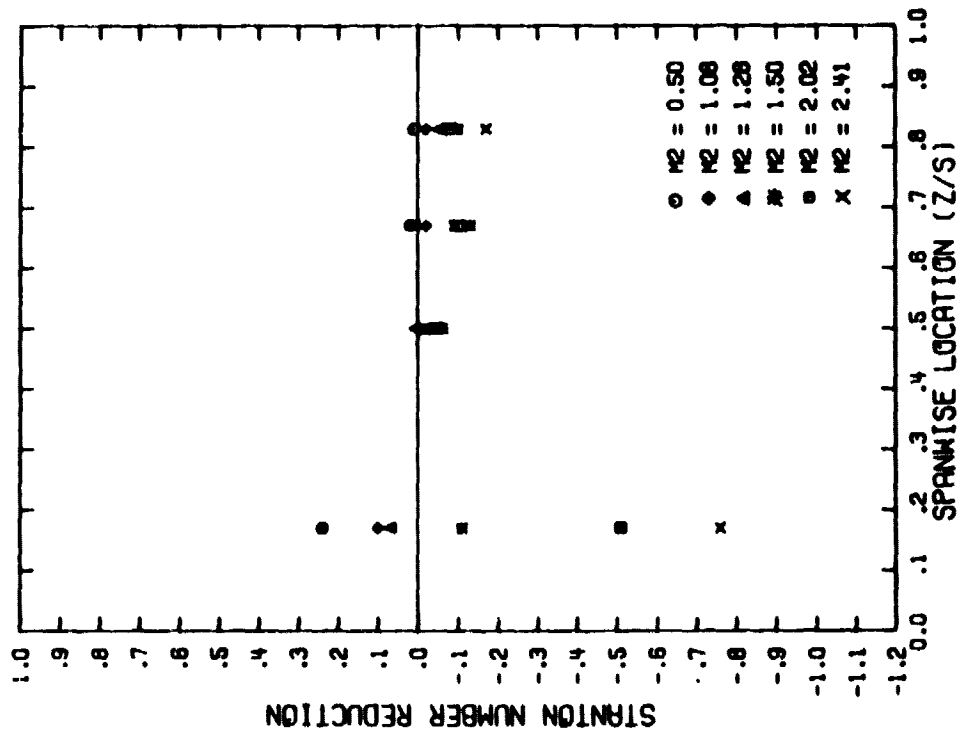


Figure A-30. Spanwise Variation of the Stanton Number Reduction with Single Row Injection ($\theta_2=22.90^\circ$, $s/d_0=10$, $(x/d_0)_2=16.5$)

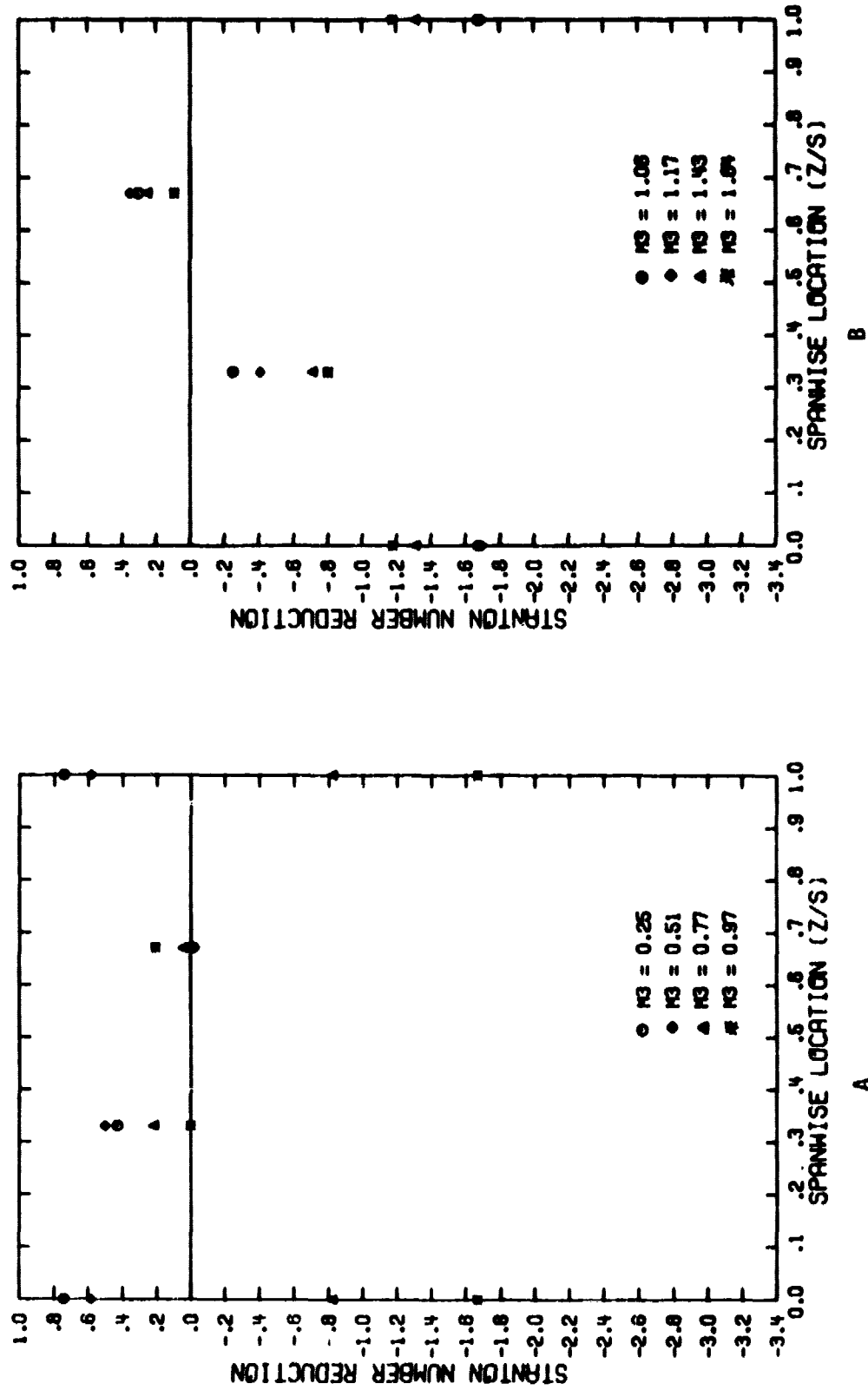


Figure A-31. Spanwise Variation of the Stanton Number Reduction with Single Row Injection
 $(\theta_3=40.8^\circ, s/d_0=5, (x/d_0)_3=1.5)$

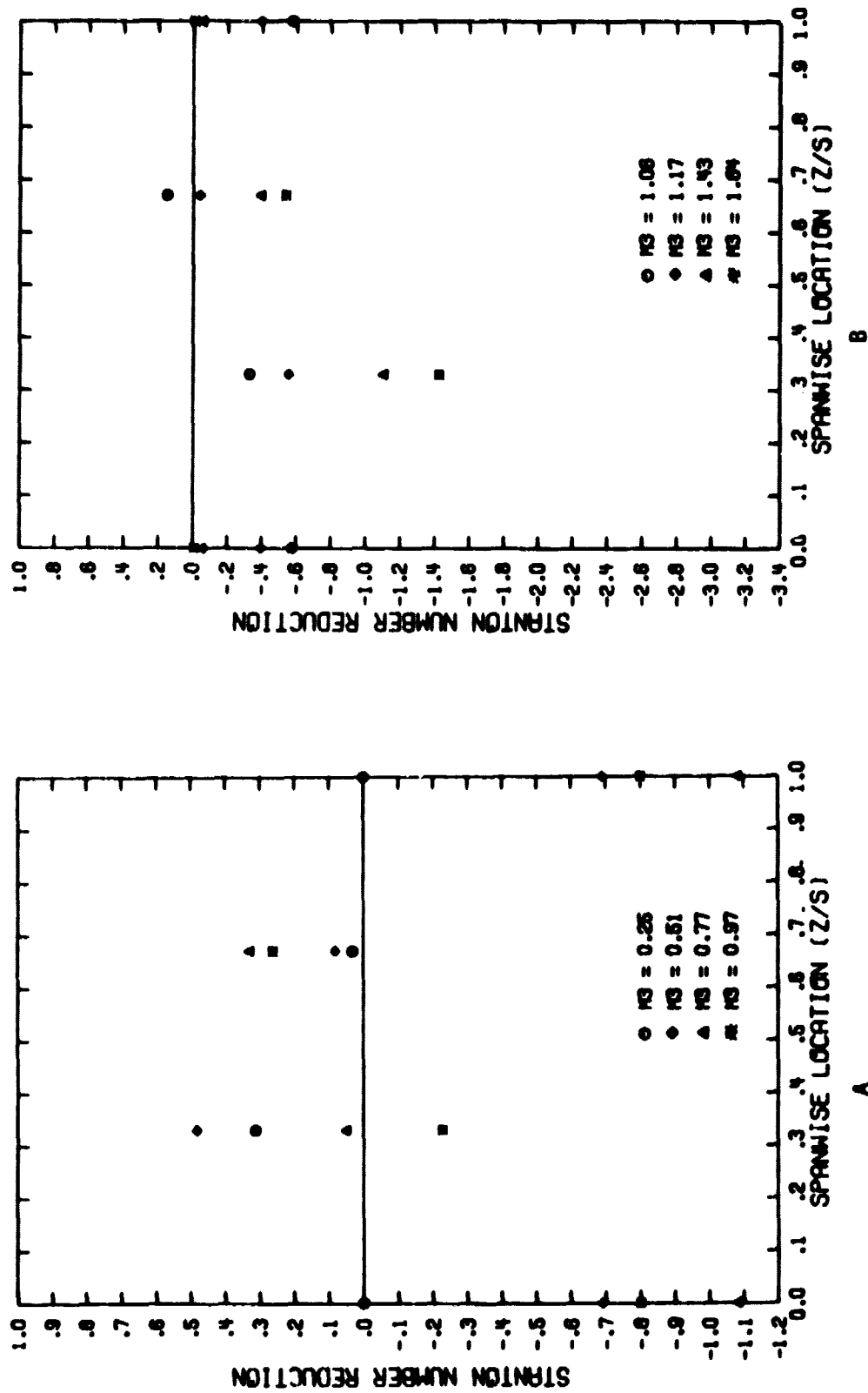


Figure A-32. Spanwise Variation of the Stanton Number Reduction with Single Row Injection
 $(\theta_3 = 40.8^\circ, s/d_0 = 5, (x/d_0)_3 = 3.5)$

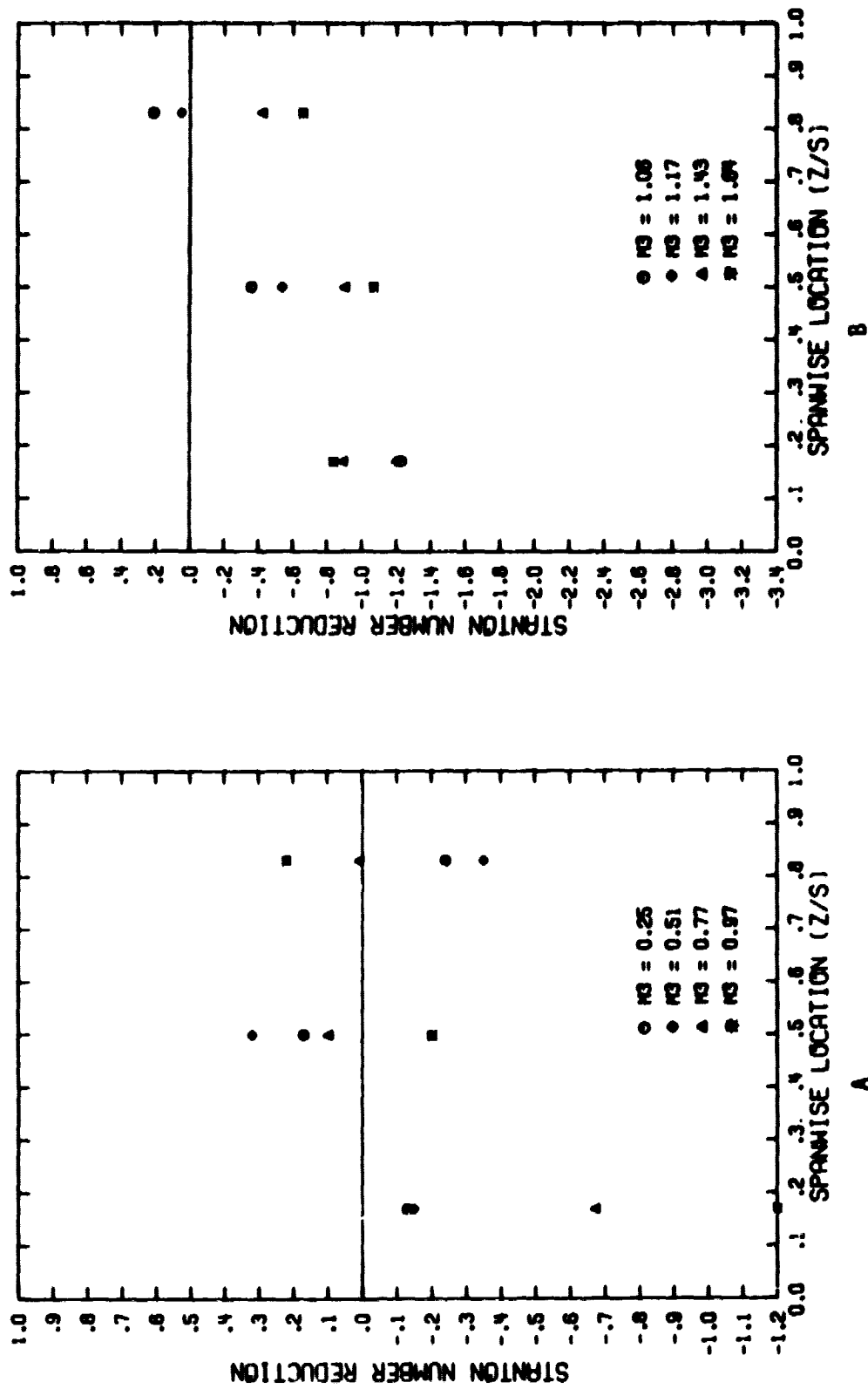


Figure A-33. Spanwise Variation of the Stanton Number Reduction with Single Row Injection
 $(\theta_3=40.8^\circ, s/d_0=5, (x/d_0)_3=6.5)$

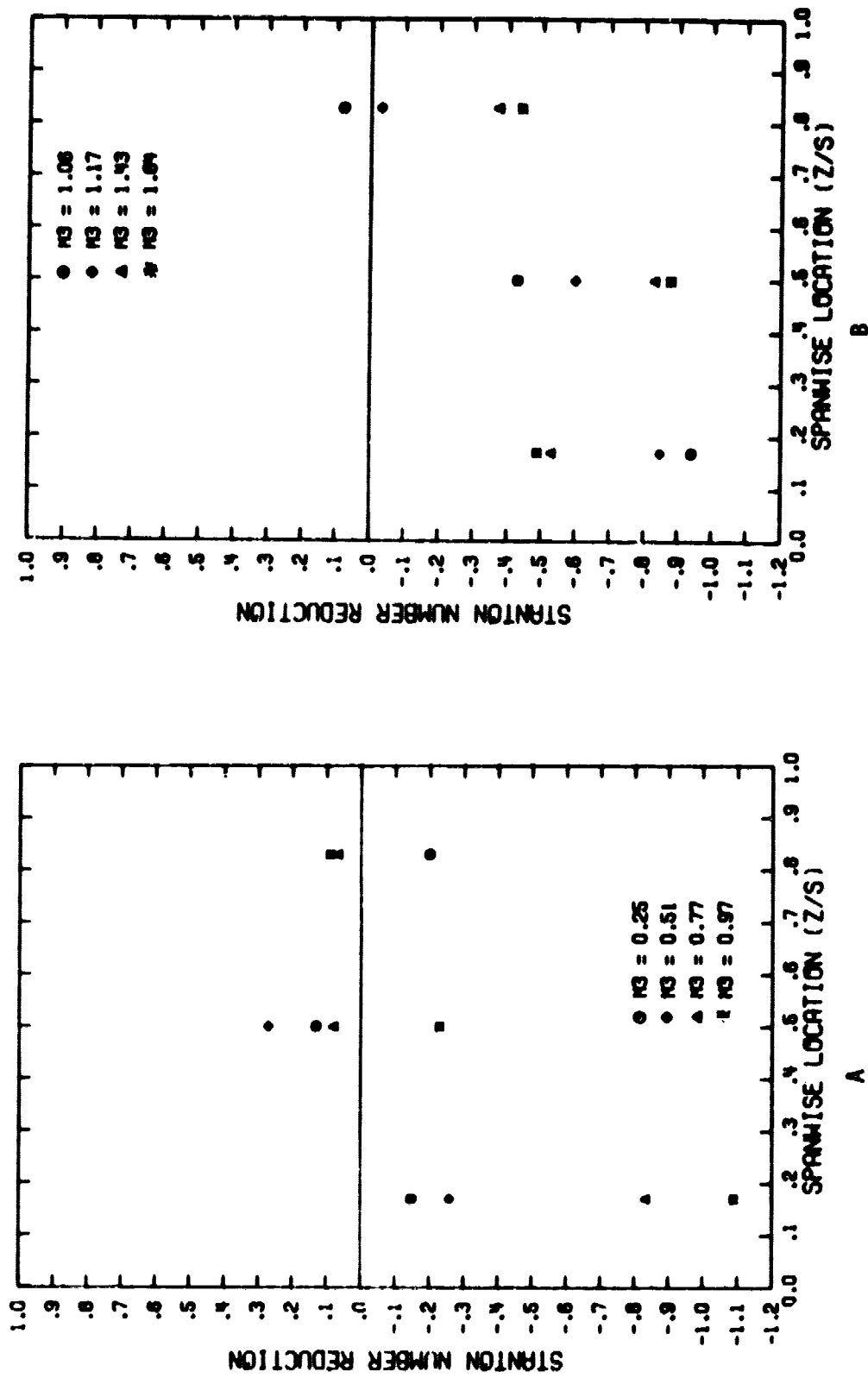


Figure A-34. Spanwise Variation of the Stanton Number Reduction with Single Row Injection
 $(\theta_3 = 40.8^\circ, s/d_0 = 5, (x/d_0)_3 = 8.5)$

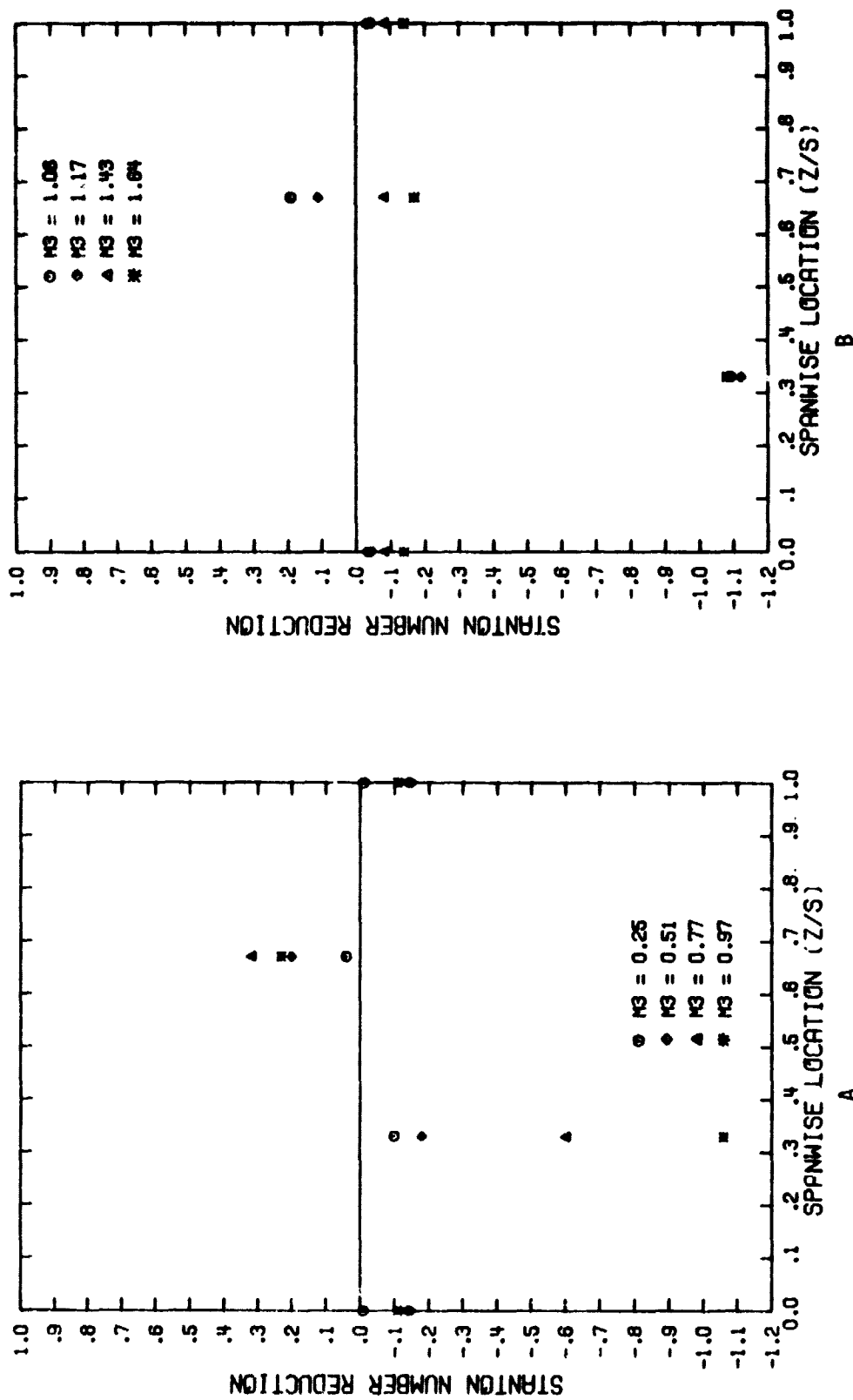


Figure A-35. Spanwise Variation of the Stanton Number Reduction with Single Row Injection
 $(\theta_3 = 40.8^\circ, s/d_0 = 5, (x/d_0)_3 = 11.5)$

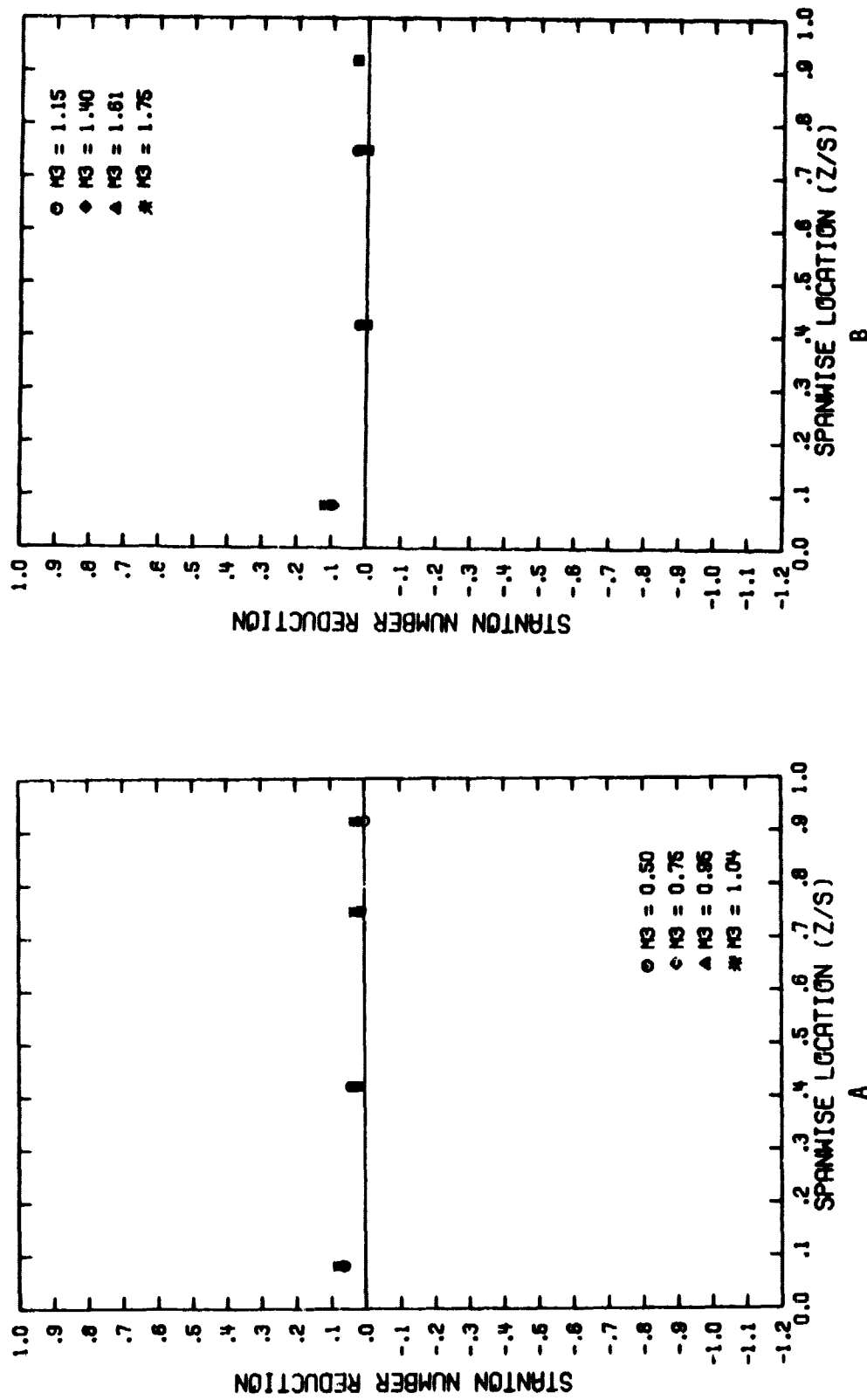


Figure A-36. Spanwise Variation of the Stanton Number Reduction with Single Row Injection
 $(\theta_3 = 40.80^\circ, s/d_0 = 10, (x/d_0)_3 = -1.5)$

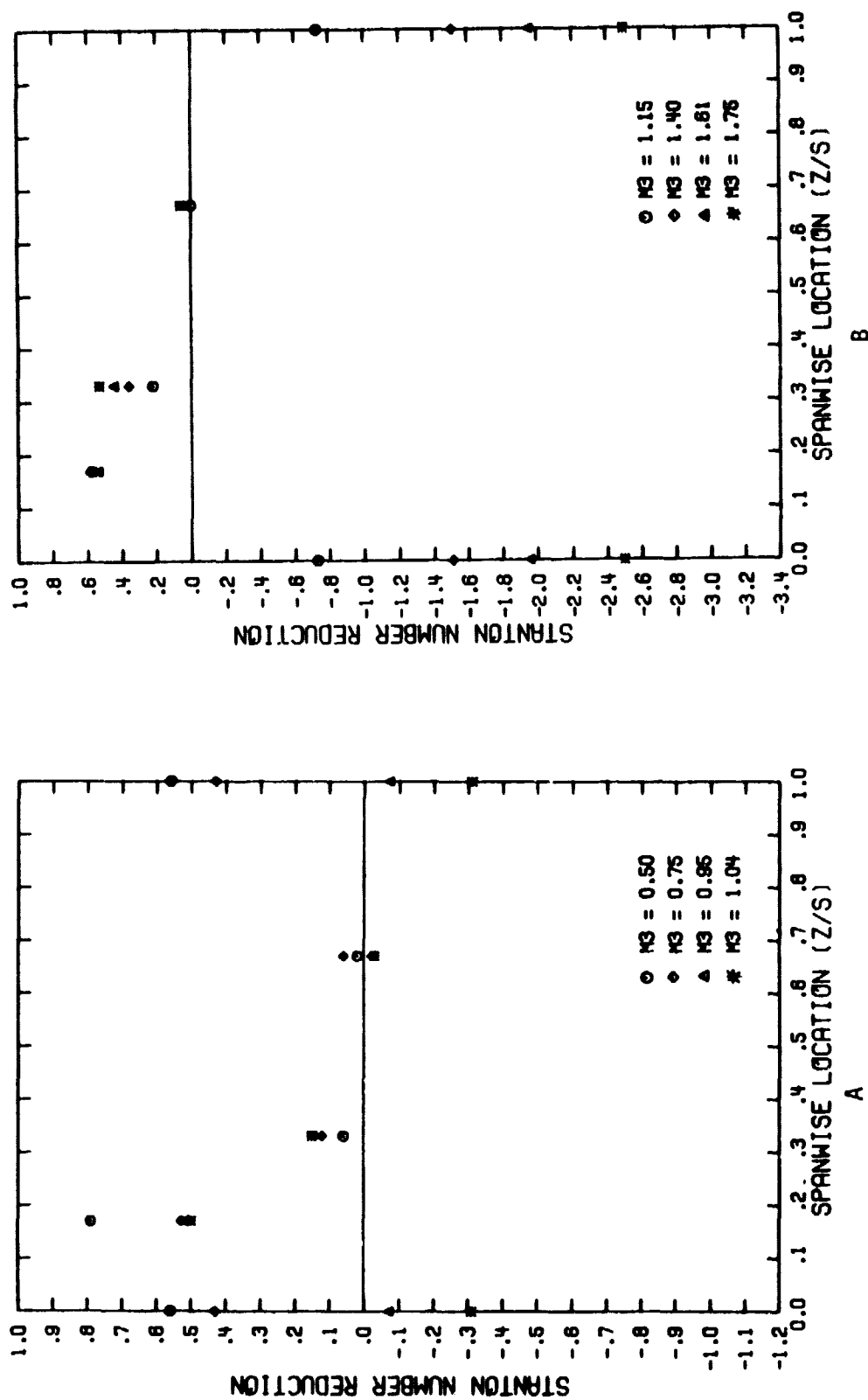


Figure A-37. Spanwise Variation of the Stanton Number Reduction with Single Row Injection
 $(\theta_3=40.8^\circ, s/d_0=10, (x/d_0)=1.5)$

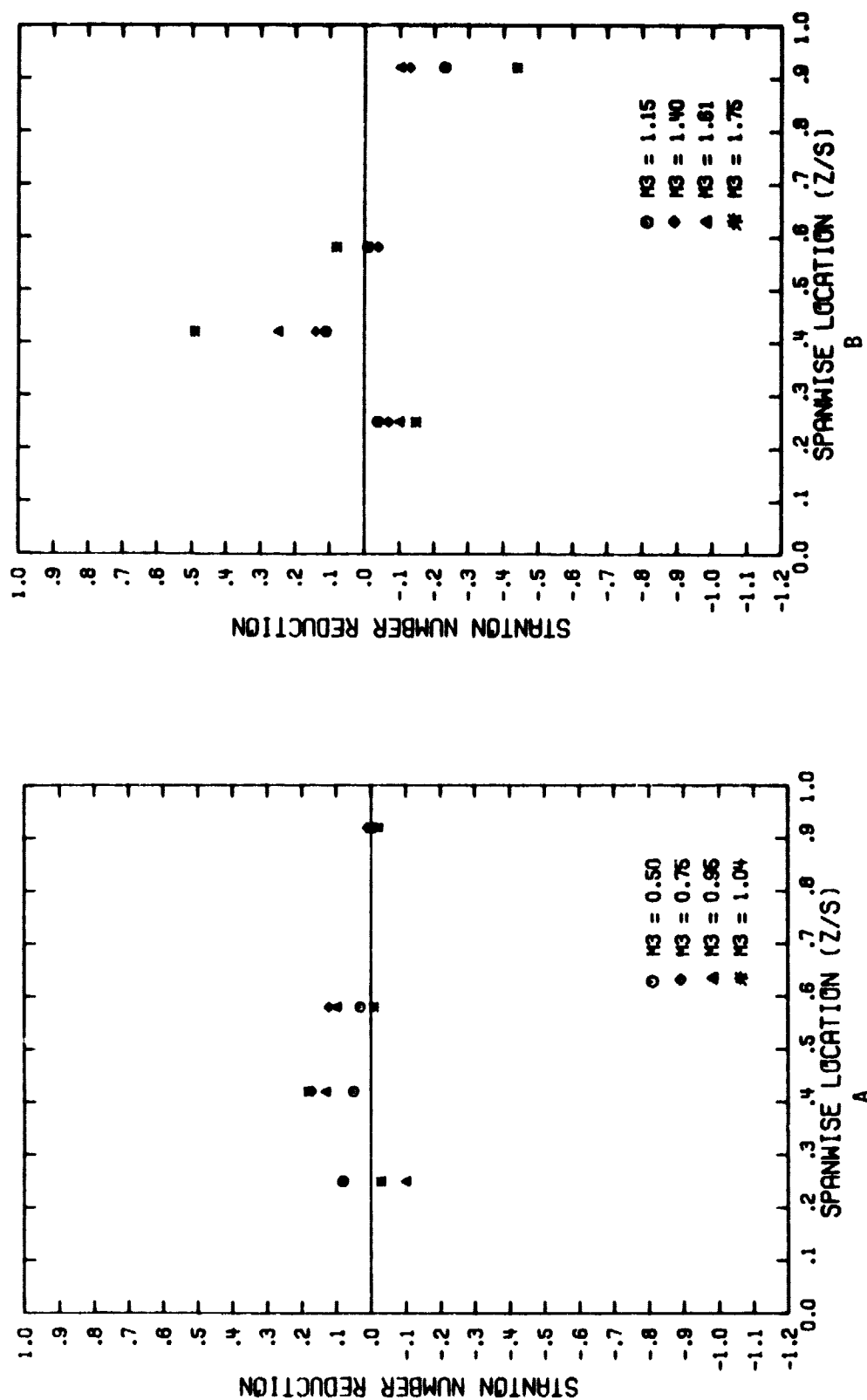


Figure A-38. Spanwise Variation of the Stanton Number Reduction with Single Row Injection
 $(\theta_3=40.80^\circ, s/d_0=10, (x/d_0)=6.5)$

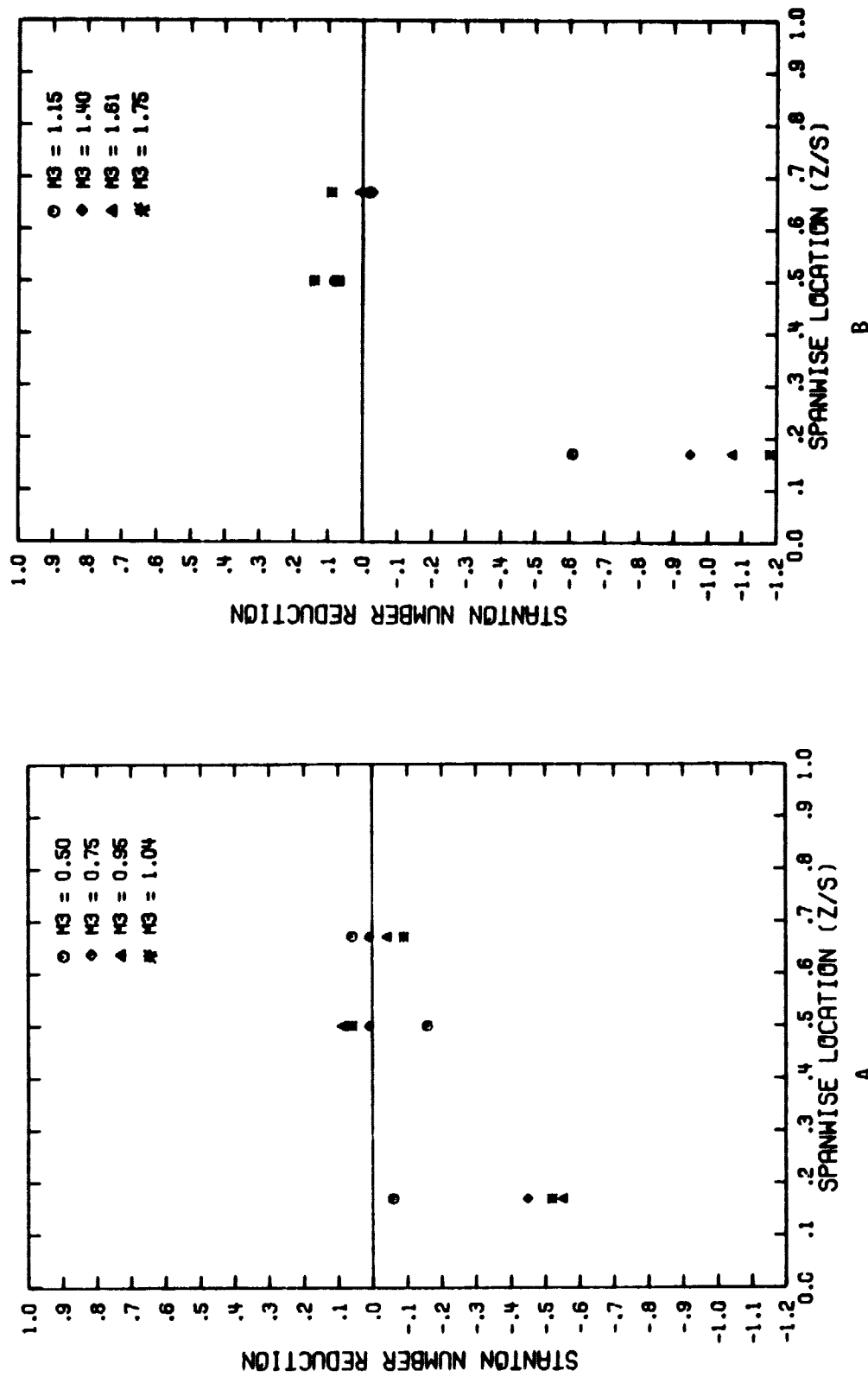


Figure A-39. Spanwise Variation of the Stanton Number Reduction with Single Row Injection
 $(\Theta_3=40.8^\circ, s/d_0=10, (x/d_0)_3=11.5)$

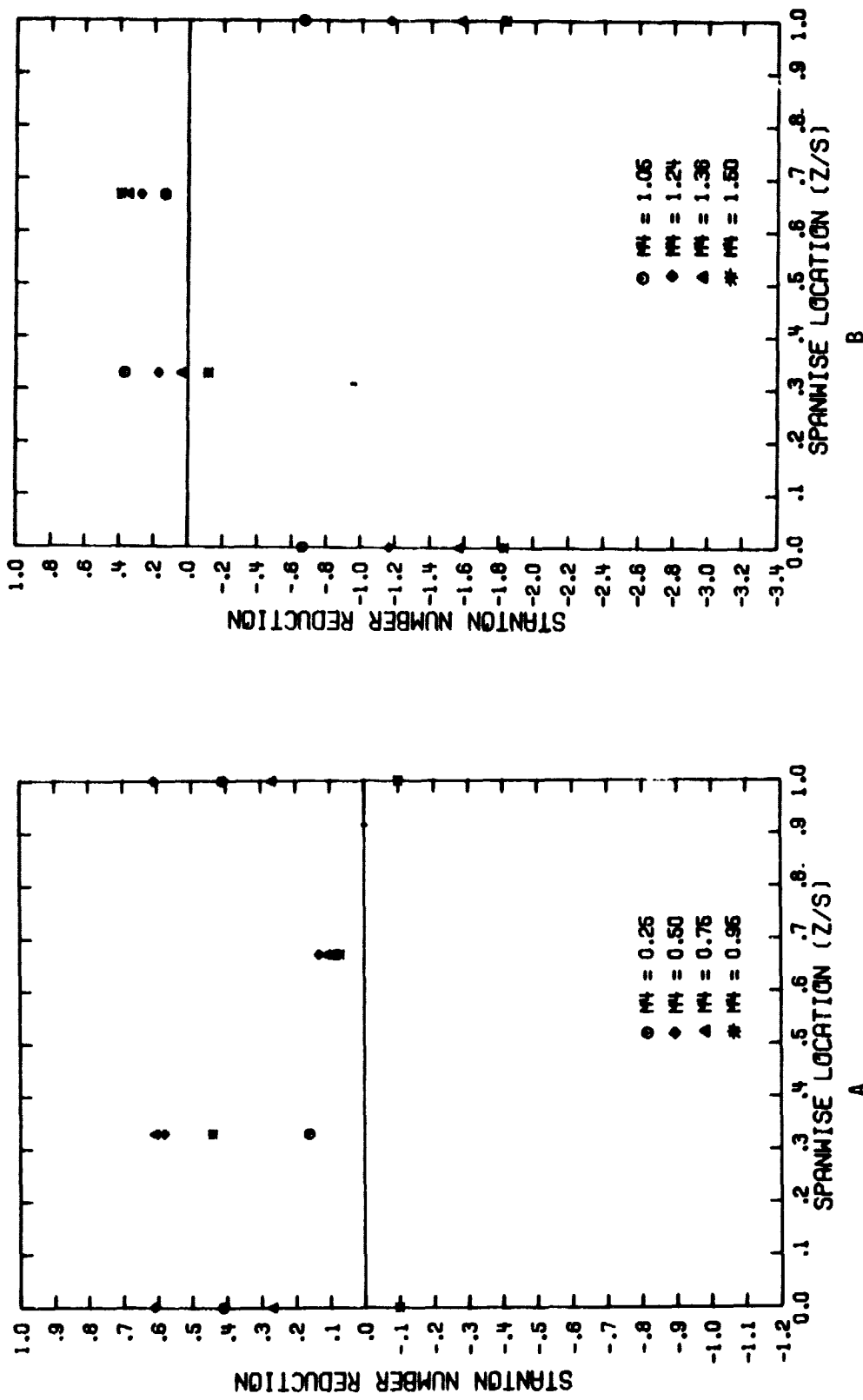


Figure A-40. Spanwise Variation of the Stanton Number Reduction with Single Row Injection
 $(\Theta_4 = 58.7^\circ, s/d_0 = 5, (x/d_0)_4 = 1.5)$

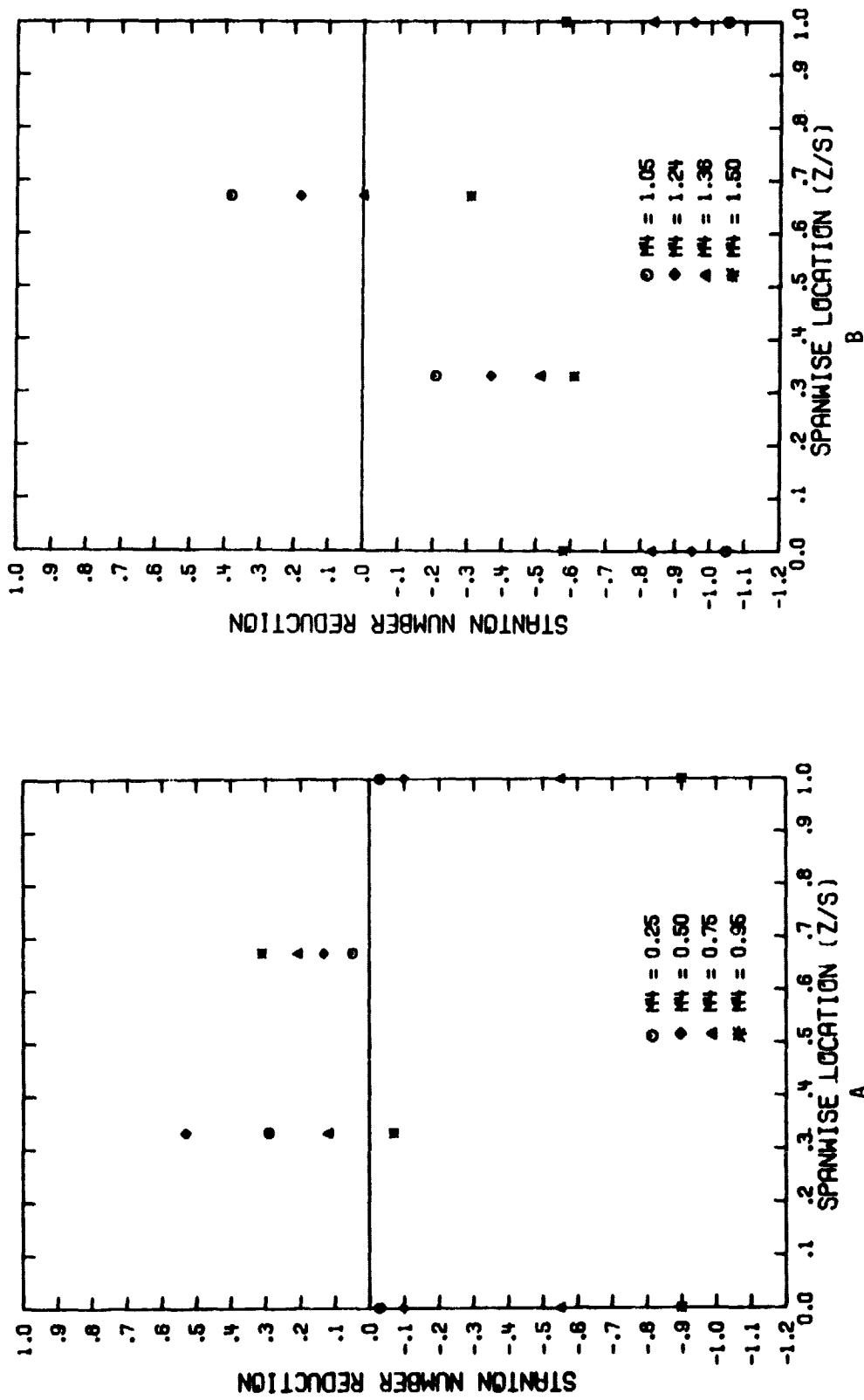


Figure A-41. Spanwise Variation of the Stanton Number Reduction with Single Row Injection
 $(\Theta_4 = 58.7^\circ, s/d_0 = 5, (x/d_0)_4 = 3.5)$

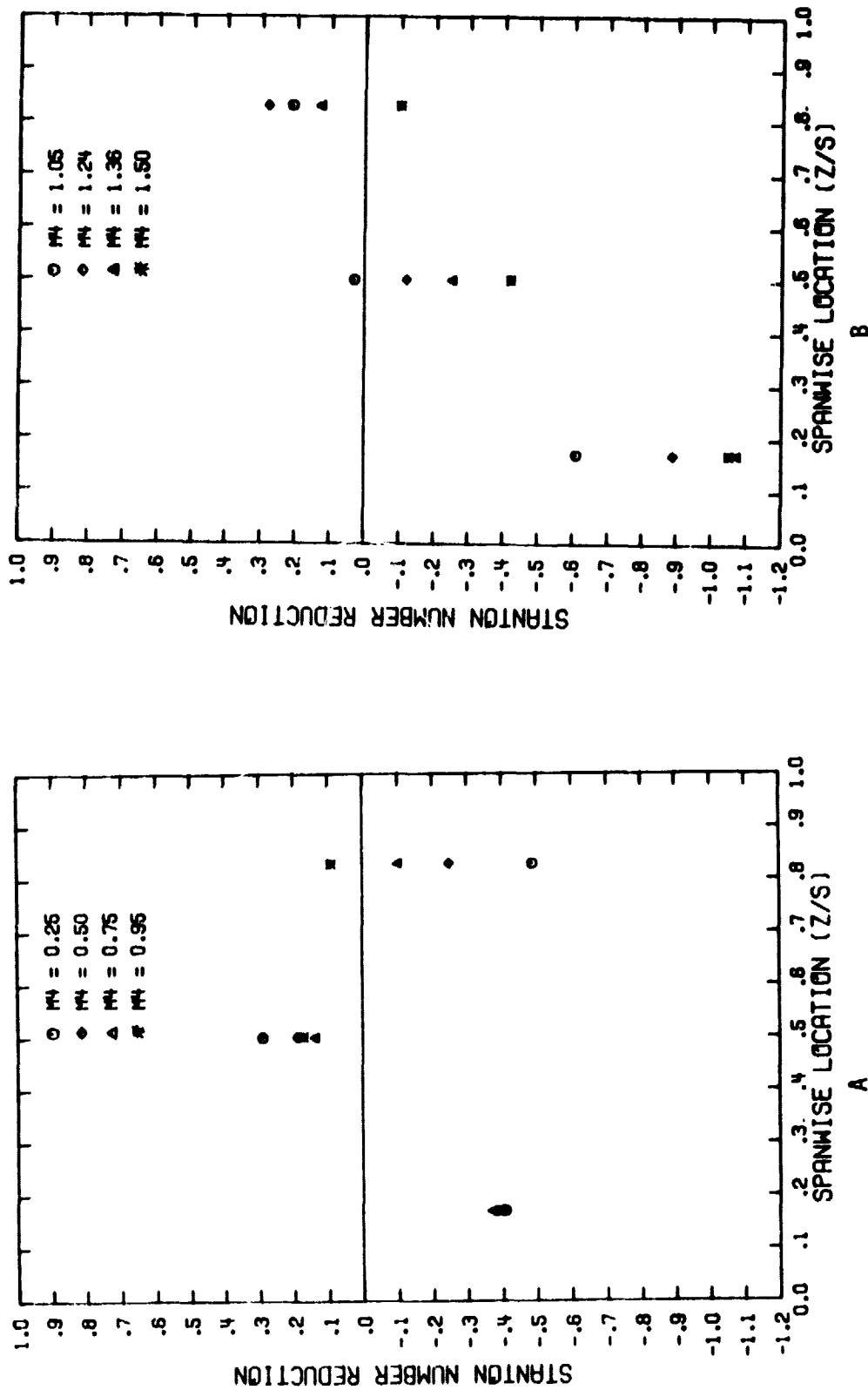


Figure A-42. Spanwise Variation of the Stanton Number Reduction with Single Row Injection
 $(\Theta_4 = 58.7^\circ, s/d_0 = 5, (x/d_0)_4 = 6.5)$

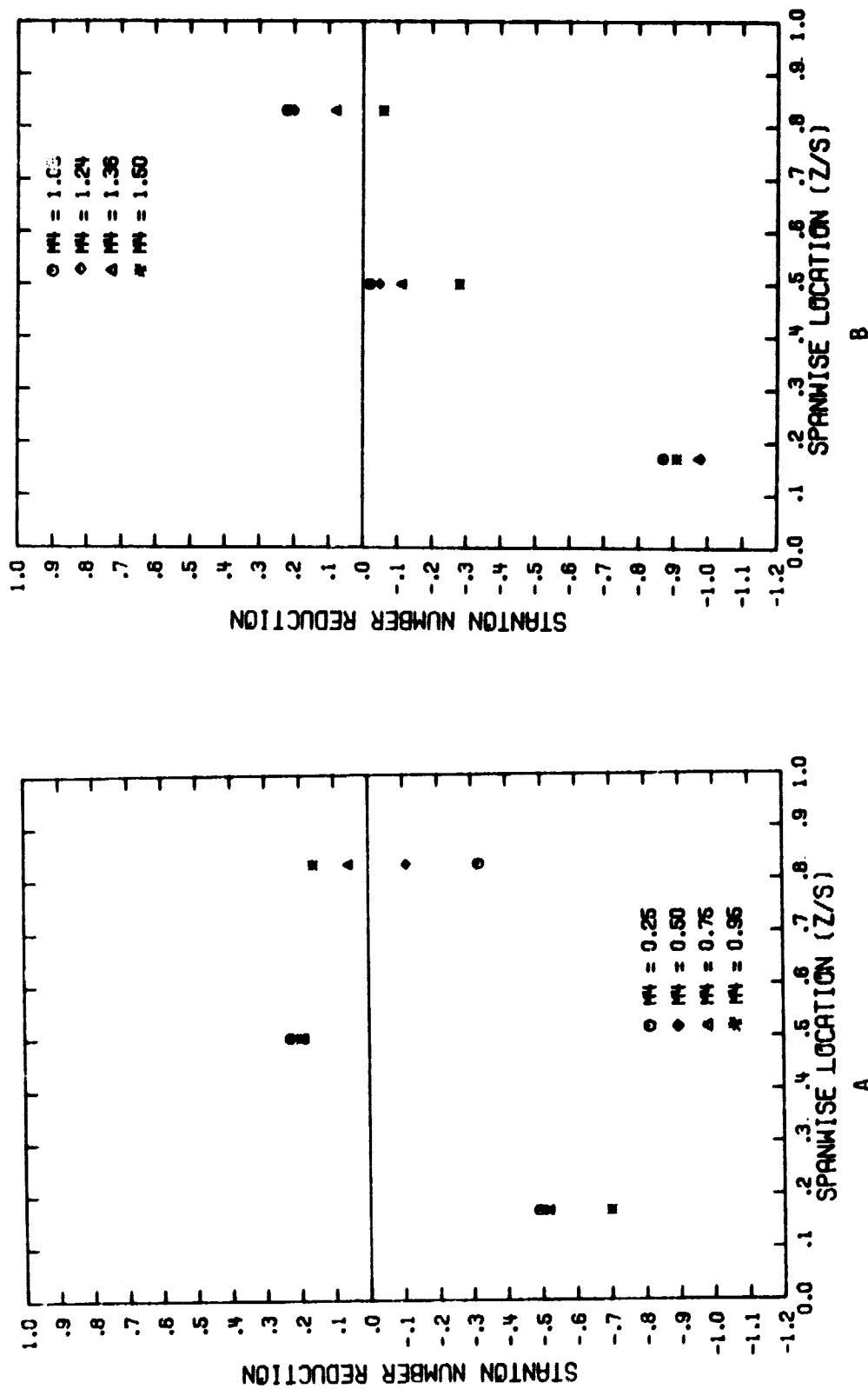


Figure A-43. Spanwise Variation of the Stanton Number Reduction with Single Row Injection
 ($\odot_4 = 58.7^\circ$, $s/d_0 = 5$, $(x/d_0)_4 = 8.5$)

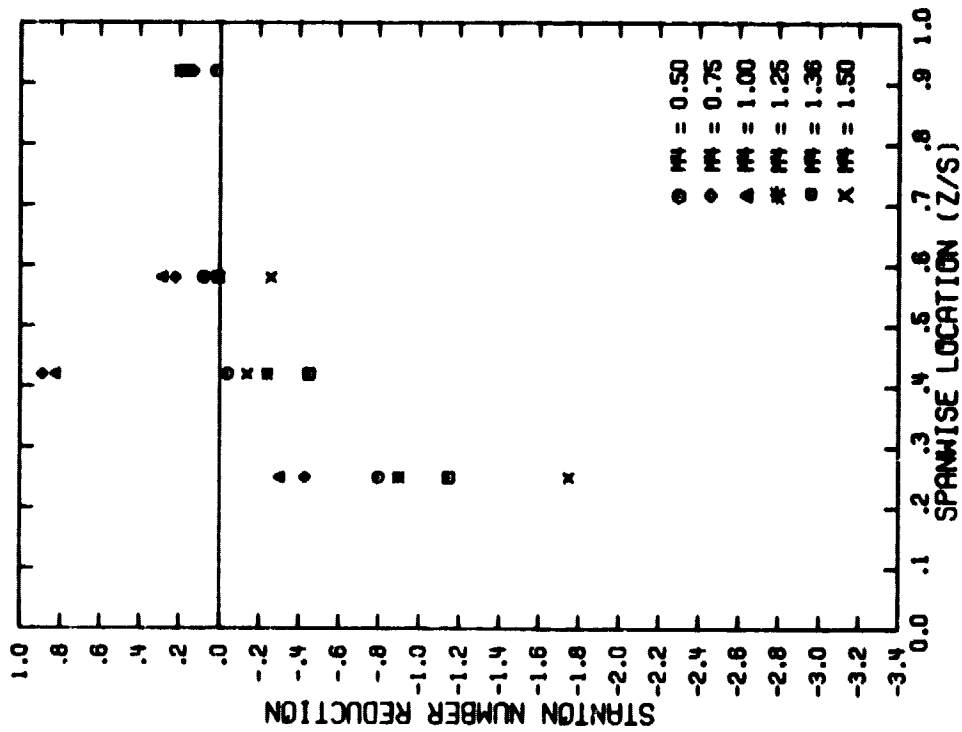


Figure A-44. Spanwise Variation of the Stanton Number Reduction with Single Row Injection ($\theta = 58.7^\circ$, $s/d_0 = 10$, $(x/d_0)/4 = 1.5$)

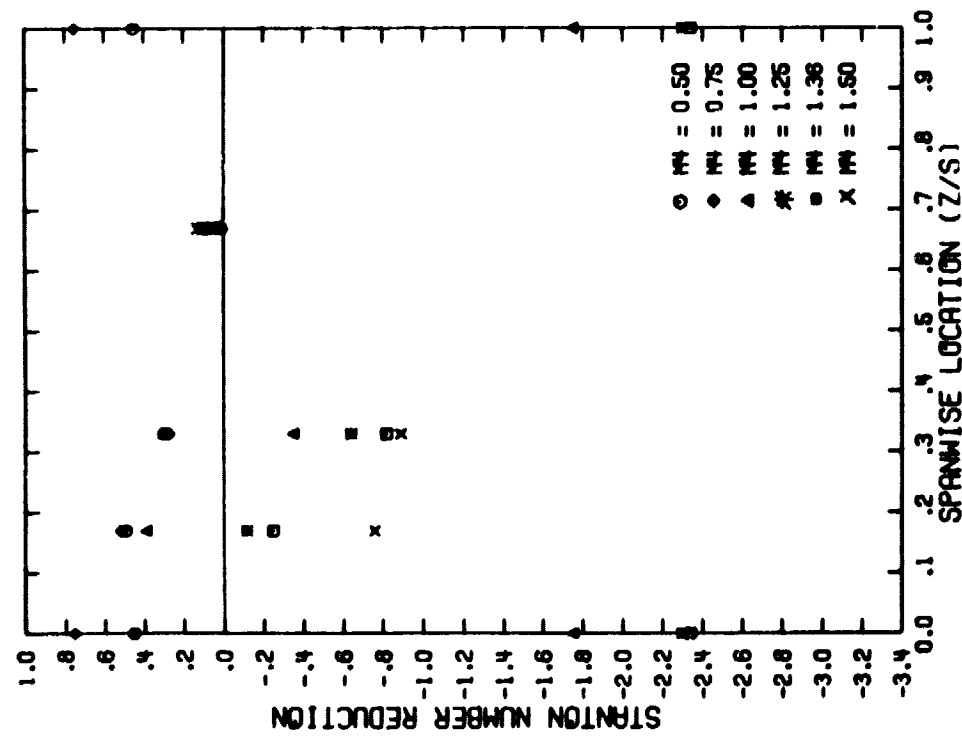


Figure A-45. Spanwise Variation of the Stanton Number Reduction with Single Row Injection ($\theta = 58.7^\circ$, $s/d_0 = 10$, $(x/d_0)/4 = 6.5$)

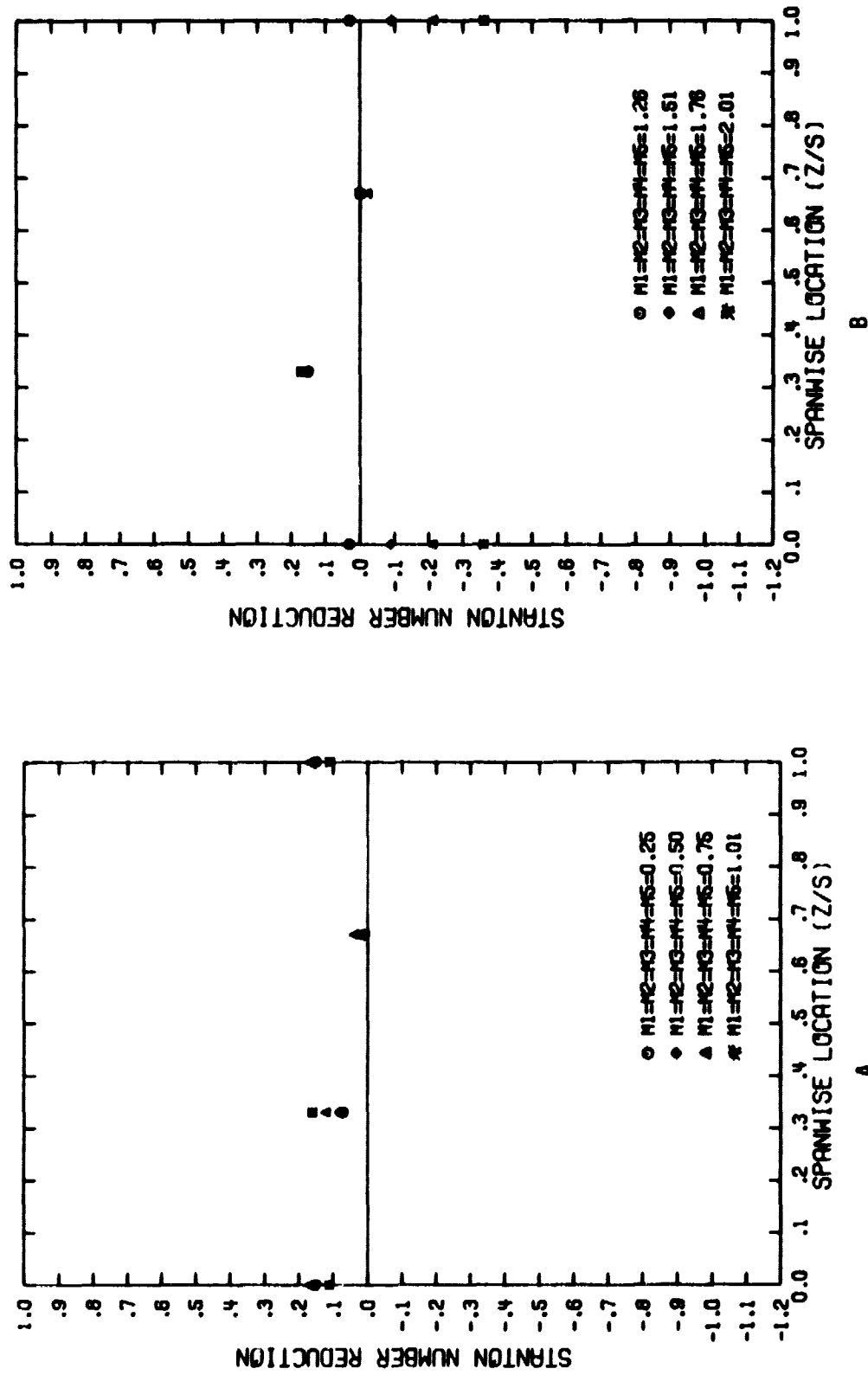


Figure A-46. Spanwise Variation of the Stanton Number Reduction with Uniform Blowing from a Five Row Configuration ($\theta_1=50^\circ$, $s/d_0=P/d_0=5$, $(x/d_0)_1=1.5$)

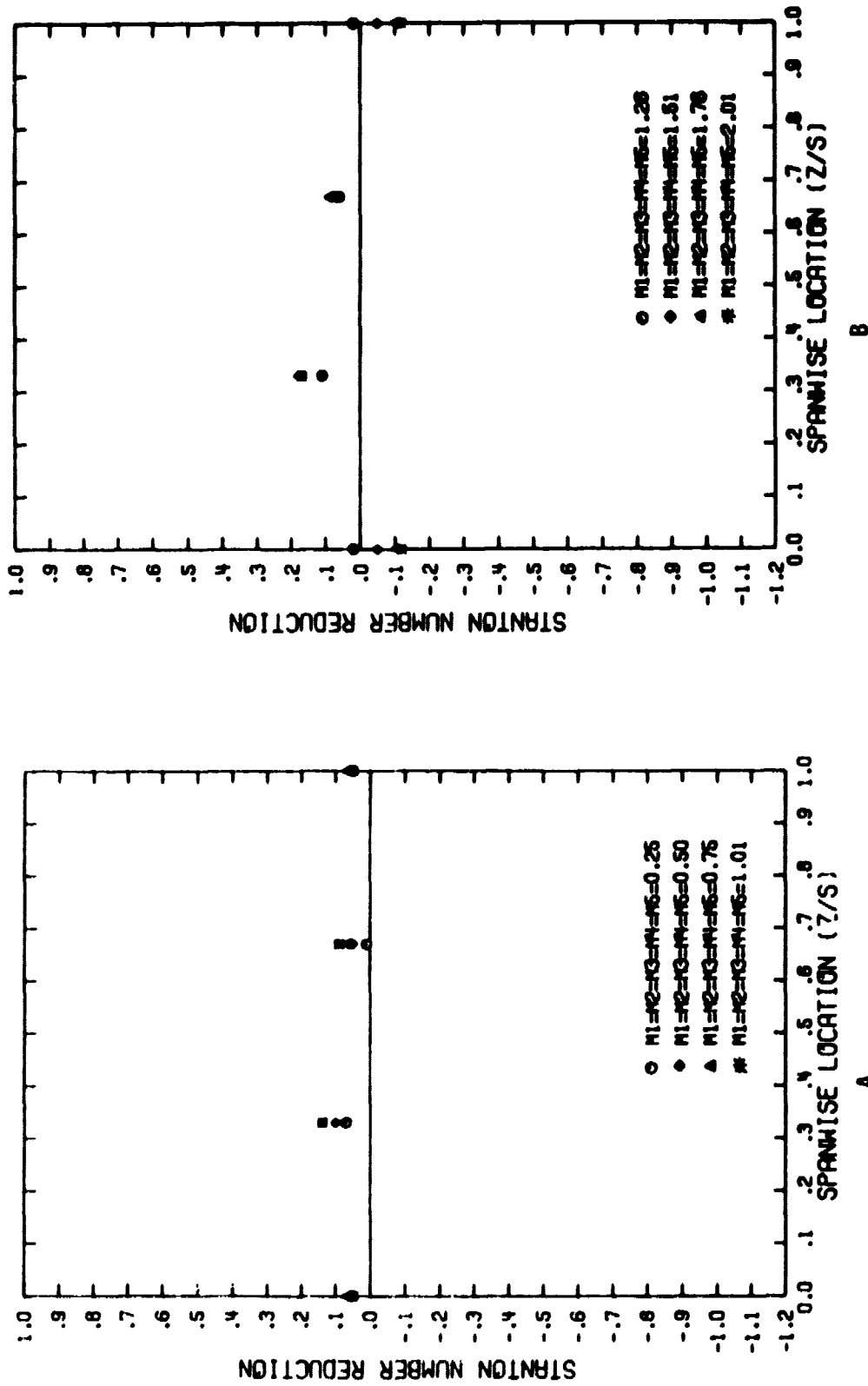


Figure A-47. Spanwise Variation of the Stanton Number Reduction with Uniform Blowing from a Five Row Configuration ($\Theta_1=50^\circ$, $s/d_0=P/d_0=5$, $(x/d_0)_1=3.5$)

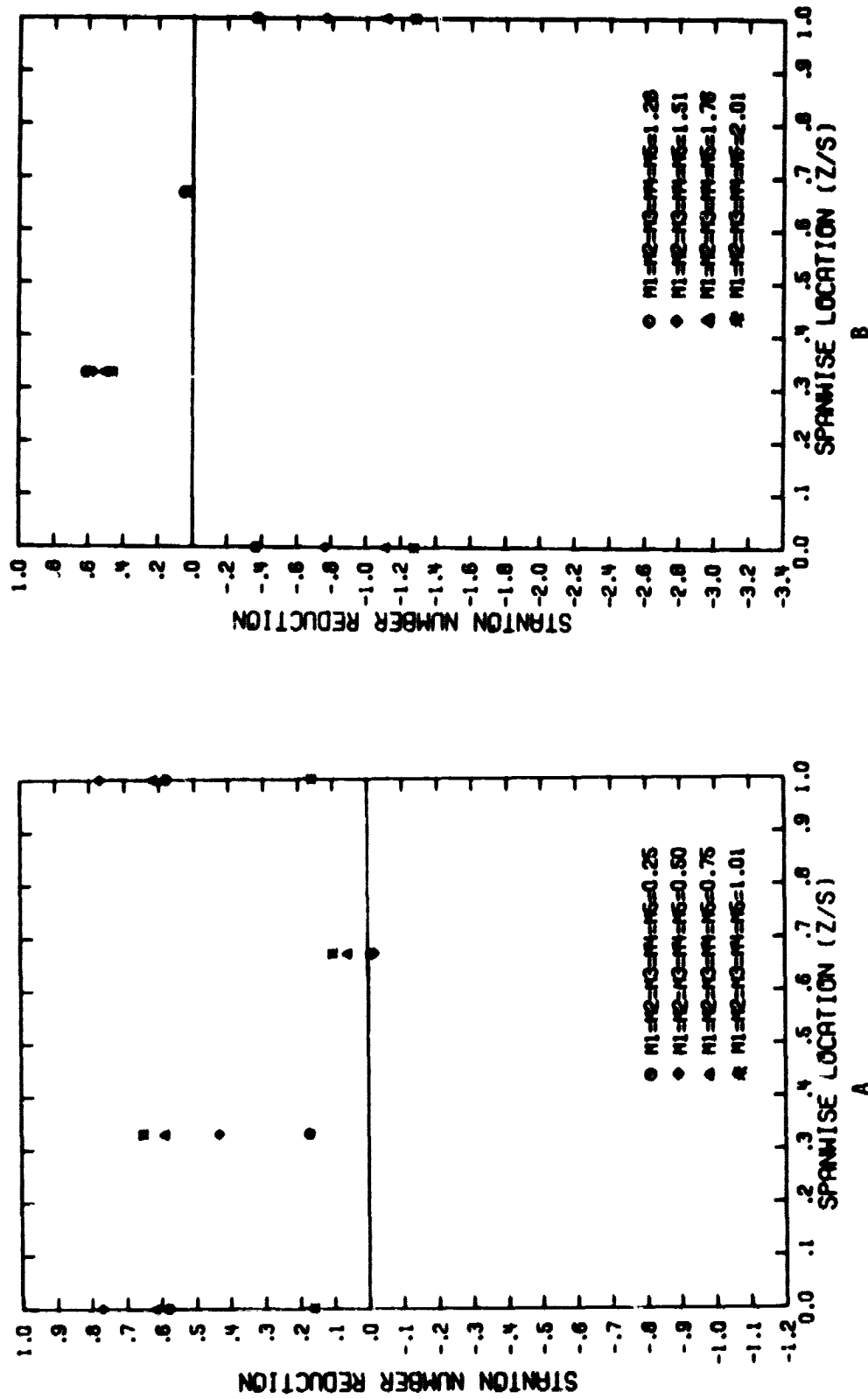


Figure A-48. Spanwise Variation of the Stanton Number Reduction with Uniform Blowing from a Five Row Configuration ($\theta_1=50^\circ$, $\theta_2=22.9^\circ$, $s/d_0=P/d_0=5$, $(x/d_0)_2=1.5$)

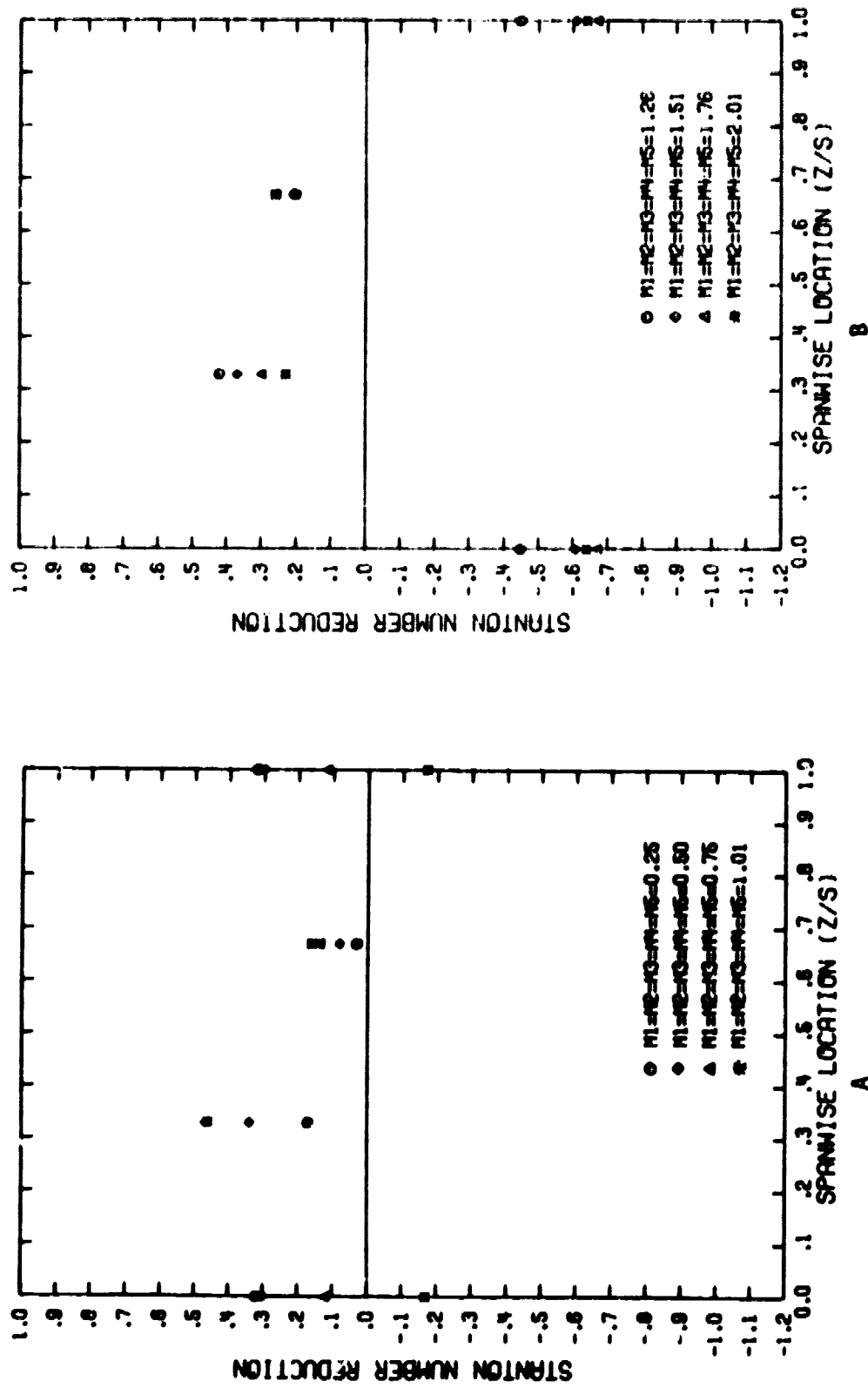


Figure A-49. Spanwise Variation of the Stanton Number: Reduction with Uniform Blowing from a Five Row Configuration ($\theta_1=5^\circ$, $\theta_2=22.9^\circ$, $s/d_0=5$, $(x/d_0)^2=3.5$)

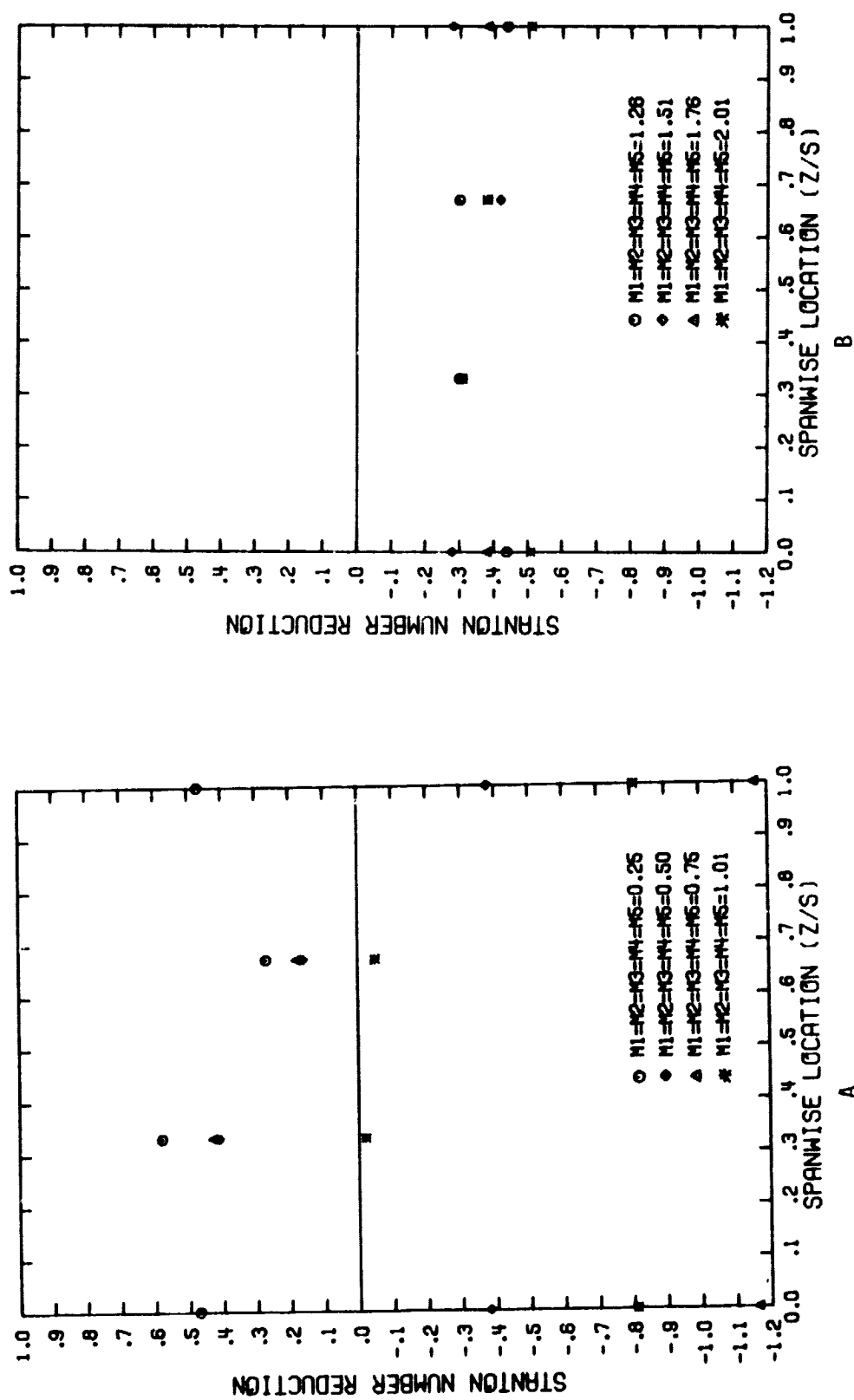


Figure A-50. Spanwise Variation of the Stanton Number Reduction with Uniform Blowing from a Five Row Configuration ($\theta_1=50^\circ$, $\theta_2=22.9^\circ$, $\theta_3=40.8^\circ$, $s/d_0=P/d_0=5$, $(x/d_0)^{1/3}=1.5$)

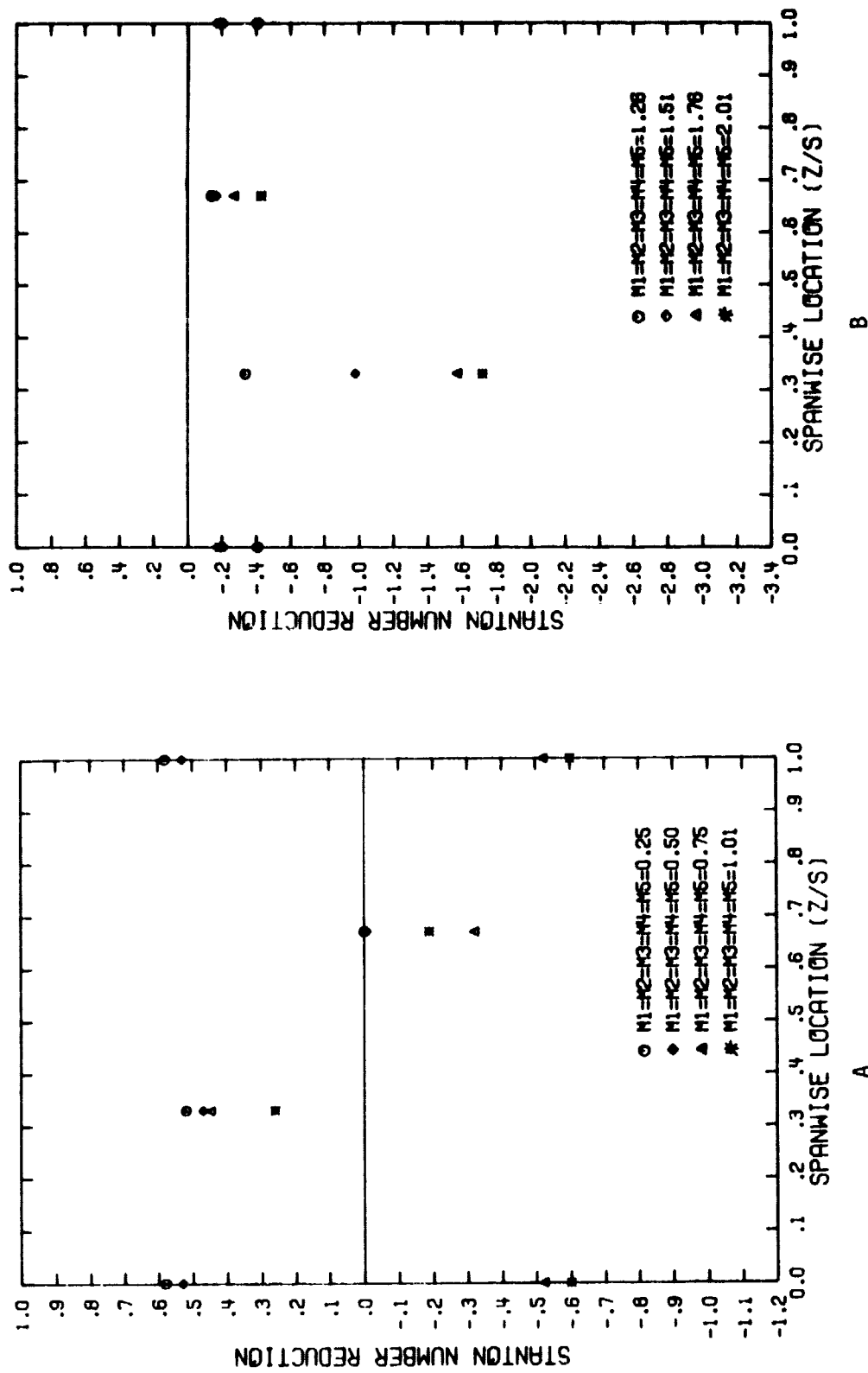


Figure A-51. Spanwise Variation of the Stanton Number Reduction with Uniform Blowing from a Five Row Configuration ($\theta_1=5^\circ$, $\theta_2=22.9^\circ$, $\theta_3=40.8^\circ$, $\theta_4=58.7^\circ$, $s/d_0=P/d_0=5$, $(x/d_0)_4=1.5$)

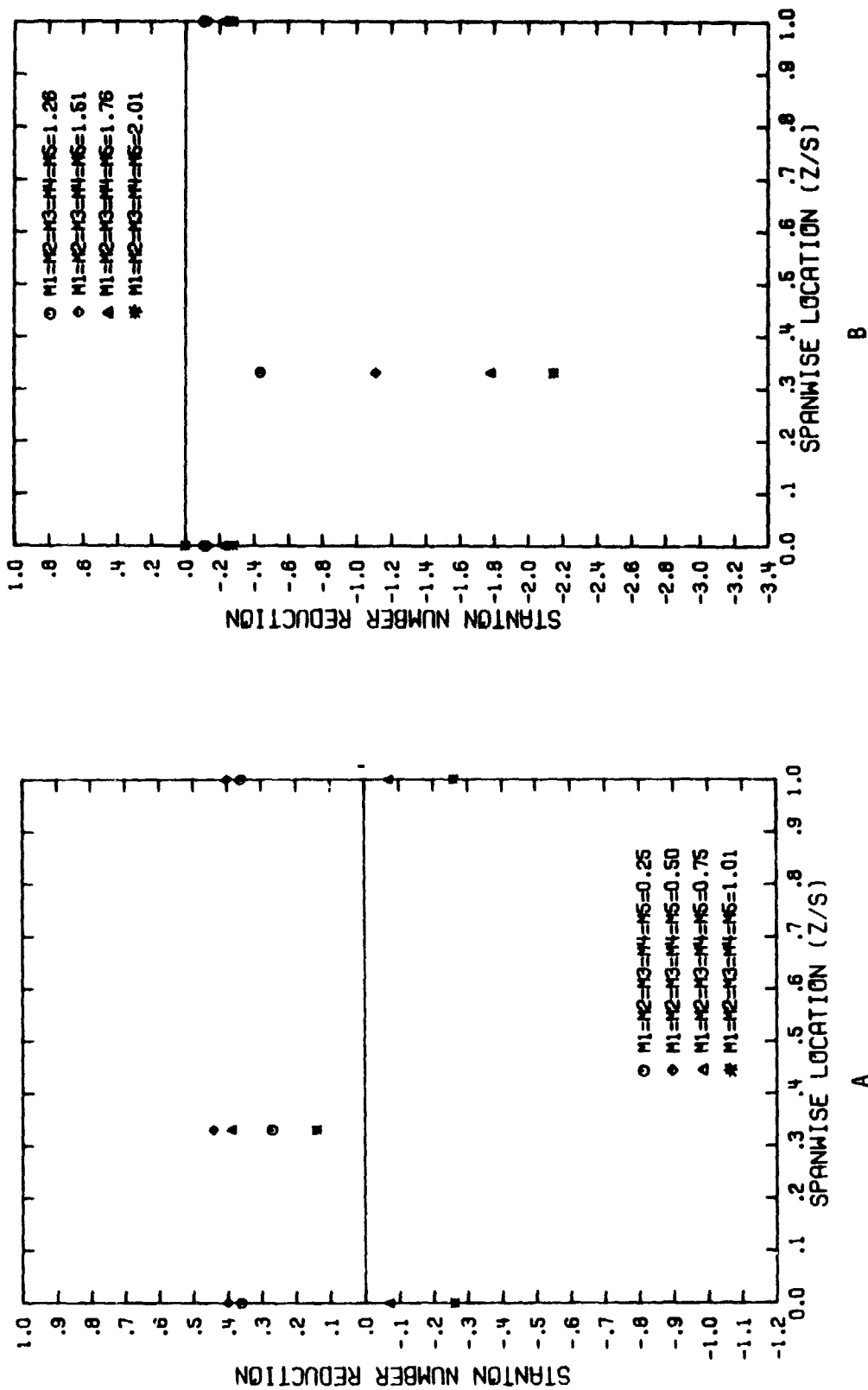


Figure A-52. Spanwise Variation of the Stanton Number Reduction with Uniform Blowing from a Five Row Configuration ($\theta_1=50^\circ$, $\theta_2=22.9^\circ$, $\theta_3=40.8^\circ$, $\theta_4=58.7^\circ$, $\theta_5=76.6^\circ$, $s/d_0=P/d_0=5$, $(x/d_0)_5=1.5$)

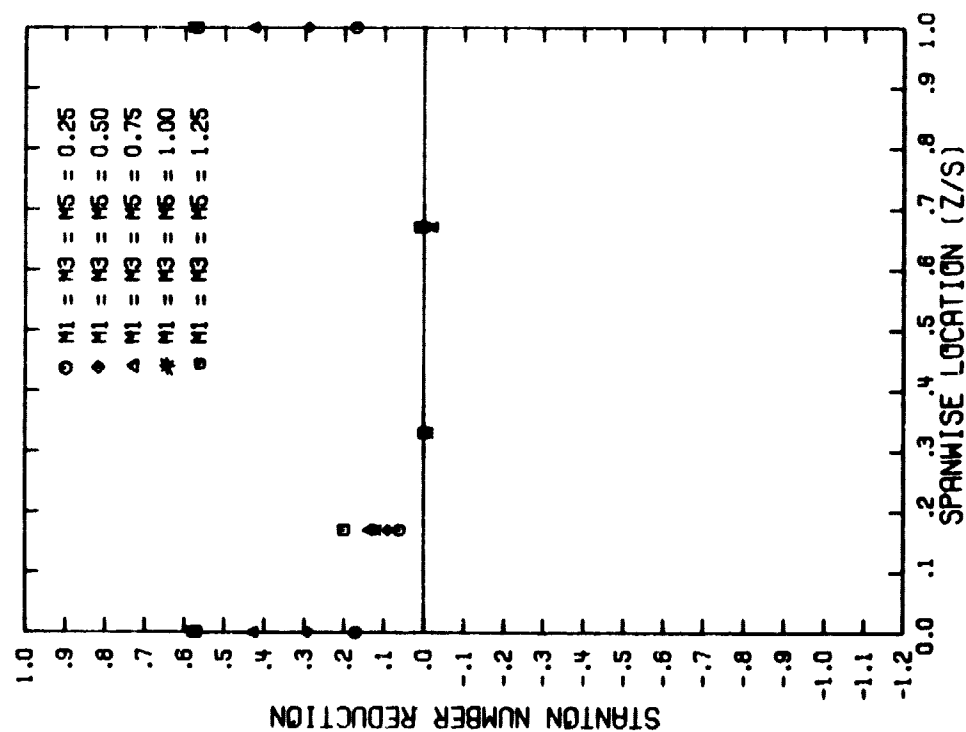
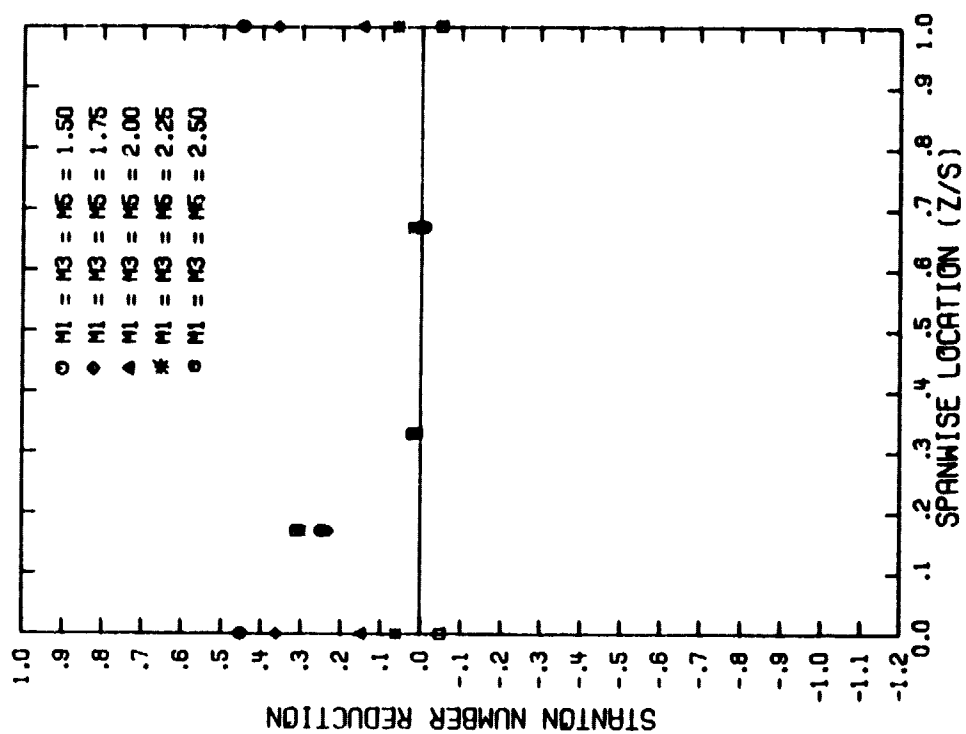


Figure A-53. Spanwise Variation of the Stanton Number Reduction with Uniform Blowing from a Three Row Configuration ($\theta_1=50^\circ$, $s/d_0=P/d_0=10$, $(x/d_0)\gamma=1.5$)

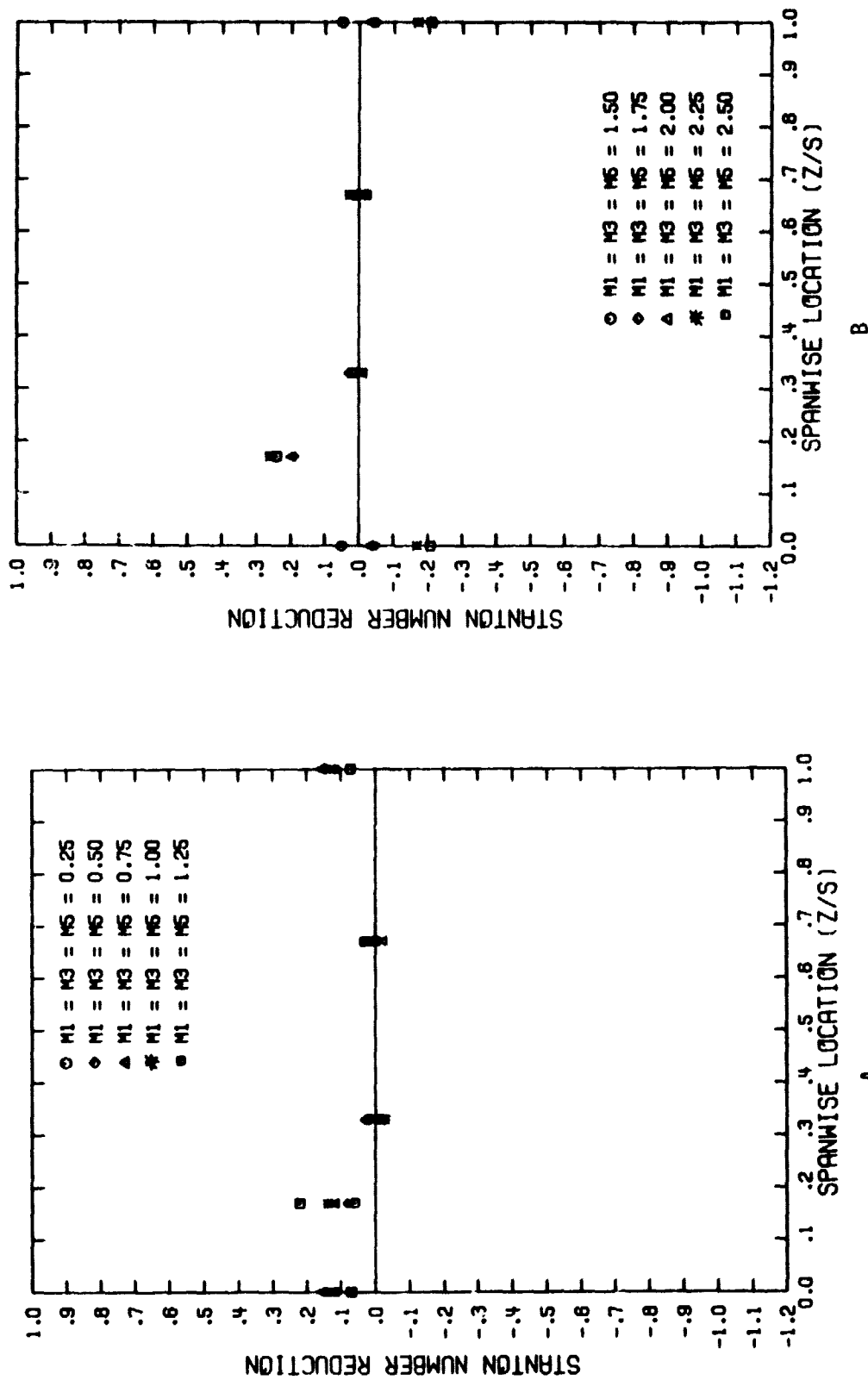


Figure A-54. Spanwise Variation of the Stanton Number Reduction with Uniform Blowing from a Three Row Configuration ($\Theta_1=5^\circ$, $s/d_0=P/d_0=10$, $(x/d_0)_1=3.5$)

ORIGINAL PAGE IS
OF POOR QUALITY

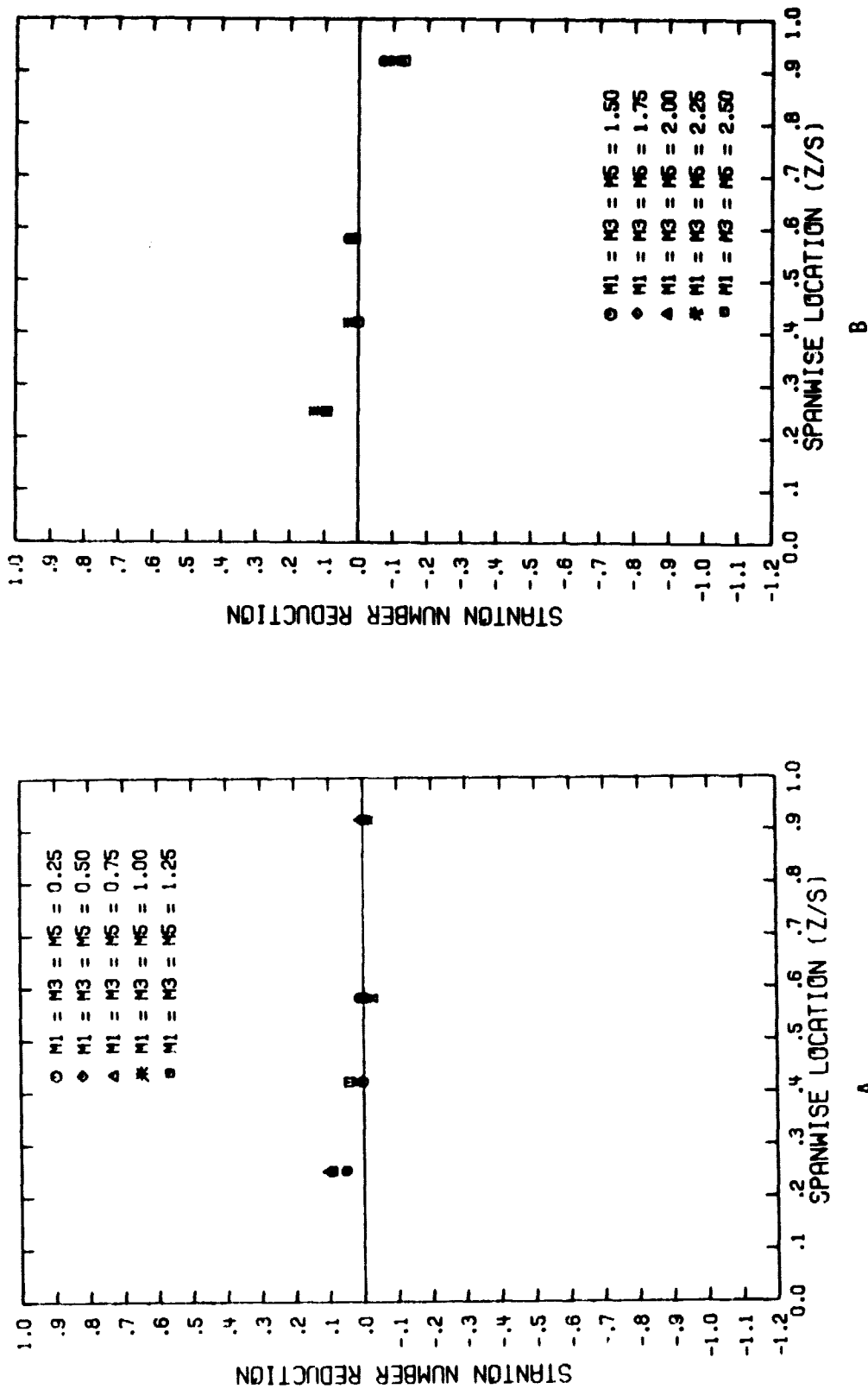


Figure A-55. Spanwise Variation of the Stanton Number Reduction with Uniform Blowing from a Three Row Configuration ($\Theta_1=50^\circ$, $s/d_0=P/d_0=10$, $(x/d_0)_1=6.5$)

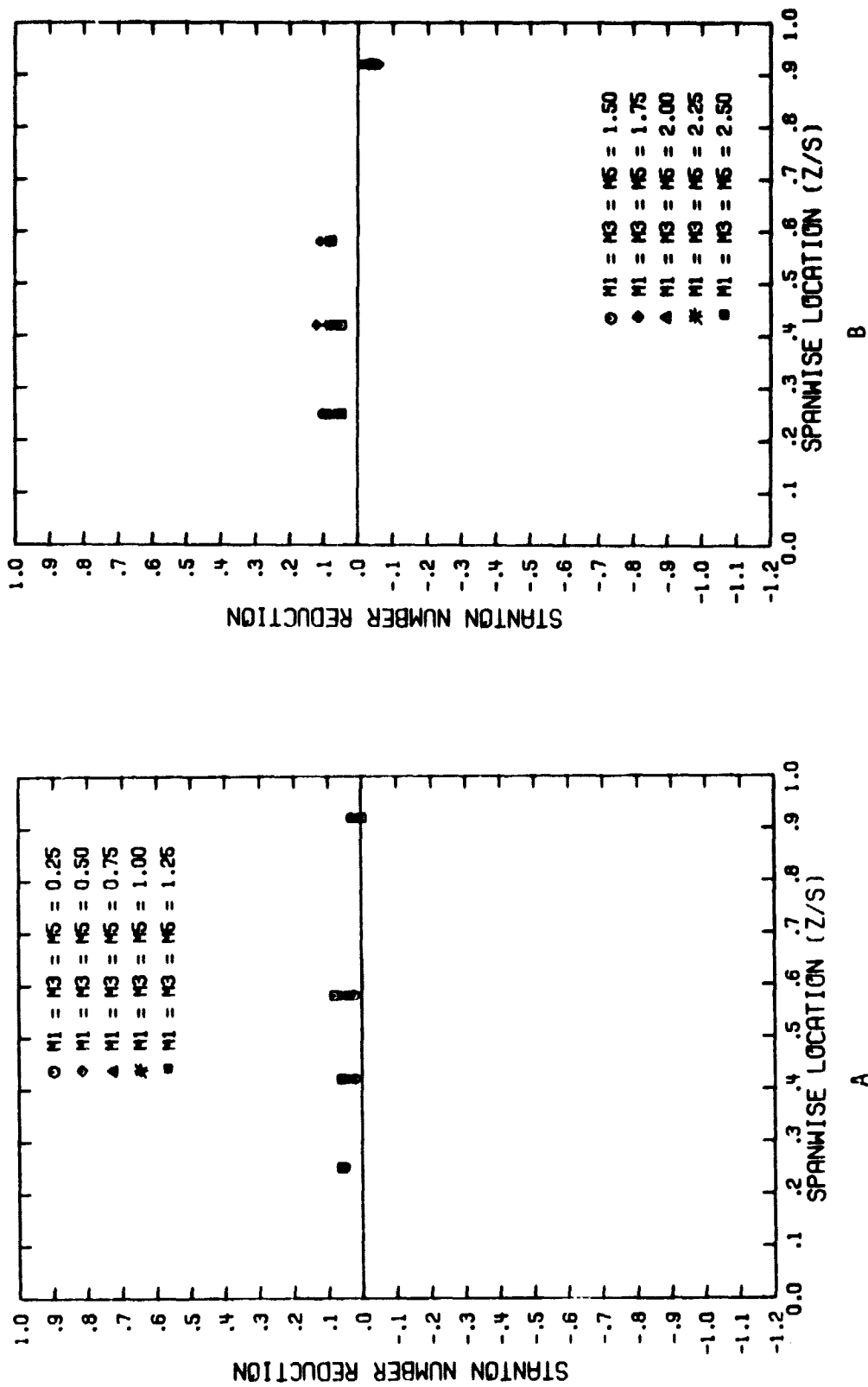


Figure A-56. Spanwise Variation of the Stanton Number Reduction with Uniform Blowing from a Three Row Configuration ($\theta_1=50^\circ$, $s/d_0=P/d_0=10$, $(x/d_0)_1=8.5$)

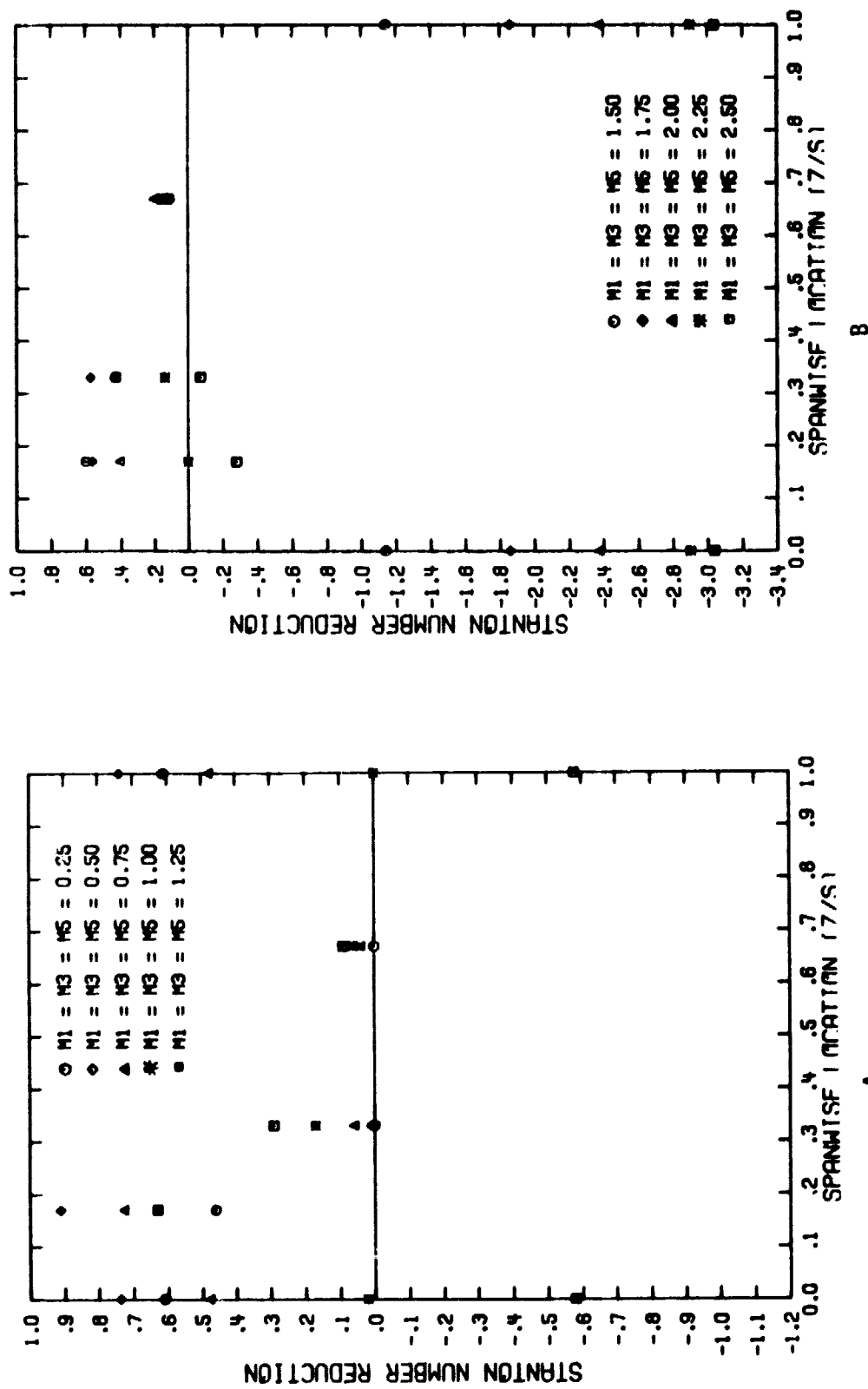


Figure A-57. Spanwise Variation of the Stanton Number Reduction with Uniform Blowing from a Three Row Configuration ($\theta_1=5^\circ$, $\theta_3=40.8^\circ$, $s/d_0=P/d_0=10$, $(x/d_0)_3=1.5$)

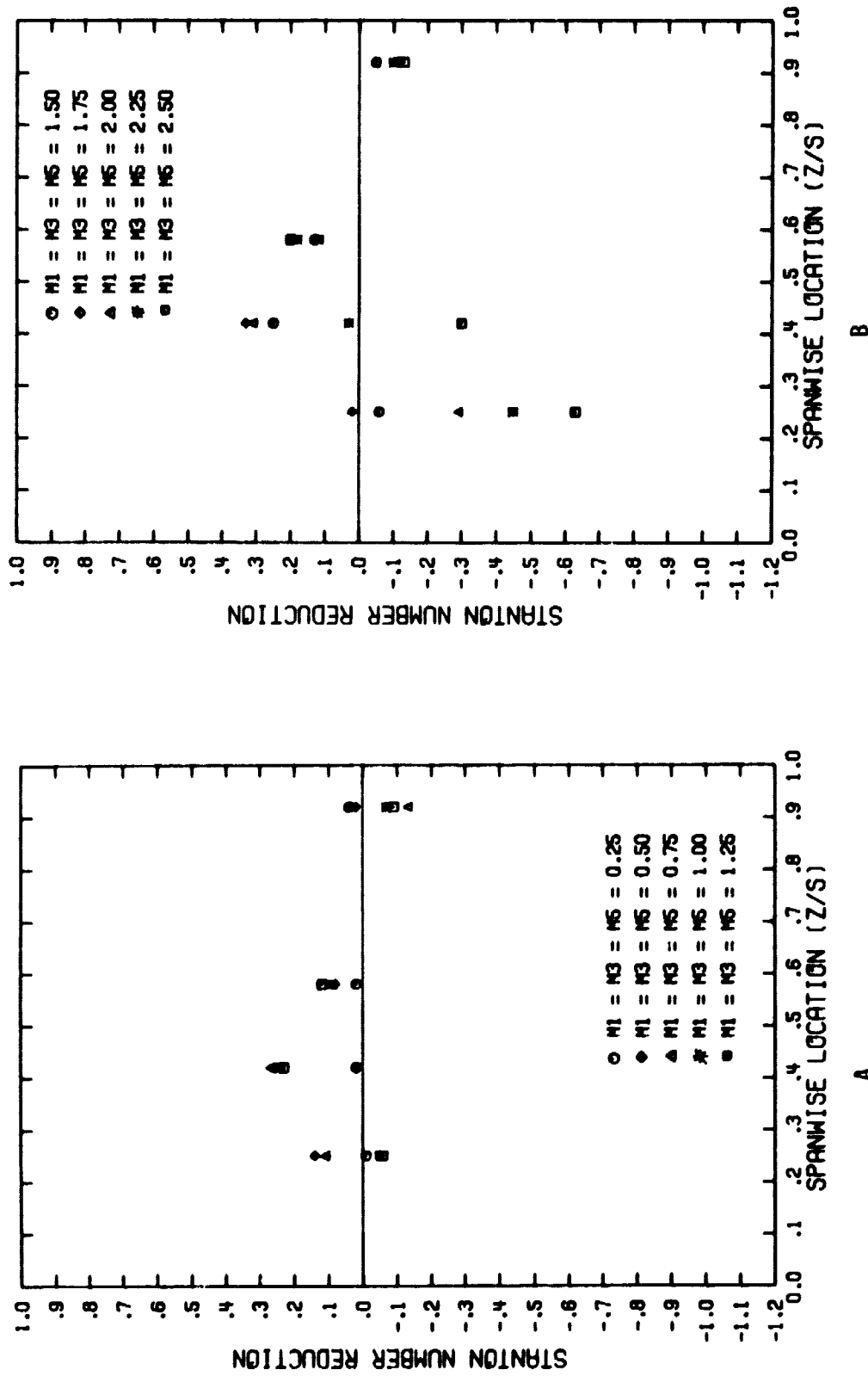


Figure A-58. Spanwise Variation of the Stanton Number Reduction with Uniform Blowing from a Three Row Configuration ($\Theta_1=5^\circ$, $\Theta_3=40.8^\circ$, $s/d_0=P/d_0=10$, $(x/d_0)^3=6.5$)

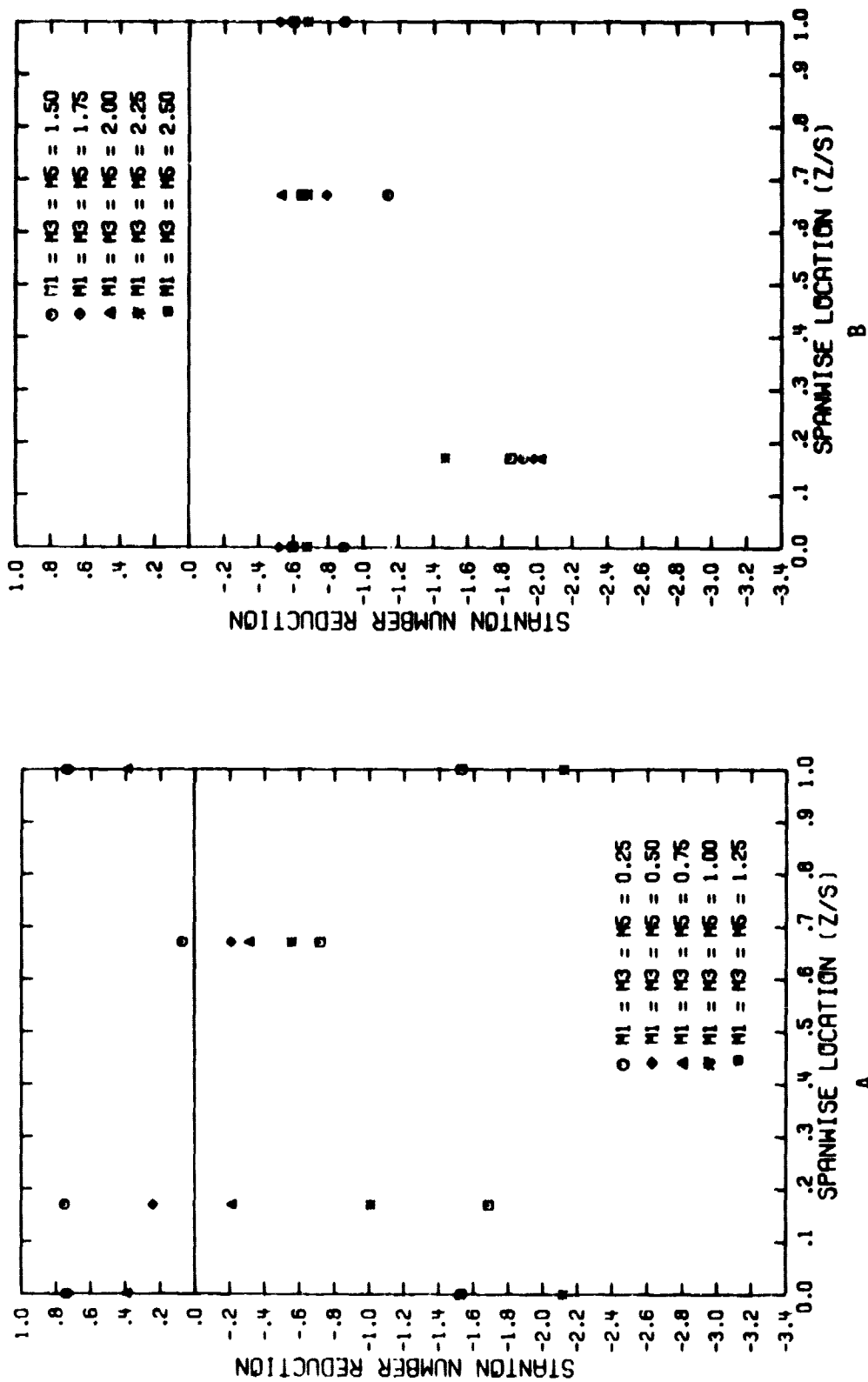


Figure A-59. Spanwise Variation of the Stanton Number Reduction with Uniform Blowing from a Three Row Configuration ($\theta_1=50^\circ$, $\theta_3=40.8^\circ$, $\theta_5=76.6^\circ$, $s/d_0=P/d_0=10$, $(x/d_0)_5=1.5$)

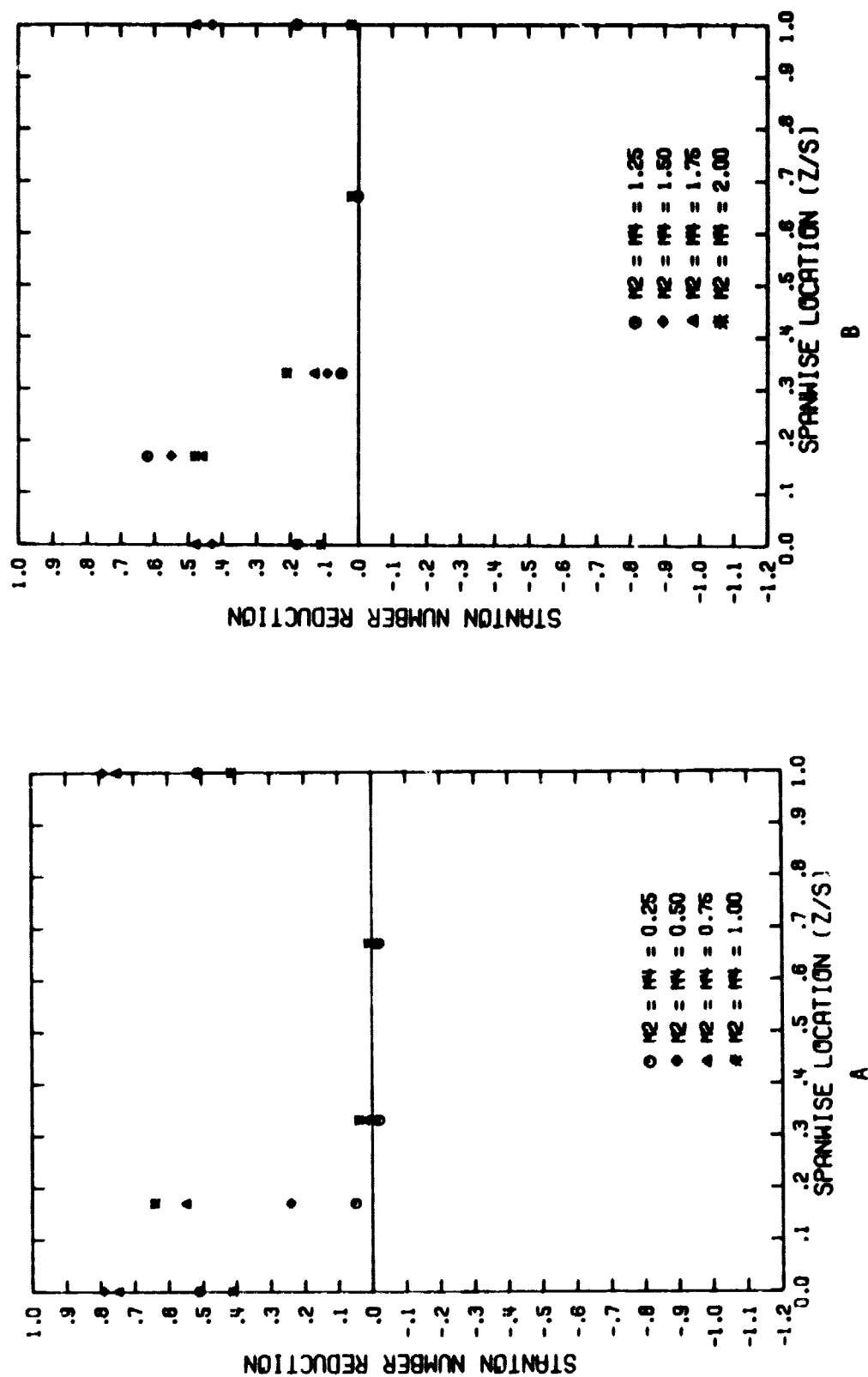


Figure A-60. Spanwise Variation of the Stanton Number Reduction with Uniform Blowing from a Two Row Configuration ($\Theta_2=22.90^\circ$, $s/d_0=P/d_0=10$, $(x/d_0)_2=1.5$)

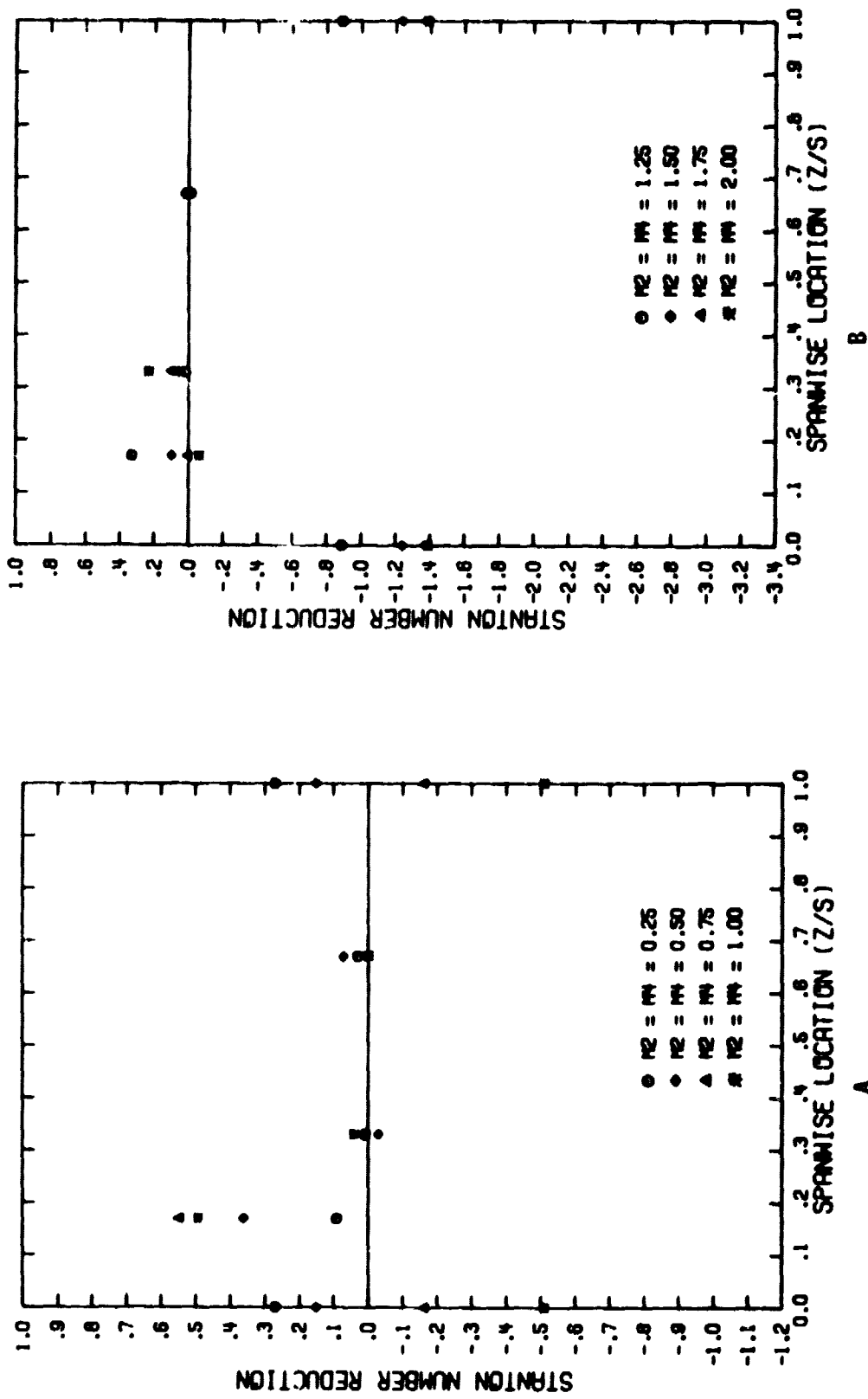


Figure A-61. Spanwise Variation of the Stanton Number Reduction with Uniform Blowing from a Two Row Configuration ($\theta_2 = 22.90^\circ$, $s/d_0 = P/d_0 = 10$, $(x/d_0)^2 = 3.5$)

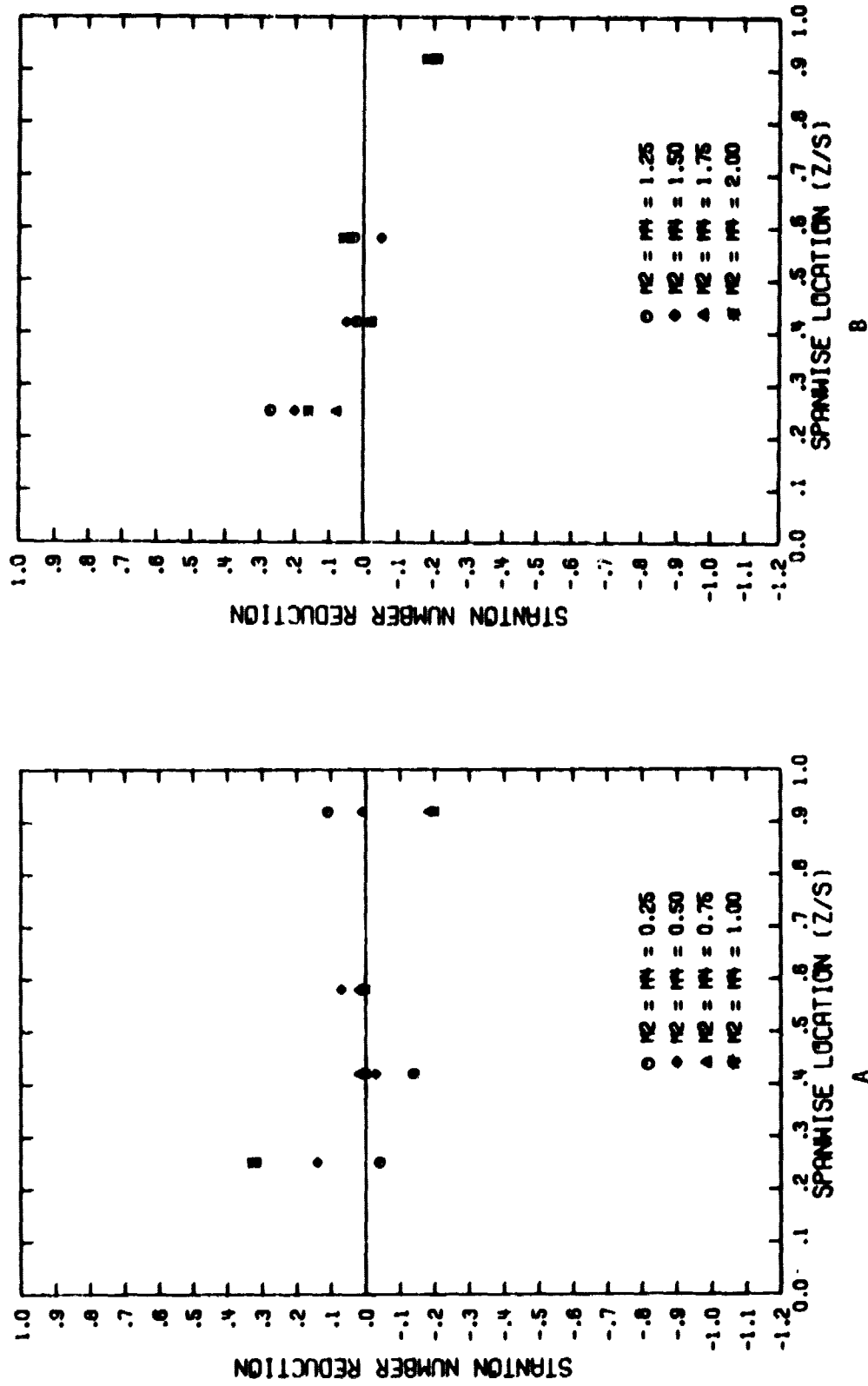


Figure A-62. Spanwise Variation of the Stanton Number Reduction with Uniform Blowing from a Two Row Configuration ($\theta_2 = 22.90^\circ$, $s/d_o = p/d_o = 10$, $(x/d_o)_2 = 6.5$)

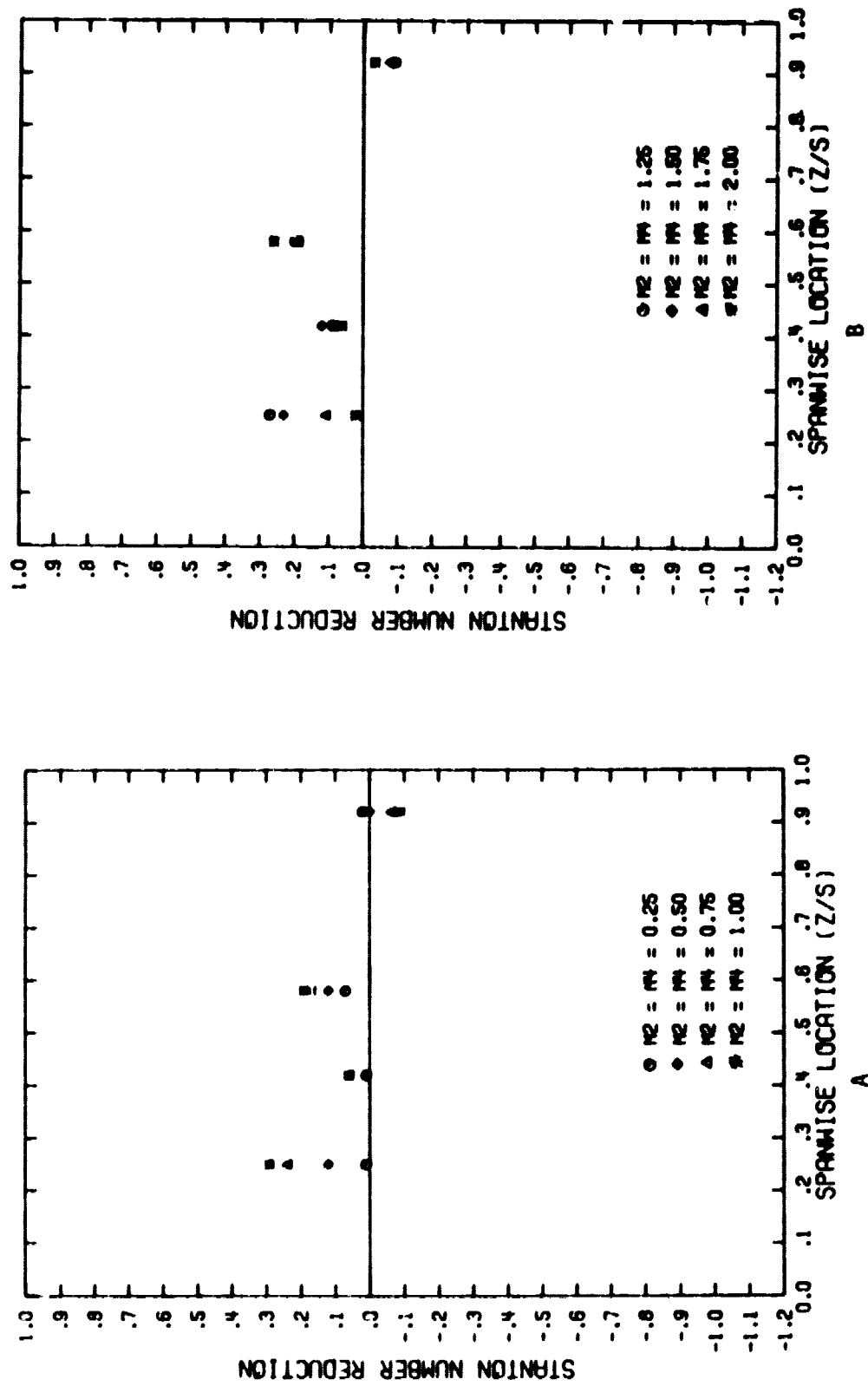


Figure A-63. Spanwise Variation of the Stanton Number Reduction with Uniform Blowing from a Two Row Configuration ($\theta = 22.9^\circ$, $s/d_0 = P/d_0 = 10$, $(x/d_0)^2 = 8.5$)

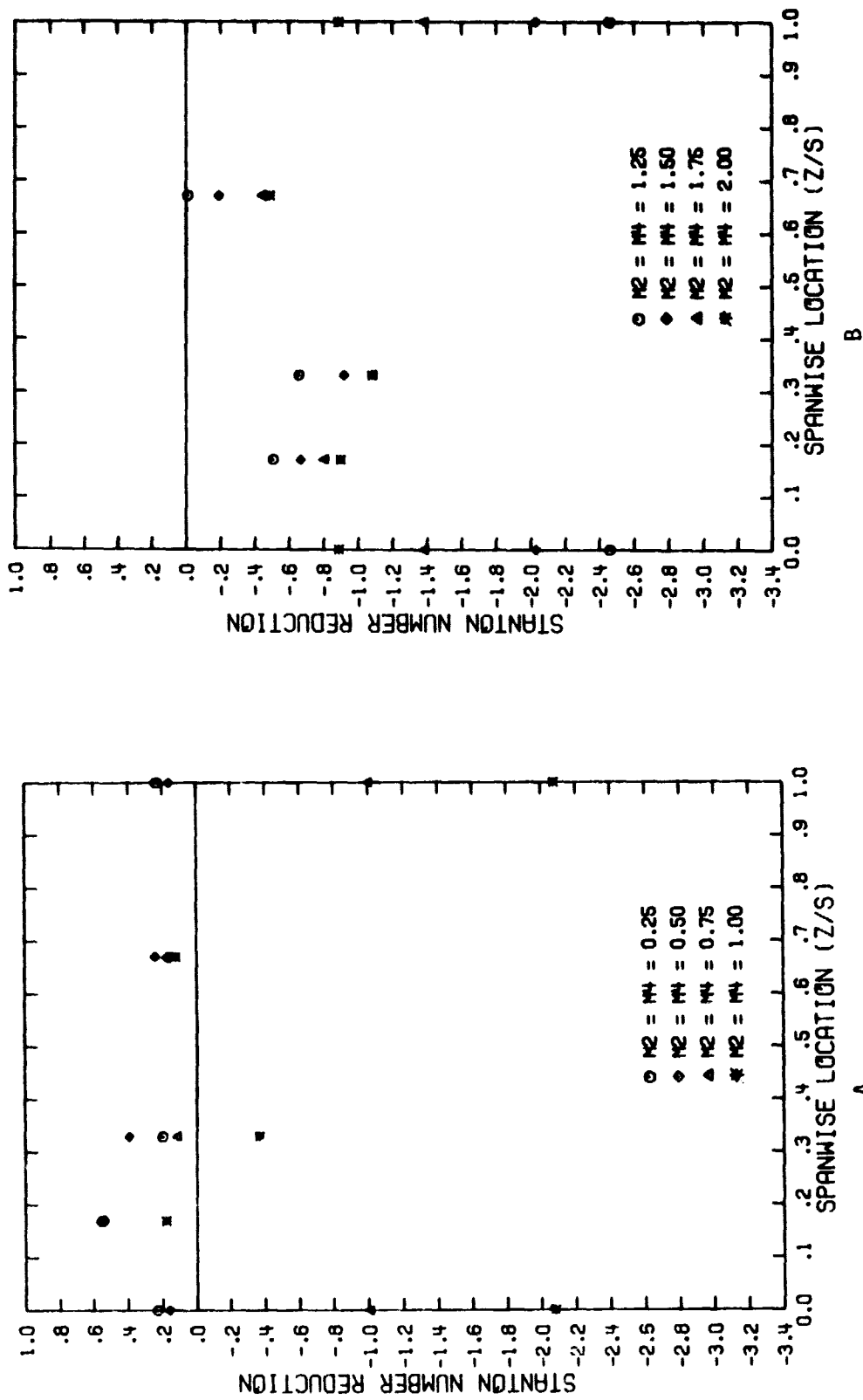


Figure A-64. Spanwise Variation of the Stanton Number Reduction with Uniform Blowing from a Two Row Configuration ($\Theta_2 = 22.9^\circ$, $\Theta_4 = 58.7^\circ$, $s/d_0 = P/d_0 = 10$, $(x/d_0)_4 = 1.5$)

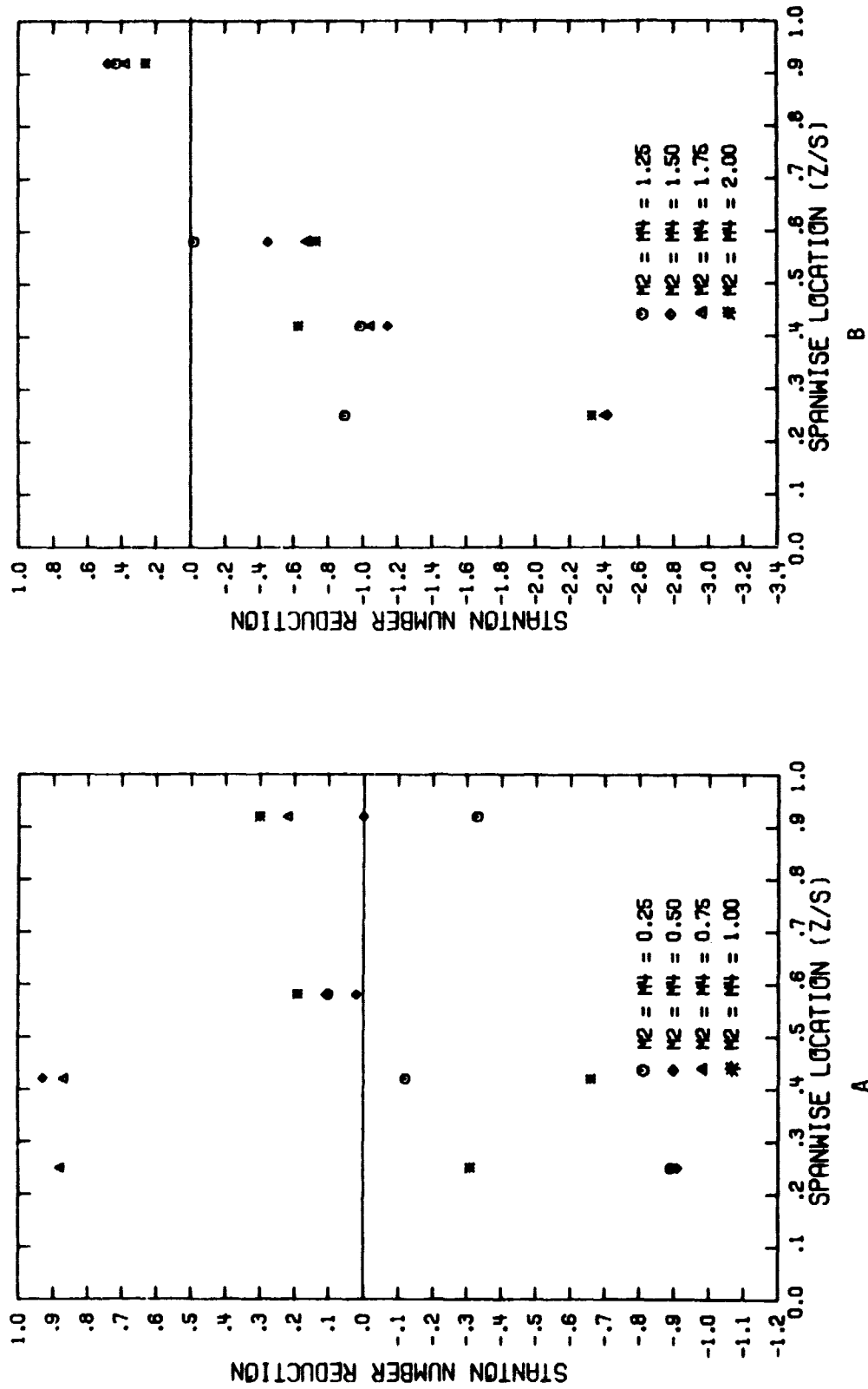


Figure A-65. Spanwise Variation of the Stanton Number Reduction with Uniform Blowing from a Two Row Configuration ($\Theta_2=22.9^\circ$, $\Theta_4=58.7^\circ$, $s/d_0=10$, $(x/d_0)_4=6.5$)

ORIGINAL PAGE IS
OF POOR QUALITY

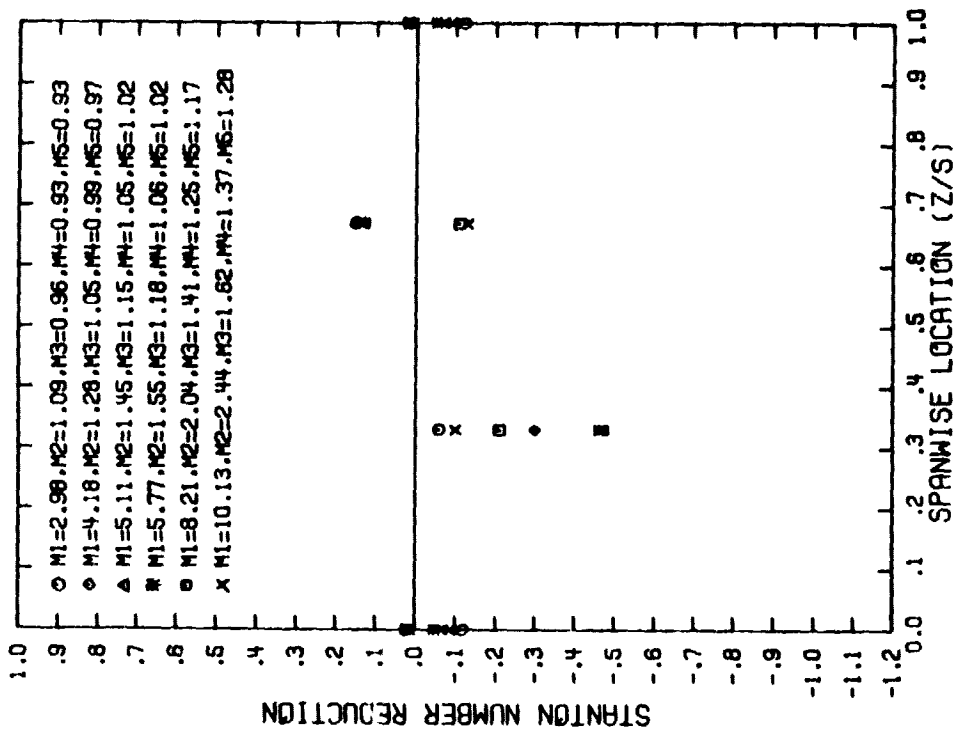


Figure A-66. Spanwise Variation of the Stanton Number Reduction with Plenum Blowing from a Five Row Configuration ($O_1=50$, $s/d_0=P/d_0=5$, $(x/d_0)_1=1.5$)

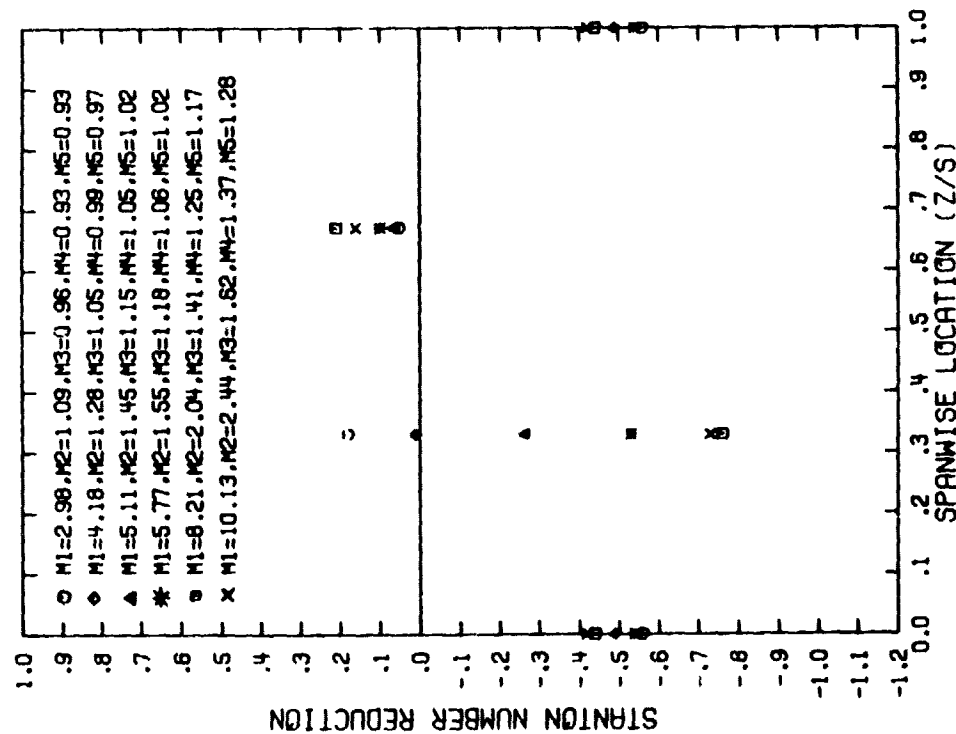


Figure A-67. Spanwise Variation of the Stanton Number Reduction with Plenum Blowing from a Five Row Configuration ($O_1=50$, $s/d_0=P/d_0=5$, $(x/d_0)_1=3.5$)

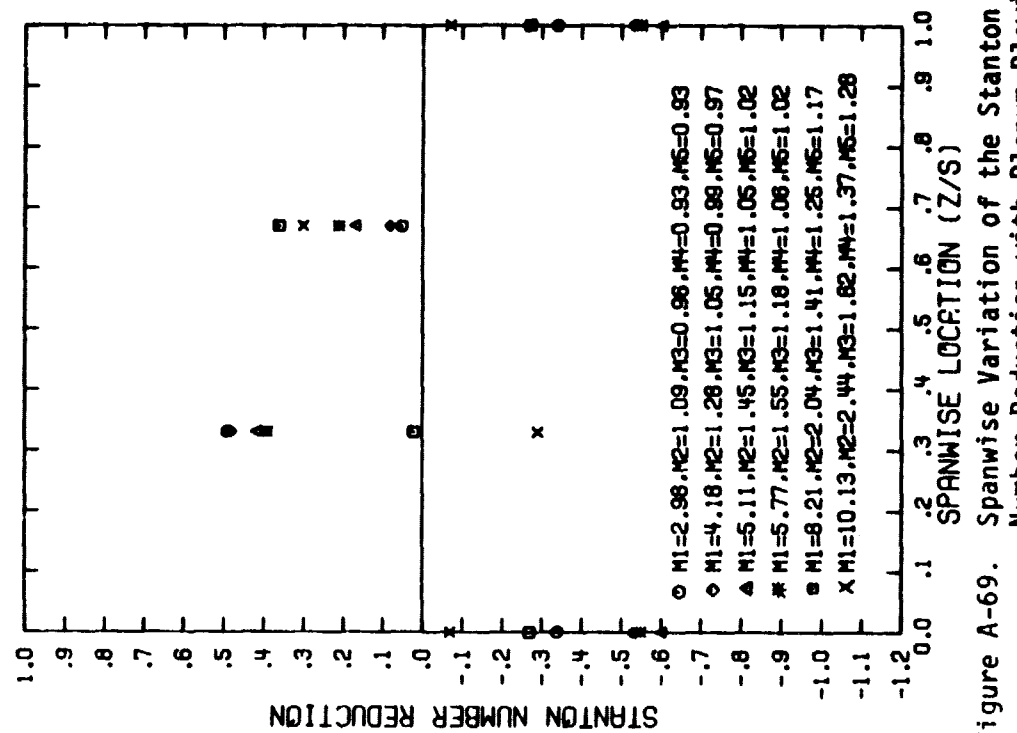


Figure A-69. Spanwise Variation of the Stanton Number Reduction with Plenum Blowing from a Five Row Configuration ($\theta_1=5^\circ$, $\theta_2=22.9^\circ$, $s/d_0=P/d_0=5$, $(x/d_0)_2=3.5$)

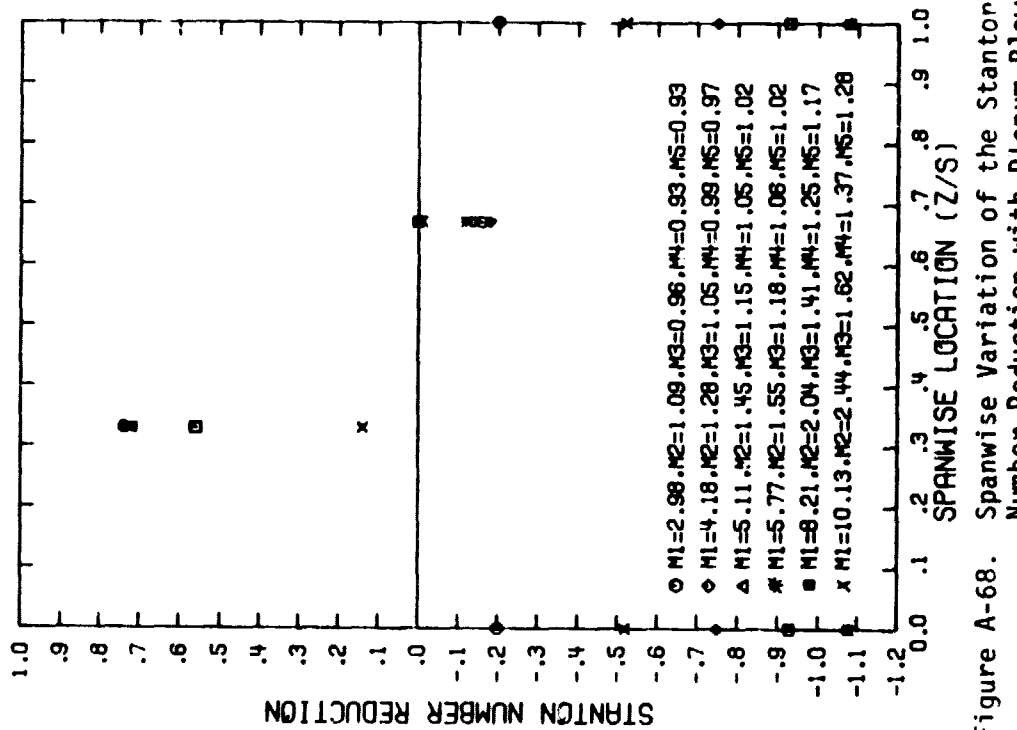


Figure A-68. Spanwise Variation of the Stanton Number Reduction with Plenum Blowing from a Five Row Configuration ($\theta_1=5^\circ$, $\theta_2=22.9^\circ$, $s/d_0=P/d_0=5$, $(x/d_0)_2=1.5$)

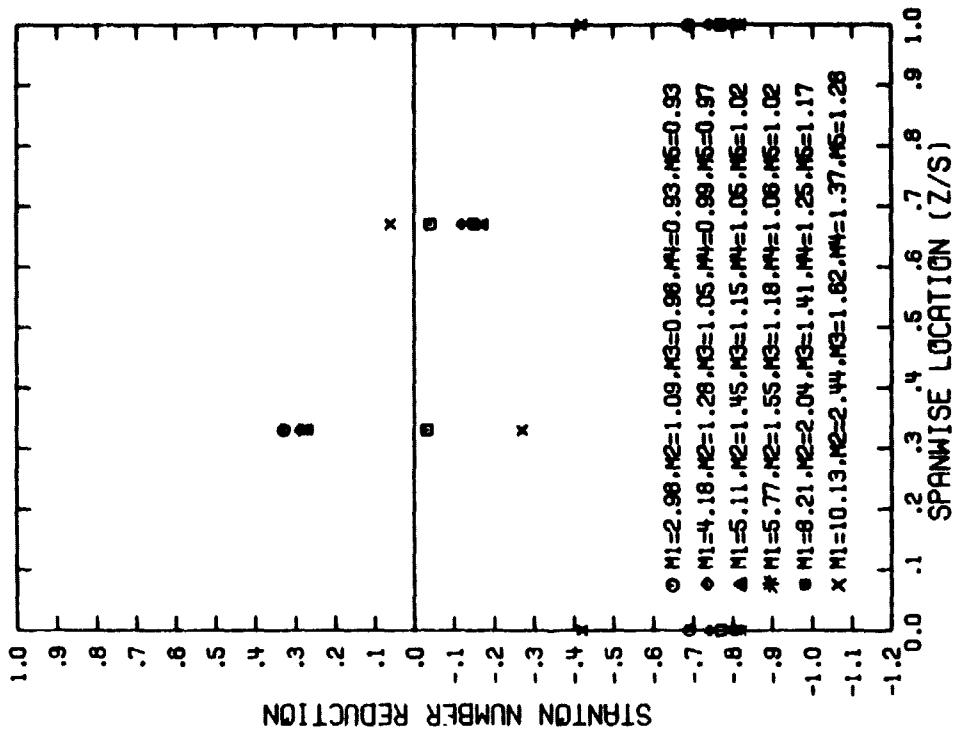


Figure A-71. Spanwise Variation of the Stanton Number Reduction with Plenum Blowing from a Five Row Configuration ($\Theta_1=50^\circ$, $\Theta_2=22.90^\circ$, $\Theta_3=40.80^\circ$, $\Theta_4=58.70^\circ$, $s/d_0=P/d_0=5$, $(x/d_0)_4=1.5$)

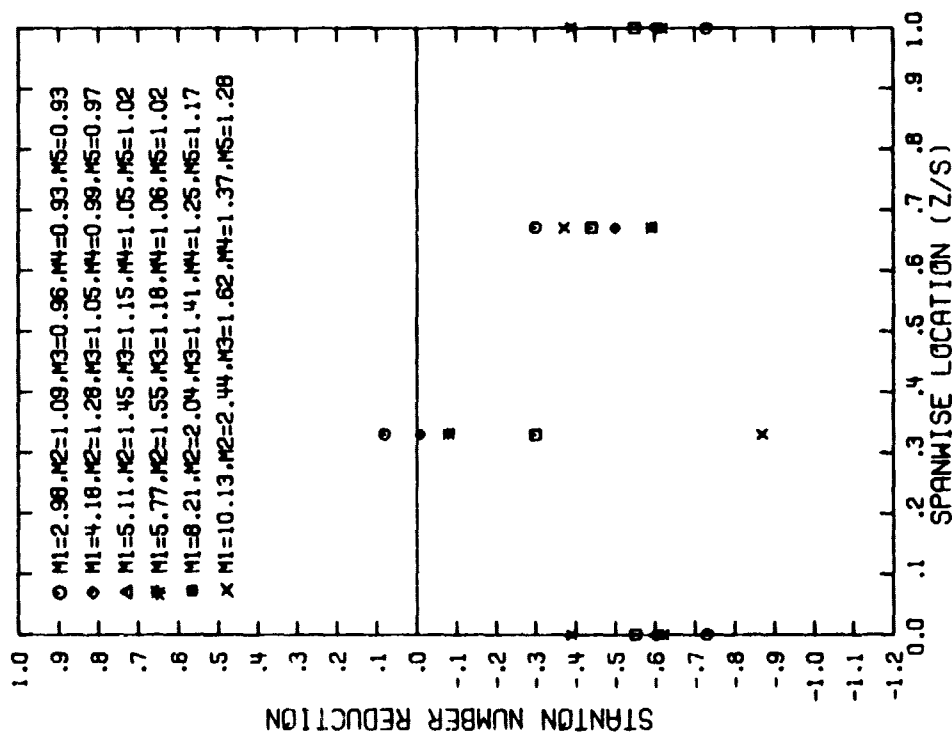


Figure A-70. Spanwise Variation of the Stanton Number Reduction with Plenum Blowing from a Five Row Configuration ($\Theta_1=50^\circ$, $\Theta_2=22.90^\circ$, $\Theta_3=40.80^\circ$, $s/d_0=P/d_0=5$, $(x/d_0)_3=1.5$)

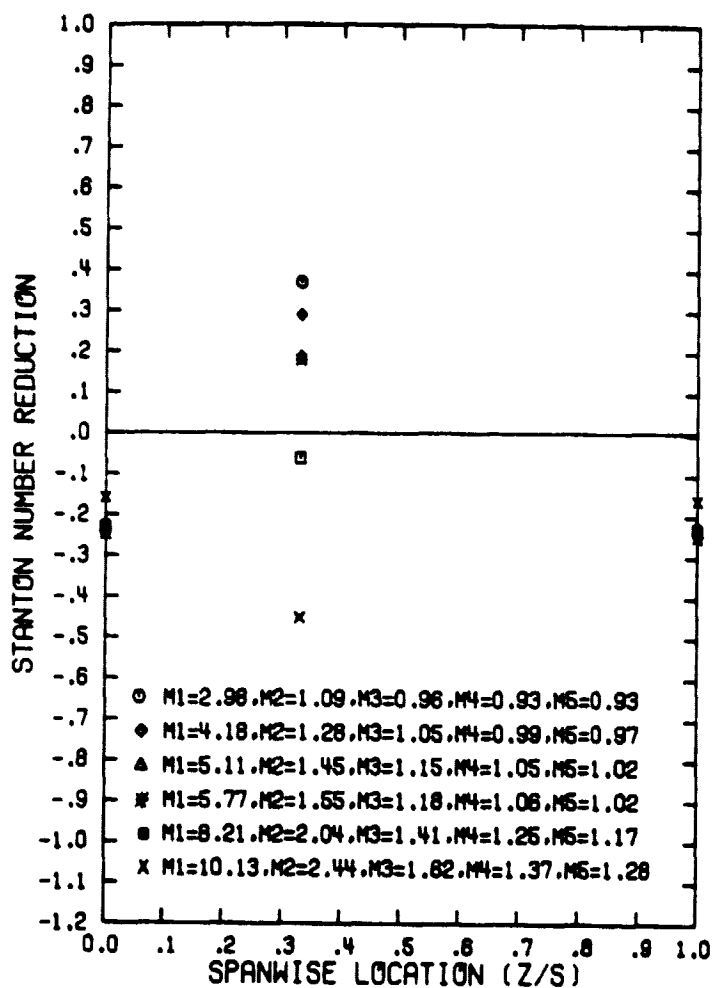


Figure A-72. Spanwise Variation of the Stanton Number Reduction with Plenum Blowing from a Five Row Configuration ($\theta_1=5^\circ$, $\theta_2=22.9^\circ$, $\theta_3=40.8^\circ$, $\theta_4=58.7^\circ$, $\theta_5=76.6^\circ$, $s/d_0=P/d_0=5$, $(x/d_0)_5=1.5$)

ORIGINAL PAGE IS
OF POOR QUALITY

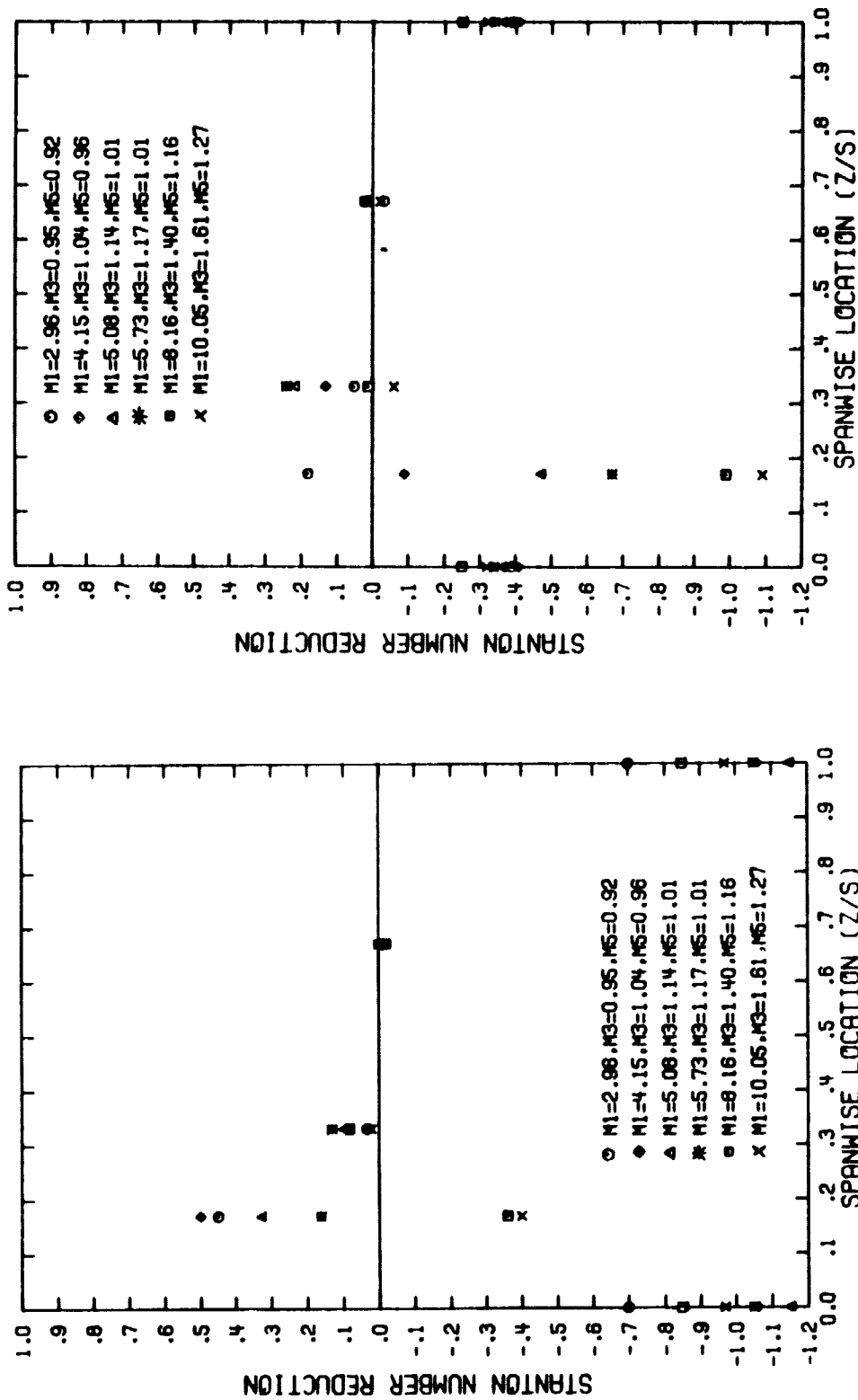


Figure A-73. Spanwise Variation of the Stanton Number Reduction with Plenum Blowing from a Three Row Configuration ($O_1=50$, $s/d_0=P/d_0=10$, $(x/d_0)_1=1.5$)

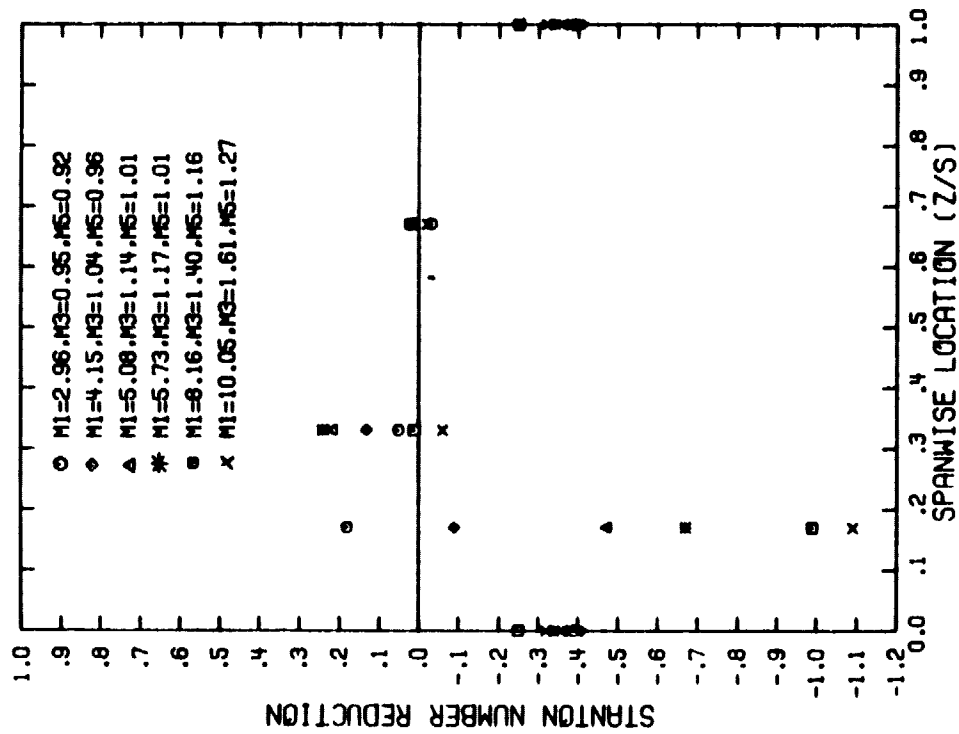


Figure A-74. Spanwise Variation of the Stanton Number Reduction with Plenum Blowing from a Three Row Configuration ($O_1=50$, $s/d_0=10$, $(x/d_0)_1=3.5$)

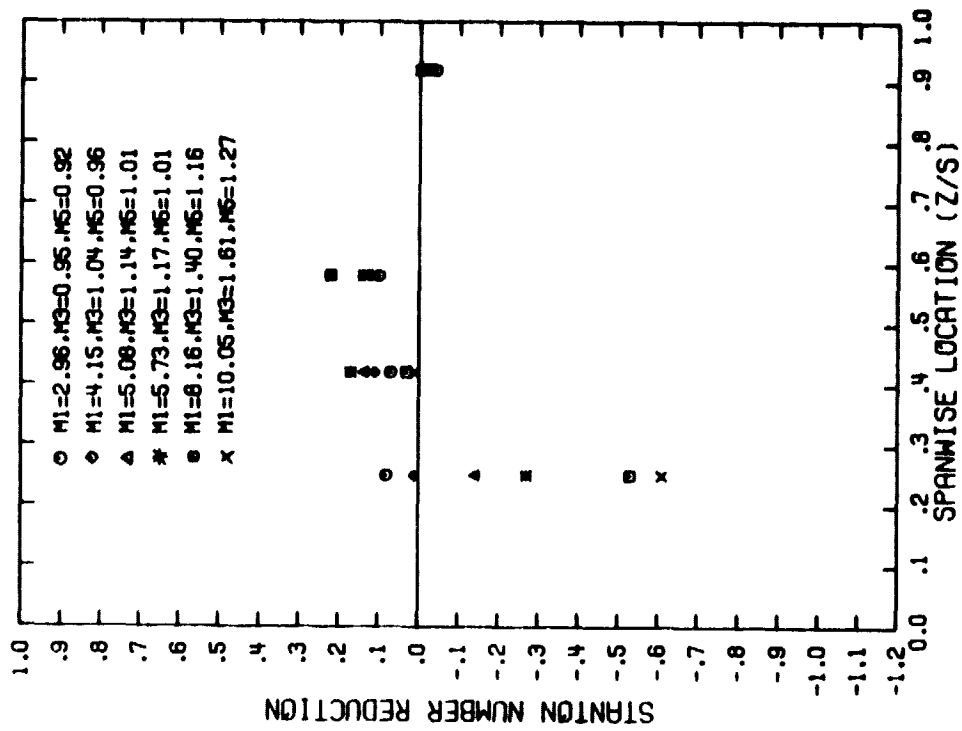


Figure A-75. Spanwise Variation of the Stanton Number Reduction with Plenum Blowing from a Three Row Configuration ($\theta_1=50^\circ$, $s/d_0=P/d_0=10$, $(x/d_0)_1=6.5$)

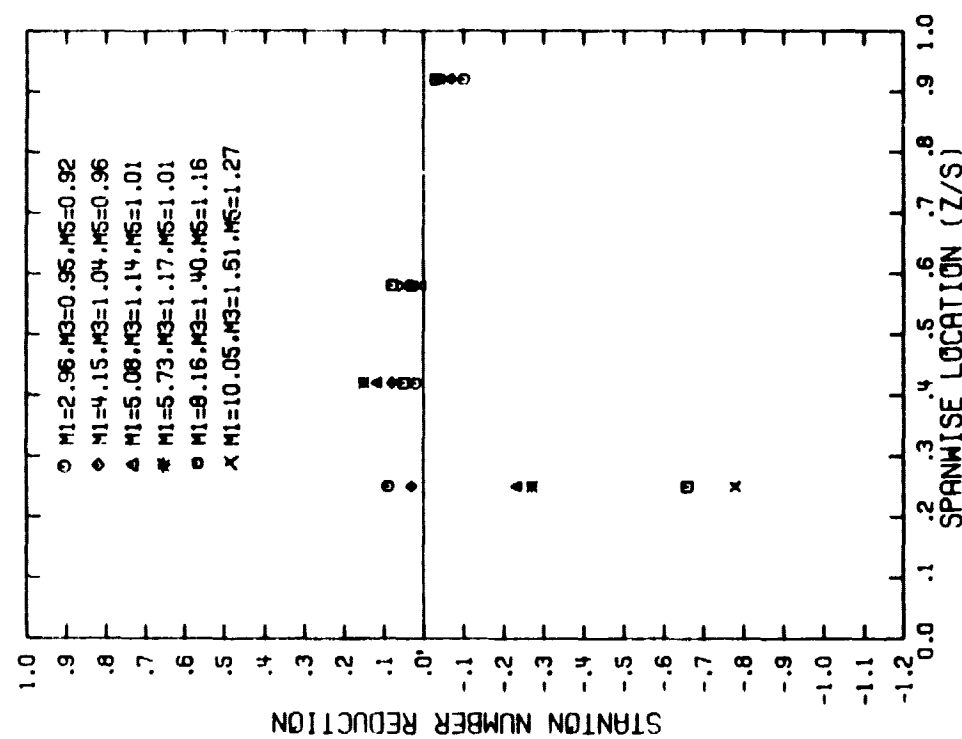


Figure A-76. Spanwise Variation of the Stanton Number Reduction with Plenum Blowing from a Three Row Configuration ($\theta_1=50^\circ$, $s/d_0=P/d_0=10$, $(x/d_0)_1=8.5$)

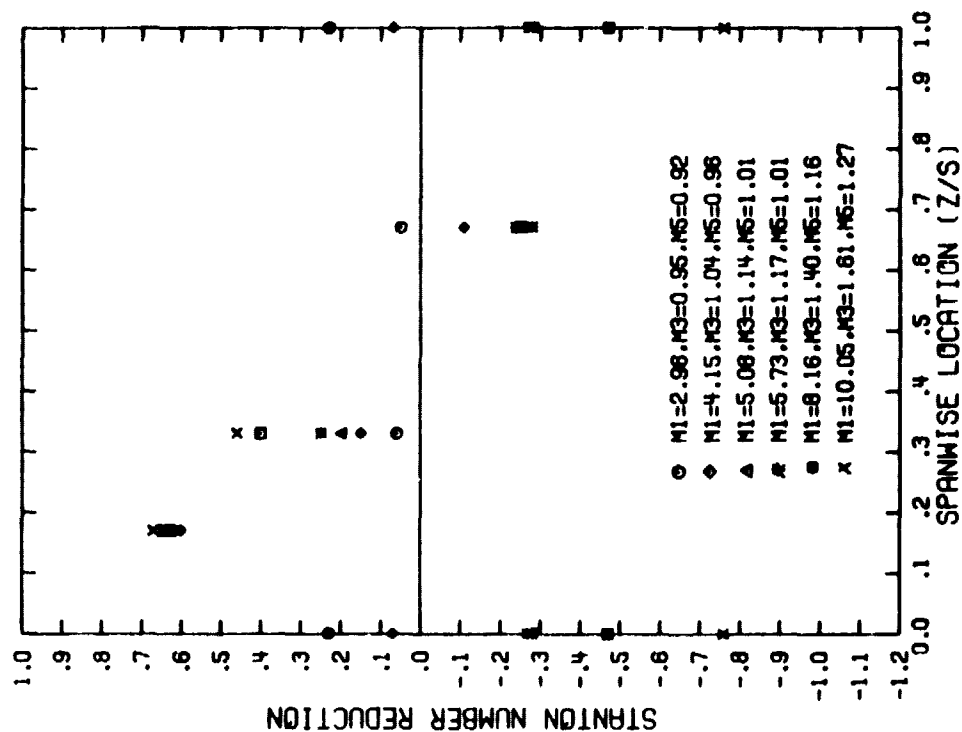


Figure A-77. Spanwise Variation of the Stanton Number Reduction with Plenum Blowing from a Three Row Configuration ($\theta_1=5^\circ$, $\theta_3=40.8^\circ$, $s/d_0=P/d_0=10$ (x/d_0)₃=1.5)

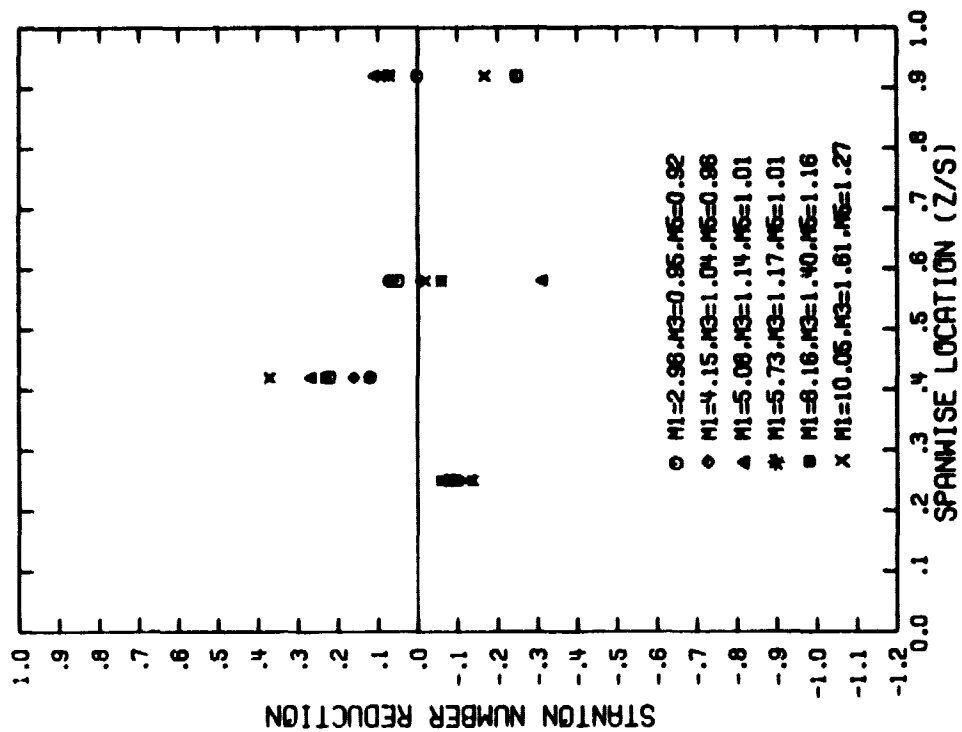


Figure A-78. Spanwise Variation of the Stanton Number Reduction with Plenum Blowing from a Three Row Configuration ($\theta_1=5^\circ$, $\theta_3=40.8^\circ$, $s/d_0=P/d_0=10$ (x/d_0)₃=6.5)

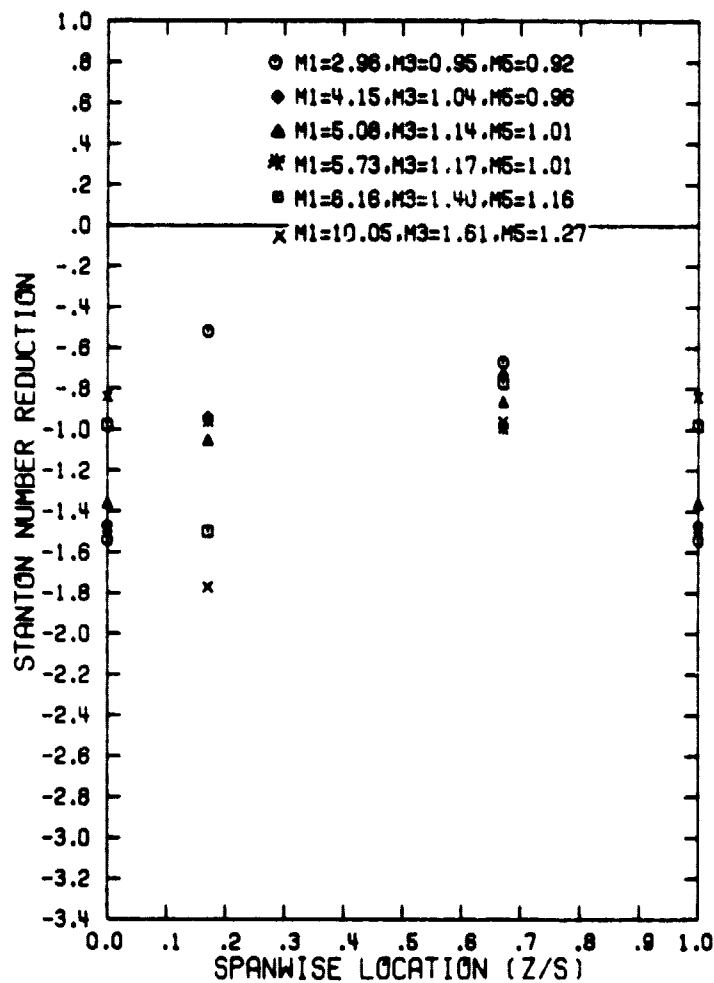


Figure A-79. Spanwise Variation of the Stanton Number Reduction with Plenum Blowing from a Three Row Configuration ($\theta_1=5^\circ$, $\theta_3=40.8^\circ$, $\theta_5=76.6^\circ$, $s/d_0=P/d_0=10$, $(x/d_0)_5=1.5$)

ORIGINAL PAGE IS
OF POOR QUALITY

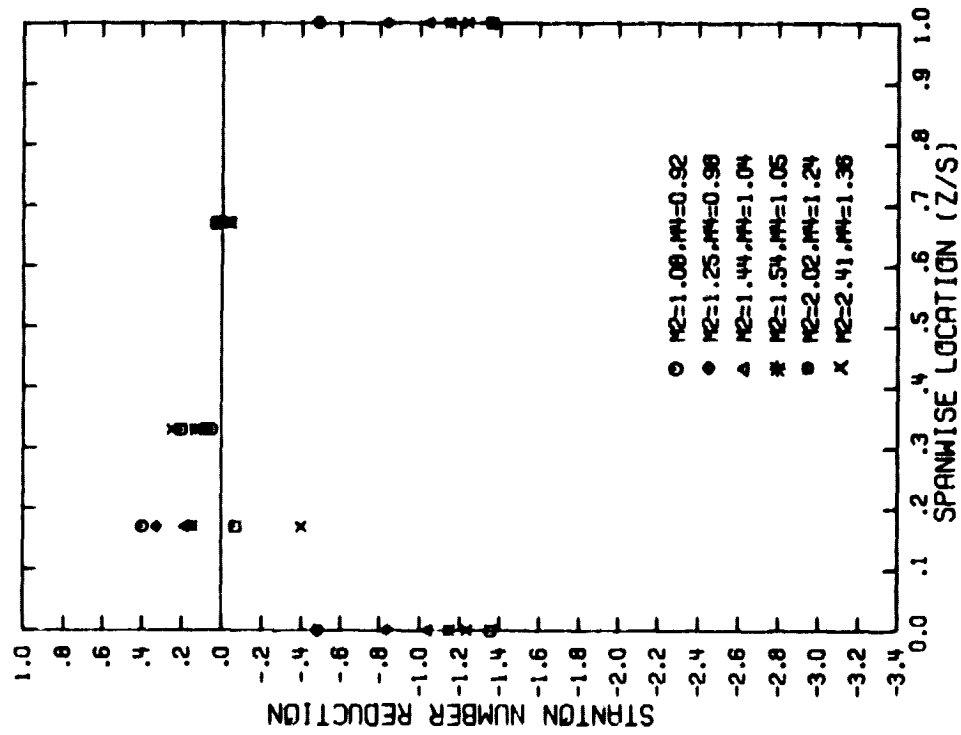


Figure A-80. Spanwise Variation of the Stanton Number Reduction with Plenum Blowing from a Two Row Configuration ($\theta_2 = 22.9^\circ$, $s/d_0 = P/d_0 = 10$, $(x/d_0)_2 = 1.5$)

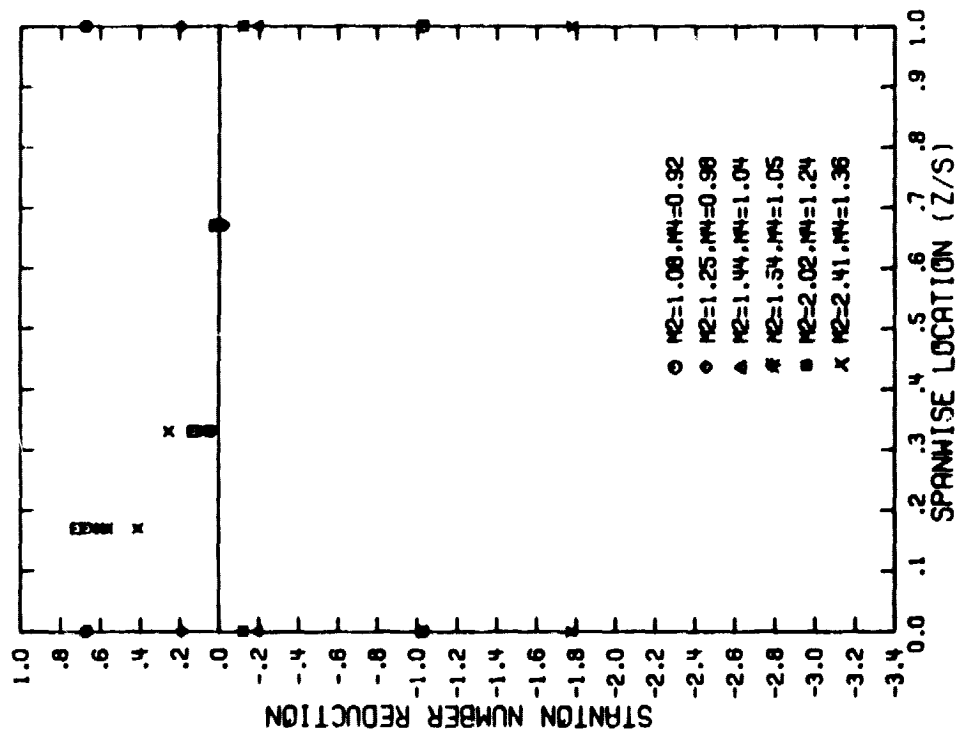


Figure A-81. Spanwise Variation of the Stanton Number Reduction with Plenum Blowing from a Two Row Configuration ($\theta_2 = 22.9^\circ$, $s/d_0 = P/d_0 = 10$, $(x/d_0)_2 = 3.5$)

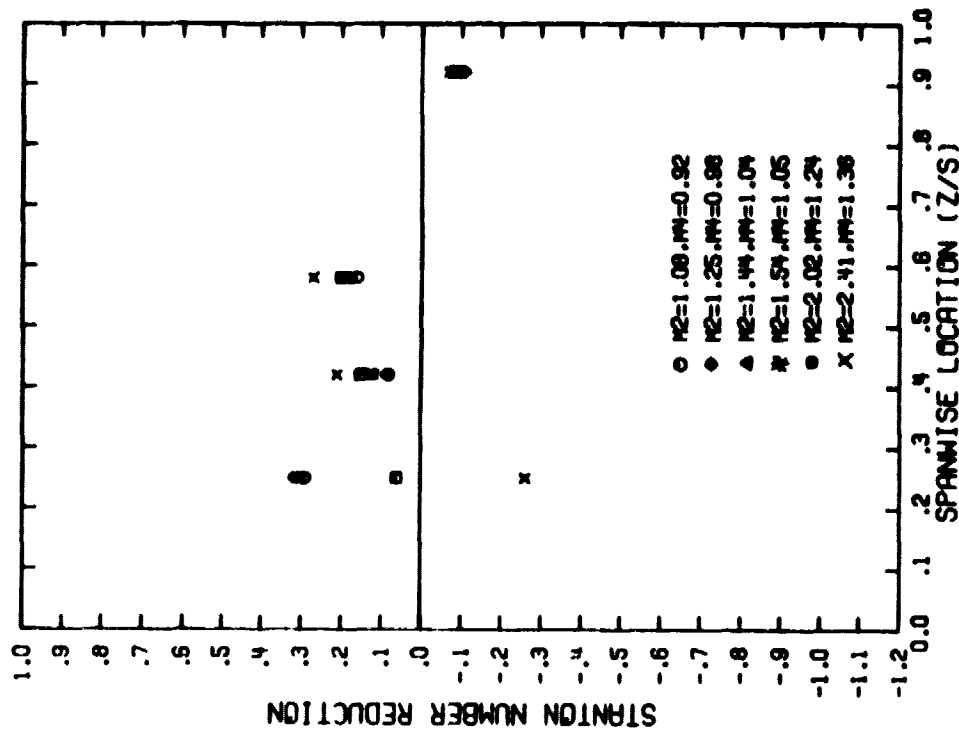


Figure A-82. Spanwise Variation of the Stanton Number Reduction with Plenum Blowing from a Two Row Configuration ($O_2=22.9^\circ$, $s/d_0=P/d_0=10$, $(s/d_0)_2=6.5$)

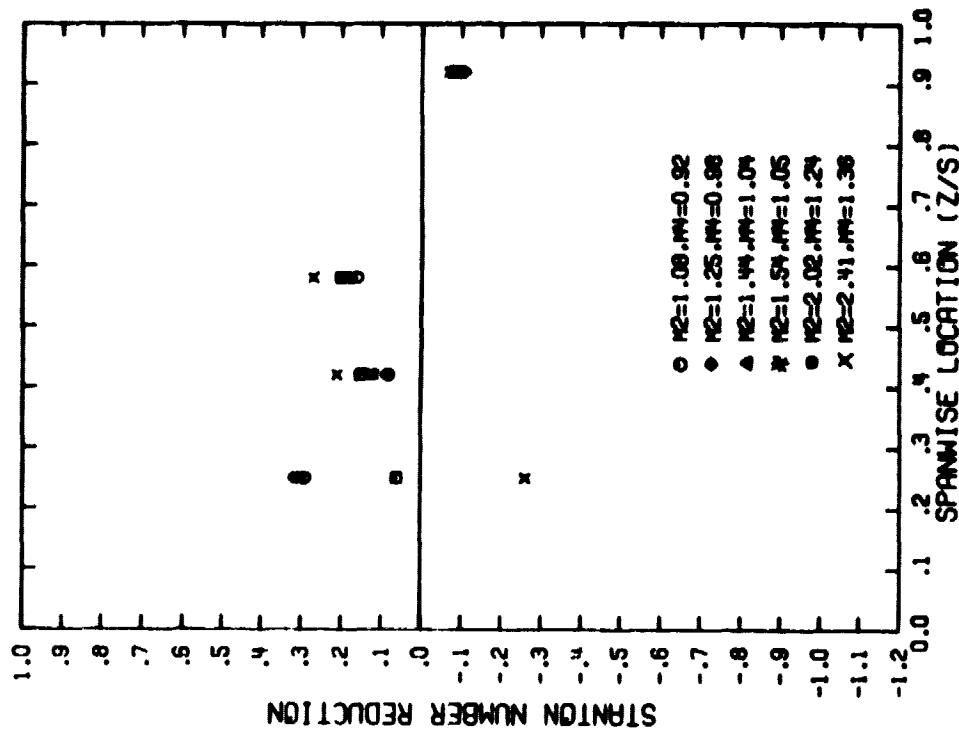


Figure A-83. Spanwise Variation of the Stanton Number Reduction with Plenum Blowing from a Two Row Configuration ($O_2=22.8^\circ$, $s/d_0=P/d_0=10$, $(x/d_0)_2=8.5$)

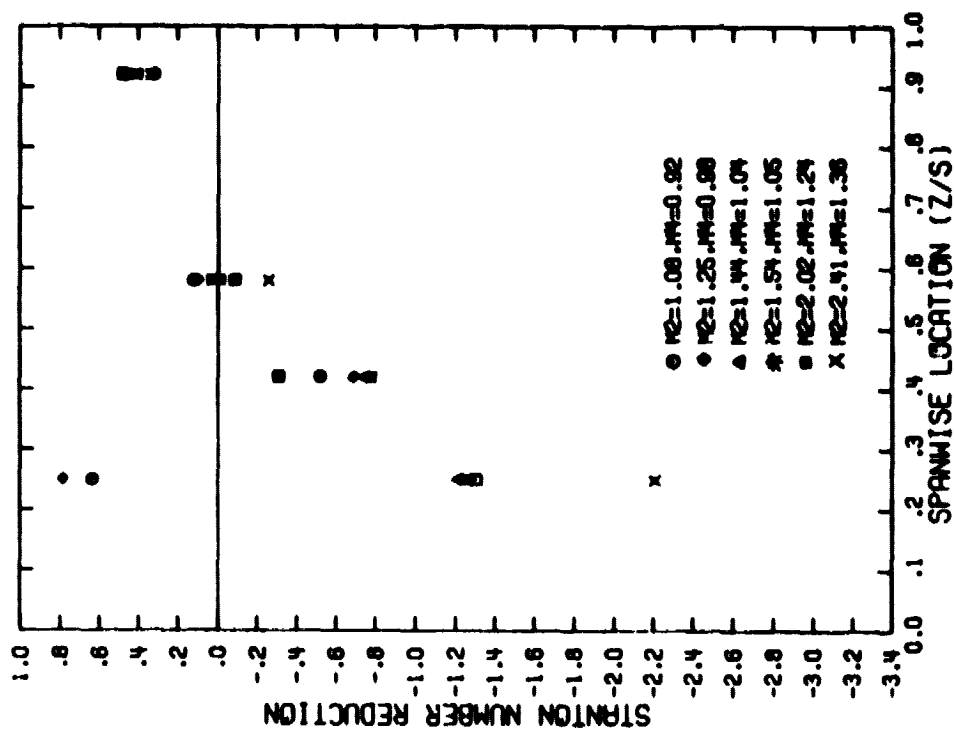


Figure A-84. Spanwise Variation of the Stanton Number Reduction with Plenum Blowing from a Two Row Configuration ($\Theta_2=22.9^\circ$, $\Theta_4=58.7^\circ$, $s/d_0=P/d_0=10$, $(x/d_0)_4=1.5$)

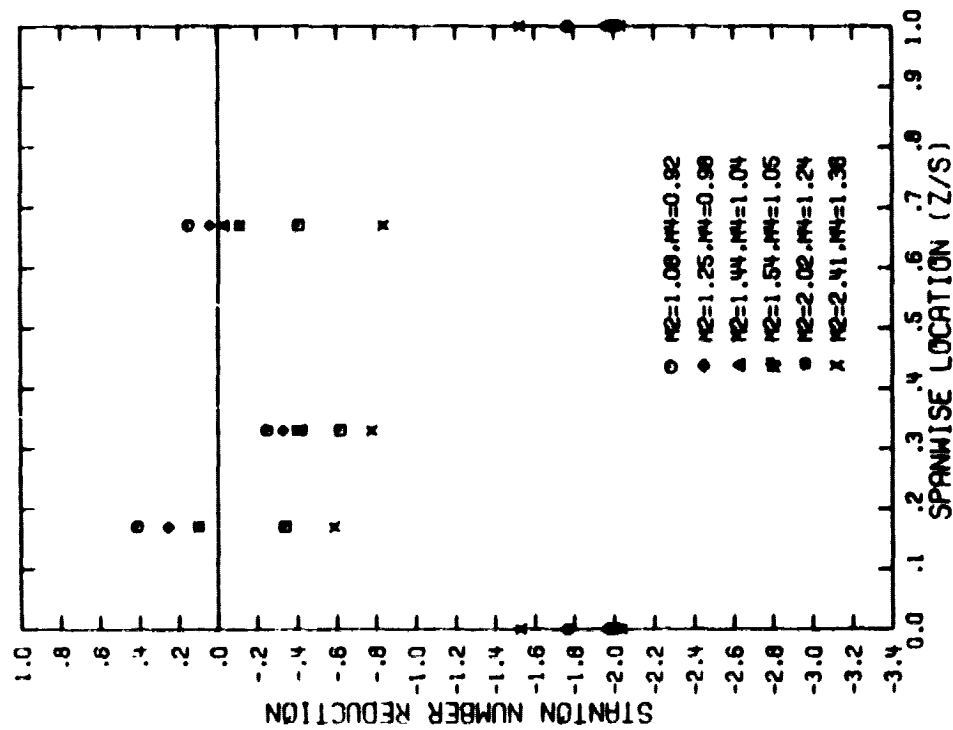


Figure A-85. Spanwise Variation of the Stanton Number Reduction with Plenum Blowing from a Two Row Configuration ($\Theta_2=22.9^\circ$, $\Theta_4=58.7^\circ$, $s/d_0=P/d_0=10$, $(x/d_0)_4=6.5$)

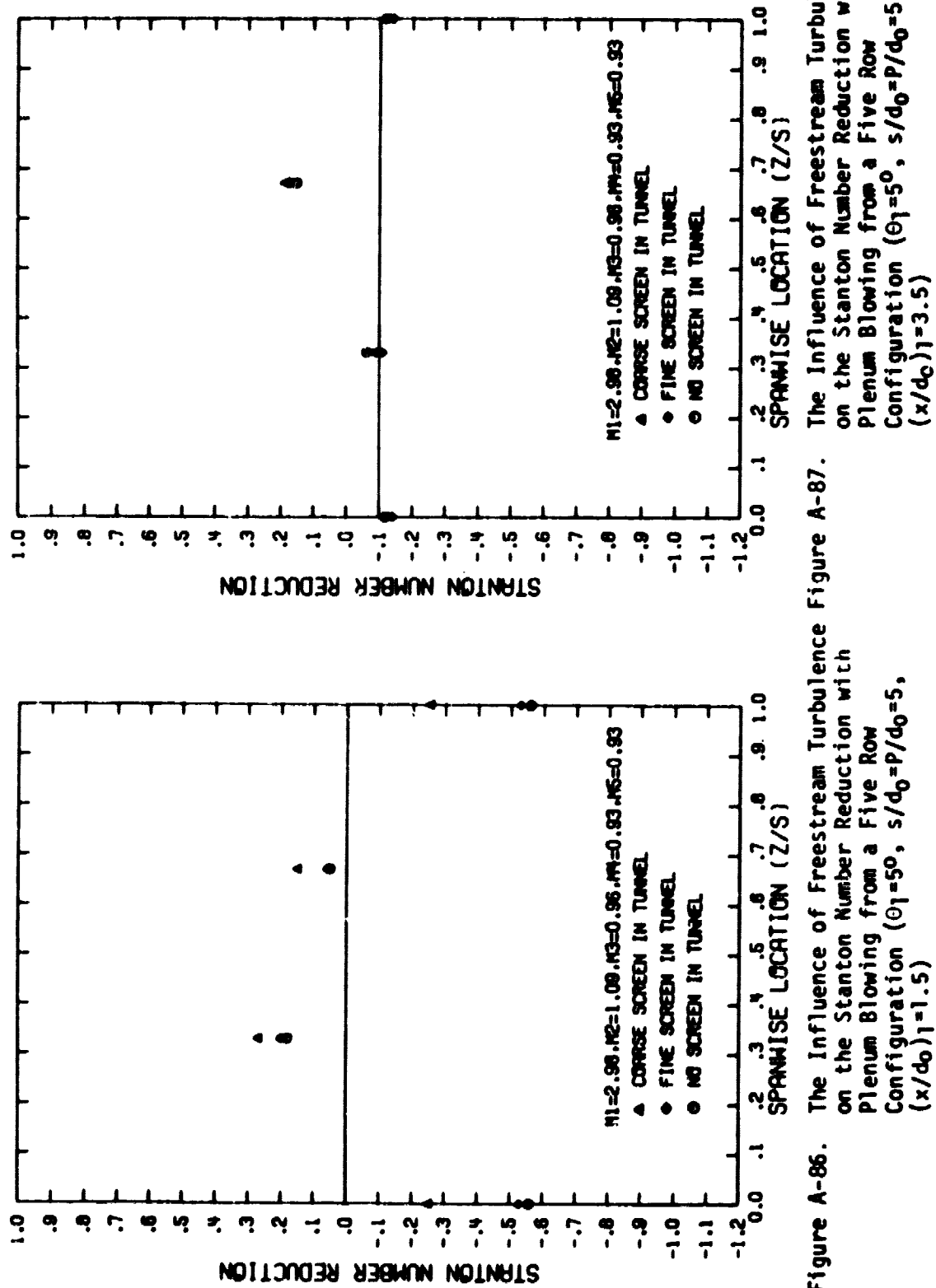


Figure A-86. The Influence of Freestream Turbulence on the Stanton Number Reduction with Plenum Blowing from a Five Row Configuration ($\theta_1 = 50^\circ$, $s/d_0 = P/d_0 = 5$, $(x/d_0)_1 = 1.5$)

Figure A-87. The Influence of Freestream Turbulence on the Stanton Number Reduction with Plenum Blowing from a Five Row Configuration ($\theta_1 = 50^\circ$, $s/d_0 = P/d_0 = 5$, $(x/d_0)_1 = 3.5$)

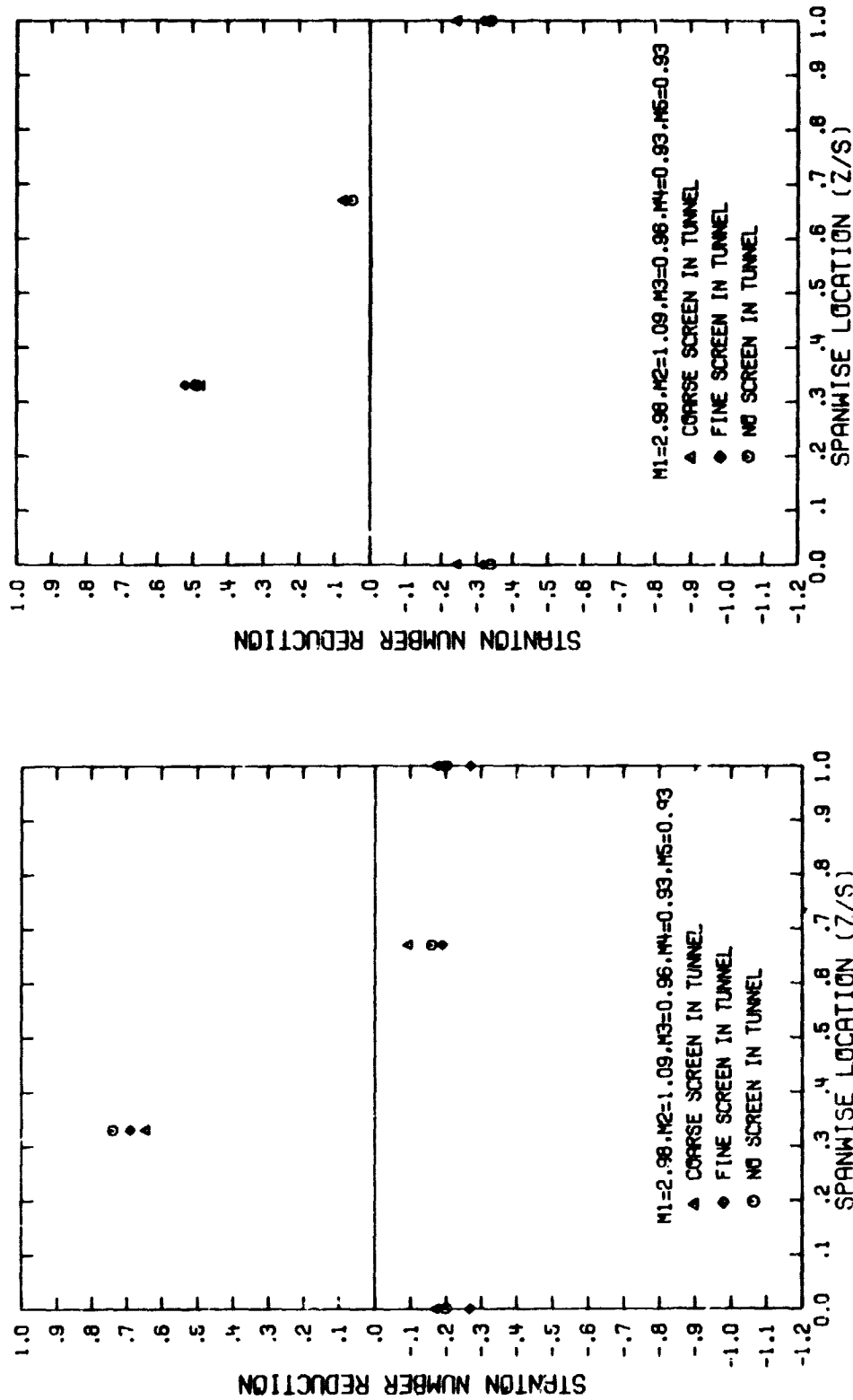


Figure A-88. The Influence of Freestream Turbulence on the Stanton Number Reduction with Plenum Blowing from a Five Row Configuration ($\theta_1=50^\circ$, $\theta_2=22.90^\circ$, $s/d_0=P/d_0=5$, $(x/d_0)_2=1.5$)

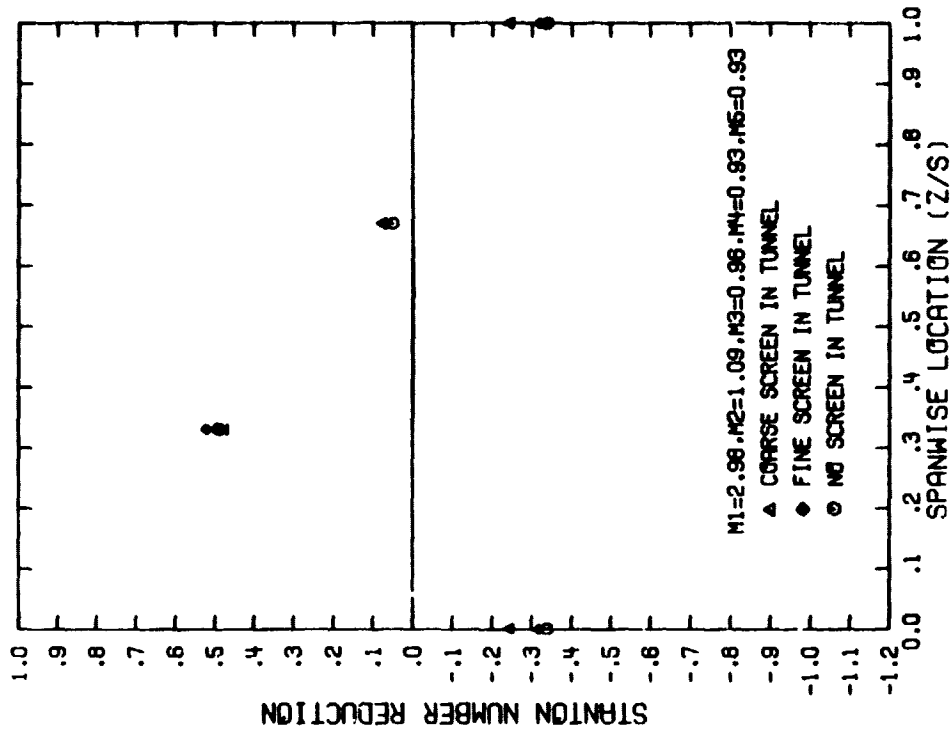


Figure A-89. The Influence of Freestream Turbulence on the Stanton Number Reduction with Plenum Blowing from a Five Row Configuration ($\theta_1=50^\circ$, $\theta_2=22.90^\circ$, $s/d_0=P/d_0=5$, $(x/d_0)_2=3.5$)

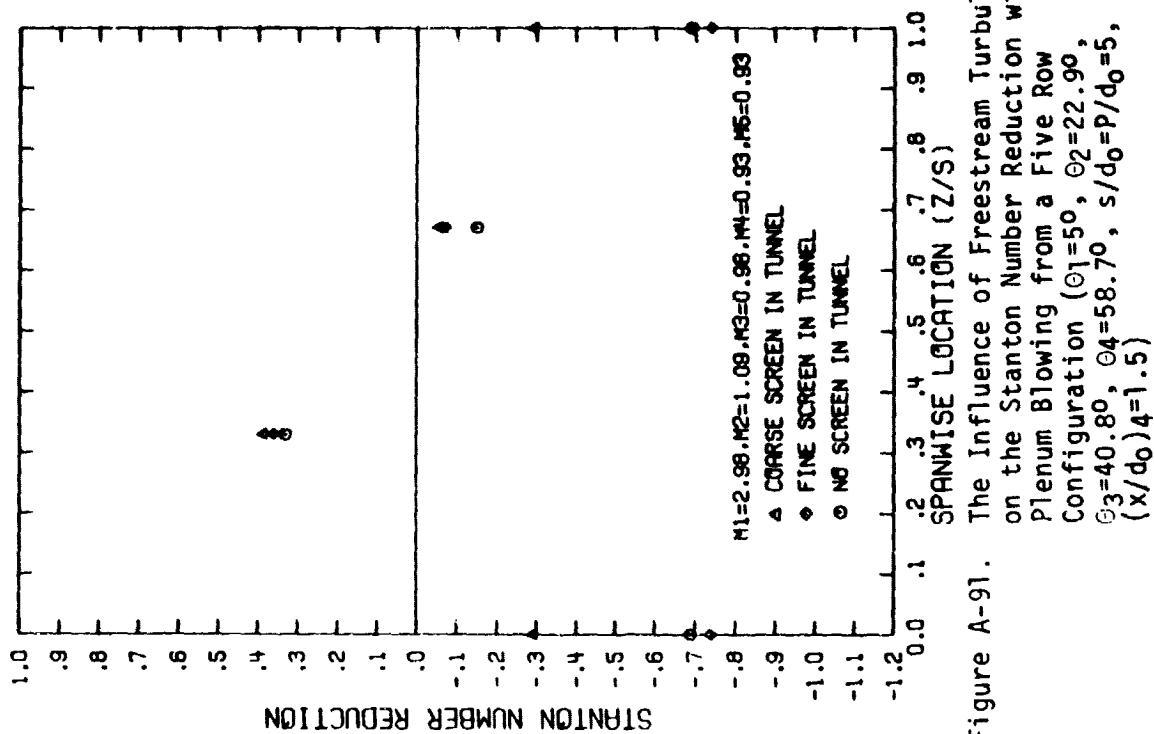


Figure A-91. The Influence of Freestream Turbulence on the Stanton Number Reduction with Plenum Blowing from a Five Row Configuration ($\theta_1=50^\circ, \theta_2=22.90^\circ, \theta_3=40.80^\circ, \theta_4=58.70^\circ, s/d_0=P/d_0=5, (x/d_0)_4=1.5$)

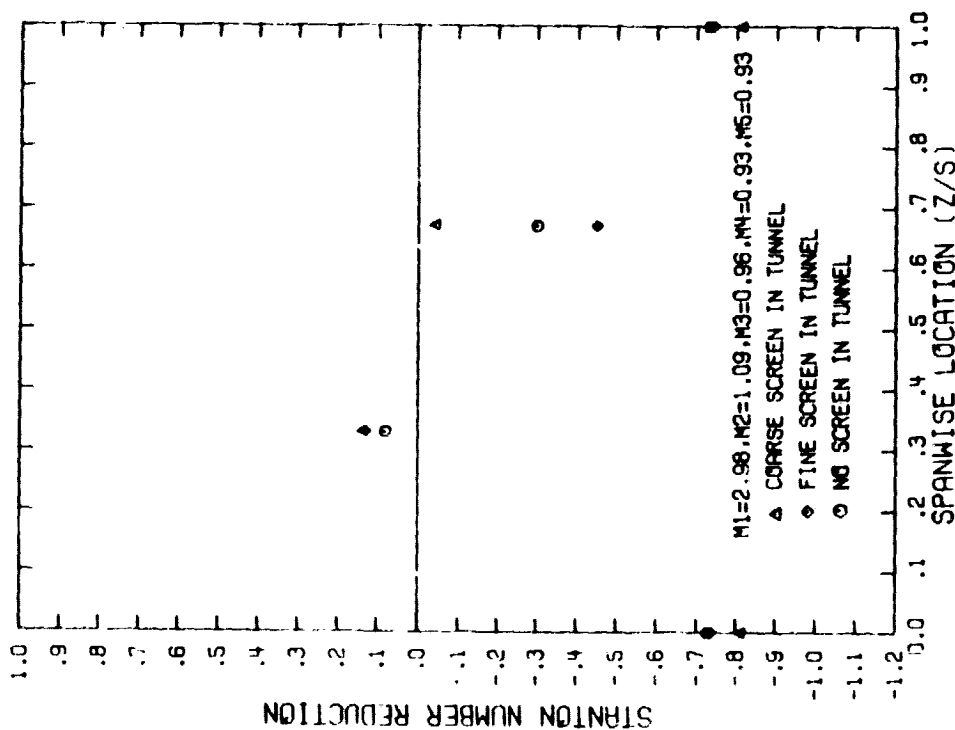


Figure A-90. The Influence of Freestream Turbulence on the Stanton Number Reduction with Plenum Blowing from a Five Row Configuration ($\theta_1=50^\circ, \theta_2=22.90^\circ, \theta_3=40.80^\circ, s/d_0=P/d_0=5, (x/d_0)_3=1.5$)

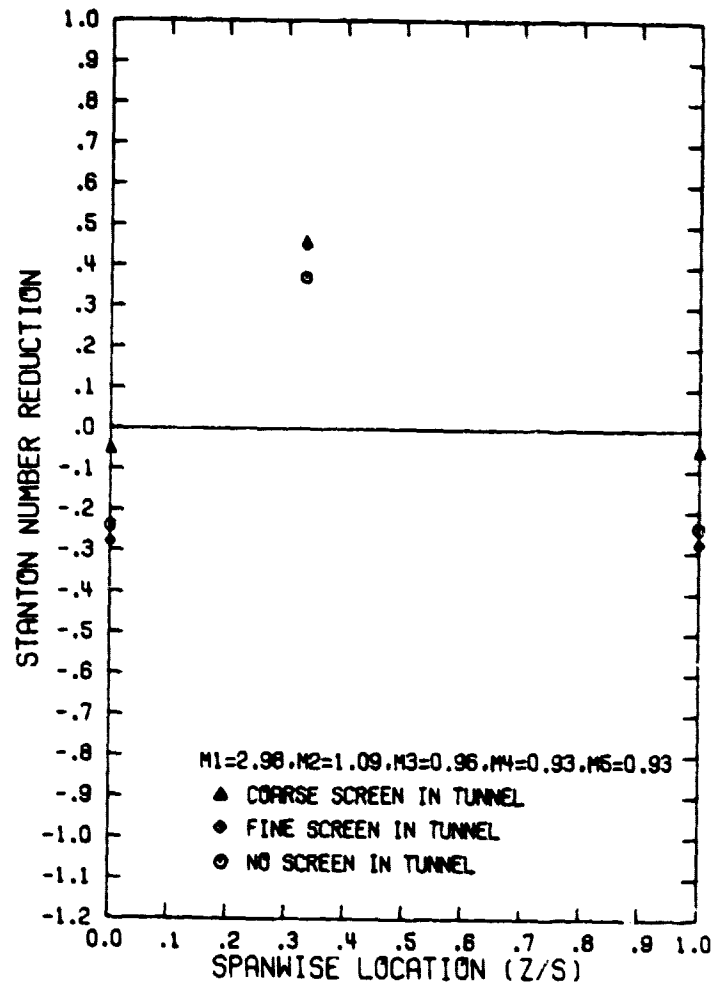


Figure A-92. The Influence of Freestream Turbulence on the Stanton Number Reduction with Plenum Blowing from a Five Row Configuration ($\theta_1=5^\circ$, $\theta_2=22.9^\circ$, $\theta_3=40.8^\circ$, $\theta_4=58.7^\circ$, $\theta_5=76.6^\circ$, $s/d_0=P/d_0=5$, $(x/d_0)_5=1.5$)

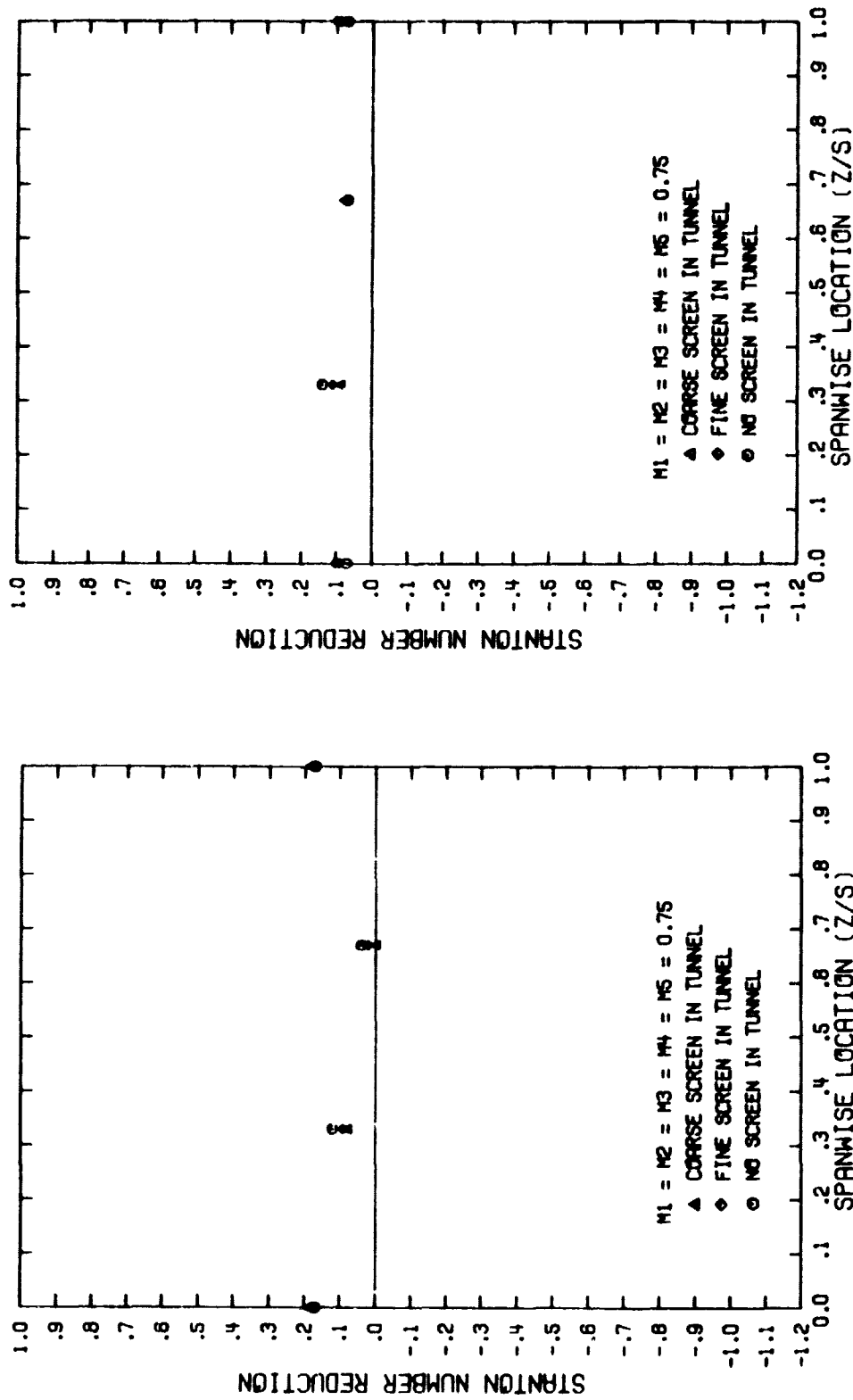


Figure A-93. The Influence of Freestream Turbulence on the Stanton Number Reduction with Uniform Blowing from a Five Row Configuration ($\theta_1=50^\circ$, $s/d_0=P/d_0=5$, $(x/d_0)_1=1.5$)

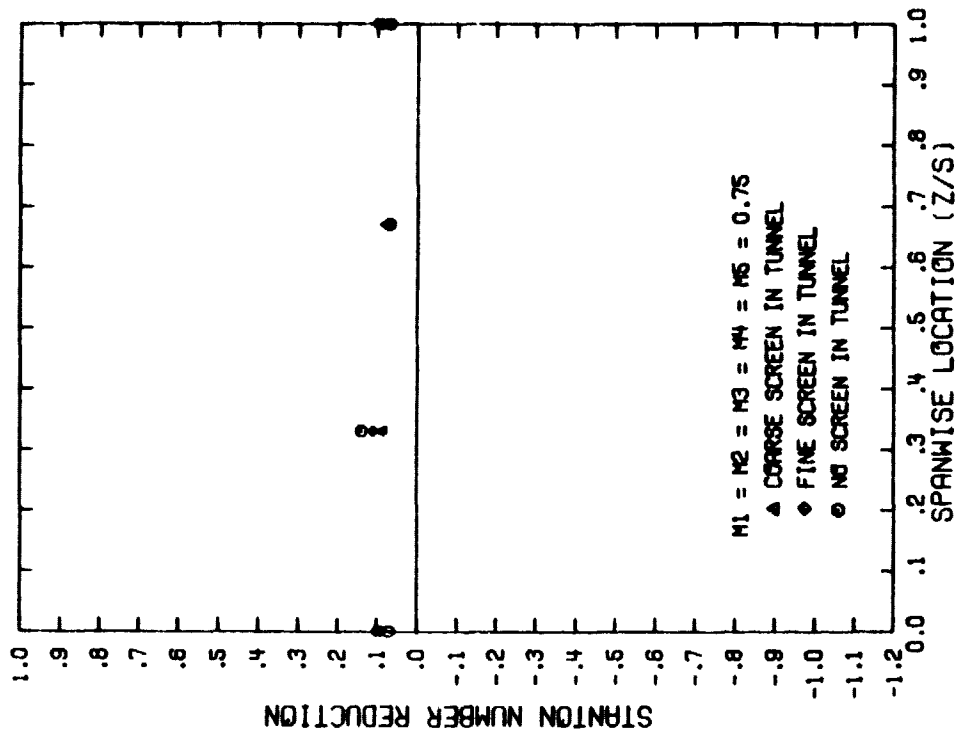


Figure A-94. The Influence of Freestream Turbulence on the Stanton Number Reduction with Uniform Blowing from a Five Row Configuration ($\theta_1=50^\circ$, $s/d_0=P/d_0=5$, $(x/d_0)_1=3.5$)

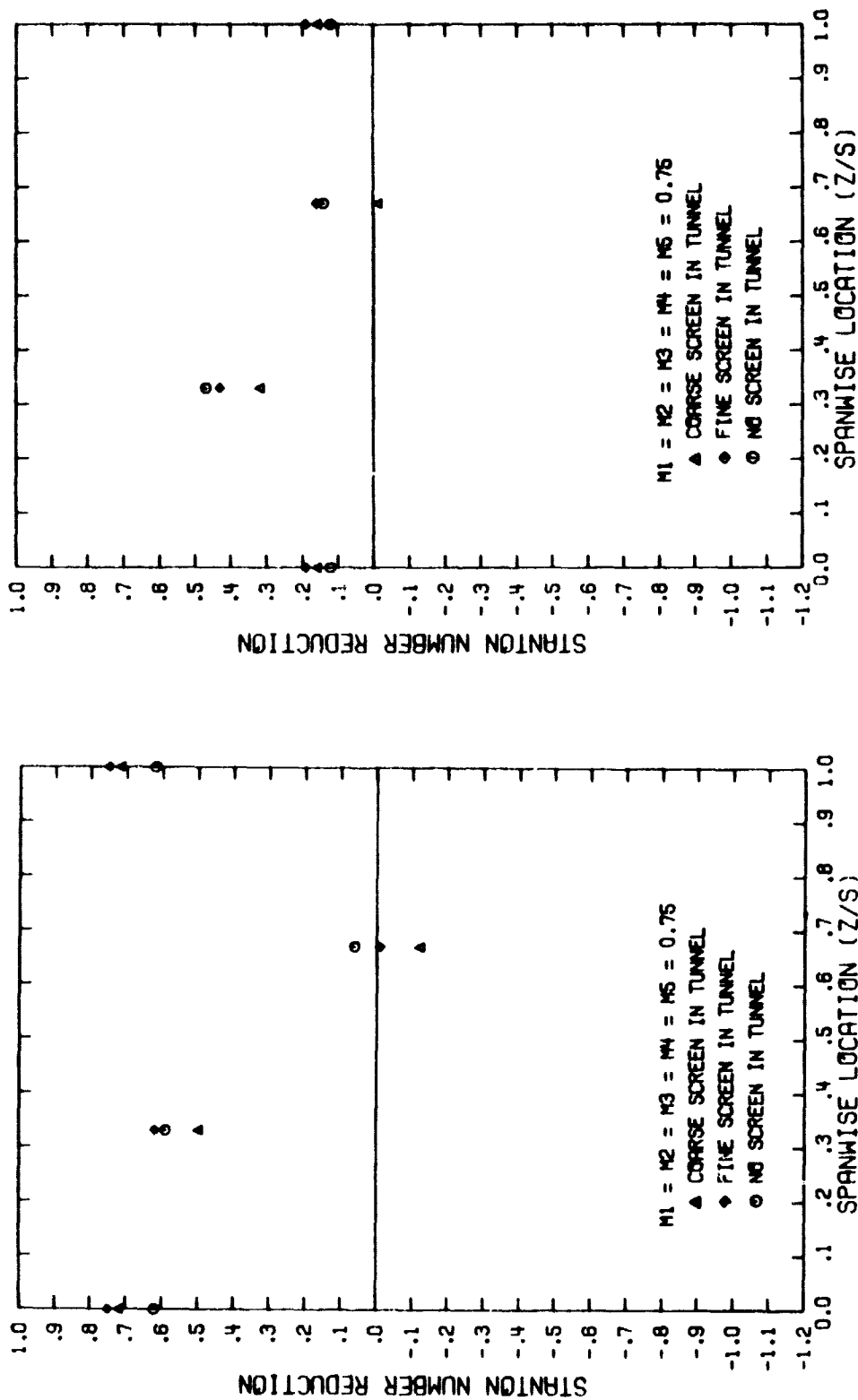


Figure A-95. The Influence of Freestream Turbulence on the Stanton Number Reduction with Uniform Blowing from a Five Row Configuration ($\theta_1=50^\circ$, $\theta_2=22.90^\circ$, $s/d_0=P/d_0=5$, $(x/d_0)_2=1.5$)

Figure A-96. The Influence of Freestream Turbulence on the Stanton Number Reduction with Uniform Blowing from a Five Row Configuration ($\theta_1=50^\circ$, $\theta_2=22.90^\circ$, $s/d_0=P/d_0=5$, $(x/d_0)_2=3.5$)

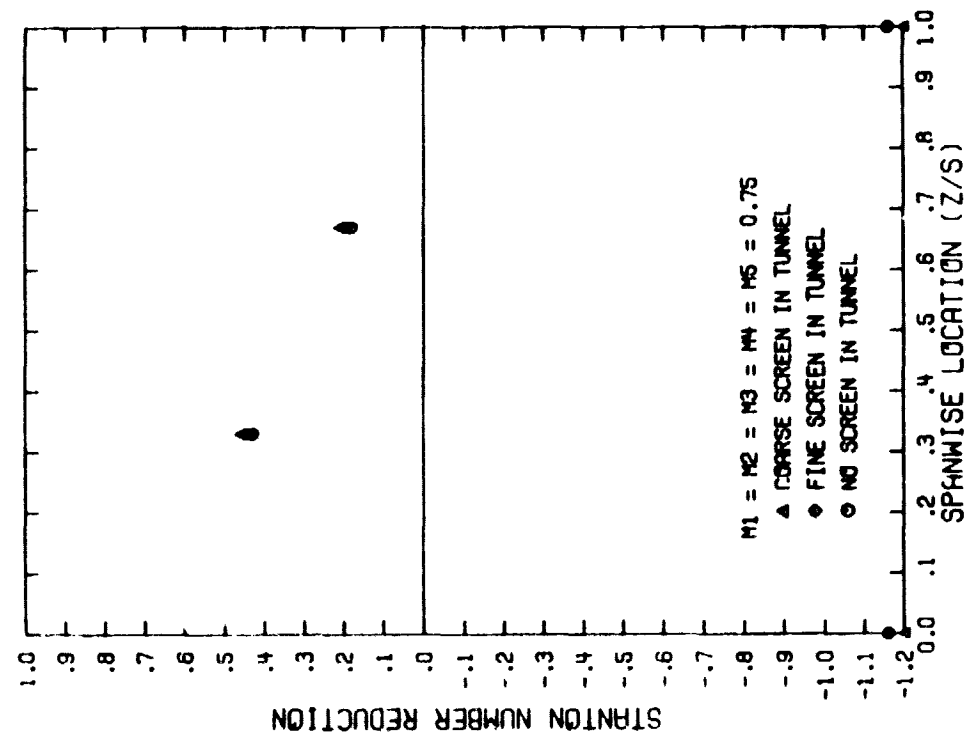


Figure A-97. The Influence of Freestream Turbulence on the Stanton Number Reduction with Uniform Blowing from a Five Row Configuration ($\Theta_1=50^\circ$, $\Theta_2=22.90^\circ$, $\Theta_3=40.80^\circ$, $s/d_0=P/d_0=5$, $(x/d_0)_3=1.5$)

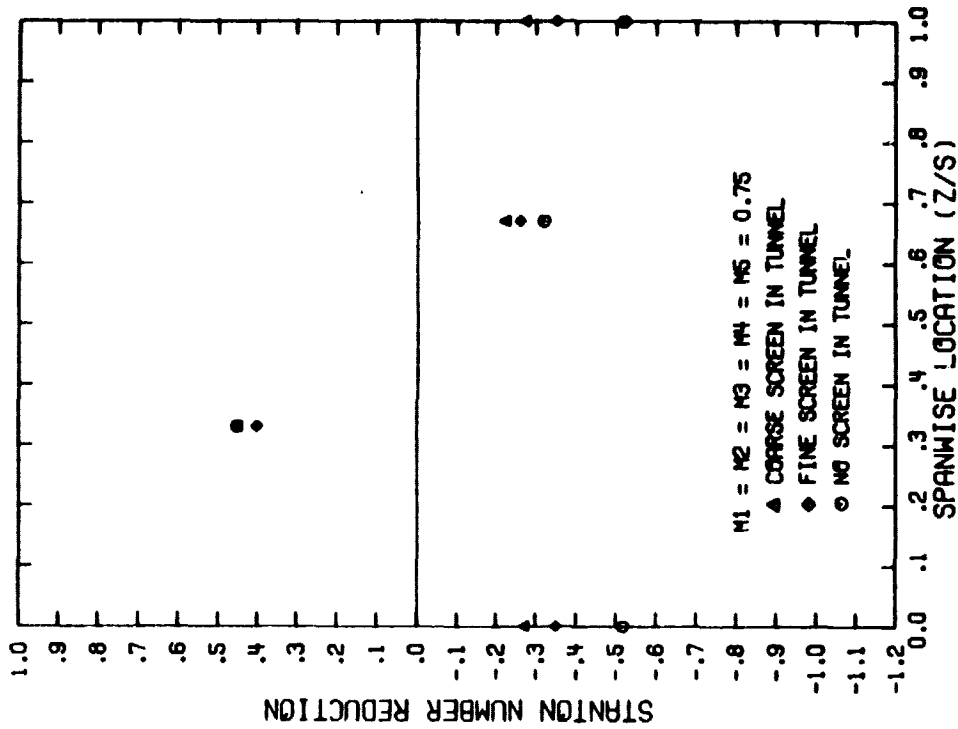


Figure A-98. The Influence of Freestream Turbulence on the Stanton Number Reduction with Uniform Blowing from a Five Row Configuration ($\Theta_1=50^\circ$, $\Theta_2=22.90^\circ$, $\Theta_3=40.80^\circ$, $\Theta_4=58.70^\circ$, $s/d_0=P/d_0=5$, $(x/d_0)_4=1.5$)

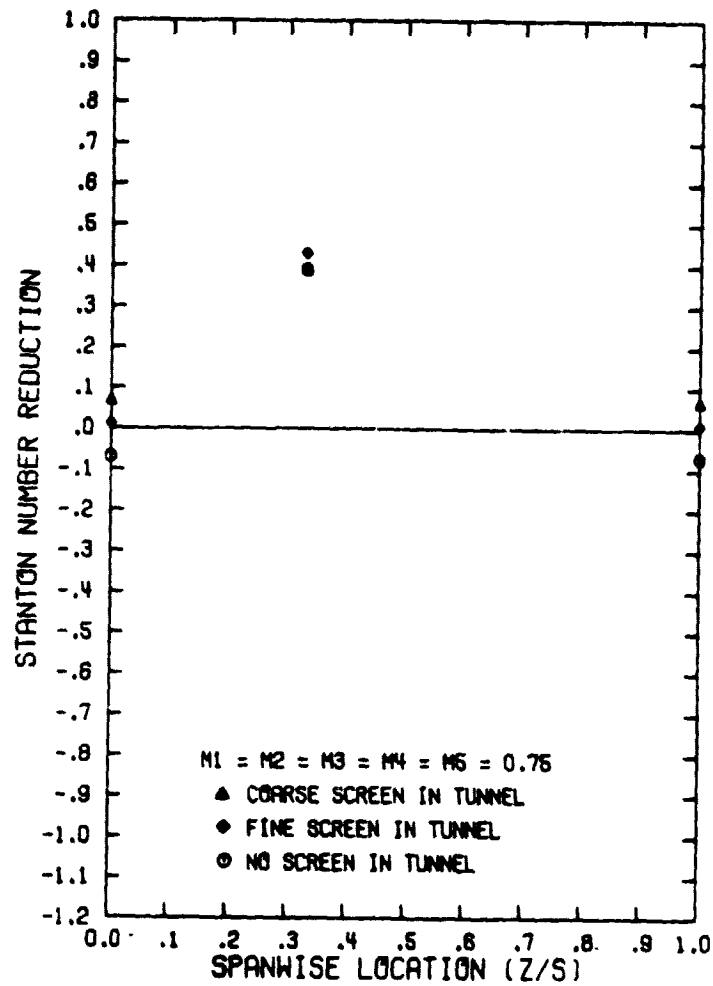


Figure A-99. The Influence of Freestream Turbulence on the Stanton Number Reduction with Uniform Blowing from a Five Row Configuration ($\theta_1=50^\circ$, $\theta_2=22.9^\circ$, $\theta_3=40.8^\circ$, $\theta_4=58.7^\circ$, $\theta_5=76.6^\circ$, $s/d_0=P/d_0=5$, $(x/d_0)_5=1.5$)